JPL PUBLICATION 85-29, VOLUME III

Proceedings of the Workshop on Identification and Control of Flexible Space Structures

Volume III

G. Rodriguez
Editor

(NASA-CR-176053) PROCEEDINGS OF THE WORKSHOP ON IDENTIFICATION AND CONTROL OF FLEXIBLE SPACE STRUCTURES, VOLUME 3 (Jet Propulsion Lab.) 463 p HC A20/MF A01 CSCL 22B G3/18
N85-31195 THRU N85-31214 Unclas 21843

April 1, 1985

NASA
National Aeronautics and
Space Administration

Jet Propulsion Laboratory
California Institute of Technology
Pasadena, California

JPL PUBLICATION 85-29, VOLUME III

Proceedings of the Workshop on Identification and Control of Flexible Space Structures

Volume III

G. Rodriguez
Editor

April 1, 1985

NASA

National Aeronautics and
Space Administration

Jet Propulsion Laboratory
California Institute of Technology
Pasadena, California

This publication was prepared by the Jet Propulsion Laboratory, California Institute of Technology, under a contract with the National Aeronautics and Space Administration.

ABSTRACT

These proceedings report the results of a workshop on identification and control of flexible space structures held in San Diego, CA, July 4-6, 1984. The workshop was co-sponsored by the Jet Propulsion Laboratory and the NASA Langley Research Center, and preceded the 1984 American Control Conference held at the same location. The main objectives of the workshop were to provide a forum to exchange ideas in exploring the most advanced modeling, estimation, identification and control methodologies to flexible space structures. The workshop responded to the rapidly growing interest within NASA in large space systems (space station, platforms, antennas, flight experiments) currently under design. The workshop consisted of surveys, tutorials, contributed papers, and discussion sessions in the following general areas: missions of current interest - space platforms, antennas, and flight experiments; control/structure interactions - modeling, integrated design and optimization, control and stabilization, and shape control; uncertainty management - parameter identification, model error estimation/compensation, and adaptive control; and experimental evaluation - ground laboratory demonstrations and flight experiment designs. Papers and lectures on these topics were presented at a total of fourteen sessions, including three panel discussions.

TABLE OF CONTENTS

VOLUME I

VOLUME II

VOLUME III

N85-31196

A STUDY ON THE CONTROL OF THIRD GENERATION SPACECRAFT*

E. J. Davison and W. Gesing
University of Toronto
Toronto, Ontario, Canada M5S 1A4

ABSTRACT

An overview of some studies which have recently been carried out in [1]-[3] on the control of third-generation spacecraft, as modelled by the MSAT space vehicle configuration, is made. This spacecraft is highly non-symmetrical and has appendages which cannot in general be assumed to be rigid. In particular, it is desired to design a controller for MSAT which stabilizes the system and satisfies certain attitude control, shape control, and possibly station-keeping requirements; in addition, it is desired that the resultant controller should be robust and avoid any undesirable "spill-over effects". In addition, the controller obtained should have minimum complexity.

The method of solution adopted to solve this class of problems is to formulate the problem as a robust servomechanism problem [5]-[7], and thence to obtain existence conditions and a controller characterization to solve the problem.

The final controller obtained for MSAT has a distributed control configuration and appears to be quite satisfactory.

INTRODUCTION

This paper summarizes studies carried out in [1]-[3] on control system structures known as third-generation spacecraft. Such spacecraft have:

(1) Large mass
(2) High power
(3) Large non-symmetric flexible appendages
(4) Precise communication RF beam control requirements.

In particular, the class of spacecraft represented by the Mobile Communications Satellite (MSAT) is used as a reference for these studies. This spacecraft has non-symmetric appendages which cannot be assumed to be rigid (see Figure 1).

There are a number of control problems associated with the attitude-control, shape-control and possibly station-keeping control for such third generation spacecraft (referred to as LFSS), which may be listed as follows:

A. The LFSS Control Problem

Problem 1: Lightly Damped, Oscillatory Plant

A LFSS has eigenvalues either at the origin or approximately distributed along the imaginary axis. One of the basic objectives that a controller must accomplish in this case is to stabilize the rigid body modes of the LFSS, and at the same time to stabilize the elastic modes of the LFSS. This is called the LFSS stabilization problem.

*This work was supported by the Department of Communications, Ottawa, Canada under contracts DOC-CR-SP-82-007, DOC-CR-SP-83-002, DOC-CR-SP-84-002.

Problem 2: Modelling

In modelling a LFSS, experience has shown that dynamic analysis may provide a framework for the modelling of the low frequency elastic modes of the LFSS in a reasonably accurate way, but that the high frequency elastic modes cannot be expected to be determined accurately, i.e. there will always be errors present in modelling the high frequency elastic modes of the LFSS. In addition, the calculation of dampening effects on the LFSS can only be done with great uncertainty.

Problem 3: The Infinite Dimensional Plant - The "Spill-Over Problem"

The classical modelling of elastic structures as continua results in the well known "infinite dimensional" system representation of a LFSS. Whether or not one adopts this infinite dimensionality representation seriously from an engineering standpoint, there is no question that the number of system elastic modes present in a LFSS is always larger than the number which any design model of a LFSS can accommodate. In trying to control the modelled rigid and elastic modes, it is essential that the controller should not cause these unmodelled high frequency elastic modes to become unstable. This is called the "Spill-Over Problem".

Problem 4: The Sensor/Actuator Placement Problem

The LFSS is intrinsically distributed, and the configuration of control hardware is not in general specified. Thus, unlike many conventional control problems, part of the LFSS control problem is in determining the number and location of sensor/actuators on the LFSS.

Problem 5: Requirement for Multivariable Control Theory

The concept of "third generation" spacecraft, unlike the first and some second generation spacecraft, precludes single-input, single-output control design. Some type of multivariable control design method is mandatory to deal with the severe interaction occurring in the system.

Problem 6: Minimization of Number of Sensors/Actuators

There is a practical limiation on the quantity of hardware that can be distributed over the LFSS vehicle. This implies in particular that one cannot assume full state feedback is available, and that the number of actuators/sensors used must be limited, i.e. one must minimize any unnecessary sensor/actuators required for LFSS control.

The following problem definition is now given:

B. The LFSS Robust Servomechanism Problem

Assume that a LFSS can be exactly described by the following finite dimensional linear time invariant model:

$$\begin{aligned} \dot{x} &= Ax + Bu + E\omega \\ y &= Cx + F\omega \\ y_m &= C_m x + F_m \omega_m \end{aligned} \tag{1}$$

where $x \epsilon R^n$ is the state, $u \epsilon R^m$ is the control (actuator inputs), $y_m \epsilon R^{r_m}$ are the measured (sensor) outputs, and $y \epsilon R^r$ are the outputs to be regulated. Here $\omega \epsilon R^{\Omega}$ are assumed to be constant unmeasurable disturbances applied to the structure, $\omega_m \epsilon R^{\Omega_m}$ are assumed to be constant unknown measurement errors and $e \triangleq y - y_{ref}$ is the error in the system where y_{ref} is a constant set-point. Thus, it is assumed that (1) may include an arbitrarily large number of elastic modes (but not infinite).

Assume now that an approximate model of (1), called the design model for (1), is given by:

$$\begin{aligned} \dot{\bar{x}} &= \bar{A}\bar{x} + \bar{B}u + \bar{E}\omega \\ y &= \bar{C}\bar{x} + \bar{F}\omega \\ y_m &= \bar{C}_m\bar{x} + \bar{F}_m\omega_m \end{aligned} \tag{2}$$

where $\bar{x} \epsilon R^{\bar{n}}$ is the state of the design model, and where $\bar{n} << n$. It is desired now to find a controller based on the design model (2), such that when it is applied to (1), the system is asymptotically stable, i.e. no spill-over occurs, and such that:

$$\lim_{t\to\infty} e(t) = 0 \quad , \qquad \forall x(0) \epsilon R^n, \quad \forall \omega \epsilon R^{\Omega}, \quad \forall \omega_m \epsilon R^{\Omega_m} \tag{3}$$

This is called the <u>LFSS Robust Servomechanism Problem,</u> which includes the following subproblems:

(1) Stabilization
(2) Station-keeping
(3) Attitude control
(4) Shape control.

THE MSAT CONTROL PROBLEM

The MSAT spacecraft is illustrated in Figure 1. It consists of four components, one of wich is rigid (the bus) and three of which are flexible (the solar array, the tower, and the reflector). The tower-reflector-hub hinge point is assumed to have a gimbal (see Figure 2).

The coordinates assumed for each of these substructures are as follows:

(1) Bus - three rigid rotations $(\theta_x, \theta_y, \theta_z)'$

(2) Tower - relative displacement of tower tip to tower root $(f^{-1}\delta_1, f^{-1}\delta_2, f^{-1}\delta_3)'$
- relative angular displacement of reflector with respect to frame fixed at tower root (with zero gimbal angles) $(\alpha_1, \alpha_2, \alpha_3)'$

(3) Reflector - two gimbal angles at tower-reflector-hub hinge point $(\beta_1, \beta_2)'$

The actuators which are assumed to be available are as follows:

(1) Eight thrusters f_i, $i=1,2,\ldots,8$, four from thrusters on the bus and four from thrusters at the reflector hinge point, aligned as shown in Figure 2.

(2) Two torquers at the reflector hub, one about each gimbal axis $(g_{\beta_1}, g_{\beta_2})'$ (see Figure 2).

In this case, a design model and an evaluation model was developed in [4], in which the design model has 18 states consisting of 5 rigid body modes (corresponding to the three rigid rotations of the bus and two gimbal angles of the reflector) together with 4 elastic modes, and the evaluation model has 32 states consisting of 5 rigid body modes and 11 elastic modes. Table 1 gives the eigenvalues of the open loop system for the two models. The models used in this study included the effect of dampening terms D, D_E (see Table 1).

TABLE 1: Open Loop Eigenvalues of MSAT Vehicle

	Standard Design Model		Evaluation Model	
	With Damping Term D Excluded	With Damping Term D Included	With Damping Term D_E Excluded	With Damping Term D_E Included
Rigid Body Modes	0 (repeated 10 times)	0 (repeated 10 times)	0 (repeated 10 times)	0 (repeated 10 times)
Elastic Body Modes	0±j0.124 0±j0.239 0±j0.556 0±j0.780	-0.000923±j0.124 -0.00170 ±j0.240 -0.00856 ±j0.556 -0.0211 ±j0.779	0±j0.124 0±j0.151 0±j0.239 0±j0.556 0±j0.690 0±j0.780 0±j1.55 0±j3.14 0±j3.96 0±j9.95 0±j14.0	-0.000923±j0.124 -0.000853±j0.151 -0.00171 ±j0.239 -0.00856 ±j0.556 -0.00553 ±j0.690 -0.0211 ±j0.780 -0.0751 ±j1.55 -0.0280 ±j3.14 -0.0528 ±j3.96 -0.524 ±j10.1 -1.17 ±j13.8

It may be noted that the elastic modes of the evaluation model interweave with the elastic modes of the design model.

A. Description of Problem to be Solved

In this case it is desired to solve the LFSS Robust Servomechanism Problem for the MSAT vehicle. In particular, there are two separate requirements for the controller to be designed for the MSAT vehicle:

Requirement I

Find a controller, based on the MSAT design model, which solves the following problems:

- Stability: stabilize the 5 rigid body modes and the 4 elastic modes of the system.
- Attitude control: regulate θ_x, θ_y, θ_z to desired constant set points θ_x^{ref}, θ_y^{ref}, θ_z^{ref} respectively, in the presence of unknown constant disturbances.

- Shape control: regulate $\beta_1+\alpha_1$, $\beta_2+\alpha_2$, $f^{-1}\delta_1$, $f^{-1}\delta_2$, $f^{-1}\delta_3$, α_3 to zero, in the presence of unknown constant disturbances.
- Spill-over problem: it is desired that the controller should satisfy the above requirements, and not cause any instability to occur with respect to any of the vehicle's elastic modes which are not included in the design model.
- Controller complexity: it is desired to minimize the number of sensors and actuators which are required to solve the problem.
- Discrete controller implementation: it is desired that the controller, when implemented digitally, should not require an excessively large sampling rate to maintain stability.

Requirement II

Apply the controller obtained, based on the MSAT design model, to the MSAT evaluation model, and verify that all objectives above are satisfied.

The outputs to be regulated in this case are given by:

$$y \triangleq (\theta_x,\theta_y,\theta_z,\beta_1+\alpha_1,\beta_2+\alpha_2,f^{-1}\delta_1,f^{-1}\delta_2,f^{-1}\delta_3,\alpha_3)' \tag{4}$$

B. Assumptions Made in Problem Formulation

In this problem, it is assumed that there is no requirement for controlling the ω_x, ω_y, ω_z rigid body modes. (Note: this assumption is not essential, e.g. [2], [3] also deals with the case of station-keeping.) It is also assumed that there is no need to include any gyroscopic terms in the design and evaluation models.

METHOD OF SOLUTION ADOPTED TO OBTAIN A CONTROLLER TO SOLVE PROBLEM

The method of approach adopted to solve this problem was based on using the results of the "robust servomechanism problem" [5]-[7], in conjunction with a parameter optimization method [8] to determine the controller's parameters, e.g. see [9] which solves a special case of the above problem when the sensors and actuators are collocated, using a decentralized control configuration. In this case, existence conditions for a solution to the problem were obtained, and a necessary controller structure developed. In particular, it was found that any controller which solves the MSAT problem specifications must consist of a "servo-compensator" [5] (unique), together with a stabilizing compensator (non-unique). In this study, the simplest possible stabilizing compensator, i.e. a stabilizing compensator consisting of only proportional and rate feedback terms, was used.

In this case, in order to satisfy the existence conditions obtained for a solution to exist to the problem, it was necessary to choose the following inputs (actuators) and measurable outputs (sensors) for the controller:

Outputs (sensors):

$$y_m \triangleq (\theta_x,\theta_y,\theta_z,\beta_1,\beta_2,\alpha_1,\alpha_2,f^{-1}\delta_1,f^{-1}\delta_2)' \tag{5}$$

Inputs (actuators):

$$u \triangleq (g^*_{c_3}, g_{\beta_1}, g_{\beta_2}, f^*_1, f^*_2, f^*_5, f^*_6)' \qquad (6)$$

where $g^*_{c_3}$, f^*_1, f^*_2, f^*_5, f^*_6 correspond to various combinations of the thrusters $f_1, f_2, \ldots, f_7, f_8$ (see Figure 2), as described in Appendix I.

FINAL CONTROLLER CONFIGURATION OBTAINED

In this case, the following distributed controller was obtained as a solution to the MSAT robust servomechanism problem, based on the MSAT design model:

$$\begin{pmatrix} g^*_{c_3} \\ g_{\beta_1} \\ g_{\beta_2} \\ f^*_1 \\ f^*_2 \end{pmatrix} = -K_1 \begin{pmatrix} \theta_x - \tilde{\theta}_x \\ \theta_y - \tilde{\theta}_y \\ \theta_z - \tilde{\theta}_z \\ \beta_1 \\ \beta_2 \end{pmatrix} - K_2 s \begin{pmatrix} \theta_x \\ \theta_y \\ \theta_z \\ \beta_1 \\ \beta_2 \end{pmatrix} - \frac{K_3}{s} \begin{pmatrix} \theta_x - \tilde{\theta}_x \\ \theta_y - \tilde{\theta}_y \\ \theta_z - \tilde{\theta}_z \\ \beta_1 + \alpha_1 \\ \beta_2 + \alpha_2 \end{pmatrix} - \frac{K_4}{s} \begin{pmatrix} f^{-1}\delta_1 \\ f^{-1}\delta_2 \end{pmatrix} \qquad (7)$$

$$\begin{pmatrix} f^*_5 \\ f^*_6 \end{pmatrix} = -\frac{K_5}{s} \begin{pmatrix} f^{-1}\delta_1 \\ f^{-1}\delta_2 \end{pmatrix}$$

where s denotes the Laplace Transform operator, where

$$\begin{pmatrix} \tilde{\theta}_x \\ \tilde{\theta}_y \\ \tilde{\theta}_z \end{pmatrix} \triangleq \left(\frac{\gamma}{s+\gamma}\right)^2 \begin{pmatrix} \theta^{ref}_x \\ \theta^{ref}_y \\ \theta^{ref}_z \end{pmatrix} \qquad (8)$$

and where K_1, K_2, K_3, K_4, K_5, γ are given as follows:

$$K_1 = \begin{bmatrix} 1.43 & 0.500 & 24.7 & 1.34 & -0.0460 \\ 0.0255 & 4.64 & 1.12 & 15.6 & -0.000439 \\ -6.81 & -0.000957 & 0.00981 & -0.000483 & 18.6 \\ 0.00326 & 38.0 & -0.231 & 14.5 & -0.00955 \\ 59.0 & -0.00916 & 0.0216 & 0.0127 & -2.40 \end{bmatrix}$$

$$K_2 = \begin{bmatrix} 28.5 & 10.0 & 494 & 26.7 & -0.920 \\ 0.510 & 92.8 & 22.3 & 312 & -0.00877 \\ -136 & -0.0191 & 0.196 & -0.00965 & 372.2 \\ 0.0653 & 760 & -4.63 & 290 & -0.191 \\ 1180 & -0.183 & 0.432 & 0.254 & -48.1 \end{bmatrix}$$

$$K_3 = \begin{bmatrix} 7.14\times10^{-4} & 2.50\times10^{-4} & 1.24\times10^{-2} & 6.68\times10^{-4} & -2.30\times10^{-5} \\ 1.28\times10^{-5} & 2.32\times10^{-3} & 5.58\times10^{-4} & 7.80\times10^{-3} & -2.19\times10^{-7} \\ -3.41\times10^{-3} & -4.79\times10^{-7} & 4.90\times10^{-6} & -2.41\times10^{-7} & 9.31\times10^{-3} \\ 1.63\times10^{-6} & 1.90\times10^{-2} & -1.16\times10^{-4} & 7.26\times10^{-3} & -4.78\times10^{-6} \\ 2.95\times10^{-2} & -4.58\times10^{-6} & 1.08\times10^{-5} & 6.34\times10^{-6} & -1.20\times10^{-3} \end{bmatrix}$$

$$K_4 = \begin{bmatrix} -0.464 & 0.0433 \\ -0.0144 & 0.0536 \\ -0.00438 & 0.201 \\ 0.136 & 0.0461 \\ -0.000753 & 1.13 \\ 0.0268 & 0.225 \\ 0.0273 & -0.226 \end{bmatrix}$$

$$K_5 = \begin{bmatrix} 0.0268 & 0.225 \\ 0.0273 & -0.226 \end{bmatrix}$$

$$\gamma = 2.0\times10^{-3}$$

This controller is just a multivariable generalization of the classical three term controller used in classical control. The controller has minimal complexity in the sense that it has minimum order feedback dynamics and has the minimum number of actuators/sensors required in order to solve the problem. It is to be noted that no a priori assumption on the distributed structure of (7) was made — the distributed structure of the controller (7) arose from the analysis automatically.

PROPERTIES OF PROPOSED CONTROLLER

The main features of the proposed controller when applied to the MSAT design model and evaluation model will now be described. The main features of interest are:

(1) The stabilization properties of the proposed controller.
(2) The steady state regulation properties of the proposed controller.

The following results are obtained:

A. Eigenvalues of Closed Loop System Using Proposed Controller

Table 2 gives a listing of all eigenvalues obtained by applying the proposed controller (7) to the MSAT design model and evaluation models.

TABLE 2: Listing of Closed Loop Eigenvalues Using Proposed Controller (7) When Applied to MSAT Design and Evaluation Models

Standard Design Model		Evaluation Model	
$-0.00047 \pm j0.0085$ $-0.0024 \pm j0.016$ $-0.0051 \pm j0.022$ $-0.0097 \pm j0.030$ $-0.010 \pm j0.031$	rigid body modes	$-0.00047 \pm j0.0085$ $-0.0024 \pm j0.016$ $-0.0051 \pm j0.023$ $-0.0097 \pm j0.030$ $-0.010 \pm j0.031$	rigid body modes
$-0.00014 \pm j0.124$ $-0.0061 \pm j0.240$ $-0.017 \pm j0.557$ $-0.029 \pm j0.780$	elastic body modes	$-0.00014 \pm j0.124$ $-0.00020 \pm j0.151$ $-0.0061 \pm j0.240$ $-0.017 \pm j0.557$ $-0.0079 \pm j0.690$ $-0.0029 \pm j0.780$ $-0.129 \pm j1.35$ $-0.067 \pm j3.16$ $-0.069 \pm j3.95$ $-0.5 \pm j8.88$ $-0.51 \pm j11.3$	elastic body modes
-5.0×10^{-4} -5.0×10^{-4} -5.0×10^{-4} -5.0×10^{-4} -5.0×10^{-4} -5.0×10^{-4} -5.0×10^{-4}	servo-compensator modes	-1.7×10^{-3} -5.0×10^{-4} -5.0×10^{-4} -5.0×10^{-4} -5.0×10^{-4} -5.0×10^{-4} -5.0×10^{-4}	servo-compensator modes
-2.0×10^{-3} -2.0×10^{-3} -2.0×10^{-3} -2.0×10^{-3} -2.0×10^{-3} -2.0×10^{-3}	feedforward controller modes	-2.0×10^{-3} -2.0×10^{-3} -2.0×10^{-3} -2.0×10^{-3} -2.0×10^{-3} -2.0×10^{-3}	feedforward controller modes

It is observed that the resultant closed loop system is asymptotically stable for both the design and evaluation models, i.e. no undesirable spill-over effects occur. It is also observed that the dominant time constant of the system is mainly associated with the servo-compensator modes. This implies that one would expect for the case of tracking, that the dominant time response of the system would be associated with the feedforward controller modes, i.e. $TC_{dom} \doteq 500$ sec $\doteq 8$ min., and for the case of disturbance rejection, that the dominant time of the system would be associated with the servo-compensator modes, i.e. $TC_{dom} \doteq 2000$ sec $\doteq 0.6$ hrs. This result is verified in the simulation studies to follow.

B. Steady-State Values of Outputs Using Proposed Controller: Tracking Case

Table 3 gives a summary of results obtained for the case of unit step function tracking, when the proposed controller (7) is applied to the MSAT design and evaluation model. It is observed that all 9 outputs of the system are asymptotically regulated to their correct values as desired.

TABLE 3: Steady-State Values of Outputs Using Proposed Controller (7) When Applied to Design and Evaluation Model - Tracking Case

	$\theta_x^{ref}=1$	$\theta_y^{ref}=1$	$\theta_z^{ref}=1$
θ_x	1	0	0
θ_y	0	1	0
θ_z	0	0	1
$\beta_1+\alpha_1$	0	0	0
$\beta_2+\alpha_2$	0	0	0
$f^{-1}\delta_1$	0	0	0
$f^{-1}\delta_2$	0	0	0
$f^{-1}\delta_3$	0	0	0
α_3	0	0	0

Note: Any $|\text{number}|<10^{-16}$ is assumed to be zero.

C. Steady-State Values of Outputs Using Proposed Controller: Disturbance Rejection Case

Tables 4 and 5 give a summary of all results obtained for the case of disturbance rejection, when the proposed controller is applied to the MSAT design and evaluation models respectively. In this case, it is assumed that a unit step function change occurs for different disturbances corresponding to $\bar{g}_{c_1},\bar{g}_{c_2},\ldots,\bar{f}_0,\bar{f}_9$ defined in Table 6. It is observed that the first 7 outputs of the system are asymptotically regulated to zero, and that the remaining two outputs are approximately equal to zero in all cases, as is desired.

D. Sampling Rate Requirements for Digital Implementation of Proposed Controller

If it is assumed that the proposed controller (7) is to be implemented digitally, then it is necessary that the sensor outputs and actuator signals be updated at a fast enough rate so as to guarantee closed loop stability, when the the controller is applied to the evaluation model. In this case, on assuming that the sensor and actuator signals are updated at the same rate, it was found that a sampling rate of at least 0.1 Hz must be used to implement the proposed controller. This requirement is not demanding.

TABLE 4: Steady-State Values of Outputs Using Proposed Controller (7) When Applied to MSAT Design Model - Disturbance Rejection Case

	$\bar{g}_{c_1}=1$	$\bar{g}_{c_2}=1$	$\bar{g}_{c_3}=1$	$\bar{g}_{\beta_1}=1$	$\bar{g}_{\beta_2}=1$	$\bar{f}_1=1$	$\bar{f}_2=1$	$\bar{f}_5=1$	$\bar{f}_6=1$	$\bar{f}_0=1$	$\bar{f}_9=1$
θ_x	0	0	0	0	0	0	0	0	0	0	0
θ_y	0	0	0	0	0	0	0	0	0	0	0
θ_z	0	0	0	0	0	0	0	0	0	0	0
$\beta_1+\alpha_1$	0	0	0	0	0	0	0	0	0	0	0
$\beta_2+\alpha_2$	0	0	0	0	0	0	0	0	0	0	0
$f^{-1}\delta_1$	0	0	0	0	0	0	0	0	0	0	0
$f^{-1}\delta_2$	0	0	0	0	0	0	0	0	0	0	0
$f^{-1}\delta_3$	2×10^{-10}	8×10^{-8}	0	0	0	3×10^{-10}	-3×10^{-10}	0	0	3×10^{-9}	-8×10^{-9}
α_3	-2×10^{-8}	8×10^{-6}	0	0	0	-1×10^{-7}	1×10^{-7}	0	0	-2×10^{-6}	3×10^{-6}

Note: Any $|\text{number}|<10^{-16}$ is assumed to be zero.

TABLE 5: Steady-State Values of Outputs Using Proposed Controller (7) When Applied to MSAT Evaluation Model - Disturbance Rejection Case

	$\bar{g}_{c_1}=1$	$\bar{g}_{c_2}=1$	$\bar{g}_{c_3}=1$	$\bar{g}_{\beta_1}=1$	$\bar{g}_{\beta_2}=1$	$\bar{f}_1=1$	$\bar{f}_2=1$	$\bar{f}_5=1$	$\bar{f}_6=1$	$\bar{f}_0=1$	$\bar{f}_9=1$
θ_x	0	0	0	0	0	0	0	0	0	0	0
θ_y	0	0	0	0	0	0	0	0	0	0	0
θ_z	0	0	0	0	0	0	0	0	0	0	0
$\beta_1+\alpha_1$	0	0	0	0	0	0	0	0	0	0	0
$\beta_2+\alpha_2$	0	0	0	0	0	0	0	0	0	0	0
$f^{-1}\delta_1$	0	0	0	0	0	0	0	0	0	0	0
$f^{-1}\delta_2$	0	0	0	0	0	0	0	0	0	0	0
$f^{-1}\delta_3$	4×10^{-5}	-3×10^{-8}	0	0	0	4×10^{-9}	-4×10^{-9}	0	0	-3×10^{-6}	-8×10^{-4}
α_3	-3×10^{-7}	5×10^{-5}	0	0	0	-7×10^{-8}	7×10^{-8}	0	0	1×10^{-6}	3×10^{-6}

Note: Any $|\text{number}|<10^{-16}$ is assumed to be zero.

SIMULATIONS OBTAINED USING PROPOSED CONTROLLER TO SOLVE MSAT PROBLEM

This section gives some typical simulations of the closed loop system obtained by using the proposed controller (7) applied to the MSAT design and evaluation models. Additional simulation studies are given in [3].

A. Example No. 1 (Attitude Control: $\theta_x^{ref}=1$)

In this example, it is assumed that the system has zero initial conditions, that there are no disturbances present, and that a unit step function change of +1 occurs in the set point for θ_x at t=0, i.e. $\theta_x^{ref}=1$, $\theta_y^{ref}=0$, $\theta_z^{ref}=0$.

Figure 3 gives a plot of all 9 output variables y given by (4) when the controller is applied to both the design and evaluation model in this case. It is observed that the system's response is almost decoupled, i.e. the output θ_x is approximately equal to its desired value of +1 at $t \doteq 50$ min, and that all other 8 outputs are barely excited.

Figure 4 gives a plot of the 7 control variables u given by (5) for this example.

B. Example No. 2 (Disturbance Rejection: $\bar{f}_5=1$)

In this example, it is assumed that the system has zero initial conditions, that all set points are identically equal to zero, and that a unit step function change of +1 occurs at t=0 corresponding to a disturbance thrust $\bar{f}_5=1$, where $\bar{f}_5$ is defined in Table 6. This example would correspond to a misaligned thruster associated with the proposed controller.

Figure 5 gives a plot of all 9 output variables y when the controller is applied to both the design and evaluation model in this case. It is observed that the elastic modes of the vehicle are now excited, and that the output variables are asymptotically regulated to zero in approximately 2.7 hours, which is consistent with the closed loop eigenvalues of the system given in Table 2.

Figure 6 gives a plot of the 7 control variables u for this example.

C. Example No. 3 (Disturbance Rejection: $\bar{f}_9=1$)

This example is similar to Example No. 2 except that it is assumed that a unit step function of +1 occurs at t=0 corresponding to a disturbance thrust $\bar{f}_9=1$, where $\bar{f}_9$ is defined in Table 6. This disturbance is representative of an arbitrary constant disturbance which may affect the system.

Figure 7 gives a plot of all 9 output variables y when the controller is applied to both the design and evaluation models in this case. It is observed that the elastic modes of the vehicle are now also excited as they were in Example No. 2, and that the output variables are satisfactorily asymptotically regulated with the same time constant as in Example No. 2.

Figure 8 gives a plot of the 7 control variables u for this example.

TABLE 6: Definition of Disturbances Assumed

$\bar{f}_1,\bar{f}_2,\bar{f}_5,\bar{f}_6,\bar{f}_0,\bar{f}_9$	Disturbance forces corresponding to the thrusters f_1,f_2,f_5,f_6,f_0,f_9 respectively of Figure 2
$\bar{g}_{\beta_1},\bar{g}_{\beta_2}$	Disturbance torques corresponding to g_{β_1},g_{β_2} respectively about the gimbal axis β_1,β_2^1
$\bar{g}_{c_1},\bar{g}_{c_2},\bar{g}_{c_3}$	Disturbance torques in the bus about the x,y,z axis respectively

ROBUST PROPERTIES OF CONTROLLER DESIGN METHOD

A study of the robustness properties of the proposed controller design method was carried out [3]. This was done by comparing the controller designs obtained using the proposed method to different design models of MSAT. It was concluded that the proposed design method appears to be quite insensitive to the type of design model used, e.g. all controllers obtained, when based on MSAT design models which had at least two dominant elastic body modes included, produced stable closed loop systems and give satisfactory tracking/regulation, when applied to the MSAT evaluation model. Other studies showed that the controller is robust with respect to evaluation models of arbitrary complexity.

CONCLUSIONS

This paper gives a brief summary of the work performed in [1]-[3]. In these studies, the control system design of a third-generation spacecraft, as modelled by the MSAT space configuration is studied. This spacecraft is highly non-symmetrical and has appendages which cannot, in general, be assumed to be rigid; the elasticity of these appendages makes the control system design particularly demanding. In particular, it is desired to design a controller for MSAT which stabilizes the system and satisfies certain attitude control, shape control and possibly station-keeping requirements. In addition, it is desired that the resultant controller should be robust and avoid any "spill-over effects", i.e. it should satisfy the problems' specifications based on only an approximate design model for MSAT being available. In addition, the controller obtained should have minimum complexity, i.e. a minimum number of sensors/actuators should be used.

The method of solution adopted to solve this class of problems was to formulate the problem as a robust servomechanism problem and thence to obtain existence conditions and a controller characterization to solve the problem. In this case, the controller obtained must contain a servo-compensator together with a stabilizing compensator.

The final controller obtained for MSAT has a distributed control configuration, and appears to be quite satisfactory, i.e. extensive testing of the controller shows that the controller is indeed robust with respect to the choice of the design model, and that it satisfies all specifications of the problem statement.

ACKNOWLEDGEMENTS

The authors are grateful to P. Hughes, A.H. Reynaud and H. Stieber for their valuable assistance in this work. This work was sponsored by the Department of Communications, Ottawa, Canada under the Scientific Authorities: H. Reynaud and H.F. Stieber.

REFERENCES

[1] Davison,E.J., Hughes,P.C., "A Study to Determine Control Techniques Applicable to Third-Generation Spacecraft", DOC Report No.: DOC-CR-SP-82-007, March 1982.

[2] Davison,E.J., "A Study to Develop Control Techniques Applicable to Third-Generation Spacecraft", DOC Report No.: DOC-CR-SP-83-002, February 1983.

[3] Davison,E.J., "A Study to Develop Control Techniques Applicable to Third-Generation Spacecraft - Part III", DOC Report No.: DOC-CR-SP-84-002, February 1984.

[4] Hughes,P.C., Sincarsin,G.B., "MSAT Structural Dynamics Model for Control System Design", DOC Report No.: DOC-CR-SP-82-054, August 1982.

[5] Davison,E.J., "Robust Control of a Servomechanism Problem for Linear Time-Invariant Multivariable Systems", IEEE Trans. on Automatic Control, Vol. AC-21, No. 1, 1976, pp. 25-34.

[6] Davison,E.J., Goldenberg,A., "Robust Control of a General Servomechanism Problem: The Servo-Compensator", Automatica, Vol. 11, 1975, pp. 461-471.

[7] Davison,E.J., "The Robust Decentralized Control of a General Servomechanism Problem", IEEE Trans. on Automatic Control, Vol. AC-21, No. 1, 1976, pp. 14-24.

[8] Davison,E.J., Ferguson,I.J., "Design of Controllers for the Multivariable Robust Servomechanism Problem Using Parameter Optimization Methods", IEEE Trans. on Automatic Control, Vol. AC-26, No. 1, 1981, pp. 93-110.

[9] West-Vukovich,G., Davison,E.J., Hughes,P., "The Decentralized Control of Large Flexible Space Structures", IEEE Trans. on Automatic Control, 1984 to appear.

APPENDIX I

Definitions of $g^*_{c_3}, f^*_1, f^*_2, f^*_5, f^*_6$

$g^*_{c_3}$ is defined in terms of thrusters f_1, f_2, f_3, f_4 as follows:

$$\begin{pmatrix} f_1 \\ f_3 \end{pmatrix} = \begin{pmatrix} 8.66 \\ 8.66 \end{pmatrix} g^*_{c_3} \qquad \text{if } g^*_{c_3} \geq 0$$

$$\begin{pmatrix} f_2 \\ f_4 \end{pmatrix} = \begin{pmatrix} 8.66 \\ 8.66 \end{pmatrix} g^*_{c_3} \qquad \text{if } g^*_{c_3} < 0$$

f^*_5, f^*_6 are defined in terms of thrusters f_5, f_6, f_7, f_8 as follows:

$$\begin{pmatrix} f_5 \\ f_7 \end{pmatrix} = \begin{pmatrix} 1 \\ 0 \end{pmatrix} f^*_5 \quad \text{if } f^*_5 \geq 0 \quad ; \quad \begin{pmatrix} f_6 \\ f_8 \end{pmatrix} = \begin{pmatrix} 1 \\ 0 \end{pmatrix} f^*_6 \quad \text{if } f^*_6 \geq 0$$

$$\begin{pmatrix} f_5 \\ f_7 \end{pmatrix} = \begin{pmatrix} 0 \\ 1 \end{pmatrix} f^*_5 \quad \text{if } f^*_5 < 0 \quad ; \quad \begin{pmatrix} f_6 \\ f_8 \end{pmatrix} = \begin{pmatrix} 0 \\ 1 \end{pmatrix} f^*_6 \quad \text{if } f^*_6 < 0$$

f^*_1, f^*_2 are defined in terms of thrusters f_1, f_2, f_3, f_4 as follows:

$$\begin{pmatrix} f_1 \\ f_2 \\ f_4 \end{pmatrix} = \begin{pmatrix} 1 & 1 \\ 1 & 0 \\ 0 & 1 \end{pmatrix} \begin{pmatrix} f^*_1 \\ f^*_2 \end{pmatrix} \qquad \text{if } f^*_1 \geq 0 \text{ and } f^*_2 \geq 0$$

$$\begin{pmatrix} f_1 \\ f_2 \\ f_3 \end{pmatrix} = \begin{pmatrix} 1 & 1 \\ 1 & 0 \\ 0 & 1 \end{pmatrix} \begin{pmatrix} f^*_1 \\ f^*_2 \end{pmatrix} \qquad \text{if } f^*_1 \geq 0 \text{ and } f^*_2 < 0$$

$$\begin{pmatrix} f_3 \\ f_4 \\ f_1 \end{pmatrix} = \begin{pmatrix} 1 & 0 \\ 1 & 1 \\ 0 & 1 \end{pmatrix} \begin{pmatrix} f^*_1 \\ f^*_2 \end{pmatrix} \qquad \text{if } f^*_1 < 0 \text{ and } f^*_2 \geq 0$$

$$\begin{pmatrix} f_2 \\ f_3 \\ f_4 \end{pmatrix} = \begin{pmatrix} 0 & 1 \\ 1 & 1 \\ 1 & 0 \end{pmatrix} \begin{pmatrix} f^*_1 \\ f^*_2 \end{pmatrix} \qquad \text{if } f^*_1 < 0 \text{ and } f^*_2 < 0$$

ORIGINAL PAGE IS
OF POOR QUALITY

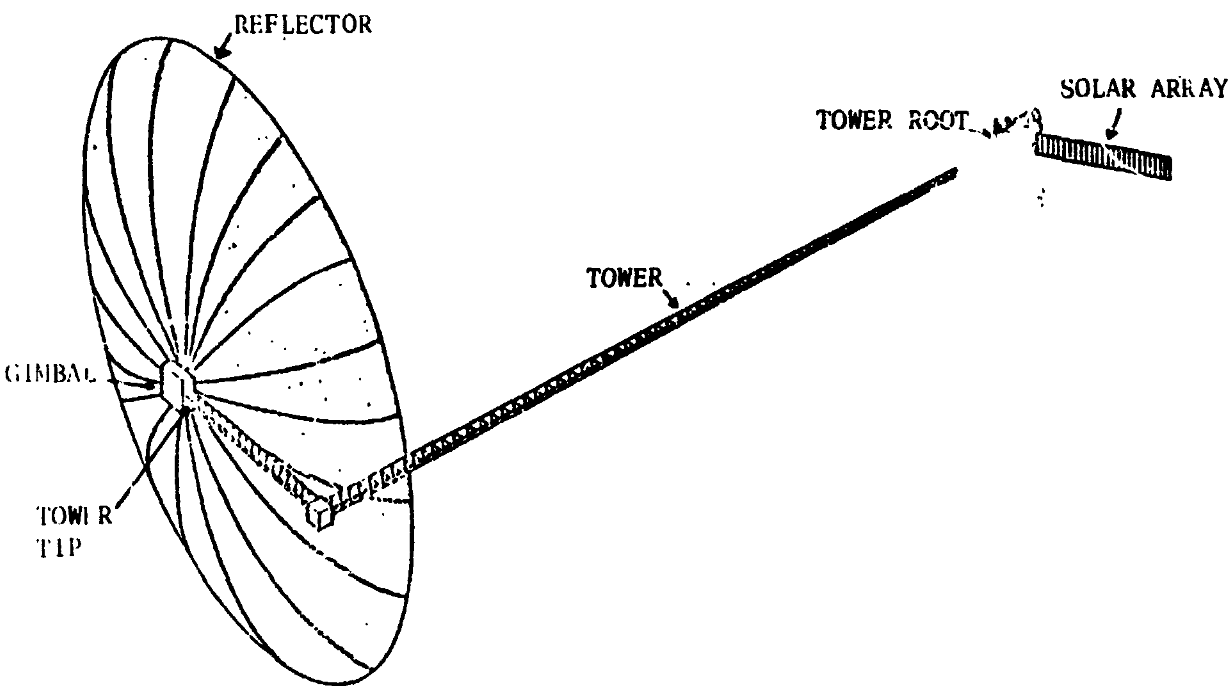

Figure 1: The MSAT configuration - a typical third generation spacecraft.

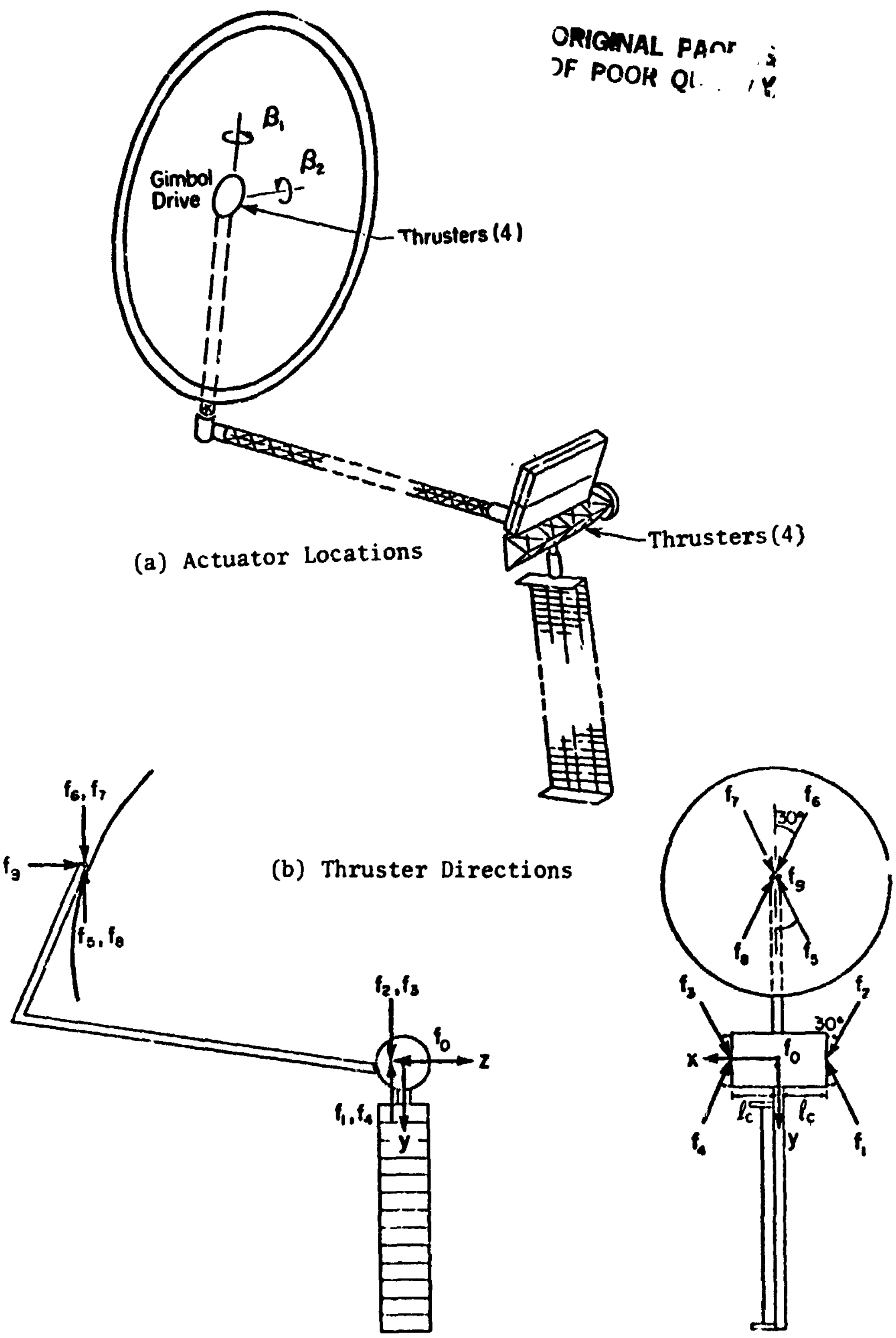

Figure 2: Assumed control inputs for MSAT spacecraft (taken from [4]).

ORIGINAL PAGE IS
OF POOR QUALITY

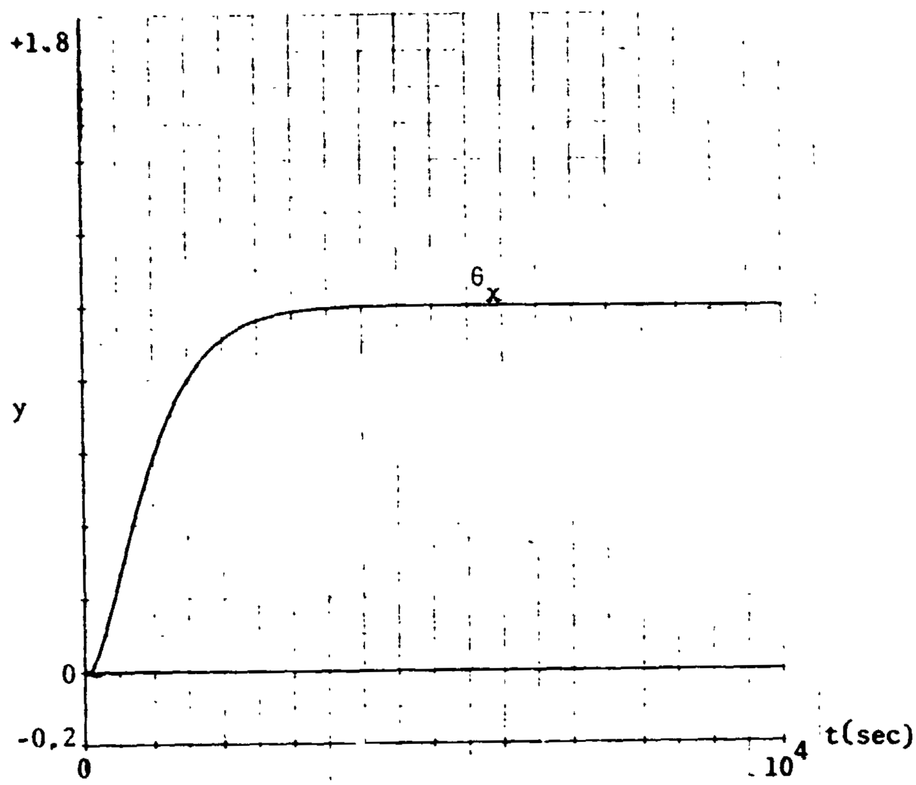

Figure 3: Plot of 9 regulated outputs y for example no. 1.

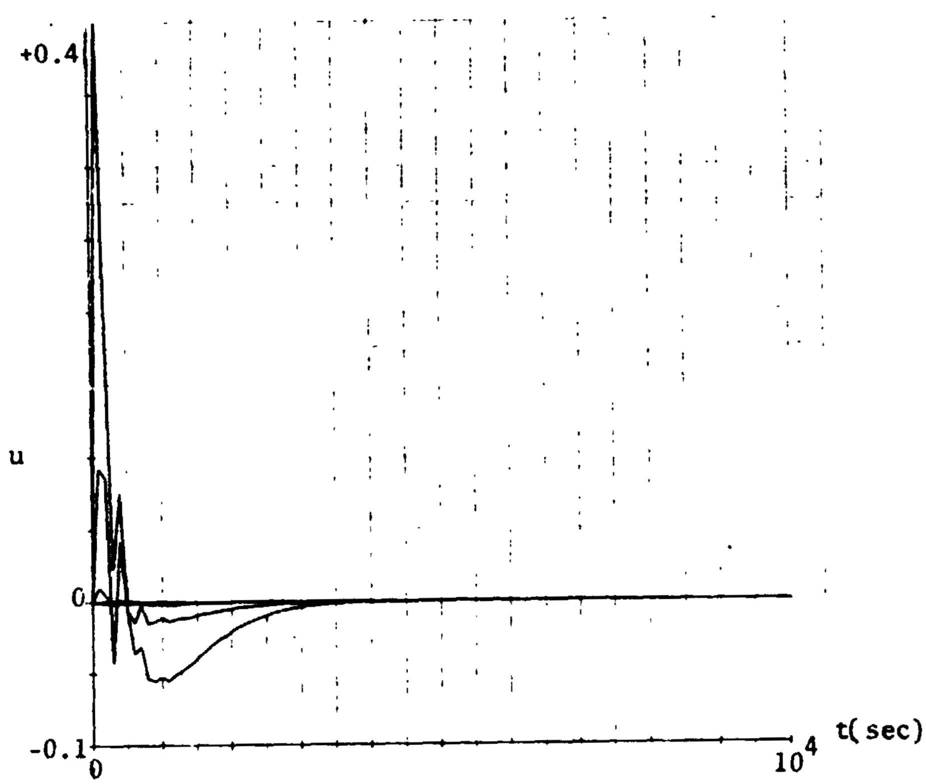

Figure 4: Plot of 7 control inputs u for example no. 1.

ORIGINAL PAGE IS
OF POOR QUALITY

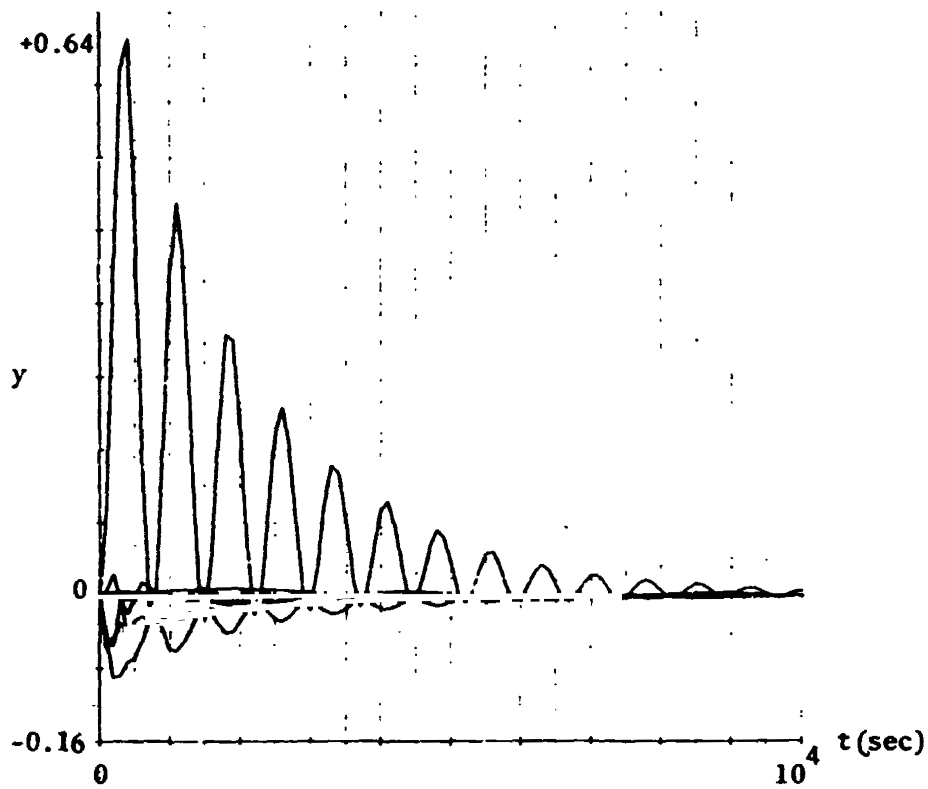

Figure 5: Plot of 9 regulated outputs y for example no. 2.

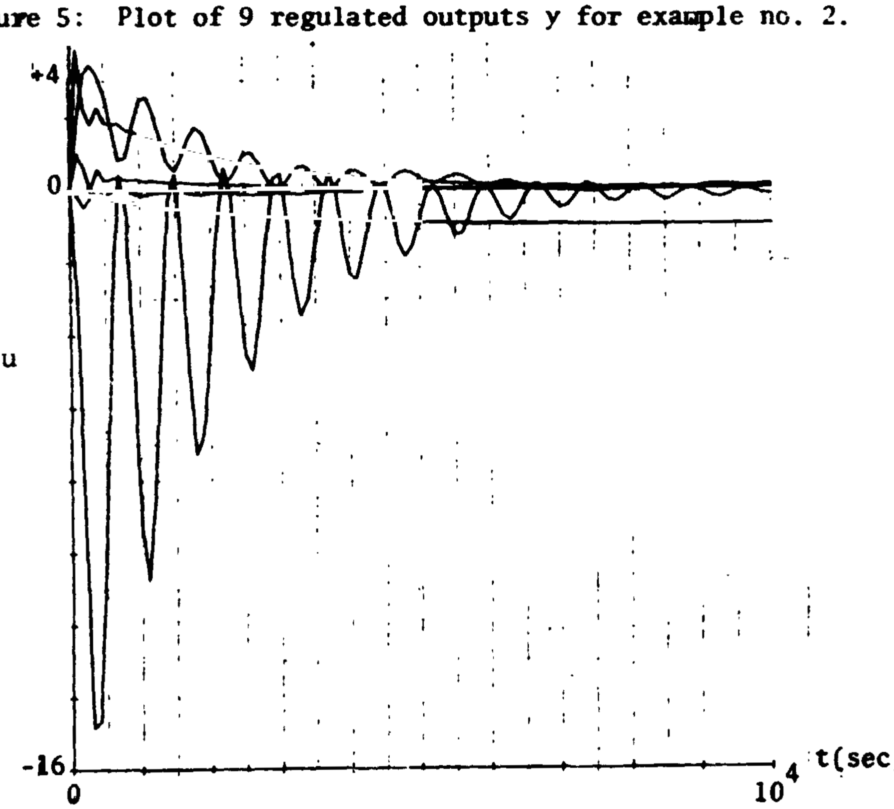

Figure 6: Plot of 7 control inputs u for example no. 2.

ORIGINAL PAGE IS
OF POOR QUALITY

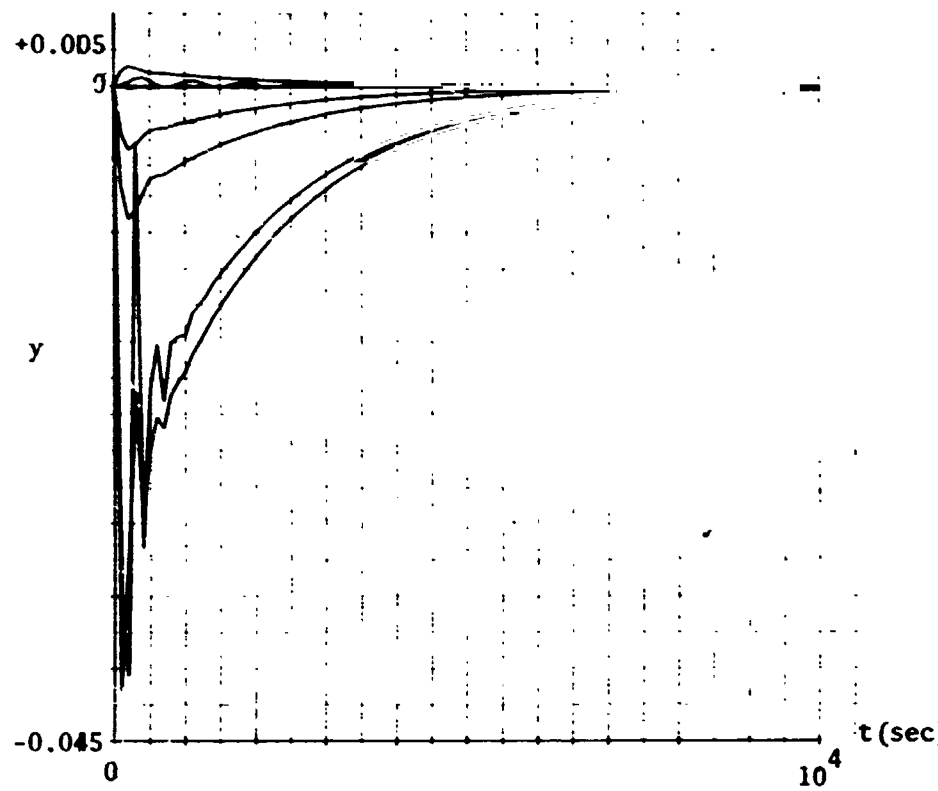

Figure 7: Plot of 9 regulated outputs y for example no. 3.

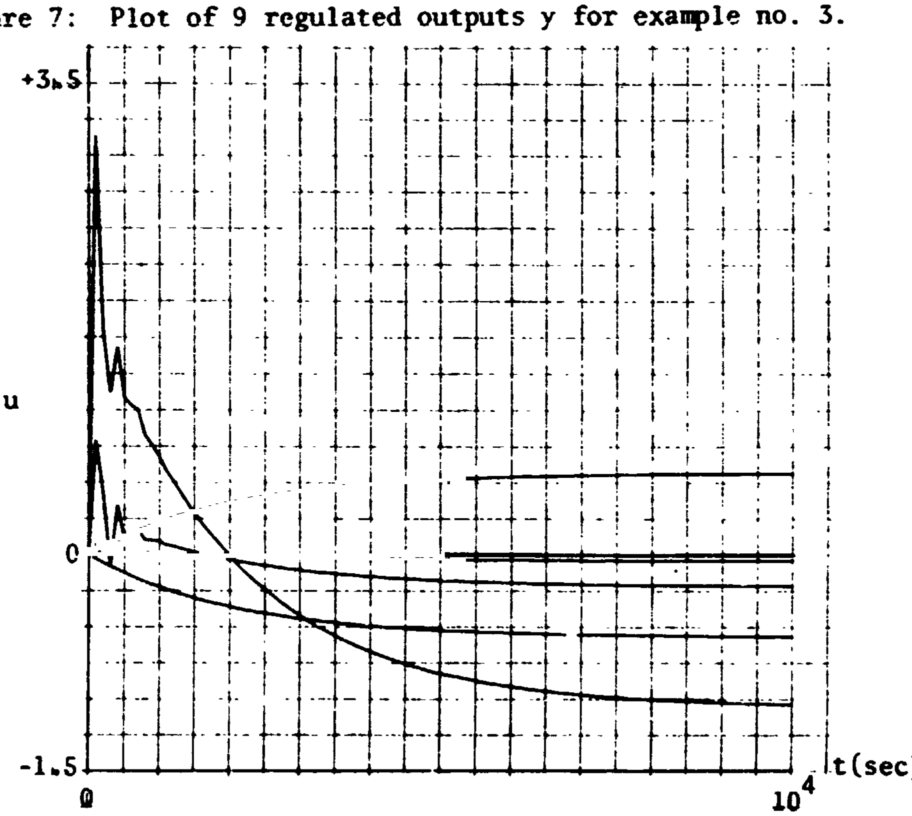

Figure 8: Plot of 7 control inputs u for example no. 3.

N85-31197

SENSOR/ACTUATOR SELECTION FOR THE CONSTRAINED VARIANCE CONTROL PROBLEM

M. L. DeLorenzo
Air Force Academy, Colorado Springs, CO 80901

R. E. Skelton
School of Aeronautics and Astronautics
Purdue University
West Lafayette, IN 47907

ABSTRACT

This paper considers the problem of designing a linear controller for systems subject to inequality variance constraints. A quadratic penalty function approach is used to yield a linear controller. Both the weights in the quadratic penalty function and the locations of sensors and actuators are selected by successive approximations to obtain an optimal design which satisfies the input/output variance constraints. The method is applied to NASA's 64 meter Hoop-Column Space Antenna for satellite communications. In addition the solution for the control law, the main feature of these results is the systematic determination of actuator design *requirements* which allow the given input/output performance constraints to be satisfied.

I. INTRODUCTION

Consider the task of controlling the linear, stochastic system

(1a) $\dot{x} = Ax + B(u+w)\ , \quad x \epsilon R^n,\ u \epsilon R^m,\ y \epsilon R^k$

(1b) $y = Cx$

(1c) $z = Mx + v, \quad z \epsilon R^\ell$

$$E\begin{pmatrix} x(0) \\ w(t) \\ v(t) \end{pmatrix} = 0\ , \quad E\begin{pmatrix} x(0) \\ w(t) \\ v(t) \end{pmatrix}(x^T(o),\ w^T(\tau),\ v^T(\tau)) = \begin{bmatrix} X_0 & 0 & 0 \\ \cdot & W\delta(t-\tau) & \\ 0 & 0 & V\delta(t-\tau) \end{bmatrix}$$

$$W = \text{diag}\ [\dots\ W_{ii}\ \dots],\quad V = \text{diag}\ [\dots\ V_{ii}\ \dots],$$

such that these four control design goals are met:

$$\text{(I)}\quad E_\infty y_i^2(t) \overset{\Delta}{=} \lim_{t\to\infty} E\, y_i^2(t) \le \sigma_i^2,\ i = 1, \dots, k$$

$$E_\infty u_i^2(t) \overset{\Delta}{=} \lim_{t\to\infty} E\, u_i^2(t) \le \mu_i^2,\ i = 1, \dots, \bar{m}$$

PRECEDING PAGE BLANK NOT FILMED

(II) *Only* $\bar{\ell} < \ell$ *sensors are used*

$$(2) \qquad \bar{z} = \begin{pmatrix} z_1 \\ \vdots \\ z_{\bar{\ell}} \end{pmatrix} = \begin{pmatrix} m_1^T x + v_1 \\ \vdots \\ m_{\bar{\ell}}^T x + v_{\bar{\ell}} \end{pmatrix} = \bar{M}x + \bar{v}$$

from the admissible set of ℓ *sensors described from* (1c)

$$(1c) \qquad z = \begin{pmatrix} z_1 \\ \vdots \\ z_{\ell} \end{pmatrix} = \begin{pmatrix} m_1^T x + v_1 \\ \vdots \\ m_{\ell}^T x + v_{\ell} \end{pmatrix} = Mx + v.$$

(III) *Only* $\bar{m} < m$ *actuators are used*

$$(3) \qquad \bar{B}(\bar{u} + \bar{w}) = \sum_{i=1}^{\bar{m}} b_i(u_i + w_i)$$

from the admissible set of m *actuators described from* (1a)

$$(4) \qquad B(u + w) = \sum_{i=1}^{m} b_i(u_i + w_i)$$

(IV) *The control* $\bar{u}(t)$ *is a linear function of the present and past measurements* $\bar{z}(\tau)$, $\tau \le t$.

Many engineering control design problems can be stated with performance constraints of the form (I). For example, large space telescopes are feasible only if the RMS pointing errors $(E_\infty y_i^2)^{1/2}$ are within certain bounds $(E_\infty y_i^2)^{1/2} \le \sigma_i$) so as to achieve diffraction-limited performance (σ_i) of the optics. The designer may also have the freedom to choose from a number of different types of sensors and actuators at a number of different locations. The locations and the types of actuators (sensors) determine the vectors b_i (m_i) in (4) and (1c).

A straight-forward approach to accommodate the bounded input/output problem (I) yields nonlinear controllers [1-2], violating goal (IV). A straight-forward approach to accommodate goals (IV) and (I) is to use a penalty function method [3-5], minimizing

$$(5) \qquad V = E_\infty \frac{1}{t}\int_0^t (\|y\|_Q^2 + \|u\|_R^2)\, d\tau \ , \qquad \|y\|_Q^2 = y^TQy$$

while adjusting Q and R until (I) is satisfied. These successive approximation schemes [3-5] presume a fixed measurement/control structure, and hence do not satisfy goals (II) and (III). It is important to unify the treatment of all four goals (I-IV) since it has been shown [6-7] they are inherently interdependent problems. In particular, for the *isolated* problems; [6] has shown the optimal sensor and actuator selection for LQG problems (5) with *fixed* (Q,R), and [3-5] have adjusted Q and R to satisfy the constrained-variance problem (I) with *fixed* sensors and actuators (i.e. fixed B, M).

Unfortunately, the optimal answer for the simultaneous solution of both problems turns out *not* to be the juxtaposition of results [6] and [3-5], due to the interdependence of the two problems.

The purpose of this paper is to present a unified treatment of the entire problem (I-IV), which we call the Constrained Variance Sensor/Actuator Selection (CVSAS) problem. Section II describes the approach. Section III gives the formulas for sensor and actuator effectiveness to deal with goals (II) and (III). Section IV presents the numerical algorithm for iteratively dealing with goal (I). Section V gives the algorithm for solving the entire problem (I-IV). Section VI illustrates the application to the Hoop-Column Antenna.

II. APPROACH

The solution of the problem with inequality constraints (I) is generally not unique. To be a bit more specific than statement (I) we define two variations of the problem. The first is called the "Constrained-Input Variance" option of the CVSAS. In this option the input constraints in (I) are *binding* and the output constraints in (I) are *relaxed*.

<u>CIVSAS: The Constrained-Input Variance, Sensor/Actuator Selection Problem</u>

Satisfy (II), (III), *and with all input-constraints binding,*

$$(6) \qquad \mu_i^{-2}E_\infty u_i^2 = 1, \quad i = 1, \ldots, \bar{m} \ ,$$

minimize (recall $y_i = c_i^Tx$*),*

$$(7a) \qquad V_y = \sum_i \sigma_i^{-2}E_\infty y_i^2 \quad \forall\ i: \ \ \sigma_i^{-2}E_\infty y_i^2 > 1 \ .$$

If however, there is no i *for which* $\sigma_i^{-2}E_\infty y_i^2 > 1$ *then minimize*

(7b) $$V_y = \sum_{i=1}^{k} \sigma_i^{-2} E_\infty y_i^2$$

with all input constraints binding (6).

Definition: *The phrase "minimal achievable output performance" for the* CIVSAS *will mean the minimum constraint violation in the sense of the minimum value of* V_y *in* (7) *with input constraints binding* (6).

The CIVSAS problem is useful when one wishes to determine the best performance achievable for a *given* power limitation on the input devices (actuators). That is, for a *given* set of μ_i the CIVSAS *finds* the minimum achievable output performance.

The second variation of the CVSAS problem is called the Constrained Output Variance Sensor/Actuator Selection (COVSAS).

COVSAS: The Constrained-Output Variance, Sensor/Actuator Selection Problem

Satisfy (II), (III), *and with all output constraints binding*

(8) $$\sigma_i^{-2} E_\infty y_i^2 = 1 \ , \quad i = 1, \ldots, k \ ,$$

minimize

(9a) $$V_u = \sum_i \mu_i^{-2} E_\infty u_i^2 \ \forall \ i: \ \mu_i^{-2} E_\infty u_i^2 > 1.$$

If however, there is no i *for which* $\mu_i^{-2} E_\infty u_i^2 > 1$ *then minimize*

(9b) $$V_u = \sum_{i=1}^{\bar{m}} \mu_i^{-2} E_\infty u_i^2$$

with all output constraints binding, (8).

Definition 2: *The phrase "minimum achievable input performance" for the* COVSAS *will mean the minimum constraint violation in the sense of* (9), *with all output constraints binding* (8).

The COVSAS is useful when one wishes to determine the necessary capabilities (design requirements) of the actuators in order to achieve the *specified* output performance. That is, for a *given* set of σ_i the COVSAS *finds* the minimum achievable input performance.

III. SENSOR/ACTUATOR EFFECTIVENESS

In this Section we temporarily assume that Q and R in (5) are *specified* diagonal matrices $Q = \text{diag}[\ldots q_i \ldots]$, $R = \text{diag}[\ldots r_i \ldots]$, and we wish to determine a ranking of the effectiveness of the admissible set of sensors and actuators for the LQG problem described by (1) and (5). To help with this task a price or "cost" is assigned to each input and output by decomposing the total system cost function (5) into contributions from each input and output. This task is called "input or output cost analysis" and from [6] we have the results

$$V = \sum_{i=1}^{m} V_i^u + \sum_{i=1}^{k} V_i^y = \sum_{i=1}^{m} V_i^w + \sum_{i=1}^{\ell} V_i^v \tag{10}$$

where V_i^u, V_i^y, V_i^w, V_i^v is the contribution in V of, respectively, the i^{th} control u_i, output y_i, noise w_i, or noise v_i, and

$$V_i^u = r_i ||g_i||^2_{\hat{X}} \qquad i = 1, \ldots, m \tag{11a}$$

$$V_i^y = q_i ||c_i||^2_{P+\hat{X}} \qquad i = 1, \ldots, k \tag{11b}$$

$$V_i^w = W_{ii} ||b_i||^2_{K+L} \qquad i = 1, \ldots, m \tag{11c}$$

$$V_i^v = V_{ii} ||f_i||^2_{L} \qquad i = 1, \ldots, \ell \tag{11d}$$

where P, K, $\hat{X}$ and L satisfy

$$0 = PA^T + AP - PM^TV^{-1}MP + BWB^T, \quad [f_1, \ldots, f_\ell] \stackrel{\Delta}{=} F = PM^TV^{-1} \tag{12a}$$

$$0 = KA + A^TK - KBR^{-1}B^TK + C^TQC, \quad [g_1, \ldots, g_m] = G^T = -KBR^{-1} \tag{12b}$$

$$0 = \hat{X}(A + BG)^T + (A + BG)\hat{X} + FVF^T \tag{12c}$$

$$0 = L(A - FM) + (A - FM)^TL + G^TRG \tag{12d}$$

The effectiveness of the i^{th} sensor is measured by

(13) $$V_i^{sens} = V_i^{v}$$

and the effectiveness of the ith actuator is measured by

(14) $$V_i^{act} \stackrel{\Delta}{=} V_i^{u} - V_i^{w}$$

These terms V_i^{sens} and V_i^{act} represent the particular combinations of the input/output costs V_i^u, V_i^w, V_i^v which are involved in the performance of each sensor and actuator. (The distinction here is that the effect of the *input* w_i can be calculated by V_i^w, but the effect of an *actuator* involves both V_i^u and V_i^w since the actuator is noisy, and this dependence is accounted for in (14)). To see that V_i^{sens} and V_i^{act} gives the appropriate measure of the effect of *deleting* the ith sensor or the ith sensor or the ith sensor or the ith actuator, refer to the numerical work in [7].

Two results from [6] add insight into the use of (13), (14).

Theorem 1, [6,7]:

For a specified (Q,R), *the optimal value of the* LQG *performance metric* (5) *cannot be reduced by the deletion of any of the admissible sensors* z_i, $i = 1, \ldots, \ell$.

Theorem 2, [6,7]:

For a specified (Q,R) *the optimal value of the* LQG *performance metric* (5) *can possibly be reduced by the deletion of some of the admissible actuators* u_i, $i = 1, \ldots, m$.

These theorems partially explain why the sensor effectiveness V_i^{sens} is a much simpler calculation than V_i^{act}. Since the magnitude of the gain on the ith sensor signal $||f_i||^2 = ||m_i||^2_{pp} V_{ii}^{-2} \to 0$ as $V_{ii} \to \infty$, an extremely noisy sensor simply will not affect the optimal LQG controller. Hence, the effectiveness of the ith sensor can be calculated by the input cost V_i^v. Section V will show how to use (13) and (14) in the solution of the COVSAS problem.

IV. THE COVLQG ALGORITHM

Now we cite an algorithm (COVLQG) to solve the COVSAS problem under the temporary assumption that $\bar{\ell} = \ell$ and $\bar{m} = m$. That is, all admissible sensors and actuators are used ($\bar{B} = B$ and $\bar{M} = M$). The COVLQG algorithm will first be stated and then its theoretical properties will be discussed.

The COVLQG algorithm (i.e. the COVSAS with $\bar{\ell} = \ell$, $\bar{m} = m$):

Step A: *Compute* P *from* (12a). *If* $\sigma_i^{-2}||c_i||_P^2 > 1$ STOP. *No solution to the* COVLQG *problem exists. Otherwise initialize*

$$q_i(o) = \sigma_i^{-2}, \quad r_i(o) = \mu_i^{-2} .$$

Discussion of Step A: The lower bound on $E_\infty y_i^2$ in an LQG problem is $E_\infty y_i^2 \geq ||c_i||_P^2$ (from the well known lower bound tr CPC^T on V in (5)), and this result is independent of the choice of $Q \geq 0$, $R > 0$.

Step B: *Compute*

$$E_\infty y_i^2 = q_i^{-1} V_i^y \quad \forall\ i:\ q_i > 0$$

$$E_\infty u_i^2 = r_i^{-1} V_i^u$$

using (11), (12). *If* $\sigma_i^{-2} E_\infty y_i^2 = 1\ \forall\ i:\ q_i > 0$ *and if* $\mu_i^{-2} E_\infty u_i^2 \geq 1\ \forall\ i = 1, \ldots m$, STOP. *The* COVLQG *solution has been found.*

Discussion of Step B: In the COVLQG option all necessary control effort is applied to force the constraints $E_\infty y_i^2 \leq \sigma_i^2$ to be binding. A formal proof that the stopping criterion of Step B indicates a solution of the COVLQG problem is given by Theorem 5 of [7].

Step C: Q *and* R *update equations: Let the iteration index be* j *and set* $q_i(j+1) = [\sigma_i^{-2} E_\infty y_i^2] q_i(j)$, $i = 1, \ldots, k$. *If* $(\varepsilon\sigma_i^2)^{-1} < q_i(j+1) < \varepsilon\sigma_i^{-2}$, *(*$\varepsilon < 0$ *small specified constant) then set* $q_i(j+1) = 0$. *If* $\sigma_i^{-2} E_\infty y_i^2 = 1\ \forall\ i:\ q_i > 0$, *then set* $r_i(j+1) = [\mu_i^{-2} E_\infty u_i^2]^{1/2} r_i(j)$, $\forall\ i:\ \mu_i^{-2} E_\infty u_i^2 < 1$. *For all other* i, *set* $r_i(j+1) = r_i(j)$. *Return to* Step B.

Discussion of Step C: The $r_i(j+1)$ of Step C are clearly adjusted toward the stopping condition of Step B ($\mu_i^{-2} E_\infty u_i^2 \geq 1$), since a reduction in r_i causes $E_\infty u_i^2$ to increase. The justification for setting $q_i = 0$ when *either* $q_i(j+1) \to 0$

or when $q_i(j+1) \to \infty$ is as follows: The tendency of q_i toward zero indicates a lack of output controllability due to a degenerate rank of C (rank $C < k$). In this case, the algorithm ceases to attempt the impossible (i.e. to force two *dependent* outputs to arbitrary values) by removing this particular y_i (the least critical one as indicated by the smallest $q_i \to 0$) from the cost function by setting its coefficient $q_i = 0$. Now let rank $C = k$. The tendency of q_i toward ∞ can result only when a stabilizable, detectable system is not output controllable, (even though $C = k$) *and* an uncontrollable output converges to a value which violates its constraint ($E_\infty y_i^2 > \sigma_i^2$). The constraint is violated the smallest amount possible since in this case the corresponding $q_i \to \infty$ on successive iterations of the update equations. When this condition is determined, such y_i's are removed from the cost function on future iterations (by setting $q_i = 0$) since it now has been established that they *cannot* be brought within specification $E_\infty y_i^2 \le \sigma_i^2$.

A similar algorithm exists for the Constrained Input Variance LQG problem (CIVLQG) and details are given in [7].

V. THE COVSAS ALGORITHM

The sensor/actuator effectiveness formulas (13), (14) derived in Section III and the COVLQG algorithm of Section IV are now integrated to solve the COVSAS problem posed in Section II.

COVSAS Algorithm:

Step 1. *Specify* $\{A,B,C,M,V,\bar{\ell},\bar{m},\sigma^2,\mu^2\}$. *Run* COVLQG *algorithm using* ℓ *actuators,* m *sensors.*

Step 2. *Compute* V_i^{sens}, V_i^{act} *from* (13), (14) *and rank sensors and actuators according to their effectiveness:*

(15a) $$V_1^{sens} \ge V_2^{sens} \ge \cdots \ge V_\ell^{sens}$$

(15b) $$V_1^{act} \ge V_2^{act} \ge \cdots \ge V_m^{act}$$

Delete the sensor and actuator with the lowest effectiveness values V_i^{sens}, V_i^{act}, *provided such deletion does not cause loss of* *controllability or observability.*‡ *Unless* $\ell < \bar{\ell} + 1$, *reset* ℓ *to* ℓ-1. *Unless* $m < \bar{m} + 1$, *reset* m to m-1. *If* $\sigma_i^{-2} E_\infty y_i^2 = 1 \ \forall\ i = 1, \ldots, k$ *and* $\forall$ i: $\mu_i^{-2} E_\infty u_i^2 > 1$, *if* $[\frac{1}{\ell} \sum_{i=1}^{\ell} \mu_i^{-2} E_\infty u_i^2]_{(j+1)\text{iteration}} <$ $[\frac{1}{\ell} \sum_{i=1}^{\ell} \mu_i^{-2} E_\infty u_i^2]_{(j+1)\text{iteration}}$ *return to* Step 1. *Otherwise STOP. A solution to the* COVSAS *has been found.*

Discussion of Step 2: Numerical experience with this algorithm suggests that more than one sensor and more than one actuator may be deleted on each iteration. In fact, for many cases the same result can be obtained by reducing ℓ to $\bar{\ell}$ and m to $\bar{m}$ on the *first* iteration. However, this *quicker* convergence can sometimes converge only to *suboptimal* answers, and the algorithm above is written in its most conservative form (deleting only one sensor and/or actuator per iteration) where convergence to optimal values is more reliable [7].

VI. CONTROL OF A SPACE ANTENNA

Fig. 1 depicts the Hoop-Column Antenna arrangement for a proposed NASA communications satellite. Stationed in a geosynchronous orbit, the objective of the antenna control system is to regulate the orientation and focus of the satellite antenna relative to its multiple feed horns (at node 10). Table 1 lists the 24 linear and angular displacements which make up the outputs y_i, $i = 1, \ldots, k$, where $k = 24$. Table 2 lists the 39 admissible sensors and Table 3 lists the 12 admissible actuators. Note that ARX2 stands for angular rate about the x axis at node 2. AX2 stands for angular displacement about axis x at node 2. Z10-Z2 stands for a rectilinear displacement between nodes 10 and 2 in the z direction. The specifications for the outputs are $\sigma_i = 22.8$ arc seconds for $i = 1, \ldots, 6$, and $\sigma_i = .158$ mm for $i = 7, \ldots, 24$. The specifications for the inputs u_i are $\mu_i = 10$ dn-cm, $i = 1, \ldots, 12$. The actuator noise is described by $W = \text{diag}\ [\ldots W_{ii} \ldots]$, $W_{ii} = .1\ (\text{dy-cm})^2$, $\forall\ i = 1, \ldots 12$. The sensor noise is $V = \text{diag}\ [\ldots V_{ii} \ldots]$, $V_{ii} = 7.615\text{x}10^{-7}\ \text{rad}^2$, $i = 1,2,3,13,14,15$, $V_{ii} = 2.5\text{x}10^{-7}\ \text{m}^2$, $i = 4, \ldots, 12, 16, \ldots, 27$, $V_{ii} = 4.76\text{x}10^{-5}\ (\text{rad/sec})^2$, $i = 28, \ldots, 39$. It is desired to limit the number of actuators to $6 = \bar{m}$ and the number of sensors to $12 = \bar{\ell}$. The dynamics of the antenna structure were described by 10 elastic modes and 3 rigid body modes. The square of the frequencies

---

‡Observability, controllability checks are particularly simple for flexible space structures using the tests in [8]. That is, rank tests of matrices $[B; AB, \ldots A^{n-1}B]$, $[C^T, A^TC^T, \ldots A^{Tn-1}C^T]$ can be *avoided*.

ω_i^2, i = 1, ..., 10 of the elastic modes are

$$(\omega_1^2, \omega_2^2, \ldots, \omega_{10}^2) = (.40579,\ 7.2090,\ 7.2362,\ 13.277,$$
$$44.834,\ 132.14,\ 142.66,\ 445.01,\ 448.69,\ 775.86)\ (\text{rad/sec})^2.$$

More complete information for the antenna model may be found in [7].

The results of the COVSAS algorithm applied to the Hoop-Column Antenna are summarized in Table 4. The 6 actuators deleted from the admissible set of Table 3 are (listed in order of deletion): u_{12}, u_9, u_6, u_{10}, u_7, u_4. The 27 sensors deleted (in order of deletion) are: z_{15}, z_3, z_6, z_{12}, z, z_{13}, z_2, z_1, z_{24}, z_{27}, z_4, z_5, z_{18}, z_{21}, z_{30}, z_{39}, z_{33}, z_7, z_8, z_{31}, z_{23}, z_{20}, z_{35}, z_{25}, z_{22}, z_{16}. Notice that even though the output constraints are still binding the total control effort is *less* using only 6 actuators, (6x5.021 = 30.12) than using 12 actuators (12x3.275 = 39.30 > 30.12). Thus, *better* performance is possible with *fewer* actuators, since for several actuators the noise effect V_i^w is greater than the signal effect V_i^u in (14) (note the negative values of V_i^{act} in Table 4).

Perhaps the most important information from the COVSAS is the determination of the minimum achievable actuator specification [illegible] from Table 5 that all of the 24 outputs are held within their design constraints (σ_i = 22.8 arc secs. for angles and σ_i = .158 mm for rectilinear displacements) by actuators which *must be designed* for the capabilities of TABLE 5. That is, the given output specifications, σ_i^2 are possible to meet if μ_i is changed (=> actuators are redesigned) (from Table 5) to $\mu_1 = 73$, $\mu_2 = 26$, $\mu_3 = 105$, $\mu_4 = 26$, $\mu_5 = 32$, $\mu_6 = 39$.

VII. CONCLUSIONS

Presented is an algorithm COVSAS which integrates the following tasks:

Selects sensors and actuators from an admissible set.

Designs a linear feedback controller which satisfies output variance constraints.

Determines *actuator design requirements* which allow the output variance constraints to be satisfied.

Numerical properties of the convergence of this algorithm are given for NASA's Hoop-Column Antenna. Additional theoretical properties of convergence of this algorithm are given in [7].

REFERENCES

[1] H. Toivonen, "Minimum Variance Control of First Order Systems with a Constraint on the Input Amplitude" IEEE Trans. Auto. Control, Vol. AC-26, No. 2, April 1981, pp. 556-558.

[2] G.C. Goodwin, "Amplitude Constrained Minimum Variance Controller, El tron. Letters, Vol. 8, pp. 181-182, 1972.

[3] P.M. Makila, T. Westerlund, and H.T. Toivonen, "Constrained Linear Quadratic Gaussian Control," 21st IEEE CDC, Orlando, FL., Dec. 1982.

[4] H. Toivonen, "Variance-Constrained Self-Tuning Control," Automatica, to appear.

[5] R.E. Skelton and M.L. DeLorenzo, "Weight Selection for Covariance Constrained LQG Regulators: Large Space Structure Application," Automatica, to appear.

[6] R.E. Skelton and M.L. DeLorenzo, "Selection of Noisy Actuators and Sensors in Linear Stochastic Systems," J. Large Scale Systems, Theory and Applications, North-Holland publishing, to appear.

[7] M.L. DeLorenzo, "Selection of Noisy Sensors and Actuators for Regulation of Linear Systems," Ph.D. Thesis, May 1983, School of Aeronautics and Astronautics, Purdue University, West Lafayette, IN. 47907.

[8] P.C. Hughes and R.E. Skelton, "Controllability and Observability of Linear Matrix-Second-Order Systems," J. Applied Mechanics, Vol. 47, No. 2, June 1980, pp. 415-420.

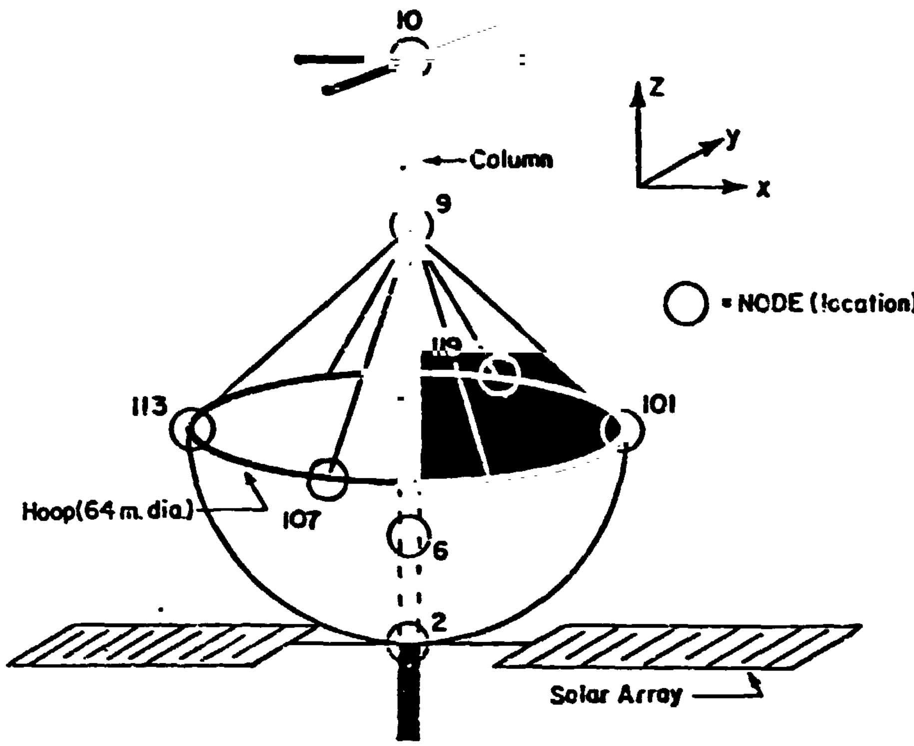

Figure 1: Hoop Column Antenna

Table 1: Hoop Column Output Description

Output #	Type	Nodal Location	Direction
1	Inertial Angle	2	X
2	"	2	Y
3	"	2	Z
4	Relative Angle Between	10 and 2	X
5	"	"	Y
6	Inertial Angle	10	Z
7	Relative Linear Disp. Between	6 and 2	X
8	"	"	Y
9	"	9 and 2	X
10	"	"	Y
11	"	10 and 2	X
12	"	"	Y
13	"	101 and 10	X
14	"	"	Y
15	"	"	Z
16	"	107 and 10	X
17	"	"	Y
18	"	"	Z
19	"	113 and 10	X
20	"	"	Y
21	"	"	Z
22	"	119 and 10	X
23	"	"	Y
24	"	"	Z

Table 2: Hoop-Column Sensor Labels

Sensor Number	Label	Sensor Number	Label	Sensor Number	Label
1	AX2	14	AY10	27	Z119-Z10
2	AY2	15	AZ10	28	ARX2
3	AZ2	16	X101-X10	29	ARY2
4	X6-X2	17	Y101-Y10	30	ARZ2
5	Y6-Y2	18	Z101-Z10	31	ARX6
6	Z6-Z2	19	X107-X10	32	ARY6
7	X9-X2	20	Y107-Y10	33	ARZ6
8	Y9-Y2	21	Z107-Z10	34	ARX9
9	Z9-Z2	22	X113-X10	35	ARY9
10	X10-X2	23	Y113-Y10	36	ARZ9
11	Y10-Y2	24	Z113-Z10	37	ARX10
12	Z10-Z2	25	X119-X10	38	ARY10
13	AX10	26	Y119-Y10	39	ARZ10

Table 3: Hoop Column Actuator Description

Actuator		torque about axis at Node location
u_1	=	T X 2
u_2	=	T Y 2
u_3	=	T Z 2
u_4	=	T X 6
u_5	=	T Y 6
u_6	=	T Z 6
u_7	=	T X 9
u_8	=	T Y 9
u_9	=	T Z 9
u_{10}	=	T X 10
u_{11}	=	T Y 10
u_{12}	=	T Z 10

Table 4: Hoop Column Output Constrained COVSAS Results

Iteration Number	Identified Sensors (V_i^{sen})	Identified Actuators (V_i^{act})	Ave Input Value (7.6)	Number of Sensors/Actuators
1	AZ10(.0004116) AZ2(.000397) Z6-Z2(0) Z9-Z2(0) Z10-Z2(0)	TZ10(-1.362) TZ9(-1.369)	3.275	39/12
2	AY1(.003362) AX10(.003358) AY2(.00226) AX2(.00226) Z113-Z10(.001942) Z119-Z10(.001884)	TZ6(-2.1405)	3.592	34/10
3	X6-X2(.01457) Y6-Y2(.01455) Z101-Z10(.0110) Z107-Z10(.0108)	TX10(-1.2055)	3.699	28/9
4	ARZ2(.02844 ARZ10(.02232) ARZ6(.02238)	TX9(-1.2917)	3.997	24/8
5	X9-X2(.0986) Y9-Y2(.0839)	TX6(-1.4793)	4.377	21/7
6	ARX6(.07648) ARX2(.07648)	----	4.829	19/6
7	Y107-Y10(.13395) XRY9(.1098)	----	4.857	17/6
8	X119-X10(.1557) X113-X10(.1555) X101-X10(.1551)	----	4.905	15/6
9	----	----	5.021	12/6

Table 5: Output-constrained Specifications

Output #	$E_\infty y_i^2$	Actuator #	$E_\infty u_i^2$ (minimum achievable)
1(AX2)	.015 sec	1 TX2	72.91 dn-cm
2(AY2)	.015 sec	2 TY2	26.145 dn-cm
3(AZ2)	11.588 sec	3 TZ2	105.47 dn-cm
4(AX10-AX2)	.001 sec	4 TY6	26.138 dn-cm
5(AY10-AY2)	.001 sec	5 TY9	31.750 dn-cm
6(AZ10)	12.000 sec	6 TY10	38.812 dn-cm
7(X6-X2)	.010 mm		
8(Y6-Y2)	.010 mm		
9(X9-X2)	.068 mm		
10(Y9-Y2)	.068 mm		
11(X10-X2)	.158 mm		
12(Y10-Y2)	.158 mm		
13(X101-X10)	.104 mm		
14(Y101-Y10)	.158 mm		
15(Z101-Z10)	.007 mm		
16(X107-X10)	.158 mm		
17(Y107-Y10)	.156 mm		
18(Z107-Z10)	.008 mm		
19(X113-X10)	.122 mm		
20(Y113-Y10)	.158 mm		
21(Z113-Z10)	.001 mm		
22(X119-X10)	.158 mm		
23(Y119-Y10)	.091 mm		
24(Z119-Z10)	.001 mm		

N85-31198

EIGENVALUE PLACEMENT AND STABILIZATION BY CONSTRAINED OPTIMIZATION

S. M. DeCaro* and D. J. Inman**
University at Buffalo
State University of New York
Buffalo, NY 14260

ABSTRACT

A pole placement algorithm is proposed which uses constrained non-linear optimization techniques on a finite dimensional model of a linear n degree of freedom system. Low order feedback control is assumed where r poles may be assigned; r being the rank of the sensor coefficient matrix. It is shown that by combining feedback control theory methods with optimization techniques, one can ensure the stability characteristics of a system, and can alter its transient response.

INTRODUCTION

One common method of approaching the problems of controlling the vibration of a structure is to employ eigenvalue (pole) placement methods. Such solutions have attracted the attention of numerous authors over the past twenty-five years, including W. M. Wonham [6], E. J. Davison [3], S. Srinathkumar [5], A. N. Andry et al [1], [2] and many others.

In exploring pole placement in dynamical systems, an inadequacy of stability considerations in contemporary algorithms was noted and thus motivated this work. It appears that the problem has not been solved or even addressed in many approaches.

If a system is controllable, one has the ability to place a predetermined number of poles. Thus, when pole placement techniques are employed, there is a limit on the number of poles that may be assigned. As is well known, the rank of the sensor coefficient matrix determines how many poles may be placed exactly. These poles may be noted as the controllable eigenvalues of the system, while the remaining may be labelled uncontrollable.

---

*Present Address: Member Technical Staff
AT&T Bell Laboratories
Whippany Road Room 3C-249
Whippany, New Jersey 07981

**Research supported by AFOSR Grant Number AFOSR 82-0242

Thus, due to restrictions inherent to every system, every pole may not be desirably placed. Therefore, one does not have control over the full order of the system. When moving the allowable eigenvalues, those which are not placed will also be affected, with the possibility of generating an unstable state.

Since an unstable system is undesirable, the ability to place a predetermined number of poles, while forcing the system to remain stable would be quite desirable to the designer. Many pole placement methods yield satisfactory assignment of the desired modes, but unfortunately can drive the remaining eigenvalues unstable. Thus, requiring iteration of the algorithms, compromising the desired choice of eigenvalues or eigenvectors, until a stable response results. With the large number of modes required in modelling flexible structures, these methods become costly and time consuming.

Hence, a pole placement method is proposed which constrains the unspecified modes to be stable by taking advantage of constrained optimization techniques. It appears that no previous work has guaranteed stable unplaced poles or has assured the magnitude of relative stability.

Several numerical examples will be presented, and results will be compared with those of Srinathkumar [5].

PROPOSED SOLUTION

The systems studied in this paper are of the mechanical type, which are second order by nature, incorporating mass, stiffness and damping parameters, where only the class of discrete systems shall be investigated.

Assuming small motions about the equillibrium point implies linearization of the equations of motion, which become

$$[M]\ddot{\underline{q}}(t) + [D+G]\dot{\underline{q}}(t) + [S+H]\underline{q}(t) = \underline{F}(t) \tag{1}$$

The forcing function vector, $\underline{F}(t)$, may then be described as

$$\underline{F}(t) = [V]\dot{\underline{q}}(t) + [P]\underline{q}(t),$$

where [V] and [P] are the velocity and position feedback matrices, respectively. $\underline{q}(t)$ is the coordinate vector, while $\dot{\underline{q}}(t)$ and $\ddot{\underline{q}}(t)$ are the first and second time derivatives of this vector.

[M] is known as the mass or inertia matrix, [D] is called the damping matrix, and [S] is the stiffness matrix. The matrix [G] may be referred to as the gyroscopic or Coriolos matrix, and [H] is the circulatory matrix.

The [M], [D], [S], [G] and [H] matrices are assumed to be time-invariant, and therefore are represented by constant values, all being of nth order, where n represents the number of degrees of freedom of the system.

Using normal state space methods by letting

$$\underline{x}(t) = \begin{bmatrix} \dot{\underline{q}}(t) \\ \hline \underline{q}(t) \end{bmatrix},$$

the n-dimensional system becomes the following 2n-dimensional model:

$$\dot{\underline{x}}(t) = \left[\begin{array}{c|c} -M^{-1}(D+G) & -M^{-1}(S+H) \\ \hline I_n & 0 \end{array}\right] \underline{x}(t) + \begin{bmatrix} B_1 \\ \hline B_2 \end{bmatrix} \underline{u}(t)$$

$$\underline{y}(t) = [C_1 \mid C_2]\underline{x}(t) \tag{2}$$

where [M] is assumed to have an inverse and $\begin{bmatrix} B_1 \\ B_2 \end{bmatrix} \underline{u}(t)$ is a representation of the system's forcing function, $\underline{F}(t)$.

More simply, equation (2) may be expressed as follows:

$$\dot{\underline{x}}(t) = [A']\underline{x}(t) + [B]\underline{u}(t), \quad \underline{x}(0) = \underline{x}_0$$

$$\underline{y}(t) = [C]\underline{x}(t)$$

where $\underline{u}(t) = [K]\underline{y}(t)$

$\underline{y}(t)$ is the output vector, [C] is a constant sensor coefficient matrix, and [K] is the feedback gain matrix. [B] may now be described as the constant coefficient matrix of actuator dynamics, and $\underline{u}(t)$ is the control vector. The following conditions hold:

i) $\underline{x} \epsilon R^{2n}$, $\underline{u} \epsilon R^{m}$, $\underline{y} \epsilon R^{r}$

ii) A', B, C are real, constant matrices of appropriate dimensions.

iii) rank B = m $\neq$ 0, rank C = r $\neq$ 0

By block diagram representation, the system described by equation (3) may be expressed as in Figure 1.

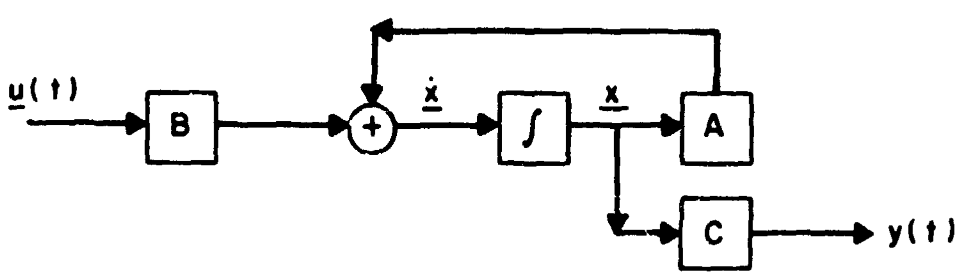

FIGURE 1

And a more revealing representation is shown in Figure 2.

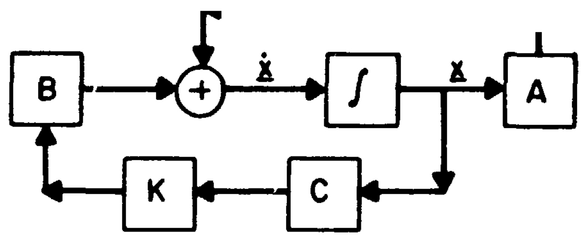

FIGURE 2

Equation (2) may be rewritten as follows:

$$\dot{\underline{x}}(t) = \left[\begin{array}{c|c} -M^{-1}(D+G) & -M^{-1}(S+H) \\ \hline I_n & 0 \end{array}\right] \underline{x}(t) + \left[\begin{array}{c} B_1 \\ \hline B_2 \end{array}\right] [K][C_1 \mid C_2]\underline{x}(t)$$

or

$$\dot{\underline{x}}(t) = \left[\begin{array}{c|c} -M^{-1}(D+G) & -M^{-1}(S+H) \\ \hline I_n & 0 \end{array}\right] \underline{x}(t) + \left[\begin{array}{c|c} B_1KC_1 & B_1KC_2 \\ \hline B_2KC_1 & B_2KC_2 \end{array}\right] \underline{x}(t)$$

$$\underline{y}(t) = [C_1 \mid C_2]\underline{x}(t) \tag{3}$$

By comparison of equations (1) and (3), one may note that this implies:

$$[B_2] = [0],$$

thus

$$\dot{\underline{x}}(t) = \left[\begin{array}{c|c} -M^{-1}(D+G) & -M^{-1}(S+H) \\ \hline I_n & 0 \end{array}\right] \underline{x}(t) + \left[\begin{array}{c|c} B_1KC_1 & B_1KC_2 \\ \hline 0 & 0 \end{array}\right] \underline{x}(t)$$

$$\underline{y}(t) = [C_1 \mid C_2]\underline{x}(t) \tag{4}$$

If we define

$$[A] = \left[\begin{array}{c|c} -M^{-1}(D+G) + B_1KC_1 & -M^{-1}(S+H) + B_1KC_2 \\ \hline I_n & 0 \end{array}\right]$$

and describe equation (4) as follows:

$$\underline{\dot{x}} = [A]\underline{x}$$

$$\underline{y} = [C]\underline{x}$$

Then, the set of equations must satisfy the eigenvalue problem, i.e.,

$$[A]\underline{v}_i = \zeta_i \underline{v}_i \tag{5}$$

where $\left\{\zeta_i\right\}_{i=1}^{2n} \equiv$ the 2n eigenvalues

and $\left\{\underline{v}_i\right\}_{i=1}^{2n} \equiv$ the corresponding eigenvectors.

By substitution of equation (4) into equation (5),

$$\zeta_i \underline{v}_i = \left[\begin{array}{c|c} -M^{-1}(D+G) & -M^{-1}(S+H) \\ \hline I_n & 0 \end{array}\right] \underline{v}_i + \left[\begin{array}{c|c} B_1KC_1 & B_1KC_2 \\ \hline 0 & 0 \end{array}\right] \underline{v}_i$$

$\underline{v}_i$ may then be defined to correspond to the above partitioning as follows:

$$\underline{v}_i = \left[\begin{array}{c} \underline{z}_i \\ \hline \underline{w}_i \end{array}\right]$$

yielding

$$\zeta_i \left[\begin{array}{c} \underline{z}_i \\ \hline \underline{w}_i \end{array}\right] = \left[\begin{array}{c|c} -M^{-1}(D+G) & -M^{-1}(S+H) \\ \hline I_n & 0 \end{array}\right] \left[\begin{array}{c} \underline{z}_i \\ \hline \underline{w}_i \end{array}\right] + \left[\begin{array}{c|c} B_1KC_1 & B_1KC_2 \\ \hline 0 & 0 \end{array}\right] \left[\begin{array}{c} \underline{z}_i \\ \hline \underline{w}_i \end{array}\right]$$

which implies

$$\zeta_i \underline{w}_i = \underline{z}_i$$

substituting,

$$\zeta_i^2 \underline{w}_i = -M^{-1}(D+G)\zeta_i \underline{w}_i - M^{-1}(S+H)\underline{w}_i + B_1KC_1\zeta_i\underline{w}_i + B_1KC_2\underline{w}_i \tag{6}$$

If we define $\{\lambda_i\}$ $i = 1,2,\ldots,r$ as the r eigenvalues to be placed, equation (6) may be expressed as

$$W\Delta^2 = -M^{-1}(D+G)W\Delta - M^{-1}(S+H)W + B_1KC_1W\Delta + B_1KC_2W$$

where $$W = [\underline{w}_1 \mid \underline{w}_2 \mid \cdots\cdots \mid \underline{w}_r]$$

and $$\Delta = \text{diag}(\lambda_1, \lambda_2, \ldots, \lambda_r)$$

By taking advantage of the generalized left inverse theorem,

$$[K] = [B_1^T B_1]^{-1}[B_1^T][W\Delta^2 + M^{-1}(D+G)W\Delta + M^{-1}(S+H)W][C_1 W\Delta + C_2 W]^{-1},$$

which is the equation describing the gain matrix needed to obtain those eigenvalues desired.

A single objective function was then determined from the set of equations described by equation (7), where the values of [K] were determined by minimizing that objective function. The constraints imposed on the system were that the real part of the eigenvalues of the closed loop system were all negative. These constraints were also modified, as was desired, to increase the stability margin.

NUMERICAL EXAMPLES

Example 1:

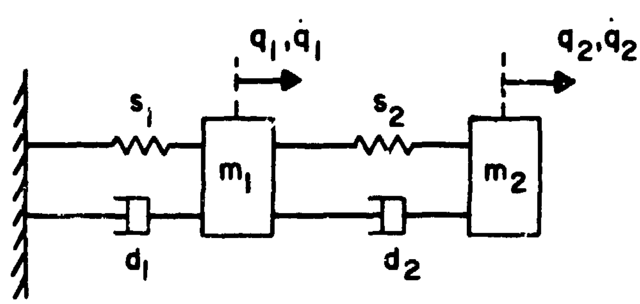

FIGURE 3

Specifications: $m_1 = m_2 = 1$

$S_1 = 4$

$S_2 = 1$

$d_1 = 2$

$d_2 = 1$

Eigenvalues of unforced system:

$$-1.666207 \pm 1.41334i$$
$$-.333783 \pm -.83265i$$

$$[C] = \begin{bmatrix} 0 & 1 & 0 & 0 \\ 1 & 0 & 0 & 0 \end{bmatrix}$$

$$[B] = \begin{bmatrix} 1 & 0 \\ 0 & 1 \\ 0 & 0 \\ 0 & 0 \end{bmatrix}$$

Desired eigenvalues:

$$\lambda_1 = -4.0 + 0i$$
$$\lambda_2 = -3.0 + 0i$$

Resulting eigenvalues using the proposed method with no additional factor for relative stability:

$$-4.000000 + 0i$$
$$-1.335420 + 0i$$
$$-.249608 + 0i$$
$$-3.000000 + 0i$$

Resulting eigenvalues using the proposed method with added factor of relative stability:

$$-4.000000 + 0i$$
$$-2.999999 + 0i$$
$$-.572543 \pm 0.74353i$$

Resulting eigenvalues using Srinathkumar method:

$$9.1256 + 0i$$
$$-.8141 + 0i$$
$$-4.0000 + 0i$$
$$-3.0000 + 0i$$

Note that the method proposed here yields the desired eigenvalues and that the unspecified eigenvalues remain stable, whereas in the Srinathkumar method an unspecified eigenvalue is moved into the right half plane.

Example 2:

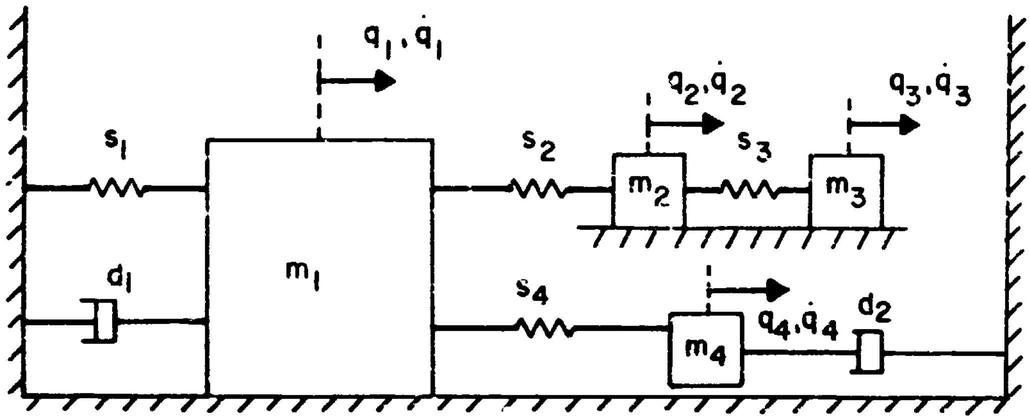

FIGURE 4

Specifications: $m_1 = 4$

$m_2 = m_3 = m_4 = 1$

$S_1 = S_2 = S_3 = S_4 = 1$

$d_1 = d_2 = .5$

Eigenvalues of unforced system:

$$
\begin{array}{l}
-.004055 \pm 1.647953i \\
-.170649 \pm 1.131418i \\
-.062364 \pm .355674i \\
-.075432 \pm .730441i
\end{array}
$$

$$[C] = \begin{bmatrix} 1 & 0 & 0 & 0 & 0 & 0 & 0 & 0 \\ 0 & 0 & 0 & 1 & 0 & 0 & 0 & 0 \end{bmatrix}$$

$$[B] = \begin{bmatrix} 1 & 0 & 0 \\ 0 & 1 & 0 \\ 0 & 0 & 1 \\ 0 & 0 & 0 \\ 0 & 0 & 0 \\ 0 & 0 & 0 \\ 0 & 0 & 0 \end{bmatrix}$$

Desired eigenvalues: $\lambda_{1,2} = -.4 \pm .5$

Resulting eigenvalues using the proposed method, where a factor for relative stability was added:

$$\begin{array}{l} -.289342 \pm 1.378583i \\ -.145451 \pm 1.171345i \\ -.400007 \pm \ .500003i \\ -.197840 \pm \ .425944i \end{array}$$

Example 3:

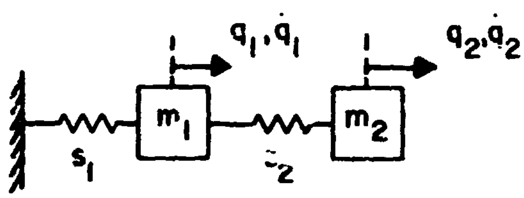

FIGURE 5

Specifications: $m_1 = m_2 = 1$

$S_1 = 3$

$S_2 = 1$

Eigenvalues of unforced system:

$$\begin{array}{l} \pm 2.074313i \\ \pm \ .835000i \end{array}$$

$$[C] = [1 \quad 1 \quad 0 \quad 0]$$

$$[B] = \begin{bmatrix} 1 & 0 \\ 0 & 1 \\ 0 & 0 \\ 0 & 0 \end{bmatrix}$$

Desired eigenvalue: $.5 + 0i$

Resulting eigenvalues using the proposed method, where factor for relative stability was added:

$$\begin{array}{l} -\ .170373 \pm 1.809097i \\ -1.817157 + 0i \\ -\ .500003 + 0i \end{array}$$

CONCLUSION

A pole placement algorithm has been proposed which used constrained non-linear programming techniques for a finite dimensional model of a linear n degree of freedom system. It has been shown that by constraining the eigenvalues of the full order system while simultaneously placing those allowable, one can ensure the stability characteristics of a system, and can alter its transient response.

Results of the Srinathkumar method were presented for Example 1, and showed how this method yielded the desired eigenvalues quite accurately, yet unfortunately forced the originally stable system unstable, therefore resulting in an undesirable response.

No previous work has guaranteed stable unplaced poles or has assured the magnitude of relative stability.

REFERENCES

[1] Andry, A. N., Shapiro, E. Y., and Chung, J. C., "Eigenstructure Assignment for Linear Systems," IEEE Transactions on Aerospace and Electronic Systems, Vol. 19, No. 5, September 1983, pp. 711-729.

[2] Andry, A. N., Shapiro, E. Y., and Chung, J. C., "Modal Control of Vibrating Systems," Proceedings of the First International Modal Analysis Conference and Exhibit, Orlando.

[3] Davison, E. J., "On Pole Assignment in Linear Systems with Incomplete State Feedback," IEEE Transactions on Automatic Control, June 1970, pp. 348-351.

[4] Meirovitch, L., Computational Methods in Structural Dynamics, Sijthoff and Noordhoff, Rockville, Maryland, 1980.

[5] Srinathkumar, S., "Eigenvalue/Eigenvector Assignment Using Output Feedback," IEEE Transactions on Automatic Control, Vol. AC-23, No. 1, February 1978, pp. 79-81.

[6] Wonham, W. M., "On Pole Assignment in Multi-Input Controllable Linear Systems," IEEE Transactions on Automatic Control, Vol. AC-12, No. 6 December 1967, pp. 660-665.

N85-31199

MATRIX TRANSFER FUNCTION DESIGN FOR FLEXIBLE STRUCTURES—AN APPLICATION

T. J. Brennan, A. V. Compito, A. L. Doran, C. L. Gustafson, and C. L. Wong
Aerospace Corporation
Los Angeles, CA 90009

ABSTRACT

The application of matrix transfer function design techniques to the problem of disturbance rejection on a flexible space structure is demonstrated. The design approach is based on parameterizing a class of stabilizing compensators for the plant and formulating the design specifications as a constrained minimization problem in terms of these parameters. The solution yields a matrix transfer function representation of the compensator. A state space realization of the compensator is constructed to investigate performance and stability on the nominal and perturbed models. The application is made to the ACOSS (Active Control of Space Structures) optical structure.

I. INTRODUCTION

The problem of flexible space structure control has motivated a great deal of research for theoreticians and practitioners of multivariable control design. In spite of the efforts directed in this area there still remains a significant gap between the multivariable theory and the control design implementation. This gap stems from two sources. The first difficulty is one of problem specification. Translation of complex system requirements and constraints into the specific mathematical cost functionals required by most design methods may be impossible in many cases. Free parameters in the chosen design methodology may not be traceable to the parameters which describe the system in terms of desired performance, plant uncertainty, hardware limitations, etc. A second roadblock to the implementation of modern control design techniques is the lack of reliable algorithms and software to perform the sophisticated mathematical manipulations required by these techniques. Recent years have shown very considerable advances in this field (see [1]) but much remains to be done.

Most of the MIMO (multi-input/multi-output) compensators which have actually left the textbook and been calculated in computers are based on state space methods, and, in particular, LQG (Linear-Quadratic-Guassian) design theory. This is due in part to the long history of development of these design techniques as well as the availability of reliable algorithms to solve matrix Riccati equations and the ease of performing most state space manipulations. Frequency domain techniques for calculating MIMO feedback systems have been avoided. The extensions of classical frequency domain concepts to MIMO systems have not been totally satisfying and calculations involving matrices of transfer functions present an entirely new set of problems. Nonetheless, frequency domain design is still appealing and certain feedback notions cannot be adequately expressed without reference to transfer functions.

We have carried through a compensator design for a flexible structure based on transfer function parameterization techniques. General theories of feedback control system parameterization have been developed by several authors ([2], [3], and [4]). The goal of a parametric approach is the selection of a set of numerical quantities, along with an acceptable range of values, which span a class of possibly acceptable compensators and, wi which, one is able to adequately express the system requirements in terms of costs and constraints. A particularly simple parameterization for stable plants was introduced by Zames, [4], and exploited for the unity feedback configuration of Figure 1 bv Desoer and Chen [5]. This is the parameterization we will implement here. The details are in section IV. Previous examples of this design approach can be found in [6] and [7].

II. ACOSS STRUCTURE

The ACOSS optical structure was developed by the Charles Stark Draper Laboratories as a control design test specimen to evaluate the design approaches developed for the DARPA ACOSS program, [8]. It was designed to exhibit the closely spaced, low frequency mode distribution expected on some future space systems. The structure is provided as a finite element model having 84 dynamic degrees of freedom (see Figure 2). In addition to the nominal structure, two perturbed structures were defined to represent plant uncertainty. The perturbed models represent mass and stiffness variations of approximately 10%. The nominal model is denoted P0, the perturbed models are P2 and P4.

The performance goal is expressed in terms of a line of sight error on a focal plane on the lower section of the truss as shown in Figure 2. The error has two angular components and a defocus component resulting from deviations in the optical path due to structural vibrations. Three rigid mirrors determine the optical path. These are assumed to be rigidly mounted to the structure. Two disturbances are defined on the structure as shown in the figure. For our design problem we are only considering the disturbance propagating from the equipment panel and we assume it has a flat PSD out to 5 Hz. The equipment panel is isolated from the structure by a spring-damper system. The residual disturbance propagation through this isolation system into the line of sight is still unacceptably high. The control problem is to further reduce this residual with active structural control.

III. MODEL SELECTION AND ACTUATOR PLACEMENT

For the current design problem we chose a 5 mode model of the structure, selecting those modes having most significant influence between disturbance and line of sight. The modal influence was determined based on ideas from internally balanced coordinates. For a description of internally balanced coordinates see [9] and for an application to modal coordinates see [10]. Given a second order model description,

$$\ddot{q}_i + 2\,\zeta_i \omega_i \dot{q}_i + \omega_i^2 q_i = \underline{g}_i^T \underline{w}\,, \qquad i = 1,\ldots,n \tag{1}$$

$$\underline{y} = \sum_{i=1}^{n} \underline{h}_i q_i \tag{2}$$

with natural damping ζ_i, frequency ω_i, inputs $\underline{w}$, and outputs $\underline{y}$, an index for ranking the modes can be calculated as the approximate "second order modes," ([10]) by

$$\sigma_i^2 = \frac{\sqrt{(\underline{g}_i^T \underline{g}_i)(\underline{h}_i^T \underline{h}_i)}}{4\,\zeta_i \omega_i} \tag{3}$$

Using the modal disturbance influence matrix for the $\underline{g}_i$'s and the line of sight measurement matrix for the $\underline{h}_i$'s the 5 highest rank modes are tabulated in Table 1. Agreeing with our intuition, these turn out to be two isolator rotations, two isolator translations, and the first bending mode of the upper truss. A description of the modes of the structure can be found in [8].

Mode	7	8	12	13	21
Frequency (Hz)	.15	.26	.58	.58	2.3

Table 1. Design Modes

The line of sight measurement matrix is a function of 21 nodal degrees of freedom. From among these 21 degrees of freedom we chose to locate three force actuators (assumed to be of the momentum exchange or proof mass type) to control the three line of sight measurements. To make this selection an appeal is again made to the approximate second order modes of equation (3).

If the forcing function on the right of (1) is $g_{ij}u$ where g_{ij} is the influence of the j^{th} actuator, $j = 1,\ldots,21$ on the i^{th} mode, $i = 1,\ldots,5$, then we denote the corresponding second order mode by σ_{ij} and define

$$\alpha_j^2 = \sum_{i=1}^{5} \sigma_{ij}^{\,2} \tag{4}$$

Here, α_j is a measure of the influence of the j^{th} actuator on the line of sight for the selected 5 mode model. We chose three actuators whose force directions span the three spatial directions and have large α_j with respect to the total 21 possible actuators. Two of the actuators selected are located on the corners of the primary mirror and the third is on the lower truss.

To complete the description of the design plant we assumed the availability of direct measurements of the line of sight. No other sensors were used for the control design. We now have a state space description of the design plant in modal coordinates,

$$\dot{x} = Fx + Gu + Dd \tag{5}$$

$$y = Hx \tag{6}$$

where u is the actuator command and d is the disturbance input.

For calculation of the compensator we need a transfer function representation of the design plant. The convenient representation for constructing state space realizations of the compensator is a polynomial matrix coprime factorization [11,12], that is, $P = ND^{-1}$ where N and D are coprime polynomial matrices. An algorithm to construct a coprime factorization from a state space description can be found in [13].

IV. DESIGN PROBLEM

The feedback configuration used for the design is shown in Figure 1. The closed loop system is referred to as $\mathcal{S}$. P is the open loop design plant, a 3x3 transfer function given from the state space equations by $H(sI-F)^{-1}G$. The inputs are u_1 and u_2 with the reference input, u_1, identically zero. The outputs are y_1 and y_2 with the line of sight represented by y_2. The disturbance propagates into the line of sight through the transfer function $\tilde{P} = H(sI-F)^{-1}D$ and may thus be represented as an additive disturbance, $\tilde{P}d$, at the plant output.

The closed loop system transfer function is defined to be

$$H_{yu} : \begin{pmatrix} u_1 \\ u_2 \end{pmatrix} \rightarrow \begin{pmatrix} y_1 \\ y_2 \end{pmatrix} . \tag{7}$$

Stability of H_{yu} can be taken to be closed loop stability. H_{yu} may be expressed in a simple parameterized form as

$$H_{yu} = \begin{bmatrix} Q & -QP \\ PQ & P(I-QP) \end{bmatrix} \tag{8}$$

where Q is referred to as the Zames parameterization, [4], with

$$Q = C(I + PC)^{-1} . \tag{9}$$

We state here the fundamental result from [5] which is the basis of this design approach.

<u>Fact</u>: For P exponentially stable and strictly proper, Q is exponentially stable and proper if and only if

(i) C is proper and

(ii) H_{yu} is exponentially stable and proper.

When this is the case the compensator is given by

$$C = Q(I - PQ)^{-1} \tag{10}$$

In other words designing stabilizing compensators for $\mathcal{S}$ is equivalent to specifying exponentially stable, proper Q.

From (8) we see that the I/O map, that is, the transfer function from u_1 to y_2 is

$$H = H_{y_2 u_1} = PQ \tag{11}$$

Given an invertible plant transfer function, P, one can see from the relation (11) that a parametrization of the closed loop system by Q is equivalent to a parameterization by H. Moreover, for P exponentially stable, Q exponentially stable implies the same for H. But since

$$Q = P^{-1}H \tag{12}$$

it becomes clear that exponential stability of H only implies exponential stability of Q when P has no unstable zeros. However, by imposing an additional condition on H, namely that H has the same right half plane zero structure as P, then parameterization by such H is equivalent to parameterization by exponentially stable Q. If a proper compensator is desired the additional constraint of properness of Q is required and will result in an excess pole over zero constraint on H which depends on P.

Parameterization by the I/O map, H, may simplify the design problem and allow the designer to more directly specify his design objective. For example, for a disturbance attenuation problem, the closed loop disturbance to output map, or sensitivity map, is simply given as $(I - H)$. In addition, in some applications, a decoupled I/O map is desirable and one is directly able to parameterize a diagonal H. This is the approach we take for this design. Calculating the transmission zeros of our design plant using the QZ algorithm [14] we find that there are no zeros in the right half plane so we may freely specify H as diag(h_i, i=1,2,3) with each h_i of the form

$$\frac{g\, p_n(s)}{p_{d_1}(s)\, p_{d_2}(s)} \tag{13}$$

where g is a gain and

$$p_n(s) = s^2 + 2\zeta_n \omega_n s + \omega_n^2 \tag{14}$$

$$p_{d_j}(s) = s^2 + 2\zeta_{d_j} \omega_{d_j} s + \omega_{d_j}^2 \tag{15}$$

This parameterization has 21 parameters consisting of the gains, and second order damping and frequency terms.

We set for ourselves a design goal of minimizing closed loop response to the disturbance over a low frequency band of 5 Hz. To achieve this we define a constrained optimization problem as follows:

Minimize

$$J = \|(I - H(j\omega))\, \tilde{P}(j\omega)\|_2 \ , \quad \omega = 10\pi \tag{16}$$

subject to

$0.01 < \zeta_n, \zeta_{d_j}$	:Stability
$0.04 < \omega_n, \omega_{d_j} < \omega_b$	:Bandwidth
$h_i(0) = 1$	:Low frequency noise rejection

The matrix under the norm of J is diagonal so we simply take the Euclidean vector norm of the diagonal. The minimization of the cost at 5 Hz and the DC unity gain constraint will result in disturbance rejection across the 5 Hz band. The $\tilde{P}$ term in the cost weights the diagonal terms in (I - H) according to the way the disturbance propagates through the structure.

In general (I - H) is the ratio of the relative uncertainty in the I/O map to the relative uncertainty in the open loop plant. More precisely

$$(\Delta H)\hat{H}^{-1} = (I-H)(\Delta P)\hat{P}^{-1} \tag{17}$$

where

$$\Delta P = \hat{P} - P \tag{18}$$

$$\Delta H = \hat{H} - H \tag{19}$$

for a "perturbed" plant $\hat{P}$ which results in a perturbed I/O map $\hat{H}$. In effect, minimization of J reduces the impact of plant uncertainties on closed loop system performance.

Having specified the optimization problem one can use numerical or analytical means to solve it. Omitting the details, we calculated a local minimum to this problem analytically. The achievable performance is clearly dependent on the bandwidth, ω_b. For a given ω_b the local minimum satisfies

$$\omega_{d_j} = \omega_b \tag{20}$$

$$p_{d_1}(s) = p_{d_2}(s) \tag{21}$$

$$\frac{2\zeta_n}{\zeta_{d_j}} = \frac{\omega_n}{\omega_{d_j}} \tag{22}$$

$$g = \frac{\omega_{d_i}^4}{\omega_n^2} \tag{23}$$

Given this solution we can adjust the bandwidth of each of the three loops to achieve a desired performance level. To achieve 0.04 reduction in each channel we have the following parameter values:

	ω_{d_i}	ζ_{d_i}	ω_n	ζ_n	g
h_1	300	1.5	10^4	100	81
h_2	600	.8	$4\text{X}10^4$	107	81
h_3	300	5	$2\text{X}10^3$	200	25

V. COMPENSATOR REALIZATION

Having arrived at parameter values we have specified the desired I/O map, H. The compensator which will produce this I/O map is

$$C = Q(I - PQ)^{-1} \tag{24}$$

$$= P^{-1}H(I - H)^{-1} . \tag{25}$$

Since the I/O map is given by diag(h_i) with each h_i of the form

$$h_i = \frac{n_i}{d_i} , \tag{26}$$

the compensator becomes

$$C = P^{-1}\mathrm{diag}\left(\frac{n_i}{d_i - n_i}\right). \tag{27}$$

We have already expressed P as a polynomial matrix coprime factorization, $P = ND^{-1}$. Thus (27) becomes

$$C = D\,N^{-1}\mathrm{diag}\left(\frac{n_i}{d_i - n_i}\right). \tag{28}$$

Since the degree of $d_i - n_i$ is 4, we can factor this polynomial into two quadratics as

$$d_i - n_i = \tilde{d}_{i_1}\tilde{d}_{i_2}, \qquad i = 1,2,3. \tag{29}$$

Hence (29) can be rewritten as

$$C = D\ \{\ \mathrm{diag}(\tilde{d}_{i_1})N\ \}^{-1}\ \mathrm{diag}\left(\frac{n_i}{\tilde{d}_{i_2}}\right) \quad . \tag{30}$$

By inspection, $\mathrm{diag}(\tilde{d}_{i_1})N$ is column-reduced [12], and has column degrees equaling those of D. Consequently $D\ \{\mathrm{diag}(\tilde{d}_{i_1})N\}^{-1}$ is proper and has a state space realization [12, Sec. 6.4]. Now, since $\mathrm{diag}(n_i/\tilde{d}_{i_2})$ also has a state space realization, the two realizations can be cascaded to yield a realization for C.

VI. RESULTS

Having computed a state space description of the compensator we are now able to determine closed loop stability for various versions of the plant simply by extracting the eigenvalues from the closed loop state equations derived from Figure 1. We find that for all three versions of the plant (P0, P2, and P4) the five mode description remains stable under feedback by our compensator.

To investigate the robustness of the design with respect to unmodeled dynamics we appended additional modes to the plant model and found that the closed loop system became unstable in almost all cases. Upon investigation of this problem we discovered that though the 5 mode design plant was minimum phase, the addition of almost any other mode or set of modes resulted in a nonminimum phase plant. Information about these unstable zeros was not available in the design plant so the resulting compensator tended to place closed loop poles at these zeros. Thus the stability problem experienced is one of modeling or model reduction. In general, any control design approach must have information about the right half plane zeros of the plant.

The performance of the closed loop system remained very consistent with the predictions made during the design stage. The steady state RSS response at 5 hz of the two angular components of the line of sight is given as a fraction of open loop response for the three models by:

P0	P2	P4
4.3×10^{-2}	5.1×10^{-2}	4.6×10^{-2}

The broadband disturbance attenuation is illustrated on the Bode plots of Figures 3 and 4 which compare open and closed loop response. Across a significant portion of the 5 Hz band the performance improvement is 3 to 4 orders of magnitude.

VII. CONCLUSIONS

We have demonstrated the applicability of a transfer function parameterization design approach for problems of broadband disturbance attenuation on flexible space structures. This methodology provides the control designer with a great deal of flexibility to meet system requirements by the choice of parameter set and selection of cost function and constraints. Although the implementation of this technique requires difficult numerical calculations involving matrix transfer functions, algorithms and software for these types of problems are already emerging. The success of this approach is dependent on an appropriate parameter selection in which to express the problem specifications. This suggests research, probably application specific, which addresses the issues of problem description and requirements interpretation in the control design process.

REFERENCES

[1] A. J. Laub, "Numerical Aspects of Control Design Computations," Computer-Aided Design and Analysis of Digital Guidance and Control Systems, NATO AGARD-LS-128, July 1983.

[2] L. Pernebo, "An Algebraic Theory for the Design of Controllers Linear Multivariable Feedback Systems," IEEE Trans. Aut. Contr., Vol. AC-26, pp. 171-194, February 1981.

[3] D. C. Youla, H. A. Jabr, and J. J. Bongiorno, Jr., "Modern Wiener-Hopf Design of Optimal Controllers - Part II: The Multivariable Case," IEEE Trans. Aut Contr., Vol. AC-21, pp.319-338, June 1976.

[4] G. Zames, "Feedback and Optimal Sensitivity: Model Reference Transformations, Multiplicative Seminorms, and Approximate Inverses," IEEE Trans. Aut. Contr., Vol. AC-26, pp. 301-320, April 1981.

[5] C. A. Desoer and M. J. Chen, "Design of Multivariable Feedback Systems with Stable Plant," IEEE Trans. Aut. Contr., Vol. AC-26, pp. 408-415, April 1981.

[6] F. P. Fernandez, "Multivariable Controller Design Using Parameter Optimization," M.I.T. master's thesis, May 1983.

REFERENCES (Continued)

[7] C. L. Gustafson and C. A. Desoer, "Controller Design for Linear Multivariable Feedback Systems with Stable Plants, Using Optimization with Inequality Constraints," Int. J. Contr., Vol. 37, No. 5, pp. 881-907, 1983.

[8] Charles Stark Draper Laboratory, "ACOSS Six (Active Control of Space Structures)," Interim Report, RADC-TR-80-377, January 1981.

[9] B. C. Moore, "Principal Component Analysis in Linear Systems: Controllability, Observability, and Model Reduction," IEEE Trans. Aut. Contr., Vol. AC-26, pp. 17-32, February 1981.

[10] C. Z. Gregory, Jr., "Reduction of Large Flexible Spacecraft Models Using Internal Balancing Theory," Proceedings of the 1983 AIAA Guidance and Control Conference, Gatlinburg, Tennessee.

[11] F. M. Callier and C. A. Desoer, Multivariable Feedback Systems, Springer-Verlag: New York - Heidelberg - Berlin, 1982.

[12] T. Kailath, Linear Systems, Prentice Hall: Englewood Cliffs, N.J., 1980.

[13] R. V. Patel, "Computation of Matrix Fraction Descriptions of Linear Time-Invariant Systems," IEEE Trans. Aut. Contr., Vol. AC-26, pp. 148-161, February 1981.

[14] A. J. Laub and B. C. Moore, "Calculation of Transmission Zeros Using QZ Techniques," Automatica, Vol 14, 1978, pp. 557-566.

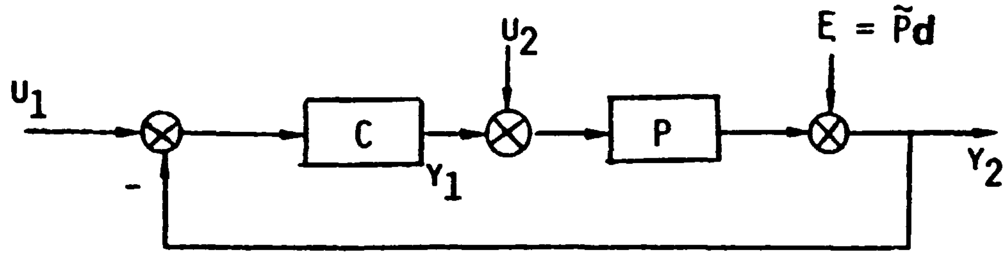

FIGURE 1. BLOCK DIAGRAM OF $\mathcal{S}$

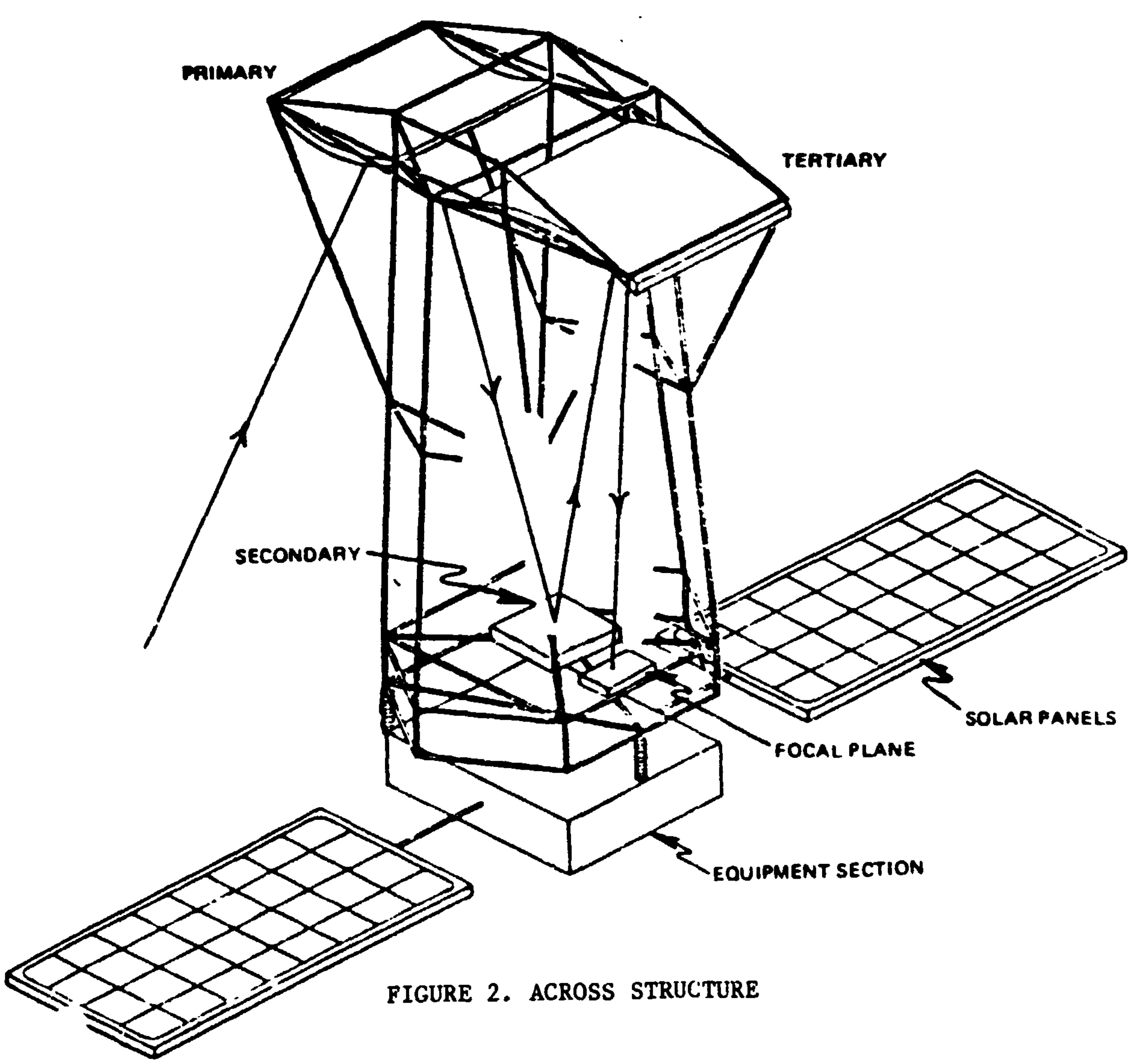

FIGURE 2. ACROSS STRUCTURE

ORIGINAL PAGE IS
OF POOR QUALITY

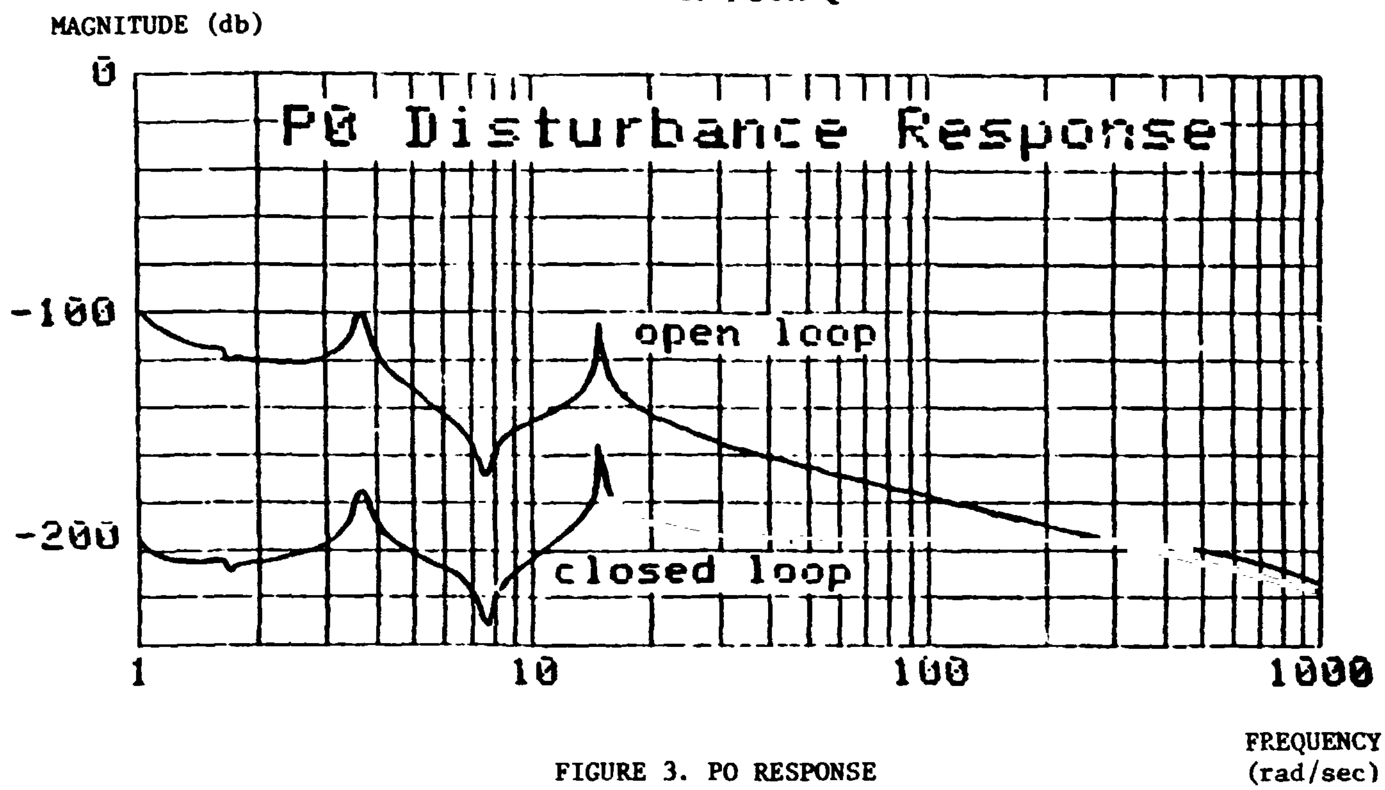

FIGURE 3. PO RESPONSE

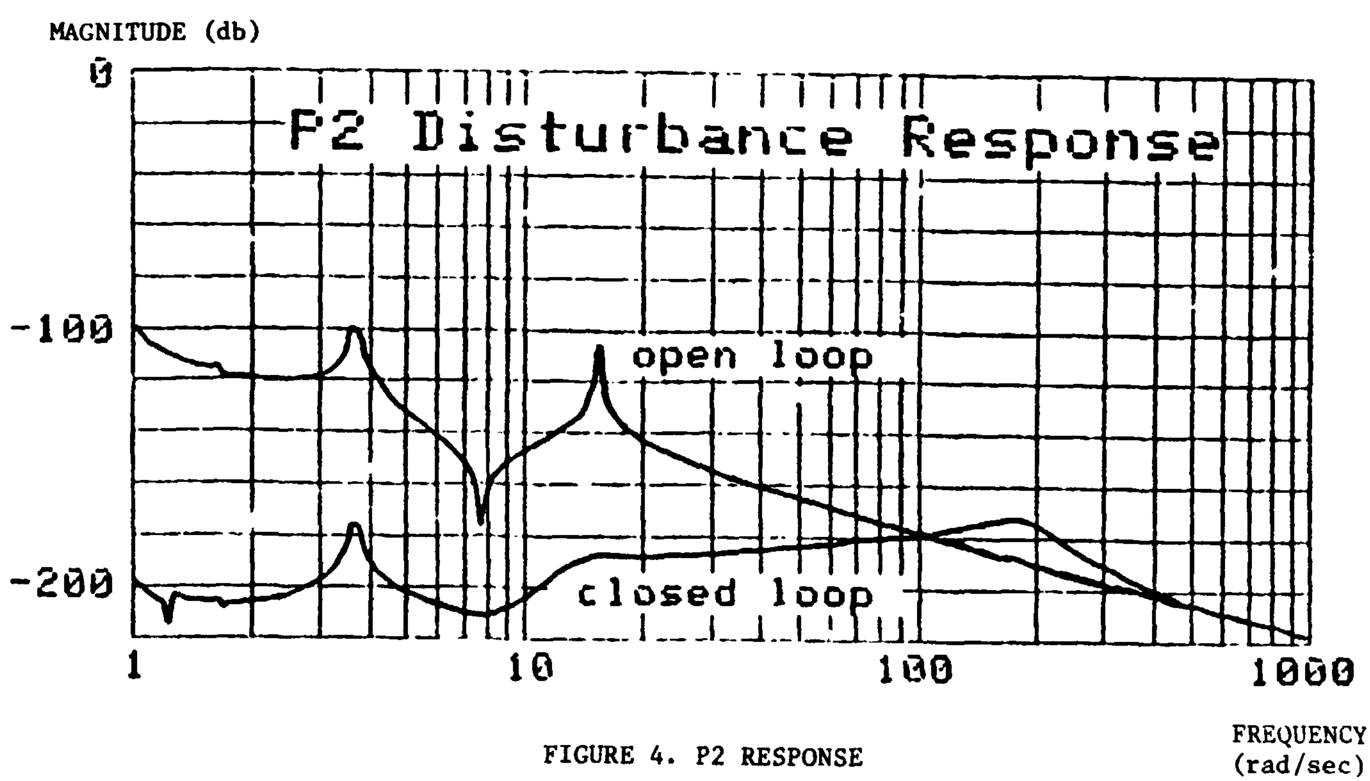

FIGURE 4. P2 RESPONSE

N85-31200

ROBUST CONTROL DESIGN FOR LARGE SPACE STRUCTURES

W. L. Eastman
McDonnell Douglas Technical Services Co.
Houston, TX 77058

J. A. Bossi
University of Washington
Seattle, WA 98195

INTRODUCTION

The control design problem for the class of future spacecraft referred to as large space structures (LSS) is by now well known [1-3]. The issue is the reduced order control of a very high-order, lightly damped system with uncertain system parameters, particularly in the high frequency modes. This paper presents a design methodology which incorporates robustness considerations as part of the design process. Combining pertinent results from multivariable systems theory and optimal control and estimation, LQG eigenstructure assignment [4] and LQG frequency-shaping, [5-7] were used to improve singular value robustness measures in the presence of control and observation spillover.

The design technique is summarized as follows. A low order LQG compensator is synthesized using the technique of recursive eigenstructure assignment to place closed-loop eigenvalues where desired. This design is evaluated for singular value performance margin and for singular value gain margin with respect to plant uncertainties (e.g., modeled dynamics). The compensator is then resynthesized using frequency-shaping concepts to improve the singular value robustness measures. The recursive eigenstructure assignment technique allows regulator close-loop eigenvalue placement at the desired locations for the plant and as required for frequency-shaping. Furthermore, the frequency-shaped compensator eigenvalues can also be assigned, thus assuring LQG compensator stability, as well as estimator stability.

This procedure using robust frequency-shaped compensation was applied to the design of the controller for a representative large space structure. Results are presented as singular value Bode plots. Comparisons are made to a recent study[8] utilizing the same large space structure model.

LQG CONTROL DESIGN FOR LSS

Control design plant modelling for LSS utilizes a high-order structural model, typically obtained by finite-element programs such as NASTRAN. The limitations of computer implementation require that the finite-element model be reduced to a design model. One approach is to truncate the high-order model into primary and residual modes, where the primary modes are to be used for control design. The modal truncation can be based on engineering judgement or on a selection criterion such as modal cost analysis [9].

The system model has the form

$$\begin{aligned} \dot{x}_p &= A_p x_p + B_p u \\ \dot{x}_R &= A_R x_R + B_R u \\ y &= C_p x_p + C_R x_R \end{aligned} \tag{1}$$

where x_p are the primary modes and x_R are the residual modes. An observer-based control design for the primary modes then has the form

$$\dot{\hat{x}}_p = A_p \hat{x}_p + B_p u + G(y - C_p \hat{x}_p) \qquad (2)$$
$$u = -K\hat{x}_p$$

Using LQG design, the gains (K, G) are selected to minimize quadratic performance indices. The terms $B_R u$ and $C_R x_R$ were identified by Balas [3] as control spillover and observation spillover respectively. These terms have the potential for interacting through the observer (2) to produce instability.

LQG theory guarantees that the reduced-order closed loop system is stable with eigenvalues of (A_p-B_pK) and (A_p-GC_p). However, no such guarantee holds for the compensator,

$$u = Hy \qquad (3)$$

which has the eigenvalues of $(A_p-B_pK-GC_p)$. This fact can be fatal for LSS reduced-order control, unless measures are taken to ensure system robustness.

ROBUSTNESS MEASURES FOR LSS

For multivariable feedback systems the emerging singular value robustness theory can be used to develop measures for stability and performance. Kosut, et al,[8] applied this theory to the large space structure control design problem, treating the residual dynamics as a perturbation. For a system with a stable nominal feedback system (based on the reduced model) and stable perturbations (due to the residual dynamics), sufficient conditions for stability are obtained when the singular value stability measures exceed the maximum perturbation due to model uncertainty. Fig. 1 defines the terminology for a large space structure control system. For an additive perturbation, Fig. 2a, the sufficient conditions for stability are

$$SM_1 = \underline{\sigma}\,[I + H(j\omega)\ G_c\ (y\omega)] > \bar{\sigma}\,[H(j\omega)\ G_R\ (j\omega)]$$

$$SM_2 = \underline{\sigma}\,[I + G_c\ (j\omega)\ H(j\omega)] > \bar{\sigma}\,[G_R\ (j\omega)\ H(j\omega)] \qquad (4)$$

where $\bar{\sigma}$ (•) indicates the maximum singular value and $\underline{\sigma}$ (•) indicates the minimum singular value. (Singular values of the complex matrix A are the positive square roots of the eigenvalues of A*A, where (•)* indicates conjugate tran-spose.) If $G_c(s)$ is minimum phase and invertible, a multiplicative perturbation can be formed, Fig. 2b, and the sufficient conditions for stability are then

$$SM_1 = \underline{\sigma}\,[I + (HG_c)^{-1}] > \bar{\sigma}\,[G_c^{-1}G_R]$$

$$SM_2 = \underline{\sigma}\,[I + (G_cH)^{-1}] > \bar{\sigma}\,[G_RG_c^{-1}] \qquad (5)$$

where the $j\omega$ arguments have been supressed. Good performance within the operating frequency region (i.e., the "control bandwidth") is provided when the performance measure

$$PM = \underline{\sigma}\,[I + G_c H] \qquad (6)$$

is large. The stability measures (4) are generalizations of Nyquist polar plot analysis; the measures (5) are generalizations of Nyquist inverse polar plot analysis. The need for large performance measure (6) is a generalization of the desirability of large loop gains.

ROBUST COMPENSATION DESIGN

The stability and performance measures presented above require stability of the nominal feedback system. In a previous work [4], the authors presented a recursive design procedure which assigns the closed-loop eigenstructure in linear quadratic regulators. At each stage, the required solution for the steady state Riccati matrix which shifts a pole or pole pair to specified values is obtained. For pole pair placement, a free parameter in the solution permits selection of closed-loop eigenvectors. This design procedure is summarized in Appendix 1.

Using duality, the procedure also applies to estimator design. By extension, the procedure can be used to design stable compensators by considering the closed-loop regulator dynamics matrix (A-BK) as the open-loop system and picking the estimator gain to place the compensator eigenstructure of (A-BK-GC).

Compensator robustness can be enhanced through the use of frequency-shaped control and estimation [5,6]. In frequency-shaped estimation, a frequency-domain performance index is considered,

$$J = E \frac{1}{2\pi} \int_{-\infty}^{\infty} [w'Q(j\omega)w + v' R(j\omega)v] \, d\omega \tag{7}$$

where w is the disturbance and v is the sensor noise. Sensor noise frequency-shaping is realized by treating v as an auto correlated noise source of the form

$$v(j\omega) = R^{1/2}(j\omega) \, v'(j\omega) \tag{8}$$

where $v'(j\omega)$ is a white noise process. In the approach used here, $Q(j\omega)$ is determined by pole placement, equivalent to injecting fictitious process noise. $R^{1/2}(j\omega)$ must be proper (not strictly proper) to maintain sensor noise weighting over the entire spectrum. Then define a pseudo-measurement

$$z' = R^{-1/2}(j\omega) \, z = R^{-1/2}(j\omega) \, Cx(j\omega) + v'(j\omega) \tag{9}$$

$R^{-1/2}(j\omega)$ can be realized in state space as

$$\begin{aligned} \dot{x}_V &= A_V x_V + B_V Cx \\ y &= C_V x_V + D_V Cx \\ z' &= C_V x_V + D_V Cx + v' \end{aligned} \tag{10}$$

This dynamic model is appended to the system dynamics to form the frequency-shaped estimator,

$$\dot{\hat{x}} = A\hat{x} + G(z' - C_V\hat{X}_V - D_V C\hat{x}) + B_c u$$

$$\dot{\hat{x}}_V = A_V\hat{x}_V + B_V C\hat{x} + G_V (z' - C_V\hat{X}_V - D_V C\hat{x}) \tag{11}$$

where z' is obtained from (10). The gains G and G_V can be picked to place the eigenvalues of (11) at those of the frequency-shaping filter (10) and the others as required for performance. A dual result can be used to develop frequency-shaped gains for the regulator.

Because frequency-shaping adds states to the compensator, an efficient choice of the loops to be shaped is desirable. Kim [7] has developed a procedure for loop selection based on the singular vectors of the return ratio matrices G_cH or HG_c. He conjectured that an input vector y in the direction of q_1, the singular vector corresponding to $\bar{\sigma}(A)$ will get the largest amplification by A. Similarly, a vector in the direction of q_n, the singular vector corresponding to $\underline{\sigma}(A)$ will get smallest amplification. Therefore, if the component of y in the direction which is closest to q_1, is reduced by a filter before it enters A, $\bar{\sigma}(A)$ is effectively reduced. $\underline{\sigma}(A)$ increased by increasing the compon[illegible] of y closest to q_n before it enters A. It can be shown that frequency-shaping introduces transmission zeros into the compensator transfer function.

DESIGN METHODOLOGY

The discussion which has been presented above suggests the following design methodology:

1. Compensator design for performance of the reduced order system.

2. Evaluation of the stability margins (4,5) against the perturbation due to the residual dynamics.

3. Selection of frequency-shaping filters to enhance stability robustness.

4. Synthesis of frequency-shaped compensator to incorporate performance and stability margins.

The recursive eigenstructure design algorithm can be used for the designs.

EXAMPLE.

The design methodology was applied to a control design for the ACOSS-1 model, also used in the comparison study [9]. The model is illustrated and the state-space data are listed in Appendix 2. As in the comparison study the first eight structural modes were retained. A regulator was designed with closed-loop poles at 20% damping; a compensator was designed with poles at critical damping. Fig. 3 illustrates stability measure (5) for the loop broken at the output. Performance is adequate at low frequencies but stability robustness is inadequate above 1 Hz.

To improve stability robustness, frequency-shaped estimation was incorporated in all three output loops using second-order low-pass filters. Fig. 4 illustrates the recovery of stability robustness while still retaining good low frequency performance, Fig. 5.

DISCUSSION

In the comparative study by Kosut, et al [8], both LQG modal control and a frequency-shaped control were investigated (along with others). LQG control was found to have poor performance as well as poor stability robustness. Frequency-shaped control was found to have adequate stability robustness, but poor low frequency performance.

The methodology presented here addresses both of these issues. Performance is achieved by pole placement design of the compensator, achieving good loop gains at low frequency. Stability robustness is achieved by adding frequency-shaping without sacrificing low frequency performance, since the gain of the frequency-shaping filters is one at low frequencies.

CONCLUSIONS

A design meth dology for control systems for large space structures has been proposed which incorporates both performance and stability robustness concerns as an integral part of the design process. Performance was achieved by placing the poles of the compensator. Stability robustness was achieved by frequency-shaping the compensator to satisfy a frequency domain stability robustness test.

An example was presented which applied the methodolgy to a system with the loop broken at the output. A full design study would also require examination of the system with the loop broken at the input, using regulator frequency-shaping to enhance robustness.

REFERENCES

1. Seltzer, S. M., "Dynamics and Control of Large Space Structures: An Overview," Jnl. of Astro. Sciences, Vol. XXVII, No. 2, pp 95-101.

2. Likins, P., "The New Generation of Dynamic Interaction Problems," Jnl. of Astro. Sciences, Vol. XXVII, No. 2, pp 103-113.

3. Balas, M., "Trends in Large Space Structure Control Theory: Fondest Hopes, Wildest Dreams," IEEE Transactions on Automatic Control, Vol. AC-27, No. 3, pp 522-535.

4. Eastman, W. L., and Bossi, J. A., "Design of Linear Quadratic Regulators with Assigned Eigenstructure," Int. Jnl. of Control, Vol 39, No. 4, 731-742.

5. Gupta, N. K., "Frequency-Shaped Cost Functionals: Extension of Linear-Quadratic-Gaussian Design Methods," Jnl. of Guidance and Control, Vol. 3, No. 6.

6. Gupta, N. K., "Robust Control/Estimator Design by Frequency-Shaped Cost Functionals," Proc. of 20th IEEE Control and Decision Conf., San Diego, CA, 1981.

7. Kim, B., "Frequency-Shaped Estimation and Robust Controller Design for Aircraft Flight Control in Wind Disrurbances," Ph. D. Thesis, University of Washington, Dept. of Aeronautics and Astronautics, Seattle, WA., 1983.

8. Kosut, R. L., Salzwedel, H., and Emami-Naeini, A., "Robust Control of Flexible Spacecraft, Jnl. of Guidance and Control, Vol. 6, No. 2.

9. Skelton, R. E., "Cost Decomposition of Linear Systems with Application to Model Reduction," Int. Inl. of Control, Vol 32, No. 6,. pp. 1031-1055.

10. Solheim, O. A., "Design of Optimal Control Systems with Prescribed Eigenvalues," Int. Jnl. of Control, Vol. 15, No. 1.

11. Strunce, R., Lin, J., Hegg, D., Henderson, T., "Actively Controlled Structure Theory," Final Report, Vol. 2 of 3, R-1338, Charles Stark Draper Lab., Cambridge, Mass, Dec. 1979.

APPENDIX 1

Recursive Eigenstructure Design

The steady-state optimal control law for the linear, time-invariant, controllable system:

$$\dot{x} = Ax + Bu \tag{A.1}$$

which minimizes the quadratic performance index,

$$J = 1/2 \int_0^\infty [x^T Qx + u^T Ru]\, dt \tag{A.2}$$

is linear state feedback

$$u = Kx = - R^{-1} B^T Sx \tag{A.3}$$

where S is the solution of the steady-state Riccati equation,

$$-SA - A^T S + SBR^{-1} B^T S - Q = 0 \tag{A.4}$$

In this appendix we summarize an interactive design technique which solves (A.4) to provide specified eigenvalues of the closed-loop system dynamics matrix A+BK and which also permits some freedom in selecting closed-loop eigenvectors. The method is reported elsewhere [4] in detail. It extends the procedure of Solheim [10] in which, for fixed R, the elements of Q providing the required pole placement are calculated directly.

The design technique is recursive; at each stage, the system dynamics matrix A in (A.1) incorporates previous state feedback. We then implement the following eigenstructure calculation:

$$X^{-1}[\Lambda - H\bar{S}]X = \bar{\Lambda} \qquad (A.5)$$

where $\Lambda = T^{-1} AT$ is block diagonal, T is the real eigenvector matrix of A, and $H = T^{-1}BR^{-1}B^TT^{-T}$ is symmetric and positive semi-definite. $\bar{\Lambda}$ is identical to Λ except for a block of shifted poles. X is the transformation from open-loop eigenvectors to closed-loop eigenvectors; it is defined as the "stage" eigenvector matrix. $\bar{S}$ is the Riccati matrix in the open-loop diagonalized coordinate system; $\bar{S}$ is chosen to shift a single pole or a pair of poles. The corresponding gain matrices, K, determined for each stage are subsequently added to obtain a final gain which achieves the same closed-loop pole locations.

To provide the required pole shift, the only non-zero elements of S correspond to the entries of Λ which are to be shifted. With this choice of S, the characteristic equation factors into the product of terms for the unshifted poles and a term for the desired shifted poles. Thus,

$$|sI - \Lambda| = D(s) \prod_{i \epsilon I} (s - \lambda_i) \qquad (A.6)$$

where I is the index set for the unshifted poles, and D(s) contains explicit elements of S, H, and the block of Λ which is to be shifted. Matching the coefficients of powers of s in D(s) to the equivalent terms in the closed-loop characteristic equation provides a set of equations in the required elements of $\bar{S}$. For the single pole shift $\Lambda_{jj} = \lambda$ to κ, the only non-zero element of $\bar{S}$ satisfies

$$\bar{S}_{jj} = \frac{\lambda-\kappa}{H_{jj}} .$$

For double pole placement it can be shown that the three required elements of $\bar{S}$ lie on the intersection of two quadric surface in a mathematical space having the three $\bar{S}$ elements as coordinates. (It can also shown that a direct solution for Q has a similar geometric interpretation.) If the corresponding submatrix of H is positive definite, the surfaces are a plane and a hyperboloid of one or two sheets; the intersection, if it exists, is always an ellipse. If the relevant submatrix of H is singular, the surfaces are planes, and the intersection is a line. The different points comprising the solution all provide the desired eigenvalue placement, but with different eigenvectors.

In ref. 4 a solution for $\bar{S}$ is presented which takes advantage of the quadric surface geometry to define a free parameter that allows design freedom in the choice of closed-loop eigenvectors. The solution for the stage eigenvector X partitions into two sets of equations. The first is a homogeneous Lyapunov equation for the submatrix corresponding to the shifted pole block in Λ. For a pole pair shift, the submatrix is 2x2. Hence, depending upon the nature of the closed-loop poles (real or complex), one or two elements of the submatrix may be chosen arbitrarily; the remaining elements then depend on the choice of elements of $\bar{S}$. The other equation is a non-homogeneous Lyapunov equation in the remaining elements of the columns of X containing the 2x2 submatrix; its solution depends upon the 2x2 submatrix, the elements of $\bar{S}$ and $\bar{\Lambda}$, and certain elements of H.

The closed-loop system eigenvector matrix is then $T_{CL} = TX$. The solution of X depends upon $\bar{S}$, which varies with the choice of the free parameter. Therefore, by recursively shifting pole pairs, design freedom exists to select closed-loop eigenvectors while providing required pole placements.

The procedure outlined above lends itself to a recursive procedure for practical multivariable regulator design. The steps in the procedure are as follows:

1. System (A.1) is placed in modal form.

2. The designer selects the control weighting matrix R, then H is calculated.

3. The designer selects a real pole or pair of poles to be shifted and their desired location; a pair, he also selects the free parameter which determines the closed-loop eigenvectors.

4. The stage gain is calculated and the closed-loop system is placed in modal form.

5. Steps 3 and 4 are repeated for other poles until the designer is satisfied.

6. The total system gain is obtained by adding the stage gains.

Clearly by duality, the same process can be applied to estimator design, permitting the development of multivariable compensators.

APPENDIX 2.

The ACOSS-1 flexible spacecraft model was developed by the Charles Stark Draper Laboratory.[10] It is representative of many radar and optical control problems, but is small enough to be tenable for research studies. The structure is a tetrahedral truss supported by three right-angle bipods. The truss members are flexible in the axial direction only. The model has 12 modes; for control design, only eight are assumed to be known.

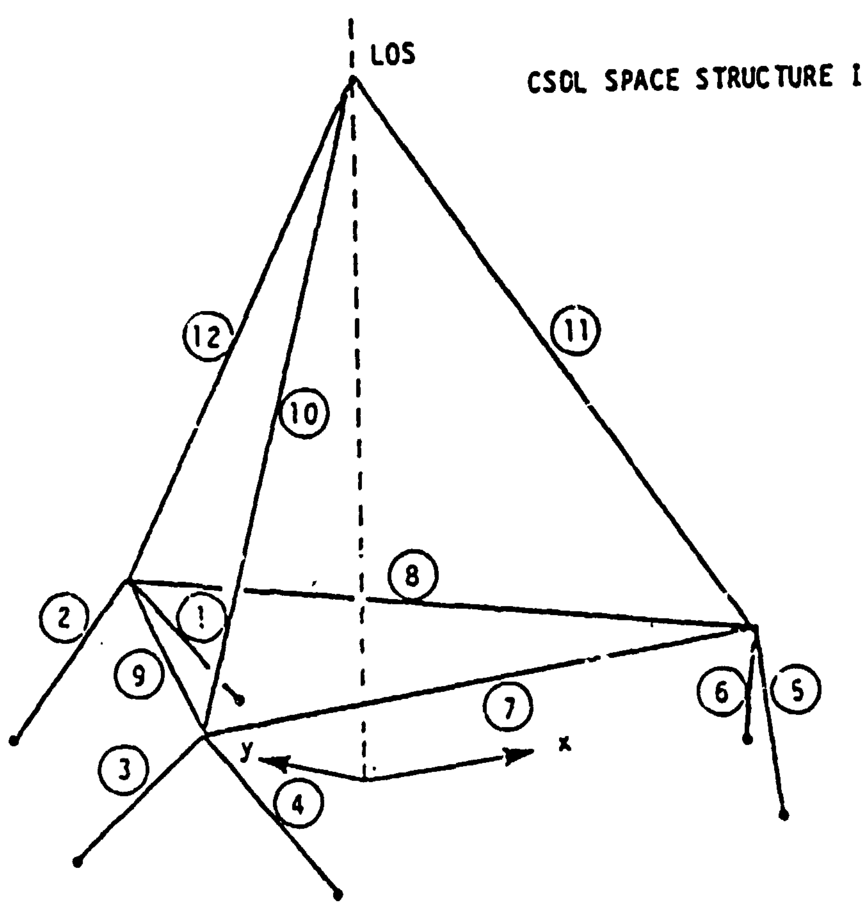

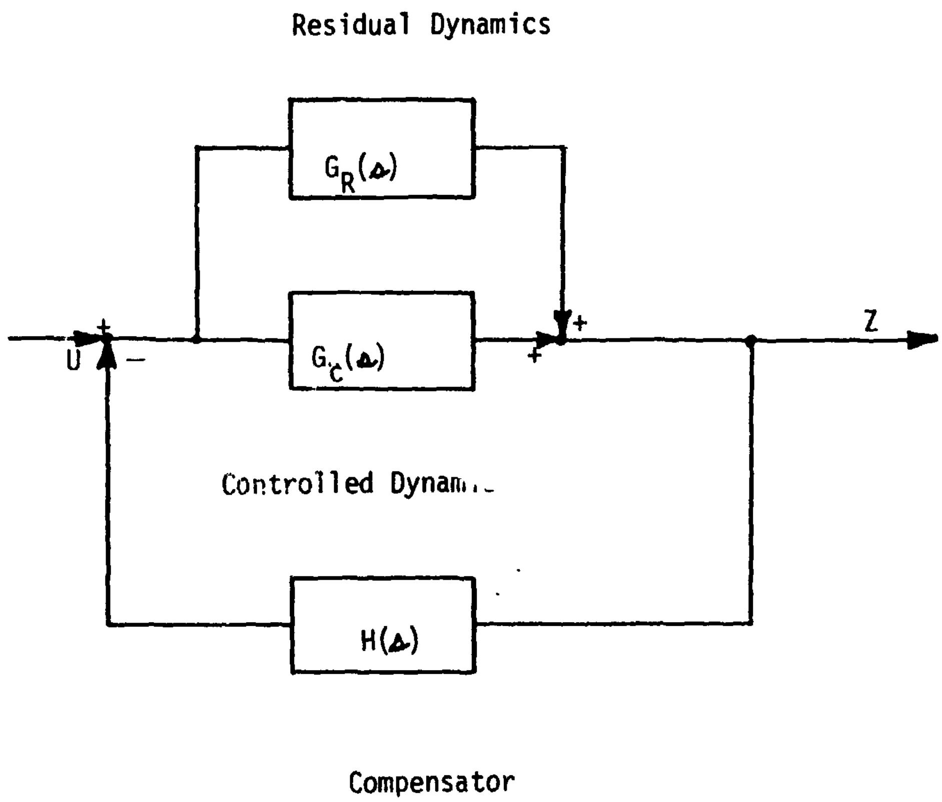

Fig. 1 - LSS Control System

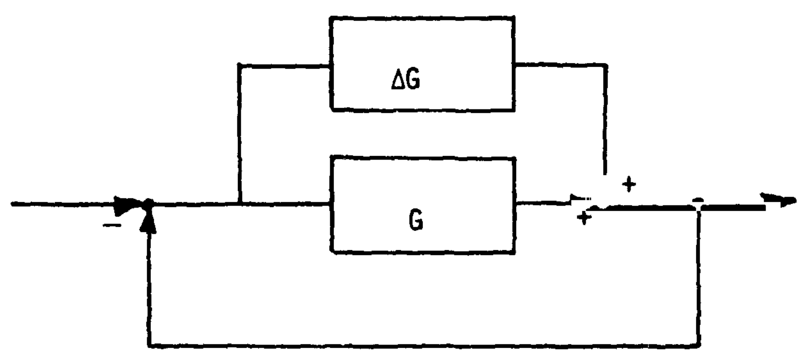

Fig. 2a - Additive Perturbation

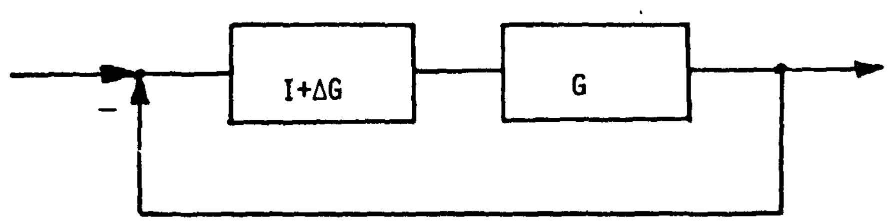

Fig. 2b - Multiplicative Perturbati

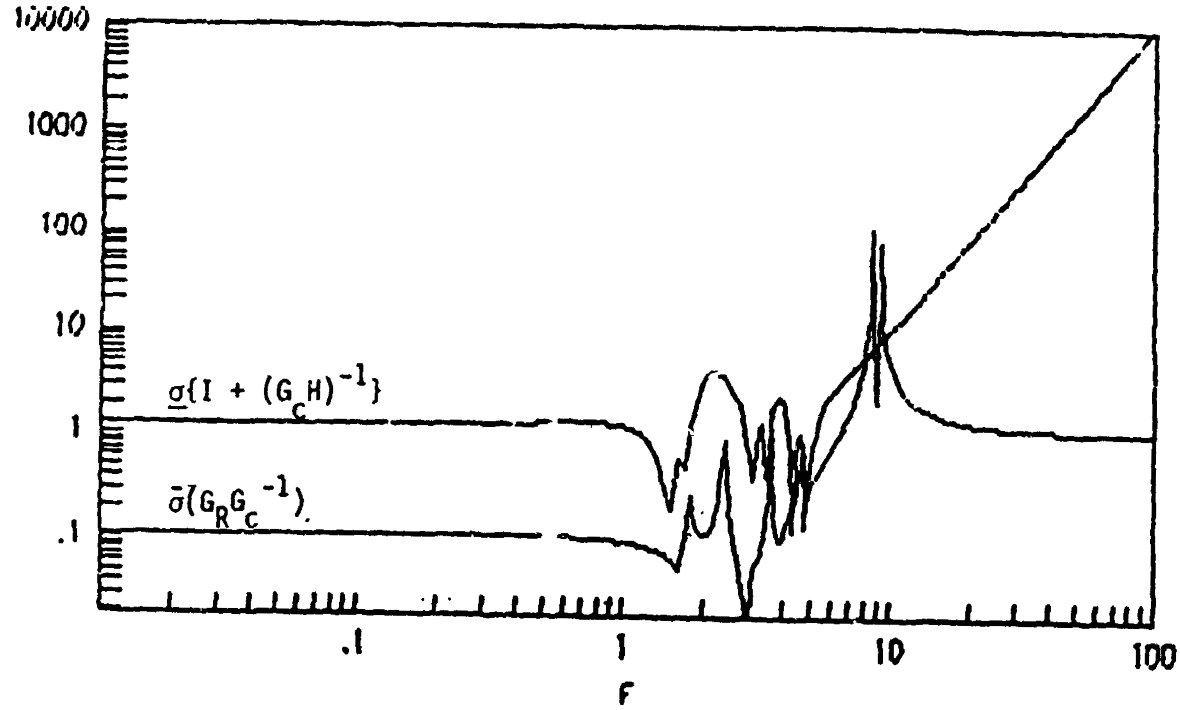

Fig. 3 Reduced - Order Control Stability Margin

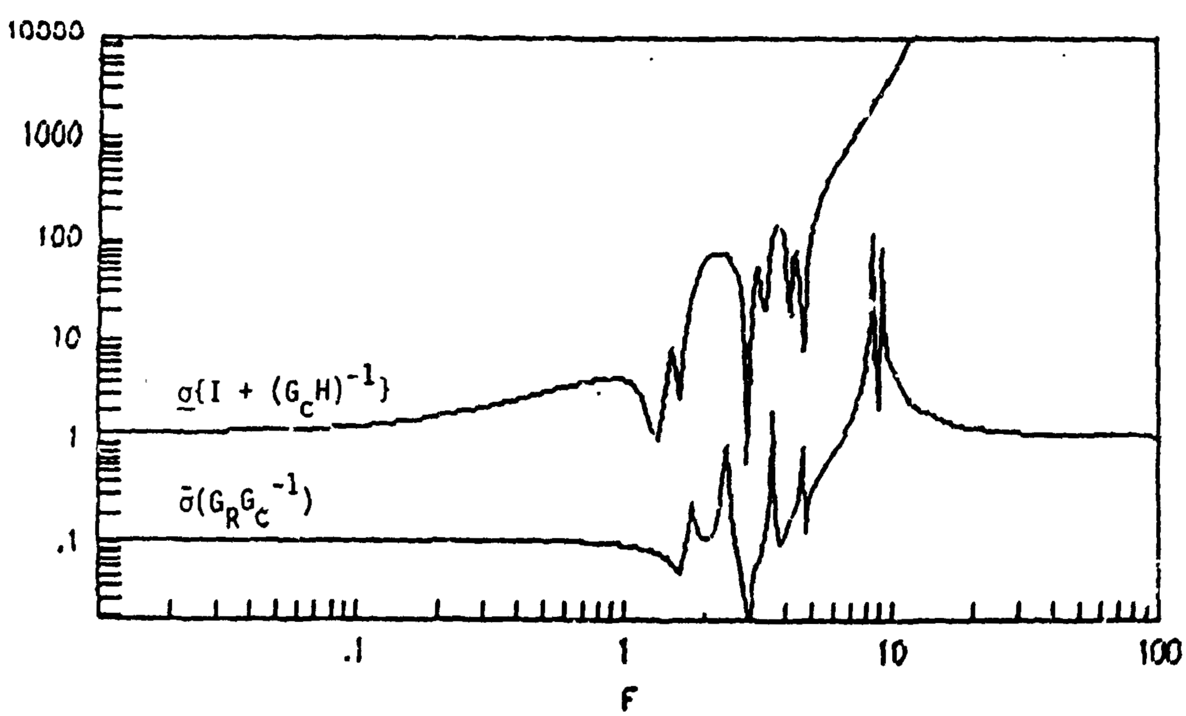

Fig. 4 Frequency - Shaped Control Stability Margin

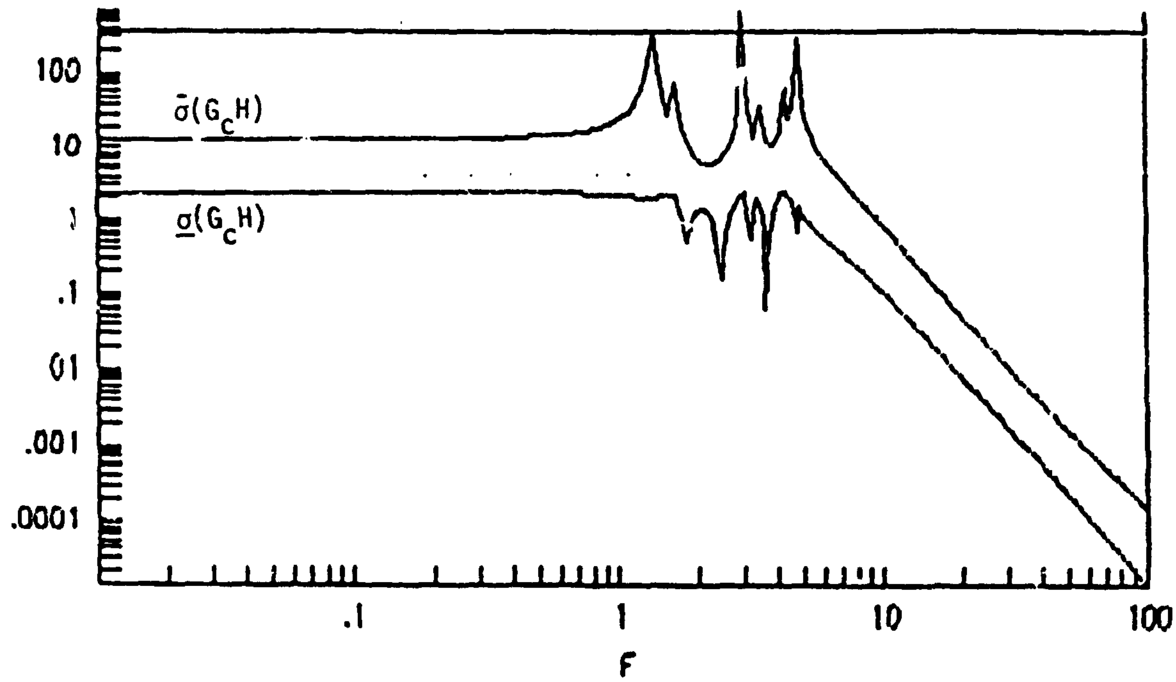

Fig. 5 Loop Gains

N85-31201

ON THE STABILITY OF COLLOCATED CONTROLLERS IN THE PRESENCE OF UNCERTAIN NONLINEARITIES AND OTHER PERILS

S. M. Joshi
NASA Langley Research Center
Hampton, VA 23665

ABSTRACT

Robustness properties are investigated for two types of controllers for large flexible space structures, which use collocated sensors and actuators. The first type is an attitude controller which uses negative definite feedback of measured attitude and rate, while the second type is a damping enhancement controller which uses only velocity (rate) feedback. It is proved that collocated attitude controllers preserve closed-loop global asymptotic stability when linear actuator/sensor dynamics satisfying certain phase conditions are present, or monotonic increasing nonlinearities are present. For velocity feedback controllers, the global asymptotic stability is proved under much weaker conditions. In particular, they have 90° phase margin and can tolerate nonlinearities belonging to the $[0,\infty)$ sector in the actuator/sensor characteristics. The results significantly enhance the viability of both types of collocated controllers, especially when the available information about the large space structure (LSS) parameters is inadequate or inaccurate.

INTRODUCTION

Large flexible space structures are infinite-dimensional systems with very small inherent energy dissipation (damping). Because of practical limitations, only finite-dimensional controllers and point actuators and sensors must be used for controlling large space structures (LSS). In addition, considerable uncertainty exists in the knowledge of the parameters. For these reasons, the design of a stable controller for a large space structure (LSS) is a challenging problem.

A class of controllers, termed "collocated controllers" [1], represents an attractive controller because of its guaranteed stability properties in the presence of plant uncertainties. Collocated attitude (CA) controllers are designed to control the rigid-body attitude as well as the structural modes, while collocated direct velocity feedback (CDVFB) controllers are designed only for enhancement of structural damping. Both types of collocated controllers guarantee stability regardless of the number of modes in the LSS model and uncertainties in the knowledge of the parameters [1], [2]. A CA controller basically consists of compatible sensor/actuator pairs placed at the same

C-2

locations, and utilizes negative definite feedback of position and velocity (e.g., LSS attitude and attitude rate). A CDVFB controller [3] is a special case of the CA controller where only rate feedback is used for damping enhancement without affecting the rigid-body modes. It has been proved in references [1], [2], [3] that, the closed-loop system is always stable in the sense of Lyapunov, and is also asymptotically stable (AS) under certain additional conditions.

Although collocated controllers have attractive stability properties with perfect (i.e., linear, instantaneous) sensors and actuators, the sensors and actuators available in practice tend to have nonlinearities and phase lags associated with them. In order to be useful in practical applications, the controller should be tolerant to nonlinearities (e.g., saturation, relays, deadzones, etc.), and to phase shifts (e.g., actuator dynamics and/or computational delays). Uncertainties usually exist in the knowledge of the nonlinearities and the phase lags. For these reasons, this paper investigates the closed-loop stability of collocated controllers in the presence of unmodeled sensor/actuator dynamics and nonlinearities. The situation is mathematically described by including an operator $\mathcal{H}$ in the feedback path. The actual input u(t) is given by:

$$u(t) = \mathcal{H} u_c(t) \tag{1}$$

where u_c is the ideal (desired) input, $\mathcal{H}$ is a nonanticipative, linear or nonlinear, time-varying or invariant operator. For CA controllers, it is proved that the closed-loop system is globally asymptotically stable if

1) $\mathcal{H}$ is linear, time-invariant (LTI) and stable with a rational transfer matrix H(s) which satisfies certain frequency-domain conditions, or

2) If $\mathcal{H}$ consists of time-invariant, strictly monotonic increasing nonlinearities belonging to the $[0, \infty)$ sector. (A function $\phi(\sigma)$ is said to belong to the $[k, h)$ sector if $\phi(0) = 0$ and $k\sigma^2 \leq \sigma\phi(\sigma) < h\sigma^2$ for all $\sigma \neq 0$).

For CDVFB controllers, it is proved that global asymptotic stability is preserved when

1) $\mathcal{H}$ is a stable nonlinear dynamic operator and satisfies certain passivity conditions, or

2) $\mathcal{H}$ is a stable LTI operator with phase within $\pm 90°$

3) $\mathcal{H}$ consists of nonlinear gains belonging to the $[0, \infty)$ sector.

These analytical results significantly enhance the stability and robustness properties of collocated controllers, and therefore increase their practical applicability.

PROBLEM FORMULATION

The linearized equations of motion of a large flexible space structure (using torque actuators) are given by:

$$A\ddot{x} + B\dot{x} + Cx = \sum_{i=1}^{m} \Gamma_i^T u_i \tag{2}$$

where

$$x = (\phi_s, \theta_s, \psi_s, q_1, q_2, \ldots, q_{nq})^T \tag{3}$$

$$A = \text{diag}\ (I_s, I_{nq\ x\ nq}) \tag{4}$$

$$B = \text{diag}\ (0_{3\ x\ 3}, D) \tag{5}$$

$$C = \text{diag}\ (0_{3\ x\ 3}, \Lambda) \tag{6}$$

$$\Gamma_i = [I_{3\ x\ 3}, \Phi_i] \tag{7}$$

$$u_i = (u_{xi}, u_{yi}, u_{zi})^T \tag{8}$$

where ϕ_s, θ_s, ψ_s denote the three rigid-body Euler angles, n_q is the number of structural modes, q_i denotes the modal amplitude of ith structural mode ($i = 1, 2, \ldots, n_q$), I_s denotes the 3 x 3 moment of inertia matrix, Ψ_i is the 3 x n_q mode-slope matrix at the ith (3-axis) actuator location. It is assumed that m, 3-axis torque actuators are used. $I_{\ell\ x\ \ell}$ denotes the ℓ x ℓ identity matrix, and diag( ) denotes a block-diagonal matrix. D is a symmetric positive definite or semidefinite matrix which represents the inherent structural damping. Since some damping, no matter how small, is always present, we assume $D > 0$ throughout this paper. Λ is an n_q x n_q diagonal matrix of squared structural frequencies

$$\Lambda = \text{diag}\ (\omega_1^2, \omega_2^2, \ldots, \omega_{nq}^2) \tag{9}$$

Assuming that m, 3-axis attitude and rate sensors (e.g., star trackers and rate gyros) are placed at the locations of the actuators, the measured 3-axis attitude y_{ai} and rate y_{ri} at actuator location i (ignoring noise) are given by:

$$y_{ai} = \Gamma_i x \tag{10}$$

$$y_{ri} = \Gamma_i \dot{x} \tag{11}$$

denoting

$$u = [u_1^T, u_2^T, \ldots, u_m^T]^T \tag{12}$$

$$\Gamma^T = [\Gamma_1^T, \Gamma_2^T, \ldots, \Gamma_m^T] \tag{13}$$

$$y_a = [y_{a1}^T, y_{a2}^T, \ldots, y_{am}^T]^T \tag{14}$$

$$y_r = [y_{r1}^T, y_{r2}^T, \ldots, y_{rm}^T]^T \tag{15}$$

where u, y_a, y_r are 3m x 1 vectors, and Γ is a 3m x (n_q + 3) matrix. The control law for the collocated attitude controller is given by:

$$u_c = u_{cp} + u_{cr} \tag{16}$$

$$u_{cp} = -G_p y_a \tag{17}$$

$$u_{cr} = -G_r y_r \tag{18}$$

where u_c represents the command input, u_{cp} and u_{cr} represent command attitude and rate inputs, and G_p, G_r are 3m x 3m feedback gain matrices.

For CDVFB controllers, the rigid-body rates are removed from the feedback signal by subtracting attitude rates at two locations. Consequently, the model used for damping enhancement has the form:

$$\ddot{q} + D\dot{q} + \Lambda q = \tilde{\Phi}^T u \tag{19}$$

where $\tilde{\Phi}$ consists of appropriate differences between the mode-slopes. The control law is given by:

$$u_c = -G_r \tilde{y}_r \tag{20}$$

where

$$\tilde{y}_r = \tilde{\Phi}\dot{q} \tag{21}$$

The control laws given above for CA and CDVFB controllers have very attractive robustness properties. It was shown in [1], [2] that, if D > 0, $G_p = G_p^T > 0$, and $G_r = G_r^T > 0$, then the closed-system is asymptotically stable (AS). The stability result holds regardless of the number of modes in the model, and regardless of inaccuracy in the knowledge of the parameters. In real life, however, nonlinearities and phase lags exist in the sensors and actuators, which invalidate these robust stability properties. The real problem then is to investigate the closed-loop stability for the case where the actual input is given by Eq. (1), where $\mathcal{H}$ is a nonanticipative, linear or nonlinear, time-varying or invariant operator. The situation is shown in Figure 1. Our approach is to make use of input-output stability concepts and Lyapunov methods. We assume throughout the paper that the problem is well-posed, and that a unique solution exists. We start by defining the terminology and the concepts, which are adopted from [4].

MATHEMATICAL PRELIMINARIES

Consider the linear vector space L_n^2 of real square-integrable n-vector functions of time t, defined as:

$$L_n^2 = \{g: R_+ \to R^n \mid \int_0^\infty g^T(t)g(t)dt < \infty\} \tag{22}$$

where R^n is the linear space of ordered n-tuples of real numbers, and R_+ denotes the interval $0 \leq t < \infty$. The scalar product is defined as

$$\langle g_1, g_2\rangle = \int_0^\infty g_1^T(t)g_2(t)dt \tag{23}$$

For $g \in L_n^2$, its norm is defined as

$$\|g\| = \langle g,g\rangle^{1/2} \tag{24}$$

Define the truncation operator P_T such that

$$g_T(t) \triangleq P_T g(t) = \begin{cases} g(t) & 0 \leq t \leq T \\ 0 & t > T \end{cases} \tag{25}$$

Define the extended space L_{ne}^2:

$$L_{ne}^2 = \{g: [R_+ \to R^n \mid g_T \in L_n^2 \; \forall T \geq 0\} \tag{26}$$

Thus L_{ne}^2 is a linear vector space of functions of t whose truncations are square-integrable on $[0,T)$ for all $T < \infty$. For g_1, $g_2 \in L_{ne}^2$, define the truncated inner product

$$\langle g_1, g_2\rangle_T = \langle g_{1T}, g_{2T}\rangle = \int_0^T g_1^T(t)g_2(t)dt \tag{27}$$

The truncated norm is defined by: $\|g\|_T = \langle g,g\rangle_T^{1/2}$.

Consider an operator $\mathcal{H}: L_{ne}^2 \to L_{ne}^2$. $\mathcal{H}$ is said to be strictly passive if there exist finite constants β and $\delta > 0$ such that

$$\langle \mathcal{H}g, g\rangle_T \geq \beta + \delta\|g\|_T^2 \quad \forall T \geq 0, \forall g \in L_{ne}^2 \tag{28}$$

$\mathcal{H}$ is passive if $\delta = 0$ in (28).

Stability With Dynamic Operator in the Loop

We consider the case where the operator $\mathcal{H}$ is linear and time-invariant (LTI), and has a finite-dimensional state-space representation. We denote $\mathcal{H}g$ by $\mathcal{H}(z_0; g)$ where z_0 is the initial state vector of $\mathcal{H}$, and assume $m = 1$ for simplicity (i.e., one 3-axis actuator).

Theorem 1. Suppose $\mathcal{H}$ is a non-anticipative, strictly stable, completely observable, LTI operator whose transfer matrix is $H(s) = \varepsilon I + \hat{H}(s)$, where $\varepsilon > 0$ and $\hat{H}(s)$ is a proper, minimum-phase, rational matrix. Under these conditions, the closed-loop system given by Eqs. (1), (2), (10), (11), (16)-(18) is asymptotically stable (AS) if

$$\hat{H}(j\omega)\,(\omega G_r - jG_p) + (\omega G_r + jG_p)\,\hat{H}^*(j\omega) \geq 0 \text{ for all real } \omega. \tag{29}$$

where * denotes the conjugate transpose.

Proof - Define the function

$$V(t) = x^T C x + \dot{x}^T A\, \dot{x} \tag{30}$$

Since $C \geq 0$, $A > 0$, $V(t) \geq 0$ for all $t \geq 0$. Differentiating V with respect to t, and using (1), (10), (11), (16)-(18),

$$\dot{V} = -\, 2\dot{x}^T B\dot{x} - 2u_{cr}^T\, G_r^{-1}\, \mathcal{H}[z_o;\, u_c] \tag{31}$$

where $\mathcal{H}$ also depends on its initial state z_0. Since $\mathcal{H}$ is linear,

$$\mathcal{H}[z_o;\, u_c] = h_o(t) + \mathcal{H}[0;\, u_c] \tag{32}$$

where $h_0(t)$ is the unforced response of $\mathcal{H}$ due to nonzero initial state. Since $\mathcal{H}$ is strictly stable, $\|h\|_0$ is finite for any finite z_0.

Substituting (32) in (31) and integrating from 0 to T, since $V(T) \geq 0$,

$$0 \leq V(T) = V(0) - 2\langle \dot{x},\, B\dot{x}\rangle_T - 2\,\langle u_{cr},\, G_r^{-1} h_o\rangle_T$$
$$-\, 2\langle u_{cr},\, G_r^{-1}\, \mathcal{H}_p u_{cp}\rangle_T \tag{33}$$

where

$$\mathcal{H}_p u_{cp} = \mathcal{H}[0;\, (G_p + sG_r)\, u_{cp}] \tag{34}$$

In (34), "s" denotes the derivative operator. ("s" is technically noncausal; however, this difficulty can be overcome by defining the derivative of a truncation at T to be equal to that of the untruncated function.) Using Parseval's theorem,

$$\langle u_{cr}, G_r^{-1} \mathcal{H}_p u_{cp} \rangle_T = \frac{1}{2\pi} \int_{-\infty}^{\infty} U_{cr_T}^{*}(j\omega)\, G_r^{-1} H(j\omega)\, [G_p + j\omega G_r]\, U_{cp_T}(j\omega) d\omega$$

$$= \frac{1}{2\pi} \int_{-\infty}^{\infty} U_{cr_T}^{*}(j\omega)\, G_r^{-1} H(j\omega)\, [\frac{G_p}{j\omega} + G_r]\, U_{cr_T}(j\omega) d\omega$$

$$= \frac{1}{2\pi} \int_{-\infty}^{\infty} U_{cr_T}^{*}(j\omega)\, [G_r^{-1} H(j\omega) (\frac{G_p}{j\omega} + G_r)$$

$$+ (\frac{G_p}{-j\omega} + G_r)\, H^{*}(j\omega)\, G_r^{-1}]\, U_{cr_T}(j\omega) d\omega$$

The matrix in the brackets is positive (from Eq. 29), and we have

$$\langle u_{cr}, G_r^{-1} \mathcal{H}_p u_{cp} \rangle_T \geq \varepsilon \, \| u_{cr} \|_T^2 \tag{35}$$

which yields (from (33)

$$0 \leq V(o) - 2 \langle \dot{q}, D\dot{q} \rangle_T - 2 \varepsilon \| u_{cr} \|_T^2 - 2 \langle u_{cr}, G_r^{-1} h_o \rangle_T \tag{36}$$

wherein we have used the fact that $\dot{x}^T B \dot{x} = \dot{q}\, D\dot{q}$. Therefore,

$$\lambda_m(D) \| \dot{q} \|_T^2 + \varepsilon \| u_{cr} \|_T^2 \leq V(o)/2 + \| u_{cr} \|_T \| G_r^{-1} \|_s \| h_o \| \tag{37}$$

where $\| \ \|_s$ denotes the spectral norm of a matrix, and λ_m denotes the smallest eigenvalue. Eq. (37) can be written as

$$\lambda_m(D) \| \dot{q} \|_T^2 + (c_1 \| u_{cr} \|_T - \frac{c_2}{2c_1})^2 \leq V(o)/2 + c_2^2/4c_1 \tag{38}$$

where $c_1 = \sqrt{\varepsilon}$ and $c_2 = \| h_o \|$ Therefore, $\lim_{t\to\infty} \dot{q}(t) = 0$, and $\lim_{t\to\infty} u_{cr}(t) = 0$. Denoting the rigid-body attitude $\alpha = (\phi_s, \theta_s, \psi_s)^T$, this implies that $\lim_{t\to\infty} \alpha(t) = 0$. Taking the limit of the closed-loop equation as $t\to\infty$,

$$\begin{bmatrix} 0 \\ \Lambda \bar{q} \end{bmatrix} = \begin{bmatrix} I \\ \phi^T \end{bmatrix} \overline{\mathcal{H}} u_{cp} \tag{39}$$

where the overhead bar denotes the limit as $t \to \infty$. From (39), $\overline{\mathcal{H} u_{cp}} = 0$ and $\bar{q} = 0$, which yields $\bar{\alpha} = 0$. Since $\mathcal{H}$ is observable and its output tends to zero, its state vector tends to zero as $t \to \infty$, and the system is asymptotically stable.

The following corollary essentially states that, for diagonal G_p, G_r, and H, it is sufficient that the phase lag of $\hat{H}(j\omega)$ is less than the phase lead introduced by the controller.

Corollary 1.1. Suppose G_p, G_r and H are diagonal and satisfy the assumptions of Theorem 1. Then the closed-loop system is globally asymptotically stable if

$$-\tan^{-1} \frac{\omega G_{ri}}{G_{pi}} \leq \text{Arg } \{\hat{H}_i(j\omega)\} \leq 180° - \tan^{-1} \frac{\omega G_{ri}}{G_{pi}} \quad \text{for all real } \omega \tag{40}$$

where Arg( ) denotes the phase angle of a complex variable.

For the case where $H_{ii}(s) = k_i/(s + a_i)$, with k_i, $a_i > 0$, condition (40) becomes

$$\frac{G_{ri}}{G_{pi}} \geq 1/a_i \tag{41}$$

Thus, for the case of first-order sensor/actuator dynamics, the system is asymptotically stable if the ratio of rate-to-proportional gain is at least equal to the magnitude of the actuator pole.

In Theorem 1 and Corollary 1.1, the transfer function of $\mathcal{H}$ was assumed to be of the form: $H(s) = \varepsilon I + \hat{H}(s)$, where $\varepsilon > 0$. That is, a direct transmission term, no matter how small, was present. From Theorem 1, the closed-loop system is AS for any $\varepsilon > 0$. Therefore, the closed-loop eigenvalues are all in the open left half-plane (OLHP). Because of continuity, it is obvious that, when $\varepsilon = 0$, the eigenvalues will not cross the imaginary axis. That is, the eigenvalues will be in the closed left half-plane (CLHP). Theorem 2 given below considers the case when $\varepsilon = 0$. It essentially shows that, if the closed-loop system with no elastic modes is AS with $\hat{\mathcal{H}}$ in the loop, then so is the system with elastic modes, provided that (29) is satisfied with H replacing $\hat{H}$.

Theorem 2. Suppose $\mathcal{H}$ is a non-anticipative, strictly stable, completely observable, LTI operator with rational transfer matrix H(s) which is proper and minimum-phase. If the closed-loop system for the rigid body model alone (i.e., Eqs. (1), (2), (10), (11), (16)-(18) with $n_q = 0$) is AS, then the entire closed loop system (i.e., with $n_q \neq 0$) is AS provided that

$$H(j\omega)\,(\omega G_r - jG_p) + (\omega G_r + jG_p)\,H^*(j\omega) \geq 0 \text{ for all real } \omega \tag{42}$$

Proof. Considering the rigid-body equations,

$$I_s\ddot{\alpha} = \mathcal{H} u_c = \mathcal{H}(u_\alpha + u_q) \tag{43}$$

where $u_\alpha = -G_p\alpha - G_r\dot{\alpha}$ and $u_q = -G_p\Phi q - G_r\Phi\dot{q}$. Thus the transfer function from $\dot{q}$ to $\dot{\alpha}$ is given by

$$M(s) = [I + H(s)\{G_p + G_r s\}]^{-1} H(s)\{G_p + G_r s\}\Phi$$

Since the closed-loop rigid-body system is strictly stable by assumption, M(s) is strictly stable and finite-gain, which implies

$$\|\dot{\alpha}\|_T \leq \gamma\|\dot{q}\|_T + \|h_m\|_T \qquad (44)$$

where γ is the gain of M and h_m is its free response. Proceeding as in the proof of Theorem 1, we can arrive at Eq. (37) wherein $\varepsilon = 0$ and n_0 is replaced by h_m. Since $u_{cr} = -G_r(\dot{\alpha} + \Phi\dot{q})$, we have from (44),

$$\|u_{cr}\|_T \leq c_1\|\dot{q}\|_T + c_2\|h_m\|_T \qquad (45)$$

where c_1 and c_2 are positive constants. Completing squares as in (38) and noting that $\|h_m\|$ is finite, it can be proved that $\|\dot{q}\|_T$ is bounded for all $T > 0$, and that $\lim_{t\to\infty}\dot{q}(t)=0$. From (45), u_{cr} also tends to zero as $t\to\infty$. The remainder of the proof is similar to that of Theorem 1.

Corollary 2.2 With the same assumptions as in Theorem 2, if G_p, G_r, and H are diagonal, then the closed-loop system is AS if (40) is satisfied with H replacing $\hat{H}$.

From Corollary 2.2, for the case where $H_{ii}(s) = k_i/(s + a_i)$ with k_i, $a_i > 0$, the closed-loop asymptotic stability is assured if $G_{pi} \leq a_i G_{ri}$ for $i = 1, 2, \ldots, m$.

The significance of the results of this section is that the stability can be assured by making the ratio of the rate-to-proportional gains sufficiently large. One has to know only the sensor/actuator characteristics, and the knowledge of the plant parameters is not required. This result is completely consistent with the result obtained in [5] for single-input, single-output systems, for small G_p and G_r, using a root-locus argument.

The next section considers the case where nonlinearities are present in the loop.

Stability in the Presence of Nonlinearities

Suppose Eq. (1) is replaced by

$$u = \psi(u_c) \qquad (46)$$

where ψ is an m-vector, one-to-one, time-invariant function, $\psi: R^m \to R^m$, as follows:

$$\psi(\sigma) = [\psi_1(\sigma_1), \psi_2(\sigma_2), \ . \ . \ . \ , \psi_m(\sigma_m)] \tag{47}$$

For this case, the stability of the closed-loop system can be investigated using Lyapunov methods. A function $\phi(\nu)$: $R^1 \to R^1$ is said to belong to the $(0, \infty)$ sector if $\phi(0) = 0$ and $\nu\phi(\nu) > 0$ for $\nu \neq 0$. ϕ is said to belong to the $[0, \infty)$ sector if $\phi(0) = 0$ and $\nu\phi(\nu) \geq 0$ for $\nu \neq 0$. [Fig. 2] Many nonlinearities encountered in practice, such as saturation, relay, dead-zones, belong to the $[0, \infty)$ sector. As in the previous section, we assume that the problem is well-posed, and that a unique solution exists, and we consider the case with one 3-axis actuator for simplicity.

Theorem 3. Consider the closed-loop system given by Eqs. (2), (10), (11), (16)-(18), and (46), where G_p and G_r are positive definite and diagonal, and each ψ_i is in the $(0, \infty)$ sector and is strictly monotonic increasing for $i = 1, 2, \ . \ . \ . \ . \ , m$. Then the closed-loop system is globally asymptotically stable.

Proof. Define

$$V(x, \dot{x}) = x^T Cx + \dot{x}^T A\dot{x} + 2 \sum_{i=1}^{3} G_{pi}^{-1} \int_o^{u_{cpi}} \psi_i(\nu) d\nu \tag{48}$$

where G_{pi} and u_{cpi} denote the iith and ith elements of G_p and u_{cp}, respectively. This form is the well-known "Lure'-type" Lyapunov function [6]. From Eqs. (4) and (6), $x^T Cx + \dot{x}^T A\dot{x} = 0$ only when $\dot{\alpha} = 0$, $q = \dot{q} = 0$. That is, this quantity can be zero when $\alpha \neq 0$. However, when $q = 0$, $u_{cpi} = G_{pi}\alpha$, which is nonzero when $\alpha \neq 0$. Thus the third term on the right hand side of (48) is positive (since ψ_i is in the $(0, \infty)$ sector) for $\alpha \neq 0$. Therefore, V is positive definite. From (48), using (2), (46), (16)-(18),

$$\dot{V} = -2\dot{x}^T B\dot{x} - 2 \sum_{i=1}^{3} u_{cri} G_{ri}^{-1} \ \psi_i(u_{cpi} \cdot u_{cri}) - G_{pi}^{-1} \psi_i(u_{cpi}) \dot{u}_{cpi} \tag{49}$$

Since $\dot{u}_{cpi} = G_{pi} G_{ri}^{-1} u_{cri}$, we have from (49):

$$\dot{V} = -2\dot{x}^T B\dot{x} - 2 \sum_{i=1}^{3} u_{cri} G_{ri}^{-1} \ [\psi_i(u_{cpi} + u_{cri}) - \psi_i(u_{cpi})] \tag{50}$$

Since ψ_i is strictly monotonic increasing,

$$\dot{V} \leq -2\dot{q}^T D\dot{q} \tag{51}$$

$\dot{V} = 0$ only when $\dot{q} = 0$ and $u_{cri} = 0$, which implies $\dot{\alpha} = 0$. Considering the closed-loop equation,

$$\begin{bmatrix} 0 \\ \Lambda q \end{bmatrix} = \begin{bmatrix} I \\ \Phi T \end{bmatrix} \ \psi(u_{cp}) \tag{52}$$

which yields $\psi_i\ (u_{cpi}) = 0$ and $\dot{q} = 0$. Since $\psi_i(v) = 0$ only at $v = 0$, this implies that $\alpha = 0$. Thus $\dot{V} \equiv 0$ only at the origin, and the system is globally asymptotically stable.

Thus the collocated controller is guaranteed to be globally asymptotically stable in the presence of monotonic increasing nonlinearities. This r ... of the nonlinearities is also called "incremental passivity." As se n t previous section, if the nonlinearities are replaced by dynamic operat s, mere incremental passivity is not sufficient for stability.

ROBUSTNESS OF VELOCITY FEEDBACK CONTROLLERS

Stability with Dynamic Operator in the Loop

Consider the case where a nonlinear dynamic operator $\mathcal{H}(z_o;\ v)$ is present in the loop. Suppose $\mathcal{H}$ is represented by the following state-space model:

$$\dot{z} = f(z,\ v,\ t),\ z(0) = z_o \tag{53}$$

$$w(t) = p(z,\ t) \tag{54}$$

where v and w are 3m x 1 vectors which are the input and the output of $\mathcal{H}$. Define the operator

$$\partial \mathcal{H}\ (z_o;\ g) = \mathcal{H}(z_o;\ g) - \mathcal{H}(z_o;\ 0) \tag{55}$$

We define $\mathcal{H}$ to be internally stable if $\| \mathcal{H}\ (z_o;\ 0) \|$ is finite for any finite z_o.

Theorem 4. Consider the system given by Eqs. (1), (19), (20) (21), where the operator $\mathcal{H}$ has the state-space representation given by (53), (54). Suppose $G_r^{-1}\partial\mathcal{H}$ is passive and $\mathcal{H}$ is uniformly observable, finite-gain, internally stable, continous operator. Then the closed-loop system is globally asymptotically stable.

Proof. Defining

$$V(t) = q^T \Lambda q + \dot{q}^T \dot{q} \tag{56}$$

$V(t) \geq 0$ for all $t \geq 0$. Differentiating V(t) with respect to t and using Eqs. (19), (20), (21) and (1),

$$\dot{V} = -2\dot{q}^T D\dot{q} - 2u_{cr}^T G_r^{-1}\ \mathcal{H}(z_o;\ u_{cr}) \tag{57}$$

Integrating from 0 to T , since $V \geq 0$,

$$0 \leq V(T) = V(0) - 2\langle \dot{q}, D\dot{q} \rangle_T - 2\langle u_{cr}, G_r^{-1} \mathcal{H}(z_o; u_{cr}) \rangle_T \tag{58}$$

which yields (after manipulation)

$$2 \lambda_m(D) \|\dot{q}\|_T^2 \leq V(0) - \beta + 2\|\dot{q}\|_T \|\tilde{\Phi}\|_s \| \mathcal{H}(z_o; 0) \| \tag{59}$$

where β is a constant (see Eq. 28).

By using a procedure similar to that in the proof of Theorem 1, it can be proved that $\|\dot{q}\|$ is bounded, and that the system is globally asymptotically stable.

The following corollary is an immediate consequence of Theorem 3.

Corollary 4.1. If $\mathcal{H}$ is a strictly stable, completely observable, LTI operator with rational, mimimum-phase transfer matrix $H(s)$, the closed-loop system of Eqs. (1), (19), (20), (21) is asymptotically stable provided that

$$H(j\omega)G_r + G_r H^*(j\omega) \geq 0 \text{ for all real } \omega \tag{60}$$

Note that the above condition is equivalent to passivity of $G_r^{-1}\mathcal{H}$.

Corollary 4.2. Under the assumptions as in Corollary 1.1, if G_r and are diagonal, the closed-loop system of Eqs. (1), (19), (20), (21) is asymptotically stable if

$$\text{Re}[H_i(j\omega)] \geq 0 \text{ for all real } \omega$$

As a result of Corollary 4.2, CDVFB controllers can tolerate stable first-order dynamics in the loop. If $H_i(s) = e^{-j\phi_i}$, we have $\text{Re}[H_i(j\omega)] \geq 0$ for $-90° \leq \phi_i \leq 90°$; therefore, CDVFL controllers have 90° phase margin.

Stability in the Presence of Nonlinearities

Suppose the operator $\mathcal{H}$ in (1) is replaced by an m-vector nonlinear function ψ as in Eq. (47), except that ψ is allowed to be time-varying. The following theorem gives sufficient conditions for global asymptotic stability.

Theorem 5. Consider the closed-loop system given by Eqs. (1), (19), (20), (21), where G_r is diagonal and positive definite, and each ψ_i belongs to the $[0, \infty)$ sector. Then the closed-loop system is globally asymptotically stable.

Proof. Starting with V as in Eq. (56),

$$\dot{V} = -2\dot{q}^T D\dot{q} - 2\sum_{i=1}^{3m} G_{ri}^{-1} u_{cri} \psi_i(u_{cri}, t) \tag{62}$$

Thus $\dot{V} < 0$, and $\dot{V} \equiv 0$ only if $\dot{q} \equiv 0$, which can happen (from the equations of motion) only when $q \equiv 0$. Therefore, the system is globally asymptotically stable.

The next theorem considers a special case when nonlinearities and first-order dynamics are simultaneously present in the loop, as shown in Fig. 3.

Theorem 6. Consider the closed-loop system given by Eqs. (1), (19), (20), (21), where $G_r > 0$ is diagonal. Suppose $\mathcal{H} = \text{diag}(\mathcal{H}_1, \mathcal{H}_2, \ldots, \mathcal{H}_m)$, where

$$\mathcal{H}_i g = \psi_i(\mathcal{G}_i g) \tag{63}$$

where each ψ_i: $R^1 \to R^1$ is a time-invariant, differentiable function belonging to the $[0, \infty)$ sector, and there exists a constant $K < \infty$ such that $|\psi_i'| < K$ over the interval $(-\infty, \infty)$. Suppose $\mathcal{G}_i$ is an LTI operator whose transfer function is: $G_i(s) = a_i(1 + p_i s)^{-1}$, $a_i > 0$, $p_i > 0$ for $i = 1, 2, \ldots, m$. Then the system is globally asymptotically stable.

Proof. Starting with V as in Eq. (56) and proceeding as in the proof of Theorem 4, we have

$$0 \le V(0) - 2\langle \dot{q}, D\dot{q}\rangle_T - 2\sum_{i=1}^{3m} G_{ri}^{-1} \langle u_{cri}, \psi_i\{\mathcal{G}_i(0; u_{cri}) + g_{oi}\}\rangle_T \tag{64}$$

where g_{oi} is the unforced response of $\mathcal{G}_i$ due to nonzero initial state. Using mean value theorem, Eq. (64) can be written as:

$$0 \le V(0) - 2\langle \dot{q}, D\dot{q}\rangle_T - 2\sum_{i=1}^{3m} \langle u_{cri}, \psi_i\{\mathcal{G}_i(0; u_{cri})\}\rangle_T$$

$$+ \langle u_{cri}, \psi_i'(\hat{u}) g_{oi}\rangle_T \tag{65}$$

where $\hat{u}$ lies in the interval bounded by $\mathcal{G}_i(0; u_{cri})$ and $\mathcal{G}_i(0; u_{cri}) + g_{oi}$. Noting that the operator $\psi_i\{\mathcal{G}_i(0; u_{cri})\}$ is passive [4], and simplifying, we have

$$\lambda_m(D)\|\dot{q}\|_T^2 \le V(0)/2 + \|\bar{\Phi}\|_s K \|\dot{q}\|_T \|g_o\| \tag{65}$$

where

$$\|g_o\| = \sum_{i=1}^{3m} \|g_{ci}\| < \infty \tag{66}$$

The remainder of the proof is similar to that of Theorem 4.

CONCLUDING REMARKS

Robustness properties were investigated for two types of controllers for large space structures, which use collocated sensors and actuators. The first type is the collocated attitude (CA) controller, which controls the rigid-body attitude and the elastic motion using negative definite feedback of measured-attitude and rate. The second type of controller is the collocated direct velocity feedback (CDVFB) controller for damping enhancement. Such controllers are known to provide closed-loop asymptotic stability regardless of the number of modes and parameter values, provided that the actuators and sensors are perfect. This robust stability property was extended further in this paper by proving that the global asymptotic stability is preserved even when sensors/actuators are not perfect. The CA controller preserves global asymptotic stablity when the sensors/actuators are represented by (i) linear, time-invariant dynamics which satisfy certain simple phase conditions, or (ii) time-invariant, monotonic increasing nonlinearities belonging to the $(0, \infty)$ sector. The CDVFB controller preserves global asymptotic stability under much weaker conditions. In particular, CDVFB controllers have 90° phase margin and are tolerant to time-varying nonlinearities in the $[0, \infty)$ sector. These global asymptotic stability results are valid regardless of the number of modes in the model and regardless of parameter values. Therefore, it can be concluded that these controllers offer viable methods for robust attitude control or damping enhancement, especially when the parameters are not accurately known. An important application of the collocated attitude controller would be during deployment or assembly of a large space structure, when the dynamic characteristics are changing, and during initial operating phase, when the dynamic characteristics are not known accurately. A robust collocated controller can provide stable interim control which can perhaps be replaced later by a high-performance controller designed using parameters estimated on orbit.

REFERENCES

1. Joshi, S. M.: A Controller Design Approach for Large Flexible Space Structures. NASA CR-165717, May 1981.

2. Elliott, L. E., Mingori, D. L., and Iwens, R. P.: Performance of Robust Output Feedback Controller for Flexible Spacecraft. Proc. 2nd Symposium on Dynamics and Control of Large Flexible Spacecraft, Blacksburg, Va., June 1979, pp. 409-420.

3. Balas, M. J.: Direct Velocity Feedback Control of Large Space Structures. Journal of Guidance and Control, Vol. 2, May-June 1979, pp. 252-253.

4. Desoer, C. A., and Vidyasagar, M.: Feedback Systems: Input-Output Properties. Academic Press, N.Y., 1975.

5. Joshi, S. M.: Design of Stable Feedback Controllers for Large Space Structures. Proc. Third VPI&SU/AIAA Symposium on Dynamics and Control of Large Flexible Spacecraft, Blacksburg, Va., June 15-17, 1981.

6. Aizerman, M. A., and Gantmacher, F. R.: Absolute Stability of Regulator Systems. Holden-Day, Inc., San Francisco, 1964.

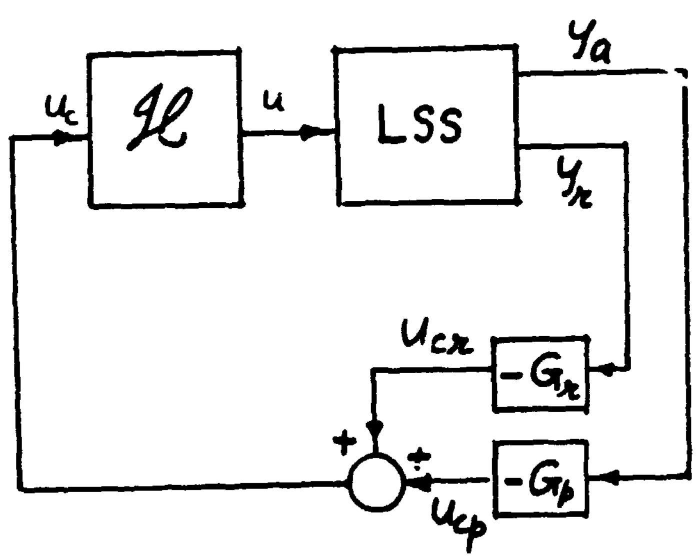

Figure 1. - Collocated Contoller

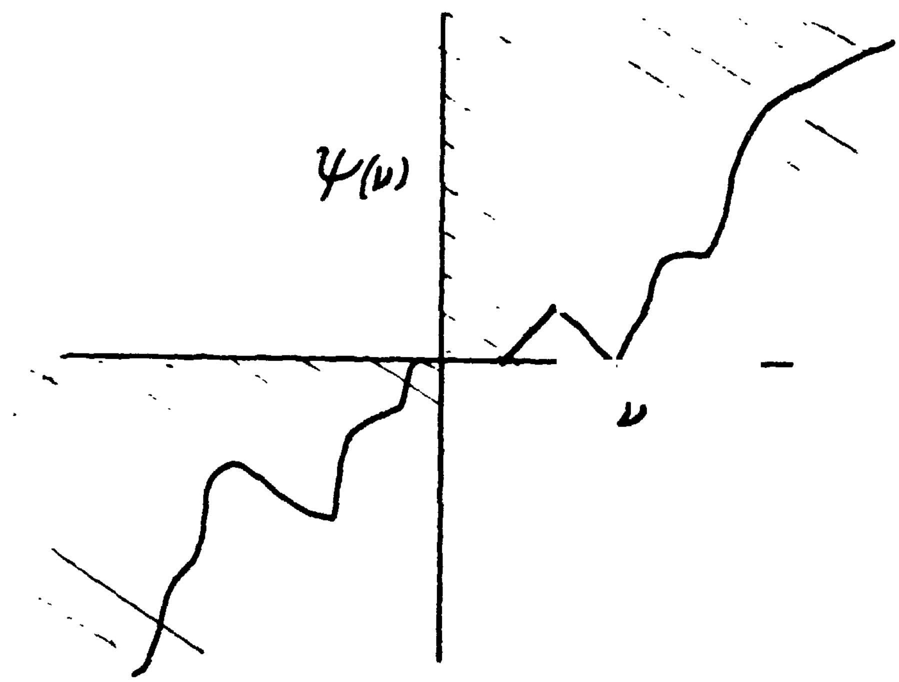

Figure 2.- Nonlinearity belonging to the $[0,\infty)$ sector

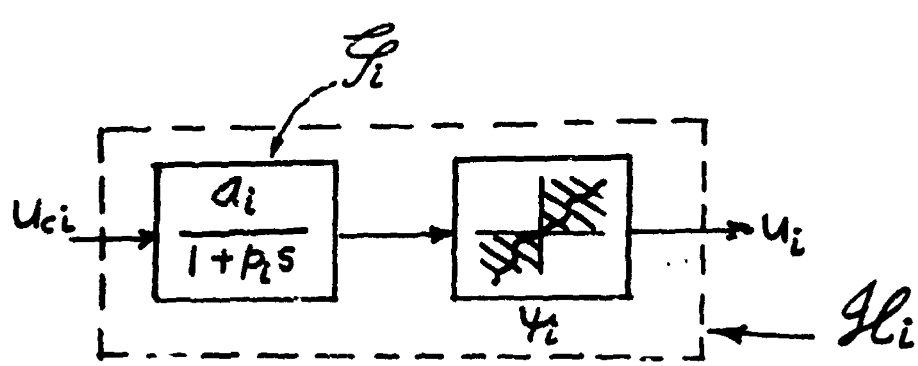

Figure 3.- Linear dynamics and nonlinearities simultaneously in the loops

N85-31202

ADAPTIVE CONTROL—ACTUAL STATUS AND TRENDS

I. D. Landau
Research Director at C.N.R.S.
GRECO "Systemes Adaptatifs"
and
Laboratoire d'Automatique de Grenoble
ENSIEG
B. P. 46, 38402 – Saint Martin d'Heres, France

ABSTRACT

Important progress in research and application of Adaptive Control Systems has been achieved in the last ten years. The techniques which are currently used in applications will be reviewed. Theoretical aspects currently under investigation and which are related to the application of adaptive control techniques in various fields will be briefly discussed. Applications in various areas will be briefly reviewed. The use of adaptive techniques for vibrations monitoring and active vibration control will be emphasized.

I. INTRODUCTION

The use of adaptive control techniques is motivated by the need of automatically adjusting the parameters of the controller when plant parameters and disturbances are unknown or change with time, in order to achieve (or to maintain) a certain index of performance for the controlled system. While this problem can be reformulated as a nonlinear stochastic control problem (the unknown parameters are considered as auxiliary states) the resulting solutions are extremely complicated. Therefore, in order to obtain something useful, it is necessary to make approximations. Adaptive control techniques can be viewed as approximations for nonlinear stochastic control problems. Model Reference Adaptive Controllers (MRAC) and Self-Tuning Regulators (STR) can be considered as two approximations among other possible approximations. These two approaches to adaptive control problems have been extensively studied and they are well understood. These approaches have been proven to be usable in practice and an important number of successful applications have been reported. However, some important theoretical problems still need further investigation and more experience utilizing these techniques in practice should be gained.

As mentioned earlier the MRAC and STR approaches can be considered as possible approximations for the solutions of some nonlinear stochastic control problems. However, when making approximations, some hypothesis should be considered which can justify these approximations. The basic hypothesis for MRAC and STR is of an algebraic nature: for any possible values of the plant (and disturbance) parameters, there exists a linear controller with a fixed complexity such that the plant plus the controller has the pre-specified characteristics. The adaptive control loop will only search for the values of the tuned parameters of a controller whose structure has been fixed using a standard control design technique.

The MRAC and STR techniques have been initially developed independently. Subsequently, connections between these two techniques have been investigated and emphasized. See Egardt (1980), Landau (1981), Landau (1982), Aström (1983). For certain classes of problems these two approaches are equivalent. It is important to note that the development of these two adaptive control techniques is largely based on the deep understanding of certain types of linear algebraic control design techniques and of an appropriate interpretation of the controller design strategy.

A brief review of the underlying concepts and configurations used for MRAC and STR is given in Section II. The linear tracking and regulation problem is reviewed in Section III and this allows the definition of the structure of the controller. The structures of various adaptive control schemes are presented in Section IV. The parameter adaptation algorithms are discussed in Section V. Applications are listed in Section VI. Current research trends are indicated in Section VII.

II. MODEL REFERENCE ADAPTIVE CONTROLLERS AND SELF-TUNING REGULATORS - BASIC PRINCIPLES.

Figure 2.1 illustrates the basic philosophy for designing a linear controller. The desired performance is specified in terms of the characteristics of a dynamic system which is a "realization" of the desired input-output behavior of the closed loop control system. The controller is designed such that the closed loop control system is characterized by the same parameters as those of the "desired" dynamic system.

Since desired performance corresponds in fact to the output of the "desired" dynamic system which is pre-specified, the design problem can be recast as in Fig. 2.2. The objective is now to design a controller such that the error between the output of the plant and the output of the reference model (the dynamic system which has the desired characteristics) is identically null for identical initial conditions and such that an eventual initial error will vanish with a certain dynamics.

These two interpretations of the linear control design in the case of a plant with unknown or varying parameters lead to two adaptive control schemes, shown in Figs. 2.3 and 2.4. Figure 2.3 is an extension of the scheme given in Fig. 2.2 and is called (explicit) MRAC. The difference between the output of the plant and the output of the reference model is a measure of the difference between the real performance and the desired one. This information is used through an "adaptation mechanism" (parameter adaptation algorithm) to directly adjust the parameters of the controller. This is a "direct" adaptive control scheme.

Figure 2.3 is an extension of the scheme considered in Fig. 2.1 in the sense that a suitable controller can be designed if a plant model is estimated on-line based on the current input-output data available. This scheme is called STR and it is inspired by the separation theorem

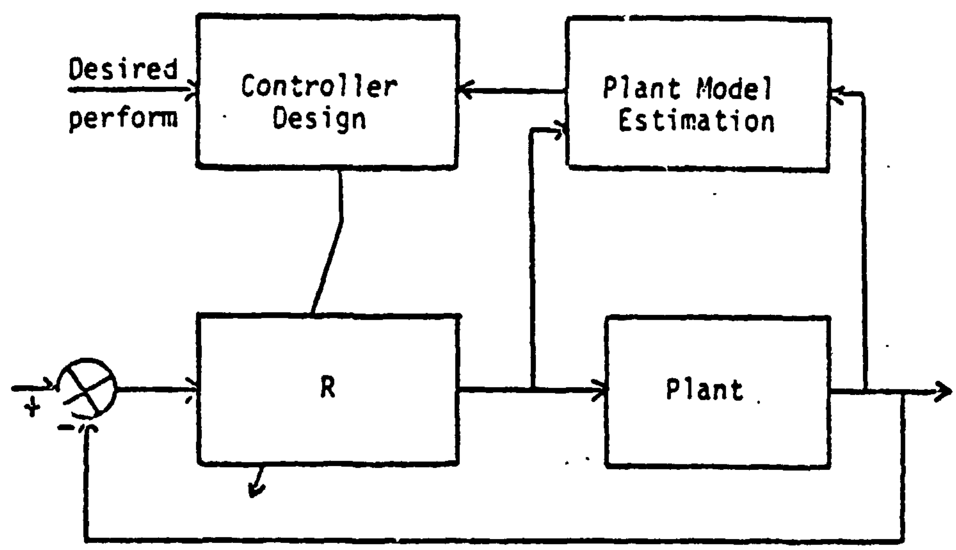

Figure 2.3

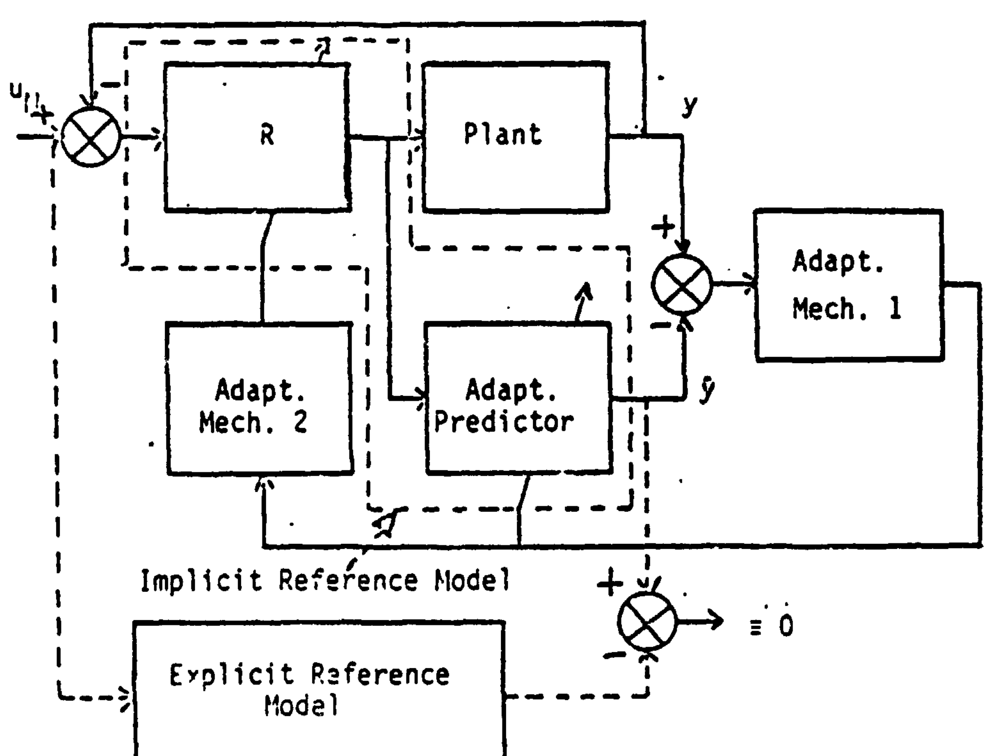

Figure 2.4

PRECEDING PAGE BLANK NOT FILMED

101 - 102

A. Minimum Phase Plants

Consider the S.I.S.O. discrete linear time invariant plant described by:

a) deterministic environment:

$$A(q^{-1})y(k+D) = B(q^{-1})u(k), \; d > 0, \; y(0) \neq 0 \tag{3.1}$$

b) stochastic environment:

$$A(q^{-1})y(k+d) = B(q^{-1})u(k) + C(q^{-1})\omega(k+d) \tag{3.2}$$

where:

$$A(q^{-1}) = 1 + a_1q^{-1} + \ldots + a_nq^{-n}$$

$$B(q^{-1}) = b_o+b_1q^{-1} + \ldots + b_mq^{-m} \qquad b_o \neq 0 \tag{3.3}$$

$$C(q^{-1})- = 1 + c_1q^{-1} + \ldots + c_nq^{-n}$$

$$C_R(q^{-1}) \; y(k+1) = 0 \tag{3.4}$$

where:

$$C_R(q^{-1}) = 1 + c_1^Rq^{-1} + \ldots + c_n^Rq^{-n} \tag{3.5}$$

is an asymptotically stable polynomial.

In order to design the controller, we will consider two strategies, one using an explicit reference model as part of the control system and the other using a 1-step ahead predictor of the plant output which together with the controller will form an implicit reference model.

Strategy 1: Explicit Reference Model

One considers an explicit reference model given by:

$$C_T(q^{-1}) \; y^M(k+1) = D(q^{-1}) \; u^M(k) \tag{3.6}$$

where $y^M(k)$ is the output of the explicit reference model. The design objective is:

$$C_R(q^{-1}) \; \varepsilon(k+1) = 0 \qquad k \geq 0 \tag{3.7}$$

where

$$\varepsilon(k) = y(k) = y^M(k) \tag{3.8}$$

is the plant model error. It is obvious that Eq. (3.7) includes the regulation objective specified by Eq. (3.4) (for $u_M(k) \equiv 0$, $\varepsilon(k) = y(k)$). Equation (3.1) with d = 1 can be rewritten as:

$$C_R(q^{-1})\ y(k+1) = [C_R(q^{-1})-A(q^{-1})]yk+1) + B(q^{-1})u(k)$$

$$= R(q^{-1})y(k) + b_o u(k) + B^*(q^{-1})u(k) \tag{3.9}$$

where

$$R(q^{-1}) = C_R(q^{-1}) - A(q^{-1}) = \sum_{i=1}^{n} (c_i^R - a_i)q^{-i+1} = r_1 + r_2 q^{-1} \dots r_n q^{-n+1} \tag{3.10}$$

$$B^*(q^{-1}) = B(q^{-1}) - b_o \tag{3.11}$$

and Eq. (3.7) becomes:

$$C_R(q^{-1})\varepsilon(k+1) = R(q^{-1})y(k) + b_o u(k) + B^*(q^{-1})u(k) - C_R(q^{-1})y_M(k+1) = 0 \tag{3.12}$$

which yields the desired control

$$u(k) = \frac{C_R(q^{-1})y^M(k+1) - R(q^{-1})y(k) - B^*(q^{-1})\ k)}{b_o} \tag{3.13}$$

Introducing the notation:

$$\phi_0^T(k) = [u(k-1)\ \dots\ u(k-m),\ y(k)\ \dots\ y(k-n+1)] \tag{3.14}$$

$$\theta_0^T = [b_1\ \dots\ b_m\ ,\ r_1\ \dots\ r_n] \tag{3.15}$$

Equation (3.15) can be written:

$$u(k) = \frac{C_R(q^{-1})y^M(k+1) - \theta_0^T\phi_0(k)}{b_o} \tag{3.16}$$

or in an equivalent form:

$$C_R(q^{-1})y^M(k+1) = \theta^T\phi(k) \tag{3.17}$$

where:

$$\phi(k)^T = [u(k),\ \phi_0^T(k)] \tag{3.18}$$

$$\theta^T = [b_o,\ \theta_0^T] \tag{3.19}$$

The resulting control scheme is given in Fig. 3.1.

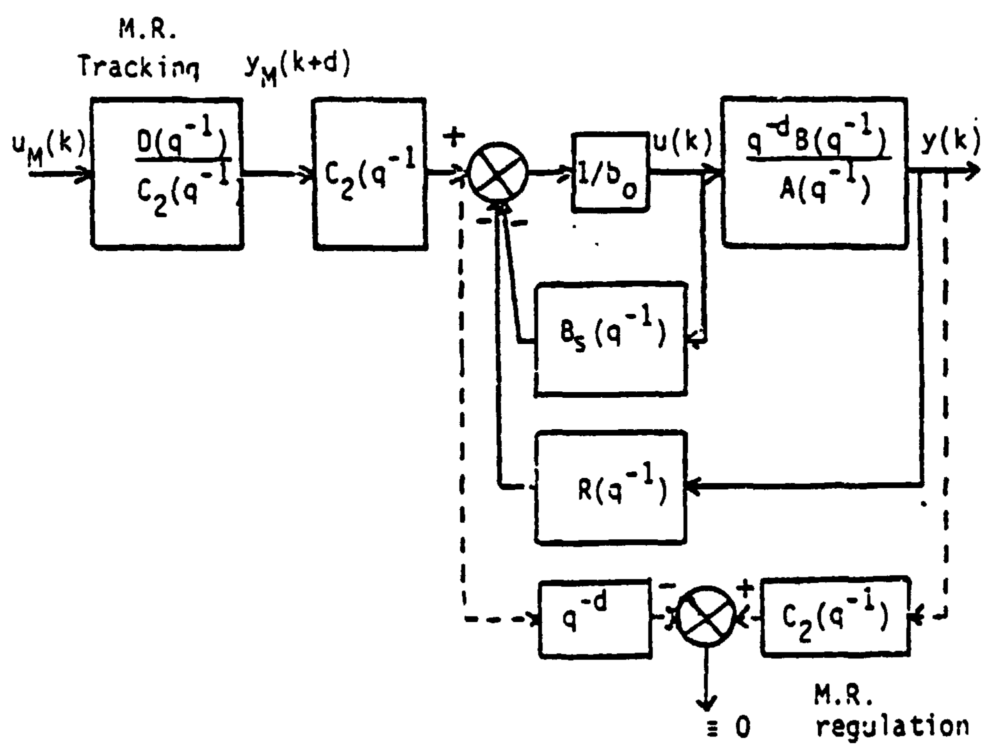

M.R.
Tracking
$y_M(k+d)$
$u_M(k)$
$\frac{D(q^{-1})}{C_2(q^{-1})}$
$C_2(q^{-1})$
+
-
-
$1/b_0$
$u(k)$
$\frac{q^{-d}B(q^{-1})}{A(q^{-1})}$
$y(k)$
$B_S(q^{-1})$
$R(q^{-1})$
q^{-d}
-
+
$C_2(q^{-1})$
$\equiv 0$
M.R.
regulation

Figure 3.1

Strategy 2: Implicit Reference Model.

This strategy is directly inspired by the separation theorem: one first designs an appropriate predictor for the plant output, and then a control will be computed such that the output of the predictor behaves as the desired output in tracking.

First step: (predictor design). The predictor will be designed such that the 1-step ahead prediction error $\hat{\varepsilon}(k+1)$ is defined by:

$$\hat{\varepsilon}(k+1) = y(k+1) - \hat{y}(k+1) \tag{3.20}$$

where $\hat{y}(k+1)$ is the predictor output and will vanish according to:

$$C_R(q^{-1})\ \hat{\varepsilon}(k+1) = 0\ ;\ k \geq 0 \tag{3.21}$$

Using Eq. (3.9), one obtains from Eq. (3.21) that the 1-step ahead predictor is characterized by:

$$C_R(q^{-1})\hat{y}(k+1) = b_o u(k) + R(q^{-1})y(k) + b^*(q^{-1})u(k) = \theta^T\ \phi(k) \tag{3.22}$$

where $R(q^{-1})$, $B^*(q^{-1})$, θ, $\phi(k)$ are given by Eqs. (3.10), (3.11), (3.18), and (3.19) respectively.

Second step: (computation of the control). The control is computed such that $\hat{y}(k+1) = y^M(k+1)$; where $y^M(k+1)$ is the desired output given by Eq. (3.6). One finally obtains:

$$C_R(q^{-1})\hat{y}(k+1) = C_R(q^{-1})y^M(k+1) = \theta^T\phi(k) \tag{3.23}$$

and the control is given by Eq. (3.17) as expected.

Because of the output of the predictor is equal to the output of the explicit reference model, the predictor plus the control will form an "implicit reference model."

B. Tracking and Regulation in Stochastic Environment

We will examine first the behavior of the controller designed in the previous section when the plant is subject to a stochastic disturbance of the type considered in Eq. (3.2). For $d = 1$ Eq. (3.2) becomes:

$$A(q^{-1})\ y(k+1) = B(q^{-1})\ u(k) + C(q^{-1})\ \omega(k+1) \tag{3.24}$$

Using the control given in Eq. (3.13) one obtains:

$$C_R(q^{-1})\ y(k+1) = C_R(q^{-1})\ y^M(k+1) + C(q^{-1})\ \omega(k+1) \tag{3.25}$$

Neglecting the effect of the deterministic disturbance (which vanishes with the dynamics defined by $C_R(q^{-1})$) one can re-write Eq. (3.25) as:

$$y(k+1) = y^M(k+1) + \frac{C(q^{-1})}{C_R(q^{-1})}\,\omega(k+1)$$

$$= \frac{D(q^{-1})}{C_T(q^{-1})}\,u^M(k) + \frac{C(q^{-1})}{C_R(q^{-1})}\,\omega(k+1) \tag{3.26}$$

Equation (3.26) shows the presence of two reference models: a deterministic one for tracking by $\frac{D(q^{-1})}{C_T(q^{-1})}$ whose input is the reference signal $u^M(k)$ and a stochastic one for regulation defined by $\frac{C(q^{-1})}{C_T(q^{-1})}$ whose input is the white noise sequence $\omega(k+1)$.

In general the objective of the design in a stochastic environment is to obtain a minimum variance tracking and regulation, i.e.:

$$E\,\{[y(k+1) - y_M(k+1)]^2\} = \min \tag{3.27}$$

From Eq. (3.26) it results straightforwardly that the objective of Eq. (3.27) is achieved if one chooses:

$$C_R(q^{-1}) = C(q^{-1}) \tag{3.28}$$

which leads to:

$$E\,\{[y(k+1) - y_M(k+1)]^2\} = E\{\omega^2(k+1)\} = \sigma^2 \tag{3.29}$$

For the case $d > 1$, the control can no longer be computed directly using the strategies given above since this will lead to a non-causal controller (future values of the output and input are involved for the computation of the control at the instant k). This problem can be avoided by using a polynomial identify which allows us always to express the output $y(k+d)$ in terms only of $y(k)$; $y(k-1)$... and $u(k)$, $u(k-1)$ ...

Consider the following polynomial identity:

$$C_R(q^{-1}) = A(q^{-1})\,S(q^{-1}) + q^{-d}R(q^{-1}) \tag{3.30}$$

which has a unique solution for the polynomials $S(q^{-1})$ and $R(q^{-1})$ for $\deg S(q^{-1}) = d-1$ where

$$S(q^{-1}) = 1 + S_1 q^{-1} \ldots S_{d-1} q^{-d+1} \tag{3.31}$$

$$R(q^{-1}) = r_1 + r_2 q^{-1} \ldots r_n q^{-u+1} \tag{3.32}$$

Using the identity of Eq. (3.30) in Eq. (3.9) for d > 1 one obtains:

$$C_R(q^{-1})y(k+d) = R(q^{-1})y(k) + b_o u(k) + B_S(q^{-1})u(k) \tag{3.33}$$

where

$$B_S(q^{-1}) = B(q^{-1})S(q^{-1}) - b_o \tag{3.34}$$

Equation (3.7) for d > 1 becomes:

$$C_R(q^{-1})\varepsilon(k+d) = R(q^{-1})y(k) + b_o u(k) + B_S(q^{-1})\, u(k) - C_R(q^{-1})\, y_M(k+d) = 0 \tag{3.35}$$

which yields the desired control

$$u(k) = \frac{C_R(q^{-1})\, y^M(k+d) - R(q^{-1})y(k) - B_S(q^{-1})u(k)}{b_o} = \frac{C_R(q^{-1})\, y^M(k+d) - \theta_o^T \phi_o(k)}{b_o} \tag{3.36}$$

The control has the same structure as for the case d = 1 except that the polynomials $R(q^{-1})$ and $B\ (q^{-1})$ are different, as well as θ_o and $\phi_o(k)$:

> Note that the strategy presented above achieves a poles-zeros placement.

C. Non-minimum Phase Plants

In this case one can no longer assume that $B(z^{-1})$ is asymptotically stable and therefore the zeros of the plant transfer function can no longer be cancelled. The basic control strategy (algebraic approach) is the poles placement technique without zeros cancelling. The basic relation for the design of the controller is the Bezout identity:

$$A(q^{-1})\, S(q^{-1}) + q^{-d}\, B(q^{-1})\, R(q^{-1}) = C_R\, (q^{-1})$$

and the controller has the structure:

$$S(q^{-1})\ u(k) = \frac{1}{\beta}\ C_R(q^{-1})\ y_M(k+d) - R(q^{-1})\ y(k)$$

$$\beta = \begin{cases} 1 \text{ if } B(1) = 0 \\ B(1) \text{ elsewhere} \end{cases}$$

For a survey of the control strategies for non-minimum phase plants, see Landau, M'Saad, Ortega (1983).

IV. STRUCTURES OF ADAPTIVE CONTROL SYSTEMS

In adaptive control schemes the fixed controller designed for the case of known parameters is replaced by an adjustable controller having the same structure, i.e., the fixed parameter vector will be replaced by an adjustable parameter vector which for the case of the design considered for minimum phase plants is given by:

$$\hat{\theta}^T(k) = [\hat{b}_o(k),\ \hat{\theta}_0^T(k)] \tag{4.1}$$

and the corresponding control law will be given (either in deterministic or stochastic environment) by:

$$u(k) = \frac{C_R(q^{-1})y^M(k+1) - \hat{\theta}_0^T(k)\phi_o(k)}{\hat{b}_o(k)} \tag{4.2}$$

or:

$$\hat{\theta}^T(k)\ \phi(k) = C_R(q^{-1})\ y^M(k+1) \tag{4.3}$$

See Fig. 4.1a.

Note that in the case of schemes using an implicit (prediction) reference model (STR) the plant predictor will be replaced by an adaptive predictor governed by:

$$C_2(q^{-1})\ \hat{y}(k+1) = \hat{\theta}^T(k)\ \phi(k) \tag{4.4}$$

and the control will be computed according to the strategy in the linear case with known parameters which will lead to Eq. (4.3). See Fig. 4.1b.

V. PARAMETER ADAPTATION ALGORITHMS

Various approaches have been considered for the development of parameter adaptation algorithms (PAA). A fairly general structure for the PAA is given by:

$$\hat{\theta}(k+1) = \hat{\theta}(k) + F_k\ \phi(k)\ \nu(k+1) \tag{5.1}$$

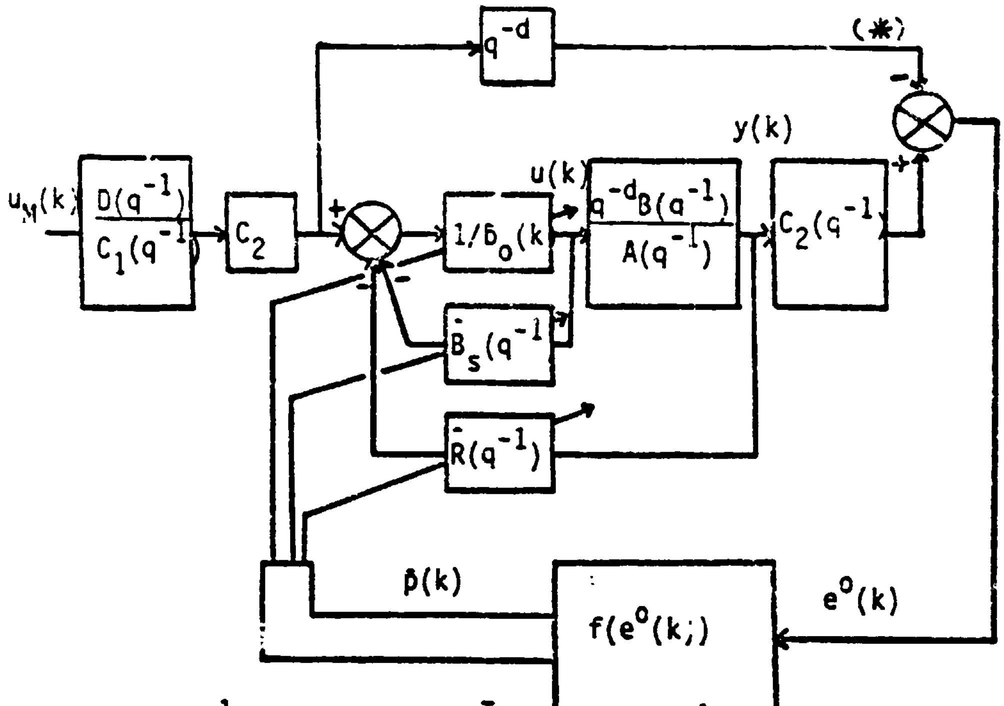

$$C_2(q^{-1})\ y_M(k+1) = \hat{p}(k)^T\ \phi(k) = C_2(q^{-1})\ \hat{y}(k+1)$$

Figure 4.1a

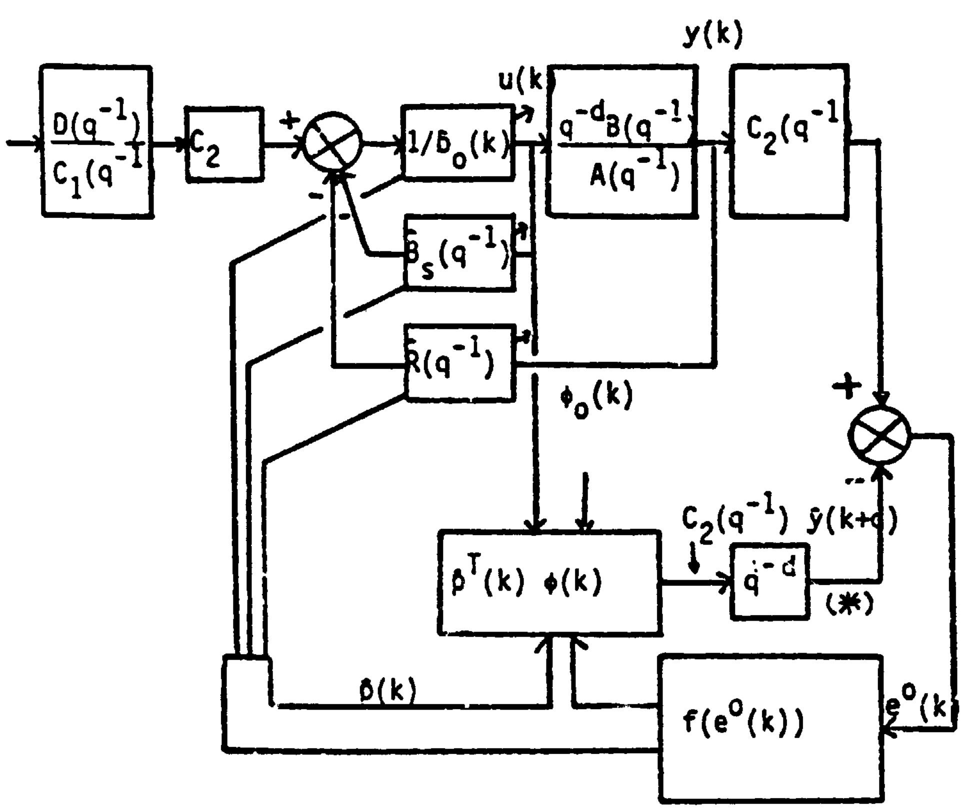

Figure 4.1b

$$\nu(k+1) = \frac{\nu^o_{k+1}}{1 + \phi(k)^T\ F_k\ \phi(k)} \tag{5.2}$$

$$F^{-1}_{k+1} = \lambda_1(k)\ F^{-1}_k + \lambda_2(k)\ \phi(k)\ \phi(k)^T \tag{5.3}$$

$$0 < \lambda_1(k) \leq 1\ ;\ 0 \leq \lambda_2(k) < 2\ ;\ F_0 > 0 \tag{5.4}$$

Using the matrix inversion lemma:

$$F_{k+1} = \frac{1}{\lambda_1(k)} [F_k - \frac{F_k\ \phi(k)\ \phi(k)^T\ F_k}{\frac{\lambda_1(k)}{\lambda_2(k)} + \phi(k)^T\ F_k\ \phi(k)}] \tag{5.5}$$

where $\hat{\theta}(k)$ is the adjustable parameter vector, $F(k)$ is the matrix adaptation gain, $\phi(k)$ is the measurement or the observation vector and $\nu^o(k+1)$ and $\nu(k+1)$ are the "a priori" and the "a posteriori" adaptation errors respect-tively. The "a priori" adaptation error is a measurable quantity which depends on $\hat{\theta}(i)$ up to the instant k, and the "a posteriori" adaptation error which enters in the adaptation algorithm is not directly measurable (it depends on $\hat{\theta}(k+1)$) but can be expressed in terms of the "a priori" adaptation error as indicated in eq. (5.2).

Different choices for $\lambda_1(k)$ and $\lambda_2(k)$ are possible leading to different types of variations of the adaptation gains. The performances of the adaptive control systems in various situations depend upon the choices of these two parameters. For details see Landau, Lozano (1981) and Landau (1983).

VI. APPLICATIONS

There are already a significant number of applications of adaptive control systems as well as a few commercial products. For references, see Aström (1983), Landau (1981), Landau, Tomizuka, Auslander (1983), Narendra, Monopoly (1980), Unbehauen (1980).

The adaptive control schemes can be used in three modes of operation:

1) Auto-tuning of a linear controller in the case of plants with unknown but constant parameters.

2) Building a gain schedule for unknown plants with dynamics depending on operating points.

3) Adapting in real-time the controller for plants with unknown and time-varying parameters.

An important remark to be made is that adaptive control algorithms cannot be used in p actice without a priori analysis of the control problem corresponding to each tentative application. This analysis should give answers to two categories of questions regarding (a) the need of adaptive control and (b) specific design requirements.

The main areas of applications are:

- Grinding
- Drying furnaces
- Cement mills
- Chemical reactors
- Distillation columns
- Diesel and explosion engines
- Heating and ventilation
- Paper machines
- Power systems
- Electrical drives
- Autopilots for ships
- Robotics
- Heat exchangers
- pH-control
- Active vibration control

An adaptive active vibrations control is described in Mote, Rahimi (1983). It uses first a recursive parameter estimation technique for estimating in real-time the parametric model of the composite vibration signal for circular plates (the vibrations frequencies). Then the parameters of the transfer from control heat to vibration frequency are estimated on-line and used for computing in real time the controller parameters.

VII. THEORY

The most complete theory is available today for the adaptive control of minimum phase plants achieving a poles-zeros placement. For this type of plant, tracking and regulation with independent objectives can be achieved both in deterministic and stochastic environments. Both MRAC and STR approaches lead in this case to "direct" adaptive control schemes.

The basic assumptions for the design of adaptive control systems for minimum-phase plants in deterministic and stochastic environments are summarized next.

- Exact knowledge of the plant delay (d).
- Knowledge of an upper bound for the degree of $A(q^{-1})$ which is the denominator of the plant transfer function.
- The zeros of the plant transfer function must lie within the unit circle.
- A lower bound of the magnitude of the leading coefficient of the plant transfer function should be known.
- The sign of the leading coefficient of the numerator plant transfer function is useful to be known (in order to avoid large adaptation transients).
- The stochastic disturbances are modeled by ARMA processes.
- Asymptotic type convergence is considered.

However, in practice some of these assumptions cannot be reasonably satisfied, in particular, the need for knowing an upper bound for the denominator degree (which in many cases simply does not exist) and the requirement that the disturbance is of ARMA type.

The use of reduced order models in adaptive control design is one of the main research topics today, and interesting results have been obtained leading to improved design techniques. See Ioannou (1983), Ortega, Landau (1983), Kosut (1983).

The case of disturbances which cannot be modeled by ARMA processes has also been considered. See, for example, Samson (1983), Peterson, Narendra (1982).

Another aspect is the extension of the adaptive control design for the multi inputs - multi outputs systems. Except for trivial cases, the extension raises important parameterization problems for MIMO plants. A survey of the various designs available can be found in Dion, Dugard (1983). More a priori knowledge on the plant structure than in the SISO case is required, and the research is directed towards the development of adaptive control schemes requiring less a priori structural information. The Hermite form of MIMO transfer matrix plays a key role in understanding the multivariable case.

The case of adaptive control of non-minimum phase plants is more complicated both from the point of view of the complexity of the adaptive control schemes and of the analysis. A survey of the adaptive control techniques for this type of plant is given in Landau, M'Saad, Ortega (1983). Most of the schemes are of "indirect" type, and the major question to be answered in order to show the convergence of the system is whether the estimated plant model converges towards the model with satisfactory properties (stabilizable). Global convergence results have been obtained, but with the requirement of using an additional persistent excitation signal, see Goodwin, Teoh, Innis (1982). The robustness of the adaptive control designs for non-minimum phase plants with respect to model reduction and ill-modeled disturbances has also been studied, see, for example, Praly (1983).

REFERENCES

Aström, K.J. (1983) Theory and applications of adaptive control, Automatica Vol. 19, No. 5.

Dion, J.M., Dugard, L., Pameterization for multivariable adaptive systems, Proc. IFAC Workshop "Adaptive Systems in Control and Signal Processing," Pergamon, Oxford.

Egardt, B. (1980) Unification of some discrete time adaptive control schemes, IEEE Trans. A.C., AC-25, 710.

Goodwin, G.C., Teoch, E.K., McInnis, B.C. (1982) Globally convergent adaptive controllers for linear systems having arbitrary zeros, Rep. University of Newcastle.

Ioannou, P. (1983) Robust redesign of adaptive control in the presence of disturbances in unmodeled dynamics, Proc. IFAC Workshop "Adaptive Systems in Control and Signal Processing," Pergamon, Oxford.

Kosut, R.L. (1983) Robustness issues in adaptive control. Ibid.

Landau, I.D. (1981) Model reference adaptive controllers and stochastic self-tuning regulators - A unified approach, Trans. ASME, Journ. D.S.M.C., Vol. 103, pp. 404-416.

Landau, I.D. (1982) Combining model reference adaptive controllers and stochastic self-tuning regulators, Automatica, Vol. 18, No. 1.

Landau, I.D., M'Saad, M., Ortega, R. (1983) Adaptive controllers for discrete time systems with arbitrary zeros, A survey. Proc. IFAC Workshop "Adaptive Systems in Control and Signal Processing," Pergamon, Oxford.

Landau, I.D., Lozano, R. (1981) Unification of discrete time explicit model reference adaptive control designs, Automatica, Vol. 17, No. 4, pp. 593-611.

Landau, I.D. (1983) Lecture notes on adaptive control.

Landau, I.D., Tomizuka, M., Auslander, D. (1983) Adaptive Systems in Control and Signal Processing, Pergamon, Oxford.

Mote, C.D., Rahimi, A. (1983) Real time vibration control of rotating circular blades by temperature control and system identification. Proc. IFAC Workshop "Adaptive Systems in Control and Signal Processing," Pergamon, Oxford.

Narendra, K.S., Monopoly, R. (1980) Applications of adaptive control, Academic Press, N.Y.

Ortega, R., Landau, I.D. (1983) Robustness of discrete adaptive controllers: Quantification and improvement, Proc. IEEE-CDC, San Antonio.

Peterson, B., Narendra, K.S. (1982) Bounded error adaptive control, IEEE Trans. A.C., AC-27.

Praly, L. (1983) Robustness of indirect adaptive control based on pole placement design, Proc. IFAC Workshop "Adaptive Systems in Control and Signal Processing," Pergamon, Oxford.

Samson, C. (1983) Stability analysis of adaptively controlled systems subject to bounded disturbances. Automatics, Vol. 19, No. 1, pp. 81-86.

Unbehauen, H. (1980) Methods and applications of adaptive control, Springer-Verlag, Berlin.

N85-31203

A NONLINEAR DUAL-ADAPTIVE CONTROL STRATEGY FOR IDENTIFICATION AND CONTROL OF FLEXIBLE STRUCTURES*

F. E. Thau
City College of The City University of New York
New York, NY 10031

ABSTRACT

A technique is presented for obtaining a control law to regulate the modal dynamics and identify the modal parameters of a flexible structure. The method is based on using a min-max performance index to derive a control law which may be considered to be a best compromise between optimum one-step control and identification inputs. Features of the approach are demonstrated by a computer simulation of the controlled modal response of a flexible beam.

I. INTRODUCTION

A class of indirect adaptive control systems proposed for the control of large space structures [1] is based on a modal decomposition of the system dynamics and may incorporate one or more on-line testing schemes [2] to determine when successful parameter identification has been achieve. The control strategy used in calculating the actuator inputs must achieve adequate regulation or tracking performance and, at the same time, provide inputs to allow adequate parameter identification. A control system designer is thus faced with the problem of devising a control strategy to ensure acceptable system performance even when on-line parameter identifiability tests have failed because the system

* This work was supported by NASA under Grant NAG-I-6.

PRECEDING PAGE BLANK NOT FILMED

configuration has changed or the environment in which the system operates has changed.

In this paper we formulate and examine the performance of a nonlinear dual-adaptive control scheme in which a sampled-data controller is designed to select a best compromise between an input signal that is optimum for mean-square system regulation and an input signal that is optimum for parameter identification. Dual control theory, originally formulated by Feldbaum [3,4], has been studied in [5-7] and in the references cited therein. A key concept introduced by Feldbaum is the dual control strategy based on a performance index that takes into account the fact that future observations on the process will be made. A controller may be able to "probe" the system for state and parameter estimation improvement, which then may improve future regulation and tracking performance. In many situations where the dual nature of stochastic control is not taken into account the controller becomes "cautious" [5,6] and tends to "turn-off". This undesirable phenomenon is avoided by the approach described below.

II. FORMULATION OF AN ADAPTIVE PERFORMANCE INDEX

The discrete-time dynamics for each mode is assumed to be described by the ARMA model

$$y(t)+a_1y(t-1)+a_2y(t-2) = b_1u(t-1)+b_2u(t-2)+e(t) \tag{1}$$

where $y(t)$ denotes modal displacement, $u(t)$ denotes modal force, and $e(t)$ is a sequence of independent, equally-distributed, normal $(0,\sigma^2)$ random variables. It is assumed that $e(t)$ is independent of $y(t-1),y(t-2),\ldots,$ $u(t-1),u(t-2),\ldots$ and that the parameters a_1,a_2,b_1,b_2 are unknown constants. If we let Y_t denote the information available to the controller at time t,

$$Y_t = \left\{y(t),y(t-1),\ldots,\ u(t-1),u(t-2),\ldots\right\} \tag{2}$$

$x(t)$ denote the modal parameter vector and $\theta(t)$ denote a modal measurement vector,

$$\begin{aligned} x^T(t) &= (a_1,a_2,b_1,b_2); \\ \theta^T(t) &= (-y(t-1),-y(t-2),u(t-1),u(t-2)) \end{aligned} \tag{3}$$

where $(\ .\ )^T$ denotes vector or matrix transpose, then (1) may be rewritten as

$$y(t) = \theta^T(t)x(t)+e(t) \tag{4}$$

where the constant parameter "dynamics" satisfies

$$x(t+1) = x(t) \tag{5}$$

It can than be shown, following the analysis of [8], that the conditional distribution of $x(t+2)$ given Y_{t+1} is normal with mean $x(t+2)$ and covariance matrix $P(t+2)$ where $x(t)$ and $P(t)$ satisfies the difference equations

$$\hat{x}(t+1) = \hat{x}(t)+K(t)(y(t)-\theta^T(t)x(t)) \tag{6}$$

$$K(t) = P(t)\theta(t)/(\sigma^2+\theta^T(t)P(t)\theta(t)) \tag{7}$$

$$P(t+1) = P(t)-(P(t)\theta(t)\theta^T(t)P(t))/(\sigma^2+\theta^T(t)P(t)\theta(t)) \tag{8}$$

Furthermore, the control law that minimizes the regulation criterion

$$V_C(u(t)) = E\left\{y^2(t+1)\mid Y_t\right\} \tag{9}$$

is given by

$$u(t) = -\frac{\sum x_i(t+1)x_3(t+1)+P_{3i}(t+1))\theta_i(t+1)}{x_3^2(t+1)+P_{33}(t+1)} \tag{10}$$

where $\sum$ denotes the sum over $i = 1$ to 4 with the value 3 excluded.

To provide bounded modal inputs that improve parameter identification accuracy while guaranteeing that the modal amplitude will not become excessively large, the controller is designed to optimize, at each sampling instant t, the following performance criterion:

$$\min_{u(t)} \max_{\lambda} [V(\lambda, u(t))] \tag{11}$$

subject to the constraints

$$u(t) \leq M, \ 0 \leq \lambda \leq 1 \tag{12}$$

where

$$V(\lambda, u(t)) = \lambda \frac{V_C(u(t))}{V_C^0} + (1-\lambda)\frac{V_I(u(t))}{V_I^0} \tag{13}$$

V_C° denotes an acceptable or desired level of regulation cost. $V_I(u(t))$ denotes and identification cost function of u(t),

$$V_I(u(t)) = \text{trace}\left[P(t+2)\right] \tag{14}$$

V_I° denotes and acceptable or desired level of identification cost. The maximization indicated in (11) yields a function V(u(t)) which, although not convex, is interpreted as specifying, for each admissible u(t), the most costly linear combination of relative regulation and relative identification cost. Minimization of V(u) thus yields the modal input that minimizes this most costly combination of relative identification and regulation performance.

III. SIMULATION RESULTS

Since $V_C(u(t))$ and trace P(t+2) are relatively simple functions of u(t) the numerical solution of the one-step optimization problem (11)-(13) at each sampling time is quite feasible. Results of simulation studies described below illustrate an interesting feature of this approach: since the parameters involved in the evaluation of $V_C(u(t))$ and $V_I(u(t))$ depend on system measurements, the optimum distribution of relative cost, $\lambda^*(u)$ depends on on-line measurement data and hence, at each sampling instant, the weighting between identification and regulation will change depending on the on-line system performance. This is in contrast to[9] in which a fixed weighting between absolute control and identification cost is used at each sample time.

In the simulation study we compare the performance of three control systems:

a) A constrained adaptive controller that minimizes (9) subject to the control magnitude constraint.
b) An optimum identification controller that minimizes (14) subject to the control magnitude constraint.
c) The one-step dual-adaptive controller based on (11)-(13).

In Figures 1-3 we present simulated modal response data for the first flexible mode of the Langley beam experiment described in [10] where we assume here that a single actuator is used. The accumulated on-line regulation cost, VT, shown in Figure 1 is defined as

$$VT(N) = \sum_{K=1}^{N} y^2(k) \tag{15}$$

and the on-line identification cost, PT, is defined as

$$PT(N) = \text{trace}\ [P(N)] \tag{16}$$

where P(N) is calculated on-line using (8). Note that for the first 10 to 15 sampling times the regulation cost of the dual-adaptive controller is close to that of the constrained minimum-variance controller and the identification cost of the dual-adaptive control system is close to that of the constrained one-step optimum identification controller. Figure 2 indicates that the dual-adaptive controller's actuator signals switch between its limits, ± 0.5, more frequently than do the actuator signals of the other controllers. This may be due to the lack of any energy constraint in the above problem formulation.

A future study will examine the performance of the energy-constrained dual-adaptive controller in comparison with energy-constrained minimum-variance and one-step optimum identification controllers. The relative regulation cost and relative identification cost defined in (13) are plotted in Figure 3 where

$$V_C^{\circ}\ (N) = \sigma^2 N \tag{17}$$

is the accumulated control cost that would be achieved if the parameters of the system where known precisely and if an unconstrained control law were used; $\sigma^2 = 10^{-4}$ was used in the simulation runs. A constant value $V_I^{\circ} = 10^{-4}$ was chosen as indicating the acceptable level of parameter identification. Figure 3 indicates that, depending on on-line measurements, the one-step identification and regulation cost at one sampling instant can have widely differing shapes from their respective distributions at other sampling times. This leads to the on-line variations in the dual-adaptive control strategy mentioned earlier.

The simulation results indication that the one-step, constrained dual-adaptive controller has the feature of providing, based on measured data, system inputs that result in parameter identification while maintaining bounded modal amplitude response.

REFERENCES

1. Montgomery, R. C. and Thau, F.E., "Adaptive and Learning Control of Large Space Structures," AIAA Guidance and Control Conference, June, 1980.

2. Sundararajan, N. and Montgomery, R. C., "Adaptive Control of a Flexible Beam Using Least Square Lattice Filters," 1983 Large Space Structures Workshop, Blacksburg, Va.

3. Feldbaum, A. A., "Dual Control Theory I - IV, Automation and Remote Control 1960, vol. 21, pp. 874, pp. 1033; 1962, vol. 22, pp. 1, pp. 109.

4. Feldbaum, A. A., Optimal Control Systems, Academic Press, New York, 1965.

5. Bar-Shalom, Y., "Stochastic Dynamic Programming: Caution and Probing, " IEEE Trans., Vol. AC - 26, No. 5, Oct. 1981, pp, 1184 - 1195.

6. Wittenmark, B., "Stochastic Adaptive Control Methods: A Survey,"Int. J. Control, Vol. 21, No. 5, pp. 705 - 730, 1975.

7. Bar-Shalom, Y. and Tse, E., "Dual Effect, Certainty Equivalence, and Separation in Stochastic Control, "IEEE Trans., Vol. AC - 19, pp. 494 - 500, Oct. 1974.

8. Astrom, K. J. and Wittenmark, B., "Problems of Identification and Control," J. Math. Anal and Appl, Vol. 34, pp. 90 - 113, 1971.

9. Wittenmark, B., "An Active Suboptimal Dual Controller for Systems with Stochastic Parameters," Auto. Contr. Theory Appl., Canada, Vol. e, pp. 13-19, 1975.

10. Thau, F. E., Montogomery, R. C., and Horner, G.C., "On-Line Structural Parameter Identification," Proc. AIAA Guidance and Control Conference, August, 1981, Albuquerque, New Mexico, pp. 530-539.

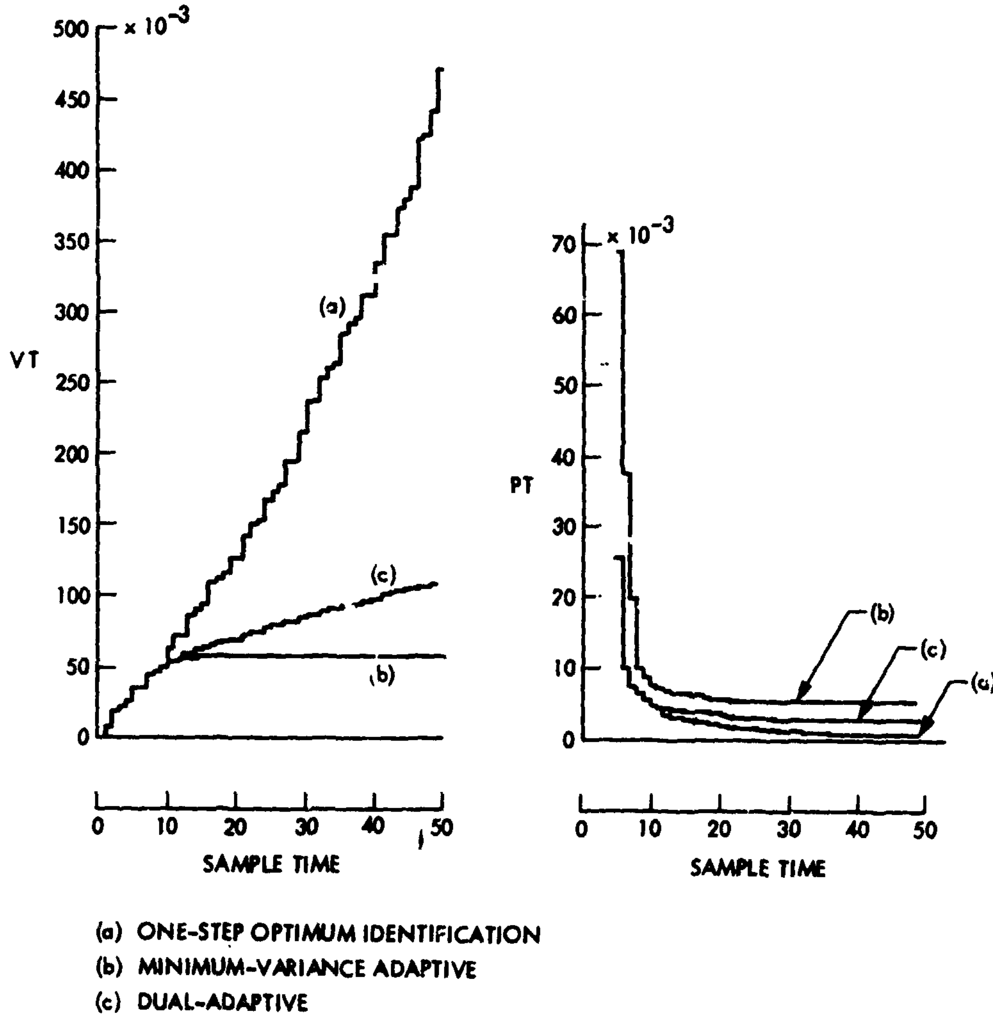

Fig. 1. On-Line Regulation and Identification Cost for Three Feedback Controllers

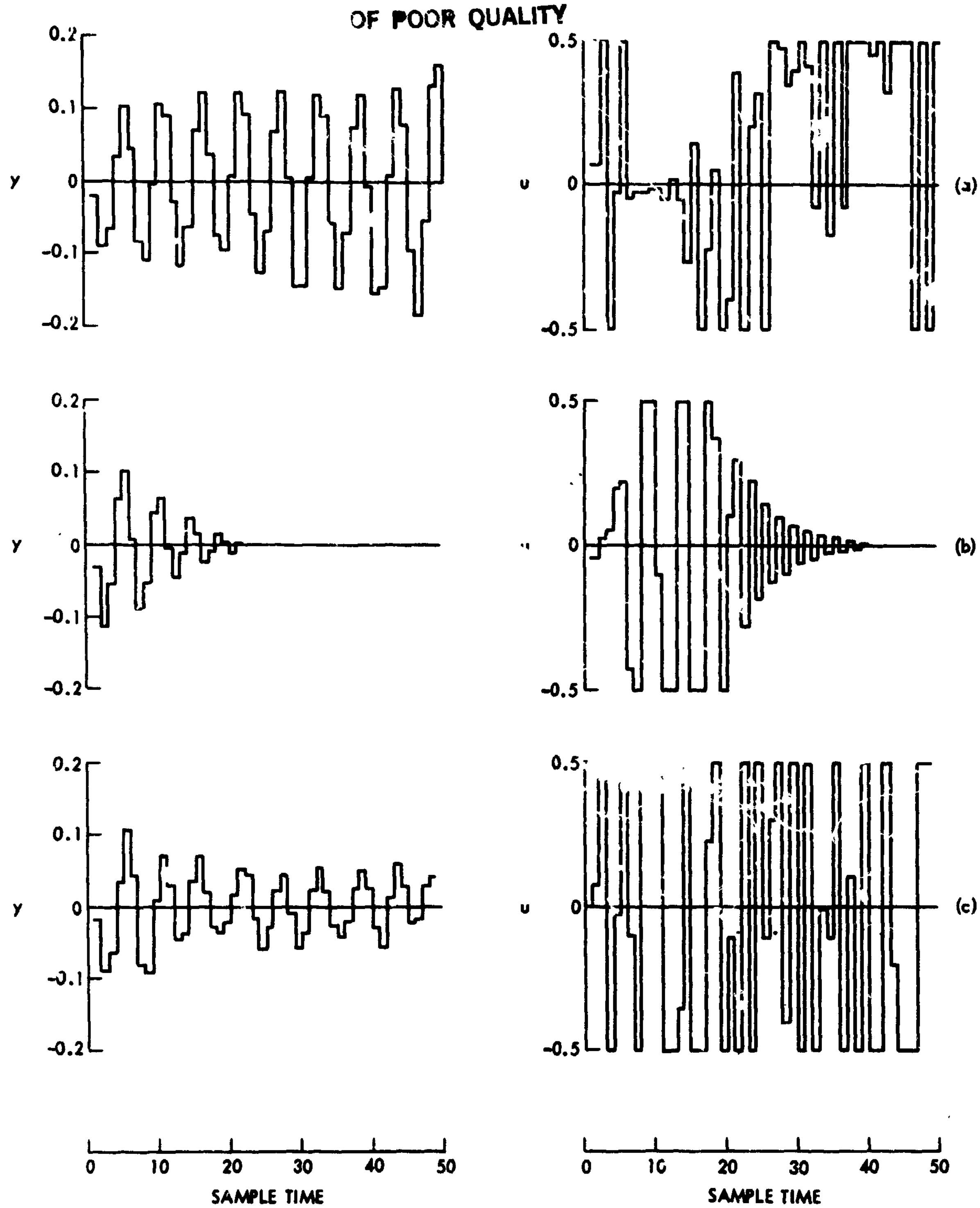

(a) ONE-STEP OPTIMUM IDENTIFICATION
(b) MINIMUM-VARIANCE ADAPTIVE
(c) DUAL-ADAPTIVE

Fig. 2. Modal Displacement and Modal Force for First Flexible Mode

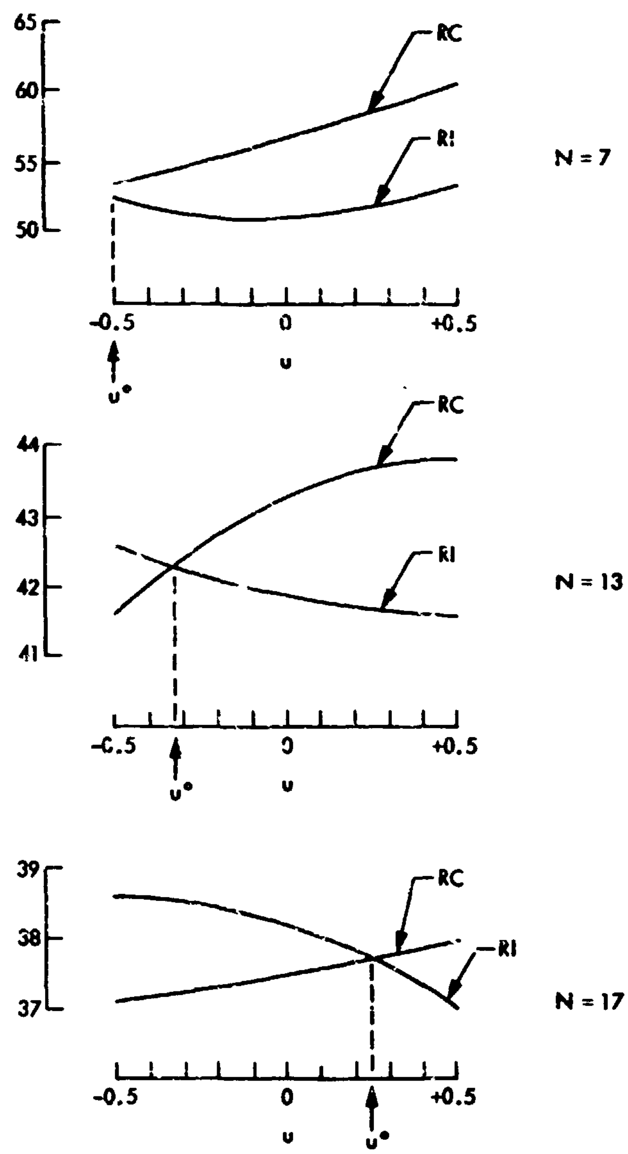

Fig 3. Relative Control Cost RC = $V_C(u)/V_C^\circ$ and Relative Identification Cost RI = $V_I(u)/V_I^\circ$ for 3 Sample Times

N85-31204

STABLE DIRECT ADAPTIVE CONTROL OF LINEAR INFINITE-DIMENSIONAL SYSTEMS USING A COMMAND GENERATOR TRACKER APPROACH

M. J. Balas, H. Kaufman, and J. Wen
Rensselaer Polytechnic Institute
Troy, NY 12180

ABSTRACT

We present a command generator tracker approach to model following control of linear distributed parameter systems (DPS) whose dynamics are described on infinite-dimensional Hilbert spaces. This method generates finite-dimensional controllers capable of exponentially stable tracking of the reference trajectories when certain ideal trajectories are known to exist for the open-loop DPS; we present conditions for the existence of these ideal trajectories. An adaptive version of this type of controller is also presented and shown to achieve (in some cases, asymptotically) stable finite-dimensional control of the infinite-dimensional DPS.

I. INTRODUCTION

By a distributed parameter system (DPS), we mean a system whose dynamical behavior with respect to external disturbances is described by partial differential equations. Of course, everything is a DPS if it is carefully scrutinized, especially if high performance is demanded, e.g., a simple electrical circuit at very high frequencies. However, lumped parameter (ordinary differential equation) approximations often suffice to describe the system behavior of many engineering systems. Indeed, such approximations are necessary for DPS controller designs to be implemented with on-line digital computers. Nevertheless, the distributed parameter nature of control problems should not be discarded prematurely; otherwise, control approaches can be generated which look good on paper but are not sufficiently robust to operate with the actual system. This has been illustrated in computer simulation and in even a few laboratory demonstrations of flexible structures, yet, it continues to be ignored in some parts of the control community. To understand the controller-structure interaction, a DPS viewpoint is essential.

The most serious difficulty of the DPS viewpoint is that it requires the mathematical ideas of infinite-dimensional function spaces and unbounded operators on these spaces; for example, see [1]-[2]. Several results in the past have been posed within this mathematical framework with the required mathematical rigor [3]. Yet, the necessary practical constraints were interpreted so that the results would be relevant to structural dynamicists and control system engineers and would make the maximum use of their experience and intuition.

With these ideas in mind, the concept of model following appears to be a procedure that yields a useful finite dimensional controller that might be designed taking into account the distributed nature of the system dynamics, whereas early model following control systems required the satisfaction of certain "Perfect Model Following" conditions which necessitated the use of a reference model having the same order as that of the process [4], the more recent output model following controller or Command Generator Tracker (CGT) as developed by Broussard [5] allows the use of a model of arbitrary order, provided that the number of controls is equal to the number of outputs being controlled. This concept in fact served as the basis for a finite dimensional adaptive controller that was used for controlling large structural systems [6, 7].

Thus since the CGT algorithm makes it possible to use a finite dimensional reference model which subsequently gives a finite dimensional controller regardless of the process order. This provides the basis for a direct adaptive controller which produces stable closed-loop operation with the class of linear distributed parameter systems considered here. The difficulties of stable adaptive distributed parameter control are detailed in, e.g., [8]-[9] and the references contained therein. In Sections 2 and 3 the nonadaptive model following controller is developed and analyzed; in Section 4, the adaptive version is presented and shown to produce a stable closed-loop. Conclusions and future directions are presented in Section 5.

2. PROBLEM FORMULATION

2.1 Process Description

The distributed parameter systems (DPS) of interest will be modeled by the following <u>state space form</u>:

$$\begin{cases} \dfrac{\partial v(t)}{\partial t} = Av(t) + Bf(t) \; ; \; v(o) = v_o & (2.1a) \\ y(t) = Cv(t) & (2.1b) \end{cases}$$

where the <u>state</u> $v(t)$ is in an infinite-dimensional real Hilbert space H with inner product $(\cdot,\cdot)$ and corresponding norm $||\cdot||$. The bounded input-output operators B and C have the <u>same finite rank</u> P, and $f(t)$, $y(t)$ represent the <u>inputs</u> for P linear actuators and the <u>outputs</u> from P linear sensors, respectively. Thus,

$$Bf(t) = \sum_{i=1}^{P} b_i \, f_i(t) \qquad (2.2)$$

and

$$y(t) = [y_1(t), \ldots, y_P(t)]^T \text{ with}$$

$$y_j(t) = (c_j, v(t)) \; ; \; 1 \le j \le P \qquad (2.3)$$

where b_i and c_j belong to H. In infinite-dimensional theory, the operator A is a closed, linear, unbounded (differential) operator with domain $D(A)$ dense in H. Furthermore, (2.1)-(2.3) represents some <u>well-posed</u> physical system, which in mathematical terms is the <u>weak formulation</u> of (2.1):

$$\begin{cases} v(t) = U(t)\, v_o + \int_0^t U(t-\tau)\, Bf(\tau)d\tau \\ y(t) = Cv(t) \;;\; t \geq 0 \end{cases} \tag{2.4}$$

where v_o is <u>any</u> initial state in H and U(t) is the C_o-semigroup of bounded operators generated on H by A. This latter means:

$$U(t+\tau) = U(t)\, U(\tau) \;;\; t \geq 0,\ \tau \geq 0 \tag{2.5a}$$

$$U(o) = I \tag{2.5b}$$

$$\lim_{t\to 0^+} [U(t) - I]\, v = 0 \;;\; v \text{ in } H \tag{2.5c}$$

$$Av = [\lim_{t\to 0^+} \frac{U(t)-I}{t}]v \;;\; v \text{ in } D(A) \tag{2.5d}$$

Note that the semigroup U(t) evolves the initial conditions v_o forward in time. When v_o is in D(A) and f(t) has continuous first derivative, v(t) also is differentiable, lies in D(A) for $t \geq 0$, and satisfies (^ 1). However, any v_o and H and any square-integrable f(t) will satisfy the weak formulation (2.4) and yield states v(t) in H for all $t \geq 0$. Consequently, (2.4) is easier to work with in infinite-dimensions and is more likely to represent the actual physical system being modeled by (2.1). This form, (2.1) or (2.4), models most practical <u>interior control problems</u> for linear DPS where the actuator and sensor influence functions are given by b_i and c_j, respectively.

For example, control of the damped wave equation on a region $\Omega \subseteq R^n$ by a single actuator and sensor is described by (for $\epsilon > 0$):

$$\begin{cases} \dfrac{\partial^2 u(x,t)}{\partial x^2} + \epsilon \dfrac{\partial u(x,t)}{\partial t} - A_o u(x,t) = b(x)\, f(t) & (2.6a) \\ y(t) = \int_\Omega c(x)\, u(x,t)\, dx & (2.6b) \end{cases}$$

where u(x,t) is the displacement from equilibrium of Ω and the influence functions b and c can be taken as approximations of Dirac delta functions at the location of the actuator and sensor. The operator A_o is the <u>Laplacian</u> given by

$$A_o u(x,t) = \sum_{\ell=1}^{n} \frac{\partial^2 u(x,t)}{\partial x_\ell^2} \tag{2.7}$$

on $D(A_o) \equiv \{u(x,t)\epsilon H_o | u(x,t)$ is smooth and $u(x,t) = 0$ on the boundary of $\Omega\}$. The domain $D(A_o)$ is dense in $H_o \equiv L^2(\Omega)$ with the usual inner product $(\cdot,\cdot)_o$. This can be put into the form (2.1) by choosing the state $v(t) = [u(x,t),$

$\frac{\partial u(x,t)}{\partial t}]^T$ in $H \equiv D(A_o^{1/2}) \times H_o$ with the <u>energy inner product</u>:

$$(v,\omega) = (A_o^{1/2}v_1, A_o^{1/2}\omega_1)_o + (v_2, \omega_2)_o \tag{2.8}$$

The operator A in (2.1) becomes

$$A = \begin{bmatrix} 0 & I \\ -A_o & -\varepsilon I \end{bmatrix} \tag{2.9}$$

and the rest follows.

Another important example is the mathematical setting for large structural systems (LSS) which may be described as a continuum by the following system of partial differential equations:

$$m(x)u_{tt}(x,t) + D_o u_t(x,t) + A_o u(x,t) = F(x,t) \tag{2.10}$$

where $u(x,t)$ represents a vector of instantaneous displacements of the structure Ω from its equilibrium position due to transient disturbances and the applied force distribution $F(x,t)$. The displacements can be translational and rotational, and the forces can be generalized to include torques, as well. The mass density $m(x)$ is positive and bounded on Ω.

The internal restoring force term $A_o u$ is generated by a time-invariant, symmetric, non-negative differential operator A_o appropriate to the LSS. The domain $D(A_o)$ of A_o contains all smooth functions satisfying the LSS boundary conditions and is dense in the infinite-dimensional Hilbert space $H_o = L^2(\Omega)$ with the usual inner product $(\cdot,\cdot)_o$ and associated norm $||\cdot||_o$. In most cases, the operator A_o is assumed to have discrete spectrum, i.e., isolated resonances; this can be expressed by the following eigen-problem:

$$A_o\phi_k = w_k^2 \phi_k \tag{2.11}$$

where w_k are the vibration mode frequencies and $\phi_k(x)$ are the corresponding vibration <u>mode shapes</u>. Of course, <u>exact expressions for this modal data are rarely known for an actual LSS</u>.

The damping term $D_o u_t$ is composed of a skew symmetric part, which represents <u>gyroscopic damping</u> due to any on-board rotors or constant spin rate of the whole LSS, and a small symmetric part which represents the internal <u>structural damping</u> and is thought to provide very low mode damping.

The applied force distribution is

$$F(x,t) = F_C(x,t) + F_D(x,t) \tag{2.12}$$

where F_D represents the external disturbance forces on the LSS (and possible nonlinearities) and F_c represents the control forces due to P actuators:

$$F_c = B_o f = \sum_{i=1}^{P} b_i(x)\ f_i(t) \tag{2.13}$$

where the actuator amplitudes are $f_i(t)$ and the actuator influence functions are $b_i(x)$ in H_o. These are usually localized or point devices so that they approximate $\delta(x-x_i)$; however, they do not have to be point devices.

Observations are obtained by P sensors

$$y = C_o u + E_o u_t \tag{2.14}$$

where $y_j(t) = (c_j,u_o) + (e_j,u_t)_o$, $1 \leq j \leq P$, with influence functions c_j for position sensors and e_j for velocity sensors in H_o. Again, these are usually localized or point devices but they do not have to be.

The LSS dynamics are defined by (2.10) and (2.14) can be put into the infinite-dimensional state space form:

$$\begin{cases} \dfrac{\partial v(t)}{\partial t} = Av(t) + Bf(t) + \Gamma f_D(t) & (2.15a) \\ y(t) = Cv(t)\ ;\ v(o) = v_o & (2.15b) \end{cases}$$

with (A,B,C) as in (2.1) and the persistent disturbance term $\Gamma f_D(t)$ obtained from F_D in (2.12). Impulsive disturbances in the structure are modeled by the initial condition v_o.

The Hille-Yosida Theorem (e.g. [1], Theo. 8, 9, p. 153), provides conditions under which an operator A generates a C_o-semigroup U(t) satisfying:

$$||U(t)|| \leq Ke^{-\sigma t},\ t \geq 0 \tag{2.16}$$

where $K \geq 1$ and σ real. The necessary and sufficient conditions are given for the resolvent operator $R(\lambda,A) \equiv (\lambda I-A)^{-1}$:

$$||R(\lambda,A)^n|| \leq \frac{K}{(\lambda+\sigma)^n}\ ;\ n = 1, 2, \ldots \tag{2.17}$$

for all real $\lambda > -\sigma$ in the resolvent set of A, $\rho(A) = \{\lambda \text{ complex } | R(\lambda,A) \text{ is a bounded operator on } H\}$. The spectrum of A, $\sigma(A) = \rho(A)^c$ is much more complicated in infinite-dimensions, but, in finite-dimensions, it consists only of the (finite number of) eigenvalues of A. We say that A is exponentially stable when $\sigma > 0$ in (2.16), i.e., the semigroup U(t) generated by A decays exponentially at the rate σ. There are many other types of stability in infinite-dimensions, but no others provide the safety of a stability margin σ; therefore, this seems to be the kind of stability of most practical interest for engineering applications where there is always some uncertainty in the model of DPS.

2.2 Model Following Control Problem Formulation

Given the DPS as defined in (2.1), it is desired to find a finite dimensional controller so that the output $y(t)$ "follows" a desirable output trajectory $y_m(t)$. This output trajectory is to be generated by the finite dimensional (asymptotically) stable reference model:

$$\dot{q} = A_m q + B_m u_m \tag{2.18a}$$

$$y_m = C_m q \; ; \; q(o) = q_o \tag{2.18b}$$

where

q is the model state vector having dimension N,

u_m is a step or reference level command with dimension P,

y_m is the output trajectory also having the dimension P,

and A_m, B_m are matrices with appropriate dimensions. It should be noted that the dimension of both y_m and u_m is the same as the dimension of the process input f and the process output y as defined in (2.1). Usually $q_o = 0$ will be chosen.

The output model following control problem to be solved is the development of an algorithm that defines the process input $f(t)$ so that the following two model following conditions (MFC) are satisfied:

MFC 1) If $y(t_1) = y_m(t_1)$, then

$y(t) \equiv y_m(t)$, for $t \geq t_1$

MFC 2) If $y(t_1) \neq y_m(t_1)$, then

$y(t)$ asymptotically will approach $y_m(t)$, i.e.

$\lim_{t \to \infty} [y(t) - y_m(t)] = 0$

3. DEVELOPMENT OF THE NONADAPTIVE MODEL FOLLOWING CONTROLLER

3.1 Solution Definition

In a manner similar to Broussard's development of the Command Generator Tracker (CGT) [5], the concept of an ideal state v^*, control f^* and output trajectory y^* will be introduced. It is required that these trajectories satisfy the process dynamics (2.1) and that the ideal output y^* be identical to the model output y_m. Thus:

$$\begin{cases} \dfrac{\partial v^*(t)}{\partial t} = Av^*(t) + Bf^*(t) & (3.1a) \\ y^*(t) = Cv^*(t) \ ; \ v^*(o) = v_o^* & (3.1b) \end{cases}$$

where the ideal state $v^*(t)$ is (as with $v(t)$) in the infinite dimensional Hilbert space H.

Furthermore

$$y^*(t) = y_m(t) = C_m q(t) \tag{3.2}$$

In a manner similar to that in [5], it will be assumed that $v^*(t)$ and $f^*(t)$ are linearly related to the model state vector $q(t)$ and command vector $u_m(t)$ as follows:

$$v^*(t) = A_{11}\ q(t) + S_{12}\ u_m \tag{3.3}$$

$$f^*(t) = S_{21}\ q(t) + S_{22}\ u_m \tag{3.4}$$

The bounded linear operators S_{11}, S_{12}, S_{21}, S_{22} will not be determined to satisfy MFC 1.

To this effect, differentiation of (3.3) with respect to t and substitution of (3.1) and (2.18) gives:

$$\frac{\partial v^*(t)}{\partial t} = S_{11}\ \dot{q} = S_{11}\ A_m q + S_{11}\ B_m u_m \tag{3.5a}$$
$$= Av^* + Bf^*$$

where

$$v_o^* = S_{11}\ q_o + S_{12}\ u_m \tag{3.5b}$$

is in D(A).

Replacing v^* and f^* on the right side of (3.5) by (3.3) and (3.4) gives:

$$S_{11}\ A_m q + S_{11}\ B_m u_m$$
$$A(S_{11}q + S_{12}\ u_m) + B(S_{21}q + S_{22}\ u_m) = \tag{3.6}$$

Now since (3.6) must be valid for all q and u_m, it is necessary that:

$$S_{11}\ A_m = AS_{11} + BS_{21} \tag{3.7}$$

$$S_{11}\ B_m = AS_{12} + BS_{22} \tag{3.8}$$

Finally the incorporation of (3.2) yields

$$y^*(t) = CS_{11}q + CS_{12}\,u_m = y_m = C_m q \tag{3.9}$$

Thus:

$$CS_{11} = C_m \tag{3.10}$$

$$CS_{12} = 0 \tag{3.11}$$

In summary then eqs. (3.7), (3.8), (3.10) and (3.11) must be solved in order to find S_{21} and S_{22} which in turn define the ideal control f^* of Eq. (3.4).

Recall however, that both MFC 1 and MFC 2 must both be satisfied. In order to satisfy MFC 2, it is useful to consider the equation for the error

$$e = v^* - v \tag{3.12}$$

which is in D(A) when v_o and v_o^* are both in D(A). Differentiation of (3.12) with respect to time gives:

$$\begin{aligned} \frac{\partial e}{\partial t} &= \frac{\partial v^*}{\partial t} \\ &= Av + Bf - (Av^* + Bf^*) \\ &= Ae + B(f - f^*) \end{aligned} \tag{3.13}$$

This equation suggests that the actual <u>model following control</u> f be defined as:

$$\begin{aligned} f &= f^* + G(y - y_m) \\ &= f^* + G\,C(v - v^*) \\ &= f^* + G\,C\,e \end{aligned} \tag{3.14}$$

Substitution of (3.14) into (3.13) gives:

$$\dot{e} = (A + B\,G\,C)e \tag{3.15}$$

where $G:R^P \to R^P$ is a bounded linear operator. Thus if G is chosen such that $(A + B\,G\,C)$ generates an exponentially stable C_o-semigroup, then the control f as defined by (3.14) will satisfy the conditions for model following.

It is important to note that this controller is clearly finite dimensional. For implementation it is only necessary to "build" a finite dimensional reference model and form the proper linear combination of its state vector and command vector. The gain operator G is also finite dimensional and should be chosen such that the decay of any transient caused by initial plant model output error is sufficiently fast. We summarize the above discussion as

Theorem 1: If (A,B,C) is exponentially output stabilizable and there exist bounded linear operators S_{11}, S_{12}, S_{21}, and S_{22} such that (3.7) - (3.8) and (3.10) - (3.11) are satisfied, then the model following control (3.4) and (3.14) satisfies the model following conditions MFC (1) and (2) and $\lim_{t\to\infty} [v(t)-v^*(t)] = 0$ when both v_o and v_o^* belong to D(A).

From [10], we see that (A,B,C) is exponentially output stabilizable if and only if $\tilde{H}_N \equiv N(C)^\perp$ and $\tilde{H}_R \equiv N(C)$ form a pair of stabilizing subspaces for (A,B). Note that dim $\tilde{H}_N$ = P which is the number of sensors (or actuators) used. The conditions for existence of the ideal trajectories (3.1) will be developed in the next subsection.

3.2 Existence of Ideal Trajectories

The existence of ideal trajectories $v^*(t)$ for the DPS (2.1) is determined by solutions S_{ij} to the operator equations (3.7) - (3.8) and (3.10) - (3.11). These can be rewritten as

$$\begin{bmatrix} A & B \\ C & 0 \end{bmatrix} \begin{bmatrix} S_{11} & S_{12} \\ S_{21} & S_{22} \end{bmatrix} = \begin{bmatrix} S_{11} & 0 \\ 0 & I \end{bmatrix} \begin{bmatrix} A_m & B_m \\ C_m & 0 \end{bmatrix} \tag{3.16}$$

where $S_{11}:R^N \to D(A)$ and $S_{12}:R^P \to D(A)$ are bounded operators with finite-rank and $S_{21}:P^N \to R^P$ and $S_{22}:R^P \to R^P$ are matrices of appropriate dimension. Note that (3.16) describes a kind of aggregation (in the sense of Aoki) for the infinite-dimensional system (2.1) into a finite-dimensional system (2.17). The existence of the ideal trajectories $v^*(t)$ in (3.1) guarantees that such an aggregation is possible, i.e. the DPS (2.1) generates the ideal trajectories which correspond to those of the finite-dimensional model (2.18).

In most situations, the ideal initial condition will be $v_o^* = 0$; hence, from (3.5b) we would choose $q_o = 0$ and $S_{12} = 0$, which correctly corresponds to (3.11). This reduces the other operator equations to the following:

$$\begin{cases} S_{11} A_m = A S_{11} + B S_{21} & (3.17a) \\ S_{11} B_m = B S_{22} & (3.17b) \\ C S_{11} = C_m & (3.17c) \end{cases}$$

we have the following:

Theorem 2: If the spectra $\sigma(A)$ and $\sigma(A_m)$ are separated by a smooth simple closed curve Γ containing $\sigma(A_m)$ in its interior and $\sigma(A)$ in its exterior, then, given any linear operator $S_{21}:R^N \to R^P$, there exists a unique bounded linear operator $S_{11}:R^N \to D(A)$ given by

$$S_{11}q = \frac{1}{2\pi i} \int_\Gamma R(\lambda,A)\ B\ S_{21}\ R(\lambda,A_m)q\,d\lambda \tag{3.18}$$

for any q in R^N.

PROOF: From (3.17a), it follows that for any $\lambda\epsilon\sigma(A)\cap\sigma(A_m)$:

$$S_{11}\ R(\lambda,A_m) - R(\lambda,A)\ B\ S_{21}\ R(\lambda,A_m) = R(\lambda,A)\ S_{11} \tag{3.19}$$

But integration of (3.19) over the curve Γ produces:

$$0 = \frac{1}{2\pi i}\int_\Gamma R(\lambda,A)\ S_{11}q\ d\lambda = \frac{1}{2\pi i}\int_C [S_{11}\ R(\lambda,A_m)q - R(\lambda,A)\ B\ S_{21}\ R(\lambda,A_m)q]d\lambda$$

$$= S_{11}q - \frac{1}{2\pi i}\int_C R(\lambda,A)\ B\ S_{21}\ R(\lambda,A_m)q\ d\lambda .$$

because Γ encloses the finite number of singularities of A_m and excludes all of the spectrum of A. Clearly, since $R(\lambda,A):H\to D(A)$, S_{11} must have its range in $D(A)$, and this is the desired result. #

Once, we have specified the matrix S_{21}, the unique operator S_{11} is determined. Satisfaction of (3.17c) could most easily be done by defining C_m to be $C\ S_{11}$. The determination of the matrix S_{22} for (3.17b) could be done from

$$S_{22} = (B^*B)^{-1}\ B^*\ S_{11}\ B_m \tag{3.20}$$

as long as B_m is chosen so that a solution exists. Note that the operator B has full rank P and so the inverse of B^*B exists.

Although the above existence result does not really require the number of actuators and sensors to be equal, this will be needed in the later sections. Also, the following alternative existence result requires it:

Theorem 3: Let zero belong to $\rho(A)$ and $C\ A^{-1}\ B$ be nonsingular on R^P, then

$$\begin{bmatrix} A & B \\ C & 0 \end{bmatrix}^{-1} = \begin{bmatrix} \Omega_{11} & \Omega_{12} \\ \Omega_{21} & \Omega_{22} \end{bmatrix} = \left[\begin{array}{c|c} A^{-1}(I-B(CA^{-1}B)^{-1}CA^{-1}) & A^{-1}B(CA^{-1}B)^{-1} \\ (CA^{-1}B)^{-1}CA^{-1} & -(CA^{-1}B)^{-1} \end{array}\right]$$

and $S_{12} = \Omega_{11}\ S_{11}\ B_m$, $S_{21} = \Omega_{21}\ S_{11}\ A_m + \Omega_{22}\ C_m$, and $S_{22} = \Omega_{21}\ S_{11}\ B_m$ where S_{11} satisfies:

$$S_{11} = \Omega_{11}\ S_{11}\ A_m + \Omega_{12}\ C_m \tag{3.21}$$

The proof of Theo. 3 can be obtained by straightforward computation using (3.16). Furthermore, note that

$$AS_{11} = A\Omega_{11} S_{11} A_m + A\Omega_{12} C_m$$

$$= (I-B\Omega_{12}) S_{11} A_m + (-B\Omega_{22}) C_m$$

$$= S_{11} A_m - B[\Omega_{12} S_{11} A_m + \Omega_{22} C_m] = S_{11} A_m - BS_{21}$$

which is the same as (3.17a); however, Theo. 3 gives a wider range of solutions than Theo. 2 since S_{12} need not be zero. The solution of (3.21) can be handled when zero belongs to (A_m) because we then have the following:

$$S_{11} A_m^{-1} = \Omega_{11} S_{11} + \Omega_{12} C_m A_m^{-1} \tag{3.22}$$

which has a unique solution S_{11} whenever the $\sigma(A_m^{-1})$ and $\sigma(\Omega_{11})$ are separated by a smooth simple closed curve (see proof of Theo. 2).

4. THE ADAPTIVE MODEL FOLLOWING CONTROLLER

4.1 Development of the Adaptive Controller

The nonadaptive control law (3.14) requires exact knowledge of the gain operators G, S_{21}, and S_{22}. These may be known to exist via mathematical structure of the DPS (A,B,C) in (2.1) (e.g. Theos. 1, 2, 3) but they may not be available in an explicit form. Consequently, we would need an adaptive version of (3.14):

$$f(t) = S_{21}(t)\ q(t) + S_{22}(t)\ u_m + G(t)\ e_y(t) \tag{4.1}$$

where

$$e_y \equiv y - y_m = y - y^* \tag{4.2}$$

We assume throughout Sec. 4.0 that the hypotheses of Theo. 1 are satisfied for the DPS (2.1). Take $e(t) \equiv v(t) - v^*(t)$ and, from (2.1), (3.1),(3.3) and (4.2), obtain (for v_o and v_o^* in D(A)):

$$\begin{cases} \dfrac{\partial e(t)}{\partial t} = A_c e(t) + B\Delta K(t)\ r(t) \\ e(o) \equiv e_o = v_o - v_o^* \end{cases}$$

where

$A_c \equiv A + BGC$ generates an exponentially stable C_o-semigroup $U_c(t)$ and

$$r(t) \equiv \begin{bmatrix} e_y(t) \\ q(t) \\ u_m \end{bmatrix}$$ belongs to R^{N+2P} and $\Delta K(t) \equiv K(t) - K_o$ where

$$K(t) = [G(t) \mid S_{21}(t) \mid S_{22}(t)] \text{ and } K_o = [G \mid S_{21} \mid S_{22}]$$

The <u>adaptive gain laws</u> we shall use are motivated by [6] and have the form:

$$\begin{cases} K(t) = K_I(t) + K_p(t) & (4.4a) \\ K_p(t)z = -\Gamma_p \, e_y(t) \, (r(t),z) & (4.4b) \\ \dot{K}_I(t)z = -\Gamma_I^{-1} \, e_y(t) \, (r(t),z) & (4.4c) \end{cases}$$

where $\dot{K}_I \equiv \frac{dK_I}{dt}$, z belongs to R^{N+2P}, and Γ_p, Γ_I are both positive definite matrices on R^P. Note that (since K_o is constant):

$$\Delta\dot{K}_I(t) = \dot{K}_I(t) = -\Gamma_I^{-1} \, e_y(t) \, (r(t),\cdot) \qquad (4.5)$$

where

$$\Delta K_I(t) \equiv K_I(t) - K_o.$$

The <u>closed-loop adaptively controlled DPS</u> is given by (4.3) and (4.5):

$$\begin{cases} \frac{\partial \bar{e}(t)}{\partial t} = \bar{A}_c \, \bar{e}(t) + \bar{F}\,(t, \bar{e}(t)) \\ \bar{e}(o) = \bar{e}_o \equiv \begin{bmatrix} e_o \\ K_I(o) \end{bmatrix} \end{cases} \qquad (4.6)$$

where
$$\bar{e}(t) \equiv \begin{bmatrix} e(t) \\ \Delta K_I(t) \end{bmatrix}, \qquad \bar{A}_c \equiv \begin{bmatrix} A_c & 0 \\ 0 & 0 \end{bmatrix}, \text{ and}$$

$$\bar{F}(t,\bar{e}(t)) \equiv \begin{bmatrix} B\Delta K(t) \, r(t) \\ -\Gamma_I^{-1} \, e_y(t) \, (r(t),\cdot) \end{bmatrix} \text{ with } e_y(t) = C\,e(t) \text{ and } r(t) = \begin{bmatrix} e_y(t) \\ q(t) \\ u_m \end{bmatrix}.$$

The state $\bar{e}(t)$ of (4.6) resides in a new Hilbert space $\bar{H}$ where $\bar{H} \equiv H \times B_2(R^{N+2P}, R^P)$ with $B_2(H_1,H_2)$ representing the Schmidt class of compact linear operators from H_1 into H_2 with inner product $(A,B) \equiv \text{tr } A^* B$ where "tr" denotes the trace of the operator; see [11] pp 262-264 for further details. The inner product on $\bar{H}$ is formed by summing those of H and B_2; we shall use the same symbols for all inner products $(\cdot,\cdot)$ and their corresponding norms $||\cdot||$. The nonlinear function $F(t,\cdot):\bar{H}\to\bar{H}$ is continuous; hence,

$$\bar{e}(t) = \bar{U}(t)\,\bar{e}_o;\ t \geq 0 \tag{4.7}$$

where $\bar{U}(t)$ is the nonlinear semigroup defined on $\bar{H}$ by (for any h in $\bar{H}$):

$$\bar{U}(t)h = \bar{U}_c(t)h + \int \bar{U}_c(t-\tau)\ \bar{F}(\tau,\bar{U}(\tau)h)d\tau \tag{4.8}$$

where

$\bar{U}_c(t) = \begin{bmatrix} U_c(t) & 0 \\ 0 & 1 \end{bmatrix}$ is the linear C_o-semigroup generated on $\bar{H}$ by $\bar{A}_c$ in (4.6). The above follows from [12] Lemma 5.2 p. 186 where further details on nonlinear semigroups are also available; consequently, the closed-loop infinite-dimensional system (4.6) is well-posed on $\bar{H}$.

4.2 Closed-Loop Stability

The stability analysis of the nonlinear infinite-dimensional system (4.6) requires the extension of Lyapunov theory to infinite-dimensional spaces. This has been done in [12]-[13] and we summarize the necessary elements here:

Def: The equilibrium point ϕ is stable for the system (4.6) if for every $\varepsilon > 0$ there exists $\delta > 0$ such that $||\bar{e}(o) - \phi|| < \delta$ implies $||\bar{e}(t) - \phi|| < \varepsilon$ for all $t \geq 0$. If, in addition to stability, there is a $\gamma > 0$ such that $||\bar{e}(o) - \phi|| < \gamma$ implies $\lim_{t\to\infty} ||\bar{e}(t)-\phi|| = 0$, then ϕ is said to be asymptotically stable for (4.6). Usually we can take $\phi = 0$. We say an equilibrium point is unstable whenever it is not stable.

Def: A continuous functional $V:\bar{H}\to R$ is a Lyapunov function for (4.6) if $V(o) = 0$ and $\dot{V}(\bar{e}) \leq 0$ for all $\bar{e}$ in $\bar{H}$ where

$$\dot{V}(\bar{e}) \equiv \limsup_{t\to 0^+} \frac{V(\bar{e}(t))-V(\bar{e})}{t} \tag{4.9}$$

where $\bar{e}$ is in $\bar{H}$ and $\bar{e}(t) = \bar{U}(t)\bar{e}$ as given in (4.7).

Lemma 1: If $V:\bar{H}\to R$ is a Lyapunov function for (4.6) with the property that

$$V(\bar{e}) \geq f_1(||\bar{e}||) \tag{4.10}$$

for all $\bar{e}$ such that $||\bar{e}|| \leq h$ (where $0 < h < \infty$) and f_1 is of class M_h (i.e. $f_1:[0,h]\to R^+$ with $f_1(o) = 0$ and f_1 strictly increasing on $[0,h]$, then the zero equilibrium point is stable for (4.6).

Lemma 2: If in addition to the hypotheses of Lemma 1, the Lyapunov function $V(\cdot)$ has the property:

$$\begin{cases} \dot{V}(\bar{e}) \leq -W(\bar{e}) \quad \text{for all } \bar{e} \text{ in } \bar{H} & (4.11a) \\ W(\bar{e}) \geq f_2(||\bar{e}||) \quad \text{for } ||\bar{e}|| \leq h & (4.11b) \end{cases}$$

where f_2 is also of class M_h, then the zero equilibrium point is asymptotically stable for (4.6).

The proofs of Lemmae 1 and 2 can be found in [13]. These results constitute Lyapunov's Direct Method on infinite-dimensional spaces.

We now have the following stability result for our adaptively controlled closed-loop system (4.6):

Theorem 4: Assume the following:

(a) In (4.3), $A_c \equiv A + BGC$ satisfies

$$(A_c v, Pv) + (Pv, A_c v) = -(Qv,v) \tag{4.12}$$

for all v in D(A) where P and Q are symmetric positive operators on H such that (for some α, β positive constants):

$$\begin{cases} ||v||^2 \leq (v,Pv) \leq \beta\, ||v||^2 & (4.13a) \\ \alpha||v||^2 \leq (Qv,v) \ (\text{i.e } Q \text{ is coercive}) & (4.13b) \end{cases}$$

for all v in H,

(b) $B^* P = C$, (4.14)

(c) the hypotheses for Theo. 1 are satisfied, and both v_o and v_o^* belong to D(A),

then $V(\bar{e}) \equiv (e,Pe) + (\Delta K_I, \Gamma_I \Delta K_I)$, with $\Delta K_I(t) \equiv K_I(t) - K_o$ and $\bar{e} \equiv \begin{bmatrix} e \\ \Delta K \end{bmatrix}$, is a Lyapunov function for (4.6) and the zero equilibrium point is stable.

PROOF: Recall that

$$\Delta K(t) = \Delta K_I(t) + K_p(t) \tag{4.15}$$

$$\Delta \dot{K}_I(t) = K_I(t) \tag{4.16}$$

Now, clearly V is a continuous functional from $\bar{H}$ into R (due to (4.13a) with V(o) = 0. Furthermore, since V is a quadratic functional, it is Frechet differentiable. Hence, from (4.6) and (4.12),

$$\dot{V}(\bar{e}) = -(Qe,e) + 2\mu \tag{4.17}$$

where $\mu \equiv [(Pe, B\Delta Kr) + (\Delta K_I, \Gamma_I \Delta \dot{K}_I)]$

From (4.16), (4.4c), and (4.15), we have

$$\begin{aligned}\mu &= (B^*Pe,\ \Delta K_r) - (\Delta K_I,\ e_y(r,\cdot))\\ &= (B^*Pe,\ \Delta K_r) - (r,\ \Delta K_I^*\ e_y)\\ &= (B^*Pe,\ \Delta K_I r) + (B^*Pe,\ K_p r) - (r,\ \Delta K_I^*\ e_y)\\ &= (\Delta K_I r,\ [B^*Pe - e_y]) + (K_p r,\ B^*Pe)\end{aligned} \tag{4.18}$$

where we have used $(A,B) \equiv \mathrm{tr}\, A^*B = \mathrm{tr}(BA^*)$. Furthermore, using (4.14) in (4.18), yields

$$\mu = (K_p r,\ e_y) = -(\Gamma_p e_y)||r||^2 \tag{4.19}$$

from (4.4b). Consequently, using (4.19) in (4.17), we obtain

$$\begin{aligned}\dot{V}(\bar{e}) &= -[(Qe,e) + 2(\Gamma_p e_y,\ e_y)||r||^2]\\ &\leq -[\alpha||e||^2 + 2\ \alpha_p||e_y||^2||r||^2] \leq 0\end{aligned} \tag{4.20}$$

where $\alpha_p \equiv \lambda_{min}(\Gamma_p)$ and we have used (4.13b).

Also, using (4.13a), we have

$$V(\bar{e}) \geq ||e||^2 + \lambda_{min}(\Gamma_I)\ ||\Delta K_I||^2$$

In other words, $f_1(\zeta) \equiv [1 + \lambda_{min}(\Gamma_I)]\zeta^2$ which is of class M_h. Therefore, the above satisfies the hypotheses of Lemma 1 and the desired result is obtained. #

Note that the use of a proportional adaptive gain (4.4b) produced the second term in (4.20); however, this term is not essential and the above argument could be simplified by omitting (4.4b) from the adaptive gain laws.

The hypotheses (a) and (b) correspond to the Kalman - Yakubovich conditions in infinite-dimensional spaces. From [13] Theo. 4.7, if for some real ω, $(Av,\ v) \leq \omega||v||^2$ for all v in D(A), then exponential output stabilization of (A,B,C) would be equivalent to satisfaction of hypotheses (2); however, there would be no guarantee that P and Q could be found in (4.12) such that (4.14) could be obtained. In finite-dimensional spaces, the Kalman - Yakubovich conditions are equivalent to the strict positive realness of the transfer function $T_c(s) = C(sI-A_c)^{-1}B$, i.e. Re $T_c(j\omega) > 0$ for all real ω; see [14] pp. 115-118. A number of papers, e.g. [15] - [17], have been written on this relationship in infinite-dimensional spaces. For example, [17] asserts that $\mathrm{Re}T_c(j\omega)$ must be coercive, which would be quite a bit stronger than what is required in finite-dimensions. This is an area that requires further investigation.

As pointed out in [9], we cannot immediately conclude asymptotic stability from (4.20) since it does not satisfy the hypotheses of Lemma 2. In finite-dimensional space, we could apply the LaSalle Invariance Principle to obtain asymptotic stability as is done in [6]; however, in infinite-dimensional spaces, it is not the case that "bounded sets are precompact" and this is essential for the LaSalle result.

The following result ([13] Theo. 5.4 p. 188) may be helpful:

Lemma 3: Let $\bar{A}_c$ in (4.6) generate the linear C_o-semigroup $\bar{U}_c(t)$ on $\bar{H}$ and $\bar{F}$ is any bounded, continuous function such that (4.6) generates a nonlinear semigroup $\bar{U}(t)$ on $\bar{H}$ (as given in (4.8)), then all bounded orbits of (4.6) are precompact if either

(a) $\bar{U}_c(t)$ is compact operator for all $t \geq 0$

or

(b) $\bar{U}_c(t)$ is exponentially stable and the function $\bar{F}$ is compact (i.e. maps bounded sets into precompact ones)

Due to the form of $\bar{A}_c \equiv \begin{bmatrix} A_c & 0 \\ 0 & 0 \end{bmatrix}$, it is not possible to satisfy (b); however, (a) may be satisfied, for example by operators A which generate holomorphic semigroups. This latter is determined by the form of damping operator in a flexible structure. Again, this is a topic for further investigation. An alternative adaptive gain law:

$$\dot{K}_I(t)v = -\Gamma^{-1} \left(e_y(r,v) + K_I(t)v\right) \tag{4.21}$$

yields:

$$\dot{V}(\bar{e}) \leq -[\alpha||e||^2 + 2||\Delta K_I||^2 + 2(\Delta K_I, K_o)]$$

which does not quite give asymptotic stability but might be modified to do so.

5. CONCLUSIONS

In this paper, we have presented a direct adaptive controller for linear distributed parameter systems (DPS) described on infinite-dimensional Hilbert spaces. The controller is based on a command generator tracker approach used in finite-dimensional spaces, e.g. [6] where it is shown to be asymptotically stable. We have shown here that, under certain conditions on the open-loop loop DPS, ideal trajectories do exist and the adaptive controller is stable, i.e. the output and gain errors remain bounded. If the further condition that A in (2.1) generates a holomorphic C_o-semigroup is imposed, then we can also conclude asymptotic stability which guarantees asymptotic tracking or model following.

A number of issues have been opened for further investigation:

(1) use of dynamic rather than output feedback stabilization;

(2) generation of asymptotic ideal trajectories by the open-loop DPS;

(3) connections between the Kalman-Yakubovich conditions and the input-output description of the DPS;

(4) development of alternative adaptive gain laws which produce asymptotic stability of the closed-loop system;

(5) exploration of reasonable conditions under which LaSalle's Invariance Principle can be used to determine asymptotic stability of the closed-loop system.

ACKNOWLEDGEMENTS

This research was supported in part by the National Science Foundation under Grant No. ECS-80-16173 and the Air Force Office of Scientific Research under Grant No. AFOSR-83-0124. Any opinions, findings, and conclusions or recommendations expressed in this publication are those of the author and do not necessarily reflect the views of NSF or AFOSR.

REFERENCES

[1] R. Curtain and A. Pritchard, Functional Analysis in Modern Applied Mathematics, Academic Press, NY, 1977.

[2] A. Balakrishnan, Applied Functional Analysis, Springer-Verlag, NY, 1976.

[3] M. Balas, "Toward A More Practical Control Theory for Distributed Parameter Systems", in Control and Dynamic Systems: Advances in Theory and Applications, Vol. 18, C.T. Leondes, editor, Academic Press, NY, 1982.

[4] H. Erzberger, "On the Use of Algebraic Methods in the Analysis and Design of Model Following Control Systems", NASA TN D-4663, 1963.

[5] J. Broussard and M. O'Brien, "Feedforward Control to Track the Output of a Forced Model", 17th IEEE Conf. on Decision and Control, Jan. 1979, pp. 1144-1155.

[6] I. Bar-Kana, H. Kaufman, M. Balas, "Model Reference Adaptive Control of Large Structural Systems", AIAA J. Guidance, Control, and Dynamics, March-April 1983, pp. 112-118.

[7] I. Bar-Kana, H. Kaufman, "Some Applications of Direct Adaptive Control to Large Structural Systems", AIAA J. Guidance, Control and Dynamics, to appear.

[8] M. Balas and C.R. Johnson, Jr., "Adaptive Control of Distributed Parameter Systems: The Ultimate Reduced-Order Problem", IEEE Conf. on Decision and Control, Ft. Lauderdale, Fl. 1979.

[9] M. Balas, "New Directions in Asymptotically Stable Finite-Dimensional Adaptive Control of Linear Distributed Parameter Systems", This Proceedings.

[10] M. Balas, "Linear Distributed Parameter Systems: Closed-Loop Exponential Stability With A Finite-Dimensional Controller", Automatica, to appear.

[11] T. Kato, Perturbation Theory For Linear Operators, Springer-Verlag, NY, 1966.

[12] J. Walker, Dynamical Systems and Evolution Equations: Theory and Applications, Plenum Press, NY, 1980.

[13] J. Walker, "On the Application of Liapunov's Direct Method to Linear Dynamical Systems", J. Math. Analy. & Appl., Vol. 53, 1976, pp. 187-220.

[14] S. Lefschetz, Stability of Nonlinear Control Systems, Academic Press, NY, 1962.

[15] V. Hiris and M. Megan, "Remarks on Hyperstability of Infinite-Dimensional Linear Systems", Int. J. Control, Vol. 35, 1982, pp. 739-747.

[16] D. Wexler, "On Frequency Domain Stability for Evolution Equations in Hilbert Spaces Via the Algebraic Riccati Equation", SIAM J. Math. Analy., Vol. 11, 1980, pp. 969-983.

[17] A. Likhtarnikov and V. Yakubovich, "The Frequency Theorem for Equations of Evolutionary Type", Sibirskii Mathematicheskii Zhurnal, Vol. 17, 1976, pp. 1069-1085.

N85-31205

SELF-TUNING ADAPTIVE CONTROLLER USING ONLINE FREQUENCY IDENTIFICATION

W. W. Chiang and R. H. Cannon, Jr.
Stanford University
Palo Alto, CA 94304

ABSTRACT

A real-time adaptive controller has been designed and tested successfully on a fourth order laboratory dynamic system which features very low structural damping and a non-colocated actuator-sensor pair. The controller, implemented in a digital minicomputer, consists of a state estimator, a set of state feedback gains, and a Frequency-Locked-Loop (FLL) for real time parameter identification . The FLL can detect the closed-loop natural frequency of the system being controlled, calculate the mismatch between a plant parameter and its counterpart in the state estimator, and correct the estimator parameter in real time. The adaptation algorithm can correct the controller error and stabilize the system for more than 50% variation in the plant natural frequency, compared with a 10% stability margin in frequency variation for a fixed-gain controller having the same performance at the nominal plant condition. After it has locked to the correct plant frequency, the adaptive controller works as well as the fixed-gain controller does when there is no parameter mismatch. The very rapid convergence of this adaptive system is demonstrated experimentally, and can also be proven with simple root-locus methods.

I. INTRODUCTION

A controller using Kalman filter and full state feedback usually has good performance, provided a very accurate model of the plant is known. But such controllers are very sensitive to parameter variation, especially when the plant has very low inherent damping, and when the sensor is not colocated with the actuator.

A two-disk laboratory model, consisting of two inertia disks connected by a torsion rod, which has a structural damping of 0.004, and with separated sensor and actuator locations was constructed to test several adaptive controller designs. The form of the equations of motion of the model is known due to the ease of analysis of the lumped system; but the lack of accurate knowledge about the natural structural frequency during controller design corresponds to a plant parameter uncertainty or variation; and this uncertainty is what the adaptive controller handles.

It has been proposed by Kopf, Brown, Marsh (Ref.1) and Macala (Ref.2) to use a Phase-Locked-Loop to implement tuned damping and notch filtered command torque, so that the feedback control force near the structural frequency can be adjusted properly according to the natural frequency of the plant. Rosenthal and Cannon (Ref.3) have implemented such a kind of controller for the two-disk experimental system.

Under the same research project, a different approach using a Frequency-Locked-Loop (FLL) to identify the plant frequency was developed. This paper describes in detail how the FLL identifies the unknown plant parameter and updates the controller in real time.

II. DESCRIPTION OF THE TWO-DISK PLANT AND FIXED-GAIN CONTROLLER

The plant to be controlled is a mechanical system which consists of two horizental steel disks connected by a vertical elastic steel rod. The two disks are supported by bearings which allow rotational motion only. A low-friction DC motor is attached to the lower disk, and an RVDT sensor detects the angular position of the upper disk.

If structural damping is neglected*, the state equation of motion of this system can be expressed as

$$\begin{pmatrix} \dot{x}_1 \\ \dot{x}_2 \\ \dot{x}_3 \\ \dot{x}_4 \end{pmatrix} = \begin{pmatrix} 0 & 1 & 0 & 0 \\ 0 & 0 & 0 & 0 \\ 0 & 0 & 0 & 1 \\ 0 & 0 & -\omega_n^2 & 0 \end{pmatrix} \begin{pmatrix} x_1 \\ x_2 \\ x_3 \\ x_4 \end{pmatrix} + \frac{1}{J} \begin{pmatrix} 0 \\ 1 \\ 0 \\ -1 \end{pmatrix} u, \tag{1}$$

where x_1 and x_3 are the position states of the rigid body mode and the structural oscillation mode respectively, x_2 and x_4 are rates of those states respectively; ω_n is the natural frequency, J is the total moment of inertia of the two disks, and u is the control torque from the DC motor.

The sensor output is

$$y = x_1 + x_3. \tag{2}$$

A first-order high-pass filter with 100 Hz cutoff frequency is used to differentiate the position sensor output and provides the pseudo-rate of the top disk.

If all the parameters of the plant are known accurately, an LQG design (Ref.4) will result in a set of state feedback gains C for regulation and estimator gains L for state estimation. However, if the plant natural frequency ω_n is not known by the controller designer, and a value ω_e is used in the estimator, the stability of the whole system has to be analyzed by augmenting the system state equations with those of the estimator states, and finding the modal frequencies and dampings of the system (Ref.5)

Using the same penalty weightings for control effort and state errors, an LQG design produces different feedback gains C and L for different natural frequencies ω_n of the plant. Analysis shows that the stability of the whole system is less sensitive to those feedback gains than to the parameter ω_e used in the estimator, since an error in the latter parameter corresponds to a modeling error, while variations in the former ones correspond to different weightings in the LQG design process. In the experiment described here, feedback gains C and L are chosen for the nominal plant frequency, and are kept constant in order to demonstrate the adaptation of the controller by correcting ω_e in the estimator.

From the analysis of the augmented system state equations, the frequency ω_c of the most unstable closed-loop mode can be found as a function of ω_n and ω_e, if all other parameters are kept constant. This function

$$\omega_c = f(\omega_e, \omega_n), \tag{3}$$

will affect the closed-loop performance of the adaptation process, and has to be taken into account in the design process. The two-disk model has a nominal frequency of 13.3 rad/sec, and the function described in equation (3) can be shown approximately as in Fig. 1, and can be approximated as

$$\omega_c - \omega_n = (\omega_n - \omega_e) + 0.6 \tag{4}$$

for $/\omega_n - \omega_e/ < 1.5$rad/sec.

III. FREQUENCY IDENTIFICATION USING FREQUENCY-LOCKED-LOOP

A Phase-Locked-Loop (PLL) was initially proposed to be used to detect the vibration frequency. PLLs have been used widely in locking onto high-frequency signals in electrical engineering applications, but it

* It is actually 0.004

is only beginning to be used in locking onto low-frequency signals in mechanical systems. A PLL has the ability to identify the phase and frequency of a signal contaminated by a relatively large amount of noise at other frequencies. Several signal components at different frequencies can be identified by using several PLLs.

The traditional PLLs are nonlinear elements for which the performance is hard to analyze and predict; and they have limited locking ranges due to their nonlinearity. Besides, PLLs are more sensitive to the phase than to the frequency of their driving signal, which makes them unsuitable for frequency identification because the identification will be disturbed by the phase in the sensor signal every time a new position command or an external disturbance is applied to the system, even though a PLL has identified the correct plant frequency already.

A modification is made to a PLL to eliminate its sensitivity to phase in the input signal and make the input/output relation linear in a larger tracking range, so that it works better for frequency identification, while retaining the other virtues of PLLs. The final product, called a Frequency-Locked-Loop (FLL), is shown schematically in Fig. 2, and its input/output relation can be seen from the functional block diagram in Fig. 3, where ω_i is the frequency of the input signal and ω_o is the output signal – the frequency detected by the FLL. Also shown in the same block diagram are ω_s, the starting oscillation frequency; $\Delta\omega$, the correction on the output; and ω_{er}, the error of the output of the FLL.

The character of the block $G(s)$ can be chosen arbitrarily by the designer as long as it can update the output frequency of the FLL according to its error ω_{er}. If a simple integrator $\frac{G}{s}$ is chosen as the element $G(s)$, then the FLL will have a pole at $-K$ where

$$K = \frac{G(a-b)}{ab}. \tag{5}$$

Parameters a and b should be determined with the following restriction

$$\omega_n > a > b > /\omega_i - \omega_o/. \tag{6}$$

In the present case,

$$\omega_n = 13.3\text{rad/sec}, \tag{7}$$

and the linear search range is chosen to be

$$/\omega_i - \omega_o/ = \frac{\omega_n}{4} = 3.3\text{rad/sec}. \tag{8}$$

The pole location $s = -K$ should be determined as the result of a compromise between speed of response and noise rejection, at the nominal locking frequency range. In this case, the parameters of the FLL are chosen as

$$a = 6.0, \qquad b = 4.0, \qquad G = 20.0, \qquad \Longrightarrow \qquad K = 1.67, \tag{9}$$

to work in the range of 1 to 3 Hz.

With parameters chosen as above, the block diagram in Fig. 3 can be simplified to the transfer function

$$Q(s) = \frac{\Omega_o(s)}{\Omega_i(s)} = \frac{K}{(s+K)}. \tag{10}$$

Fig. 4(a) shows the test result of the FLL output when the frequency of the input signal is changed stepwisely. The response for small input change (the first change in Fig. 4(a)) is similar to the step response of a first-order filter with pole at $-K$, as shown in Fig. 4(b). The response for a larger input change (the second change in Fig. 4(a)) experienced some nonlinearity at the beginning because its internal structure is not linear; however, the FLL still tracked the input signal and provided the correct output in a reasonable time.

IV. CORRECTION OF PARAMETER ERROR IN THE CONTROLLER

Because eigenvalues are properties of the system, they are independent of the instantaneous value of state variables and are influenced only by changes of parameters. The relation between ω_e and ω_c, as shown in Eqn. 4, can be expressed as in Fig. 5. Using the difference between $(\omega_o - 0.6)$ and ω_e to update – through the integrator $\frac{H}{s}$ – the parameter ω_e in the controller, the closed loop dynamics of the parameter variation, identification, and correction can be expressed as in Fig. 6. The characteristic equation of the closed parameter adaptation loop is

$$1 + \frac{HK}{(s+H)(s+K)} = 0, \tag{11}$$

or,

$$s(s+K) + (s+2K)H = 0, \tag{12}$$

which can be written in Evan's form as

$$\frac{s(s+K)}{(s+2K)} = -H. \tag{13}$$

The root locus of Eqn. 13 vs. the positive value of H with $K = 1.67$ is shown in Fig. 7, and the value of $H = 9.9$ is chosen obviously to maximize the adaptation rate. The change of the slope in Fig. 1 corresponds to a variation in the gain in Eqn. 4, and Eqn. (11) can be modified as

$$1 + \frac{rHK}{(s+H)(s+K)} = 0, \tag{14}$$

where $2 > r > 0$, and the root locus shown in Fig. 8 guarantees the stability of the system over the range of the gain "r".

Any sensor measurement, controller state variable, or linear combination thereof can be chosen as the input signal to drive the FLL, so long as the signal contains the modal frequency of interest (the larger the better!). The error between the sensor rate and the estimate of it is chosen to drive the FLL, since there is less error signal if all parameters in the controller are correct.

The FLL must be turned off if its input signal is too small, in order to reject the influence from random noise.

A PDP-11/23 minicomputer was used to implement the controller and the FLL at 25 Hz sample rate. The test results of this adaptive system are summerized in the following section.

V. EXPERIMENTAL RESULTS

Fig. 9 shows the natural oscillation of the uncontrolled disk system. The frequency of oscillation is 2.11 Hz. with 0.004 damping. (The long-period motion is caused because the disk system is hung from the ceiling with a long steel wire to reduce the axial thrust on bearings. This mode is approximated as a rigid body mode in the controller design analysis.)

Fig. 10 shows the step response of a nonadaptive control system designed with the LQG method. The response is very good (Fig. 10) when there is no modeling error in the controller design. However, as Fig. 11 shows, the system becomes unstable when there is 10% modeling error in frequency in the designing of the nonadaptive controller.

When the FLL is used in the adaptive control, the system can detect and correct a controller's parameter error of 50% or more in frequency. Figs. 12 (a) through (f) show the sensor output in different tests. The instability due to the initial parameter error is shown when the control system was just turned on, and the system was then stabilized after the adaptation algorithm had corrected the controller's error. The initial turn on of the control system and the time when position commands are changed are marked on those recordings.

Fig. 13 shows the comparison of the impulsive disturbance response, between the nonadaptive controller with no modeling error and the adaptive one after its parameter error has been corrected. The comparison shows almost no difference between their performances.

VI. DISCUSSION

(A) Frequency-Locked-Loop

The FLL is a nonlinear element, but its input/output relation is almost linear. It behaves linearly for 40% changes in input signal frequency, and still works for 100% change in frequency in the nonlinear region. The test recorded in Fig. 4 attests to the discussion above. The linear range can be chosen by selecting parameters properly.

The FLL still works when the amplitude of its input signal is as weak as two quantization intervals of the A/D converter, if it is free of noise and bias; but in real applications it must be turned off at small level of input signal to reduce the effect of noise.

The FLL can identify the plant characteristic in a small window of the frequency spectrum, so that the effects of other parts of the system dynamics do not have to be taken into account if they are not critical to the overall performance. It can only detect modes that are either only slightly damped or unstable, since they can provide oscillatory signals for detection; however, heavily damped modes are usually robust to parameter uncertainty and don't need adaptive control.

(B) Parameter Error Correction Loop

The parameter error correction scheme can be determined by root-locus analysis, or even by the LQG method, since the FLL has a linear characteristic.

Fig. 12 shows some small-amplitude vibration building up due to the lack of signal to lock the FLL, but the parameter estimate error was soon corrected and vibration suppressed.

By examining the response to command change and to disturbances, it is found that the Self-Tuning Adaptive Controller behaved almost the same as the correct fixed optimal controller, except for the few cycles of vibration at the beginning when the parameter error was being corrected.

It is better to use the error of an estimated sensor output to drive the FLL, since it is undisturbed by the control force during a new command change if the model is correct.

Both the identification and error correction are running in real time while the controller is doing its job. Any change in the plant can be tracked and adapted to rapidly.

VII. CONCLUSION

The use of FLL in identifying system vibration frequency and adapting controller parameters is promising. All kinds of controllers, such as Kalman filter and state feedback, band-pass, or notch filters can have their parameter errors corrected in a similar way. It is expected that system with many vibration modes can be handled with several FLLs.

ACKNOWLEDGMENTS

The research reported upon here was sponsored by the National Aeronautics and Space Administration through the Langley Research Center and the Jet Propulsion Laboratory. The authors also appreciated the advice and help from Dan E. Rosenthal who was doing the other part of the research under the same NASA contract.

REFERENCE

(1) Edward H. Kopf, Thomas K. Brown and Elbert L. Marsh, "Flexible Stator Control on the Galileo Spacecraft", paper 79-161, AAS/AIAA Astrodynamics Specialist Conference, Provincetown, MASS/ June 25-27, 1979.

(2) G. A. Macala, "Tuned Feedback Damping: Phase-Locked-Loop Design, Analysis, and Performance Results", Engineering Memorandun 343-470, Jet Propulsion Laboratory, June 5, 1980.

(3) Dan E. Rosenthal and Robert H. Cannon, Jr., "Experiments with Adaptive Control of Flexible Structures", to be published in the Journal of The Astronautical Sciences, 1984.

(4) A. E. Bryson, Jr. & Y-C Ho, "Applied Optimal Control", Hemisphere Publishing Co., 1975.

(5) Daniel B. DeBra, "Estimation in Satellite Control", Proceedings of the Ninth International Symposium on space Technology and Science, Tokyo, 1971.

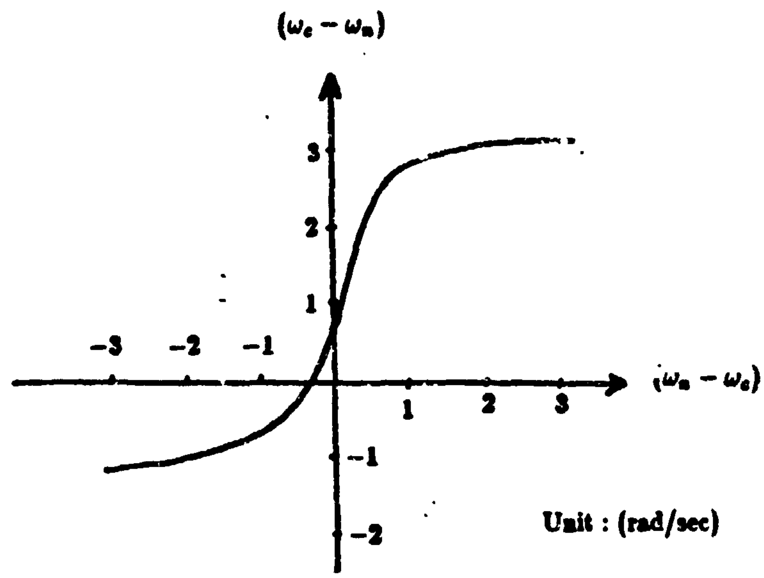

Fig. 1 Relationship between ω_n, ω_e, and ω_s.

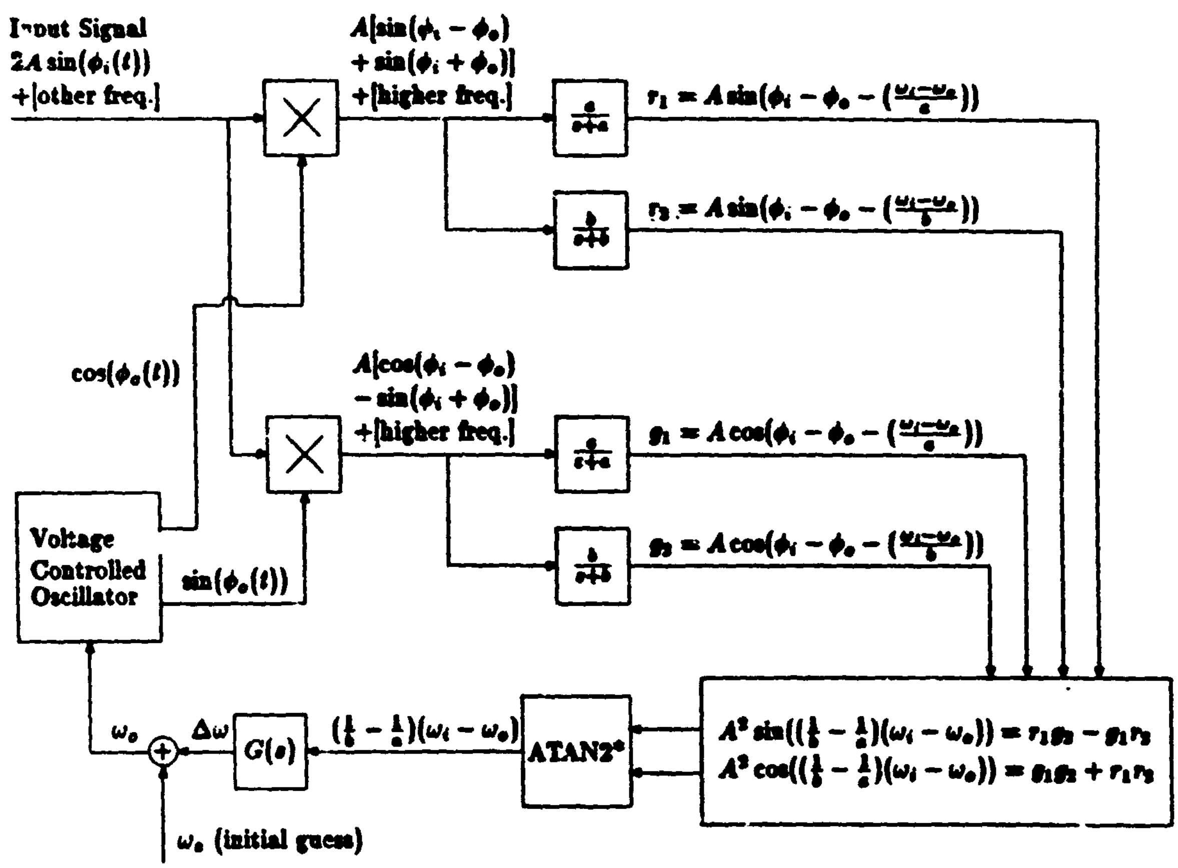

Choose $a > b$

*ATAN2 is a FORTRAN arctangent function which keeps tracking the correct quadrant of the angle.

Fig. 2 ... Diagram of the FLL Implementation.

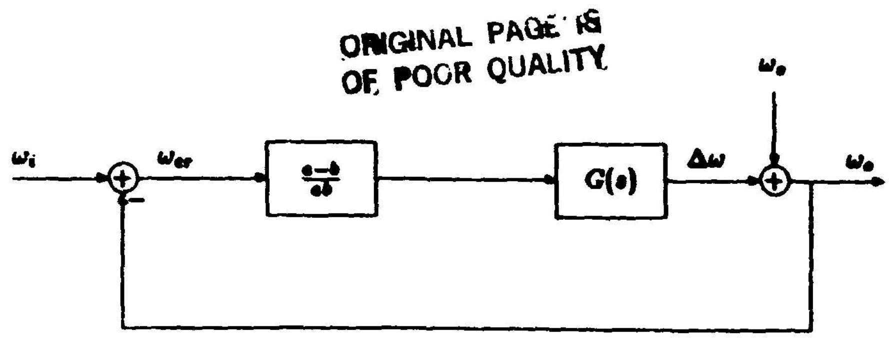

Fig. 3 Functional Block Diagram of the FLL.

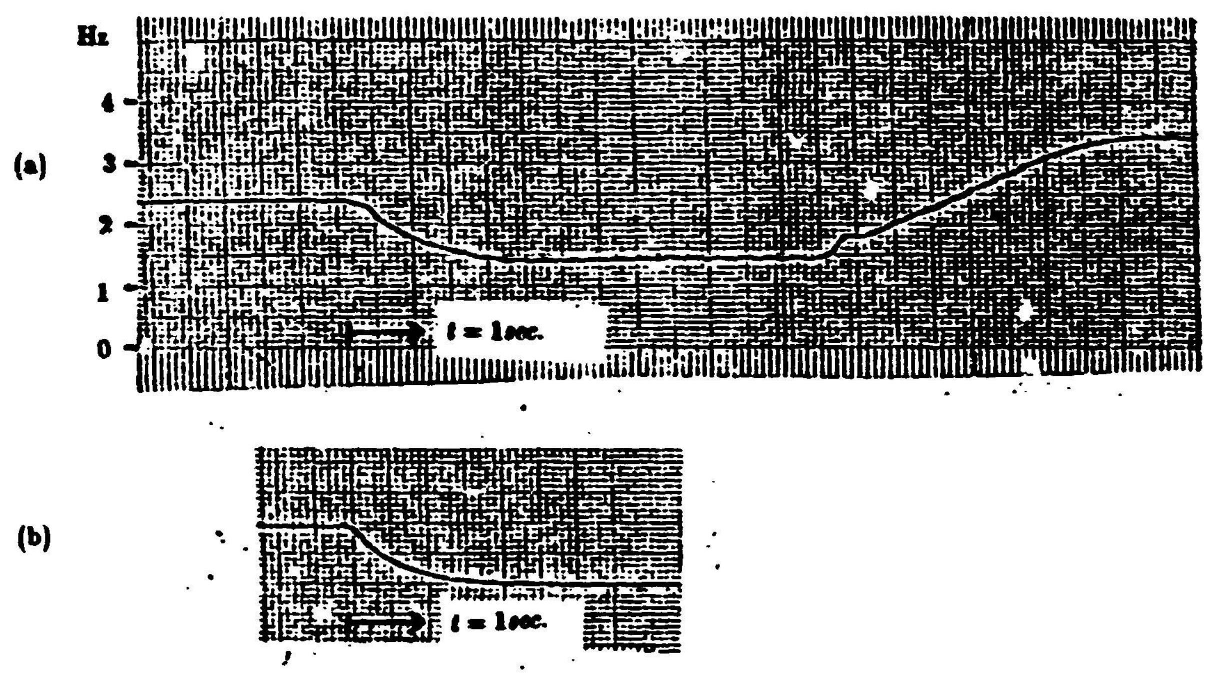

Fig. 4 Step Response of the FLL (a), Compared with That of a First-Order System (b) with Pole at $s = -1.67\text{sec}^{-1}$.

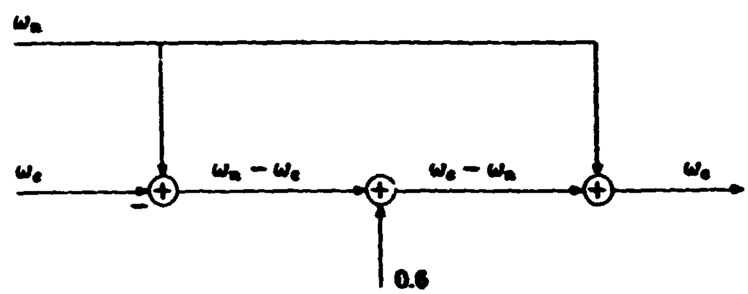

Fig. 5 Block Diagram of the Relation Between ω_n, ω_c, and ω_e.

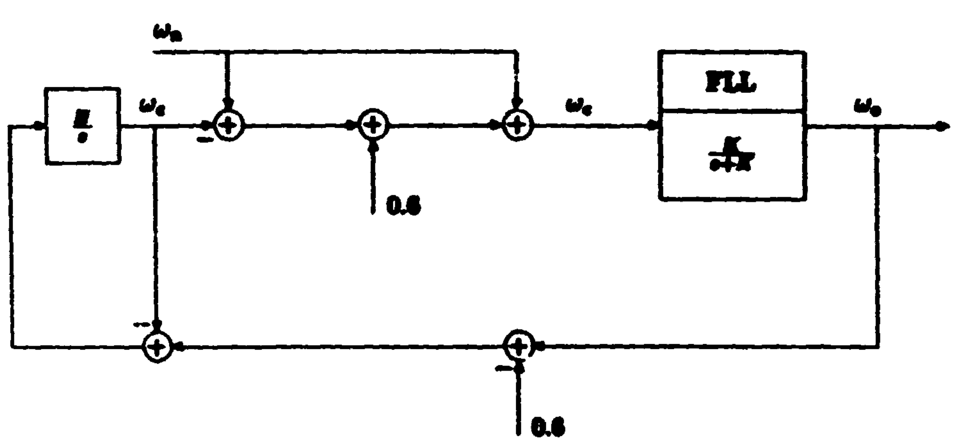

Fig. 6 Closed-Loop Dynamics of Parameter Variation, Identification, and Correction.

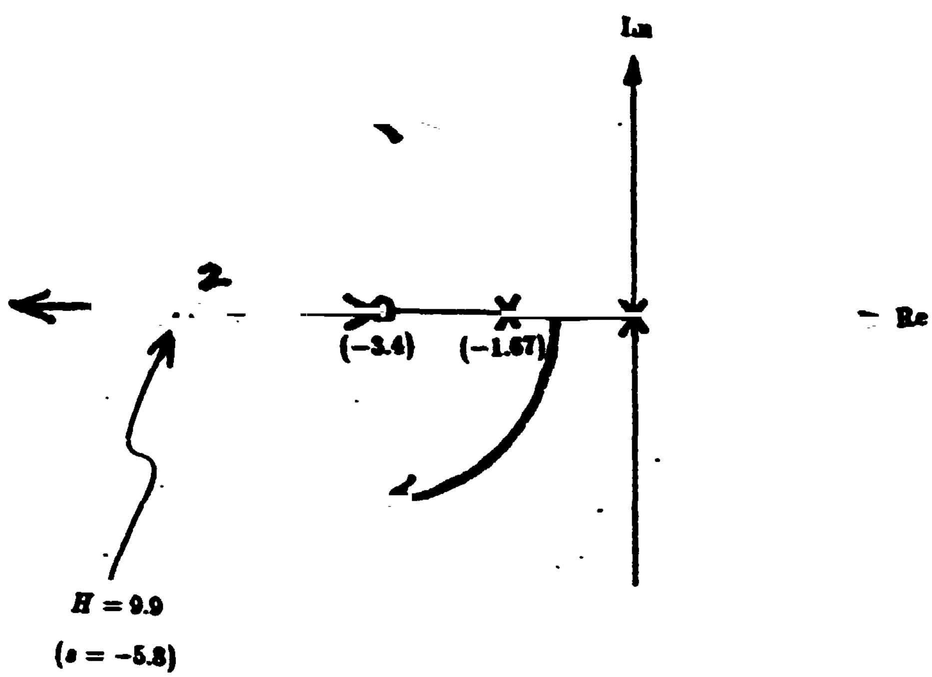

Fig. 7 Variation of Poles of the Closed Parameter Loop versus the Selection of the Value of H.

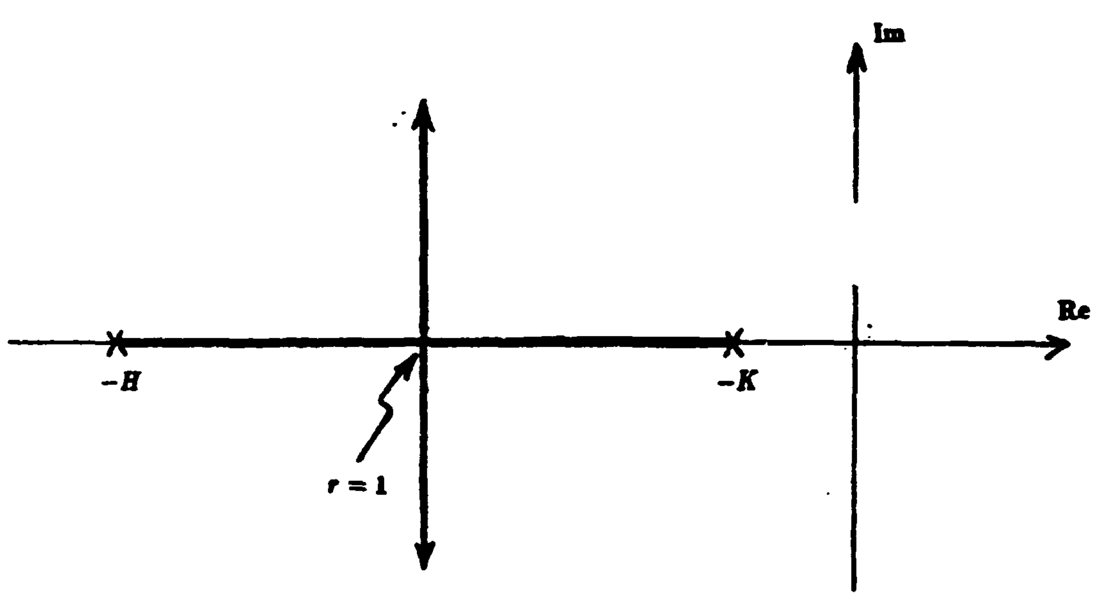

Fig. 8 Variation of Poles of the Closed Parameter Loop versus r, the Changing Slope in Fig. 1.

ORIGINAL PAGE IS
OF POOR QUALITY

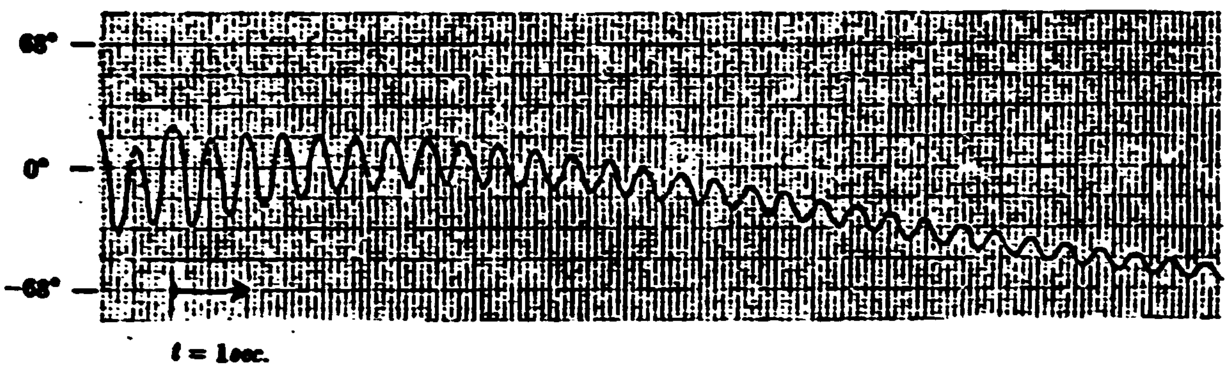

Fig. 9 Natural Vibration of the Plant (Opened Loop) at 2.11 Hz. with Damping = 0.004.
* The long-period motion is caused because the disk system is hung from the ceiling with a long steel wire to reduce the axial thrust on bearings.

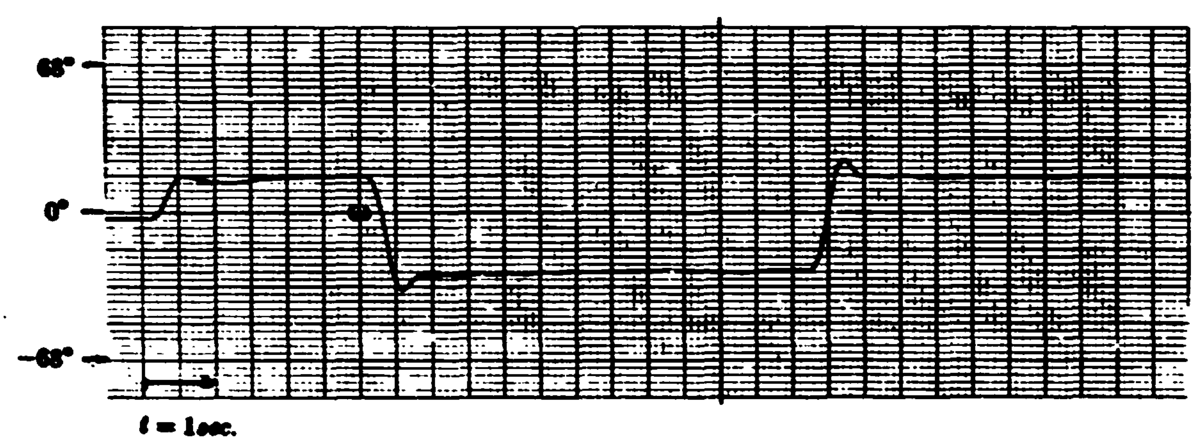

Fig. 10 Step Response of the Closed Loop with a Fixed "Optimal Controller".
(No model error in the Kalman filter.)

ORIGINAL PAGE IS
OF POOR QUALITY

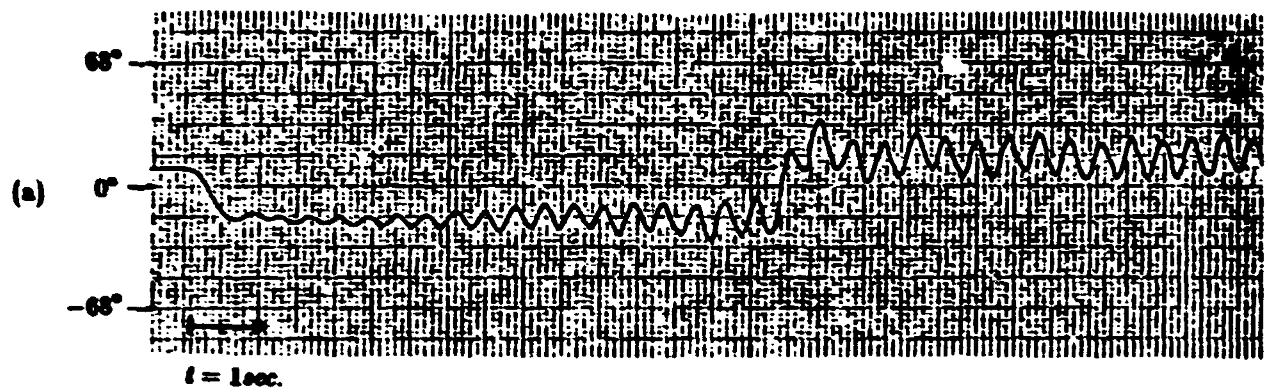

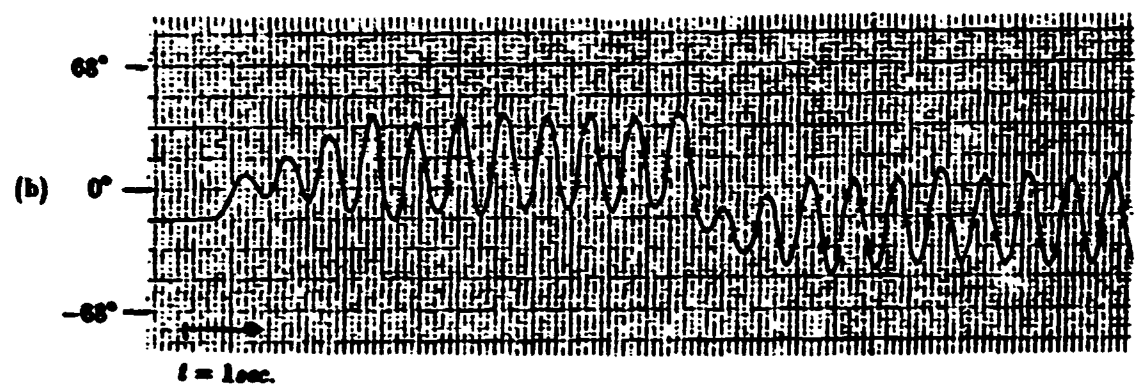

Fig. 11 Step Response of Closed Loop with Fixed "Optimal Controllers".
(a) Vibration frequency was assumed to be 1.9 Hz. (-10% error in frequency) in Kalman Filter.
(b) vibration frequency was assumed to be 2.5 Hz. (+20% error).

ORIGINAL PAGE IS
OF POOR QUALITY

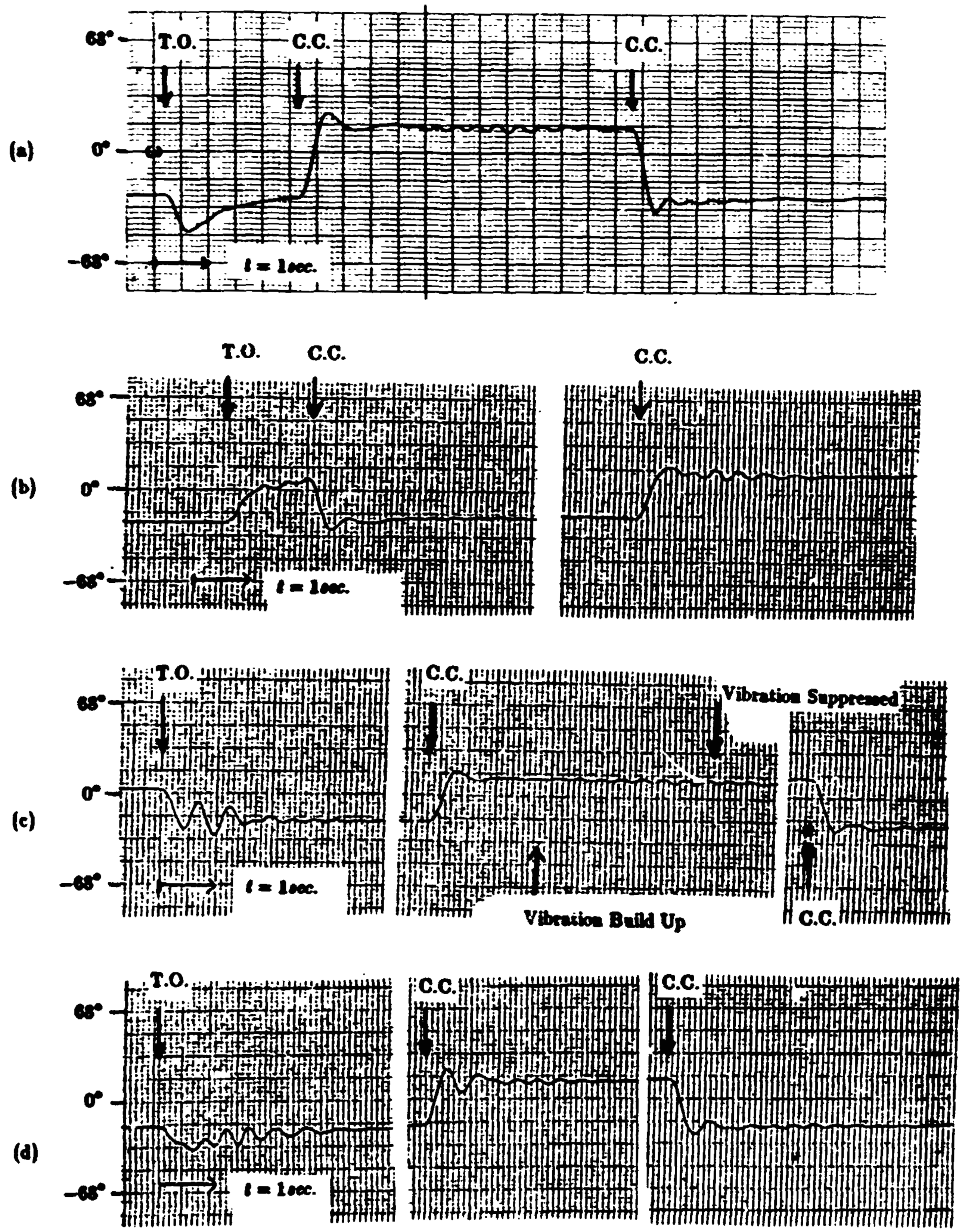

ORIGINAL PAGE IS
OF POOR QUALITY

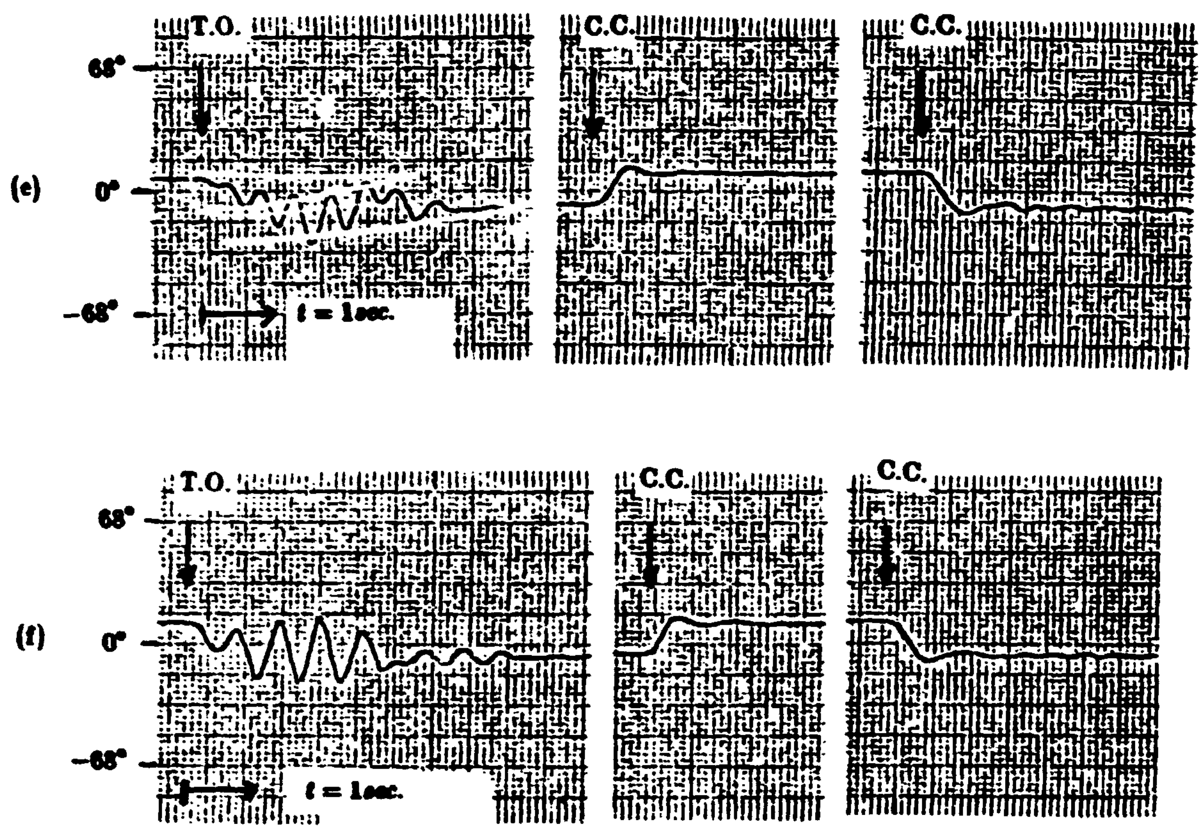

* T.O. : initial turned on.
C.C. : step command change.

Fig. 12 Step Response of the Adaptive Controller with FLL Detecting Initial Modeling Error in Plant Frequency.
(a) no error.
(b) −10% error.
(c) +25% error.
(d) −25% error.
(e) −50% error.
(f) +50% error.

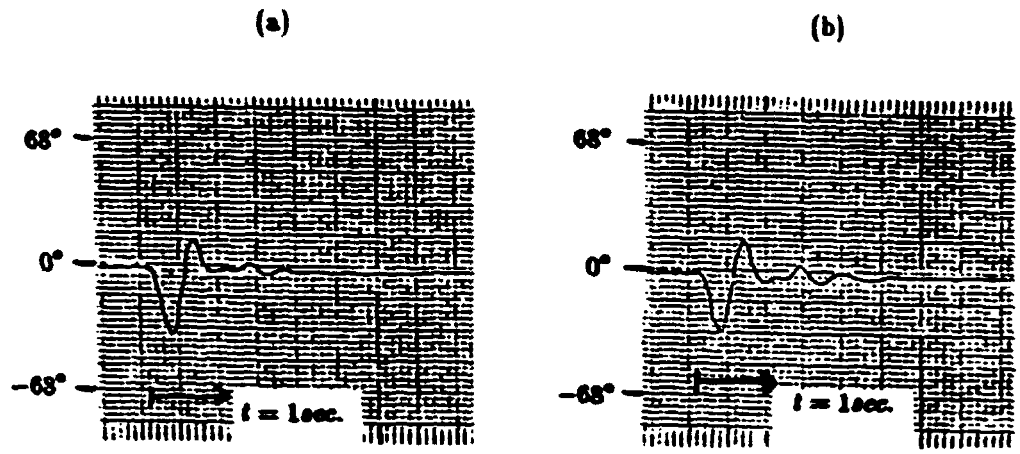

Fig. 13 Comparison of the Impulsive Disturbance Response between (a) the Nonadaptive Controller with No Modeling Error and (b) the Adaptive One after Its Parameter Error Has Been Corrected.

N85-31206

ADAPTIVE FILTERING FOR LARGE SPACE STRUCTURES—A CLOSED-FORM SOLUTION

H. E. Rauch and D. B. Schaechter
Lockheed Palo Alto Research Laboratory
Palo Alto, CA 94304

ABSTRACT

In a previous paper Schaechter proposes using an extended Kalman filter to estimate adaptively the (slowly varying) frequencies and damping ratios of a large space structure. The present paper shows that the time-varying gains for estimating the frequencies and damping ratios can be determined in closed-form so it is not necessary to integrate the matrix Riccati equations. After certain approximations, the time-varying adaptive gain can be written as the product of a constant matrix times a matrix derived from the components of the estimated state vector. This is an important savings of computer resources and allows the adaptive filter to be implemented with approximately the same effort as the non-adaptive filter. The success of this new approach for adaptive filtering has been demonstrated using synthetic data from a two mode system.

I. INTRODUCTION

Adaptive estimation and control techniques are being studied for their future application to the real-time control of large space structures, where uncertain or changing parameters may destabilize standard control system designs. In a recent paper Schaechter [1] proposes using an extended Kalman filter to estimate adaptively the (slowly varying) frequencies and damping ratios of a large space structure. For a system with N states and M (slowly varying) parameters the extended Kalman filter requires integration of an N+M by N+M nonlinear matrix Riccati equation to determine the covariance and gain for the filter. Schaechter introduces approximations which allow the integration of the nonlinear matrix Riccati equation to be replaced by integration of a smaller set of linear matrix equations. The N states of the system are estimated using constant gains determined off-line. The time-varying gains for estimating the (slowly varying) set of M parameters are determined on-line by integrating an M by N set of linear matrix equations.

The contribution of the work presented here is to show that the time-varying gains for estimating the (slowly varying) frequencies and damping ratios can be determined in closed-form so it is not necessary to integrate the M by N set of linear matrix equations. This is an important savings of computer resources and allows the adaptive filter to be implemented with approximately the same effort as the non-adaptive filter. In particular, after certain approximations the time-varying adaptive gain can be written as the product of a constant matrix times a matrix derived from the components of the estimated state vector. The constant matrix is determined off-line just as the constant gains for estimating the state are determined off-line.

The success of this new approach for adaptive filtering has been demonstrated on a computer simulation using synthetic data from a two mode system. Work in progress is applying the new approach to a much larger system using experimental data. The theoretical development and preliminary experimental results are presented in the paper.

II. FORMULATION WITHOUT ADAPTIVE FILTERING

The standard state variable formulation of the dynamic equations of motion are shown below where the dot indicates derivative, x is the state vector, u is the control vector, z is the measurement vector, and w and v are dynamic noise and measurement noise. [2]

$$\dot{x} = Fx + Gu + \Gamma w \tag{1}$$

$$z = Hx + v$$

When the dynamic system is precisely known, a state estimator of the following form may be constructed where $\hat{x}$ indicates the estimate of the state x and K is the gain matrix.

$$\dot{\hat{x}} = F\hat{x} + Gu + K(z - H\hat{x}) \tag{2}$$

The differential equation for the estimation error $\tilde{x} = x - \hat{x}$ is obtained by subtracting Eq. (2) from Eq. (1).

$$\dot{\tilde{x}} = (F - KH)\tilde{x} + \Gamma w - Kv \tag{3}$$

The differential matrix equation for the covariance of the estimation error P follows where R and Q are from the covariance of the measurement noise v an the dynamic noise w.

$$P = E(\tilde{x}\tilde{x}^T)$$

$$\dot{P} = (F - KH)P + P(F - KH)^T + \Gamma Q \Gamma^T + KRK^T \tag{4}$$

The optimal gain matrix K is chosen to minimize the trace of the estimate error covariance to give the usual result

$$K = PH^T R^{-1} \tag{5}$$

Notice that for a precisely known dynamic system, the estimation gains may be precomputed, even in the event of a time varying system. The analysis used with the adaptive filter closely parallels the development without adaptive filtering.

III. ADAPTIVE FORMULATION AND SOLUTION

Adaptive control may be required when the model in Eq. (1) is unknown, uncertain, or dependent upon a changing system configuration. The modifications that need to be made in Eq. (1) in order to include the effects of an uncertain parameter are given below where the vector parameter a has a dynamics matrix C with dynamic noise w_a,

$$
\begin{aligned}
\dot{x} &= F(a)x + Gu + \Gamma w \\
\dot{a} &= Ca + w_a \\
z &= Hx + v
\end{aligned}
\tag{6}
$$

As can be seen from Eq. (6), the system dynamics are now a function of the vector parameter a. In this formulation, the vector parameter a represents small changes from a nominal value so the average value of a is zero. These parameters are assumed to be slowly varying so that they may be adjoined to the state vector. An adaptive state estimator may be written so both the state vector and the vector of parameters are updated using the measurements.

$$
\begin{aligned}
\dot{\hat{x}} &= F(a)\hat{x} + Gu + K_x(z - H\hat{x}) \\
\dot{\hat{a}} &= C\hat{a} + K_a(z - H\hat{x})
\end{aligned}
\tag{7}
$$

Let the symmetric matrices P_x and P_a represent the covariance of the error in the estimates for x and a, respectively, and let the rectangular matrix P_{ax} represent the cross-covariance of the errors in the estimates of x and a. It is necessary to calculate these covariance matrices in order to determine the optimal gains K_x and K_a. The optimal gains are selected to minimize the trace of the covariance of the estimation error and have the following values,

$$
\begin{aligned}
K_x &= P_x H^T R^{-1} \\
K_a &= P_{ax} H^T R^{-1}
\end{aligned}
\tag{8}
$$

Proceeding as before, and assuming the estimation error $\tilde{a} = a - \hat{a}$ is small, gives the vector differential equation for the error,

$$
\begin{aligned}
\dot{\tilde{x}} &= (F - K_x H)\tilde{x} + \left(\frac{\partial F}{\partial \hat{a}}\hat{x}\right)\tilde{a} + \Gamma w - K_x v \\
\dot{\tilde{a}} &= - K_a H \tilde{x} + C\tilde{a} + w_a - K_a v
\end{aligned}
\tag{9}
$$

The matrix differential equations for the covariance are:

$$dP_x/dt = (F-K_xH)\,P_x + P_x\,(F-K_xH)^T$$
$$+ Q + K_xRK_x^T$$
$$+ (F_a\hat{x})\,P_{ax} + P_{ax}^T(F_a\hat{x})^T$$
$$dP_{ax}/dt = CP_{ax} + P_{ax}(F-K_xH)^T$$
$$+ P_a(F_a\hat{x})^T - K_aHP_x$$
$$+ K_aRK_x^T$$
$$dP_a/dt = CP_a + P_aC^T + Q_a$$
$$- K_aHP_{ax}^T - P_{ax}(K_aH)^T + K_a RK_a^T \qquad (10)$$

where $\qquad F_a = \partial F/\partial a$

and $\qquad R$, Q, and Q_a are covariances of v, Γw, and w_a (without delta function).

The remainder of this analysis will show approximations which can be used to reduce the computational effort needed to calculate the covariance matrices and the optimal gains when the covariance matrix P_a is very small (of order ϵ) and the covariance matrix P_{ax} is also very small (of order ϵ). The gain K_a will be very small (of order ϵ) because it is calculated from P_{ax}.

The differential equation for the covariance matrix P_x will involve some small terms, but most of the terms are larger and constant. If the last two terms in the differential equation for P_x are neglected (because they are small terms of order ϵ), it is possible to calculate the steady-state constant value of the covariance P_x. From the constant value of the covariance P_x the constant gain K_x can be determined. As one might suspect, the constant gain K_x has the same value as it would have if there were no errors in estimating the parameters a.

Because the covariance matrices P_{ax} and P_a are of order ϵ, many of the te[illegible] in the differential equation for P_a are of order ϵ squared. If the last [illegible] terms in the differential equation for P_a are neglected (because they are v[illegible] small terms of order ϵ squared), it is possible to calculate the steady-state value of the covariance P_a (to order ϵ). As one might suspect, the constant steady-state value obtained for P_a is the same value which would have been obtained if K_a were zero.

All that remains is to calculate the time-varying covariance P_a so that the needed gain K_a can be determined. Because the gain K_x has been [illegible] to equal $P_xH^TR^{-1}$, the last two terms in the differential equation for P_{ax} cancel out. For the remaining analysis it will be assumed there are N state variables so the first N/2 variables (designated [illegible]he N/2 length vector x*) correspond to mode position, and the last N/2 variables (designated by the N/2 length vector x**) correspond to velocity of mode position. The differential equations for the dynamics of the mode variables without any forcing or disturbing terms are presented below where A* corresponds to the damping terms ($-2\xi\omega$) and A** corresponds to the frequency terms ($-\omega^2$). Notice both A* and A** are diagonal N/2 by N/2 matrices.

$$
\begin{aligned}
dx/dt &= Fx \\
dx^*/dt &= x^{**} \qquad\qquad (11) \\
dx^{**}/dt &= A^*x^* + A^{**}x^{**}
\end{aligned}
$$

Let there be N parameters in the vector a and arrange the order of the parameters a so that the first N/2 parameters are the same as the elements of the diagonal matrix A* and the last N/2 parameters are the same as the elements of the diagonal matrix A**. Furthermore, assume the N-by-N symmetric covariance matrix P_a associated with these parameters is diagonal and composed of diagonal sub-matrices P_a* and P_a**. With these assumptions, the partial derivative can be written in a particularly simple way where x* and x** represent diagonal matrices with the diagonal elements equal to the vectors x* and x**

$$
F\hat{x} = \begin{bmatrix} 0 & I \\ A^* & A^{**} \end{bmatrix} \begin{bmatrix} x^* \\ x^{**} \end{bmatrix}
$$

$$
\begin{aligned}
F_a x &= \partial[F\hat{x}]/\partial_a \\
&= \begin{bmatrix} 0 & 0 \\ [x^*] & [x^{**}] \end{bmatrix}
\end{aligned}
$$

$$
P_a = \begin{bmatrix} P_a{}^* & 0 \\ 0 & P_a{}^{**} \end{bmatrix}
$$

$$
F_a x\, P_a = \begin{bmatrix} 0 & 0 \\ P_a{}^* & P_a{}^{**} \end{bmatrix} \begin{bmatrix} [x^*] & 0 \\ 0 & [x^{**}] \end{bmatrix} = P_a{}^{***} \cdot [\hat{x}] \qquad (12)
$$

One further assumption is that the dynamics matric C (for the parameters a) is diagonal and equal to the scalar c_0 times the identity matrix I. With those assumptions, the differential equation for the cross covariance P_{ax} can be written as follows where $\bar{x}$ is a diagonal matrix made up of the elements of x.

$$dP_{ax}/dt = P_{ax}(F-K_x H+C)^T$$

$$+ (P_a^{***}\left[\bar{x}\right])^T$$

where $$C = c_0 I$$

and $$P_a^{***} = \begin{bmatrix} 0 & 0 \\ P_a^{*} & P_a^{**} \end{bmatrix} \qquad (13)$$

The remainder of the analysis will deal with the cross-covariance matrix P_{xa} which is the transpose of the covariance matrix P_{ax}. The differential equation for the cross-covariance P_{xa} can be written as follows:

$$dP_{xa}/dt = F^* P_{xa} + P_a^{***}\left[\hat{x}\right]$$

where $$F^* = F - K_x H + C \qquad (14)$$

The linear matrix differential equation for P_{xa} has particularly desirable characteristics. All the terms in the differential equation are known constants (because the gain K_x and the covariance P_a are known and constant) except for driving terms due to estimates of the state $\hat{x}$. If the approximation is made that the derivative of the forcing terms $\hat{x}$ is equal to the dynamics matrix F times $\hat{x}$, then, except for transient terms, the solution to the linear matrix differential equation for P_{xa} can be written in closed form as a linear combination of the forcing terms $\hat{x}$. This is similar to the result in elementary linear differential equations where the general solution is composed of the sum of the homogeneous solution due to the unforced differential equation and the particular solution due to the forcing function.

Because the forcing function $\left[\hat{x}\right]$ is a diagonal matrix, the first element $\hat{x}_1$ is the forcing term for the first column of the solution for the matrix P_{ax}, the second element $\hat{x}_2$ is the forcing term for the second column of the matrix P_{ax}, and so on. Let P_i be a vector which represents the i-th column of the matrix P_{ax}. The linear matrix-vector differential equation for the i-th column can be written as follows where P_{ai} is a scalar which is the i-th element of the diagonal matrix P_a and $\hat{x}_i$ is a scalar which is the i-th element of $\hat{x}$ and P_i^* is is the i-th column of the matrix P_a^{***} which is all zeroes except for entries equal to the diagonal elements of P_a

$$dP_i/dt = F^* P_i + P_i^* \hat{x}_i \tag{15}$$

The solution for the vector P_i is assumed to be composed of the sum of two vectors. The first vector is the constant vector E_i times the scalar $\hat{x}_j$ (corresponding to the estimate of the position of the mode) and the second vector is the constant vector G_i times the scalar $\hat{x}_k$ (corresponding to the estimate of the velocity of the appropriate mode).

$$P_i = E_i \hat{x}_j + G_i \hat{x}_k \tag{16}$$

where for $i \leq N/2$ then $j = i$ and $k = i + N/2$

for $i > N/2$ then $j = i - N/2$ and $K = i$

The derivative of the vector P_i can be calculated directly if it assumed the derivative of the vector $\hat{x}$ is equal to $F\hat{x}$ with A_j^* and A_j^{**} being scalars which represent the j-th element of the representative diagonal matrices which make up F.

$$\begin{aligned} dP_i/dt &= E_i d\hat{x}_j/dt + G_i d\hat{x}_k/dt \\ &= E_i \hat{x}_k + G_i A_j^* \hat{x}_j + G_i A_j^{**} \hat{x}_k \end{aligned} \tag{17}$$

Substituting the expression for the assumed form of the vector P_i and the expression for the derivative of the vector P_i into the differential equation, gives the following equations where δ_{ij} is a discrete delta function which is unity if i equals j and zero otherwise.

$$\begin{aligned} &G_i A_j^* \hat{x}_j + (E_i + G_i A_j^{**}) \hat{x}_k \\ &= F^* E_i \hat{x}_j + F^* G_i \hat{x}_k + \delta_{ij} P_j^* \hat{x}_j + \delta_{ik} P_k^* \hat{x}_k \end{aligned} \tag{18}$$

Collecting all terms which multiply the scalar $\hat{x}_j$ gives one vector equation and collecting all terms which multiply the scalar $\hat{x}_k$ gives a second vector equation. These are two vector equations and two unknown vectors E_i and G_i.

$$\begin{aligned} G_i A_j^* &= F^* E_i + \delta_{ij} P_j^* \\ E_i + G_i A_j^{**} &= F^* G_i + \delta_{ik} P_k^* \end{aligned} \tag{19}$$

The expression for E_i obtained from the second equation is substituted into the first equations to give a single equation with the unknown vector G_i

$$G_i A_j^* = F^*(F^* G_i - G_i A_j^{**} + \delta_{ik} P_k^*) + \delta_{ij} P_j^* \tag{20}$$

Since A_j^* and A_j^{**} are both scalars, it is possible to solve directly for the unknown vector G_i where I is the identity.

$$G_i = (IA_j^* + F^* A_j^{**} - F^* F^*)^{-1}(\delta_{ij} P_j^* + \delta_{ik} F^* P_k^*) \tag{21}$$

In the same way, the expression for G_i obtained from the first equation is substituted into the second equation to give a single equation with the unknown vector E_i.

$$A_j^* E_i = (F^* - IA_j^{**})\ (F^* E_i + \delta_{ij}\ P_j^*) + A_j^* \delta_{ik} P_k^* \tag{22}$$

It is again possible to solve directly for E_i.

$$E_i = (IA_j^* + F^* A_j^{**} - F^* F^*)^{-1} \left[\delta_{ij}(F^* - IA_j^{**})P_j^* + \delta_{ik} A_j^* P_k^*\right] \tag{23}$$

Thus the two unknown vector quantities E_i and G_i can be determined from known quantities so the covariance vector P_i and the approximation for the covariance matrix P_{ax} can be determined.

IV. SIMULATION RESULTS WITH TWO MODES

The new, simplified adaptive formulation was first tested with a single mode system. After encouraging results were obtained with one mode, a two-mode system was examined. The two-mode system used in the simulation studies is shown in Figure 1.

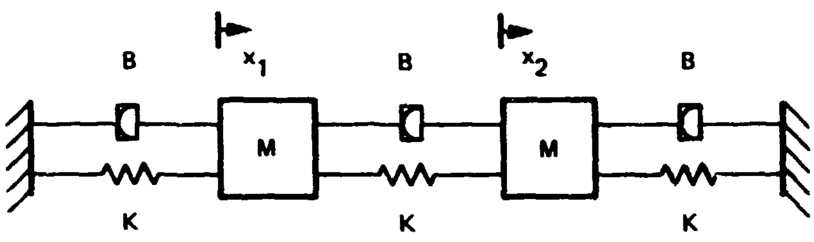

FIG. 1 TWO-MODE SYSTEM

The system consists of two masses, M, three springs, K, and three viscous dampers, B. For this study, M=1, K=1, and B=0.10. Control forces may be applied to both masses, random external forces disturb both masses, and noisy measurements of the position of both masses are available. The measurements are used for estimating the state vector, and for estimating the parameter vector. The differential equations representing this system are:

$$
\begin{aligned}
&M\ddot{x}_1 + 2B\dot{x}_1 - B\dot{x}_2 + 2Kx_1 - Kx_2 = f_1 + w_1 \\
&M\ddot{x}_2 + 2B\dot{x}_2 - B\dot{x}_1 + 2Kx_2 - Kx_1 = f_2 + w_2 \\
&z_1 = x_1 + v_1 \\
&z_2 = x_2 + v_2
\end{aligned}
\tag{24}
$$

The natural frequencies and damping ratios of this system are:

$$
\begin{aligned}
\omega_1 &= 1 & \zeta_1 &= 0.05 \\
\omega_2 &= 1.732 & \zeta_2 &= 0.0869
\end{aligned}
$$

where the low frequency mode is the common mode motion of the two masses. The spectral densities of both the process and measurement disturbances (Q and R) are 0.0163. Two hundred position measurements of both the masses were made during a sixty second computer simulation. This sixty second duration was selected to assure about ten oscillations of the lowest frequency mode. The sample rate was selected to give about ten samples per cycle of the highest frequency mode. The value of the correlation time constant for the parameters that are to be estimated was 250 seconds (so C_o is 1/250). This value is much larger than the time constants of the system. The selection of a "large" value is important in order to allow the adaptive filter to average values over several cycles of the system. The fol' wing table gives a summary of the test cases. In each case, both the standard, non-linear extended Kalman filter, and the simplified extended Kalman filter described in this paper were run in order to make comparisons. In all of the cases studied thus far, these two cases were indistinguishable, except for a small, initial transient. This transient effect is attributed to beginning the standard extended Kalman filter covariance integration with values slightly different from the steady state values.

CASE 1	ω_1 unknown ω_2 unknown	ζ_1 known ζ_2 known	no noise
CASE 2	ω_1 unknown ω_2 unknown	ζ_1 unknown ζ_2 unknown	no noise
CASE 3	ω_1 unknown ω_2 unknown	ζ_1 unknown ζ_2 unknown	noise

The results are shown i the following figures and are discussed below. In Case I the starting estimates for the natural frequencies were chosen to be 10% in error with ω_1 estimated to be 0.9 (rather than 1.0, and ω_2 estimated to be 1.559 rather than 1.732). The damping parameters were exact, and no noise was present in the system. The results for the estimate of ω_1 (Fig. 2) show that the modal frequency is very readily identified from the measurements, inspite of the 10% initial error in the estimate. As the system response diminishes, less information is available for updating the parameters. Consequently, with no new information coming into the system, the parameter estimate begins to return to its nominal value (0.9) with the selected time constant of 250 sec. The estimate of ω_2 behaves similarly.

In Case II, the objective was the same as in Case I with the additional problem of simultaneously estimating the damping parameters. The initial estimates of the damping parameters were zero. The results of the poor initial guess of the damping parameter are evident in Fig. 3. The estimate of the modal frequency tends to be lightly damped, but in all other aspects, the estimate of ω_1 appears to have the same features that were present in Case I. As has been found in past studies [1], the estimate of the damping parameter itself is quite poor. This is due to the fact that the position measurement contains very little damping information.

Case III is identical to Case II with the addition of both process and measurement disturbances. Surprisingly, this case yielded the best results, as is evident in Figures 4 and 5. The effects of the noise are clearly visible in the figures. However, in contrast with the previous two cases, the process noise continues to excite the system after the transient effect of the initial conditions have subsided. The result is that the measurements continue to provide information on the parameters for the duration of the simulation. Since the higher frequency mode is more heavily damped, and is less perturbed by the external disturbance, the improvement in the natural frequency estimate of mode two is not as dramatic.

CONCLUSIONS

This paper has developed approximations which allow dramatic reductions in the on-line computational requirements of the extended Kalman filter. Numerical simulations of this technique have validated the approach for two simple spring-mass systems. It was found that the full non-linear extended Kalman filter and the closed-form adaptive filter developed in this paper gave virtually identical results. Work is currently in progress to apply this approach to a much larger system using experimental data, rather than simulated data.

REFERENCES

(1) SCHAECHTER, D. B., "Adaptive Control for Large Space Structures", AIAA Guidance and Control Conference, Gatlinburg, Tennessee, paper no. 83-2246, August 15-17, 1983.

(2) BRYSON, A. E. and HO, Y. C., Applied Optimal Control, Blaisdell, Waltham Massachusetts, 1969.

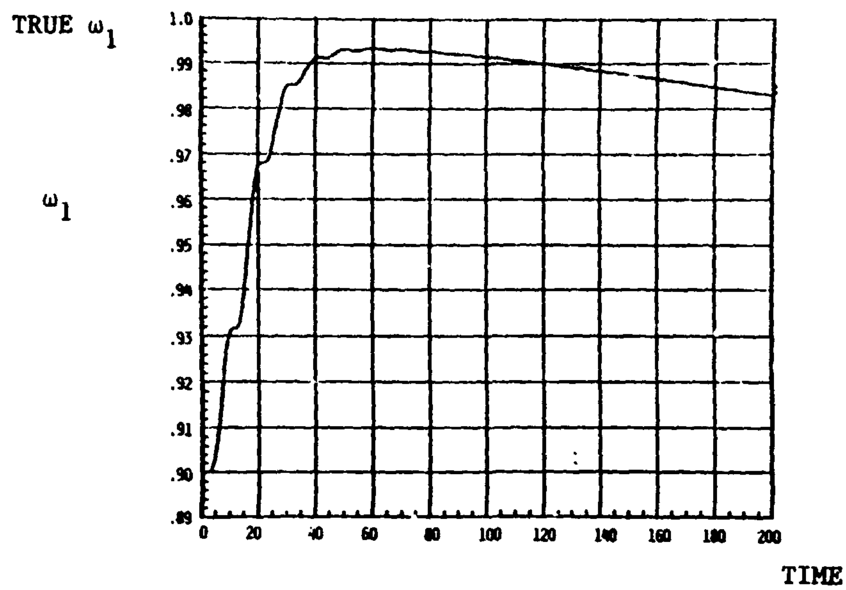

FIGURE 2 Estimate of ω_1 (CASE I)

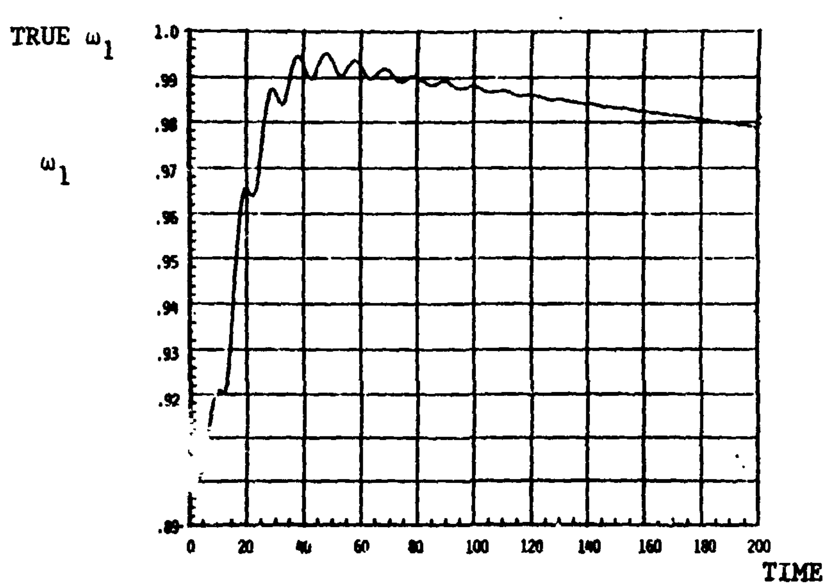

FIGURE 3 Estimate of ω_1 (CASE II)

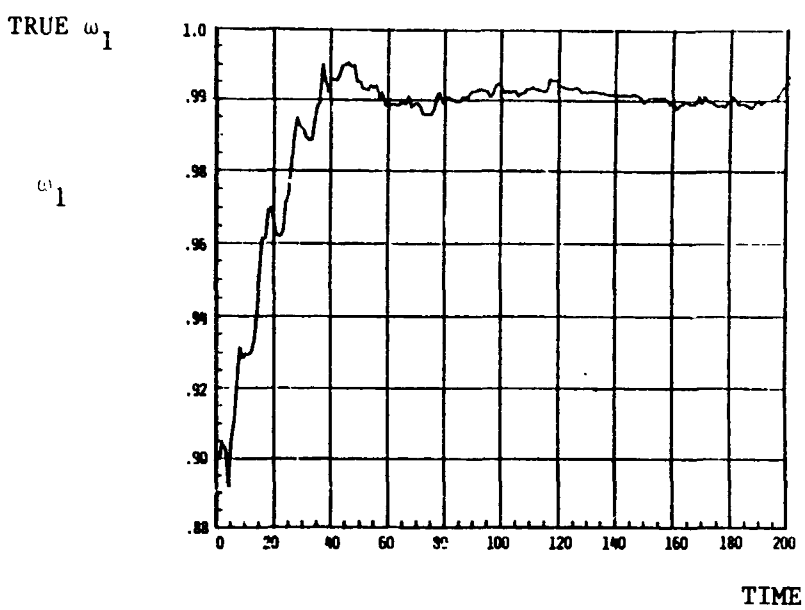

FIGURE 4 Estimate of ω_1 (CASE III)

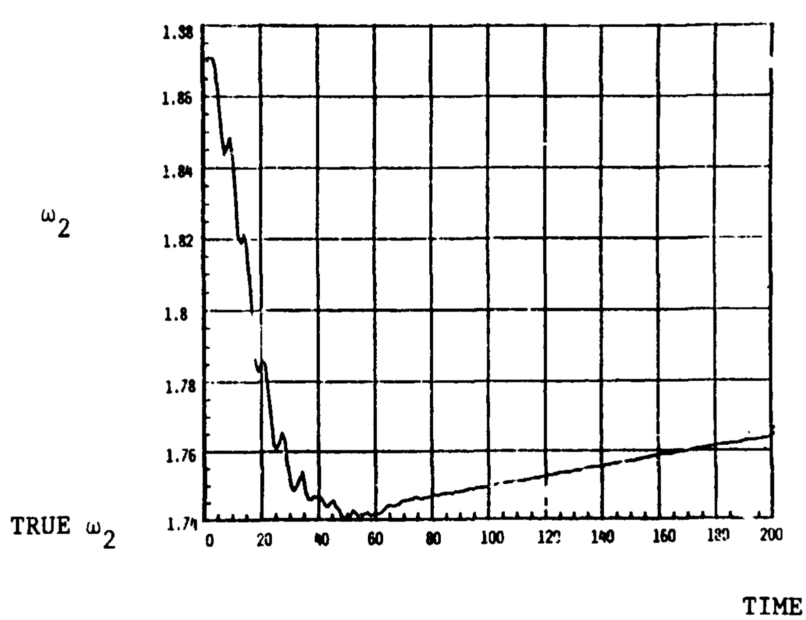

FIGURE 5 Estimate of ω_2 (CASE III)

N85-31207

ROBUST ADAPTIVE CONTROL

K. S. Narendra and A. M. Annaswamy
Yale University
New Haven, CT 06520

ABSTRACT

The paper discusses several concepts and results in robust adaptive control and is organized in three parts. The first pa... surveys existing algorithms. Different formulations of the problem and theoretical solutions that have been suggested are reviewed here. The second part contains new results related to the role of persistent excitation in robust adaptive systems and the use of hybrid control to improve robustness. In the third part promising new areas for future research are suggested which combine different approaches currently known.

1. INTRODUCTION

The stable adaptive control of linear time invariant plants, in what is now termed "the ideal case", was resolved in 1980 [1-4]. The assumptions made in [1-4] regarding the plant to prove global stability are quite stringent. Specifically, knowledge of the sign of the high frequency gain K_p, the relative degree n^* and an upper bound n on the order of the plant transfer function are assumed to be known. Further it is assumed that the zeros of the plant transfer function lie in the left half plane, the plant parameters are constant (though unknown) and the system is disturbance free. However, in practice, these assumptions are rarely met. No actual plant is truly linear, finite dimensional or noise free. Further, in practical situations, the rationale for using adaptive control is to compensate for large variations in plant parameters. In the presence of such deviations from ideal conditions, the algorithms suggested in [1-4] no longer assure the boundedness of the signals in the adaptive loop. This accounts for the wide interest in the past few years in what is termed robust adaptive control to achieve satisfactory performance in the prese..ce of both modeling and operating uncertainties. This paper attempts to survey some of the modest gains that have been made in this direction, presents some new results for improving robustness and discusses promising directions for future research.

Adaptive systems are special classes of nonlinear systems and many questions which arise in such systems can be stated as problems in the stability theory of differential equations. In particular, questions of robustness can be addressed using amply discussed results on practical stability and total stability. Since such results are bound to find increased application in adaptive systems, some of the more frequently used concepts, definitions and theorems are collected in section 2.

Recent years have witnessed many contributions to the robustness problem. Among these some assume additional prior information regarding the un..rtainties to suitably modify the adaptive algorithms [5-9] while others ass... that the reference inputs possess properties which make the ideal system e..ponentially

 PRECEDING PAGE BLANK NOT FILMED

stable. In all cases it is shown that boundedness of solutions is assured when the true situation deviates in specific ways from the ideal. Some of these analytical results which are currently known are presented in section 3.

Sections 4 and 5 contain some new results on persistent excitation and hybrid adaptive control which are relevant to the problem of robustness. In section 4 a nonlinear error equation of second order is discussed in detail. While the ideal system is uniformly asymptotically stable it is shown that unbounded solutions can result if the disturbance is sufficiently large. It is also shown that by increasing the degree of persistent excitation of the reference input the overall system can be made practically stable. Section 5 discusses hybrid control algorithms recently introduced by the authors [10]. The same algorithms can also be modified to adaptively control discrete plants by updating control parameters infrequently. Some plausible arguments are given towards the end of the section as to why such algorithms may be more robust than continuous algorithms when external bounded disturbances are present.

Finally, in section 6, possible ways of combining known methods are discussed in the hope that it will stimulate research in these new directions. While no hard results exist in these areas the suggestions are based on extensive simulation studies.

2. MATHEMATICAL PRELIMINARIES AND STABILITY RESULTS

Some well known concepts and results of stability theory which find frequent application in the analysis of adaptive systems are included in this section. While they can be readily found in any good text [11-13] we present them here for easy reference as well as to place some of the problems discussed in the following sections in proper perspective. We start with the definitions of uniform asymptotic and exponential stability of the solution $x = 0$ of an equation $\dot{x} = f(x,t)$, $f(0,t) = 0$. We assume that f is continuous and satisfies conditions which guarantee the existence and uniqueness of solutions and continuity of their dependence on the initial conditions. The general solution of the differential equation is denoted as $p(t,x_0,t_0)$ with $p(t_0,x_0,t_0) = x_0$.

(i) Definition (Uniform Asymptotic Stability): The equilibrium $x = 0$ of the differential equation $\dot{x} = f(x,t)$ is uniformly asymptotically stable if it is uniformly stable and for some $\varepsilon_1 > 0$ and all $\varepsilon_2 > 0$ there is a $T(\varepsilon_1,\varepsilon_2) > 0$ such that $\|x_0\| < \varepsilon_1$ implies $\|p(t,x_0,t_0)\| < \varepsilon_2$ for all $t \geq t_0 + T$.

(ii) Definition (Exponential Stability): The equilibrium state of the equation $\dot{x} = f(x,t)$ is exponentially stable if two positive constants α and β which are independent of the initial values exist such that for sufficiently small initial values, $\|p(t,x_0,t_0)\| < \beta\|x_0\|e^{-\alpha(t-t_0)}$.

A linear time-invariant system with $f(x,t) = Ax$ where A is a constant matrix is asymptotically stable if the eigenvalues of A are in the open left half of the complex plane. Asymptotic, uniform asymptotic and exponential stability are equivalent in this case. For linear time-varying systems, asymptotic stability does not imply uniform asymptotic stability whereas the latter is equivalent to exponential stability. For linear systems, all stability properties hold in the large. In general, for nonlinear systems exponential stability implies uniform asymptotic stability but not vice versa. If $f(x,t)$ is autonomous or periodic in t, all stability properties are uniform.

In robust adaptive control we are interested in deducing the properties of the solutions of a perturbed system (S_p) from the behavior of the solutions of an unperturbed system (S). These are described by the differential equations

$$\dot{x} = f(x,t) \quad (S) \; ; \qquad \dot{x} = f(x,t) + g(x,t) \quad (S_p) \tag{1}$$

Let the equilibrium state of (S) be exponentially stable. If $\|g(x,t)\| < L\|x\|$ for sufficiently small b and δ, and $\|x\| < \delta$, then the equilibrium state of (S_p) is also exponentially stable [11]. In physical situations the condition $g(0,t) = 0$ required above is not generally met and this gives rise to the concept of total stability.

(iii) Definition (Total Stability) [11]: The equilibrium state $x = 0$ of (S) is totally stable if for every $\varepsilon > 0$ two positive numbers $\delta_1(\varepsilon)$ and $\delta_2(\varepsilon)$ exist such that every solution $p(t,x_0,t_0)$ of (S_p) satisfies $\|p(t,x_0,t_0)\| < \varepsilon$, $t \geq t_0$ provided $\|x_0\| < \delta_1$ and $\|g(x,t)\| < \delta_2$.

In the Russian literature this is also referred to as stability under persistent disturbances. The uniform asymptotic stability of the unperturbed system implies total stability [11] and is frequently used to prove robustness of adaptive systems in the presence of sufficiently small perturbations. Recently the magnitude constraint on $\|x_0\|$ in the definition of total stability has been relaxed by Anderson and Johnstone [8] at the expense of stronger conditions on $f(x,t)$.

In practical systems we are interested in the uniform boundedness of the solutions in the presence of perturbations as well as in the magnitudes of this bound. This leads to the concept of practical stability defined below.

(iv) Definition (Practical Stability) [12]: Let $Q_0 = \{x \mid \|x\| < \delta_1\}$ be open set in $\mathbb{R}^n$ and $\delta_2 > 0$ a constant such that $\|g(x,t)\| < \delta_2$ for all x and $t \geq t_0$. If the solutions of (S_p) lie within a closed bounded set $Q \supset Q_0$ for $x_0 \in Q_0$ then the system (S) is said to be practically stable.

Total stability assures the existence of Q_0 and δ_2 relative to which the system (S) is practically stable but provides no way of estimating the size of Q_0 or the magnitude of δ_2. In adaptive control applications this is not adequate. One is more interested in determining an estimate of Q from a knowledge of δ_2.

An alternative method for treating the effect of perturbations is by considering them as bounded independent functions of time. This leads to the well known concept of bounded input - bounded output (BIBO) stability.

(v) Definition (BIBO Stability): A system $\dot{x} = f(x,u,t)$ with $f(\cdot,0,t) = 0$ is BIBO stable if for every $\alpha \geq 0$ and every $a \geq 0$ there is a $\beta = \beta(\alpha,a)$ such that $\|p_u(\tau,x_0,t_0)\| \leq \beta$ for all $\tau \geq t_0$ for every initial condition (x_0,t_0) with $\|x_0\| \leq \alpha$ and $\sup_t \|u(t)\| \leq a$, where $p_u(\cdot,x_0,t_0)$ is the solution of the system with input $u(\cdot)$.

A linear system $\dot{x} = A(t)x + b(t)u$ is BIBO stable if the homogeneous part is uniformly asymptotically stable. This is a property which is frequently used in robust adaptive control using the concept of persistent excitation. In contrast to the above, uniform asymptotic stability of a nonlinear system does not imply BIBO stability. An example of this was given by Desoer et al [14]. A similar situation arises in the discussion of robustness of a second order nonlinear system in section 4.

Stability Problems in Adaptive Systems: The study of the stability of adaptive systems (as shown in the following sections) can be conveniently carried out using a set of nonlinear time-varying error differential equations. Even in the "ideal" or disturbance free case the time-variations arise due to the presence of the reference input $r(\cdot)$. The following are some noteworthy features of many of the stability questions which arise in adaptive systems.

(i) In the ideal case, a Lyapunov function $V > 0$ with $\dot{V} \leq 0$ can be found. The negative semi-definiteness of $\dot{V}$ cannot be avoided and is a result of the adaptive law used.

(ii) As a result of (i) even the unforced (autonomous) system is uniformly stable. Even when the reference input is persistently exciting, $\dot{V} \leq 0$ but the system can be shown to be uniformly asymptotically stable [15]. We note that LaSalle's theorem cannot be directly applied to prove this since the system is nonautonomous.

(iii) Since the system is exponentially stable with a persistently exciting reference input, Malkin's theorem can be used to conclude that the solutions will be bounded for some initial set Q_0 and perturbation of magnitude $\leq \delta_2$. However, very little can be said directly about either Q_0 or δ_2.

(iv) Another consequence of the semidefiniteness of $\dot{V}$ is that assuring even the boundedness of solutions using Lyapunov's Direct method for given bounds on perturbations is no longer trivial. Some of these cases are considered in section 3. In section 4 it is shown that even when the reference input is persistently exciting, if the disturbance is large the solutions can be unbounded. Alternately, for a given bound on the disturbance the persistent excitation can be made sufficiently large to assure the boundedness of the solutions.

3. RECENT RESULTS IN ADAPTIVE CONTROL

In this section we attempt to survey briefly some of the theoretical results currently known in the area of robust adaptive control. The aim of the section is to provide an understanding of the qualitative ideas that led to these results as well as the analytical tools used in deriving them. Since the ideal system forms the starting point of all perturbation analyses, we shall briefly outline the statement of the problem and the proof of stability in this case. Further, while several stable adaptive algorithms have been suggested in the literature, we shall discuss the proof of stability using only the algorithm proposed in [16]. The proofs using all the other algorithms follow along similar lines.

a) Ideal System: The plant to be controlled is described by the state equations

$$\dot{x}_p = A_p x_p + b_p u \quad ; \quad y_p = c_p^T x_p \tag{2}$$

and a reference model is described by

$$\dot{x}_m = A_m x_m + b_m r \quad ; \quad y_m = c_m^T x_m \tag{3}$$

where x_p, u and y_p are respectively the state input and output of the plant and x_m and y_m are the state and output of the model. The transfer functions of the plant and model are

$$W_p(s) = c_p^T(sI-A_p)^{-1}b_p = \frac{K_p Z_p(s)}{R_p(s)} \quad ; \quad W_m(s) = c_m^T(sI-A_m)^{-1}b_m = \frac{K_m}{R_m(s)}$$

The following assumptions are made regarding $W_p(s)$ and $W_m(s)$

(i) $Z_p(s)$, $R_p(s)$ and $R_m(s)$ are monic polynomials of degrees m, n and $n^*=n-m$

(ii) $Z_p(s)$ and $R_m(s)$ are strictly stable polynomials

and (iii) r is a piecewise continuous uniformly bounded reference input.

The objective is to control the plant in such a fashion that the output error between plant and model $e_1 \triangleq y_p - y_m$ tends to zero asymptotically, while the signals and parameters of the system remain uniformly bounded. It is now well known that knowledge of the exact relative degree n^* of the plant, an upper bound n on its order, the sign of the gain K_p and the condition that $Z_p(s)$ be Hurwitz as given in (ii) are needed to solve the problem. n^* enables the model to be constructed while the value of n determines the order of the controller to be used. The sign of K_p and the constraint on $Z_p(s)$ are needed to prove the stability of the overall system.

Structure of Controller: In the following we shall assume that K_p is known and $K_p = K_m = 1$. To meet the control objective a controller described by the following equations is used:

$$\dot{\omega}^{(1)} = F\omega^{(1)} + gu \quad ; \quad \dot{\omega}^{(2)} = F\omega^{(2)} + gy_p \quad ; \quad u = \theta^T\omega + r \tag{4}$$

where F is an asymptotically stable nxn matrix, (F,g) is controllable, $\omega^T = [\omega^{(1)^T}, \omega^{(2)^T}]$ and $\theta(t)$ is a 2n dimensional parameter vector which is to be adjusted adaptively. It is well known [17] that a unique constant vector θ^* exists such that the transfer function of the plant together with the controller matches that of the model exactly, when $\theta(t) \equiv \theta^*$. The aim of the adaptive law is to adjust $\theta(t)$ in such a manner that the overall system is globally stable and $\lim_{t\to\infty} e_1(t) = 0$.

While several special cases of the adaptive control problem have been considered, we discuss below the general case when $W_p(s)$ has a relative degree $n^* \geq 2$. If $\theta(t) - \theta^* \triangleq \phi(t)$, then ϕ is the parameter error vector and the output of the plant can be expressed as

$$y_p(t) = W_m(s)[r(t) + \phi^T(t)\omega(t)] \tag{5}$$

The Adaptive Scheme: To generate the adaptive law an auxiliary error signal $y_a(t)$ is added to $e_1(t)$ to generate an augmented error $\varepsilon_1(t)$. If

$$y_a(t) \triangleq [\theta^T(t)W_m(s)I - W_m(s)\theta^T(t)]\omega(t) \tag{6}$$

then

$$\phi^T(t)\zeta(t) = e_1(t) + y_a(t) = \varepsilon_1(t) \tag{7}$$

where $W_m(s)I\omega = \zeta$. The adaptive law for updating $\theta(t)$ then depends on the augmented error $\varepsilon_1(t)$ and the signal $\zeta(t)$ and is given by

$$\dot{\phi}(t) = \dot{\theta}(t) = \frac{-\varepsilon_1(t)\zeta(t)}{1 + \zeta^T(t)\zeta(t)} \tag{8}$$

This has been shown to result in global stability of the adaptive loop [16].

Proof of Global Stability: If $V(\phi) = 1/2\ \phi^T\phi$, the adaptive law (8) yields

$$\dot{V}(\phi) = \frac{-\varepsilon_1^2(\phi)}{1 + \zeta^T(t)\zeta(t)}$$

from which it follows that

(i) ϕ and $\dot{\phi}$ are uniformly bounded

(ii) $\dot{\phi} \in L^2$ (9)

and (iii) $\varepsilon_1(t) = \nu(t)[1 + \zeta^T(t)\zeta(t)]^{1/2}$, $\nu \in L^2$

Since the complete proof is too long and involved to be included here in its entirety we merely outline the principal steps involved.

(a) Since the parameter vector is bounded by (i) it is first shown that

$$\sup_{\tau\leq t}|y_p(\tau)| \sim \sup_{\tau\leq t}\|\omega^{(2)}(\tau)\| \sim \sup_{\tau\leq t}\|\omega(\tau)\| \sim \sup_{\tau\leq t}\|\zeta(\tau)\| \tag{10}$$

Here $\sim$ is an equivalence relation and implies that the corresponding signals in (10) grow at the same rate [18].

(b) Since $\dot{\phi} \in L^2$ it can be shown that $y_a(t)$ grows at a slower rate than $\sup_{\tau\leq t}\|\omega(\tau)\|$ denoted by $y_a(t) = o[\sup_{\tau\leq t}\|\omega(\tau)\|]$. (11)

(c) From (5), (9-iii) and (11) it follows that

$$e_1 = W_m\phi^T\omega = \nu[1 + \zeta^T\zeta]^{1/2} + o[\sup_{\tau\leq t}\|\omega(\tau)\|] \tag{12}$$

(d) Since $\nu \in L^2$ using equation (4) we conclude that $\sup_{\tau\leq t}\|\omega^{(2)}(\tau)\| = o\ \sup_{\tau\leq t}\|\omega(\tau)\|$ which contradicts (10).

Hence all the signals in the system are uniformly bounded and $\lim_{t\to\infty} e_1(t) = 0$.

The importance of demonstrating the boundedness of $\phi(t)$ and $\dot{\phi} \in L^2$ in the proof of stability is worth noting. [In some cases it may be possible to show that $\lim_{t\to\infty} \dot{\phi}(t) = 0$, which serves the same purpose.] The former assures that the relevant signals in (10) grow at the same rate while the latter is used to prove that $|y_p(t)|$ and $\|\omega_2(t)\|$ should grow at different rates if the adaptive control is used, leading to a contradiction.

Asymptotic Stability of the Ideal System: Once the boundedness of all the signals in the adaptive system has been established, interest shifts to the convergence of the parameter vector $\theta(t)$ to its desired value θ^* or equivalently of $\phi(t)$ to the null vector. Since the adaptive law (8) can be represented as

$$\dot{\phi}(t) = \frac{-\zeta(t)\zeta^T(t)}{1 + \zeta^T(t)\zeta(t)}\,\phi(t) \tag{13}$$

the conditions that have to be imposed on $\zeta(t)$ to accomplish this is of interest. Following the results of Morgan and Narendra [19] if $\dfrac{\zeta(t)}{\sqrt{1 + \zeta^T(t)\zeta(t)}}$ is persistently exciting $\lim_{t\to\infty} \phi(t) = 0$ and the convergence is exponential. Since $W_m(s)I\omega = \zeta$, a sufficient condition for $\zeta(\cdot)$ to be persistently exciting is that $\omega(\cdot)$ is persistently exciting [15]. Hence conditions under which $\omega(\cdot)$ will be persistently exciting have been investigated by several authors [15,20-22].

Persistent Excitation (PE) of $\omega(t)$ and $\omega^*(t)$: Early results on the convergence of the parameter vector to the null vector were stated in terms of the PE of $\omega(t)$. However since $\omega(t)$ is a dependent variable within the adaptive loop, very little can be said directly about its persistent excitation. Hence attempts were made to express this condition in terms of the PE of signals in the model which are at the discretion of the designer. Since the adaptive system and model transfer functions are identical when $\theta(t) \equiv \theta^*$, the model can be parametrized in such a fashion that a signal ω^* in it would correspond to the signal $\omega(t)$ in the adaptive loop. Further since the model is time invariant, conditions on $r(t)$ which would assure the PE of $\omega^*(t)$ can be derived. If $\tilde{\omega}(t) \triangleq \omega(t) - \omega^*(t)$, the adaptive law assures that $\lim_{t\to\infty} \tilde{\omega}(t) = 0$. Hence, in the ideal case the PE of $\omega^*(t)$ ensures the PE of $\omega(t)$ and hence the convergence of the parameter vector $\theta(t)$ to its true value.

Comments:

(i) The above arguments have focussed attention on several interesting questions related to persistent excitation and transformations under which the property is preserved [15].

(ii) The convergence of $\tilde{\omega}(t)$ to 0 is used above to show the PE of $\omega(t)$ and hence the convergence of $\phi(t)$ to 0. This is no longer possible when an external disturbance is present since even the boundedness of the signals is not assured in such a case.

(iii) From the results of several authors it is now known that an almost periodic reference input with n-distinct frequencies results in the PE of $\omega(t)$.

b) Adaptation Under Perturbations: The adaptive control system described in section (3a) assumed ideal conditions. The plant was linear and time-invariant and no external disturbances were present. In addition, considerable prior knowledge of plant transfer characteristics was assumed to help in setting up a reference model and deriving stable adaptive laws. As mentioned earlier, plants are rarely strictly linear or finite dimensional and in many practical situations the need for adaptive control arises due to large parameter variations. Also, external input and output disturbances are invariably present in real systems. Hence there is a definite need to extend the theory developed for the ideal case to situations with modeling errors and external disturbances. Some of the schemes that have been proposed in recent years to achieve robustness in the presence of such perturbations are briefly reviewed in this section and some new results are reported in sections 4 and 5.

The basic adaptive system in the ideal case is only uniformly stable. This implies that bounded perturbations can theoretically produce unbounded outputs. When the reference input is persistently exciting, the nonlinear system is uniformly asymptotically stable in the large and exponentially stable when the initial state x_0 lies in a finite ball around the origin. The latter fact allows BIBO results to be derived using theorems of the type described by Malkin, provided the perturbations are sufficiently small. However, as pointed out in section 2, very little can be said using such an approach about the effect of bounded perturbations of a specified maximum amplitude on the global behavior of the solutions of the adaptive system. In addition to such perturbation methods a few global methods have also been used to derive results in robust adaptive systems. The principal concepts involved in deriving some of these are discussed below.

(i) Use of Dead-Zone [5]: The problem statement is similar to that given for the ideal system with the exception that $y_p = c_p^T x_p + v_1$ where v_1 is a bounded disturbance. Using the same adaptive law (8) as in the ideal case, the error equations can be expressed as

$$\phi^T(t)\zeta(t) + v(t) = \varepsilon(t) \tag{14}$$

and

$$\dot{\phi}(t) = \frac{-\Gamma\varepsilon(t)\zeta(t)}{1 + \zeta^T(t)\Gamma\zeta(t)} \qquad \text{(adaptive law)}$$

where v is an equivalent output disturbance due to v_1. The difficulty arises due to the presence of $v(t)$ in (14). When $\mathrm{sgn}[\phi^T\zeta + v] = \mathrm{sgn}[\phi^T\zeta]$ the adaptation is in the right direction. Otherwise the parameter vector may be adjusted away from its desired value. This implies that problems of convergence may arise when $\varepsilon(t)$ is of the order of the vound v_0 of $v(t)$. The modification in the algorithm suggested in [5] is to use a dead-zone so that the adaptive parameters are not adjusted when $\varepsilon(t)$ lies inside it. Hence the overall system operates in two modes-- a linear time-invariant mode when $|\varepsilon(t)| \leq v_0 + \delta$ (for some constant $\delta > 0$) and an adaptive mode otherwise. In [5] it is shown that such an algorithm results in a system with bounded signals. Further, adaptation takes place for only a finite time. This implies that in practice the system will converge to a linear time-invariant system in a finite time after which the output error will lie entirely in the dead-zone and hence adaptation ceases entirely.

(ii) Bound on $\|\theta^*\|$: An alternate approach to the bounded disturbance problem was taken by Kreisselmeier and Narendra [6]. While the statement of the problem as well as the structure of the controller are identical to that in (i), it is assumed that no knowledge of a bound on the disturbance is available. Instead, it is assumed that the desired vector θ^* has a norm less than a specified value $\|\theta^*\|_{max}$. Hence the search procedure can be confined essentially to the set $S:\{\theta \mid \|\theta\| \leq \|\theta^*\|_{max}\}$. The adaptive law used to update $\theta(t)$ is identical to that in the ideal case when θ lies in the interior of S and is modified when it reaches the boundary of S, or lies outside it. In [6] it is shown that such a scheme results in the boundedness of all signals in the system.

Apart from the obvious differences between the schemes suggested in [5] and [6], there are mathematical differences in the proof that are worth stressing. As in [1-4], the proofs of stability in [5] use limiting arguments as $t \to \infty$ to show that $\dot{\phi} \in L^2$. Such a procedure cannot be used in [6], since $\phi(t)$ does not tend to any limit as $t \to \infty$. Hence all arguments are based on the analysis of the behavior of the system over a finite interval. As shown in section 6 the approaches in [5] and [6] complement each other and can be combined to have wider application in adaptive systems in the future.

(iii) The σ-modification Scheme: In approaches (i) and (ii) certain prior information is assumed to implement the adaptive laws. In contrast to this, a scheme suggested by Ioannou and Kokotovic [7] assures boundedness of all signals in the system, without any assumptions regarding the bounds on either the disturbance or the control parameters. However, to the authors' knowledge, the method has been shown to result in global boundedness only for the special case when the reference model is strictly positive real.

The method is based on the following simple ideas. If $V(e,\phi)$ is a quadratic Lyapunov function candidate, the time derivative $\dot{V}(e,\phi)$, along a trajectory, is generally a quadratic function of e and hence is negative semidefinite. When a disturbance is present, $\dot{V}(e,\phi)$ has the general form $-e^TQe + e^T\alpha v$, where $Q = Q^T > 0$, α is a constant vector and v is a bounded disturbance. Very little can be concluded regarding stability from this and accounts for the modifications suggested in [5] and [6]. In [7], an additional term $-\sigma\theta$ is used in the adaptive law, as a result of which $\dot{V}(e,\phi)$ becomes negative definite outside a bounded region in the (e,ϕ) space. From this it is concluded that all signals in the system are bounded.

(iv) Adaptive Systems and Time-Varying Plants: The methods outlined in sections 3b(i-iii) deal with the global behavior of the adaptive systems when bounded perturbations are present. In contrast to this Anderson and Johnstone [8] examine adaptive control problems where the assumptions made regarding the system deviate slightly from the ideal. While [8] addresses primarily the problem of time-varying plant parameters the authors claim that the same methods with remarkably little change allow examination of the effect of measurement noise, plant nonlinearity and undermodelling of the plant order.

As in our discussions in section (3a), the authors first consider the ideal system and demonstrate uniform or exponential stability in the presence of persistent excitation. For the various types of perturbations considered, their aim is then to show that the resulting equations can be cast in such a form that the total stability of the overall system can be demonstrated using modifications of Malkin's theorems. However, as mentioned earlier, the theorems are useful primarily for establishing the existence of robustness in the presence of sufficiently small perturbations rather than for providing guidance in the choice of the control input to assure boundedness of solutions when the class of perturbations is specified.

4. PERSISTENT EXCITATION AND ROBUSTNESS

In the last section, we discussed two approaches of studying the robustness problem in adaptive systems. The approach in 3-d assumed that the perturbations were sufficiently small and derived BIBO results local in nature, using Malkin's theorem, whereas in 3a-3c the approach was global in nature and used additional information regarding plant dynamics and the external perturbations. Also, the first approach made use of the PE of the reference input which was not needed in the second.

In this section, we present some new results which demonstrate global boundedness of all signals in the adaptive system in the presence of bounded disturbances when the reference input is sufficiently persistently exciting. We show that by analyzing a set of nonlinear error differential equations, we can establish the global robustness behavior of the adaptive systems. In particular, it is shown that if the persistent excitation of the model output is larger than the disturbance, the solutions will be globally bounded and that if the maximum amplitude of the disturbance is greater than that of the model output, the system can have unbounded solutions. The basic idea is stated here by considering the adaptive control of a first order plant and studying the corresponding second order nonlinear differential equations in detail. The same methodology is applicable to the general adaptive control problem.

Nonlinear Error Equations: The plant to be adaptively controlled, the corresponding reference model and the resulting error equations are as follows:

$$\begin{aligned}
&\text{Plant:} && \dot{y}_p = a_p y_p + u + v; \quad u = \theta y_p + r \\
&\text{Model:} && \dot{y}_m = -y_m + r \\
&\text{Error Equations:} && \dot{e}_1 = -e_1 + \phi y_p + v \\
&\text{Adaptive Law:} && \dot{\phi} = -e_1 y_p
\end{aligned} \tag{15}$$

where r is the reference input, v is a bounded input disturbance, e_1 is the output error defined as $e_1 \triangleq y_p - y_m$ and ϕ is the parameter error. In the ideal case, when $v(t) \equiv 0$, by considering

$$\begin{aligned}
\dot{e}_1(t) &= -e_1(t) + \phi(t)y_p(t) \\
\dot{\phi}(t) &= -e_1(t)y_p(t)
\end{aligned} \tag{16}$$

it immediately follows that the system is uniformly stable and if $y_p(t)$ is persistently exciting, the system is exponentially stable. When a disturbance

$v(t)$ is present, it is tempting to proceed as in the ideal case and require $y_p(t)$ in (15) to be persistently exciting so that the unperturbed system is exponentially stable resulting in a bounded error vector for bounded perturbations. Since stability of the overall system has not been established, $y_p(t)$ cannot be assumed to be bounded and proving that it is PE becomes specious. Hence we have to express the right hand side of (15) in terms of the model output $y_m(t)$ which is an independent variable rather than the dependent variable $y_p(t)$. This results in the following nonlinear error differential equations:

$$\begin{aligned} \dot{e}_1(t) &= -e_1(t) + \phi(t)y_m(t) + \phi(t)e_1(t) + v \\ \dot{\phi}(t) &= -e_1(t)y_m(t) - e_1^2(t) \end{aligned} \tag{17}$$

By analyzing the above nonlinear differential equation, we demonstrate the global behavior of the adaptive system in the presence of $v(t)$.

The Ideal System: In the absence of external perturbations, the nonlinear system

$$\begin{aligned} \dot{e}_1(t) &= -e_1(t) + \phi(t)y_m(t) + \phi(t)e_1(t) \\ \dot{\phi}(t) &= -e_1(t)y_m(t) - e_1^2(t) \end{aligned} \tag{18}$$

can be shown to be uniformly asymptotically stable in the large as follows: If $W(e_1,\phi) = \frac{1}{2}[e_1^2 + \phi^2]$, the time-derivative $\dot{W}[e_1,\phi] = -e_1^2 \leq 0$. Hence the system $e_1(t)$ and $\phi(t)$ are uniformly bounded for all $t \geq t_0$, if $W[e_1(t_0),\phi(t_0)] < \infty$. Since $e_1 \in L^2$ and $\dot{e}_1$ is bounded, $\lim_{t\to\infty} e_1(t) = 0$. The nonlinear vector $[\phi e_1, -e_1^2]^T$ can be considered to be the input to the linear part which is exponentially stable if $y_m(t)$ is PE. As $e_1 \to 0$ as $t \to \infty$, this input tends to zero and hence $x(t) \to 0$ as $t \to \infty$ where $x \triangleq [e_1,\phi]^T$. Since all the arguments are independent of the initial time t_0 and the magnitude of the initial conditions, the system is u.a.s.l. It is also worth noting that when $y_m(t)$ is PE, the linear part of (18) is exponentially stable but the nonlinear system is exponentially stable only when the initial state $x(t_0)$ lies in a finite ball around the origin and not globally exponentially stable.

Perturbed System: To provide some insight into the behavior of the nonlinear system, we shall discuss three cases where the perturbed nonlinear system (17) is autonomous.

Case (i) $y_m(t) \equiv 0$: When $v(t) \equiv 0$, the system is uniformly stable. If $v(t) \equiv v_{max}$, $\lim_{t\to\infty} \phi(t) = -\infty$ and $\lim_{t\to\infty} e_1(t) = 0$.

Case (ii) $y_m(t) \equiv y_{max}$: The unforced system in this case is autonomous and, by LaSalle's theorem, is u.a.s.l. since the largest invariant set in $E = \{x | e_1^2 = 0\}$ is the origin. However, since the system is nonlinear, it no longer follows that a bounded input will result in a bounded output. If, for example, $v(t) \equiv -v_{max}$, where $v_{max} > y_{max}$, we can show that $\lim_{t\to\infty} e_1(t) = -y_{max}$ and $\lim_{t\to\infty} \phi(t) = -\infty$.

Case (iii) $y_m(t) \equiv y_{max}, y_{max} > v_{max}$: The system is Lagrange stable. When $v(t) \equiv -v_{max}$, the system has an equilibrium state at $(0, \frac{v_{max}}{y_{max}})$ which is u.a.s.l. Similarly when $v(t) \equiv v_{max}$, the system has an equilibrium state at $(0, -\frac{v_{max}}{y_{max}})$.

The above special cases reveal that the behavior of the nonlinear system is very much dependent on y_{max} and v_{max}. In particular, when $y_m(t) \equiv y_{max}$ and $v(t) \equiv -v_{max}$, the system has unbounded solutions when $v_{max} > y_{max}$ and all solutions are bounded when $y_{max} > v_{max}$. The results also carry over to the general case when both $v(t)$ and $y_m(t)$ are time-varying and are stated in the following main theorem of the paper. (Fig. 1)

Theorem 1: Let $|y_m(t)| \leq y_{max}$, $|v(t)| \leq v_{max}$ and $y_m(t)$ be a smooth persistently exciting signal in the sense described in [23]. This implies that positive numbers T_0, ε_0 and δ_0 exist such that given any $t_1 \geq 0$, there exists a $t_2 \in [t_1, t_1 + T_0]$, with $[t_2, t_2 + \delta_0] \subset [t_1, t_1 + T_0]$ and $\frac{1}{T_0} \left| \int_{t_2}^{t_2+\delta_0} y_m(\tau)d\tau \right| \geq \varepsilon_0$. Then

(a) If $y_{max} < v_{max}$, by choosing an input $v(t)$ as

$$
\begin{aligned}
v(t) &= -\mathrm{sgn}(y_m(t))v_{max} && \text{when } |e_1(t)| \geq y_{max} \\
&= \mathrm{sgn}(e_1(t))v_{max} && |e_1(t)| < y_{max}
\end{aligned}
$$

where $\mathrm{sgn}(a(t)) \triangleq \frac{a(t)}{|a(t)|}$ when $a(t) \neq 0$ and is equal to unity when $a(t) = 0$, there exist initial conditions for which $\lim_{t\to\infty} \phi(t) = -\infty$ and $e_1(t)$ approaches asymptotically the region $|e_1| \leq y_{max} + \varepsilon$, where ε is an arbitrary positive constant.

(b) If $\varepsilon_0 > v_{max} + \delta$ where δ is any arbitrary positive constant, then all the solutions of the differential equation (17) are bounded.

Proof:

a) Let D_1 be the open domain enclosed by the line $e_1 = -v_{max}$ and the curve $\phi = \frac{e_1 + v_{max}}{e_1 + y_{max}}$ with $\phi \leq 0$. When $y_m(t) \equiv y_{max}$ and $v(t) = -v_{max}$ all solutions that start on the boundary $\partial(D_1)$ enter D_1. Since the system is autonomous and contains no singularities in D_1, all solutions originating D_1 are unbounded and $\lim_{t\to\infty} \phi(t) = -\infty$, $\lim_{t\to\infty} e_1(t) = -y_{max}$.

For a time-varying signal $y_m(t)$ the proof of unboundedness is related to the above autonomous case. Consider the solution of the differential equation with initial condition $(0,\phi_0)$ with $\phi_0 < \frac{-v_{max}}{y_{max}}$, with $y_m(t) \equiv y_{max}$ and $v(t) \equiv -v_{max}$. Let Γ_+ denote the open curve along which the trajectory lies for all $t \geq 0$. Similarly let Γ_- denote the curve along which the solution lies for all $t \geq 0$ when $v(t) = v_{max}$ and $y(t) = -y_{max}$. Let $\Gamma(\phi_0) = \Gamma_+ \cup \Gamma_-$. $\Gamma(\phi_0)$ divides the plane into two open regions D_2 and D_2^c where $(0,\phi) \in D_2$ if $\phi < \phi_0$. Then all solutions of the differential equation with $|y_m(t)| \leq y_{max}$ and $|v(t)| \leq v_{max}$ with initial conditions on $\Gamma(\phi_0)$ lie either in $\Gamma(\phi_0)$ or enter D_2. Since this is true for every ϕ_0, the solutions are unbounded and $\lim_{t\to\infty} \phi(t) = -\infty$.

b) Let $x \triangleq [e_1,\phi]^T$. Let D denote the region in $\mathbb{R}^2$ $D \triangleq \{x \,|\, |e_1| \leq v_{max}\}$ and let D^c denote the complement of D. If $W(x) = 1/2\, x^T x$, the time derivative of W along a trajectory is $\dot{W}(x) = -e_1^2 + e_1 v < 0$ for $x \in D^c$. Hence $\|x\|$ decreases in D^c and can increase only in D. We wish to show that a constant c exists so that if $\|x(t_0)\| = c_1 \geq c$ over an interval $[t_0, t_0 + T_0]$, then $\|x(t_0 + T_0)\| < c_1$.

If $\|x(t_0)\| = c_0$, integrating the equation for $\dot{e}_1$ in (17) it can be shown that if $x(t_0) \in D$, then $x(t_1) \in D^c$ for some $t_1 \in [t_0, t_0 + T_0]$ if $c_0 > \frac{v_{max}}{\sin\theta}$, where $\cot\theta = \frac{2[T+1]}{(\varepsilon_0 - v_{max})T}$. Hence under the conditions specified in the theorem, the trajectory invariably enters D^c during every period T_0. By increasing $\|x(t_0)\|$ monotonically, the trajectory can be made to lie in a subdomain of D^c for a finite time Δ with $0 < \Delta < \delta_0$ over every period. Since $\|x(t)\|$ decays exponentially in this subdomain, a constant $c > c_0$ exists satisfying the conditions of the theorem.

Comments: 1. The positive limit set of any solution x(t) lies in D.

2. ε_0 will be referred to as the degree of persistent excitation. By the theorem, the solutions are bounded if $\varepsilon_0 > v_{max}$ but the nature of the limit set depends on T_0, ε_0 and δ_0.

3. From the theorem it follows that for a given bound v_{max} on the perturbations, the system can be made robust by increasing the degree of persistent excitation. Note that this is an example of practical stability.

4. The conditions for boundedness and unboundedness of solutions are given in this case in terms of $y_m(t)$. For design purposes it is more appropriate to express them in terms of the reference input r(t).

5. HYBRID ADAPTIVE CONTROL

In continuous adaptive systems of the type described in the previous sections, the plant operates in continuous time and the controller parameters are adjusted continuously. Recent advances in microprocessor and related digital computer technology favor the use of discrete systems in which signals are defined at discrete instants. Practical systems on the other hand may contain both discrete and continuous elements. Such systems may be described as hybrid systems. In a recent report [10] the authors have developed analytical models of hybrid ystems in which control parameters are adjusted in discrete time even as the continuous plant signals are processed in real time. The same algorithms can also be extended to control discrete time plants so that the overall discrete system operates on two time scales - a fast time scale in which the system operates and a slow time scale in which the control parameters are updated. We shall refer to such a system as a discrete hybrid system.

In this section we describe briefly one of the hybrid adaptive algorithms and demonstrate global stability in the ideal case of an adaptive system which uses such an algorithm. The behavior of a discrete hybrid system is then discussed when bounded external disturbances are present. Using the results of the previous section, arguments are put forward as to why hybrid schemes should result in more robust systems and simulation results are presented to show that this is indeed the case.

a) Hybrid Error Model: In this section we consider the first of several hybrid error models given in [10] and discuss its properties. Similar results can also be derived in all the other cases. The error model is described by the equation

$$\phi_k^T u(t) = e_1(t) \qquad t \in [t_k, t_{k+1}), \qquad k \in N \tag{19}$$

where $u: \mathbb{R}^+ \to \mathbb{R}^m$, $e_1: \mathbb{R}^+ \to \mathbb{R}^1$ are piecewise continuous functions which are referred to as the input and output functions of the error model. $\{t_k\}$ is a monotonically increasing unbounded sequence in $\mathbb{R}^+$ with $0 < T_{min} \leq T_k \leq T_{max} < \infty$ for $k \in N$ where $T_k = t_{k+1} - t_k$. When $T_k = T$, a constant, we shall call T the sampling period. $\phi: \mathbb{R}^+ \to \mathbb{R}^m$ is a piecewise constant function, referred to as the parameter error vector and assumes values $\phi(t) = \phi_k$, $t \in [t_k, t_{k+1})$, where ϕ_k is a constant vector.

It is assumed that ϕ_0 (and hence ϕ_k) is unknown, the values $u(t)$ and $e_1(t)$ can be observed at every instant t and $\Delta\phi_k \triangleq \phi_{k+1} - \phi_k$ can be adjusted at $t = t_{k+1}$. The objective is to determine an adaptive law for choosing the sequence $\{\Delta\phi_k\}$ using all available input-output data so that $\lim_{t\to\infty} e_1(t) = 0$.

Theorem 2: If in the error equation (19) the vector ϕ_k is updated according to the adaptive law

$$\Delta\phi_k = \frac{-1}{T_k}\int_{t_k}^{t_{k+1}} \frac{e_1(\tau)u(\tau)}{1 + u^T(\tau)u(\tau)}\, d\tau \tag{20}$$

then

(i) if $u(t)$ and $\dot{u}(t)$ are uniformly bounded in $\mathbb{R}^+$ $\lim_{t\to\infty} e_1(t) = 0$

(ii) if in addition to the conditions in (i) u is persistently exciting over an interval T_{min}, $\lim_{k\to\infty} \phi_k = 0$

(iii) If $u \in L_e^\infty$ then $e_1(t) = \rho(t)[1 + u^T u]^{1/2}$, $\rho \in L^2$.

Proof: If $V(k) = \frac{1}{2}\phi_k^T\phi_k$, using the adaptive law (20) we obtain $\Delta V(k) = -\frac{1}{2}\phi_k^T [2I - R_k]R_k\phi_k \leq 0$

where
$$R_k = \frac{1}{T_k}\int_{t_k}^{t_{k+1}} \frac{u(\tau)u^T(\tau)}{1 + u^T(\tau)u(\tau)}\, d\tau \,.$$

Hence $V(k)$ is a Lyapunov function and assures the boundedness of ϕ_k. Since $\sum_{k=1}^{\infty} \Delta V(k) < \infty$ it follows that $\lim_{k\to\infty} \Delta V(k) = 0$. Hence

$$\lim_{k\to\infty} \phi_k^T R_k \phi_k = \lim_{k\to\infty} \frac{1}{T_k}\int_{t_k}^{t_{k+1}} \frac{e_1^2(\tau)}{1 + u^T(\tau)u(\tau)}\, d\tau = 0.$$

(i) If u is bounded, e_1 is bounded and $e_1 \in L^2$. If $\dot{u}$ is bounded $\lim_{t\to\infty} e_1(t) = 0$.

(ii) If u is persistently exciting R_k is uniformly positive definite and hence $\phi_k \to 0$ as $k \to \infty$.

(iii) If u grows in an unbounded fashion with $u \in L_e^\infty$, $e_1 = \rho\sqrt{1 + u^T u}$ where $\rho \in L^2$.

Comments: In the three cases given in theorem 2 the first two assume that the input u is uniformly bounded and the corresponding results are applicable to the identification problem. The third case which treats unbounded inputs is applicable to the control problem.

The fact that T_k need not be a constant is also worth noting. As shown in section 6 a time-varying period may be used to improve the transient response of the system.

b) Stable Hybrid Adaptive Control - Ideal Case: The hybrid adaptive algorithm described in the preceding section can be used to adjust the control parameters of a hybrid adaptive system. Using an approach very similar to that used in section 3 for a continuous time system the overall system can be shown to be globally stable. Using the same notation as in section 3 we have for the adaptive law

$$\Delta\phi_k = -\frac{1}{T_k}\int_{t_k}^{t_{k+1}} \frac{\epsilon_1(\tau)\zeta(\tau)}{1 + \zeta^T(\tau)\zeta(\tau)}\, d\tau$$

From the analysis in the previous section we conclude that

(i) the parameter error vector ϕ_k is bounded

and (ii) $\epsilon_1 = \rho\sqrt{1 + \zeta^T\zeta}$ where $\rho \in L^2$,

which conditions are the same as those obtained for the continuous case. Condition (i) assures that the signals y_p, $\omega^{(2)}$, $\|\omega(t)\|$ and $\|\zeta(t)\|$ grow at the same rate. Condition (ii) results in $|y_p(t)| = o \sup_{\tau\leq t}\|\omega(\tau)\|$ which contradicts the previous assertion proving the boundedness of all the signals.

The similarity between the continuous and hybrid systems also extends to cases when external bounded disturbances are present and the methods described in sections 3 and 4 apply to the hybrid case as well. However, as shown in the following section, the use of averaged values over an interval rather than instantaneous values, results in more robust control.

c) Adaptive System with Two Time Scales: The hybrid adaptive algorithm developed in section 5a and applied to hybrid adaptive systems in section 5b can also be s·· modified for discrete hybrid systems or discrete systems with two time ·es, shown below.

Let the output error $e_1(k) \in \mathbb{R}^1$ and the parameter error vector $\phi(k) \in \mathbb{R}^n$ be related by the error equation

$$\phi^T(k)w(\ell) = e_1(\ell) \qquad k,\ell \in N, \quad \ell \in [kT,(k+1)T] \tag{21}$$

where $\phi(k)$ is a constant vector over the interval $[kT,(k+1)T]$, $T \in N$ and denotes the period of the interval and $w(\ell) \in \mathbb{R}^n$ is an input vector. Using information collected over the entire interval, the parameter error vector $\phi(k)$ is updated at time $(k+1)T$ using the adaptive law

$$\phi(k+1) - \phi(k) \triangleq \Delta\phi(k) = -1/T \sum_{i=kT}^{(k+1)T-1} \frac{e_1(i)w(i)}{1+w(i)^Tw(i)}$$

$$= -R(k)\phi(k) \tag{22}$$

where $R(k) \triangleq 1/T \sum_{kT}^{(k+1)T-1} \frac{w(i)w(i)^T}{1+w(i)^Tw(i)}$.

In [10] it is shown that $V(k) = 1/2\, \phi^T(k)\phi(k)$ is a Lyapunov function for the system (21) from which it follows that $\phi(k)$ is bounded if $\phi(0)$ is bounded and

$$\lim_{i\to\infty} \frac{e_1(i)}{[1+w(i)^Tw(i)]^{1/2}} = 0 \qquad i \in N \tag{23}$$

If the adaptive law (22) is used in a control system to update the parameters, equation (23) can be used to demonstrate global stability [10].

When an external disturbance v is present the error equation (23) have to be modified as

$$\phi^T(k)w(\ell) + v(\ell) = e_1(\ell) \qquad \ell \in [kT,(k+1)T] \tag{24}$$

Using the same adaptive law as before, the error equation has the form

$$\Delta\phi(k) = -R(k)\phi(k) + \sum_{i=kT}^{(k+1)T-1} \frac{w(i)v(i)}{1+w(i)^Tw(i)} \tag{25}$$

$$= -R(k)\phi(k) + s(k)$$

where $s(k) \triangleq \sum_{i=kT}^{(k+1)T-1} \frac{w(i)v(i)}{1+w(i)^Tw(i)}$.

The matrix R(k) and the vector s(k) in algorithm (25) are averaged values over an interval rather than instantaneous values. Hence the equivalent system may be considered to have more persistently exciting inputs in its homogeneous equation and a smaller magnitude of perturbation (if the mean value of the disturbance is small). Due to both reasons the outputs tend to be smaller. Simulation results shown in Fig. 2 indicate the dramatic improvement in performance.

6. NEW DIRECTIONS

The criteria for judging the performance of an adaptive control system are no different from those used for any conventional control system and include stability speed and accuracy of response. In the preceding sections methods using persistent excitation of reference input, and nonlinear and hybrid adaptive algorithms were described which would make the overall system stable under perturbations. A judicious combination of these different methods may improve the robustness of the system substantially and result in schemes which are practically attractive. Some of these combinations as well as extensions of known methods which appear promising are given below.

(i) Robustness of n^{th} Order System Using Persistent Excitation: A detailed analysis of a first order adaptive system containing a single control parameter was given in section 4. When a disturbance is present it was shown that a sufficiently large persistently exciting reference input would also result in bounded solutions. Further studies have revealed that similar conclusions can be drawn regarding higher order systems and research is currently being done to determine the bounds on the solutions.

(ii) Hybrid Adaptive Control: In the adaptive control system described in section 5, it was shown that the sampling interval T_k could itself be time-varying provided it lay in a bounded interval $[T_{min}, T_{max}]$ with $T_{min} > 0$. In practical systems it appears possible to adjust T_k on line to improve the transient response of the [illegible]n.

(iii) Dead-Zone, Persistent Excitation and Plant Identification: A sufficiently large dead-zone in the adaptive algorithm was shown to result in bounded solutions in section 3. The results in section 4 indicated that boundedness of solutions could also be achieved by increasing the PE of the reference input. It therefore appears likely that the same results can be achieved using a combination of a smaller dead-zone and a smaller degree of persistent excitation. Simulation studies have shown that this is indeed the case and attempts are being made to demonstrate this theoretically.

When the reference input is persistently exciting and the adaptive loop is stable, the plant parameters can be estimated on-line and used in second level adaptation to reduce the dead-zone further. Hence combining a dead-zone with PE of reference inputs appears to be of both theoretical and practical interest.

(iv) $\|\theta^*\|_{max}$ and Persistent Excitation: As in (iii) a persistently exciting input enables θ^* to be estimated and hence an attempt could be made to use the information to decrease the region of search.

(v) σ-modification and Persistent Excitation: The σ-modification scheme, in its basic form, described in section 3 is unappealing, since the parameter error can be large if $\|\theta^*\|$ is large. Using identification methods as in (iii) and (iv) and estimating θ^* on line, second level adaptive procedures may result in a smaller bias.

The second level adaptation problems stated in (ii)-(v) while practically attractive, lead to stability questions in more complex nonlinear systems. Further, it is worth pointing out that all of them consider external disturbances rather than perturbations in plant dynamics. The reduced order problem which deals with the design of a low order controller to adaptively control a higher order plant is generally agreed to be the single most important theoretical question in the field of adaptive control. While considerable research is being carried out in this area, it is acknowledged that even a proper formulation of this problem is a formidable one. It is felt that the answers to some of the questions raised in this section will contribute significantly towards this end.

Acknowledgment

The work reported here was supported by the National Science Foundation under grant ECS-8300223.

REFERENCES

1. K.S. Narendra, Y.H. Lin and L.S. Valavani, "Stable Adaptive Controller Design - Part II: Proof of Stability," IEEE Trans. on Autom. Control, AC-25, pp. 440-448, June 1980.

2. A.S. Morse, "Global Stability of Parameter Adaptive Control Systems," IEEE Trans. on Autom. Control, AC-25, pp. 433-439, June 1980.

3. K.S. Narendra and Y.H. Lin, "Stable Discrete Adaptive Control," IEEE Trans. on Autom. Control, AC-25, pp. 456-461, June 1980.

4. G.C. Goodwin, P.J. Ramadge and P.E. Caines, "Discrete Time Multivariable Adaptive Control," IEEE Trans. on Autom. Control, AC-25, pp. 449-456, June 1980.

5. B.B. Peterson and K.S. Narendra, "Bounded Error Adaptive Control," IEEE Trans. on Autom. Control, AC-27, pp. 1161-1168, Dec. 1982.

6. G. Kreisselmeier and K.S. Narendra, "Stable Model Reference Adaptive Control in the Presence of Bounded Disturbances," IEEE Trans. on Autom. Control, AC-27, pp. 1169-1175, Dec. 1982.

7. P.A. Ioannou and P V. Kokotovic, "Robust Redesign of Adaptive Control," IEEE Trans. on Autom. Control, AC-29, pp. 202-211, March 1984.

8. B.D.O. Anderson and R.M. Johnstone, "Adaptive Systems and Time Varying Plants," Int. Journal of Control, vol. 37, No. 2, pp. 367-377, 1983.

9. B.D.O. Anderson and R.M. Johnstone, "Robust Lyapunov Stability Results and Adaptive Systems," Proc. 20th IEEE CDC, San Diego, pp. 510-515, Dec. 1981.

10. K.S. Narendra, I.H. Khalifa and A.M. Annaswamy, "Error Models for Stable Hybrid Adaptive Systems - Part II," Tech. Report No. 8404, Center for Systems Science, Yale University, New Haven, Ct., Feb. 1984 (To be published in IEEE

Transactions on Automatic Control).

11. W. Hahn, Theory and Application of Lyapunov's Direct Method with Applications, Academic Press, New York, 1961

12. J.P. LaSalle and S. Lefschetz, Stability by Lyapunov's Direct Method with Applications, Academic Press, New York, 1961.

13. Krasovskii, Stability of Motion, Stanford University Press, Stanford, 1963.

14. C.A. Desoer, R. Liu and L.V. Auth, Jr., "Linearity vs. Nonlinearity and Asymptotic Stability in the Large," IEEE Trans. on Circuit Theory, pp. 117-118, March 1965.

15. K.S. Narendra and A.M. Annaswamy, "Persistent Excitation and Robust Adaptive Systems," Tech. Report No. 8302, Center for Systems Science, Yale University, New Haven, Ct., Aug. 1983.

16. K.S. Narendra and Y.H. Lin, "Design of Stable Model Reference Adaptive Controllers," Applications of Adaptive Control, pp. 69-130, Academic Press, New York, 1980.

17. K.S. Narendra and L.S. Valavani, "Stable Adaptive Controller Design-Direct Control," IEEE Trans. on Autom. Control, AC-23, pp. 570-583, Aug. 1978.

18. K.S. Narendra, A.M. Annaswamy and R.P. Singh, "A General Approach to the Stability Analysis of Adaptive Systems," Tech. Report No. 8402, Center for Systems Science, Yale University, New Haven, Ct., Jan. 1984 (To be published in International Journal of Control).

19. A.P. Morgan and K.S. Narendra, "On the Uniform Asymptotic Stability of Certain Linear Nonautonomous Differential Equations," SIAM Journal of Control and Optimization, vol. 15, pp. 5-24, Jan. 1977.

20. B.D.O. Anderson and C. Richard Johnson, Jr., "Exponential Convergence of Adaptive Identification and Control Algorithms," Automatica, vol. 18, pp. 1-13, 1982.

21. S. Dasgupta, B.D.O. Anderson and A.C. Tsoi, "Input Conditions for Continuous Time Adaptive Systems Problems," Proc. of the 22nd IEEE CDC, San Antonio, Dec. 1983.

22. S. Boyd and S.S. Sastry, "On Parameter Convergence in Adaptive Control," Tech. Report, June 1983.

23. A.P. Morgan and K.S. Narendra, "On the Stability of Nonautonomous Differential Equations $\dot{x} = [A + B(t)]x$ with Skew-Symmetric Matrix $B(t)$," SIAM Journal of Control and Optimization, vol. 15, pp. 163-176, Jan. 1977.

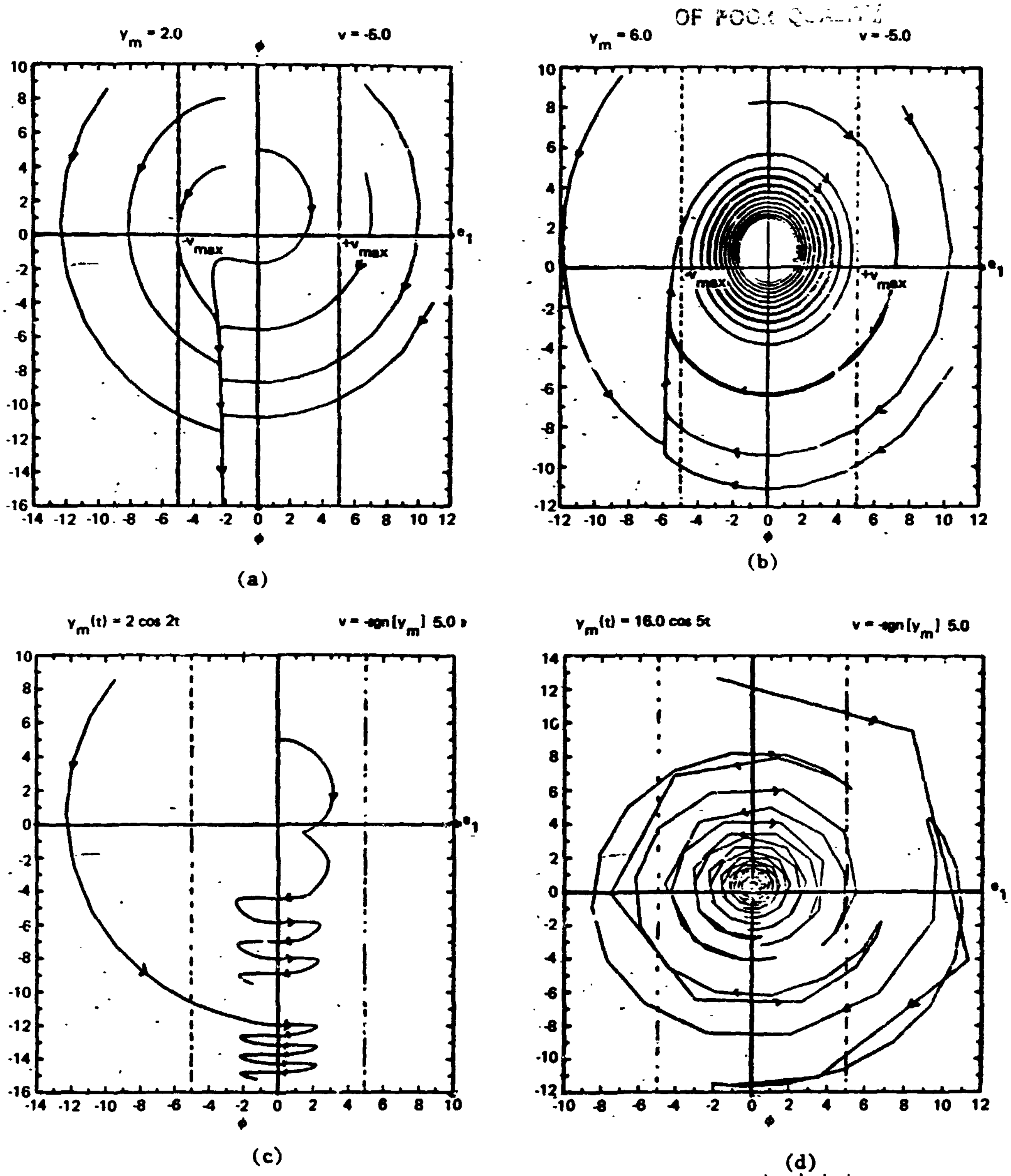

$$\dot{e}_1 = -e_1 + \phi(e_1 + y_m) + v$$

$$\dot{\phi} = -e_1(e_1 + y_m)$$

Fig. 1: Persistent Excitation and Robustness.

(a) autonomous case $|y_m|<|v|$ unstable

(b) autonomous case $|y_m|>|v|$ stable

(c) non-autonomous case $y_{max} < v_{max}$ unstable

(d) non-autonomous case $\varepsilon_0 > v_{max}$ stable

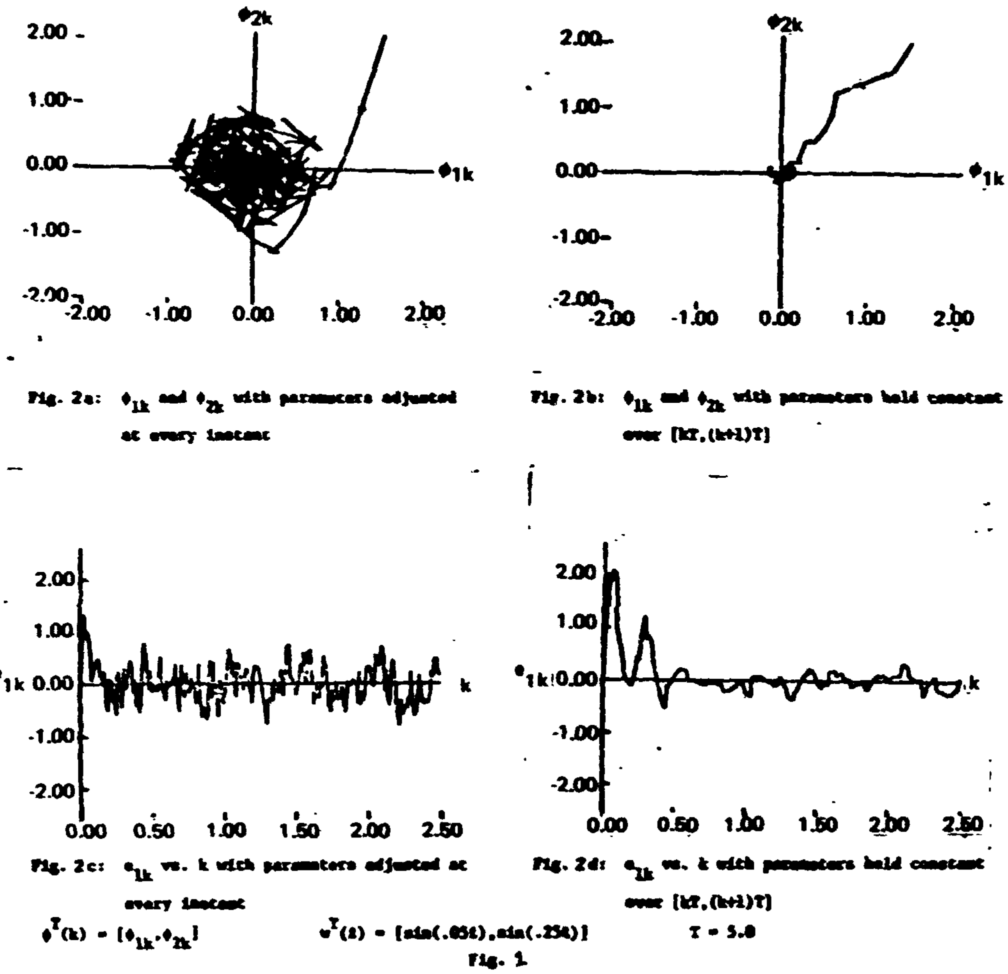

Fig. 2: Improved Robustness Using Hybrid Control

N85-31208

MAXIMUM LIKELIHOOD ESTIMATION WITH EMPHASIS ON AIRCRAFT FLIGHT DATA

K. W. Iliff* and R. E. Maine**
NASA Ames Research Center
Dryden Flight Research Facility
Edwards, CA 93523

ABSTRACT

Accurate modeling of flexible space structures is an important field that is currently under investigation. Parameter estimation, using methods such as maximum likelihood, is one of the ways that the model can be improved. The maximum likelihood estimator has been used to extract stability and control derivatives from flight data for many years. Most of the literature on aircraft estimation concentrates on new developments and applications, assuming familiarity with basic estimation concepts. This paper presents some of these basic concepts. The paper briefly discusses the maximum likelihood estimator and the aircraft equations of motion that the estimator uses. The basic concepts of minimization and estimation are examined for a simple computed aircraft example. The cost functions that are to be minimized during estimation are defined and discussed. Graphic representations of the cost functions are given to help illustrate the minimization process. Finally, the basic concepts are generalized, and estimation from flight data is discussed. Specific examples of estimation of structural dynamics are included. Some of the major conclusions for the computed example are also developed for the analysis of flight data.

INTRODUCTION

Accurate modeling of flexible space structures is an important area that is currently under investigation. The mathematical modeling of these structures can be improved using parameter estimation. Such techniques have been successfully used to estimate aircraft stability and control derivatives and refine aircraft mathematical models. Some of the experience gained in the aircraft problem can be applied directly to analysis of flexible space structures.

The maximum likelihood estimator has been used to obtain stability and control estimates from flight data for nearly 20 years. The results of many applications have been reported worldwide. Reference 1 contains a representative list of some of these reports. Several good texts (including Refs. 2 and 3) contain thorough treatments of the theory of maximum likelihood estimation. Experience reports (Refs. 1, 4, and 5) pointing out practical considerations for

*Senior Staff Scientist.

†Aerospace Engineer.

applying the maximum likelihood estimator have also been published. Stability and control derivatives estimated from flight data are currently required for correlation studies with predictive techniques, handling qualities documentation, design compliance, aircraft simulator enhancement and refinement, and control system design. Correlation, simulation, and control system design applications (including the space shuttle) are discussed in Ref. 6. Current studies have concentrated on estimation model structure determination (Refs. 7 and 8), equation error with state reconstruction (Refs. 9 to 11), and maximum likelihood estimation in the frequency domain (Refs. 12 and 13).

Most of the reports in the estimation area concentrate on new developments and applications, assuming familiarity with the basic concepts of maximum likelihood estimation. In this paper some of these basic concepts are reviewed, concentrating on simple, idealized models. These simple models provide insights applicable to a wide variety of real problems.

This paper also presents some of the basics of maximum likelihood estimation as applied to the aircraft problem. It briefly discusses the maximum likelihood estimator and the aircraft equations of motion that the estimator uses. The basic aspects of minimization and estimation are then examined in detail for a simple computed aircraft example. Finally, the discussion is expanded to the general aircraft estimation problem including specific examples of estimation of structural dynamics.

SYMBOLS

A,B,C,D,F,G	system matrices
a_N	normal acceleration positive upward, g
a_x	longitudinal acceleration, g
a_y	lateral acceleration, g
a_z	normal acceleration positive upward, g
b	reference span, ft
C_ℓ	coefficient of rolling moment
C_n	coefficient of yawing moment
C_X	coefficient of axial force
C_Y	coefficient of side force
C_Z	coefficient of normal force
$f(\cdot)$, $g(\cdot)$	general functions

GG^*	measurement noise covariance matrix
g	acceleration due to gravity, ft/sec^2
H	approximation to the information matrix
I_x, I_y, I_z, I_{xz}	moment of inertia about subscripted axis, slug-ft^2
i	general index
J	cost function
K_β	sidewash factor
L	rolling moment divided by I_x, deg/sec^2
L'	rolling moment, ft-lb
L_{YJ}	rolling moment due to yaw jet, ft-lb
M	pitching moment divided by I_y, deg/sec^2
m	mass, slug
N	number of time points or cases or yawing moment divided by I_z, deg/sec^2
n	state noise vector or number of unknowns
$\hat{p}_g$	estimated roll rate due to turbulence, deg/sec
p	roll rate, deg/sec
q	pitch rate, deg/sec
$\bar{q}$	dynamic pressure, lb/ft^2
R	innovation covariance matrix
r	yaw rate, deg/sec
S	reference area, ft^2
T	time increment, sec
t	time, sec
u	control input vector
V	forward velocity, ft/sec

x	state vector
$x_{a_y}, y_{a_y}, z_{a_y}$	distance between lateral accelerometer and the center of gravity along the appropriate axis, ft
z	observation vector
$\tilde{z}_\xi$	predicted Kalman-filtered estimate
α	angle of attack, deg
β	angle of sideslip, deg
$\hat{\beta}_g$	estimated angle of sideslip due to turbulence, deg
Δ	time sample interval, sec
δ	control deflection, deg
δ_a	aileron deflection, deg
δ_e	elevon deflection, deg
δ_r	rudder deflection, deg
η	measurement noise vector
θ	pitch angle, deg
μ	mean
ξ	vector of unknowns
σ	standard deviation
τ	time, sec
ϕ	transition matrix or bank angle, deg
ψ	integral of transition matrix, or heading angle, deg
ω	frequency, rad/sec

Subscripts:

$p,q,r,\alpha,\dot{\alpha},\beta,\dot{\beta}, \delta,\delta_a,\delta_r,\delta_e$	partial derivative with respect to subscripted quantity
0	bias or at time zero
m	measured quantity

Other nomenclature:

~	predicted estimate
^	estimate
*	transpose
'	indicates moment in ft-lb

MAXIMUM LIKELIHOOD ESTIMATION

The concept of maximum likelihood is discussed in this section. First the general heuristic problem is discussed, and then the specific equations for obtaining maximum likelihood estimates for the aircraft problem are given. In the following sections, both the concepts and the computations involved in a simple but realistic example are discussed in detail.

The aircraft parameter estimation problem can be defined quite simply in general terms. The system investigated is assumed to be modeled by a set of dynamic equations containing unknown parameters. To determine the values of the unknown parameters, the system is excited by a suitable input, and the input and actual system response are measured. The values of the unknown parameters are then inferred based on the requirement that the model response to the given input match the actual system response. When formulated in this manner, the problem of identifying the unknown parameters can be easily solved by many methods; however, complicating factors arise when application to a real system is considered.

The first complication results from the impossibility of obtaining perfect measurements of the response of any real system. The inevitable sensor errors are usually included as additive measurement noise in the dynamic model. Once this noise is introduced, the theoretical nature of the problem changes drastically. It is no longer possible to exactly identify the values of the unknown parameters; instead, the values must be estimated by some statistical criterion. The theory of estimation in the presence of measurement noise is relatively straightforward for a system with discrete time observations, requiring only basic probability.

The second complication of real systems is the presence of state noise. State noise is random excitation of the system from unmeasured sources, the standard example for the aircraft stability and control problem being atmospheric turbulence. If state noise is present and measurement noise is neglected, the analysis results in the regression algorithm.

When both state and measurement noise are considered, the problem is more complex than in the cases that have only state noise or only measurement noise. Reference 14 develops a mixed continuous/discrete maximum likelihood formulation that allows for both state and measurement noise. This formulation has a continuous system model with discrete sampled observations.

The final problem for real systems is modeling. It has been assumed throughout the above discussion that for some value (called the "correct" value) of the unknown parameter vector, the system is correctly described by the dynamic model. Physical systems are seldom described exactly by simple dynamic models, so the question of modeling error arises. No comprehensive theory of modeling error is available. The most common approach is to ignore it: Any modeling error is simply treated as state noise or measurement noise, or both, in spite of the fact that the modeling error may be deterministic rather than random. The assumed noise statistics can then be adjusted to include the contribution of the modeling error. This procedure is not rigorously justifiable, but, combined with a carefully chosen model, it is probably the best approach available.

With the above discussion in mind, it is possible to make a more precise, mathematically probabilistic statement of the parameter estimation problem. The first step is to define the general system model (aircraft equations of motion). This model can be written in the continuous/discrete form as

$$x(t_0) = x_0 \tag{1}$$

$$\dot{x}(t) = f[x(t),u(t),\xi] + F(\xi)n(t) \tag{2}$$

$$z(t_i) = g[x(t_i),u(t_i),\xi] + G(\xi)\eta_i \tag{3}$$

where x is the state vector, z is the observation vector, f and g are system state and observation functions, u is the known control input vector, ξ is the unknown parameter vector, n is the state noise vector, and η is the measurement noise vector. The state noise vector is assumed to be zero-mean white Gaussian and stationary, and the measurement noise vector is assumed to be a sequence of independent Gaussian random variables with zero mean and identity covariance. For each possible estimate of the unknown parameters, a probability that the aircraft response time histories attain values near the observed values can then be defined. The maximum likelihood estimates are defined as those that maximize this probability. Maximum likelihood estimation has many desirable statistical characteristics; for example, it yields asymptotically unbiased, consistent, and efficient estimates (Ref. 15).

If there is no state noise and the matrix G is known, then the maximum likelihood estimator minimizes the cost function

$$J(\xi) = \frac{1}{2}\sum_{i=1}^{N}[z(t_i) - \tilde{z}_\xi(t_i)]^*(GG^*)^{-1}[z(t_i) - \tilde{z}_\xi(t_i)] \tag{4}$$

where GG^* is the measurement noise covariance matrix, and $\tilde{z}_\xi(t_i)$ is the computed response estimate of z at t_i for a given value of the unknown parameter vector ξ. The cost function is a function of the difference between the measured and computed time histories.

If Eqs. (2) and (3) are linearized (as is the case for the stability and control derivatives in the aircraft problem),

$$x(t_0) = x_0 \tag{5}$$

$$\dot{x}(t) = Ax(t) + Bu(t) + Fn(t) \tag{6}$$

$$z(t_i) = Cx(t_i) + Du(t_i) + G\eta_i \tag{7}$$

For the no-state-noise case, the $\tilde{z}_\xi(t_i)$ term of Eq. (4) can be approximated by

$$\tilde{x}_\xi(t_0) = x_0(\xi) \tag{8}$$

$$\tilde{x}_\xi(t_{i+1}) = \phi\tilde{x}_\xi(t_i) + \psi[u(t_i) + u(t_{i+1})]/2 \tag{9}$$

$$\tilde{z}_\xi(t_i) = C\tilde{x}_\xi(t_i) + Du(t_i) \tag{10}$$

where

$$\phi = \exp\,[A(t_{i+1} - t_i)]$$

$$\psi = \int_{t_i}^{t_{i+1}} \exp\,(A\tau)\,d\tau\, B$$

When state noise is important, the nonlinear form of Eqs. (1) to (3) is intractable. For the linear model defined by Eqs. (5) to (7), the cost function that accounts for state noise is

$$J(\xi) = \frac{1}{2}\sum_{i=1}^{N}[z(t_i) - \tilde{z}_\xi(t_i)]^*R^{-1}[z(t_i) - \tilde{z}_\xi(t_i)] + \frac{1}{2}N\,\ln\,|R| \tag{11}$$

where R is the innovation covariance matrix. The $\tilde{z}_\xi(t_i)$ term in Eq. (11) is the Kalman-filtered estimate of z, which, if the state noise covariance is zero, reduces to the form of Eq. (4). If there is no state noise, the second term of Eq. (11) is of no consequence (unless one wishes to include elements of the G matrix as unknowns), and R can be replaced by GG* which makes Eq. (11) the same as Eq. (4).

To minimize the cost function $J(\xi)$, we can apply the Newton-Raphson algorithm which chooses successive estimates of the vector of unknown coefficients, $\hat{\xi}$. Let L be the iteration number. The L + 1 estimate of $\hat{\xi}$ is then obtained from the L estimate as follows:

$$\hat{\xi}_{L+1} = \hat{\xi}_L - [\nabla_\xi^2 J(\hat{\xi}_L)]^{-1}[\nabla_\xi^* J(\hat{\xi}_L)] \tag{12}$$

The first and second gradients are defined as

$$\nabla_\xi J(\xi) = -\sum_{i=1}^{N} [z(t_i) - \tilde{z}_\xi(t_i)]^*(GG^*)^{-1}[\nabla_\xi \tilde{z}_\xi(t_i)] \tag{13}$$

$$\nabla_\xi^2 J(\xi) = \sum_{i=1}^{N} [\nabla_\xi \tilde{z}_\xi(t_i)]^*(GG^*)^{-1}[\nabla_\xi \tilde{z}_\xi(t_i)]$$

$$-\sum_{i=1}^{N} [z(t_i) - \tilde{z}_\xi(t_i)]^*(GG^*)^{-1}[\nabla_\xi^2 \tilde{z}_\xi(t_i)] \tag{14a}$$

The Gauss-Newton approximation to the second gradient is

$$\nabla_\xi^2 J(\xi) \cong \sum_{i=1}^{N} [\nabla_\xi \tilde{z}_\xi(t_i)]^*(GG^*)^{-1}[\nabla_\xi \tilde{z}_\xi(t_i)] \tag{14b}$$

The Gauss-Newton approximation, which is sometimes referred to as modified Newton-Raphson, is computationally much easier than the Newton-Raphson approximation because the second gradient of the innovation never needs to be calculated. In addition, it can have the advantage of speeding the convergence of the algorithm, as is discussed in the SIMPLE AIRCRAFT EXAMPLE section.

Figure 1 illustrates the maximum likelihood estimation concept. The measured response of the aircraft is compared with the estimated response, and the difference between these responses is called the response error. The cost functions of Eqs. (4) and (11) include this response error. The Gauss-Newton computational algorithm is used to find the coefficient values that maximize the cost function. Each iteration of this algorithm provides a new estimate of the unknown coefficients on the basis of the response error. These new estimates of the coefficients are then used to update the mathematical model of the aircraft, providing a new estimated response and, therefore, a new response error. The updating of the mathematical model continues iteratively until a convergence criterion is satisfied. The estimates resulting from this procedure are the maximum likelihood estimates.

The maximum likelihood estimator also provides a measure of the reliability of each estimate based on the information obtained from each dynamic maneuver. This measure of the reliability, analogous to the standard deviation, is called the Cramèr-Rao bound (Ref. 16) or the uncertainty level. The Cramèr-Rao bound as computed by current programs should generally be used as a measure of relative accuracy rather than absolute accuracy. The bound is obtained from the approximation of the information matrix, H. This matrix equals the approximation to the second gradient given by Eq. (14b). The bound for each unknown is the square root of the corresponding diagonal element of H. That is, for the ith unknown, the Cramèr-Rao bound is $\sqrt{H(i,i)}$.

The Maine-Iliff formulation (Ref. 14) and minimization algorithm discussed above are implemented with the Iliff-Maine code (MMLE3 maximum likelihood estimation program). The program and computational algorithms are described fully in Ref. 17. All the computations shown and described in the remainder of the paper use the algo-rithms exactly as described in Ref. 17.

AIRCRAFT EQUATIONS OF MOTION

For the discussion that follows in later sections of this paper, some knowledge of the aircraft equations of motion is assumed. To clarify some of that discussion, the aircraft equations are discussed briefly in this section.

First, the axis system on which the aircraft equations of motion are based is discussed. Figure 2(a) shows the aircraft reference body-axis system and the conventional control surfaces. The origin of the body-axis system is at the center of gravity. The sign convention for this axis system is defined by the right-hand rule with the x-axis defined as positive forward on the aircraft. The longitudinal acceleration (a_x) and nondimensional axial force coefficient (C_X) are defined along this axis, and the roll rate (p) and rolling moment (L') are defined about this axis. The y-axis is defined as positive out the right wing. The lateral acceleration (a_y) and nondimensional side force coefficient (C_Y) are defined along this axis, and the pitch rate (q) and pitching moment (M') are defined about this axis. The z-axis is defined as positive out the bottom of the aircraft. The normal acceleration (a_z) and nondimensional normal force coefficient (C_Z) are defined along this axis, and the yaw rate (r) and yawing moment (N') are defined about this axis. The normal acceleration is sometimes defined as positive upward but is then referred to as a_N. The three moments (L', M', and N') are usually divided by the corresponding moments of inertia (I_x, I_y, and I_z), and are then referred to without the prime as L, M, and N. These quantities are nondimensionalized (C_ℓ, C_m, and C_n, respectively) for use in the equations of motion soon to be discussed. The primary control about the roll axis (x-axis) is the aileron (δ_a), about the pitch axis (y-axis) is the elevator (δ_e), and about the yaw axis (z-axis) is the rudder (δ_r). Some aircraft have other controls, but in this paper these will only be defined where they are discussed (the reaction control jets on the space shuttle, for example).

The Euler angles ϕ, θ, and ψ define the aircraft attitude with respect to the earth. These angles define the rotations which transform earth-fixed axes to the aircraft reference body-axis system of Fig. 2(a). The order of rotation must be about the z-axis (ψ), then the y-axis (θ), and finally the x-axis (ϕ) for the aircraft equations of motion that will be written subsequently.

For stability and control analysis, the velocity of the aircraft with respect to the air (not with respect to the earth) is of primary interest. Figure 2(b) shows the relationship between the aircraft axis system and the flow angles. The flow angle in the x-z plane is the angle of attack (α), and the flow angle in the x-y plane is the angle of sideslip (β). A more rigorous and detailed definition is required for the derivation of the equations of motion, but the above definitions are sufficient to define the following equation of motion.

Generalized nonlinear equations of motion are given in detail in Ref. 17, which fully describes the Iliff-Maine code (MMLE3 program). All computations and aircraft examples in this paper use the linearized form for the lateral-directional equations. These equations are given below and referred to in the remainder of the paper.

$$\dot{\beta} = \frac{\bar{q}s}{mV}(C_Y + \dot{\beta}_0) + \frac{g}{V}\cos\theta\sin\phi + p\sin\alpha - r\cos\alpha \tag{15}$$

$$\dot{p}I_x - \dot{r}I_{xz} = \bar{q}sbC_\ell + qr(I_y - I_z) + pqI_{xz} \tag{16}$$

$$\dot{r}I_z - \dot{p}I_{xz} = \bar{q}sbC_n + pq(I_x - I_y) - qrI_{xz} \tag{17}$$

$$\dot{\phi} = p + r\cos\phi\tan\theta + q\sin\phi\tan\theta + \dot{\phi}_0 \tag{18}$$

where

$$C_Y = C_{Y_\beta}\beta + C_{Y_p}\frac{pb}{2V} + C_{Y_r}\frac{rb}{2V} + C_{Y_\delta}\delta + C_{Y_0} \tag{19}$$

$$C_\ell = C_{\ell_\beta}\beta + C_{\ell_p}\frac{pb}{2V} + C_{\ell_r}\frac{rb}{2V} + C_{\ell_\delta}\delta + C_{\ell_0} + C_{\ell_{\dot{\beta}}}\frac{\dot{\beta}b}{2V} \tag{20}$$

$$C_n = C_{n_\beta}\beta + C_{n_p}\frac{pb}{2V} + C_{n_r}\frac{rb}{2V} + C_{n_\delta}\delta + C_{n_0} + C_{n_{\dot{\beta}}}\frac{\dot{\beta}b}{2V} \tag{21}$$

where the δ term is summed over all controls.

The observation equations are

$$\beta_m = K_\beta\,\beta - \frac{z_\beta}{V}p + \frac{x_\beta}{V}r \tag{22}$$

$$p_m = p \tag{23}$$

$$r_m = r \tag{24}$$

$$\phi_m = \phi \tag{25}$$

$$a_{y_m} = \frac{\bar{q}s}{mg}C_Y - \frac{z_{a_y}}{g}\dot{p} + \frac{x_{a_y}}{g}\dot{r} - \frac{y_{a_y}}{g}(p^2 + r^2) \tag{26}$$

$$\dot{p}_m = \dot{p} + \dot{p}_0 \tag{27}$$

$$\dot{r}_m = \dot{r} + \dot{r}_0 \tag{28}$$

The state, control, and observation vectors for the lateral-directional mode can then be defined as

$$x = (\beta\ p\ r\ \phi)^* \tag{29}$$

$$u = (\delta_a\ \delta_r)^* \tag{30}$$

$$z = (\beta_m\ p_m\ r_m\ \phi_m\ a_{y_m}\ \dot{p}_m\ \dot{r}_m)^* \tag{31}$$

SIMPLE AIRCRAFT EXAMPLE

The basic concepts involved in a parameter estimation problem can be illustrated by using a simple example representative of a realistic aircraft problem. The example chosen here is representative of an aircraft that exhibits pure rolling motion from an aileron input. This example, although simplified, typifies the motion exhibited by many aircraft in particular flight regimes, such as the F-14 aircraft flying at high dynamic pressure, the F-111 aircraft at moderate speeds with the wing in the forward position, and the T-37 aircraft at low speed.

Derivation of an equation describing this motion is straightforward. Figure 2(c) shows a sketch of an aircraft with the x-axis perpendicular to the plane of the figure (positive forward on the aircraft). The rolling moment (L'), roll rate (p), and aileron deflection (δ_a) are positive as shown. For this example, the only state is p and the only control is δ_a. The result of summing moments is

$$I_x\dot{p} = L'(p, \delta_a) \tag{32}$$

The first-order Taylor expansion then becomes

$$\dot{p} = L_p p + L_{\delta_a}\delta_a \tag{33}$$

where

$$L' = I_x L$$

Since the aileron is the only control, it is notationally simpler to use δ instead of δ_a for the discussion of this example. Equation (33) can then be written as

$$\dot{p} = L_p p + L_\delta \delta \tag{34}$$

An alternate approach that results in the same equation is to combine Eq. (16) with Eq. (20), substituting for C_ℓ, and then eliminate the terms that are zero for our example. This yields

$$\dot{p}I_x = \bar{q}sb\ C_{\ell_p} \frac{pb}{2V} + C_{\ell_\delta}\delta \tag{35}$$

where p is the roll rate and δ is the aileron deflection. Rearranging terms, the equation can be put into the dimensional derivative form of Eq. (34).

Equation (34) is a simple aircraft equation where the forcing function is provided by the aileron and the damping by the damping-in-roll term, L_p. In subsequent sections we examine in detail the parameter estimation problem where Eq. (34) describes the system. For this single-degree-of-freedom problem, the maximum likelihood estimator is used to estimate either L_p or L_δ or both for a given computed time history.

We will assume that the system has measurement noise, but no state noise as in Eqs. (1), (2), and (3). Equation (4) then gives the cost function for maximum likelihood estimation. The weighting GG^* is unimportant for this problem, so let it equal 1. For our example, Eqs. (2) and (3) become $x_i = p_i$ and $z_i = x_i$. Therefore, Eq. (4) becomes

$$J(L_p, L_\delta) = \frac{1}{2} \sum_{i=1}^{n} [p_i - \tilde{p}_i(L_p, L_\delta)]^2 \tag{36}$$

where p_i is the value of the measured response p at time t_i and $\tilde{p}_i(L_p, L_\delta)$ is the computed time history of $\tilde{p}$ at time t_i for $L_p = \hat{L}_p$ and $L_\delta = \hat{L}_\delta$. Throughout the rest of the paper, where computed data (not flight data) are used, the measured time history refers to p_i, and the computed time history refers to $\tilde{p}_i(L_p, L_\delta)$. The computed time history is a function of the current estimates of L_p and L_δ, but the measured time history is not.

The most straightforward method of obtaining p_i is with Eqs. (3) and (8). In terms of the notation stated above,

$$\tilde{p}_{i+1} = \phi\tilde{p}_i + \psi(\delta_i + \delta_{i+1})/2 \tag{37}$$

where

$$\phi = \exp(L_p\Delta)$$

$$\psi = \int_0^\Delta \exp(L_p\tau)\, d\tau\, L_\delta = \frac{L_\delta[1 - \exp(L_p\Delta)]}{L_p}$$

and Δ is the length of the sample interval $(t_{i+1} - t_i)$. Simplifying the notation

$$\delta_{i+1/2} = (\delta_i + \delta_{i+1})/2 \tag{38}$$

then

$$\tilde{p}_{i+1} = \phi\tilde{p}_i + \psi\delta_{i+1/2} \tag{39}$$

The maximum likelihood estimate is obtained by minimizing Eq. (36). The Gauss-Newton method described earlier is used for this minimization. Equation (12) is used to determine successive values of the estimates of the unknowns during the minimization.

For this simple problem, $\hat{\xi} = [\hat{L}_p\ \hat{L}_\delta]^*$ and successive estimates of $\hat{L}_p$ and $\hat{L}_\delta$ are determined by updating Eq. (12). The first and second gradients of Eq. (12) are defined by Eqs. (13) and (14). The complete set of equations is given in Ref. 17.

The entire procedure can now be written for obtaining the maximum likelihood estimates for this simple example. To start the algorithm, an initial estimate of L_p and L_δ is needed. This is the value of $\hat{\xi}_0$. With Eq. (12), ξ_1 and subsequently $\hat{\xi}_L$ are defined by using the first and second gradients of $J(L_p, L_\delta)$ from Eq. (36). The gradients for this particular example from Eq. (13) and (14b) are

$$\nabla_\xi J(\hat{\xi}_L) = -\sum_{i=1}^{N} (p_i - \tilde{p}_i)\nabla_\xi \tilde{p}_i \tag{40}$$

$$\nabla_\xi^2 J(\hat{\xi}_L) \cong \sum_{i=1}^{N} (\nabla_\xi \tilde{p}_i)^*(\nabla_\xi \tilde{p}_i) \tag{41}$$

With the specific equations defined in this section for this simple example, we can now proceed in the next section to the computational details of a specific example.

Computational Details of Minimization

In the previous section we specified the equations for a simple example and described the procedure for obtaining estimates of the unknowns from a dynamic maneuver. In this section we give the computational details for obtaining the estimates. Some of the basic concepts of parameter estimation are best shown with computed data where the correct answers are known. Therefore, in this section we study two examples involving computed time histories. The first example is based on data that have no measurement noise, which results in estimates that are the same as the correct value. The second example contains significant measurement noise; consequently, the estimates are not the same as the correct values. Throughout the rest of the paper, where computed data are used, the term "no-noise case" is used for the case with no noise added and "noisy case" for the case where noise has been added.

Since we are studying a simple computed example, it is desirable to keep it simple enough to complete some or all of the calculations on a home computer or, with some labor, on a calculator. With this in mind, the number of data points needs to be kept small. For this computed example, 10 points (time samples) are used. The simulated data, which we refer to as the measured data, are based on Eq. (34). We use the same correct values of L_p and L_δ (-0.2500 and 10.0, respectively) for both examples. In addition, the same input (δ) is used for both examples, the sample interval (Δ) is 0.2 sec, and the initial conditions are zero. Tables of all the significant intermediate values are given with each example. These values are given to four significant digits, although to obtain exactly the same values with a computer or calculator requires the use of 13 significant digits, as in the computation of these tables. If the four-digit numbers are used in the computation, the answers will be a few tenths of a percent off, but will still serve to illustrate the minimization accuracy. In both examples, the initial values of L_p and L_δ (or $\hat{\xi}_0$) are -0.5 and 15.0, respectively.

Example With No Measurement Noise

The measurement time history for no measurement noise (no-noise case) is shown in Fig. 3. The aileron input starts at zero, goes to a fixed value, and then returns to zero. The resulting roll-rate time history is also shown. The values of the measured roll rate to 13 significant digits are given in Table 1 along with the aileron input.

Table 2 shows the values for $\hat{L}_p$, $\hat{L}_\delta$, and J for each iteration, along with the values of ϕ and ψ needed for calculations of $\tilde{p}_i$. In three iterations the algorithm converges to the correct values to four significant digits for both L_p and L_δ. $\hat{L}_\delta$ overshoots slightly on the first iteration and then comes quickly to the correct answer. $\hat{L}_p$ overshoots slightly on the second iteration.

Figure 4 shows the match between the measured data and the computed data for each of the first three iterations. The match is very good after two iterations. The match is nearly exact after three iterations.

Although the algorithm has converged to four-digit accuracy in L_p and L_δ, the value of the cost function, J, continues to decrease rapidly between iterations 3 and 4. This is a consequence of using the maximum likelihood estimator on data with no measurement noise. Theoretically, using infinite accuracy the value of J at the minimum should be zero. However, with finite accuracy the value of J becomes small but never quite zero. This value is a function of the number of significant digits that are being used. For the 13-digit accuracy used here, the cost eventually decreases to approximately 0.3×10^{-28}.

Example With Measurement Noise

The data used in this example (noisy case) are the same as those used in the previous section, except that pseudo-Gaussian noise has been added to the roll rate. The time history is shown in Fig. 5. The signal-to-noise ratio is quite low in this example, as is readily apparent by comparing Figs. 3 and 5. The exact values of the time history to 13-digit accuracy are shown in Table 3. The values of $\hat{L}_p$, $\hat{L}_\delta$, ϕ, ψ, and J are shown for each iteration in Table 4. The algorithm converges in four iterations. The behavior of the coefficients as they approach convergence is much like the no-noise case. The most notable results of this case are the converged values of $\hat{L}_p$ and $\hat{L}_\delta$, which are somewhat different from the correct values. The match between the measured and computed time history is shown in Fig. 6 for each iteration. No change in the match is apparent for the last two iterations. The match is very good considering the amount of measurement noise.

In Fig. 7, the computed time history for the correct values of L_p and L_δ is compared to that for the noisy-case estimates of L_p and L_δ. Because the algorithm converged to values somewhat different than the correct values, the two computed time histories are similar but not identical.

The accuracy of the converged elements can be assessed by looking at the Cramèr-Rao inequality (Refs. 16 and 17) discussed earlier. The Cramèr-Rao bound can be obtained from the following approximation to the information matrix.

$$H = 2(J_{minimum})(\nabla_\xi^2 J)^{-1}/(N-1)$$

The Cramèr-Rao bounds for L_p and L_δ are the square roots of the diagonal elements of the H matrix, or $\sqrt{H(1,1)}$ and $\sqrt{H(2,2)}$, respectively. The Cramèr-Rao bounds are 0.1593 and 1.116 for $\hat{L}_p$ and $\hat{L}_\delta$, respectively. The errors in L_p and L_δ are less than the bounds.

Cost Functions

In the previous section we obtained the maximum likelihood estimates for computed time histories by minimizing the values of the cost function. To fully understand what occurs in this minimization, we must study in more detail the form of the cost functions and some of their more important characteristics. In this section, the cost function for the no-noise case is discussed briefly. The cost function of the noisy case is then discussed in more detail. The same two time histories studied in the previous section are examined here. The noisy case is more interesting because it has a meaningful Cramèr-Rao bound and is more representative of aircraft flight data.

First we will look at the one-dimensional case where L_δ is fixed at the correct value, because it is easier to grasp some of the characteristics of the cost function in one dimension. Then we will look at the two-dimensional case, where both L_p and L_δ are varying. It is important to remember that everything shown in this paper on cost functions is based on computed time histories that are defined by Eq. (36). For every time history we might choose (computed or flight data), a complete cost function is defined. For the case of n variables, the cost function defines a hypersurface of n + 1 dimensions. It might occur to us that we could just construct this surface and look for the minimum, avoiding the need to bother with the minimization algorithm. This is not a reasonable approach because, in general, the number of variables is greater than two. Therefore, the cost function can be described mathematically but not pictured graphically.

One-Dimensional Case

To illustrate the many interesting aspects of cost functions, it is easiest to first look at cost functions having one variable. In an earlier section, the cost function of L_p and L_δ was minimized. That cost function is most interesting in the L_p direction. Therefore, the one-variable cost function studied here is $J(L_p)$. All subsequent discussions are for $J(L_p)$ with L_δ equal to the correct value of 10. Figure 8 shows the cost function plotted as a function of L_p for the case where there is no measurement noise (no-noise case). As expected for this case, the minimum cost is zero and occurs at the correct value of $L_p = -0.2500$. It is apparent that the cost increases much more slowly for a more negative L_p than for a positive L_p. In fact, the slope of the curve tends to become less negative where L_p is more negative than -1.0. Physically this makes sense since the more negative values of L_p represent cases of high damping, and the positive L_p represents an unstable system. Therefore, the p_i for positive L_p becomes increasingly different from the measured time history for small positive increments in L_p. For very large damping (very negative L_p) the system would show essentially no response. Therefore, large increases in damping result in relatively small changes in the value of $J(L_p)$.

In Fig. 9, the cost function based on the time history with measurement noise (noisy case) is plotted as a function of L_p. The correct value of L_p (-0.2500) and the value of L_p (-0.3218) at the minimum of the cost (3.335) are both indicated on the figure. The general shape of the cost function in Fig. 9 is similar to that shown in Fig. 8. Figure 10 shows the comparison between the cost functions based on the time histories with and without measurement noise. The comments relating to the cost function of the no-noise case also apply to the cost function based on the noisy case. Figure 10 shows clearly that the two cost functions are shifted by the difference in the value of L_p at the minimum and increased by the difference in the minimum cost. One would expect only a small difference in the value of the cost when far from the minimum. This is because the "estimated" time history is so far from the measured time history that it becomes irrelevent as to whether the measured time history has noise added. Therefore, for large values of cost, the difference in the two cost functions should be small in comparison to the total cost.

Figure 11 shows the gradient of $J(L_p)$ plotted as a function of L_p for the noisy case. This is the function for which we were trying to find the zero (or equivalently, the minimum of the cost function) using the Gauss-Newton method of a previous section. The gradient is zero at $L_p = -0.3218$, which corresponds to the value of the minimum of $J(L_p)$.

The difference between the Newton-Raphson method (Eq. (14a)) and the Gauss-Newton method (Eq. (14b)) of minimization has been mentioned previously.

For this simple one-dimensional case, we can easily compute the second gradient both with the second term of Eq. (14a) (Newton-Raphson), and without the second term (Gauss-Newton, Eq. (14b)). Figure 12 shows a comparison between the Newton-Raphson and the Gauss-Newton approximation second gradients. The Gauss-Newton second gradient (dashed line) always remains positive because it is the sum of quadratic terms (squared for the one-dimensional example). The Newton-Raphson second gradient can be positive or negative, depending upon the value of the second partial with respect to L_p. Other than the difference in sign for the more negative L_p, the two curves have similar shapes.

As stated earlier, the Gauss-Newton method can be shown to be superior to Newton-Raphson in certain cases. We can demonstrate obvious cases of this with our example. An easy way to select a spot where problems with the Newton-Raphson method will occur is to look for places where the second gradient (slope of the gradient) is near zero or negative. Figure 11 has such a region near $L_p = -1.0$. If we choose a point where the gradient slope is exactly zero, we are forced to divide by zero in Eq. (12) with the Newton-Raphson method. This point is at $L_p = -1.13$ in Fig. 12. If the value of the slope of the gradient is negative, then the Newton-Raphson method will go to very negative values of L_p. For very negative values of L_p, the cost becomes asymptotically constant and the gradient becomes nearly zero. In that region, the Newton-Raphson algorithm would diverge towards negative infinity. If the slope of the gradient is positive but small, we still have a problem with the Newton-Raphson method. Figure 13 shows the first iteration starting from $L_p = -0.95$ for both Gauss-Newton and Newton-Raphson. The Newton-Raphson method selects a point where the tangent of the gradient at $L_p = -0.95$ intersects the zero line. This results in the selection of an L_p of approximately 2.6 in the first iteration. From that value it requires many iterations to return to the actual minimum. On the other hand, the Gauss-Newton method selects a value for L_p of approximately -0.09 and converges to the minimum to four-digit accuracy in two more iterations. With more complex examples a comparison of the convergence properties of the two algorithms becomes more difficult to visualize, but the problems are generalizations of the situation we have observed with the one-dimensional example.

The usefulness of the Cramèr-Rao bound was discussed in the Example With Measurement Noise section. At this point it is useful to digress briefly to discuss some of the ramifications of the Cramèr-Rao bound for the one-dimensional case. The Cramèr-Rao bound only has meaning for the noisy case. In the noisy example, the estimate of L_p is -0.3218 and the Cramèr-Rao bound is 0.0579. The calculation of the Cramèr-Rao bound was defined in the previous section for both one-dimensional and two-dimensional examples. The Cramèr-Rao bound is an estimate of the standard deviation of the estimate. One would expect the scatter in the estimates of L_p to be of about the same magnitude as the estimate of the standard deviation. For the one-dimensional case discussed here, the range (L_p (-0.3218) plus or minus the Cramèr-Rao bound (0.0579)) nearly includes the correct value of L_p (-0.2500). If noisy cases are generated for many time histories (adding different measurement noise to each time history), then the sample mean and sample standard deviation of the estimates for these cases can be calculated. Table 5 gives the sample mean, sample standard deviation, and the standard deviation of the sample mean (standard deviation divided by the square root of the number of cases) for 5, 10, and 20 cases. The sample mean, as expected, gets closer to the correct value of -0.2500 as the number of cases increases. This is also reflected by the decreasing values in column 4 of Table 5, which are estimates of the error in the sample mean. Column 3 of Table 5 shows the sample standard deviations, which indicate the approximate accuracy of the individual estimates. This standard deviation, which stays more or less constant, is approximately equal to the Cramèr-Rao bound for the noisy case being studied here. In fact, the Cramèr-Rao bounds for each of the 20 noisy cases used here (not shown in the table) do not change much from the values found for the noisy case being studied. Both of these results are in good agreement with the theoretical characteristics (Ref. 16) of the Cramèr-Rao bounds and maximum likelihood estimators in general.

The examples shown here indicate the value of obtaining more sample time histories (maneuvers). More samples improve confidence in the estimate of the unknowns. The same result holds true in analyzing actual flight time histories (maneuvers); thus it is always advisable to obtain several maneuvers at a given flight condition to improve the best estimate of each derivative.

The size of the Cramèr-Rao bounds and of the error between the correct value and the estimated value of L_p is determined to a large extent by the length of the time history and the amount of noise added to the correct time history. For the example being studied here, it is apparent from Fig. 5 that the amount of noise being added to the time history is large. The effect of the power of the measurement noise (GG^*, Eqs. (3) and (4)) on the estimate of L_p (that is, $\hat{L}_p$) for the time history is given in Table 6. The estimate of L_p is much improved by decreasing the measurement noise power. A reduction in the value of G to one-tenth of the value in the noisy example being studied yields an acceptable estimate of L_p. For flight data, the measurement noise is reduced by improving the accuracy of the output of the measurement sensors.

Two-Dimensional Case

In this section the cost function (which is dependent on both L_p and L_δ) is studied. The no-noise case is examined first, followed by the noisy case.

No-noise case. Even though the cost function is a function of only two unknowns, it is much more difficult to visualize than the one-unknown case. The cost function over a reasonable range of L_p and L_δ is shown in Fig. 14. The cost increases very rapidly in the region of positive L_p and large values of L_δ. The reason is just an extension of the argument for positive L_p given in the previous section. The shape of the surface can be depicted in greater detail if we examine only the values of the cost function less than 200 for L_p less than 1.0. Figure 15 shows a view of this restricted surface from the upper end of the surface. The minimum must lie in the curving valley that gets broader as we go to the far side of the surface. Now that we have a picture of the surface, we can look at the isoclines of constant cost on the L_p-versus-L_δ plane. These isoclines are shown in Fig. 16. The minimum of the cost function is inside the closed isocline. The steepness of the cost function in the positive-L_p direction is once again apparent. Inside the closed isocline the shape is more nearly elliptical, indicating that the cost is nearly quadratic here, so fairly rapid convergence in this region would be expected. The L_p axis becomes an asymptote in cost as L_δ approaches zero. The cost is constant for $L_\delta = 0$ because no response would result from any aileron input. The estimated response is zero for all values of L_p, resulting in constant cost.

Figure 16 shows the region of the minimum value of the cost function, which, as seen in the earlier example (Table 2), occurs at the correct values for L_p and L_δ of -0.2500 and 10, respectively. This is also evident by looking at the cost function surface shown in Fig. 17. The surface has its minimum at the correct value. As expected, the value of the cost function at the minimum is zero.

Noisy case. As shown before in the one-dimensional case, the primary difference between the cost functions for the no-noise and noisy cases was a shift in the cost function. In that instance, the noisy case was shifted so that the minimum was at a higher cost and a more negative value of L_p. In the two-dimensional case, the no-noise and noisy cost functions exhibit a similar shift. For two dimensions the shift is in both the L_p and L_δ directions. The shift is small enough that the difference between the two cost functions is not visible at the scale shown in Fig. 14 or from the perspective of Fig. 15. Figure 18 shows the isoclines of constant cost for the noisy case. The figure looks much like the isoclines for the no-noise case shown in Fig. 16. The difference between Figs. 16 and 18 is a shift in L_p of about 0.1. This is the difference in the value of L_p at the minimum for the no-noise and noisy cases. Heuristically, one can see that the same would be true for cases with more than two unknowns. The primary difference between the two cost functions is near the minimum.

The next logical part of the cost function to examine is near the minimum. Figure 19 shows the same view of the cost function for the noisy case as was shown in Fig. 17 for the no-noise case. The shape is roughly the same as that shown in Fig. 17, but the surface is shifted such that its minimum lies over $L_p = -0.3540$ and $L_\delta = 10.24$, and is shifted upward to a cost function value of approximately 3.3.

To get a more precise idea of the cost of the noisy case near the minimum, we once again need to examine the isoclines. The isoclines (Fig. 20) in this region are much more like ellipses than they are in Figs. 16 and 18. We can follow the path of the minimization example used before by including the results from Table 4 on Fig. 20. The first iteration ($L = 1$) brought the values of L_p and L_δ very close to the values at the minimum. The next iteration essentially selected the values at the minimum when viewed at this scale. One of the reasons the convergence is so rapid in this region is that the isoclines are nearly elliptical, demonstrating that the cost is very nearly quadratic in this region. If we had started the Gauss-Newton algorithm at a point where the isoclines are much less elliptical (as in some of the border regions in Fig. 18), the convergence would have been much slower initially, but much the same as it entered the nearly quadratic region of the cost function.

Before concluding our examination of the two-dimensional case, we need to examine the Cramèr-Rao bound. Figure 21 shows the uncertainty ellipsoid, which is based on the Cramèr-Rao bounds defined in an earlier section. The relationships between the Cramèr-Rao bound and the uncertainty ellipsoid are discussed in Ref. 16. The uncertainty ellipsoid almost includes the correct value of L_p and L_δ. The Cramèr-Rao bound for L_p and L_δ can be determined from the projection of the uncertainty ellipsoid onto the L_p and L_δ axes, and compared with the values given earlier, which were 0.1593 and 1.116 for L_p and L_δ, respectively.

ESTIMATION USING FLIGHT DATA

In the previous several sections we examined the basic mechanics of obtaining maximum likelihood estimates from computed examples with one or two unknown parameters. Now that we have a grasp of these basics, we can explore the estimation of stability and control derivatives from actual flight data. For the computationally much more difficult situation usually encountered using actual flight data, we will obtain the maximum likelihood estimates with the Iliff-Maine code (MMLE3 program) described in Ref. 17. The equations of motion that are of interest are given in the AIRCRAFT EQUATIONS OF MOTION section of this paper; the remainder of the equations are given in Ref. 17.

In general, flight data estimation is fairly complex, and codes such as the Iliff-Maine code must usually be used to assist in the analysis. However, one must still be cautious about accepting the results; that is, the estimates must fit the phenomenology, and the match between the measured and computed time histories must be acceptable. This is true in all flight regimes, but one must be particularly careful in potential problem situations such as (1) in separated flow at high Mach numbers or high angle of attack, (2) with unusual aircraft configurations such as the oblique wing (Ref. 18), or (3) with modern high-performance aircraft with high-gain feedback loops. In any of the above cases, one should be particularly careful where there are even small anomalies in the match. These anomalies may indicate ignored terms in the equations of motion, separated flow, nonlinearities, sensor problems, insufficient resolution (Ref. 1), sensor location (Ref. 1), time or phase lags (Refs. 1 and 19), or any of a long list of other problems.

The following brief examples are intended to show how the above caveats and the computed examples of previous sections can be used to assist in the analysis. In the computed example, the desirability of low-noise sensors, an adequate model, and several maneuvers at a given flight condition is shown.

Hand Calculation Example

Sometimes evaluation of a fairly complex flight maneuver can be augmented with a simple hand calculation. One example of this can be found for the space shuttle. The space shuttle is a large double-delta-winged vehicle designed to enter the atmosphere from space and land horizontally. The entry control system consists of 12 vertical reaction-control-system (RCS) jets (six up-firing and six down-firing), 8 horizontal RCS jets (four left-firing and four right-firing) 4 elevon surfaces, a body flap, and a split rudder surface. The locations of these devices are shown in Fig. 22. The vertical jets and the elevons are used for both pitch and roll control. The jets and elevons are used symmetrically for pitch control and asymmetrically for roll control. The space shuttle control system is described briefly in Ref. 6.

The shuttle example used here is from a maneuver obtained at a Mach number of approximately 21 and an angle of attack of approximately 40°. The controls being used for this lateral-directional maneuver are the differential elevons and the side-firing jets (yaw jets). The maneuver is shown in Fig. 23. Equations (15) to (31) describe the equations of motion. A simplified approach can be used to determine some of the derivatives by hand. The approach is one that has been used since the beginning of dynamic analysis of flight maneuvers. In particular, for this maneuver the slope of the rates can be used to determine the yaw jet control derivatives. This is possible for this example, even with a high-gain feedback system, because the yaw jets are essentially step functions, and the slope of the rates p and r can be determined before the vehicle and the differential elevon (aileron) responses become significant. The rolling moment due to yaw jet (L_{YJ}) is particularly important for the shuttle (Ref. 6 discusses the essential nature of flight-determined L_{YJ} in the redefinition of entry maneuvers) and is, in general, more difficult to obtain than the more dominant yawing moment due to yaw jet. Therefore, as an illustrative example, L_{YJ} is determined by hand. Figure 24 shows yaw jet activity and smoothed roll rate plotted at expanded scales. The equation for L_{YJ} is given by

$$L_{YJ} = \dot{p}I_X/(\text{Number of yaw jets}) \tag{42}$$

$$\dot{p} \cong \Delta p/\Delta t = \frac{0.07}{57.3} \div (0.1) \tag{43}$$

Therefore, given that $I_X \cong 900{,}000$ slug-ft^2, and the number of yaw jets is 4, $L_{YJ} \cong 2750$ ft-lb.

The same maneuver was analyzed with MMLE3, and the resulting match is shown in Fig. 25. The match is very good except for a small mismatch in p at about 6 sec. This small mismatch was studied separately with MMLE3 and found to be caused by a nonlinearity in the aileron derivative. The value from MMLE3 for L_{YJ} is 2690 ft-lb, which for the accuracy used here is essentially the same value as obtained by the simplified method. The aileron derivatives would be difficult to determine as accurately as the yaw jet derivatives. Although good estimates can seldom be obtained with the slope method discussed here, rough estimates can usually be obtained to gain some insight into values obtained with MMLE3 (or any other maximum likelihood program). These rough estimates can then be used to help explain unexpected values of estimates from an estimation program.

Sometimes a flight example becomes too complex to allow anything other than qualitative estimates to be determined by hand. The example shown in Fig. 26 is the determination of the rudder derivative for the F-8 aircraft with the yaw augmentation system on. This example, taken from Ref. 20, includes an aileron pulse and a rudder pulse. Although an independent pilot rudder pulse is input during the maneuver, the rudder is largely responding to the lateral acceleration feedback. When the rudder is moving, several other variables are also moving, thus making it difficult to use the simplified approach just discussed. However, $C_{n_{\delta_r}}$ can be roughly determined when the rudder moves, approximately 1.7 sec from the start of the maneuver. Most of the slope of yaw rate is probably caused by the rudder, but a poor estimate would be obtained using the hand calculation.

Cost Function for Full Aircraft Problem

The analysis of a lateral-directional maneuver obtained in flight typically has from 15 to 25 unknown parameters (as shown in Eqs. (15) and (31)), in contrast to the one or two in the simple aircraft example. This makes detailed examples unwieldy and any graphic presentation of the cost function impossible. Therefore, in this section we are primarily examining the estimation procedure and the process of the minimization.

For our flight example, we have chosen a lateral-directional maneuver, with both aileron and rudder inputs, that has 17 unknown parameters. The data are from the oblique wing aircraft (Ref. 18) with the wing unskewed during the maneuver. This example was chosen because it is a typical maneuver. The time history of the data and the subsequent output of MMLE3 have been published in Ref. 21. Some results of the analysis are shown in Table 7. The match between the measured time history (solid lines) and the estimated (calculated) time history (dashed lines) is shown as a function of iteration in Fig. 27. Figures 27(a) to (e) are for iterations 0 to 4, respectively. Table 7 shows that the cost remains unchanged after four iterations. A similar result was obtained for the two-dimensional simple aircraft example in Fig. 6 and Table 4.

Of the many things the analyst must consider in obtaining estimates, the two most important ones are how good is the match and how good is the convergence. A satisfactory match and monotor convergence are necessary, but not sufficient, conditions for a successful analysis. Figure 27(e), although not perfect, is a very good match. The convergence can best be evaluated by looking at the normalized cost in the last row of Table 7. The cost has converged rapidly and monotonically in four iterations, and it remains at the converged cost. These factors are convincing evidence that the convergence is complete. Therefore, the criteria of match and convergence are satisfied in our example. In some cases we might encounter cost that does not converge rapidly (in four to six iterations) or monotonically, or stay "exactly" at the minimum value. These situations usually indicate at least a small problem in the analysis. These problems, if found, are usually traced to an instrumentation or data aquisition problem, an inadequate mathematical model, or a maneuver that contains a marginal amount of information.

Table 7 also shows that the startup values of all the coefficients are zero for the control and bias variables. Wind tunnel estimates could have been used for starting values, but the convergence of the algorithm is not very dependent on the startup values. As part of the startup algorithm, the MMLE3 program normally holds the derivatives of the state variables constant until after the first iteration, as is evident in Table 7.

Figure 27(a) shows the match between the measured and computed data for the startup values. The match is very poor because the startup values for the control derivatives are all zero, so the only motion is in response to the initial conditions. The control derivatives and biases are determined on the first iteration, resulting in the much improved match shown in Fig. 27(b). The match after two iterations, shown in Fig. 27(c), is improved as the program further modifies the control derivatives and, for the first time, adjusts the derivatives affecting the natural frequency (C_{n_β} and C_{ℓ_β}). By the third iteration (Fig. 27(d)), the improvement in the match is almost complete, because minor adjustments to the frequency are made and the damping derivatives are changed. Fig. 27(e) shows the match when all but the most minor derivatives have ceased to change.

Several general observations can be made based on this well behaved example. The strong or most important coefficients have essentially converged in three iterations. The same effect was seen in the simple example — that is, L_δ converged faster than L_p (Table 4). Some of the less important or second-order coefficients have only converged to two places after three iterations and are still changing by one digit in the fourth place at the end of six iterations. Another observation is that for some coefficients (C_{ℓ_r}, $C_{n_{\delta_a}}$, and $C_{\ell_{\delta_r}}$) even though the sign is wrong after the first iteration, the algorithm quickly selects their correct values once the important derivatives have stabilized.

In general, if the analysis of a maneuver has gone well, we do not need to spend much time inspecting a table analogous to Table 7. However, if there have been problems in convergence or in the quality of the fit, a detailed inspection of such a table may be necessary. The data may show an important coefficient going unstable at an early iteration, which could cause problems later. If the starting values are grossly in error, the algorithm is driven a long way from reasonable values and then for many reasons does not behave well. Occasionally the algorithm alternately selects from two diverse set of values of two or more coefficients on successive iterations, behaving as if the shape of the cost function were a narrow multidimensional valley analogous to but more extreme than the two-dimensional valley shown in Figs. 18 and 20.

Cramèr-Rao Bounds

The earlier sections regarding the computed example have shown that the Cramèr-Rao bound is a good indicator of the accuracy of an estimated parameter. The Cramèr-Rao bounds can be used in a similar, but somewhat more qualitative, fashion on flight data. The Cramèr-Rao bounds that are included in MMLE3 (as well as many other maximum likelihood estimation programs) have been useful in determining whether estimates are good or bad. The aircraft example discussed here has been reported previously (for example, in Refs. 1 and 16). However, this example of the use of the Cramèr-Rao bound in the assessment of flight-derived estimates is pertinent to the thrust of this paper. Figure 28 shows estimates of C_{n_p} as a function of angle of attack for the PA-30 twin-engine general aviation aircraft (Ref. 22) at three flap settings. There is a significant amount of scatter, which makes the reliability of the information on C_{n_p} questionable. The data shown are the estimates from the MMLE3 program, which also provides the Cramèr-Rao bounds for each estimate. Past experience (Ref. 1) has shown that if the Cramèr-Rao bound is multiplied by a scale factor (the result sometimes being called the uncertainty level (Refs. 1 and 16)) and plotted as a vertical bar with the associated estimate, it helps in the interpretation of flight-determined results. Figure 29 shows the same data as Fig. 28, with the uncertainty levels now included as vertical bars. The estimates with small uncertainty levels (Cramèr-Rao bounds) are the best estimates, as was discussed earlier in the section on Cramèr-Rao bounds for the one-dimensional case. The fairing shown in Fig. 29 goes through the estimates with small Cramèr-Rao bounds and ignores the estimates with large bounds. One can have great confidence in the fairing of the estimates, because the fairing is well defined and consistent when the Cramèr-Rao bound information is included. In this particular instance, the estimates with small bounds were from maneuvers where the aileron forced the motion, and the large bounds were from maneuvers where the rudder forced the motion. Therefore, in addition to aiding in the fairing of the estimates, the Cramèr-Rao bounds help show that the aileron-forced maneuvers are superior for estimating C_{n_p} for the PA-30 aircraft.

This example illustrates that the Cramèr-Rao bounds are a useful tool in assessing flight-determined estimates, just as they were found useful for the simple aircraft example with computed data.

Atmospheric Turbulence (State Noise)

Atmospheric turbulence (state noise) cannot always be avoided in flight; therefore, it is desirable to be able to obtain stability and control derivatives in the presence of turbulence. In addition, an estimate of the turbulence time history can be of interest, particularly in the implementation of turbulence suppression systems.

Many years ago it was demonstrated that the stability and control derivatives can be adequately determined with maximum likelihood estimation techniques for maneuvers performed in smooth air. If these techniques, which do not account for turbulence, are applied to data obtained in turbulence, not only are the resulting matches of the time histories unsatisfactory but the estimated coefficients are unacceptable (Refs. 23 to 25). The technique described in Refs. 14, 23, and 25 can account for the effect of turbulence. With this technique, maximum likelihood estimates of the stability and control derivatives as well as estimates of the turbulence time histories are obtained by minimizing the cost function given by Eq. (11). Results of the application of the technique to longitudinal maneuvers obtained in turbulence have been reported previously (Refs. 23 to 25).

The lateral-directional equations (Eqs. (15), (16), (17), (18), and (29)) can be modified in a manner similar to that used to modify the longitudinal equations in Refs. 23 to 25. The turbulence (state noise) model is the Dryden expression, which is described in Ref. 26. The Iliff-Maine code (Ref. 17) can be used to obtain the maximum likelihood estimates where state noise is present.

Thirty-eight seconds of data from the PA-30 aircraft flying in turbulence was analyzed at 50 samples/sec. The best match that could be obtained with the maximum likelihood estimation method that does not account for turbulence is shown in Fig. 30. The match is unacceptable and resulted in poor estimates of the stability and control derivatives. Figure 31 shows the match obtained with the maximum likelihood estimation technique that accounts for turbulence (Refs. 14 and 17). The match is excellent and the maneuver provided acceptable estimated stability and control derivatives. It is also of interest to compare the power spectra of the estimated turbulence time histories. The power spectrum of the turbulence component affecting angle of sideslip, $\hat{\beta}_g$, is shown in Fig. 32. Figure 33 presents the power spectrum of the turbulence component affecting roll rate, $\hat{p}_g$. The slopes of the asymptotes shown in Figs. 32 and 33 are those defined by the Dryden expression given in Ref. 26. Good agreement is shown between the power spectra and the asymptotes for $\hat{\beta}_g$ and $\hat{p}_g$.

The algorithm used here is based on a linearized system described by Eqs. (5) to (7) and solved by minimizing the cost function given by Eq. (11). The system need not resemble that for the aircraft stability and control problem other than in the requirement for linearity. Therefore, many formulations for the structural problem are written in the form of Eqs. (5) to (7), and the algorithm under discussion can be directly applied with these formulations.

ESTIMATION FOR SIMPLE STRUCTURAL PROBLEM

The problem of the flexible space structure is most fully characterized as a distributed parameter system with its associated distributed system control laws. The model will vary depending upon changes in its configuration or its environment, such as solar heating. As in most cases, the preferred solution is the simplest successful approach. The lumped system approach is much simpler and computationally far more efficient than the fully distributed parameter system approach. For example, structural mode control based on current state-of-the-art approaches has proved very successful. Admittedly, the aircraft structure is heavier than most spacecraft, but many aircraft structures are highly complex, consisting of many substructures within the main structure. To the novice, many of the space structures currently being investigated appear simpler than modern, large aircraft. If the lumped parameter system approach used for the aircraft problem is found to be inadequate, it seems likely that distributed parameter estimation codes will evolve to whatever complexity is necessary to solve the flexible space structure problem.

This paper has discussed some of the experience gained from the application of aircraft stability and control analysis to flight data. The codes used for this analysis are for lumped parameter systems in the time domain. The codes have been used successfully for structural problems and are fully adaptable to the frequency domain if that is found to be preferable.

Although few results have been obtained for time-domain structural analysis at the Ames Dryden Flight Research Facility, some superficial experience in structural time-domain analysis has been obtained. The following two examples show how the techniques being used for stability and control analysis can be applied to simple structural problems. The preceeding section discussed the incorporation of state noise in the model. The following examples do not include the use of state noise, but state noise, if warranted, could easily be incorporated in the types of examples to be discussed.

Estimation of Structural Characteristics

All aircraft have observable structural modes. These modes usually cause no difficulty in estimating stability and control derivatives because the structural frequencies are higher than the aerodynamic frequencies. In general, if the structural frequencies are higher than the highest aerodynamic frequency by more than a factor of 5 to 10, they can be neglected unless their amplitude is so large as to mask measurements desired for the aerodynamic analysis. However, if one or more structural modes are affecting the aerodynamic modes, as may occur in large aircraft, these structural modes must be included in the mathematical model being analyzed.

Even though no completely satisfactory practical results are available that account for structural modes and their interactions with the aerodynamics, it is interesting to assess the time-domain maximum likelihood analysis of the structural modes independent of any interaction. This can be done where a structural mode is observed and no significant coupling is apparent.

Figure 34 shows a structural mode on the lateral acceleration of an aircraft where little effect was observed for structural-aerodynamic coupling. The frequency of the mode is high enough that the mode does not interact with the aerodynamic modes. Therefore, the stability and control derivatives were obtained separately and held constant for the succeeding analysis. The analysis consisted of using the maximum likelihood estimation program MMLE 3 (Ref. 17) with a sixth-order model that included the lateral-directional aerodynamic modes plus one structural mode. The dynamic pressure and the velocity were allowed to vary in the analysis. The structural mode frequency and damping were estimated as linear functions of dynamic pressure. The initial conditions were also estimated. A structural mode frequency of 7.84 Hz was chosen to start the estimation process. The comparison between the original data and the match obtained with the maximum likelihood estimation method is shown in Fig. 35. The two time histories are in good agreement at the beginning of the maneuver and at the end of the maneuver, but they are 180° out of phase at a time of approximately

0.3 sec. The match shown in Fig. 35 suggests that the maximum likelihood estimator has reached a local minimum but not the global minimum. Multiple minima are not normally a problem when obtaining the stability and control derivatives of aircraft with the maximum likelihood estimation method.

The reason for the multiple minima is demonstrated by the following simple scalar example. Let the noiseless measured response be $z(t) = \sin(\omega_0 t)$ and the estimated response be $\tilde{z}_\xi = \sin(\omega t)$, where ω is the only unknown coefficient. Then, by Eq. (4), the cost function becomes

$$J(\omega,T) = \int_0^T \left[\sin(\omega_0 t) - \sin(\omega t)\right]^2 dt$$

$$= t - \frac{1}{4\omega_0} \sin(2\omega_0 T) - \frac{1}{4\omega} \sin(2\omega T)$$

$$- \frac{2\omega}{\omega^2 - \omega_0^2} \quad \frac{\omega_0}{\omega} \sin(\omega T) \cos(\omega_0 T) - \cos(\omega T) \sin(\omega_0 T)$$

If T is chosen to represent 10 cycles, as shown in Fig. 35, then for an ω_0 of 1 rad/sec, T equals 20π. In Fig. 36, the cost function $J(\omega,20\pi)$ is shown as a function of ω. The global minimum is at an ω of 1 rad/sec, as it should be, but there are many local minima at increments of approximately 0.05 rad/sec. If a value of less than 0.97 or greater than 1.03 were chosen for a starting estimate of ω, the algorithm would converge to a local minimum. If a value of between 0.98 and 1.02 were chosen, it would converge to the global minimum. Therefore, for this example where 10 cycles were observed, the starting value of ω must be less than 3 percent from the correct anwser to converge to the global minimum.

Figure 37 shows a sine wave for the global minimum along with a sine wave with a frequency that varies 10 percent from the global minimum. The sine waves are in phase at the beginning and end, and 180° out of phase in the middle. These data appear similar to those shown for flight data in Fig. 35. If only one or two cycles were used for the analysis, the problem illustrated in Fig. 37 would be minimized. This is apparent in Fig. 38 where only the first cycle of Fig. 37 is shown.

If T is chosen to represent only one cycle and ω_0 remains equal to 1 rad/sec (as in Fig. 38), then T equals 2π. The cost function $J(\omega,2\pi)$ is presented as a function of ω in Fig. 39. The global minimum is correctly at an ω of 1 rad/sec, but now the algorithm converges to the global minimum if ω is started within approximately 25 percent of the correct value.

Knowing the sensitivity of the algorithm when a record with many lightly damped cycles is being analyzed, the data of Fig. 34 can be reanalyzed starting closer to the observed frequency. Starting the maximum likelihood estimation method with an ω of 9.0 results in the fit shown in Fig. 40. This is an acceptable fit of the data.

Based on the preceding results, if data are to be analyzed where many cycles of a structural mode are present, the structural mode frequency, ω, must be closely approximated before starting the estimation process.

Structural Modes in Space

In the process of analyzing aircraft flight data, the authors have frequently observed results that clearly exhibit unmodeled dynamics. The unmodeled dynamics could be caused by many phenomena, such as higher-order aerodynamic modes or structural modes. These modes can usually be ignored and left unmodeled because they have no effect on the results of primary interest in the analysis. If the unmodeled modes cannot be ignored, then the system equations must be revised to include the unmodeled modes.

The authors have not yet found it necessary to model structural modes for data obtained in space in the process of obtaining control derivatives for the space shuttle. However, the structural modes have been observed. Figure 41 shows the response of the space shuttle to the firing of a roll jet and a yaw jet at an altitude of 430,000 ft. The space shuttle configuration and the location of the RCS jets are shown in Fig. 22. The changes in the rigid-body rates and lateral acceleration caused by the jet firings are apparent in Fig. 41. The structural modes are also excited by the jets, as evidenced by the increased ringing in each signal at the time of the jet firings. The roll jet firing has little effect on the rigid-body response for the yaw rate and lateral acceleration; however, the yaw jet results in a rigid-body response for all the signals chosen. This maneuver was analyzed to obtain control derivatives for the rigid-body response described by Eqs. (15) to (31). The resulting match between the measured and computed response is shown in Fig. 42. The estimated control derivatives are in good agreement with those obtained from the maneuvers. The unmodeled structural dynamic modes are evident, but it is apparent that the modes will have little effect on the rigid-body control derivatives. The differences between the measured and computed rigid-body responses (the residuals) for the time close to when the jets were fired are shown in Fig. 43. The data shown here are for a sample interval of 0.006 sec. Some persistent structural ringing is shown for the two rates and the lateral acceleration. However, when a jet is fired, the increased structural response is evident. The structural coefficients can be extracted directly from the residual as they were for the example in the previous section. It appears that there may be some contamination caused by the rigid-body response at the instant the jets fire. If so, this contamination can be eliminated in one of two ways: either analyze the portion of the maneuver a tenth of a second after the jet fires, or adapt the equations of motion to include the structural dynamics in addition to the rigid dynamics. The structural dynamics depicted in Fig. 43 have not been analyzed, but the procedure is straightforward. The procedure used on this case was the same as that used on the example in the preceeding section. It is apparent, however, that more than one structural mode would need to be included in the model.

All the analysis techniques discussed in this paper apply to the analysis of this space shuttle example. If state noise is included in the mathematical model, then the linear form of Eqs. (5) to (7) would be required. In general, if the structural partial differential equation can be expressed in the linear form of Eqs. (5) to (7) (with or without state noise), the structural modes can be analyzed readily with the MMLE 3 program (Ref. 17) in the time domain. If the analyst prefers, the problem can be expressed in the linear constant coefficient form and analyzed in the frequency domain, as described in Ref. 12. The relative advantages and disadvantages of time-domain analysis as compared with frequency-domain analysis are also discussed in that reference. If the equations are nonlinear, but in the form of Eqs. (1) to (3), then maximum likelihood estimates can be obtained in the time domain.

CONCLUDING REMARKS

The computed simple aircraft example showed the basics of minimization and the general concepts of cost functions themselves. In addition, the example demonstrated the advantage of low measurement noise, multiple estimates at a given condition, and the Cramèr-Rao bounds, and the quality of the match between the measured and computed data. The flight data showed that many of these concepts still hold true even though the dimensionality of the cost function makes it impossible to plot or visualize. In addition, the techniques used for the aircraft problem were shown to be applicable to the flexible structure problem.

REFERENCES

1. Iliff, K. W., "Aircraft Identification Experience," AGARD-LS-104, 1979, pp. 6-1 to 6-35.

2. Goodwin, Graham C., and Payne, Robert L., Dynamic System Identification: Experiment Design and Data Analysis, Academic Press, New York, 1977.

3. Sorenson, Harold W., Parameter Estimation; Principles and Problems, Marcel Dekker, Inc., New York, 1980.

4. Klein, V., "On the Adequate Model for Aircraft Parameter Estimation," CIT, Cranfield Report Aero No. 28, Mar. 1975.

5. Hamel, P., "Determination of Stability and Control Parameters From Flight Testing," AGARD-LS-114, 1981, pp. 10-1 to 10-42.

6. Iliff, Kenneth W., and Maine, Richard E., "NASA Dryden's Experience in Parameter Estimation and Its Use in Flight Test," AIAA Paper 82-1373, Atmospheric Flight Mechanics Conference, San Diego, Calif., Aug. 1982.

7. Gupta, N. K., Hall, Earl W., and Trankle, T. L., "Advanced Methods of Model Structure Determination from Test Data," AIAA Paper 77-1170, 1977.

8. Trankle, T. L., Vincent, J. H., and Franklin, S. N., "System Identification of Nonlinear Aerodynamic Models," The Techniques and Technology of Nonlinear Filtering and Kalman Filtering, AGARD-AG-256, 1982.

9. Klein, V., and Schiess, J. R., "Compatibility Check of Measured Aircraft Responses Using Kinematic Equations and Extended Kalman Filter," NASA TN D-8514, 1977.

10. Bach, R. E., and Wingrove, R. C., "Applications of State Estimation in Aircraft Flight Data Analysis," AIAA Paper 83-2087, 1983.

11. Mulder, J. A., Jonkers, H. L., Horsten, J. J., Breeman, J. H., and Simons, J. H., "Analysis of Aircraft Performance, Stability and Control Measurements," AGARD-LS-104, 1979, pp. 5-1 to 5-87.

12. Klein, Vladislav, "Maximum Likelihood Method for Estimating Airplane Stability and Control Parameters From Flight Data in Frequency Domain," NASA TP-1637, 1980.

13. Fu, K. H., and Marchand, M., "Helicopter System Identification in the Frequency Domain," Ninth European Rotorcraft Forum, Paper 96, Stresa, Italy, Sept. 13-15, 1983.

14. Maine, Richard E., and Iliff, Kenneth W., "Formulation and Implementation of a Practical Algorithm for Parameter Estimation with Process and Measurement Noise," SIAM J. Appl. Math., vol. 41, 1981, pp. 558-579.

15. Balakrishnan, A. V., Communication Theory, McGraw-Hill Book Co., c.1963.

16. Maine, Richard E., and Iliff, Kenneth W., "The Theory and Practice of Estimating the Accuracy of Dynamic Flight-Determined Coefficients," NASA RP-1077, 1981.

17. Maine, Richard, E., and Iliff, Kenneth W., "User's Manual for MMLE3, A General FORTRAN Program for Maximum Likelihood Parameter Estimation," NASA TP-1563, Nov. 1980.

18. Maine, Richard E., Aerodynamic Derivatives for an Oblique Wing Aircraft Estimated From Flight Data by Using a Maximum Likelihood Technique," NASA TP-1336, 1978.

19. Steers, Sandra Thornberry and Iliff, Kenneth W.; "Effects of Time-Shifted Data on Flight-Determined Stability and Control Derivatives," NASA TN D-7830, 1975.

20. Shafer, M. F., "Flight-Determined Correction Terms for Angle of Attack and Sideslip," AIAA Paper 82-1374, 1982.

21. Maine, Richard E., "Programmer's Manual for MMLE3, A General FORTRAN Program for Maximum Likelihood Parameter Estimation," NASA TP-1690, 1981.

22. Fink, Marvin P., and Freeman, Delma C., Jr., "Full-Scale Wind-Tunnel Investigation of Static Longitudinal and Lateral Characteristics of a Light Twin-Engine Airplane," NASA TN D-4983, 1969.

23. Iliff, K. W.; "Identification and Stochastic Control With Application to Flight Control in Turbulence," UCLA-ENG-7340, School of Engineering and Applied Science, Univ. Calif., Los Angeles, Calif., May 1973.

24. Iliff, Kenneth W., "An Aircraft Application of System Identification in the Presence of State Noise," New Directions in Signal Processing in Communication and Control, J. K. Skwirzynski, ed., Noordhoff International Publishing (Leyden, The Netherlands), c.1975, pp. 529-541.

25. Iliff, Kenneth W.; "Estimation of Characteristics and Stochastic Control of an Aircraft Flying in Atmospheric Turbulence," Proceedings of AIAA 3rd Atmospheric Flight Mechanics Conference, c.1976, pp. 26-38.

26. Chalk, C. R., Neal, T. P., Harris, T. M., Pritchard, F. E., and Woodcock, R. J., "Background Information and User Guide for MIL-F-8785B(ASG), "Military Specification — Flying Qualities of Piloted Airplanes," AFFDLTR-69-72, Air Force Flight Dynamics Lab., Wright-Patterson Air Force Base, Aug. 1969.

Table 1 Values of computed time history with no measurement noise

i	δ, deg	p, deg/sec
1	0	0
2	1	0.9754115099857
3	1	2.878663149266
4	1	4.689092110779
5	1	6.411225409939
6	1	8.049369277012
7	1	9.607619924937
8	0	10.11446228200
9	0	9.621174135646
10	0	9.151943936071

Table 2 Pertinent values as a function of iteration

L	$\hat{L}_p(L)$	$\hat{L}_\delta(L)$	$\phi(L)$	$\psi(L)$	J_L
0	-0.5000	15.00	0.9048	2.855	21.21
1	-0.3005	9.888	0.9417	1.919	0.5191
2	-0.2475	9.996	0.9517	1.951	5.083×10^{-4}
3	-0.2500	10.00	0.9512	1.951	1.540×10^{-9}
4	-0.2500	10.00	0.9512	1.951	1.060×10^{-14}

Table 3 Values of computed time history with added measurement noise

i	δ, deg	p, deg/sec
1	0	0
2	1	0.4875521781881
3	1	3.238763570696
4	1	3.429117357944
5	1	6.286297353361
6	1	6.953798550097
7	1	10.80572930119
8	0	9.739367269447
9	0	9.788844525490
10	0	7.382568353168

Table 4 Pertinent values as a function of iteration

L	$\hat{L}_p(L)$	$\hat{L}_\delta(L)$	$\phi(L)$	$\psi(L)$	J_L
0	-0.5000	15.00	0.9048	2.855	30.22
1	-0.3842	10.16	0.9260	1.956	3.497
2	-0.3518	10.23	0.9321	1.976	3.316
3	-0.3543	10.25	0.9316	1.978	3.316
4	-0.3542	10.24	0.9316	1.978	3.316
5	-0.3542	10.24	0.9316	1.978	3.316

Table 5 Mean and standard deviations for estimates of L_p

Number of cases, N	Sample mean, $\mu(\hat{L}_p)$	Sample standard deviation, $\sigma(\hat{L}_p)$	Sample standard derivation of the mean, $\sigma(\hat{L}p)/\sqrt{N}$
5	-0.2668	0.0739	0.0336
10	-0.2511	0.0620	0.0196
20	-0.2452	0.0578	0.0129

Table 6 Estimate of L_p and Cramèr-Rao bound as a function of the square root of noise power

Square root of noise power	Estimate of L_p	Cramèr-Rao bound
0.0	-0.2500	-------
0.01	-0.2507	0.00054
0.05	-0.2535	0.00271
0.10	-0.2570	0.00543
0.2	-0.2641	0.0109
0.4	-0.2783	0.0220
0.8	-0.3071	0.0457
1.0	-0.3218	0.0579
2.0	-0.3975	0.1248
5.0	-0.6519	0.3980
10.0	-1.195	1.279

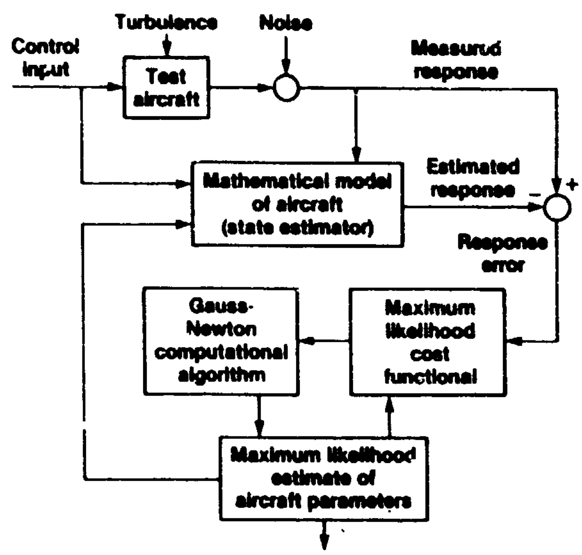

Fig. 1 Maximum likelihood estimation concept.

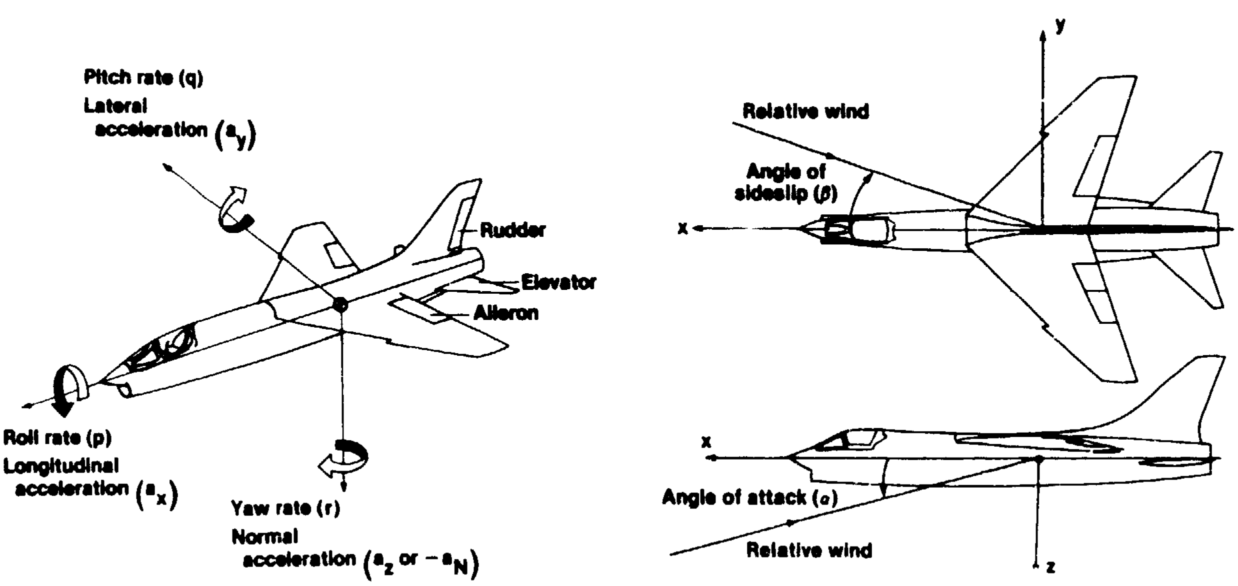

(a) Measurement and control surface definitions.

(b) Flow angle definitions.

Fig. 2 Aircraft axis system.

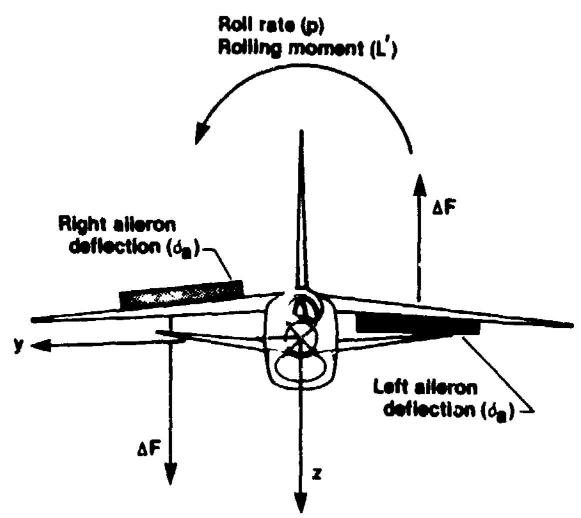

(c) Simplified aircraft nomenclature.

Fig. 2 Concluded.

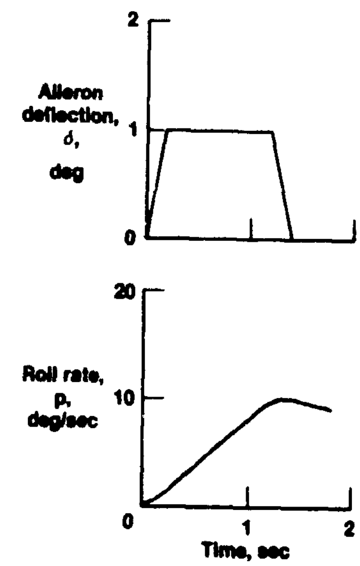

Fig. 3 Time history with no measurement noise.

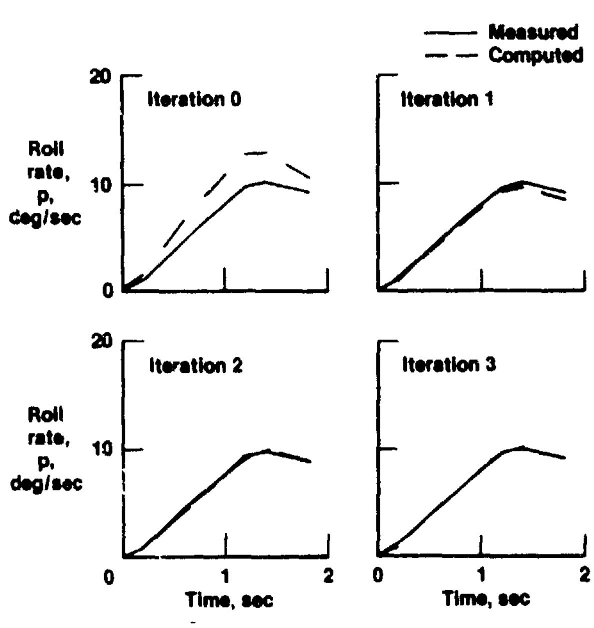

Fig. 4 Comparison of measured and computed data for each of the first three iterations.

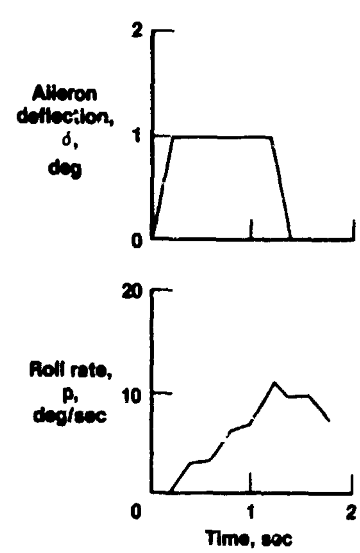

Fig. 5 Time history with measurement noise.

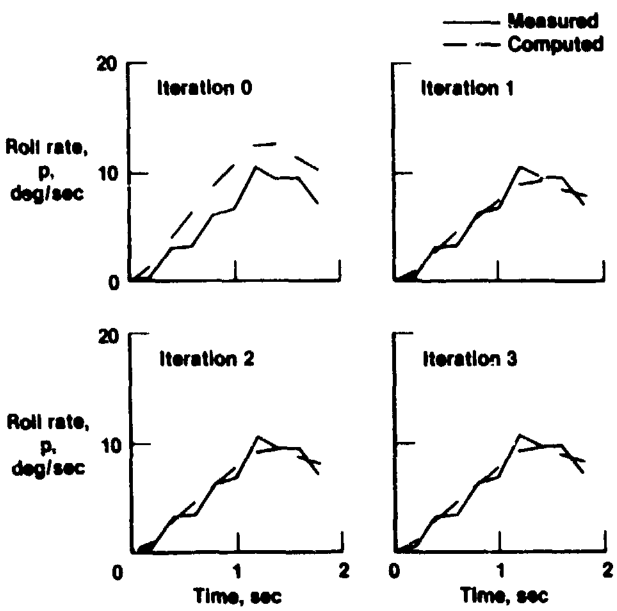

Fig. 6 Comparison of measured and computed data for each iteration.

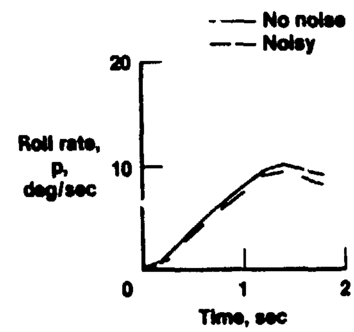

Fig. 7 Comparison of estimated roll rate from no-noise and noisy cases.

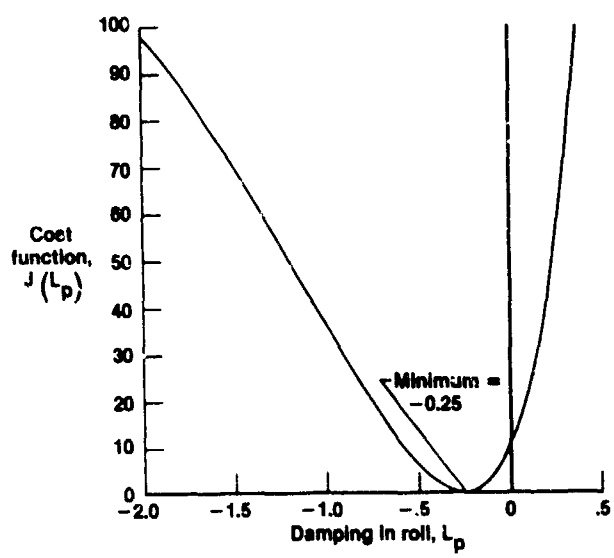

Fig. 8 Cost function ($J(L_p)$) as a function of L_p for no-noise case.

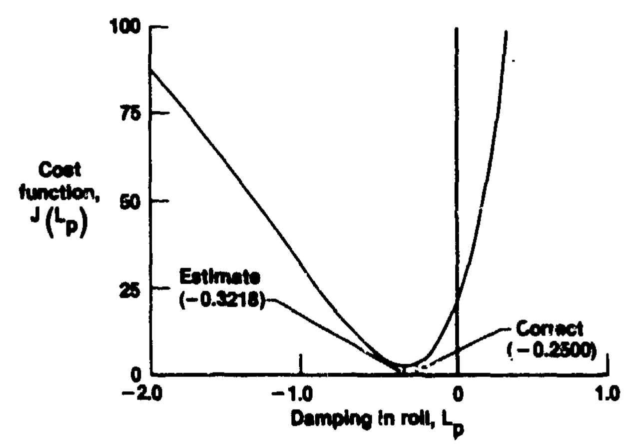

Fig. 9 Cost function as a function of L_p for noisy case.

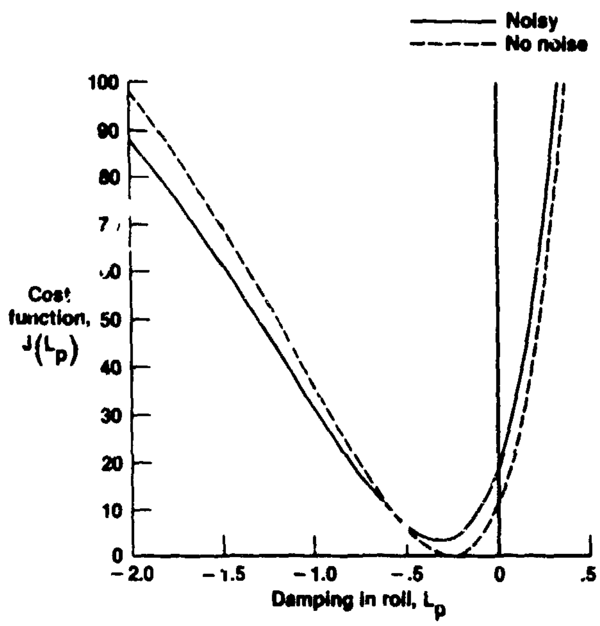

Fig. 10 Comparison of the cost functions for the no-noise and noisy cases.

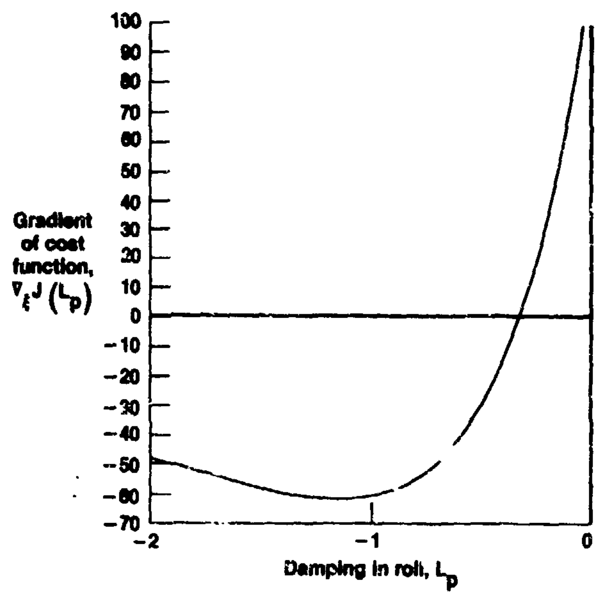

Fig. 11 Gradient of $J(L_p)$ as a function of L_p for noisy case.

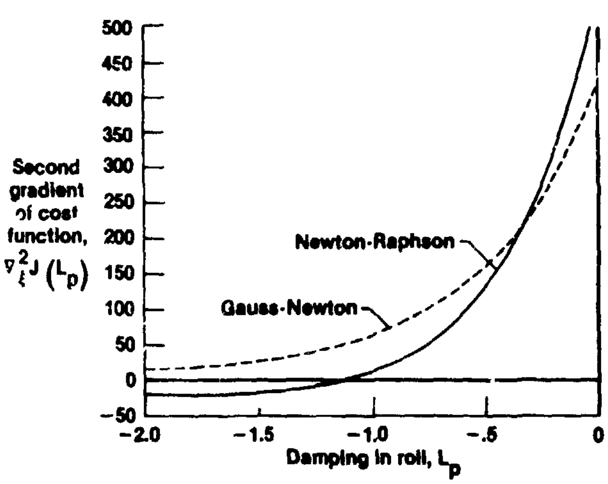

Fig. 12 Comparison of Newton-Raphson and Gauss-N values of the second gradient the noisy case.

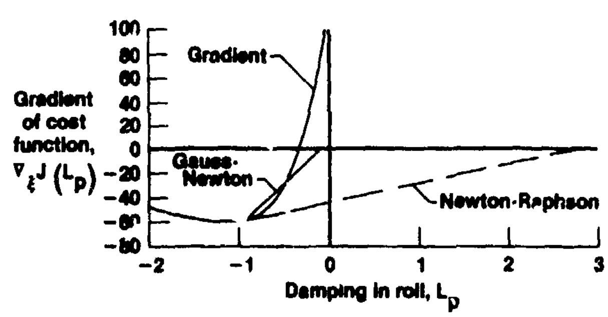

Fig. 13 Comparison of first iteration step size for the Newton-Raphson and Gauss-Newton algorithms for the noisy case.

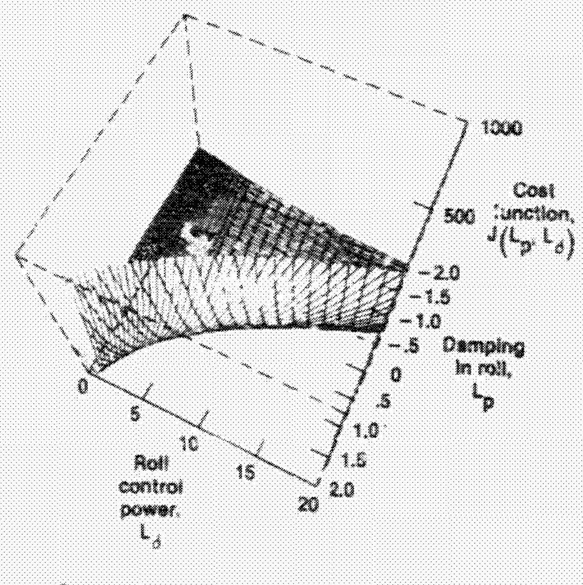

Fig. 14 Large-scale view of cost function surface.

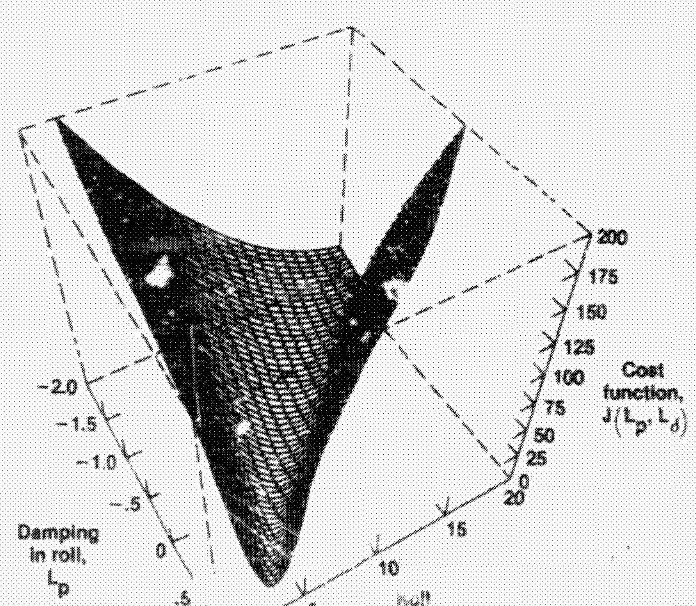

Fig. 15 Restricted view of cost function surface.

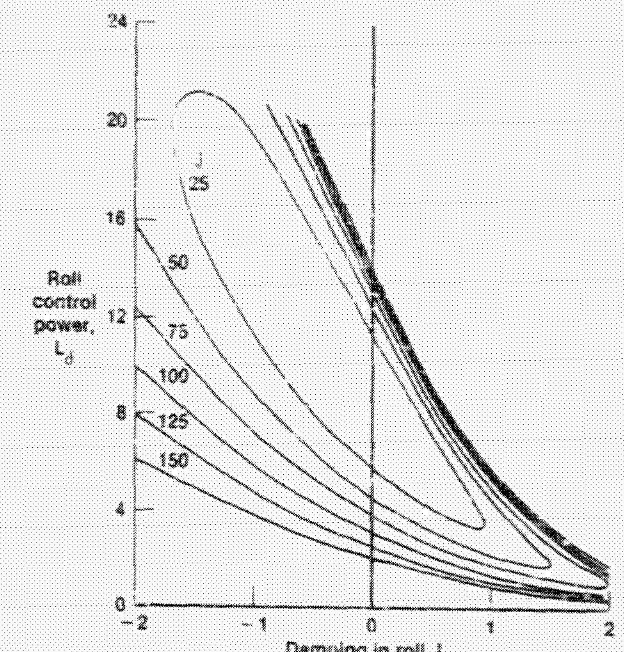

Fig. 16 Isoclines of constant cost of L_p and L_δ for the no-noise case.

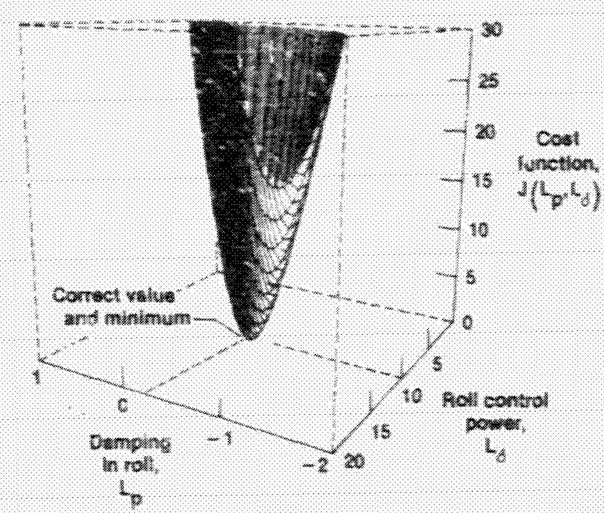

Fig. 17 Detailed view of cost function surface for no-noise case.

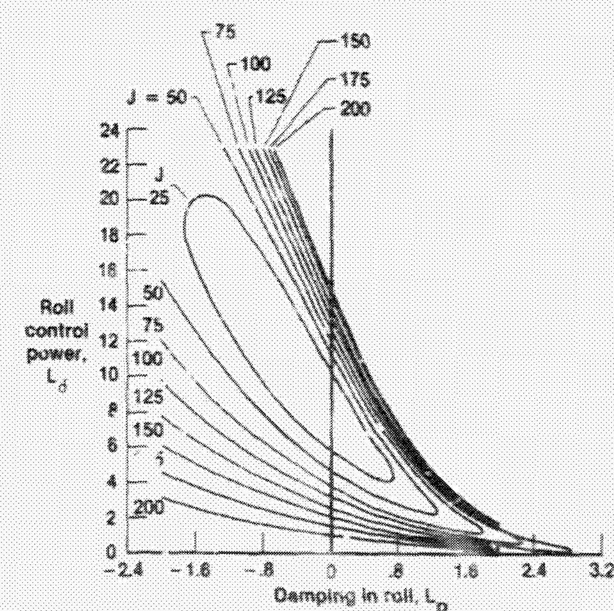

Fig. 18 Isoclines of constant cost in L_p and L_δ for the noisy case.

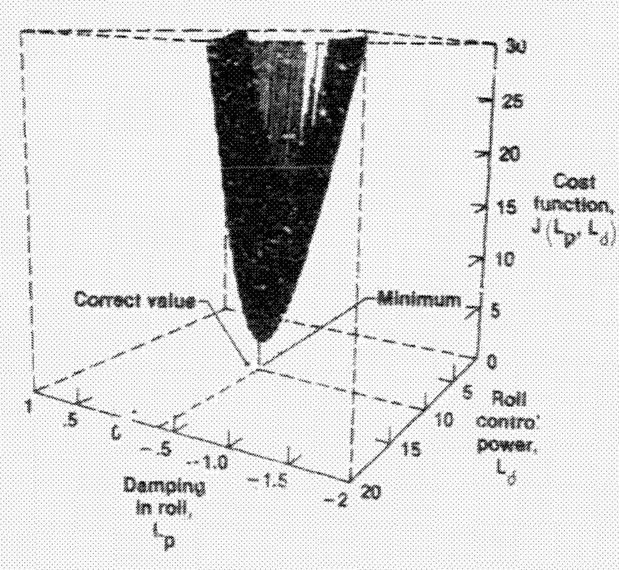

Fig. 19 Detailed view of cost function surface for noisy case.

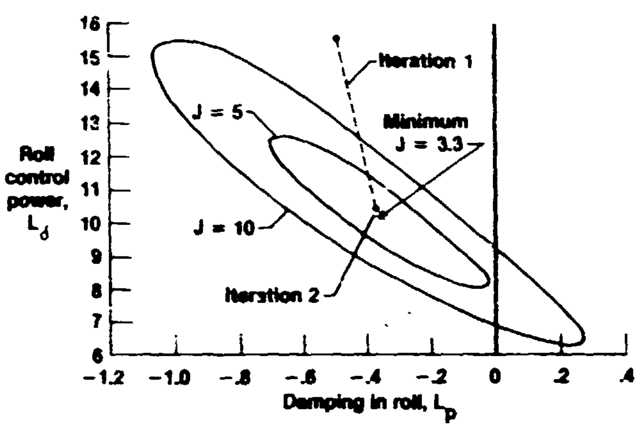

Fig. 20 Isoclines of constant cost for region near minimum for noisy case.

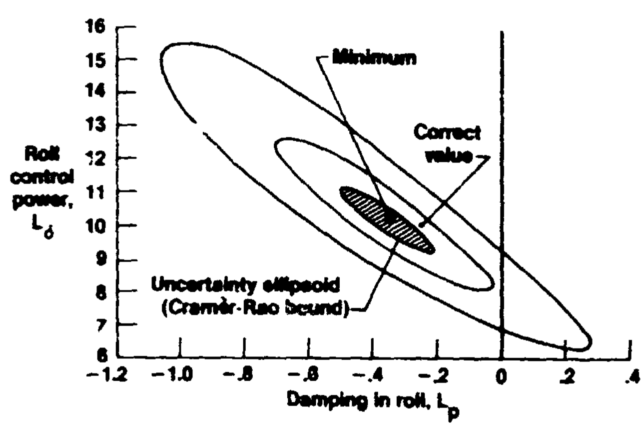

Fig. 21 Isoclines and uncertainty ellipsoid of the cost function for the noisy case.

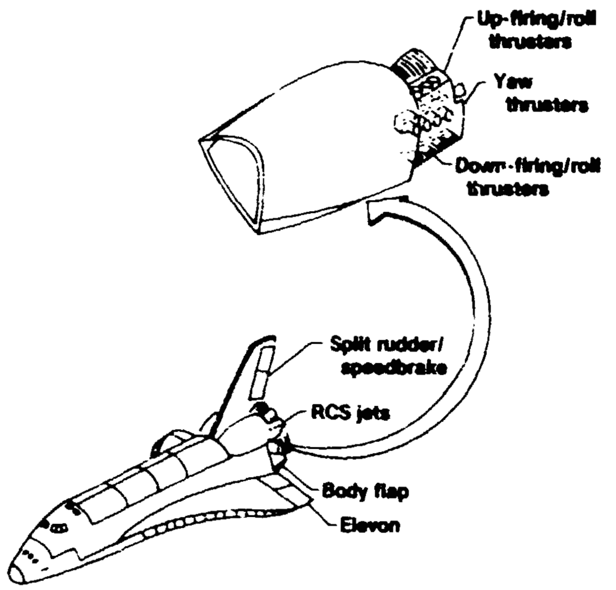

Fig. 22 Space shuttle configuration.

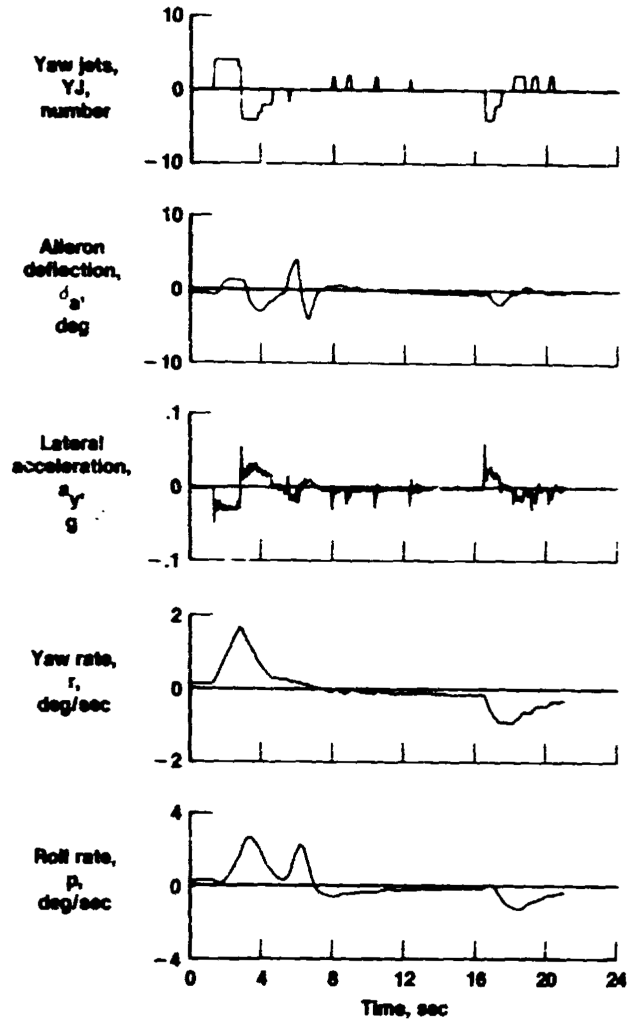

Fig. 23 Lateral-directional space shuttle maneuver at a Mach number of 21.

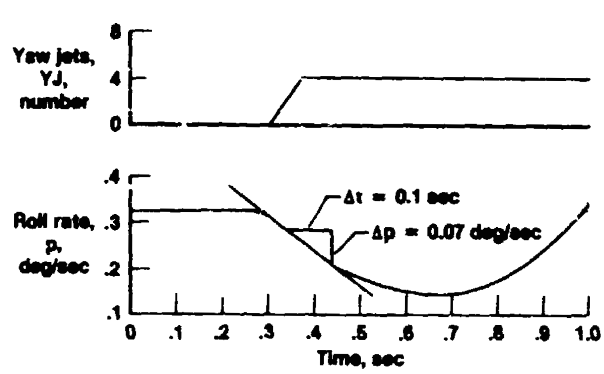

Fig. 24 Examples of obtaining L_{YJ} by simple calculations for the shuttle data from Fig. 23.

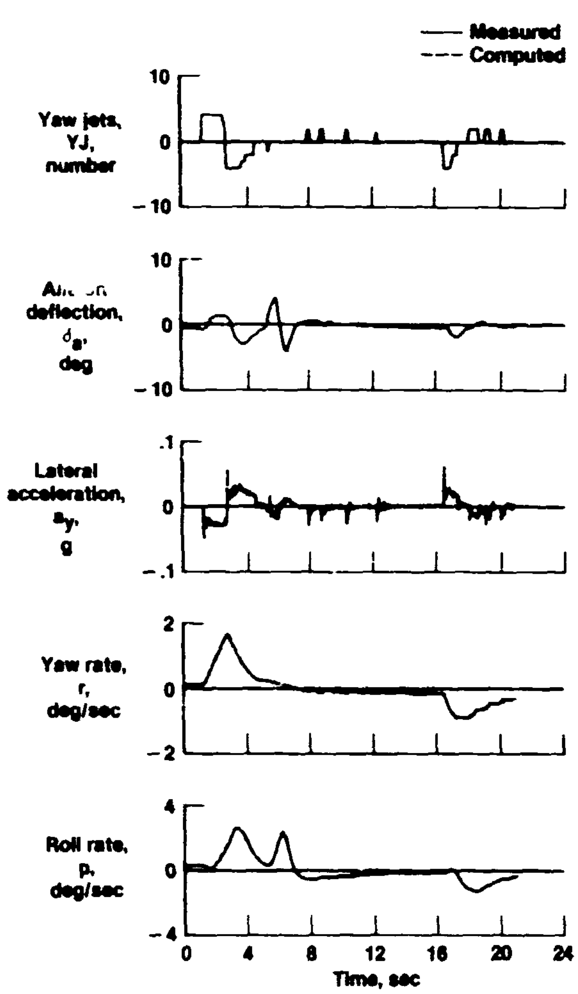

Fig. 25 MMLE3 match of maneuver shown in Fig. 23.

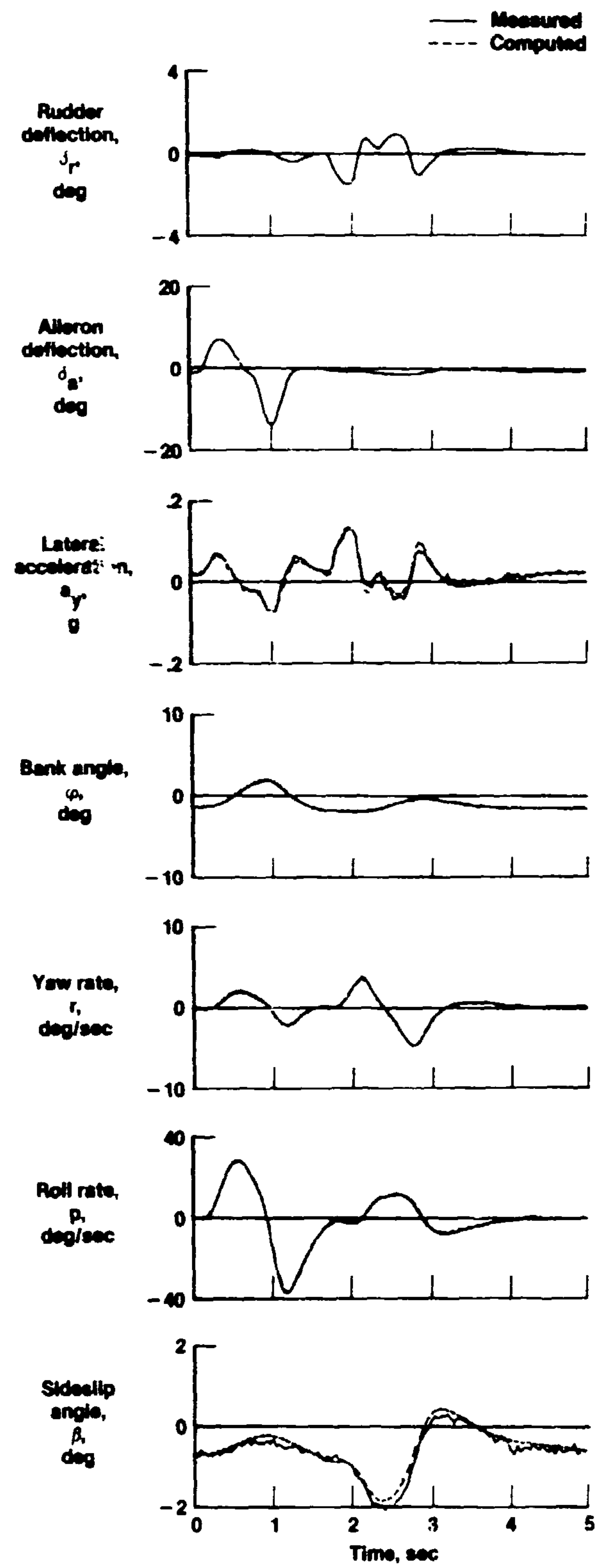

Fig. 26 Lateral-directional maneuver from F-8 aircraft with augmentation on.

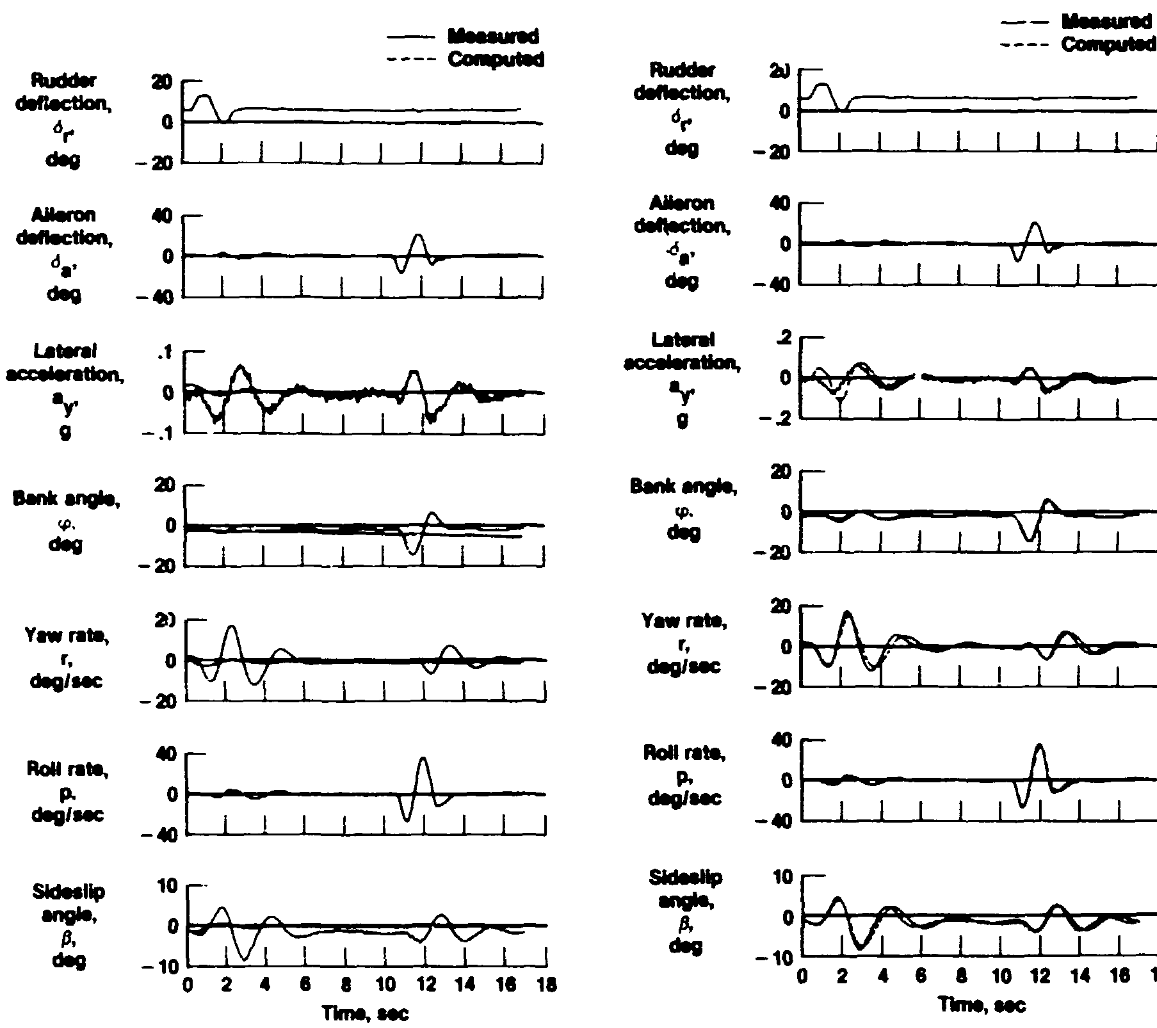

(a) Zero iteration. *(b) One iteration.*

Fig. 27 Match between measured and computed time histories as a function of iteration.

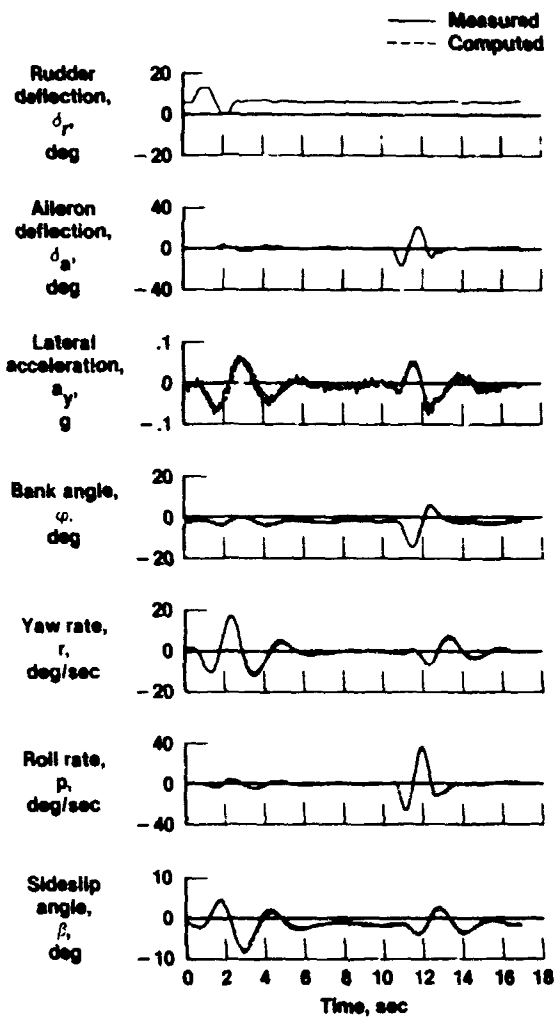

(c) Two iterations.

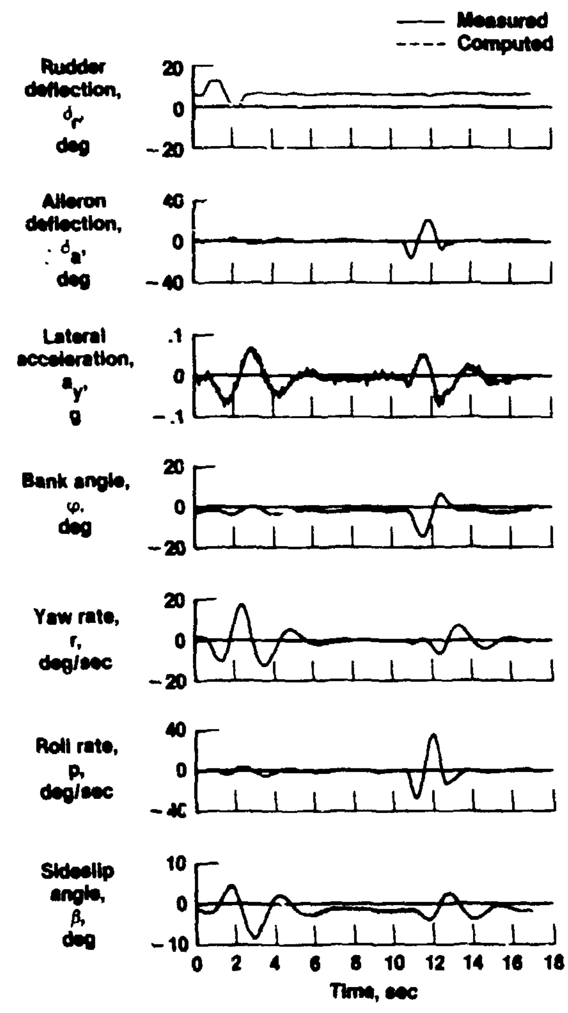

(d) Three iterations.

Fig. 27 Continued.

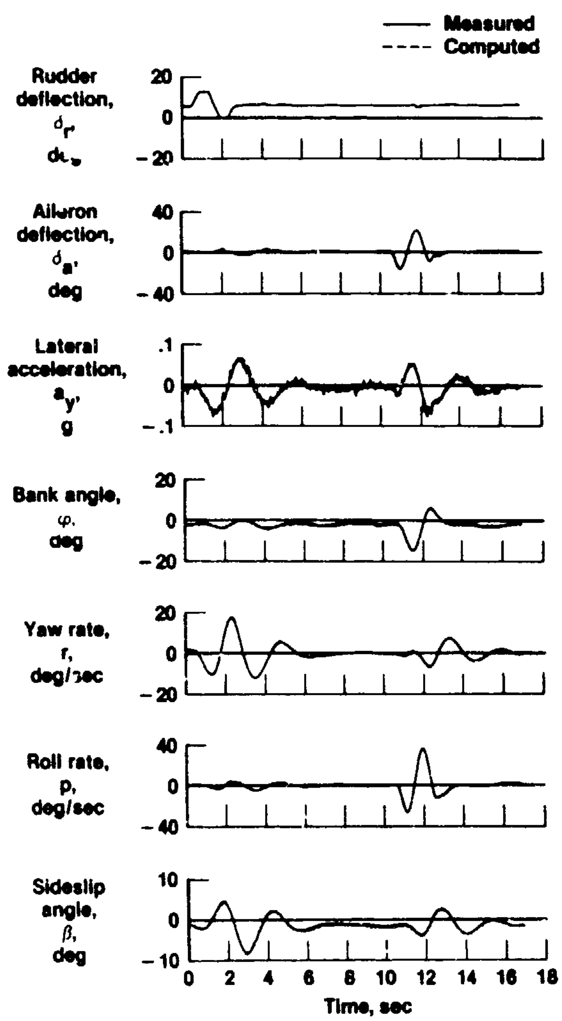

(e) Four iterations.

Fig. 27 Concluded.

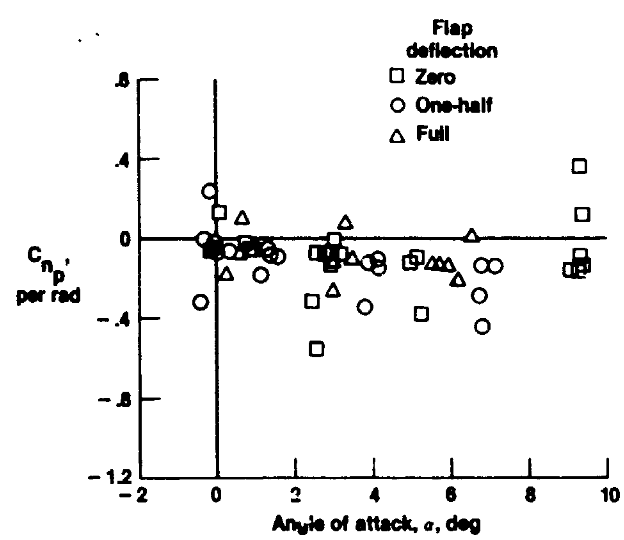

Fig. 28 Variations of C_{n_p} with angle of attack without uncertainty levels.

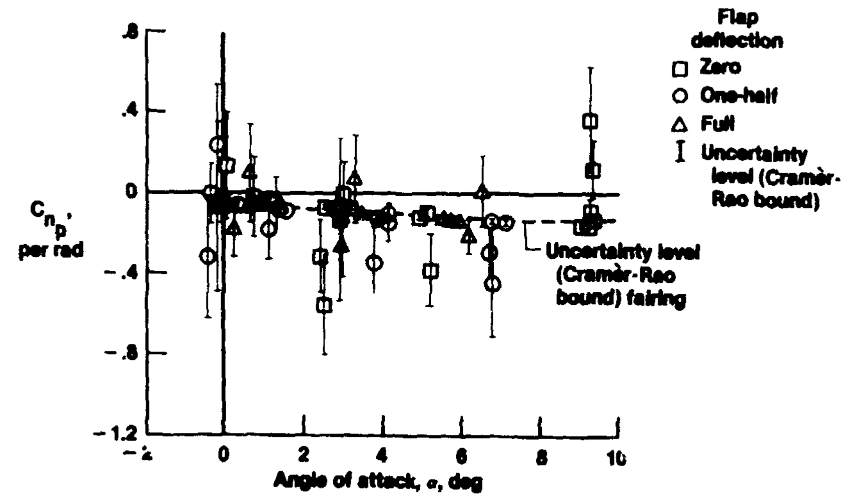

Fig. 29 Variations of C_{n_p} with angle of attack with uncertainty levels.

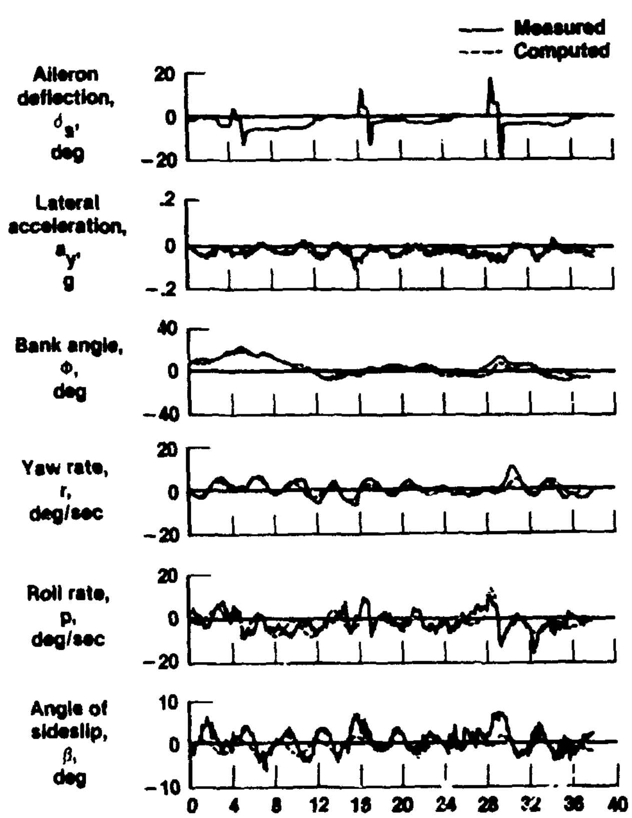

Fig. 30 Match of flight data obtained in turbulence (state noise) and computed data obtained from maximum likelihood estimator that does not account for turbulence.

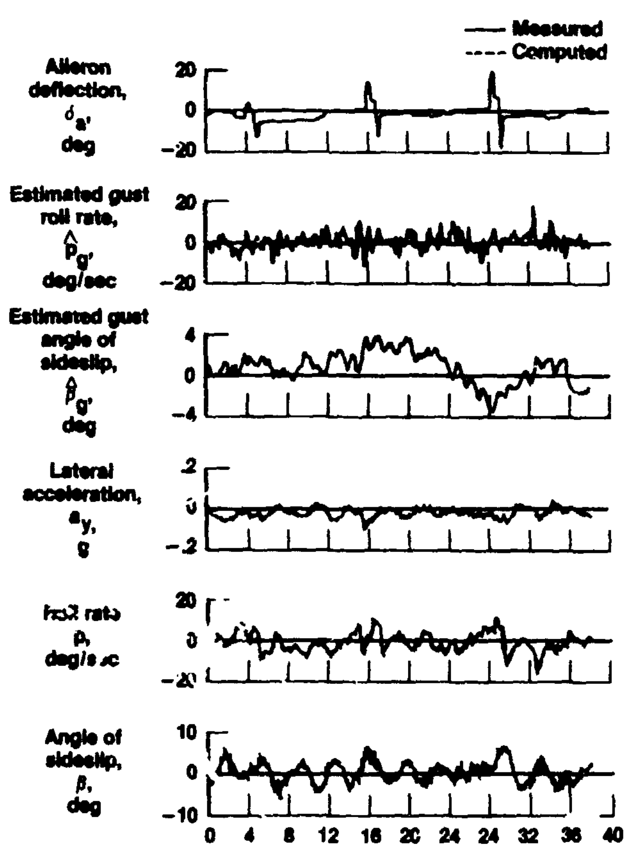

Fig. 31 Match of flight data obtained in turbulence (state noise) and computed data obtained from a maximum likelihood estimator that accounts for turbulence.

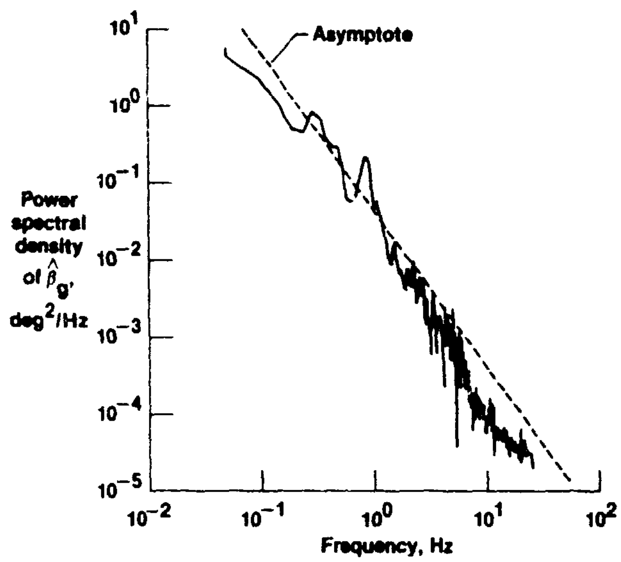

Fig. 32 Power spectral density of $\hat{\beta}_g$ obtained from maneuver shown in Fig. 31.

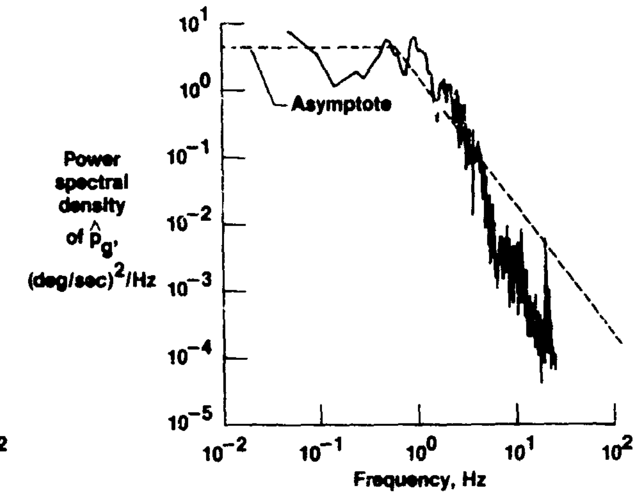

Fig. 33 Power spectral density of $\hat{p}_g$ obtained from maneuver shown in Fig. 31.

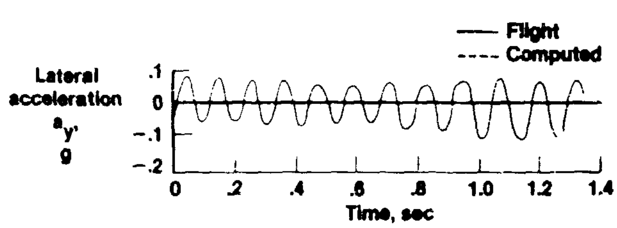

Fig. 34 Structural mode oscillation observed on the lateral acceleration.

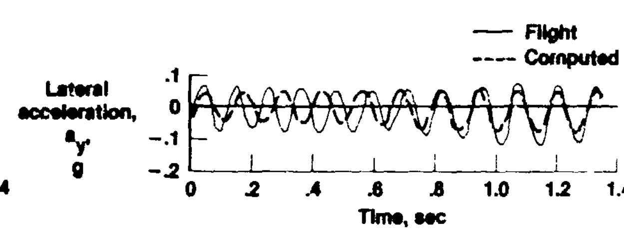

Fig. 35 Match of measured and computed lateral acceleration obtained when maximum likelihood estimator converged to local minimum.

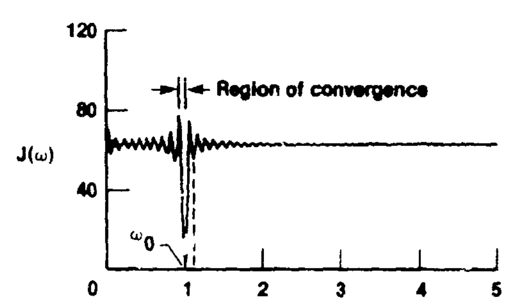

Fig. 36 Cost functional for 10 cycles of data as function of frequency, showing close proximity of local minima to global minimum.

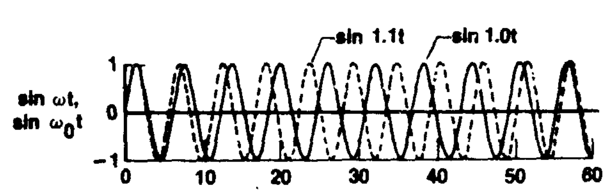

Fig. 37 Simple scalar example illustrating a local minimum similar to that shown for flight data in Fig. 35.

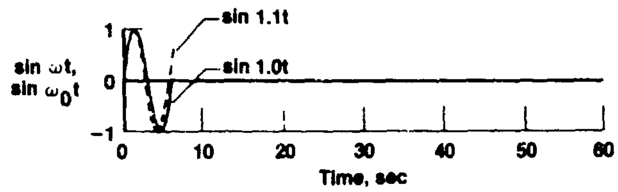

Fig. 38 Simple scalar example showing only the first cycle.

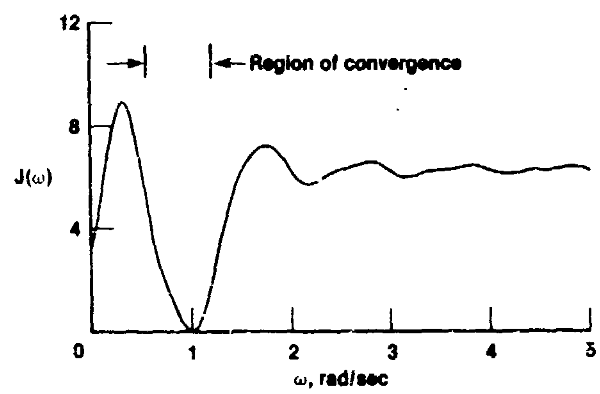

Fig. 39 Cost function for one cycle of data as function of frequency, showing wide region of convergence for global minimum.

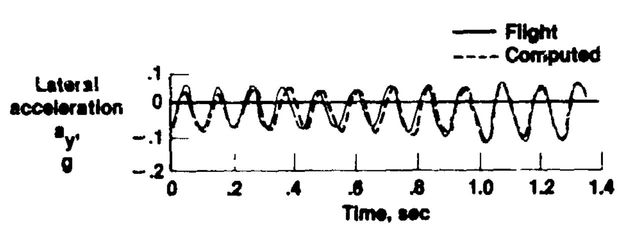

Fig. 40 Acceptable match of measured and computed lateral acceleration.

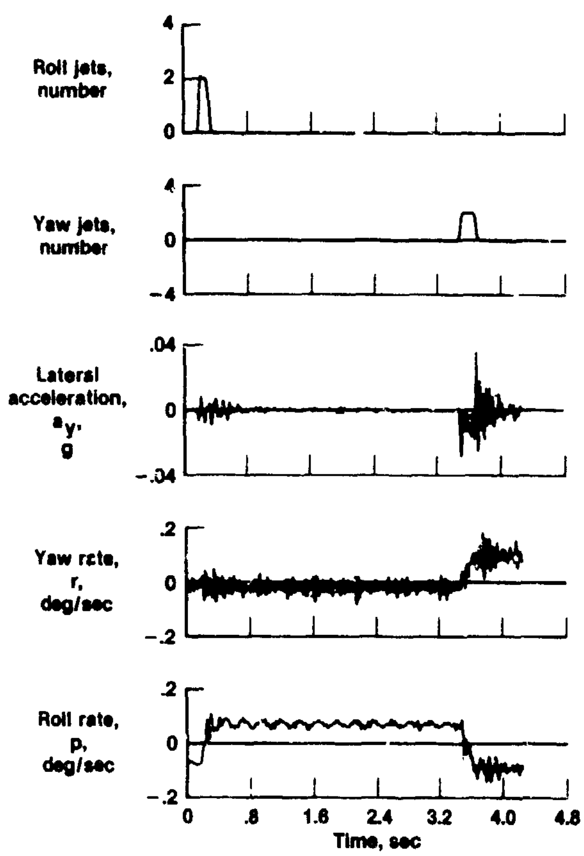

Fig. 41 Dynamic response of space shuttle to firing of roll and yaw jets at an altitude of 430,000 ft.

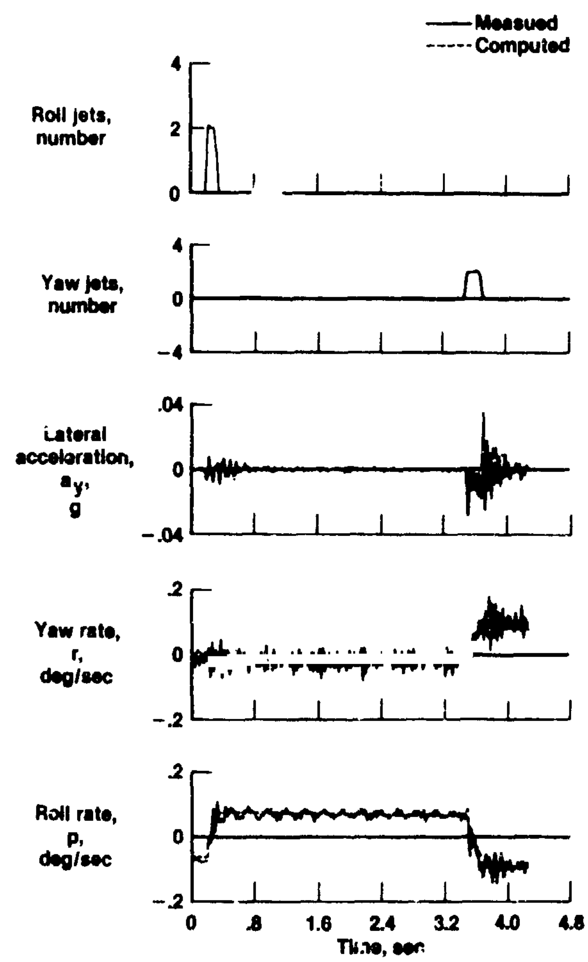

Fig. 42 Maximum likelihood match of rigid-body response of the space shuttle.

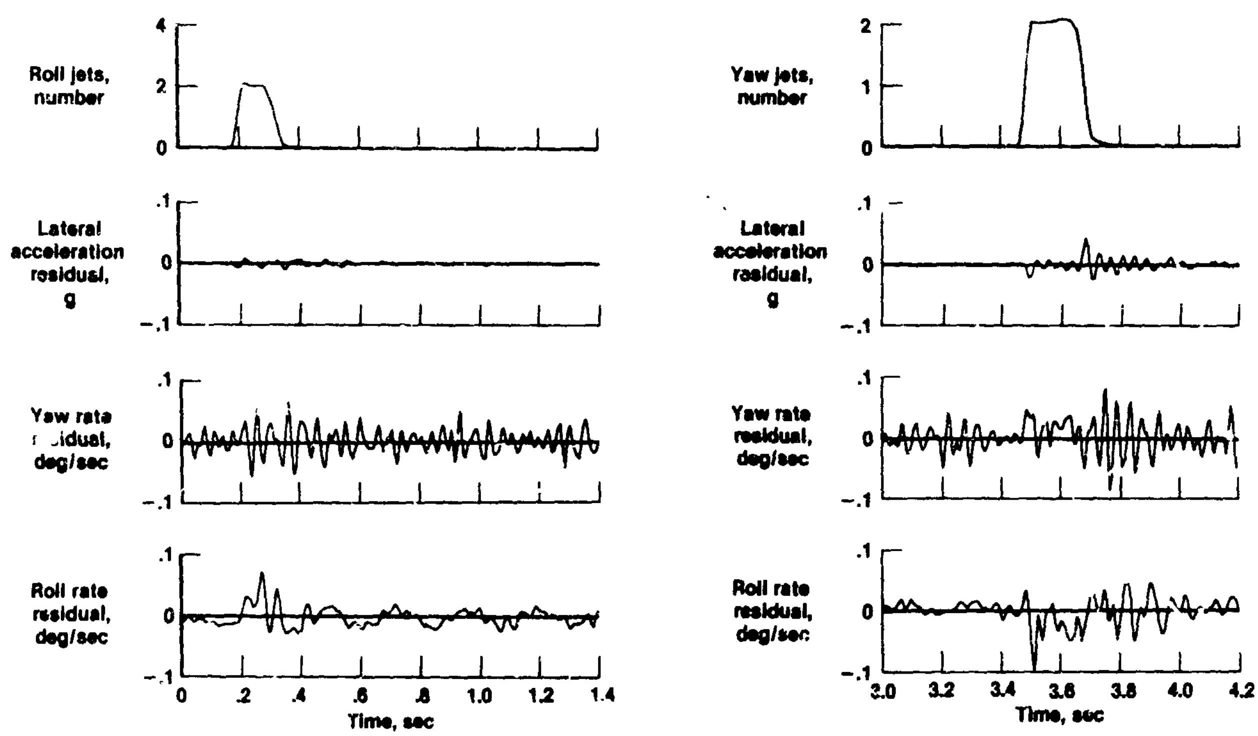

(a) Roll jet. *(b) Yaw jet.*

Fig. 43 Differe[illegible]en measured and computed rigid-body response (residual) for [illegible] shuttle. Altitude = 430,000 ft; dynamic pressure = 0.

N85-31209

OPTIMAL SENSOR LOCATIONS FOR STRUCTURAL IDENTIFICATION

F. E. Udwadia
University of Southern California
Los Angeles, CA 90089-0242

J. A. Garba
Jet Propulsion Laboratory
California Institute of Technology
Pasadena, CA 91109

SUMMARY

The optimum sensor location problem, OSLP, may be thought of in terms of the set of systems, S, the class of input time functions, I, and the identification algorithm (estimator) used, E. Thus, for a given time history of input, the technique of determining the OSL requires, in general, the solution of the optimization and the identification problems simultaneously. However, this paper introduces a technique which uncouples the two problems. This is done by means of the concept of an efficient estimator for which the covariance of the parameter estimates is inversely proportional to the Fisher Information Matrix.

INTRODUCTION

The problem of structural identification in structural engineering is one which has received considerable attention from several researchers in the recent past (Refs. 1-4). Though various methods have been developed for identifying the different parameters that characterize a structure from records obtained in them under various loading conditions, few investigators, if any, have looked at the question of where to locate sensors in a structure to acquire data for "best" parametric identification (Ref. 5). The problem of optimally locating sensors in a structural system arises from considerations of: (1) minimizing the cost of instrumentation; and (2) efficiently detecting structural changes in the system with a view to acquiring improved assessment of structural integrity.

The problem addressed in this paper can be stated as follows: Given m sensors, where should they be located in a structure so that records obtained from those locations yield the "best" estimates of the unknown parameters?

In the past, the optimal sensor location problem (OSLP) was solved by positioning the given number of sensors in the system, using the records obtained at those locations with a specific estimator, and repeating the procedure for different sensor locations. The set of locations which yield the "best" parameter estimates would then be selected as optimal. The estimates obtained, of course, would naturally depend upon the type of estimator used. Thus the optimal locations are estimator dependent, and an exhaustive search needs to be performed for each specific estimator. Such a procedure, besides being highly computationally intensive, suffers from the major drawback of not yielding any physical insight into why certain locations are preferable to others.

Recently, work on the solution of the OSLP was done by Shah and Udwadia (Ref. 5). In brief, they used a linear relationship between small perturbations in a finite dimensional representation of the system parameters and a finite sample of observations of the system time response. The error in the parameter estimates are minimized, yielding the optimal locations. In this paper, we develop a more direct approach to the problem which is both computationally superior, and throws considerable light on the rationale behind the optimal selection process.

We uncouple the optimization problem from the identification problem using the concept of an efficient estimator (e.g., the maximum likelihood estimator as time becomes very large). For such an estimator the covariance of the parameter estimates is a minimum. Using this technique and motivated by heuristic arguments, a rigorous formulation and solution of the OSLP is presented. The method is applied to a building structure modelled as a general linear dynamic system. For the N degree of freedom system considered, the methodology for selecting $m (m < N)$ of the nodal displacements for purposes of measurement is presented.

Sample calculations are made for a simple building structure modelled as a two-degree-of-freedom system subjected to base excitations. The optimal sensor location for the identification of: (a) the mass ratio; and (b) the stiffness ratio is investigated.

The results indicate that the OSLP depends on:

1) the class of systems, S, to which the structure belongs;

2) the type of excitation;

3) the actual system parameters involved; and

4) the parameters to be identified.

THEORY

Consider a system modelled by the equation

$$M\ddot{X} + C\dot{X} + KX = F(t) \tag{1}$$

where M, C, and K are the (NXN) mass, damping and stiffness matrices, $F(t)$ is an (NX1) vector containing inertial forces and externally applied loads and X is the N-vector of nodal displacements. Let θ_M, θ_C and θ_K be vectors containing the various parameters related to the mass matrix, the damping matrix and the stiffness matrix, respectively, which need to be identified. For convenience, we collect these quantities in the parameter vector, θ, defined as

$$\theta^T = \left[\theta_M^T \middle| \theta_C^T \middle| \theta_K^T\right]$$

where the superscript T indicate matrix transpose. If the M, C and K are symmetric each of the three subvectors has a maximum dimension of $N(N+1)/2$.

Given m sensors $(m < N)$, we then need to find where to locate them so that the covariance of the estimate, $\hat{\theta}$, is a minimum. Assume further that the measurement vector $Z(t)$ can be expressed as

$$Z_i(t) = g_i[X(\theta,t)] + N_i(t) \quad , \quad i = 1,2,\ldots,N \tag{2}$$

where Z_i is the ith component of $Z(t)$, and the functionals g_i represent the "measurement process". The dependence of the response X on the parameter vector θ is explicitly noted The measurement noise $N_i(t)$ is taken as non-stationary Gaussian White noise with a variance of $\psi^2(t)$. Therefore,

$$E\left[N_i(t_1)N_j(t_2)\right] = \psi^2(t_1)\,\delta_K(i-j)\,\delta_D(t_1-t_2) \quad . \tag{3}$$

where δ_K and δ_D stand for the kroneker and the dirac-delta functions, respectively. A total of m out of N responses need to be selected so that they contain the most information about the system parameters and are maximally sensitive to any changes in the parameter values. This "selection" process can be represented by an m-dimensional vector Y such that

$$Y(t) = SZ(t) \tag{4}$$

where S is the $(m \times N)$ upper triangular selection matrix with each row containing null elements except for one which is unity. The m different components of Z selected to be measured are so ordered in vector Y, that if the element in the i-th row and k-th column of S is unity, the (i+1)-ith row has unity in its ℓ-th column with $\ell > k$. The matrix S has the property that $P = S^TS$ in an (NXN) diagonal matrix with unity in its i-th row if, and only if, Z_i is selected to be measured. The elements of P are otherwise zero. Hence, one can write

$$Y(t) = Sg[X(\theta,t)] + SN(t) \tag{5A}$$

$$\triangleq H[X(\theta,t)] + V(t) \tag{5B}$$

If g_i is linearly related to the response X_j, in general, then

$$H[X(\theta,t)] = SRX \tag{6}$$

where $R(t)$ can be thought of as a dynamic gain matrix. In the case that g_i is related to the response X_i only, then matrix R will reduce to a diagonal matrix, $\left[\diagdown\, \rho_j \,\diagdown\right]$.

The problem of locating sensors in an optimal manner then reduces to determining the selection matrix S, or alternatively, finding the m locations in P that should be unity. These locations must be so chosen as to obtain the "best" parameter estimates.

SOME MOTIVATING THOUGHTS AND THE FISHER INFORMATION MATRIX

Consider a case in which one tries to estimate only one parameter, θ_1 (to be identified) involved in a dynamic system model with only one sensor provided. Therefore, one wants to ideally choose a location i (out of N possible such locations) such that the measurement $y_i(t)$, $i\varepsilon[1,N]$, $t\varepsilon(0,T)$ at location i yields the best estimate of the parameter θ_1. Heuristically, one should place the sensor at such a location that the time history of measurements obtained at that location is most sensitive to any changes in the parameter θ_1. Hence, in equation (5B) it is really the slope of $H[X(\theta_1,t)]$ with respect to θ_1 that needs to be maximized. However, since only the absolute magnitude of this slope is of interest, it is logical to want to find i (or equivalently determine the selection matrix S described previously) such as to maximize $(\partial H/\partial\theta_1)^2$ over the interval (0,T) during which the response is to be measured. This leads to maximizing the following integral:

$$q_i = \int_0^T \left(\frac{\partial H}{\partial \theta_1}\right)^2 dt \quad . \tag{7}$$

When there is more than one parameter to be estimated, and the number of sensors is greater than unity, this intuitive approach needs to be extended in a more rigorous manner. In such cases recourse to mathematical treatment is necessary, and we shall see that such treatment will be in agreement with our heuristic solution outlined above.

To further understand the problem, let us look at it from another angle, namely, the concept of an efficient unbiased estimator. For such as estimator the covariance of the estimates is a minimum. Furthermore, it can be shown that for any unbiased estimator of θ,

$$E\left[(\theta-\hat{\theta})(\theta-\hat{\theta})^T\right] \geq \left[\int_0^T \left(\frac{\partial H}{\partial \theta}\right)^T \left(\frac{\partial H}{\partial \theta}\right) / \psi^2(t)dt\right]^{-1} \tag{8}$$

where $\hat{\theta}$ is the estimate of θ and the matrix $[\partial H/\partial\theta]_{ij} \triangleq \partial H_i/\partial\theta_j$. If the estimator is "efficient", the above inequality becomes an equality. This means that the left-hand side of inequality (8) takes its lowest value (minimum covariance). Hence,

$$E\left[(\theta-\hat{\theta})(\theta-\hat{\theta})^T\right] = \left[\int_0^T \left(\frac{\partial H}{\partial \theta}\right)^T \left(\frac{\partial H}{\partial \theta}\right) / \psi^2(t)dt\right]^{-1} \tag{9}$$

The term inside the bracket on the right-hand side of the equation (9) is known as the Fisher Information Matrix, Q(T). Thus, maximizing Q(T) would indeed lead to a minimization of the covariance of the estimate, $\hat{\theta}$.

We note then that the m sensor locations need to be so chosen that a suitable norm of the matrix Q(T) given by

$$Q(T) = \int_0^T \left(\frac{\partial H}{\partial \theta}\right)^T \left(\frac{\partial H}{\partial \theta}\right) / \psi^2(t)dt \tag{10}$$

is maximized. This constitutes an extension of equation (7), which we heuristically derived earlier for the scalar case, to the vector situation. Introducing equation (6) in equation (10) one may write

$$Q(T) = \int_0^T \frac{X_\theta^T R^T P R X_\theta}{\psi^2(t)}\, dt, \tag{11}$$

where the ij element of X_θ can be written as:

$$\left[X_\theta\right]_{ij} = \frac{\partial x_i}{\partial \theta_j}, \quad i \in [1,N], \; j \in (1,m)$$

where $X = \{x_i\}_N$ and $\theta = \{\theta_i\}_L$. We note that the Fisher Matrix is symmetric and is dependent on the length of the record available, as well as the locations of the sensors as determined by the matrix P.

If the m locations where the sensors are to be placed are denoted by s_k, $k = 1,2,\ldots,m$, then

$$P = \sum_{k=1}^{m} I_{s_k} \tag{12}$$

where the $(N \times N)$ diagonal matrix I_{s_k} has all its elements equal to zero except the element of the s_k row, which is unity. Noting that P is a diagonal matrix, equation (11) can be simplified to yield

$$Q[T;s_1,s_2,\ldots,s_m;S,\theta;I] = \sum_{k=1}^{m} \int_0^T \frac{X_\theta^T r_{s_k}^T r_{s_k} X_\theta dt}{\psi^2(t)} \tag{13}$$

where r_{s_k} is the s_k row of the matrix R. Also in eq. (13) explicit mention is made of the dependence of the Fisher Matrix on the time length T of the available data, the system S, the parameter vector θ, and the time-variant input I. If the matrix R is diagonal, with diagonal elements $\rho_1,\ldots,\rho_N$, then the ij element of the matrix Q, after some manipulation, reduces to

$$Q_{ij}\left[T;s_1,s_2,\ldots,s_m;S,\theta;I\right] = \sum_{k=1}^{m} \int_0^T \left[\frac{\partial x_{s_k}}{\partial \theta_i}\,\frac{\partial_{s_k}}{\partial \theta_j}\left(\frac{\rho(t)_{s_k}}{\psi(t)}\right)^2\right] dt. \tag{14}$$

Each element of Q_{ij} represents the cross-sensitivity of measurement with respect to the response x_{s_k} of node s_k.

The optimal sensor locations are then obtained by picking m locations s_k, $k = 1,2,\ldots,m$, out of a possible N, so that a suitable norm of the matrix Q is maximized (e.g., the trace norm, etc...). This may be specified by the condition

$$\max_{s_k \, \varepsilon(1,N)} \left|\left| Q\left[T; s_1, s_2, \ldots, s_m; S, \theta; I\right]\right|\right| . \tag{15}$$

Although there are several matrix norms which could be used, perhaps the most useful and physically meaningful in this context is the trace norm. In order not to detract the reader from the basic methodology we defer an exhaustive treatment of suitable matrix norms to a later communication.

The methodology presented up to this point is valid for both linear and non-linear systems since the criterion developed in equation (13) was derived using only equations (5) and (9). We will now indicate its application to linear multi-degree-of-freedom systems.

APPLICATION TO LINEAR DYNAMIC SYSTEMS

Consider the N-degree-of-freedom dynamic system whose governing differential equation of motion is given by eq. (1), together with $X(t_0) = X_0$, $\mathring{X}(t_0) = \mathring{X}_0$, where X_0 and $\mathring{X}_0$ are the given initial conditions for the system. Assume the system to be classically damped. Introducing

$$X(t) = \Phi\eta(t) \tag{16}$$

where Φ is the $(N \times N)$ weighted modal matrix and $\eta(t)$ is the N-vector of generalized coordinates we get

$$\ddot{\eta} + 2\xi_N\omega_N\dot{\eta} + \Lambda\eta = \Phi^T F(t), \quad \eta(t_0) = \phi^T M X_0, \ \mathring{\eta}(t_0) = \phi^T M \mathring{X}_0, \tag{17}$$

where the $(N \times N)$ diagonal matrix Λ is given by

$$\left[\diagdown \Lambda \diagdown\right] = \Phi^T K \Phi = \left[\diagdown \omega_N^2 \diagdown\right], \text{ and } \xi_N = \left[\diagdown \xi_i \diagdown\right].$$

The solution of equation (17) is given as

$$\eta_i(t) = \eta_{0_i} u_i(t-t_0) + \dot{\eta}_{0_i} v_i(t-t_0) + \int_{t_0}^{t} h_i(t-\tau) p_i(\tau) d\tau \tag{18}$$

where η_{0_i} and $\dot{\eta}_{0_i}$ are initial conditions and

$$u_i(t) = \mathrm{EXP}\left(-\xi_i \omega_i t\right) \left[\mathrm{Cos}\omega_{d_i} t + \frac{\xi\omega_i}{\omega_{d_i}} \mathrm{Sin}\omega_{d_i} t \right] ,$$

$$v_i(t) = \frac{1}{\omega_{d_i}} \mathrm{EXP}\left(-\xi_i \omega_i t\right) \mathrm{Sin}\omega_{d_i} t,$$

$$h_i(t) = v_i(t),$$

$$\omega_{d_i} = \omega_i \sqrt{1 - \xi_1^2} , \quad \text{and}$$

$$p_i(t) = \Phi^T F(t), \quad i = 1,2,\ldots,N.$$

Also, differentiating equation (1) with respect to θ, yields

$$M\ddot{X}_\theta + C\dot{X}_\theta + KX_\theta = F_\theta(t) - \left(\widehat{M_\theta \ddot{X}} + \widehat{C_\theta \dot{X}} + \widehat{K_\theta X}\right); \; X_\theta(0) = 0, \; \dot{X}_\theta(0) = 0$$

where

$$\left[X_\theta\right]_{ij} = \frac{\partial x_i}{\partial \theta_j} \quad , \qquad \text{with}$$

$$\widehat{M_\theta \ddot{X}} = [M_{\theta_1} \ddot{X} \vdots M_{\theta_2} \ddot{X} \vdots M_{\theta_j} \ddot{X} \vdots M_{\theta_L} \ddot{X}]$$

$$i = 1,\ldots,N, \quad \text{and} \quad j = 1,\ldots,L.$$

Introducing

$$X_\theta = \Phi z \tag{19}$$

yields

$$\ddot{z} + 2\xi_N \omega_N \dot{z} + \Lambda z = G(t) \tag{20}$$

where

$$G(t) = \Phi^T \left[F_\theta - \left(\widehat{M_\theta \ddot{X}} + \widehat{C_\theta \dot{X}} + \widehat{K_\theta X}\right)\right] . \tag{21}$$

Equation (21) can further be simplified to give

$$G(t) = \phi^T \left[F_\theta - \left(\widehat{M_\theta \Phi \ddot{\eta}} + \widehat{C_\theta \Phi \dot{\eta}} + \widehat{K_\theta \Phi \eta}\right)\right] \tag{22}$$

where $\dot{\eta}$ and $\ddot{\eta}$ can be obtained by differentiation of eq. (18). This may be shown as follows

$$\dot{\eta}_i(t) = \eta_{0_i} W_i\left(t-t_0\right) + \dot{\eta}_{0_i} Y_i\left(t-t_0\right) + \int_{t_0}^{t} \bar{h}_i(t-\tau) p_i(\tau) d\tau \tag{23}$$

where

$$W_i(t) = -\mathrm{EXP}\left(-\xi_i \omega_i t\right) \left[\omega_{d_i} + \frac{\left(\xi_i \omega_i\right)^2}{\omega_{d_i}}\right] \mathrm{Sin}\,\omega_{d_i} t \quad ,$$

$$Y_i(t) = \mathrm{EXP}\left(-\xi_i \omega_i t\right) \left[\mathrm{Cos}\,\omega_{d_i} t - \left(\frac{\xi_i \omega_i}{\omega_{d_i}}\right) \mathrm{Sin}\,\omega_{d_i} t\right] \quad ,$$

$$\bar{h}_i(t) = Y_i(t), \qquad \text{and}$$

$$p_i(t) = \Phi^T F(t), \qquad i = 1,2,\ldots,N.$$

Also

$$\ddot{\eta}_i(t) = \eta_{0_i} \bar{W}_i\left(t-t_0\right) + \dot{\eta}_{0_i} \bar{Y}_i\left(t-t_0\right) + \int_{t_0}^{t} \bar{\bar{h}}_i(t-\tau) p_i(\tau) d\tau \tag{24}$$

where

$$\bar{W}_i(t) = \mathrm{EXP}\left(-\xi_i \omega_i t\right) \left\{ \left[\frac{\left(\xi_i \omega_i\right)^3}{\omega_{d_i}} + \omega_{d_i} \left(\xi_i \omega_i\right)\right] \mathrm{Sin}\,\omega_{d_i} t - \left[\omega_{d_i}^2 + \left(\xi_i \omega_i\right)^2\right] \mathrm{Cos}\,\omega_{d_i} t \right\} \quad ,$$

$$\bar{Y}_i(t) = \mathrm{EXP}\left(-\xi_i\omega_i t\right)\left\{\left[\frac{\left(\xi_i\omega_i\right)^2}{\omega_{d_i}} - \omega_{d_i}\right] \mathrm{Sin}\omega_{d_i} t\right.$$

$$\left. - 2\xi_i\omega_i \mathrm{Cos}\omega_{d_i} t\right\} \quad ,$$

$$\bar{\bar{h}}_i(t) = \bar{Y}_i(t),$$

$$p_i(t) = \phi^T F(t), \qquad i = 1,2,\ldots,N.$$

Therefore, substituting equations (23) and (24) into equation (22) gives G(t). Consequently the solution of equation (20) can be written as:

$$z_{ij}(t) = \int_{t_0}^{t} h_i(t-\tau)G_{ij}(\tau)d\tau \tag{25}$$

where $h_i(t)$ is the same as that of eq. (18). Notice that the initial conditions in eq. (20) are zero. This is due to the fact that the initial conditions of (18) are known constants.

If we assume that [C] is expressed as a linear combination of [K] and [M], then eq. (22) can further be simplified. Namely,

$$C = 2\alpha K + 2\beta M, \tag{26}$$

where α and β are known constants. Hence in equation (17), the percentage of damping, ξ_N, can be expressed as:

$$\xi_i = \alpha\omega_i + \frac{\beta}{\omega i} \quad , \quad i = 1,2,\ldots,N \tag{27}$$

To further simplify equation (22) under this assumption, let us consider the following three cases:

1) The vector θ contains only θ_M, i.e., only estimation of mass parameters is undertaken. Then

$$G(t) = \phi^T [F_\theta - \widehat{M_\theta \phi(\ddot{\eta}+2\beta\dot{\eta})}] \quad . \tag{28A}$$

2) The vector θ contains only the subvector θ_K. Then

$$G(t) = \phi^T[F_\theta - \widehat{K_\theta \phi(\eta+2\alpha\dot{\eta})}] \tag{28B}$$

3) Finally if the vector $\theta = [\alpha\ \beta]^T$,

$$G(t) = \langle \phi^T F_\alpha - 2\Lambda\dot{\eta},\ \phi^T F_\beta - 2I\dot{\eta} \rangle^T \tag{29}$$

If the input F(t) is not a function of θ, then F_θ would be omitted all through this discussion. Once the solution of equation (25) is obtained, the Fisher Matrices may be obtained as in equation (13). Hence

$$Q = \sum_{k=1}^{m} \int_0^T \frac{z^T \Phi^T r_{s_k}^T r_{s_k} \Phi z}{\psi^2(t)}\, dt \tag{30}$$

We note that the summation form of relation (30) is particularly amenable to the maximization of the trace norm of Q.

EXAMPLE

To illustrate some of the ideas of the previous section, consider the problem of finding the optimal sensor location (OSL) in a structural system modelled by the two-degree-of-freedom system (shown in Figure 1) which is subjected to the base excitation of $f(t)$.

The governing differential equation of motion can be expressed as

$$\ddot{M} + C\dot{X} + KX = -W\, f(t) \tag{31}$$

where $X = \langle x_1\ x_2 \rangle^T$, $C = \alpha K$, $W = \langle Am\ m \rangle^T$ and the matrices M and K are

$$M = \begin{bmatrix} A & 0 \\ 0 & 1 \end{bmatrix} m \ , \text{ and } K = \begin{bmatrix} B+1 & -1 \\ -1 & 1 \end{bmatrix} k \ .$$

A case study for locating sensors to best identify (1) the mass ratio, A, of the first to the second floor and (2) the stiffness ratio, B, of the first to the second floor, will be presented.

Let s_1 denote the lower mass location and s_2 the upper mass location. The selection between the locations can be equated to determining the one non-zero element of the [1x2] selection matrix, S, with the measurement H(t) defined by

$$H(t) = SX + V(t) \ ,$$

where, V(t) is Stationary Gaussian White Noise (S G W N) with $\psi(t)=\psi_o$.

If S = [1 0] the lower mass is selected for measurement; if S = [0 1] the upper mass is selected. The location s_1 would then be preferred over the location s_2 for identifying the parameter A, if $Q[T,s_1] > Q[T,s_2]$, where T is the time that the measurement is taken,

$$Q_1[T] \triangleq Q_1[T,s_1] = \frac{1}{\psi_o^2} \int_0^T \left(\frac{\partial x_1}{\partial A}\ \frac{\partial x_2}{\partial A} \right) \begin{bmatrix} 1 & 0 \\ 0 & 0 \end{bmatrix} \begin{Bmatrix} \frac{\partial x_1}{\partial A} \\ \frac{\partial x_2}{\partial A} \end{Bmatrix} dt$$

$$= \frac{1}{\psi_o^2} \int_0^T \left(\frac{\partial x_1}{\partial A} \right)^2 dt, \tag{32A}$$

and

$$Q_2(T) \triangleq Q[T,s_2] = \frac{1}{\psi_o^2} \int_0^T \begin{pmatrix} \frac{\partial x_1}{\partial A} & \frac{\partial x_2}{\partial A} \end{pmatrix} \begin{bmatrix} 0 & 0 \\ 0 & 1 \end{bmatrix} \begin{Bmatrix} \frac{\partial x_1}{\partial A} \\ \frac{\partial x_2}{\partial A} \end{Bmatrix} dt$$

$$= \frac{1}{\psi_o^2} \int_0^T \left(\frac{\partial x_2}{\partial A}\right)^2 dt \; . \tag{32B}$$

Since only one parameter is being estimated the Fisher matrices reduce to scalars.

The dependence of the OSL on various types of the base excitations can be studied now. Let us for this presentation consider ground acceleration in the form of a delta function, i.e., $f(t) = \delta(t)$.

In this case, closed form solutions for Q_1 and Q_2 can be obtained.

For the OSL problem for the "best" (minimum covariance) identification of the parameter A (given the parameters B and α) using an impulsive base excitation, Figure 2-A shows the plots of the ratio of the information matrices $Q_1(T)/Q_2(T)$, for T = 50 secs, for various values of the parameters A (which is to be identified) and $\alpha^* \triangleq \alpha\omega_o$, where $\omega_o \triangleq \sqrt{k/m}$. Points on the graph with ordinates greater than unity indicate the optimal location to be the lower mass level and vice versa. The graphs indicate that the optimal location in most cases, for the range of A considered, is the upper mass level. However, we observe that for some small values of A and α^* the OSL is the lower level. We note, interestingly enough, that the optimal sensor location for identification of A actually depends not only on the actual values of B and α which are presumably known, but also on the value of the parameter A itself which is to be identified! Thus to be able to ascertain the optimal sensor location some a priori assessment of A is necessary.

Figure 2-B shows that the optimal location for identification of the parameter B (given A and α), using an impulsive base input, is again the upper mass level for the range of B values considered. For larger B values, however, and $\alpha^*>0.05$, the trend appears to be more and more in favor of the upper mass. This seems intuitively correct, for as B becomes larger, the lower part of the system becomes stiffer and the OSL would be the upper mass level.

Figure 2-C is associated with the OSLP for estimating the parameter B using a sinusoidal base excitation, $f(t) = a \sin \omega t$. The figure shows that as the normalized driving frequency $\gamma = \omega/\omega_o$ varies, the OSL changes. For this example the Fisher Matrices can be computed in closed form. For the estimation of B, (given A and $\alpha^* = 0$) the dimensionless driving frequency $\gamma = \sqrt{1+1/A}$ yields no information on B from records at either of the two mass levels. The responses at the two mass levels yield identical amounts of information on B at $\gamma = 0$ and $\gamma = \sqrt{2}$ for $A \neq 1$, as indicated by the values of $Q_1/Q_2 = 1$ at these frequencies. The value of $Q_1/Q_2 = 0$ at $\gamma = 1$ is indicative of the fact that the upper mass level is a far better location for a sensor when estimating B with $\alpha^* = 0$. Figure 2-D shows the mean value of the ratio Q_1/Q_2 for a random Gaussian white noise base excitation together with the 1-σ band. The OSL appears to be at the upper mass level for identification of A.

CONCLUSIONS AND DISCUSSION

This paper presents a general methodology for determining the optimal sensor locations in dynamic systems for obtaining records which would enable the "best" (minimum covariance) identification of a given set of unknown parameters in the system. The technique utilizes the concept of an efficient estimator to uncouple the identification from the optimization problem. In order to present the basic idea in as clear a fashion as possible, we have restricted the discussion in this sequel to linear systems.

The method has been illustrated by application to a two degree of freedom system. Though the results presented here for the simple system chosen form only a first step towards acquiring a detailed understanding of the OSL problem, the following conclusions appear to be relevant at this time:

(1) The OSL for a given system heavily depends on the class of forcing functions used for obtaining response data. In this study, an impulsive base motion is considered.

(2) The OSL for linear dynamic systems is independent of the amplitude of the forcing function.

(3) The OSL depends in general on all the values of system parameters. For instance, the OSL for estimating A with minimum covariance depends not only on the actual parameter values B and α but on the value of A itself for the system! This implies that the OSL problem associated with identifying a given parameter (or a set of parameters) in a dynamic system necessitates the knowledge of some a priori estimates of the unknown parameter(s).

(4) The results of our simple example show that the OSL problem may yield solutions which may be difficult to predict on purely heuristic grounds. The OSL appears to depend, even for this relatively simple problem, in a rather complex manner on the actual parameter values of the system and the nature of the base excitation.

REFERENCES

1) Evkhoff, P., "Process Parameter and State Identification", Proc. IFAC Congress, London, 1966.

2) Hart, G.C. ed., "Dynamic Response of Structures: Instrumentation, Testing and System Identification", ASCE/EMD Specialty Conference Proceedings, U.C.L.A., 1976.

3) Hudson, D.E., "Dynamic Testing of Full Scale Structures", Earthquake Engineering, Prentice Hall, pp. 127-149.

4) Udwadia, F.E. and Shah, P.C., "Identification of Structures Through Records Obtained During Strong Ground Shaking", ASME, Journal of Engineering for Industry, Vol. 98, No. 4, 1976, pp. 1347-1362.

5) Shah, P.C. and Udwadia, F.E., "A Methodology for Optimal Sensor Locations for Identification of Dynamic Systems", Journal of Applied Mechanics, Vol. 45, March 1978.

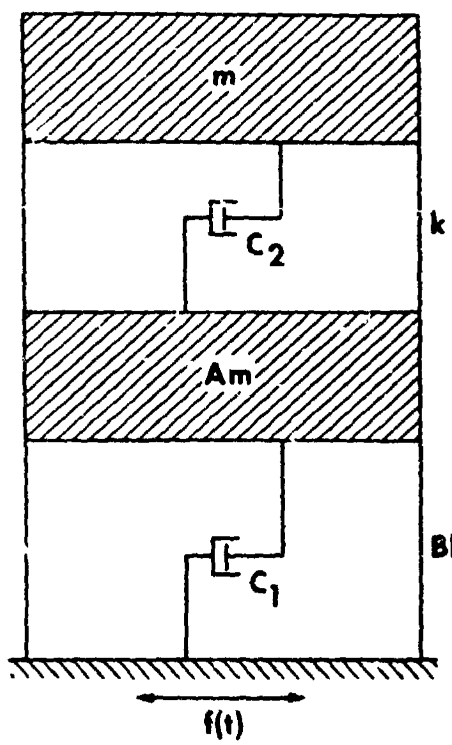

Figure 1. 2-degree-of-freedom generic structural system.

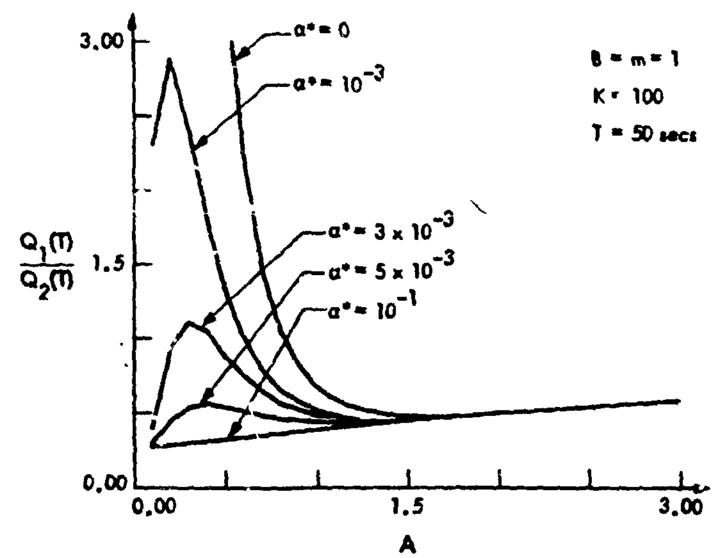

Figure 2-A. Variation of Q_1/Q_2 for various values of the parameter A. Q_1/Q_2 greater than unity indicates that optimal is at lower mass.

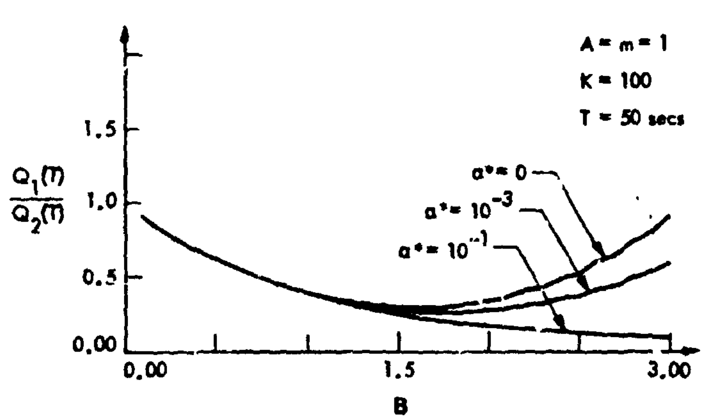

Figure 2-B. Variation of Q_1/Q_2 for various values of B.

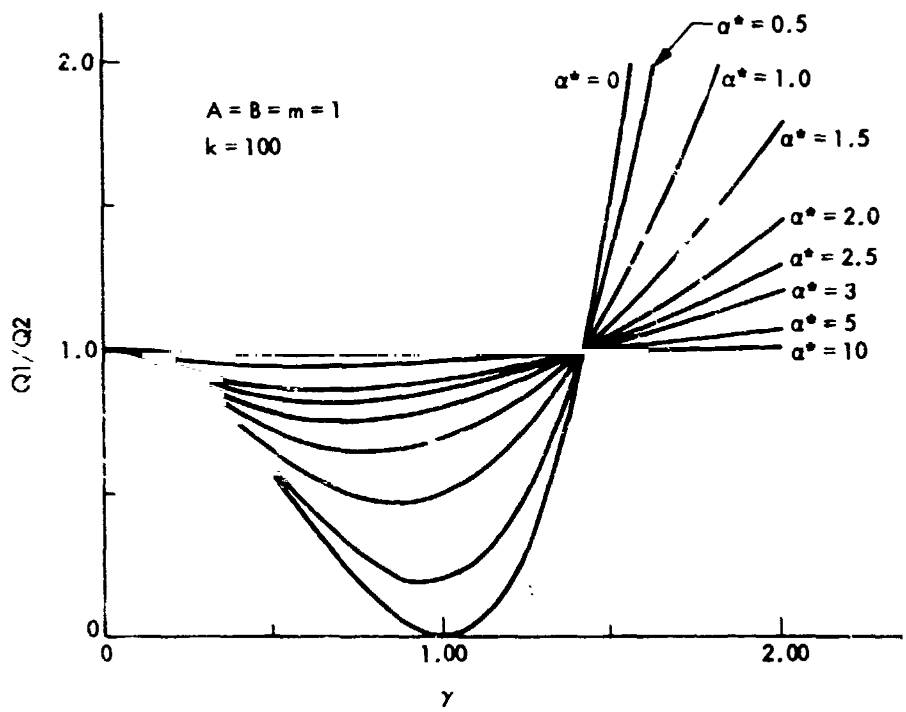

Figure 2-C. Variation of Q_1/Q_2 with $\gamma \triangleq \omega/\omega_o$ for different α^* given A=B=m=1, k=100 and f(t) = Sinωt.

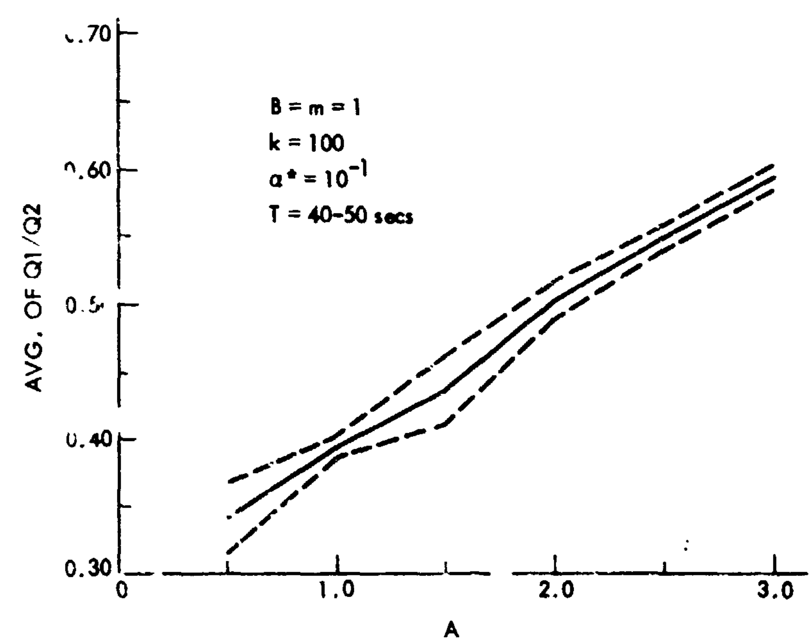

Figure 2-D. Variations in the mean value of $Q_1(T)/Q_2(T)$ and the 1-σ band with different values of A, when B=m=1, k=100, α^*=0.1. The input is Gaussian White Noise. Integration was done over a ten second period.

N85-31210

COMBINED STATE AND PARAMETER ESTIMATION FOR A STATIC MODEL OF THE MAYPOLE (HOOP/COLUMN) ANTENNA SURFACE

H. T. Banks
Lefschetz Center for Dynamical Systems
Brown University
Providence, RI 02912

P. K. Lamm
Southern Methodist University
Dallas, TX 75275

E. S. Armstrong
NASA Langley Research Center
Hampton, VA 23665

ABSTRACT

Parameter and state estimation techniques are discussed for an elliptic system arising in a developmental model for the antenna surface of the Maypole Hoop/Column antenna. A computational algorithm based on spline approximations for the state and elastic parameters is given and numerical results obtained using this algorithm are summarized.

I. INTRODUCTION

Results are presented from a Langley program directed towards developing computationally efficient identification techniques for flexible systems modeled by partial differential equations with an emphasis on large space structures. Initial efforts have been directed towards extending the spline-based theory and computational techniques used by the first two authors [1]-[6] in solving identification problems with delay and partial differential equation models in one spatial variable to solve distributed problems in several spatial variables. Additionally, in order to support Langley's technology development program [7] in large space antennae, a parameter and state estimation algorithm has been derived for a prototype distributed model of the Maypole (Hoop/Column) antenna reflector surface [8]. The next section describes the Hoop/Column antenna and presents the identification problem being considered. The state and parameter estimation approach is then outlined and discussed in the context of the Hoop/Column application. Subsequent sections include mathematical details of the antenna application and numerical results.

II. THE MAYPOLE (HOOP/COLUMN) ANTENNA

For the purpose of technology development, the NASA Large Space Systems Technology (LSST) program office has pinpointed focus missions and identified future requirements for large space antennas for communications, earth sensing, and radio astronomy [7]. In this study, particular emphasis is placed on mesh deployable antennas in the 50-120 meter diameter category. One such antenna is the Maypole (Hoop/Column) antenna shown for the 100m point-design in Figures 1 and 2. This antenna concept is being developed by the Harris Corporation, Melbourne, Florida, under contract to the Langley Research Center [8].

The Hoop/Column antenna consists of a knitted gold-plated molybdenum wire reflective mesh stretched over a collapsible hoop that supplies the rigidity necessary to maintain a circular outer shape. The annular membrane-like reflector surface surrounds a telescoping mast which provides anchoring locations for the mesh center section (Fig. 1). The mast also provides anchoring for cables that connect the top end of the mast to the outer hoop and the bottom end of the mast to 48 equally spaced radial graphite cord truss systems woven through the mesh surface [8]. Tensions on the upper (quartz) cables and outer lower (graphite epoxy) cables are counter balanced to provide stiffness to the hoop structure. The inner lower cables produce, through the truss systems, distributed surface loading to control the shape of four circular reflective dishes (Figs. 1 and 2) on the mesh surface.

After deployment or after a long period of operation, the reflector surface may require adjustment. Optical sensors are to be located on the upper mast which measure angles of retroreflective targets placed on the truss radial cord edges on the antenna surface. This information can then be processed using a ground-based computer to determine a data set of values of mesh surface location at selected target points. If necessary, a new set of shaping (control) cord tensions can be fed back to the antenna for adjustment.

It is desirable to have an identification procedure which allows one to estimate the antenna mesh shape at arbitrary surface points and the distributed loading from data set observations. It can also be anticipated that environmental stresses and the effects of aging will alter the mesh material properties. The identification procedure must also allow one to address this issue.

Considering the antenna to be fully deployed and in static equilibrium, a distributed mathematical model which describes the antenna surface deviation from a curved equilibrium configuration is under investigation (for preliminary findings, see [9]). Using a cylindrical coordinate system with the z-axis along the mast, it is expected that the resulting model will entail a system of coupled second-order linear partial differential equations in two spatial variables. The coefficients of these equations are functions of the material properties of the stretched mesh. The derivation and computer software for this model are still under development. In the meantime, a simpler developmental (prototype) problem has been solved which is descriptive of the original problem.

For the developmental problem, the loading is assumed to be normal to the horizontal plane containing the hoop rim, and the mesh surface is assumed to be described by the static two-dimensional stretched membrane equation [10] with variable stiffness (elastic) coefficients and appropriate boundary conditions for the Hoop/Column geometry. Mathematically, in polar coordinates, we have

$$-\frac{1}{r}\frac{\partial}{\partial r}\left[rE(r,\Theta)\frac{\partial u}{\partial r}\right]-\frac{1}{r^2}\frac{\partial}{\partial \Theta}\left[E(r,\Theta)\frac{\partial u}{\partial \Theta}\right]=f(r,\Theta) \tag{1}$$

where $u(r,\Theta)$ is the vertical displacement of the mesh from the hoop plane, $f(r,\Theta)$ is the distributed loading force per unit area, and $E(r,\Theta) > 0$ is the distributed stiffness (elastic) coefficient of the mesh surface (force/unit length). Equation (1) is to be solved over the annular region $\Omega = [\varepsilon,R] \times [0,2\pi]$. Appropriate boundary conditions are

$$\begin{aligned} u(\varepsilon,\Theta) &= u_0 \\ u(R,\Theta) &= 0 \end{aligned} \tag{2}$$

along with the periodicity requirement

$$u(r,0) = u(r,2\pi) \ , \tag{3}$$

where R is the radius from the mast center to the circular outer hoop, ε is the radius from the mast to the beginning of the mesh surface (see Fig. 2), and u_0 is the coordinate at $r = \varepsilon$ of the mesh surface below the outer hoop plane.

We further assume that the distributed loading along with a data set of vertical displacements, $u_m(r_i,\Theta_j)$, at selected points (r_i,Θ_j) on the mesh surface is known. Given this information, the developmental problem is to estimate the material properties of the mesh as represented by $E(r,\Theta)$ and produce state estimates of the surface represented by $u(r,\Theta)$ at arbitrary (r,Θ) points within Ω. The procedure applied to solve this problem is discussed in the next section.

III. THE SYSTEM IDENTIFICATION APPROACH

The first two authors and their colleagues have derived techniques for approximating the solutions to systems identification and control problems involving delay equation models and partial differential equation models in one spatial variable and have used them in a variety of applications [11],[12]. The Hoop/Column application requires an extension of the theory and numerical algorithms to elliptic distributed systems in several spatial variables. The approach, when specialized to the system identification problem, may be summarized as follows: (1) select a distributed parameter formulation containing unknown parameters for a specific system; (2) mathematically "project" the formulation down onto a finite dimensional subspace through some approximation procedure such as finite differences, finite elements, etc.; (3) solve the identification problem within the finite dimensional subspace obtaining an estimate dependent upon the order of the approximation embodied in the subspace; (4) successively increase the order of the approximation and, in each case, solve the identification problem so as to construct a sequence of parameter and state estimates ordered with increasing refinement of the approximation scheme; (5) seek a mathematical theory which provides conditions under which the sequence of approximate solutions approaches the distributed solution as the subspace dimension increases with a convergent underlying sequence of parameter estimates.

In applying this approach to the developmental problem, the stiffness function is parametrized in terms of cubic splines of fixed order; this converts the estimation of $E(r,\theta)$ into a finite dimensional parameter estimation problem. After writing the energy functional generic to the membrane equation, the Galerkin procedure is used to project the distributed formulation onto a finite dimensional state subspace spanned by tensor products of linear spline functions defined over Ω. The approximate displacement (state estimate) thus obtained is expressible in terms of the spline basis functions. The Galerkin procedure in this case yields algebraic equations which define the displacement approximation coordinates in terms of the unknown $E(r,\theta)$ parameters. In order to solve the approximating parameter estimation problem, the parameters defining $E(r,\theta)$ are chosen so that a least squares measure of the fit error between the observed and predicted (by the estimated state) data set is minimized. Finally, following steps (4) and (5) an algorithm is constructed to determine the order of the linear spline approximation above which little or no further improvement is obtained in the unknown quantities as one increases the dimension of the subspaces. Details of this system identification approach are presented in the following sections.

IV. FINITE DIMENSIONAL APPROXIMATIONS

Prior to applying the Galerkin procedure [13,14] to perform the finite dimensional approximation for the developmental problem, the boundary conditions (2) are converted to homogeneous form by introducing the new dependent variable

$$y(r,\theta) = u(r,\theta) - \left(\frac{r - R}{\varepsilon - R}\right) u_0 \tag{4}$$

Equation (1) then becomes

$$-\frac{1}{r}\frac{\partial}{\partial r}\left(rE(r,\theta)\frac{\partial y}{\partial r}\right) - \frac{1}{r^2}\frac{\partial}{\partial \theta}\left(E(r,\theta)\frac{\partial y}{\partial \theta}\right) = f(r,\theta) + \frac{1}{r}\frac{\partial}{\partial r}\left(\frac{rE(r,\theta)u_0}{\varepsilon - R}\right) \tag{5}$$

with boundary conditions

$$\begin{aligned} y(\varepsilon,\theta) &= 0 \\ y(R,\theta) &= 0 \\ y(r,0) &= y(r,2\pi) \ . \end{aligned} \tag{6}$$

Following the standard formulation (see [13,14]) for the weak or variational form of (5), the energy functional $\hat{E}$ associated with (5) is

$$\hat{E}(z) = \int_0^{2\pi} \int_\varepsilon^R \left[\frac{1}{2} E(r,\theta)\nabla z \cdot \nabla z - \tilde{f}(r,\theta)z\right] r\,dr\,d\theta \ , \tag{7}$$

where ∇ is the gradient in polar coordinates which, in the form used here, is equivalent to

$$\left(\frac{\partial}{\partial r}, \frac{1}{r}\frac{\partial}{\partial \theta}\right)^T . \tag{8}$$

The function $\tilde{f}$ is given by

$$\tilde{f}(r,\theta) = f(r,\theta) + \frac{1}{r}\frac{\partial}{\partial r}\left(\frac{rE(r,\theta)u_0}{\varepsilon - R}\right) \tag{9}$$

and the vertical displacement $z(r,\theta)$ of the mesh surface away from the hoop equilibrium plane is a function satisfying the boundary conditions (6) and possessing first derivatives on Ω in the distributional sense (we denote this by $z \in H^1_{0,per}(\Omega) \equiv Z$). The first variation $\delta\hat{E}$ of $\hat{E}$ about the function $y(r,\theta)$ is given by

$$\delta\hat{E}(y;v) = \int_0^{2\pi}\int_\epsilon^R \{E(r,\theta)\nabla y \cdot \nabla v - \tilde{f}(r,\theta)v\}\ r dr d\theta$$

$$= \int_0^{2\pi}\int_\epsilon^R \{E(r,\theta)\nabla y \cdot \nabla v - [f(r,\theta)v + E(r,\theta)\tilde{k} \cdot \nabla v]\}\ r dr d\theta \qquad (10)$$

where

$$\tilde{k} = \begin{pmatrix} \hat{k} \\ 0 \end{pmatrix} = \begin{pmatrix} \frac{u_0}{R-\epsilon} \\ 0 \end{pmatrix} \qquad (11)$$

and v is an arbitrary function in $Z = H^1_{0,per}(\Omega)$.

Given a finite dimensional subspace $\hat{Z}$ of Z, the Galerkin procedure defines the approximation $\hat{y}$ as the solution in $\hat{Z}$ of

$$\int_0^{2\pi}\int_\epsilon^R \{E(r,\theta)\nabla\hat{y} \cdot \nabla\hat{v}\}\ r dr d\theta = \int_0^{2\pi}\int_\epsilon^R \{f(r,\theta)\hat{v} + E(r,\theta)\tilde{k} \cdot \nabla\hat{v}\}\ r dr d\theta \qquad (12)$$

for all $\hat{v}\epsilon\hat{Z}$.

For computational efficiency, the basis functions used for the representations of $\hat{y}$ in (12) are taken as tensor products of linear B-splines ([13], p. 27; [14], p. 100). Thus $\hat{v}$ and $\hat{y}$ are in the space spanned by

$$v_{ij}^{M,N}(r,\theta) = \alpha_i^M(r)\beta_j^N(\theta)\ , \quad (i = 1,\ldots,M-1;\ \ j = 1,\ldots,N)\ , \qquad (13)$$

where $\alpha_i^M = \alpha_i^M(r)$, $(i = 1,\ldots,M-1)$, and $\beta_j^N = \beta_j^N(\theta)$, $(j = 1,\ldots,N-1)$, are standard linear B-splines with knots uniformly spaced over $[\epsilon,R]$ and $[0,2\pi]$, respectively, modified to satisfy the appropriate boundary conditions. The elements $\{\alpha_i^M\}$ are modified to satisfy homogeneous boundary conditions while β_N^N has been altered to satisfy periodic boundary conditions [15].

For $y^{M,N}(r,\Theta)$ within the subspace spanned by $v_{ij}^{M,N}$ we can write

$$y^{M,N}(r,\theta) = \sum_{i=1}^{M-1} \sum_{j=1}^{N} \alpha_i^M(r) w_{ij}^{M,N} \beta_j^N(\theta) . \tag{14}$$

Replacing $\hat{y}(r,\Theta)$ in (12) by $y^{M,N}(r,\Theta)$ from (14) and successively setting $v(r,\Theta) = v_{ij}^{M,N}(r,\Theta)$ for $i = 1,\ldots,M-1$ and $j = 1,\ldots,N$ leads to a set of high-order linear algebraic equations for the $w_{ij}^{M,N}$ coordinates.

We avoid sparse matrix methods in solving the $w_{ij}^{M,N}$ equation by imposing a separability condition:

$$E(r,\theta) = E_1(r)E_2(\theta) . \tag{15}$$

As shown in [15], condition (15) reduces the $w_{ij}^{M,N}$ calculation to the solution of the matrix equation

$$\tilde{B}^M\, W^{M,N}\, \tilde{A}^N + \tilde{D}^M\, W^{M,N}\, \tilde{C}^N = \tilde{E}^{M,N} \tag{16}$$

with

$$W^{M,N} = \left(w_{ij}^{M,N}\right) \tag{17}$$

$$\tilde{A}^N = \left(\int_C^{2\pi} E_2(\theta)\beta_j^N(\theta)\beta_q^N(\theta)d\theta\right) \tag{18}$$

$$\tilde{B}^M = \left(\int_\varepsilon^R E_1(r)\left[\frac{d}{dr}\,\alpha_i^M(r)\right]\left[\frac{d}{dr}\,\alpha_p^M(r)\right] rdr\right) \tag{19}$$

$$\tilde{C}^N = \left(\int_0^{2\pi} E_2(\theta)\left[\frac{d}{d\theta}\,\beta_j^N(\theta)\right]\left[\frac{d}{d\theta}\,\beta_q^N(\theta)\right] d\theta\right) \tag{20}$$

$$\tilde{D}^M = \left(\int_\varepsilon^R E_1(r)\,\frac{\alpha_i^M(r)\ \alpha_p^M(r)}{r}\,dr\right) \tag{21}$$

and

$$\tilde{\mathcal{E}}^{M,N} = \left(\int_0^{2\pi}\int_\varepsilon^R f(r,\theta)\alpha_i^M(r)\ \beta_j^N(\theta)\,r\,dr\,d\theta\right.$$

$$\left.+\int_0^{2\pi}\int_\varepsilon^R E(r,\theta)\hat{k}\beta_j^N(\theta)\left[\frac{d}{dr}\ \alpha_i^M(r)\right]\ r\,dr\,d\theta\right)\ , \tag{22}$$

where, in (17)-(22), $i,p = 1,\ldots,M-1$ and $j,q = 1,\ldots,N$.

Equation (16) is rewritten in the equivalent form

$$\left[(\tilde{D}^M)^{-1}\tilde{B}^M\right]W^{M,N} + W^{M,N}\left[\tilde{C}^N(\tilde{A}^N)^{-1}\right] = (\tilde{D}^M)^{-1}\tilde{E}^{M,N}(\tilde{A}^N)^{-1} \tag{23}$$

and solved by the Bartels-Stewart algorithm [16].

In order to estimate, via a numerical scheme, the functional coefficients E_1 and E_2, we parametrize these functions so that identification is performed over a finite-dimensional parameter set. To this end, let

$$E_1(r) = \sum_{k=1}^{M_1} \nu_k\lambda_k(r) \tag{24}$$

$$E_2(\theta) = \sum_{j=1}^{N_1} \delta_j\mu_j(\theta) \tag{25}$$

where ν_k and δ_j are scalar parameters and λ_k and μ_j are cubic B-spline functions defined [13, p. 61] over $[\varepsilon,R]$ and $[0,2\pi]$, respectively, whose orders are independent of M and N. The basic spline functions are modified so that μ_j and its derivatives satisfy periodic boundary conditions.

We turn next to the computer implementation of the identification scheme.

V. COMPUTATIONAL PROCEDURE

Appealing to the ideas found in previous sections, we now detail an algorithm for estimating the coefficients ν_k, $k = 1,\ldots, M_1$ and δ_j, $j = 1,\ldots, N_1$, for $E(r,\theta)$ that provide the "best fit" between estimations of the state u and observed data u_m obtained from various sample points on the surface. We may equivalently consider data for y by making the transformation

$$y_m(r_i,\theta_j) = u_m(r_i,\theta_j) - \left(\frac{r_i - R}{\varepsilon - R}\right) u_0 \tag{26}$$

for $i = 1,\ldots, L_r$ and $j = 1,\ldots, L_\theta$.

A parameter estimation algorithm may be organized into the following steps.

1. Select an order of approximation for the cubic spline elements λ_k, $k = 1,\ldots, M_1$ and μ_j, $j = 1,\ldots, N_1$, used to represent E_1 and E_2. Set $n = 1$.

2. Select M and N, the number of the linear spline basis elements used to represent $u^{M,N}$ (and $y^{M,N}$).

3. Assume a nominal set of values for

$$\nu = \left(\nu_1, \nu_2,\ldots, \nu_{M_1}\right) \tag{27}$$

and

$$\delta = \left(\delta_1, \delta_2,\ldots, \delta_{N_1}\right) . \tag{28}$$

4. Calculate the coefficient matrices in (23) and solve for $w^{M,N}(\nu,\delta)$.

5. Calculate, from (14), $y^{M,N}(r_i,\theta_j;\ \nu,\delta)$ and evaluate

$$J^{M,N}(\nu,\delta) = \sum_{i=1}^{L_r} \sum_{j=1}^{L_\theta} \left[y^{M,N}(r_i,\theta_j;\ \nu,\delta) - y_m(r_i,\theta_j)\right]^2 . \tag{29}$$

6. Proceed to step 8 if $J^{M,N}(\nu,\delta)$ is sufficiently small. Otherwise, through an optimization procedure, determine a new pair $(\hat{\nu},\hat{\delta})$ which decreases the value of $J^{M,N}$. If no such pair can be found, go to step 8.

7. Set $(\nu,\delta) = (\hat{\nu},\hat{\delta})$ and return to step 4.

8. Preserve the current values of $J^{M,N}$ and the corresponding (ν,δ) pair as the n^{th} entry in a sequence of these pairs, ordered with increasing M and N.

9. Proceed to step 10 if sufficient data has been obtained to analyze the sequences. Otherwise, set $n = n + 1$ and return to step 2 with increased M and N. The current values of (ν,δ) will be used as initial values for the next optimization process.

10. From analysis of the numerical sequences, select the (M,N) entry which indicates the best numerical results. The corresponding parameter estimate (ν,δ) pair yields $E(r,\theta)$ which determines the material properties of the antenna mesh. The matrix $w^{M,N}(\nu,\delta)$, when used in conjunction with (14), determines a state approximation $y^{M,N}$ for the shape of the antenna surface.

A convergence theory for the identification algorithm may be found in [15]. Numerical results are described in the next section.

VI. NUMERICAL RESULTS

Experimental data for the Hoop/Column antenna is not available at this time. Therefore, synthetic data is constructed to demonstrate the preceding algorithm.

As shown in Figure 2, the parent reflector has four separate areas of illumination on its surface. Each area is assumed to have the same parabolic shape. For $0 \le \theta \le \frac{\pi}{2}$ and $\varepsilon \le r \le R$.

$$u^0(r,\theta) = \begin{cases} \dfrac{u_0(R - r)}{R - \varepsilon}\left[k\left(\dfrac{r - \varepsilon}{R}\right) q_2(\theta) + 1\right], & 0 \le \theta \le \dfrac{\pi}{36} \\[2ex] \dfrac{u_0(R - r)}{R - \varepsilon}\left[k\left(\dfrac{r - \varepsilon}{R}\right) q_1(\theta) + 1\right], & \dfrac{\pi}{36} \le \theta \le \dfrac{17\pi}{36} \\[2ex] \dfrac{u_0(R - r)}{R - \varepsilon}\left[k\left(\dfrac{r - \varepsilon}{R}\right) q_3(\theta) + 1\right], & \dfrac{17\pi}{36} \le \theta \le \dfrac{\pi}{2} \end{cases} \tag{30}$$

where

$$q_1(\Theta) = \sin\Theta + \cos\Theta \ . \qquad (31)$$

The functions $q_2(\Theta)$ and $q_3(\Theta)$ are cubic polynomial fits used to ensure smoothness in regions of O near $\Theta = \frac{\pi}{2}, \pi, \frac{3\pi}{2}, 2\pi$. Formulae for $q_2(\Theta)$ and $q_3(\Theta)$ may be found in [15]. The parameter $k > 0$, a stretch factor used to perturb the surface below the conic $(k = 0)$ shape is taken as 0.25.

For the complete surface, we define, for $\varepsilon \leq r \leq R$,

$$\bar{u}(r,\Theta) = \begin{cases} u^0(r,\Theta) \ , & 0 \leq \Theta \leq \frac{\pi}{2} \\ u^0\left(r,\Theta - \frac{\pi}{2}\right), & \frac{\pi}{2} \leq \Theta \leq \pi \\ u^0(r,\Theta - \pi) \ , & \pi \leq \Theta \leq \frac{3\pi}{2} \\ u^0\left(r,\Theta - \frac{3\pi}{2}\right), & \frac{3\pi}{2} \leq \Theta \leq 2\pi \ . \end{cases} \qquad (32)$$

It is expected that the mesh will be stiffest near the outer hoop $(r = R)$ and around the inner radius $(r = \varepsilon)$. For this reason we choose a known value of $E_1(r)$ as

$$\bar{E}_1(r) = 2\hat{\tau} - \hat{\tau}\sin\left[\pi\frac{(r-\varepsilon)}{(R-\varepsilon)}\right] \qquad (\varepsilon \leq r \leq R) \qquad (33)$$

where $\hat{\tau}$ is a constant dependent on the mesh material. The stiffness in the angular direcion is expected to be uniform with

$$\bar{E}_2(\Theta) \equiv \hat{\tau} \ . \qquad (34)$$

From data provid :8] for the 100-meter point design, a reasonable value for $\hat{\tau}$ (given in units $\sqrt{N/m}$) is

$$\hat{\tau} = 3.391 \ ; \qquad (35)$$

similarly, other parameters are calculated to be $u_0 = -7.5m$, $\varepsilon = P.235m$ and $R = 50m$.

A 10 x 24 grid of data points $u_m(r_i,\theta_j)$ is calculated by evaluating $\overline{u}(r,\theta)$ at points (r_i,θ_j) with

$$r_i = \varepsilon + i\ \frac{(\ell - \varepsilon)}{11} \qquad (i = 1,2,\ldots,L_r = 10) \tag{36}$$

$$\theta_j = [7.5° + (j - 1)\ 15°]\ \frac{\pi}{180} \qquad (j = 1,2,\ldots,L_\theta = 24)\ . \tag{37}$$

Values of θ_j correspond to data taken along every other radial cord truss system with reflectors assumed located on the gore edges. Distributed loads are obtained by substituting (32)-(34) into (1) and evaluating $f(r,\theta)$.

In the examples of the identification process to be presented, an equal number of linear spline basis functions are used in both r and θ directions. That is, $M = N + 1$ for an increasing sequence of N-values. The cubic spline approximations (24) and (25) are used with fixed $M_1 = N_1 = 4$ to represent $E_1(r)$ and $E_2(\theta)$. The IMSL version (ZXSSQ) of the Levenberg-Marquardt algorithm [17] is employed to minimize $J^{M,N}$ given by (29). For the first choice of N, nominal (ν,δ) parameter values to initialize the Levenberg-Marquardt algorithm are obtained by finding those (ν,δ) coordinates which cause (24) and (25) to best approximate assumed functions $E_1^0(r)$ and $E_2^0(\theta)$ chosen as guessed forms for $\overline{E}_1(r)$ and $\overline{E}_2(\theta)$, respectively. For larger N, the latest previously obtained set of converged coordinates is used as nominal parameters. Numerical calculations are performed on a CDC Cyber 170-series digital computer using default values of the IMSL convergence parameters.

Two measures of identification scheme performance are employed. The quantity

$$\hat{J}^{M,N} = \left(\frac{J^{M,N}}{L_r L_\theta}\right)^{1/2} \tag{38}$$

is used as a measure of state estimation accuracy. Additionally,

$$R^{M,N} = \frac{\left|E^{M,N} - \overline{E}\right|}{\left|\overline{E}\right|} \times 100\% \tag{39}$$

measures the relative error between the true

$$\overline{E}(r,\theta) = \overline{E}_1(r)\overline{E}_2(\theta) \tag{40}$$

and the estimated $E(r,\theta)$ denoted by

$$E^{M,N}(r,\theta) = E_1^{M,N}(r)E_2^{M,N}(\theta) \tag{41}$$

which is calculated from (24) and (25) using the $(M,N)^{th}$ level of state approximation obtained at step 8 of the computational procedure. In (39), $|\cdot|$ denotes the L_2 norm on $[\epsilon,R] \times [0,2\pi]$. $R^{M,N}$ provides a measure of parameter estimation accuracy.

Convergence in the sense that

$$R^{M,N} \to 0$$

and

$$\hat{J}^{M,N} \to 0$$

as

$$(M,N) \to \infty$$

depends on the ability of the cubic spline approximates (24) and (25) to accurately represent $\overline{E}_1(r)$ and $\overline{E}_2(\theta)$. An exact pointwise fit can be obtained for $\overline{E}_2(\theta)$ by choice of the 4 δ-coefficients in (25). However, $\overline{E}_1(r)$ can at best be approximated to

$$\frac{\left|E_1(r) - \overline{E}_1(r)\right|}{\left|\overline{E}_1(r)\right|} = 1.23\%$$

relative error by (24) and (27) with $M_1 = 4$. Consequently, entries in the $(R^{M,N}, \hat{J}^{M,N})$ sequence can be expected to cease decreasing past some (M,N) value. Less realistic examples in which (24) and (25) exactly fit simpler

-4

$\overline{E}_1(r)$ and $\overline{E}_2(\theta)$ functions, and $\hat{J}^{M,N}$ and $R^{M,N}$ monotonically decrease with increasing (M,N) can be found in [15]. Also, using the best cubic spline fits to $\overline{E}_1(r)$ and $\overline{E}_2(\theta)$ obtained from (24) and (25) to define $E(r,\theta)$, along with the exact $f(r,\theta)$ data, we observed that

$$\hat{J}^{M,N} = 0.087$$

uniformly in (M,N). The following numerical results show that the parameter estimates from the identification procedure tend to improve (reduce) this $\hat{J}^{M,N}$ value at the expense of $R^{M,N}$.

<u>Example 1</u>: Estimate $E_2(\theta)$ holding $E_1(r)$ fixed at the best cubic spline estimate of $\overline{E}_1(r)$ using (24). Nominal parameters for the $N = 4$ starting value are obtained by fitting (25) to

$$E_2^0(\theta) = 1 + \frac{1}{2}\cos\theta \ .$$

Four δ-parameters are estimated and results summarized below.

N	$\hat{J}^{M,N}$, m	$R^{M,N}$, %	CP time, sec
4	0.0390	5.13	8
6	0.0384	5.57	23
8	0.0322	5.69	86
10	0.0347	6.01	105
12	0.0330	5.83	132

Essentially no improvement in state estimate was obtained past $N = 8$. The $E_2^{M,N}(\theta)$ tended to 3.591 instead of $\overline{E}_2(\theta) \equiv 3.391$. The ≈ 0.20 bias is attributed to the inability of (24) to exactly fit $\overline{E}_1(r)$.

Example 2: Estimate $E_1(r)$ holding $E_2(\theta)$ fixed at the best cubic spline estimate of $\overline{E}_2(\theta)$ using (25). Nominal parameters for the $N = 4$ starting value are obtained by fitting (24) to

$$E_1^0(r) \doteq 1$$

Four ✱-parameters are estimated and results summarized below.

N	$\hat{J}^{M,N}$, m	$R^{M,N}$, %	CP time, sec
4	0.0355	32.25	22
6	0.0343	24.5	41
8	0.0270	4.39	75
10	0.0293	13.17	103
12	0.0275	8.08	130
14	0.0273	7.44	168
16	0.0271	7.59	222
18	0.0267	7.68	292
20	0.0264	8.03	370
22	0.0260	7.91	460
24	0.0267	8.11	578
26	0.0250	7.49	751
28	0.0203	7.58	847
30	0.0259	7.71	1050

From a state estimation viewpoint, $N = 28$ provides the best accuracy. Overall, considering state, parameter and ease of computation, $N = 8$ is best. Figure 3 shows the character of $E_1^{M,N}(r)$ for selected values of N.

Example 3: Estimate both $E_1(r)$ and $E_2(\theta)$. Nominal parameters are obtained as before for $N = 4$ from

$$E_1^0(r) \equiv 5$$

$$E_2^0(\theta) = 1 - \frac{1}{4} \sin \theta$$

For each N, the first coefficient, δ_1, is held fixed at its initial value. Seven parameters are estimated.

N	$\hat{J}^{M,N}$, m	$R^{M,N}$, %	CP time, sec
4	0.0356	32.24	40
6	0.0341	28.71	67
8	0.0270	4.42	168
10	0.0293	13.18	209
12	0.0275	8.09	256
14	0.0273	7.45	337
16	0.0271	7.59	411
18	0.0267	7.69	490
20	0.0264	8.04	567
22	0.0262	7.90	651
24	0.0260	8.12	768
26	0.0260	7.47	945

Again, from overall considerations, $N = 8$ gives the best results.

VII. CONCLUDING REMARKS

In all examples we have been able to successfully estimate the surface shape of the model antenna. Similar results have been obtained where random noise (approximately 5% noise level) has been added to the data. These and other findings may be found in Section VI of [15].

ACKNOWLEDGMENTS

Research reported here was supported in part by NASA Grant NAG-1-258 for the first and second authors, in part by NSF Grant MCS-8205355 and in part by AFOSR Grant 81-0198 for the first author, and NSF Grant MCS-8200883 for the second author. Parts of the efforts reported were carried out while the first two authors were in residence at the Institute for Computer Applications in Science and Engineering, NASA Langley Research Center, Hampton, VA, which is operated under NASA Contracts No. NAS1-15810 and No. NAS1-16394.

REFERENCES

[1] Banks, H. T., "Algorithms for Estimation in Distributed Models With Applications to Large Space Structures." Proc. Workshop on Applications of Distributed System Theory to the Control of Large Space Structures, JPL-Calif. Inst. Tech., Pasadena, CA, July 14-16, 1982.

[2] Banks, H. T., and Crowley, J. M., "Parameter Estimation in Timoshenko Beam Models," Lefschetz Center for Dynamical Systems Report No. 82-14, Brown University, Providence, RI, June 1982; J. Astr. Sci., Vol. 31, pp. 381-397, 1983.

[3] Banks, H. T., Crowley, J. M., and Kunisch, K., "Cubic Spline Approximation Techniques for Parameter Estimation in Distributed Systems," IEEE Trans. Auto. Control, Vol. AC-28, No. 7, pp. 773-786, July 1983.

[4] Banks, H. T., and Daniel, P. L., "Parameter Estimation of Nonlinear Nonautonomous Distributed Systems," Proc. 20th IEEE Conf. on Decision and Control, San Diego, CA, pp. 228-232, 1981.

[5] Banks, H. T., and Kunisch, K., "An Approximation Theory for Nonlinear Partial Differential Equations With Applications to Identification and Control," Lefscnetz Center for Dynamical Systems Rept. 81-7, Brown University, Providence, RI, 1981; SIAM J. Control and Optimization, Vol. 20, pp. 815-849, 1982.

[6] Banks, H. T., and Daniel, P. L., "Estimation of Variable Coefficients in Parabolic Distributed Systems," LCDS Rept. #82-22, Sept. 1982, Brown University, IEEE Trans. Auto. Control, to appear.

[7] Russell, R. A., Campbell, T. G., and Freeland, R. E., "A Technology Development Program for Large Space Antennas," Paper No. IAF-80A33, Presented at Thirty-First International Astronautical Congress of the International Astronautical Federation, Tokyo, Japan, Sept. 21-28, 1980.

[8] Sullivan, M. R., "LSST (Hoop/Column) Maypole Antenna Development Program," Parts I and II, NASA CR-3558, June 1982.

[9] Banks, H. T., and Majda, G., "Modeling of Flexible Surfaces: A Preliminary Study," ICASE Rept. No. 83-19, Hampton, VA, May 1983; J. Math Modeling, to appear.

[10] Sagan, H., Boundary and Eigenvalue Problems in Mathematical Physics, John Wiley & Sons, Inc., 1966.

[11] Banks, H. T., "Distributed System Optimal Control and Parameter Estimation: Computational Techniques Using Spline Approximations," Lefschetz Center for Dynamical Systems Rept. 82-6, Brown University, Providence, RI, 1982; in Proc. 3rd IFAC Symposium on Control of Distributed Parameter Systems, Toulouse, France, S.P. 21-S.P. 27, June 29-July 2, 1982.

[12] Banks, H. T., "A Survey of Some Problems and Recent Results for Parameter Estimation and Optimal Control in Delay and Distributed Parameter Systems," In Volterra and Functional Differential Equations (K. B. Hannsgen, et al., eds.), Marcel Dekker, New York, pp. 3-24, 1982.

[13] Strang, G., and Fix, G. J., An Analysis of the Finite Element Method, Prentice-Hall, Inc., 1973.

[14] Schultz, M. H., Spline Analysis, Prentice-Hall, Englewood Cliffs, NJ, 1973.

[15] Banks, H. T., Daniel, P. L., and Armstrong, E. S., "A Spline-Based Parameter and State Estimation Technique for Static Models of Elastic Surfaces," ICASE Rept. No. 83-25, Hampton, VA, June 1983.

[16] Bartels, R. H., and Stewart, G. W., "Algorithm 432 - A Solution of the Matrix Equation AX + XB = C," Commun. ACM, Vol. 15, pp. 820-826, Sept. 1972.

[17] More, J. J., "The Levenberg-Marquardt Algorithm," Implementation and Theory in Numerical Analysis (G. A. Watson, ed.), Lecture Notes in Mathematics 630, Springer-Verlag, 1977.

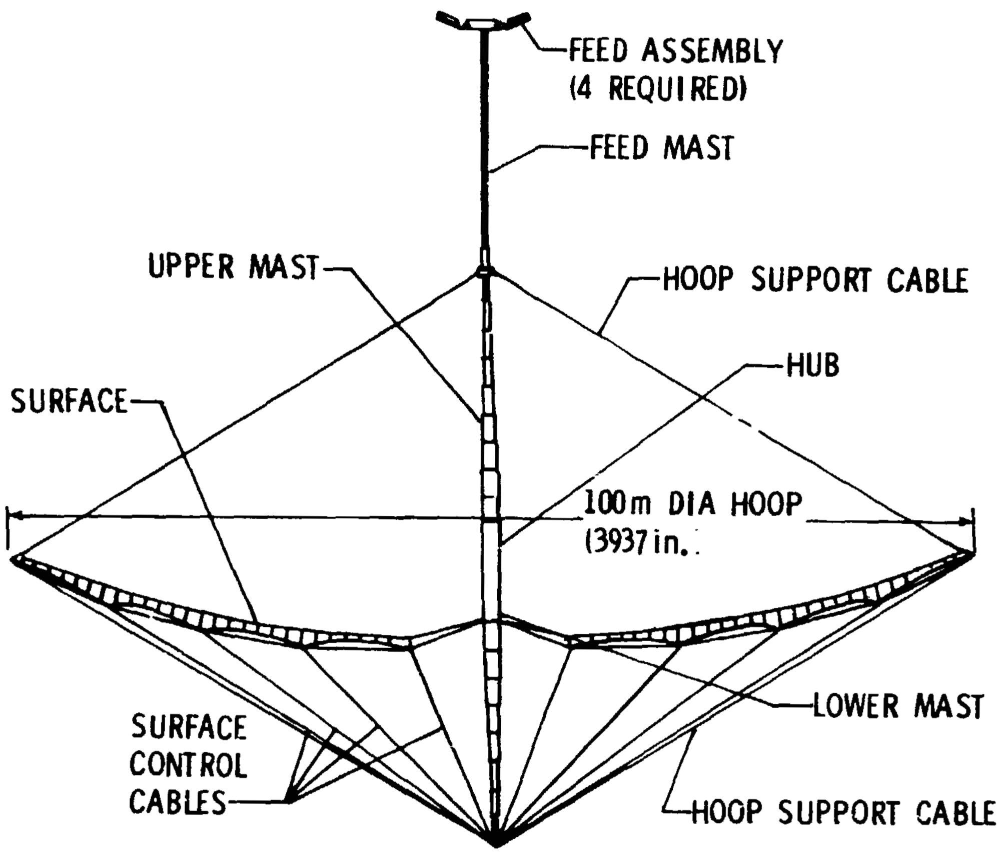

Figure 1.- Side View of Maypole (Hoop/Column) Antenna.

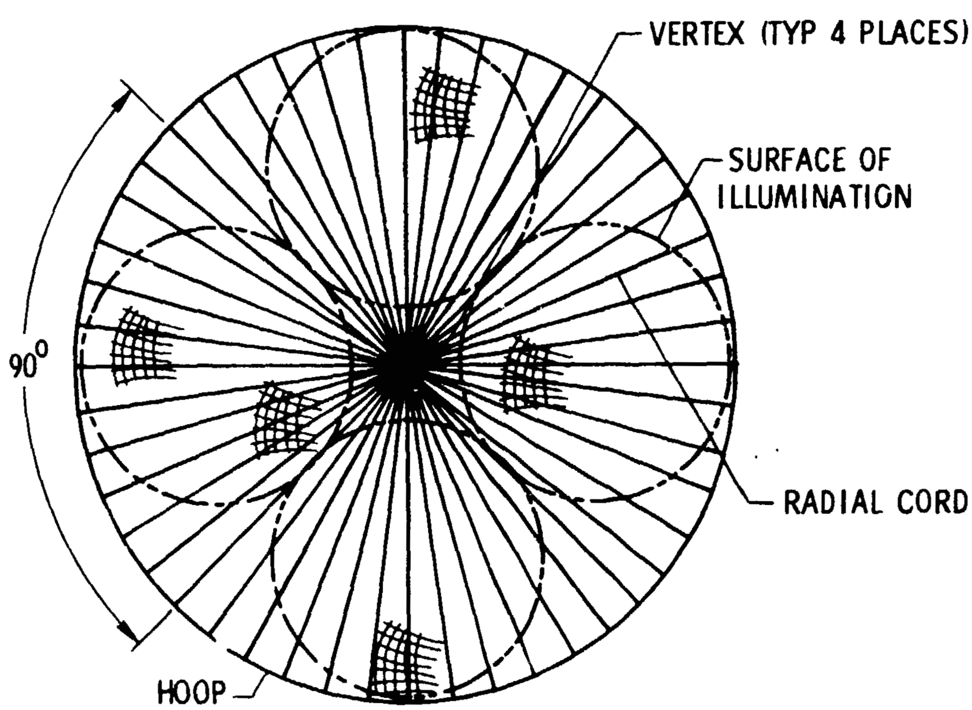

Figure 2.- Maypole (Hoop/Column) Antenna Reflector Surface.

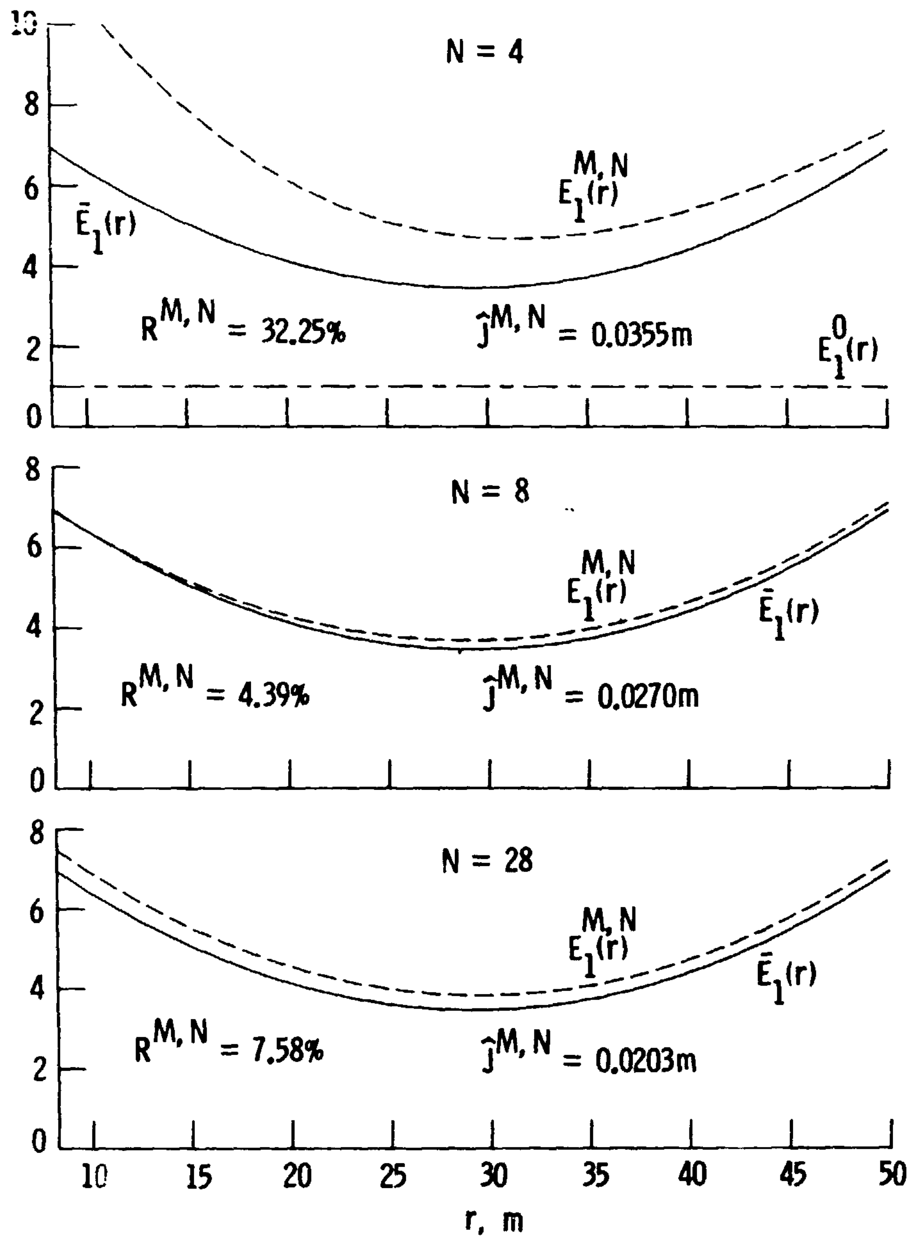

Figure 3.- Estimate $E_1(r)$ with $E_2(\theta)$ fixed.

N85-31211

EXPERIMENTAL VERIFICATION OF IDENTIFICATION ALGORITHMS FOR CONTROL OF FLEXIBLE STRUCTURES

B. Sridhar, J.-N Aubrun, and K. R. Lorell
Lockheed Palo Alto Research Laboratory
Palo Alto, CA 94304

ABSTRACT

This paper describes an on-going simple laboratory experiment, referred to as the Beam Control Experiment (BCE), which has the essential features of a large flexible structure. The experiment is used to develop and evaluate identification and control algorithms which look promising in the active control of high performance large space structures. Some results on the maximum likelihood identification of the parameters of the beam-actuator-sensor assembly from experimental data is presented in the paper.

I. INTRODUCTION

One of the major problems in the design of control systems which operate in the presence of a flexible structure is obtaining accurate information about the plant dynamics. In particular, knowledge of the frequencies, damping ratios and mode shapes of the flexible modes is critical to the successful design of a high performance system. System identification is an iterative process, the success of which depends upon the choice of algorithm and system model, the choice of inputs to excite the system, and the quality of output data. A careful integration of these items is especially critical in the case of large flexible structures.

In this paper we describe the development and performance testing of a simple laboratory model of a jitter control system designed to provide a stable image with optical components mounted on a flexible structure. The study will be carried out in three stages: (a) identification with simulated data, (b) identification with real data, and (c) comparison of closed loop performance with simulated results. Results from the first two stages are reported in this paper.

This paper is organized as follows: Section 2 describes the experimental set-up and a mathematical model for the BCE is developed in Section 3. A brief description of the maximum likelihood estimation (MLE) algorithm is presented in Section 4. Results on the identification of the parameters of the BCE using both simulated and experimental data are discussed in Section 5. A summary and future work is described in Section 6.

II. BEAM CONTROL EXPERIMENT

The idea behind this experiment (Fig. 1) is to demonstrate the interaction between the control of an optical system, symbolized by a laser beam, and control of a flexible structure, represented by a flexible aluminum beam to which passive and active mirrors are attached. These mirrors bounce the laser beam toward a desired target. The interesting control problem stems from the fact that the active mirror is in fact part of a proof-mass actuator. Thus, any attempt to control the laser beam will tend to disturb the aluminum beam, thereby also disturbing the laser beam. This intricate coupling is quite a challenge for a classical design but more amenable to modern techniques. The other aspect of the experiment is the use of a commercially available cated microprocessor (ISI MCP-100) capable of handling at maximum a 32-·· e Kalman filter at a 2000-Hz sampling rate. Such implementation, aside f ı its laboratory usefulness, bring control technology one step further toward real space implementation, and the experience gained is valuable.

The schematic of the experiment is shown in Figs. 2 and 3. The laser beam bounces first on a mirror situated near the middle point of the vertical aluminum beam, then on a mirror attached to the tip of a pivoted proof-mass actuator (PPM). The laser beam finally reaches a photodetector, which measures the laser beam position. A beam splitter provides a visual display of the jitter by projecting the spot on a remote screen.

Two sensors are used in the experiment: the photodetector measuring the line-of-sight (LOS) error, and the PPM rate sensor measuring the relative velocity of the proof-mass.

A preliminary experiment had been performed earlier (Ref. 1) using commercially available software for identification and control synthesis. Only one sensor was used (position) and the control system was able to significantly damp out the beam vibrations; thus stabilizing the line-of-sight. However, in order to eliminate the static error and achieve a higher performance, a better model is needed and thus more sophisticated identification techniques are sought to that end.

For purposes of identification, a known control force is applied to the beam using the proof-mass actuator. The control force time-history and the beam position and relative rate outputs are recorded on a Nicolet 4094 digital oscilloscope. Special software transfers the input and output data from the Nicolet 4094 to a Harris 800 computer where the identification algorithms were exercized. Thus an efficient link between hardware tests and sophisticated computer analyses (Fig. 4) was established.

III. MATHEMATICAL MODEL

In this Section, a state space model of the system is developed. The mathematical form of this model will be used both for simulation and identification of the parameters of the BCE.

The angular displacement, θ_a, of the proof-mass actuator is limited to to a few degrees. For small angles the force and torque applied by the actuator are given by the equations (Reference 2)

$$T = I\ddot{\theta}_a \tag{1}$$

$$f_a = mb\ddot{\theta}_a \tag{2}$$

where m is the mass of the proof-mass actuator, b is the distance from the center of mass to the proof-mass pivot and I is the centroid inertia of the proof-mass actuator. The dynamics of the aluminum beam will be defined in terms of the principal modes and mode shapes. Let q_i be the modal amplitude of the i^{th} mode and define:

ω_i = angular velocity of the i^{th} mode

ζ_i = damping of the i^{th} mode

ϕ_i = translational mode shape of the i^{th} mode at the beam tip (where the PPM is mounted)

and ϕ_i^R = rotational mode shape of the i^{th} mode at this tip. Let ϕ_{im} and ϕ_{im}^R be the corresponding values for the mode shapes where the mirror is mounted on the flexible beam. The modal equations for the beam are:

$$\ddot{q}_i + 2\zeta_i \omega_i \dot{q}_i + \omega_i^2 q_i = -\phi_i f_a - \phi_i^R T \qquad i = 1,2,..M \quad (3)$$

where M is the number of modes represented in the model. Due to the actuator dynamics, the control force f_c applied to the actuator is related to f_a by the equation

$$rf_a = rf_c - (K + mgb)(\theta_a - \theta_t) - D(\dot{\theta}_a - \dot{\theta}_t) \quad (4)$$

where r = lever arm of the actuator

g = acceleration due to gravity

K = spring constant of the actuator

D = damping constant of the actuator

and θ_t = rotation of the beam tip

The rotation of the beam tip can be expressed in terms of the modal amplitudes by

$$\theta_t = \sum_i^M \phi_i^R q_i \quad . \quad (5)$$

Equations (1) - (5) can be reduced to the set of equations

$$\ddot{\theta}_a = -(K + mgb)/I\ \theta_a - D/I\ \dot{\theta}_a + K/I\ \Sigma\ \phi_i^R q_i + D/I\ \Sigma\ \phi_i^R \dot{q}_i + \frac{r}{I} f_c \tag{6}$$

and

$$\ddot{q}_i = -A_i\ \theta_a - C_i\ \dot{\theta}_a - 2\ \zeta_i\ \omega_i\ \dot{q}_i - \omega_i^2 q_i + A_i\ \Sigma\ \phi_i^R q_i + C_i\ \Sigma\ \phi_i^R \dot{q}_i$$
$$+ B_i\ f_c \tag{7}$$

where

$$A_i = -K\ (I\ \phi_i^R + mb\phi_i)/I \tag{8}$$

$$B_i = A_i\ r/K \tag{9}$$

and $$C_i = A_i\ D/K \tag{10}$$

Let y_1 be the displacement of the laser beam from the reference point (i.e., this is a measurement of the L.O.S. error). Let y_2 be the relative angular rate between the actuator and the beam tip. Then,

$$y_1 = 2\ \left[\Sigma\ \phi_{im}\ q_i - (\ell_1 + \ell_2)\ \Sigma\ \phi_{im}^R\ q_i + \ell_2\theta_a\right] \tag{11}$$

and

$$y_2 = \dot{\theta}_a - \dot{\theta}_t = \dot{\theta}_a - \Sigma\ \phi_i^R\ q_i \tag{12}$$

where ℓ_1 is the distance between the mirror on the beam and the mirror on the proof-mass actuator and ℓ_2 is the distance between the photodetector and the mirror on the proof-mass actuator (See Fig. 3).

Equations 6, 7, 11, and 12 give a state space representation of the input/output behavior of the BCE with $\left[\theta_a\ \dot{\theta}_a\ q_1\ \dot{q}_1\ .\ .\ .\ q_M\ \dot{q}_M\right]$ as the state vector.

For a single mode model the equations are given by

$$\dot{x} = Fx + Gu \tag{13}$$

$$y = Hx \tag{14}$$

where

$$F = \begin{bmatrix} 0 & 1 & 0 & 0 \\ -\omega_a^2 & -D/I & \omega_a^2\ \phi_1^R & D/I\ \phi_1^R \\ 0 & 0 & 0 & 1 \\ -A_1 & -C_1 & -\omega_1^2+A_1\phi_1^R & C_1\phi_1^R - 2\ \zeta_1\omega_1 \end{bmatrix} \quad (15)$$

$$G = \begin{bmatrix} 0 & r/I & 0 & B_1 \end{bmatrix}^T \quad (16)$$

and

$$H = \begin{bmatrix} 2\ \ell_2 & 0 & 2\ (\phi_{1m} - (\ell_1 + \ell_2)\ \phi_{1m}^R) & 0 \\ 0 & 1 & 0 & -\phi_1^R \end{bmatrix} \quad (17)$$

where $\omega_a^2 = (K + mgb)/I$. (18)

Also, define $\zeta_a = \dfrac{D}{2\sqrt{I(K+mgb)}}$. (19)

The F, G and H matrices depend on the unknown parameters ($\omega_a, D, \omega_1, \zeta_1, \phi_1, \phi_1^R, \phi_{1m}, \phi_{1m}^R$) and the known parameters (I, m, b, r, ℓ_1 and ℓ_2). The values of the known parameters are tabulated in Table 1. In this model the number of unknown parameters is equal to (6M+2) where M is the number of modes.

I	$4X10^{-4}$ $Kg\text{-}m^2$
m	0.07895 Kg
b	0.06985 m
r	0.021 m
ℓ_1	0.165 m
ℓ_2	0.217 m

Table 1. Known Parameters of the BCE

IV. MAXIMUM LIKELIHOOD ESTIMATION (MLE)

There are several methods available for the estimation/identification of parameters Figure 6 shows the main components of an identification method. The system to be identified and a mathematical model, $M(p)$, of the system is excited by a known input u. An error function, $L(p,e)$, is formed from the outputs of the system and the model. Identification is the process of adjusting the model parameters p to minimize the error function. The choice of $M(p)$, $L(p,e)$ and the adjusting mechanism for p lead to different identification algorithms. In this paper, we shall restrict our attention to the maximum likelihood estimation of parameters.

The MLE can be applied to a large class of problems and has good statistical convergence and accuracy properties. In addition, MLE is well suited for identifying physical parameters of the system. This is a drawback with most recursive algorithms. The main disadvantage of MLE is the amount of computation. However, the amount of computation can be reduced significantly by taking into account the special features of the dynamics of the large space structures.

The flow of computation in the MLE is shown in Fig. 7. The mathematical model for the system is assumed to be

$$x = F(p)\ x + G(p)u + \omega \tag{20}$$

$$y = H(p)\ x + \nu \tag{21}$$

where x is the n-dimensional state vector, y the p-dimensional output vector and u the m-dimensional input vector. ω and represent the process and measurement noise respectively. The matrices F, G and H depend on p, the vector of unknown system parameters. An input signal $[u(t),\ o < t < t_N]$ has been applied to the system and the output y of the system has been observed at discrete times t_O, t_1, . . . t_N. Further, it is assumed that $x(o)$ and ω are zero-mean gaussian random variables with

$$\text{cov}\ (x(o)) = P(o) \tag{22}$$

$$\text{cov}\ (\omega) = Q \tag{23}$$

and

$$\text{cov}\ (\nu) = R \tag{24}$$

The identification problem consists of estimating the parameters p from the experimental data $u(t_i)$, $y(t_i)$, $i = 1,2,...N$. Let $\hat{x}$ be the state estimate, $\hat{y}$ the output estimate, and $e(t_k)$ be the output error

where

$$e(t_k) = y(t_k) - \hat{y}(t_k). \tag{25}$$

The negative log likelihood function, v(p,e), can be written as

$$V(p,e) = - \log L(p,e) = \sum_{i=1}^{N} e^T(i)\, B^{-1}(i)\, e(i) + \log |B(i)| \tag{26}$$

The maximum likelihood estimate of the parameters p is obtained by maximizing the likelihood function L(p,e) (or by minimizing V(p,e)). This nonlinear minimization problem has to be solved by numerical methods and makes the MLE computationally intensive. The computational aspects of MLE are discussed in Reference 4.

V. IDENTIFICATION RESULTS

Numerical results on the identification of the parameters will be presented in two steps. First results from the identification of simulated data will be shown. This will be followed by results from experimental data.

a. Simulation Results: Identification with simulated data was done to get a better understanding of the dynamics of the BCE, to provide guidelines to set up the experiment and to test the MLE software. The system was simulated using 4 modes and was excited by a "bang-bang" type input with an amplitude of ±0.1 Newton. Figure 8 shows the laser beam position and relative velocity output from the simulation. This input/output simulated data was used to identify a single mode beam model of the system (see equations 13-17). The negative log likelihood function V(p,e) was probed at a few points to see its variation with parameter p. Figure 9 shows the variation of the likelihood surface with ω_a and ω_1. The surface is well-behaved in these two variables. The damping terms ζ_a and ζ_1 were set to the simulatior values and only parameters (ω_a. ω_1, ϕ_1, ϕ_1^R, ϕ_{im} and ϕ_{im}^R) were allowed to vary. Table 2 shows the results based on simulated data. There is good agreement between simulated and estimated values. Now we are ready to try the identification with experimental data.

b. Experimental Results: The aluminum beam was excited by applying to the proof-mass actuator a sinusoidal force with a linearly varying frequency (so-called "chirp" excitation). Figure 10 shows the control force f_c. The position and rate measurements are shown in Figure 11. As before, the single mode model will be used as a starting point for the identification of parameters (ω_a, D, ω_1, ζ_1, ϕ_1, ϕ_1^R, ϕ_{im}, ϕ_{im}^R). Initially, the MLE had convergence problems. These were related to one or more of the following causes: 1) large differences between the values of some of the actual BCE parameters and those of the original simulation, 2) bias in the input force and position measurements, and 3) error in rate measurement calibration.

The bias was accounted for simply by subtracting a constant from the force input and position output. The error in rate calibration was taken into account by defining a scale factor α. This results in a new H matrix where

$$H = \begin{bmatrix} 2\ell_2 & 0 & 2(\phi_{im} - (\phi_{im} - (\ell_1+\ell_2)\ \phi_{im}^{R}) & 0 \\ 0 & \alpha & 0 & -\phi_1^{R}\ \alpha \end{bmatrix} \quad (27)$$

The scale factor was estimated along with the other 8 parameters. The estimated values are shown in Table 3. The model parameters shown in Table 3 for "simulation values" were obtained from an extremely simplified model of the aluminum beam (cantilevered with a point mass at tip). Thus, it is not surprising that some of the values obtained from the identification are very different. In particular, values of rotational mode shapes are quite sensitive to local inertias and masses.

Parameter	Simulated Data	Estimate (Simulation Data)	Estimate (Experimental Data)
ω_a	46.36	45.5	37.18
ω_1	54.63	54.58	40.32
ζ_a	0.005	.005*	85E-4
ζ_1	0.005	.005*	0.01
ϕ_1	3.328	3.49	7.48
ϕ_1	-13.51	-13.61	-110.0
ϕ_{im}	1.068	0.98	21.0
ϕ_{im}^{R}	-10.6	-10.3	2.49
α	1.0	1.0*	0.80

*These parameters were set to their simulation values.

Table 3 Results with Experimental Data

Figure 11 shows a comparison between the measured and estimated values of the outputs. The estimated values were generated for the prameter set which resulted from identification using experimental data (Table 3). Figure 11a shows the measured and estimated values of the position. Figure 11b is a blow-up of the same curve to show the difference between measured and estimated values. Figures 11c and 11d show curves similar to 11a and 11b for the rate measurement. There is very good agreement between the model output and the experimental data.

This model will be validated by taking the direct approach. In the third stage of the experiment, a control system will be designed using the identified model. The predicted behavior of the control system will be compared with its experimental behavior.

VI. CONCLUSIONS AND SUMMARY

In this paper, we have described a laboratory experiment which has the salient features of controlling an optical system located on a flexible structure. The experiment will be used as a test bed for designing control and identification algorithms for large space structures. The parameters of a model suitable for designing a control system were identified using maximum likelihood estimation. The real test of a model is of course how well it satisfies the goal of modelling. Currently, we are designing a control system based on this model and the results of this final stage will be reported in another paper.

VII. REFERENCES

1. S. C. Shah, R. A. Walker and D. B. Varvell, A Control Design Workstation, IEEE Control Systems Society Symposium on Computer-Aided Control System Design Sept. 28-30, 1983, Cambridge, Mass.

2. J.-N. Aubrun and G. Margulies, Low-Authority Control Synthesis for Large Space Structures, NASA Contractor Report NAS1-14887-Task 11 May 1982.

3. K. J Astrom, Maximum Likelihood and Prediction Error Methods, Automatica Vol. 16, pp 551-574, 1980.

4. N. K. Gupta and R. K. Mehra, Computational Aspects of Maximum Likelihood Estimation and Reduction in Sensitivity Function Calculations, IEEE Transactions on Automatic Control, AC-19, No. 6, 1974.

ORIGINAL PAGE IS
OF POOR QUALITY

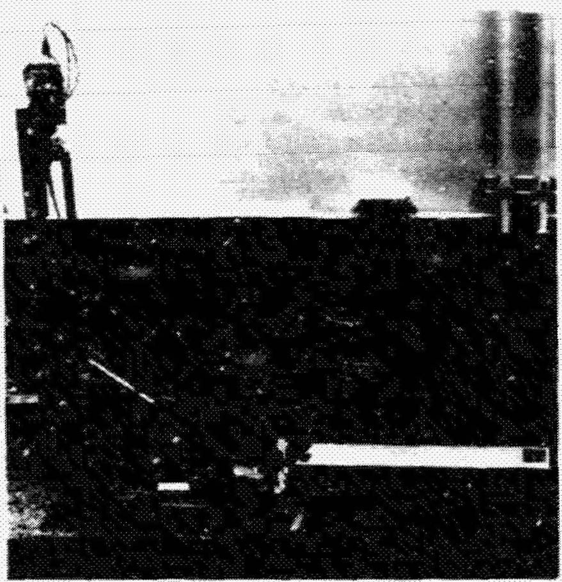

FIG. 1 BEAM CONTROL EXPERIMENT

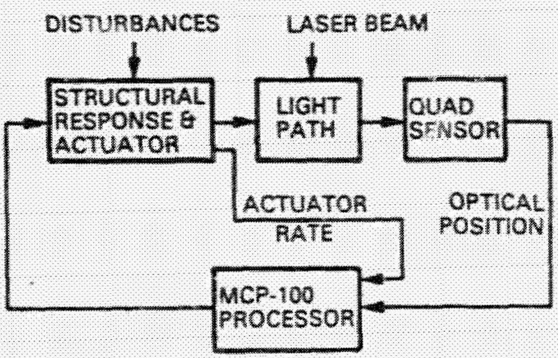

FIG. 3 BEAM CONTROL SCHEMATIC

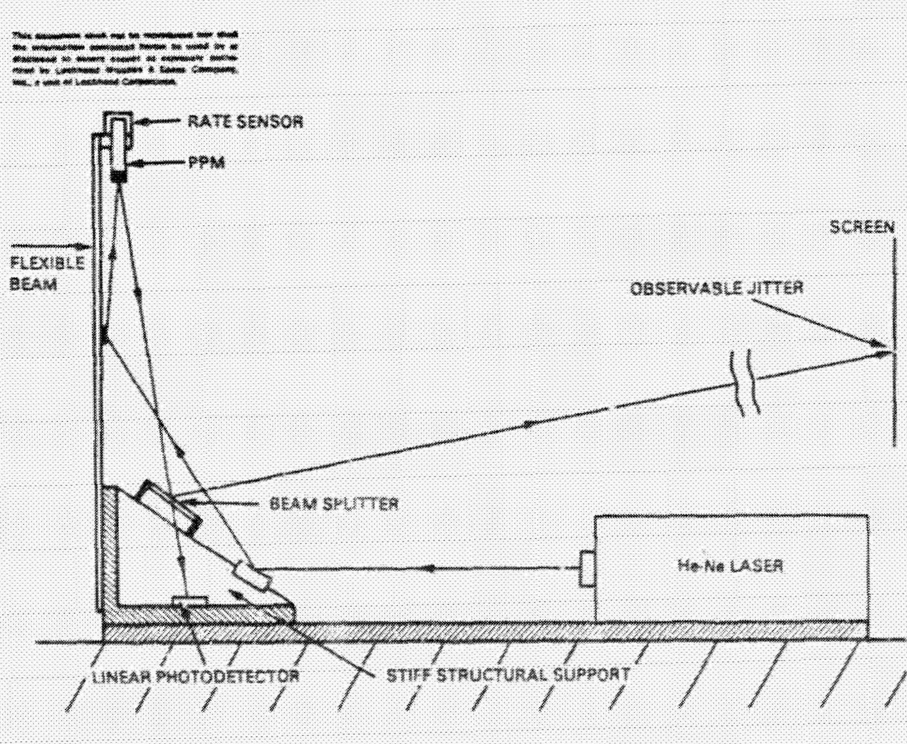

FIG. 2 BEAM CONTROL DIAGRAM

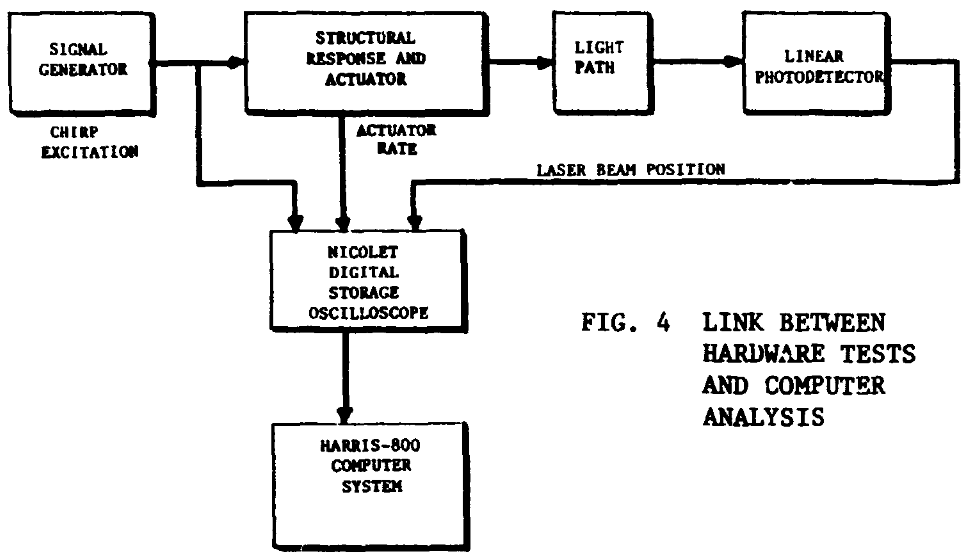

FIG. 4 LINK BETWEEN HARDWARE TESTS AND COMPUTER ANALYSIS

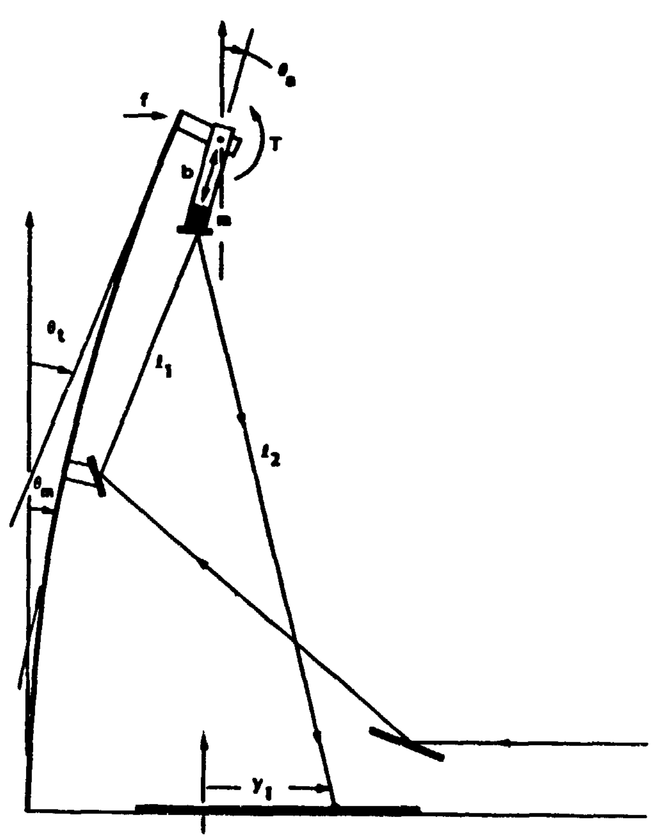

FIG. 5 BEAM EXPERIMENT GEOMETRY

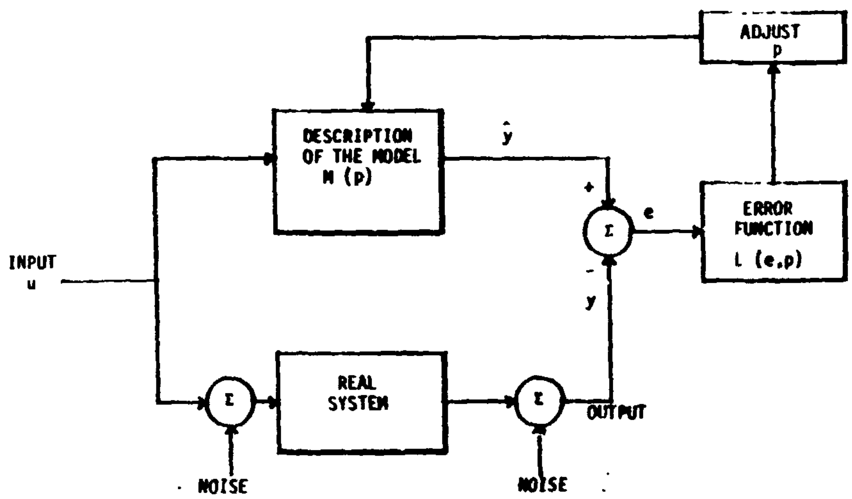

FIG. 6 COMPONENTS OF AN IDENTIFICATION SCHEME

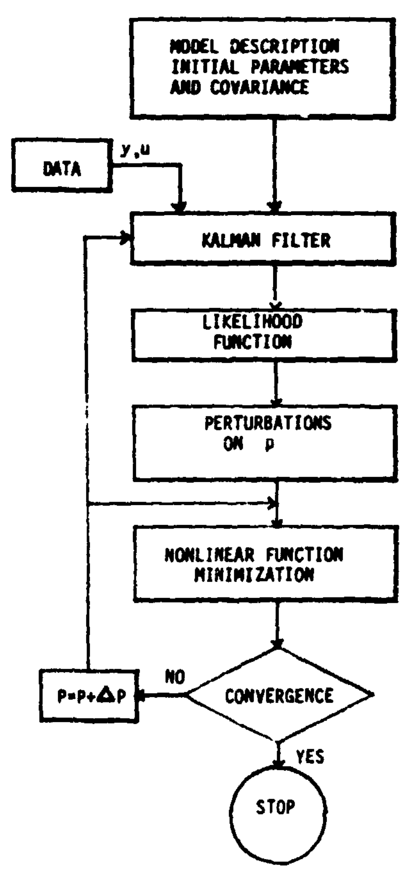

FIG. 7 COMPUTATIONS IN THE MLE

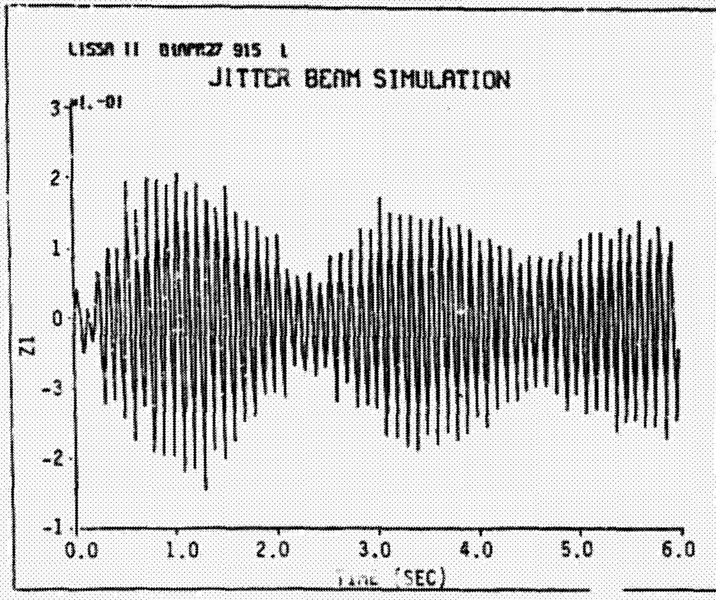

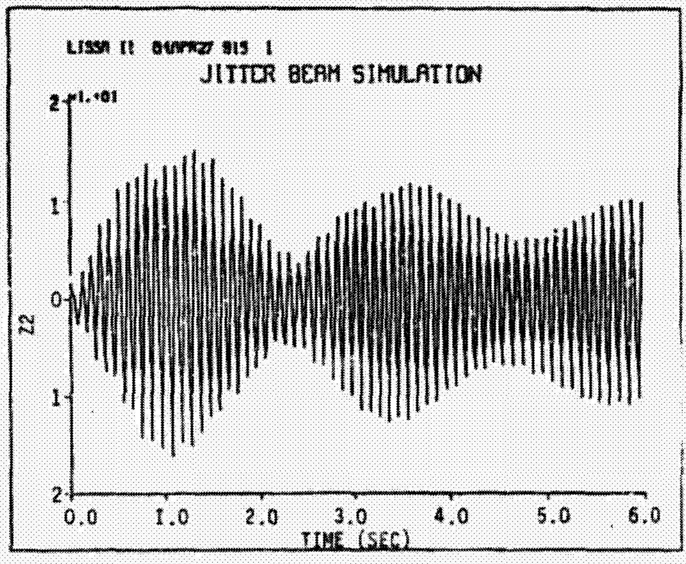

FIG. 8 BEAM POSITION AND RELATIVE ANGULAR RATE

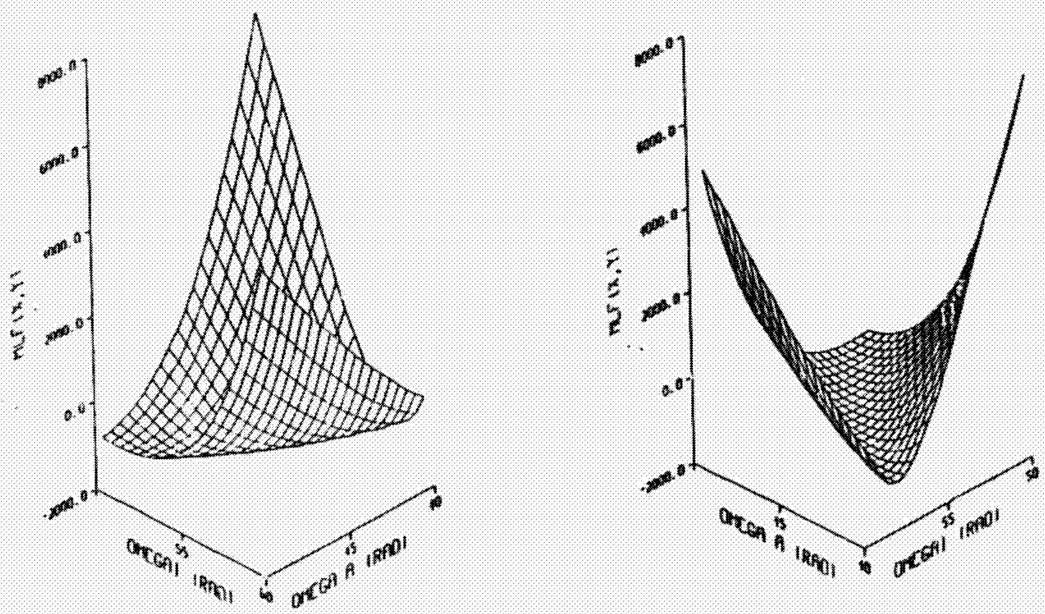

FIG. 9   MAXIMUM LIKELIHOOD SURFACE

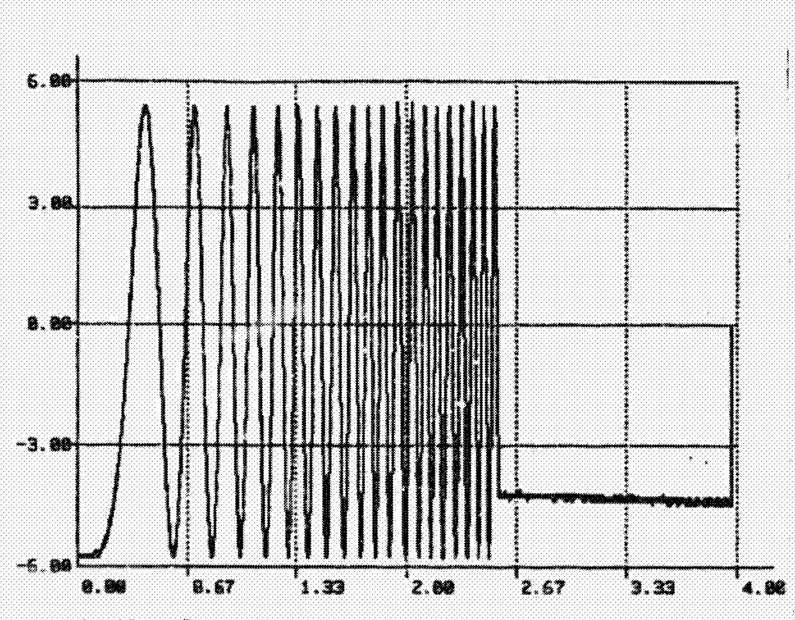

FIG. 10   BEAM EXCITATION INPUT

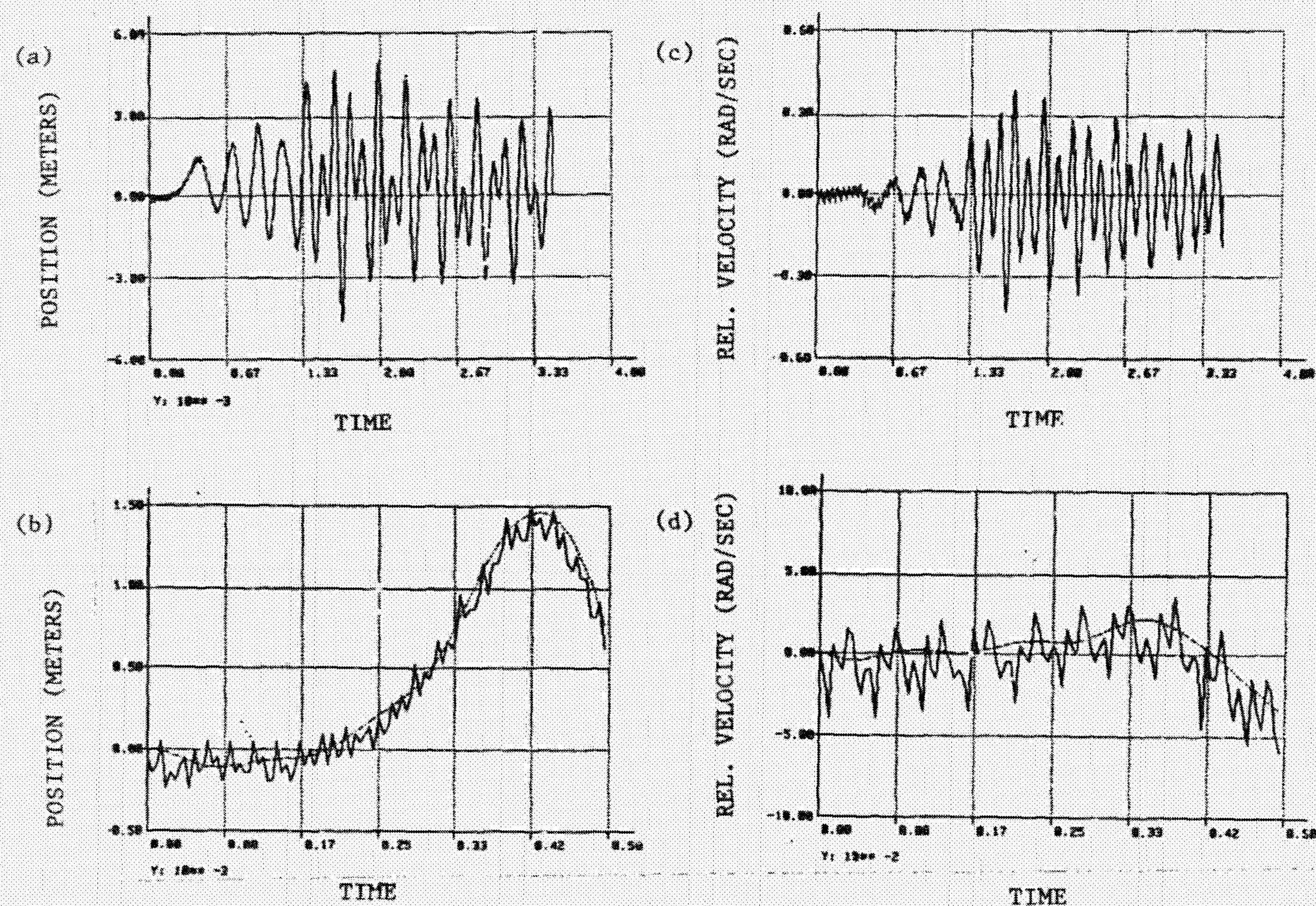

FIG. 11 COMPARISON BETWEEN ESTIMATED AND MEASURED OUTPUTS

N85-31212

AN EIGENSYSTEM REALIZATION ALGORITHM (ERA) FOR MODAL PARAMETER IDENTIFICATION AND MODEL REDUCTION

J. N. Juang and R. S. Pappa
NASA Langley Research Center
Hampton, VA 23665

ABSTRACT

A method, called the Eigensystem Realization Algorithm (ER ... s developed for modal parameter identification and model reduction of dynamic systems from test data. A new approach is introduced in conjunction with the singular value decomposition technique to derive the basic formulation of minimum order realization which is an extended version of the Ho-Kalman algorithm. The basic formulation is then transformed into modal space for modal parameter identification. Two accuracy indicators are developed to quantitatively identify the system modes and noise modes. For illustration of the algorithm, examples are shown using simulation data and experimental data for a rectangular grid structure.

I. INTRODUCTION

The state space model has received considerable attention for system analyses and design in recent control and systems research programs One of these areas, in particular, is control of large space structures. In order to design controls for a dynamic system it is necessary to have a mathematical model which will adequately describe the system's motion. The process of constructing a state space representation from experimental data is called system realization.

During the past two decades, numerous algorithms for the construction of state space representations of linear systems have appeared in the control literature. Among the first were the works of Gilbert [1] and Kalman [2], introducing the important principles of realization theory in terms of the concepts of controllability and observability. Both techniques use the transfer function matrix to solve the realization problem. Ho and Kalman [3] approached this problem from a new viewpoint. They showed that the minimum realization problem is equivalent to a representation problem involving a sequence of real matrices known as Markov parameters (pulse response functions). By minimum realization is meant the smallest state-space dimension among systems realized that has the same input-output relations within a specified degree of accuracy. Questions regarding the minimum realization from various types of input-output data and the generation of minimum partial realization are studied by Tether [4], Silverman [5], and Rossen and Lapidus [6] using Markov parameters. Rossen and Lapidus [7] successfully applied Ho-Kalman [3] and Tether [4] methods to chemical engineering systems. A common weakness of the above schemes is that effects of noise on the data analysis were not evaluated. Zeiger and McEwen

[8] proposed a combinition of the Ho-Kalman algorithm [3] with the singular value decomposition technique for the treatment of noisy data. However, no theoretical or numerical studies were reported in Reference [8]. Among follow-up developments along similar lines, Kung [9] presented and algorithm in conjunction with the singular value decomposition technique to incorporate the presence of the noise. Note that the singular value decomposition technique [10-11] has been widely recognized as being very effective and numerically stable. Although several techniques of minimum realization are available in the literature, formal direct application to the modal parameter identification for flexible structures was not yet addressed.

In the structures field, the finite-element technique is used almost exclusively for constructing analytical models. This approach is well established and normally provides a model accurate enough for structural design purposes. Once the structure is built, static and dynamic tests are performed. These test results are used to refine the finite-element model, which is then used for final analyses. This traditional approach to analytical model development may not be accurate enough for use in designing a vibration control system for flexible structures. Another approach is to realize a model directly from the experimental results. This requires the construction of a minimum-order model from the test data that characterizes the dynamics of the system at the selected control and measurement positions. The present state-of-the-art in structural modal testing and data analysis is one of controversy about the best technique to use. Classical test techniques, which may provide only good frequency and moderate mode shape accuracy, are often considered adequate for finite-element model verification purposes. On the other hand, advanced data analysis techniques which offer significant reductions in test time and improved accuracy , have been available [12-16] but are not yet fully used. For example, Ibrahim [13] presented a method based on state space for the direct identification of modal parameters from free responses. Recently, Void and Russell [16] presented a method using frequency response functions and time domain analysis which can also identify repeated eigenvalues. A comparison of contemporary methods using data from the Galileo spacecraft test is provided by Chen [17].

Although structural dynamics techniques are generally successful for ground data, further incorporation with work from the controls discipline is needed to solve modal parameter identification/control problem. For example, it is known from control theory [18] that a system with repeated eigenvalues and independent mode shapes is not identifiable by single input and single ouput. Methods which allows only one initial condition (input) at a time [13], will miss repeated eigenvalues. Also, if the realized system is not of a minimum order and matrix inversion is used for constructing an oversized state matrix, numerical errors may become dominant.

Under the interaction of structure and control disciplines, the objective of this paper is to introduce an Eigensystem Realization Algorithm (ERA) for modal parameter identification and model reduction for dynamical systems from test data. The algorithm consists of two major parts, namely, basic formulation of the minimum order realization and modal parameter identification. In the section of basic formulation, the Hankel matrix which represents the data structure for Ho-Kalman algorithm is generalized to allow random distribution of Markov parameters generated by free decay reponses. A unique approach based on this generalized Hankel matrix is developed to extend the Ho-Kalman algorithm in combination with the singular value decomposition technique [10-11]. Through the use of the generalized Hankel matrix, a linear model is realized for dynamical system matching the input and output relationship. The realized system model is then transformed into modal space for modal parameter identifications. As part of ERA, two accuracy indicators, namely, the modal amplitude coherence and the modal phase collinearity, are developed to quantify the system modes and noise modes. The degree of modal excitation and observation are evaluated. The ERA method thus forms the basis for a rational choice of model size determined by the singular values and accuracy indicators.

Two examples are given to illustrate the ERA method. The first example uses simulated data from an assumed structure. The effect of repeated eigenvalues on the parameter identification is shown. The second example uses experimental data from a simple grid structure. Comparison of the ERA results with a finite element model of the grid is performed. Experimental results for a more complex structure--the Galileo spacecraft--are shown in Ref. [19].

II. BASIC FORMULATIONS

A finite-dimensional, discrete time, linear, time-invariant dynamical system has the state-variable equations

$$x(k+1) = Ax(k) + Bu(k) \tag{1}$$

$$y(k) = Cx(k) \tag{2}$$

where x is an n dimensional state vector, u is an m dimensional control input, and y is an p dimensional output or measurement vector. The integer k is the sample indicator. The transition matrix A characterizes the dynamics of the system. For flexible structures, it is a representation of mass, stiffness and damping properties. The problem of system realization is then the following. Given the measurement functions y(k), construct constant matrices [A, B, C] such that the functions y are reproduced by the state-variable equations. With different sets of inputs and outputs, several cases can be obtained. The simplest case, namely, single input and single output, is treated first to allow the reader familiar with notations for the treatment of multi-input and multi-output cases.

Single input and single output

For the system (1) with free pulse-response (or initial-state-response), the time-domain description is given by the function known as Markov parameter

$$y(k) = CA^{k-1}B \quad [\text{or } y(k) = CA^{k}x(0)] \tag{3}$$

where x(0) is the system initial conditions and k is an integer. Note that the matrix B is a column vector (single input) whereas the matrix C is a row vector (single output). For free initial-state-response, the matrix B only represents the information of initial conditions rather than the control influence matrix as shown in Eq.(1). The problem of system realization is to construct matrices [A, B, C] in terms of the measurement function $y(k)$ such that the identities of Eq.(3) hold. Now observe that

$$\bar{y}(k) = VA^{k-1}B \quad [\text{ or } \bar{y}(k) = VA^{k}x(0) \ ] \tag{4}$$

where

$$\bar{y}(k) = \begin{bmatrix} y(k) \\ y(k+1) \\ \cdot \\ \cdot \\ \cdot \\ y(k+n-1) \end{bmatrix} ; \quad \text{and} \quad V = \begin{bmatrix} C \\ CA \\ \cdot \\ \cdot \\ \cdot \\ CA^{n-1} \end{bmatrix} \tag{5}$$

Assume that this nth order system has no repeated eigenvalues. There exists a row vector C from observability theory (Ref. 18) such that V has rank n. Consequently, rearranging Eq. (4) becomes

$$\bar{y}(k+1) = VA^{k}B = VAV^{-1}\bar{y}(k) \tag{6}$$

Given the sequence of measurement vectors $\bar{y}(k+1)$, the generalized Hankel matrix $H(k)$ is defined as

$$H(k-1) = [\bar{y}(k), \bar{y}(k+1), \ldots, \bar{y}(k+n)] = \begin{bmatrix} y(k) & ,y(k+1) & ,\ldots, & y(k+n-1) \\ y(k+1) & ,y(k+2) & ,\ldots, & y(k+n) \\ \cdot & \cdot & & \cdot \\ \cdot & \cdot & & \cdot \\ y(k+n-1) & ,y(k+n) & ,\ldots, & y(k+2n-2) \end{bmatrix} \tag{7}$$

It immediately follows from Eq.(6) that

$$H(k) = VAV^{-1}H(k-1) = VA^{k}V^{-1}H(0) \tag{8}$$

or from Eq. (4) that

$$H(k) = VA^{k}[B, AB, \ldots, A^{k-1}B] = VA^{k}W \tag{9}$$

where W is a controllability matrix (Ref. 18). Again if the system with order n has no repeated eigenvalues, there exists a column vector B such that W has rank n. This means that $H(k)$ is invertible if the system is controllable and observable. Letting $k = 1$, Eq. (8) will then determine the state matrix A in the following way

$$VAV^{-1} = H(1)H^{-1}(0) \tag{10}$$

To rigorously prove this result, define E as the column vector $E^{T}=[1,0,\ldots,0]$. The measurement function $y(k+1)$ can then be written by

$$y(k+1) = E^{T}H(k)E = E^{T}H(k)H^{-1}(0)H(0)E = E^{T}[H(1)H^{-1}(0)]^{k}H(0)E \tag{11}$$

with the aid of Eqs. (8) and (10). Hence by Eq. (3), the triple $[H(1)H^{-1}(0), H(0)E, E^{T}]$ is a realization in the sense that if the triple [A, B, C] in the system equations (1) and (2) is replaced by the $[H(1)H^{-1}(0), H(0)E, E^T]$, the measurement functions $y(k)$ are reproduced as proved in Eq. (11). In other words, state variable equations (1) and (2) are transformed to the following equations

$$\bar{x}(k+1) = H(1)H^{-1}(0)\bar{x}(k) + H(0)Eu(k) \tag{12}$$

$$y(k) = E^T\bar{x}(k) \tag{13}$$

where $\bar{x}(k) = V^{-1}x(k)$. (14)

Let us summarize the case as follows.

A finite-dimensional, discrete time, linear time invariant dynamical system with a single input and a single output is realizable if the state matrix A has no repeated eigenvalues, and the system is controllable and observable.

Multi-input and Multi-output

The time-domain description for this case is given by the pulse-response (or initial-state-reponse) function known as Markov parameter

$$Y(k) = CA^{k-1}B \quad (\text{or } Y(k) = CA^k[x_1(0), x_2(0), \ldots, x_m(0)]) \tag{15}$$

where $x_i(0)$ represents the ith set of initial condition and k is an integer. Note that B is a nxm matrix and C is a pxn matrix. The problem of system realization is that, given the functions $Y(k)$, construct constant matrices [A, B, C] in terms of $Y(k)$ such that the identities of Eq. (15) hold. The algorithm begins by forming the rxs block matrix (generalized Hankel matrix)

$$H_{rs}(k-1) = \begin{bmatrix} Y(k) & ,Y(k+t_1) & ,\ldots,Y(k+t_{s-1}) \\ Y(j_1+k) & ,Y(j_1+k+t_1) & ,\ldots,Y(j_1+k+t_{s-1}) \\ \cdot & \cdot & \cdot \\ \cdot & \cdot & \cdot \\ Y(j_{r-1}+k) & ,Y(j_{r-1}+k+t_1) & ,\ldots,Y(j_{r-1}+k+t_{s-1}) \end{bmatrix} \tag{16}$$

where $j_i(i=1,\ldots,r-1)$ and $t_i(i=1,\ldots,s-1)$ are arbitrary integers. For the system with initial-state-response measurements, simply replace $H_{rs}(k-1)$ by $H_{rs}(k)$. It is easy to prove from Eq. (15) that Eq. (9) also holds for this multi-input and multi-output case,

$$H_{rs}(k) = V_r A^k W_s \quad ; \; V_r = \begin{bmatrix} C \\ CA^{j_1} \\ \cdot \\ \cdot \\ CA^{j_{r-1}} \end{bmatrix} \text{ and } W_s = [B, A^{t_1}B, \ldots, A^{t_{s-1}}B] \tag{17}$$

where V_r and W_s are respectively the observability and controllability matrices in a general sense. Note that V_r and W_s are rectangular matrices with dimensions rp x n and n x ms respectively. Assume that there exist a matrix $H^\#$ satisfying the relation

$$W_s H^{\#} V_r = I_n \tag{18}$$

where I_n is an identity matrix of order n. Define 0_p as a null matrix with order p, $E_p^T = [I_p, 0_p, \ldots, 0_p]$ and $E_m^T = [I_m, 0_m, \ldots, 0_m]$. In view of Eqs. (16) and (18), the measurement function $Y(k+1)$ can be obtained through either of two algorithms A1 and A2. The algorithm A1 is

$$\begin{aligned} Y(k+1) &= E_p^T H_{rs}(k) E_m = E_p^T V_r A^k W_s H^{\#} V_r W_s E_m \\ &= E_p^T [V_r A W_s H^{\#}]^k V_r W_s E_m \\ &= E_p^T [H_{rs}(1) H^{\#}]^k H_{rs}(0) E_m \end{aligned} \tag{19}$$

and the algorithm A2 is

$$\begin{aligned} Y(k+1) &= E_p^T H_{rs}(k) E_m = E_p^T V_r W_s H^{\#} V_r A^k W_s E_m \\ &= E_p^T V_r W_s [H^{\#} V_r A W_s]^k E_m \\ &= E_p^T H_{rs}(0) [H^{\#} H_{rs}(1)]^k E_m \end{aligned} \tag{20}$$

Hence, by Eq.(15), $[H_{rs}(1)H^{\#}, H_{rs}(0)E_m, E_p^T]$ or $[H^{\#}H_{rs}(1), E_m, E_p^T H_{rs}(0)]$ is a realization. There is no doubt that the matrix $H^{\#}$ plays a major role in solutions (19) and (20). What is $H^{\#}$? Observe that, from Eqs. (17) and (18),

$$H_{rs}(0) H^{\#} H_{rs}(0) = V_r W_s H^{\#} V_r W_s = V_r W_s = H_{rs}(0) \tag{21}$$

$H^{\#}$ is a pseudo-inverse of $H_{rs}(0)$ in a general sense. When the rank of $H_{rs}(0)$ equals to the column number of $H_{rs}(0)$, then $H^{\#}=[[H_{rs}(0)]^T H_{rs}(0)]^{-1}[H_{rs}(0)]^T$. If the rank equals to the row number, then $H^{\#}=[H_{rs}(0)]^T[H_{rs}(0)[H_{rs}(0)]^T]^{-1}$. The matrix $H_{rs}(1)H^{\#}$ has been used in structural dynamics area to identify system modes and frequencies.[13] Both are special cases representing either single input or single output which can not realize a system that has repeated eigenvalues, or a noise-free system unless the system order is a priori known. A general solution for $H^{\#}$ is given below.

For an nth order system, find the nonsingular matrices P and Q such that[10,11]

$$H_{rs}(0) = P D Q^T \tag{22}$$

where the rpxn matrix P and the nxms matrix Q^T are isometric matrices (all the columns are orthonormal), leaving the singular values of $H_{rs}(0)$ in the diagonal matrix D with positive elements $[d_1, d_2, \ldots, d_n]$. The rank n of $H_{rs}(0)$ is determined by testing the singular values for zero (relative to desired accuracy)[12] which will be described in the next section. Define

$$H_{rs}(0) = P D Q^T = [P D][Q^T] = P_d Q^T \tag{23}$$

Each of the four matrices $[P_d^T, Q^T, W_s, V_r^T]$ has rank and row number n. By Eq.(17) with k=0,

$$V_r W_s = H_{rs}(0) = P_d Q^T \tag{24}$$

Multiplying on the left by P_d^T and solving for Q^T yields

$$TW_s = (P_d^T P_d)^{-1} P_d^T V_r W_s = Q^T \tag{25}$$

T is nonsingular because if $U = W_s Q(Q^T Q)^{-1} = W_s Q$, then TU= I by Eq. (25). Since TU = I = UT for nonsingular T and U then

$$W_s[Q(P_d^T P_d)^{-1} P_d^T] V_r = I_n \tag{26}$$

Hence, by Eq. (18)

$$H^{\#} = [Q][(P_d^T P_d)^{-1} P_d^T] = [Q][D^{-1} P^T] = Q P_d^{\#} \tag{27}$$

The dimension of matrices Q and $P_d^{\#}$ with rank n are respectively msxn and nxrp. To this end, summarize the case as follows.

A finite-dimensional, discrete time, linear time-invariant dynamical system with multi-input and multi-output is realizable in terms of the measurement function if the system is controllable and observable.

Note that no restrictions on system eigenvalues are given for this case. In other words, this technique can realize a system with repeated eigenvalues. The system (1) with this realization will be transformed into the following equation

$$\overline{x}(k+1) = H_{rs}(1) H^{\#} \overline{x}(k) + H_{rs}(0) E_m u \tag{28}$$

$$y(k) = E_p^T \overline{x}(k) \tag{29}$$

where $x(k) = V_s H^{\#} x(\overline{k})$. Or (30)

$$\overline{x}(k+1) = H^{\#} H_{rs}(1) \overline{x}(k) + E_m u \tag{31}$$

$$y(k) = E_p^T H_{rs}(0) \overline{x}(k) \tag{32}$$

where $\overline{x}(k) = W_s x(k)$ (33)

The realizations (28)-(33) are not of minumum order, since the dimension of $\overline{x}$ is the number of either columns or rows of the matrix $H_{rs}(0)$ which is larger than the order n of the state matrix A for multi-input and multi-output cases.

With the aid of Eqs.(17), (18) and (27), a minimum order of realization can be obtained from

$$
\begin{aligned}
Y(k+1) &= E_p^T H_{rs}(k) E_m = E_p^T V_r A^k W_s E_m \\
&= E_p^T V_r W_s H^\# V_r A^k W_s H^\# V_r W_s E_m \\
&= E_p^T H_{rs}(0) Q P_d^\# V_r A^k W_s Q P_d^\# H_{rs}(0) E_m \\
&= E_p^T H_{rs}(0) Q [P_d^\# H_{rs}(1) Q]^k P_d^\# H_{rs}(0) E_m \\
&= E_p^T P_d [P_d^\# H_{rs}(1) Q]^k Q^T E_m
\end{aligned} \tag{34}
$$

where Eq.(23) has been used to obtain the last equality. This is the basic formulation of realization for ERA.

The triple $[P_d^\# H_{rs}(1)Q,\ Q^T E_m,\ E_p^T P_d]$ is a minimum realization, since the order n of $P_d^\# H_{rs}(1)Q$ equals to the dimension of the state vector x. The same solution in a different form for the case where $j_i = t_i = i$ $(i=1,\ldots,r-1)$ can be obtained by completely different approach as shown in Refs. [3 & 20]. The system (1) with this realization is written as

$$\bar{x}(k+1) = P_d^\# H_{rs}(1) Q \bar{x}(k) + Q^T E_m u \tag{35}$$

$$y(k) = E^T P_d \bar{x}(k) \tag{36}$$

where

$$x(k) = W_s Q \bar{x}(k) \tag{37}$$

A simple exercise such as replacing Y(k+1) by Y(k) in Eqs.(19), (20) and (34) shows that all the algorithms developed above are also true for the realization of a system with initial-state-response.

Examination of Eqs. (19), (20) and (34) reveals that algorithms (A1) and (A2) are special cases of ERA. A1 is formulated by inserting the identity matrix (18) into the right hand side of the state matrix A as shown in Eq. (19). On the other hand, A2 is obtained by inserting the identify matrix (18) into the left hand side of the state matrix A as shown in Eq. (20). However the algorithm ERA is formed by inserting the identity matrix (18) into both sides of the state matrix A as shown in Eq. (34). Because of the different insertion, A1 and A2 do not minimize the order of the state transition matrix. Mathematically, if the singular value decomposition technique is not included in the computational procedures, A1 and A2 can not be numerically implemented, unless a certain degree of artificial noise and/or system noise are present. Noises tend to make up the rank deficiency of the generalized Hankel matrix $H_{rs}(0)$ for algorithms A1 and A2. Since the degree of noise presence is generally unknown, algorithms A1 and A2 are not recommended.

III. MODAL PARAMETER IDENTIFICATION AND MODEL REDUCTION

The presence of almost unavoidable noise and structural nonlinearity introduces uncertainty about the rank of the generalized Hankel matrix and, hence, about the dimension of resulting realization. By employing the singular value decomposition (SVD) technique, the rank structure of the Hankel matrix can be quantitatively displayed. The set of singular values can be used to judge the distance of the matrix with determined order to a lower-order one. Therefore, the structure of the generalized Hankel matrix can be properly exploited to efficiently solve the realization problem. These include an excellent numerical performance, stability of the realization and flexibility in determining order-error tradeoff.

Assume that, by Eq. (22)

$$D = \text{Diag.}\ [d_1, d_2, \ldots, d_n, d_{n+1}, \ldots, d_N] \tag{38}$$

with

$$d_1 \geq d_2 \geq \ldots \geq d_n \geq d_{n+1} \geq \ldots \geq d_N \tag{39}$$

If the matrix $H_{rs}(0)$ has a rank n then all the singular values $d_i (i=n+1,\ldots,N)$ should be zero. When singular values $d_i (i=n+1,\ldots,N)$ are not exactly zero but very small, then one can easily recognize that the matrix $H_{rs}(0)$ is not far away from a n-rank matrix. However, there can be real difficulties in determining a gap between the computed last nonzero singular value and what should be effectively considered zero, when measurement noise is present. Possible sources of the noise can be attributed to the measurement signal, computer round-off and instrument imperfections.

Look at the singular value d_n of the matrix $H_{rs}(0)$. Choose a number δ based on measurement errors incurred in estimating the elements of $H_{rs}(0)$ and/or round-off errors incurred in a previous computation to get them. If δ is chosen as "zero threshold" such that $\delta < d_n$, then the matrix $H_{rs}(0)$ is considered to have rank n. Unless information about the certainty of the measurement data are given, the number δ is defined as a function of the precision limit in the computer machine. For example, $\delta = d_n/d_1$ cannot exceed the precision limit. Further details are found in Ref. [11].

After the test of singular values, assume that the matrix $[P_d^{\#} H_{rs}(k) Q]$ has rank n. Find the eigenvalues z and eigenvectors ψ such that

$$\psi^{-1} [P_d^{\#} H_{rs}(k) Q] \psi = z \tag{40}$$

The modal damping rates and damped natural frequencies are simply the real and imaginary parts of s, after transformation from the z- to the s- plane using the relationship

$$s = [(\ln z) \pm 2j\pi\ ] / (k\Delta\tau) \tag{41}$$

where $\Delta\tau$ is the data sampling interval and j is an integer. Note that k is generally chosen as 1 for simplicity. Although z and ψ are in complex domain, computation of Eq.(40) can be performed in the real domain (Ref. 21) since the state matrix realized for most flexible structures has independent eigenvectors.

The triple $[\ z,\ \psi^{-1} Q^T E_m,\ E_p^T P_d \psi\ ]$ is obviously a minimum order of realization simply by observing Eq. (34). $E_p^T P_d \psi$ is called sensor modal displacements and $\psi^{-1} Q^T E_m$ initial modal amplitudes. To quantify the system modes and noise modes, two indicators are developed as follows.

Modal Amplitude Coherence γ

If the information about the uncertainties of the measurement is minimum, the rank thus determined by the SVD becomes larger than the number of excited and observed system modes to represent the presence of noises in modal space. In modal parameter identification, the indicator referred to as modal amplitude coherence is developed to quantitatively distinquish the system and noise modes. Based on the accuracy parameter, the degree of the modal excitation (controllability) is estimated.

The modal amplitude coherence is done by calculating the coherence between each modal amplitude history and an idea one formed by extrapolating the initial value of the history to latter points using the identified eigenvalue. Let the control input matrix (initial condition) be expressed

$$\psi^{-1}Q^T E_m = [b_1, b_2, \ldots, b_n]^* \tag{42}$$

where * means transpose and complex conjugate, and the 1 x m column vector b_j corresponds to the system eigenvalue $s_j (j=1,\ldots,n)$. Consider the sequence

$$\bar{q}_j^* = [b_j^*, \exp(t_1 \Delta\tau s_j) b_j^*, \ldots, \exp(t_{s-1} \Delta\tau s_j) b_j^*] \tag{43}$$

which represents the ideal modal amplitude in complex domain containing informations of the magnitude and phase angle with time step $\Delta\tau$. Now, define vectors q_j such that

$$\psi^{-1}Q^T = [q_1, q_2, \ldots, q_n]^* \tag{44}$$

The complex vector q_j represents the modal amplitude time history from the real measurement data obtained by the decomposition of the Hankel matrix. Let γ_j be defined as the coherence parameter for the jth mode, satisfying the relation

$$\gamma_j = |\bar{q}_j^* q_j| / (|\bar{q}_j^* q_j| |\bar{q}_j^* q_j|)^{1/2} \tag{45}$$

where | | represents the absolute value. The parameter γ_j takes only the values between 0 and 1. $\gamma_j \to 1$ as $\bar{q}_j \to q_j$ indicates that the realized system eigenvalue s_j and the initial modal amplitude b_j are very close to the true values for the jth mode of the system. On the other hand, if γ_j is far away from the value 1, the jth mode is a noise mode. However, to make a clear cut between the system modes and noises requires further studies. Obviously, the parameter γ_j quantifies the degree to which the modes were excited by a specific input, i.e. the degree of controllability.

Modal Phase Collinearity μ

For lightly damped structure, normal mode behavior should be observed, An indicator referred to as the modal phase collinearity is developed to measure the strength of linear functional relationship between the real part and the imaginary part of the sensor modal displacement (mode shape) for each mode. Based on the accuracy indicator, the degree of the modal observation is estimated. Define

$$E_p^T P_d \psi = [c_1, c_2, \ldots, c_n] \tag{46}$$

where $c_j (j=1,2,\ldots,n)$ is the sensor modal displacement corresponding to the jth realized mode. Let the column vector $\underset{\sim}{1}$ of order p be

$$\underset{\sim}{1}^T = [1,1,\ldots,1] \tag{47}$$

in which p is the number of sensors. Now compute the following quantities for the jth mode shape.

$$\bar{c}_j = c_j^T \underset{\sim}{1}/p \tag{48}$$

$$c_{rr} = [\mathrm{Real}(c_j - \bar{c}_j \underset{\sim}{1})]^T [\mathrm{Real}(c_j - \bar{c}_j \underset{\sim}{1})] \tag{49}$$

$$c_{ri} = [\mathrm{Real}(c_j - \bar{c}_j \underset{\sim}{1})]^T [\mathrm{Imag}(c_j - \bar{c}_j \underset{\sim}{1})] \tag{50}$$

$$c_{ii} = [\mathrm{Imag}(c_j - \bar{c}_j \underset{\sim}{1})]^T [\mathrm{Imag}(c_j - \bar{c}_j \underset{\sim}{1})] \tag{51}$$

$$e = (c_{ii} - c_{rr})/2c_{ri} \tag{52}$$

$$\theta = \arctan[e + \mathrm{sgn}(e)(1 + e^2)^{1/2}] \tag{53}$$

where Real( ) and Imag( ) respectively are the real part and imaginary part of the complex vector ( ), and sgn( ) is the sign of the scalar ( ). The modal phase collinearity μ_j for the jth mode is then defined as (Ref.22)

$$\mu_j = \{ c_{rr} + c_{ri}[2(e^2+1)\sin^2(\theta)-1]/e \}/(c_{rr}+c_{ii}) \; ; \; j=1,2,\ldots,n \tag{54}$$

This indicator checks the deviation from 0^o - 180^o behavior for components of jth identified sensor modal displacement. The parameter μ_j takes only the values between 0 and 1. $\mu_j \rightarrow 1$ indicates that the accuracy of the modal displacement is high. On the other hand, if μ_j is away from 1, the jth mode is either a noise mode or high damping is present.

Model Reduction

The dynamical system is composed of an interconnection of all the ERA identified modes. The accuracy indicators allow one to determine the degree of individual mode participation. Model reduction can then be made by truncating all the modes with low accuracy indicators. The accuracy of the complete modal decomposition process can be examined by comparing a reconstruction of Y(k) formed by Eq.(35) with the orginal free decay responses, using the reduced model.

IV. SUMMARY OF ERA

A flowchart of the procedures to be followed to use ERA in system model identification is presented in figure 1. The computational steps are summarized as follows:

1. Construct a block-Hankel matrix $H_{rs}(0)$ by arranging the measurement data into its rows with given r, s, t_i ($i = 1, 2, \ldots, s-1$) and j_i ($i = 1, 2, \ldots, r-1$), (Eq. 16).

2. Decompose $H_{rs}(0)$ using singular value decomposition (Eq. 23).

3. Determine the order of the system by examining the singular values of the Hankel matrix $H_{rs}(0)$ (Eq. 38).

4. Construct a minimum-order realization (A, B, C) using a shifted block-Hankel matrix (Eq. 34).

5. Find eigensolutions of the realized state matrix (Eq. 40) and compute the modal damping rates and frequencies. (Eq. 41).

6. Calculate the coherence parameter (Eq. 45) and the collinearity parameter (Eq. 54) to quantify system modes and noise modes.

7. Determine the reduced system model based on accuracy indicators, reconstruct function Y(k) (Eq. 35) and compare with measurement data.

Note that the determination of r, s, t_i and j_i in Step 1 above requires further development. This determination is related to the choice of the measurement data to minimize the size of the Hankel matrix $H_{rs}(0)$ with the rank unchanged.

V. EXAMPLES: SIMULATION AND EXPERIMENT RESULTS

To illustrate the ERA method, two examples are given. First, a numerical problem will be posed and solved for an assumed structure with distinct and repeated frequencies. Second, experimental data for a simple, two-dimensional, grid structure as shown in Fig. 2 is used and realized in terms of a linear system. Experimental results are compared with those predicted by a finite element model.

Numerical Simulation

Figure 2 shows a representation of a typical flexible structure. The dynamical equation for this typical structure with initial-state-response in terms of system modes in modal space can be written as:

$$dg/dt = \Lambda\, g \tag{55}$$

$$y = \mathcal{C}\, g \tag{56}$$

where Λ is a canonical matrix with the diagonal blocks $\{\Lambda_1, \ldots, \Lambda_k\}$,

g is the generalized modal amplitude and C is the generalized sensor influence matrix. The quasi-diagonal matrix Λ_j (j=1,---,k) has the matrix form

$$\Lambda_j = \begin{bmatrix} \delta_j & \omega_j \\ -\omega_j & \delta_j \end{bmatrix} \tag{57}$$

The complex values $\delta_j \pm i\omega_j$ are the eigenvalue of the frame structure.

Given a model described as in Eq. (55), results of some numerical simulation using the ERA scheme can be summarized in the sequel. Two cases will be given including systems with and without repeated eigenvalues. The numerical test is performed by taking as "data" y the output values of the solution of a model with the form (55) whose parameters Λ, C and initial condition $g(t_0)$ are known. In the analysis of physical systems, experimental methods generate the measurement data y. It is then desired to realize a system by using the data y and compare with the known model.

Case I: A model with distinct eigenvalues

Assume that parameters such as bending rigidity, mass density and damping coefficient of the assumed structure are adjusted to give

$$\Lambda_j = \begin{bmatrix} -0.01xj & j \\ -j & -0.01xj \end{bmatrix}; \quad j = 1, 2, 3, 4, 5 \tag{58}$$

To illustrate applications of ERA in a single input and single output case, A sensor is chosen and located to give

$$\bar{C} = [1,0,1,0,1,0,1,0,1,0] \tag{59}$$

Let the initial condition for free decay responses be

$$g^T(t_0) = [0,1,0,1,0,1,0,1,0,1] \tag{60}$$

Then the functions y with a sample time interval 0.05 second generated from the model (55) with known parameters (58), (59) and (60) are used as measurement data for the ERA procedure.

Using $j_i = t_i = i$ and r=s=90 in Eq. 16, the ERA realization of a dynamical system is

$$C = [0.709,2.529,-0.347,-1.706,0.814,-1.183,-1.382,-0.276,1.129,1.257] \tag{61}$$

$$g^T(t_0)=[0.103,0.367,-0.114,-0.563,0.395,-0.574,-0.696,-0.139,0.396,0.440] \tag{62}$$

and Λ is identical to that shown in Eq. (58) with the accuracy close to the precision limit of the computer. In the process of realization, the number $\delta = d_n/d_1$ as defined in Eq. (38) is set to be 10^{-12}. The singular values of the generalized Hankel matrix $H_{rs}(0)$ are

$$D = [49.86, 44.84, 33.69, 27.64, 23.69, 21.04, 13.57, 10.95, 6.374, 5.508] \tag{63}$$

All the values d_j ($j = 11, \ldots, 90$) which has the number d_j/d_1 less than 10^{-12} are considered to be zero. The rank of the Hankel matrix $H_{rs}(0)$ is obviously ten which is identical to the order a priori given in Eq.(58). The realized state matrix is a minimum order of 10 and the eigensolutions are obtained from this 10 x 10 matrix. All the parameters for modal amplitude coherence (Eq.45) and modal phase collinearity (Eq. 54) are 100%. Although Eqs. (61) and (62) are a different realization from the system (59) and (60), they are equivalent in the sense that a unitary transformation and normalization will make them equal.

By forming the matrices V in Eq. (5) and W in Eq. (9) with the aids of Eqs.(58)-(60), the reader can see that this realization is controllable and observable.

Case II: A model with repeated eigenvalues and independent eigenvectors

Assume now that the system model is represented by

$$\Lambda_1 = \Lambda_2 = \begin{bmatrix} -0.01 & 1.0 \\ -1.0 & -0.01 \end{bmatrix} \tag{64}$$

and

$$\Lambda_j = \begin{bmatrix} 0.01xj & j \\ -j & -0.01xj \end{bmatrix} \qquad j = 3, 4, 5 \tag{65}$$

Using the same process as last case, the ERA realization simply miss the repeated eigenvalue Λ_1. The result is expected since, by control theory for a linear system, single input or single output does not make a system with repeated eigenvalues and independent eigenvectors controllable or observable. It can be verified that the matrices V in Eq. (5) and W in Eq. (9) formed by Eqs. (59), (60), (64) and (65) have rank 8. Multi-input and multi-output must be used to realize such a system. Let two sensors be chosen and located such that

$$C = \begin{bmatrix} 1,0,1,0,1,0,1,0,1,0 \\ 0,0,1,0,1,0,1,0,1,0 \end{bmatrix} \tag{66}$$

and two initial conditions for free decay responses

$$g^T(t_0) = \begin{bmatrix} 0,1,0,1,0,1,0,1,0,1 \\ 0,0,0,1,0,1,0,1,0,1 \end{bmatrix} \tag{67}$$

Note that the rows in Eqs. (66) and (67) are independent. For each initial condition, a series of "measurement" function y with a sample time interval 0.05 second can be generated from the model (55) where each y in this case is a vector with two elements for two different sensors. The free decay function Y in Eq. (15) is then a 2 x 2 matrix. Using that $j_i = t_i = i$ and $r = s = 45$ for Eq. (16), the ERA realization for a dynamical system is then

$$C = \begin{bmatrix} 0.135,-1.686,0.155,-0,172,0.111,-0.032,0.099,0.035,0.195,0.177 \\ \\ -0.004,0.107,0.142,-0.136,0.111,-0.032,0.099,0.035,0.195,0.177 \end{bmatrix} \tag{68}$$

$$g^T(t_0) = \begin{bmatrix} -0.014,-0.457,3.840,-3.692,8.338,-2.406,8.9\text{[illegible]},3.181,2.818,2.554 \\ -0.051,\ 0.092,3.605,-3.508,8.338,-2.406,8.956,3.181,2.818,2.554 \end{bmatrix} \tag{69}$$

where Λ is identical to that shown in Eqs.(64-65). The singular values D are

$$D = [70.16,44.32,37.97,25.25,11.18,9.050,7.950,3.873,0.127,0.026] \tag{70}$$

The same error window $\delta = d_n/d_1$ as last is used. All the parameters for modal amplitude coherence and modal phase colinearity are 100%. Again, Eqs. (68-69) and Eqs. (66-67) are equivalent in the sense that a unitary transformation and normalization will make them equal. The reader can easily verify that this realization is controllable and observable.

Sample Experimental Results

A sample set of modal identification results that have been obtained from laboratory test data using ERA are included in this section. The test article, shown in Fig. 2, is a 7 ft by 10 ft flexible grid structure that will be used at NASA Langley for vibration control experimentation. It is constructed of overlapping aluminum bars of 1/4 in. by 2 in. cross section, riveted together at one-foot intervals. Four rivets are used at each joint to provide a tight connection. The structure is suspended from a stiff overhead beam using two short cables attached to the top horizontal member. The results to be shown are from a preliminary dynamics test of the grid. It was conducted by exciting the structure with an airjet and measuring the free vibration response using nine non-contacting proximity sensors. The response sensors were attached to a stiff frame located adjacent to the grid for the measurement of out-of-plane motions. Eight different excitation frequencies corresponding to resonant responses were used. The sampling rate was 32 samples per second.

The ERA analysis was performed using a single matrix of data from all nine response measurements and eight initial conditions. Each response function Y as shown in Eq. (16) was thus a 9 x 8 matrix. The Hankel matrix H_{rs} of 72 rows by 400 columns was formed to perform the analysis. Table 1 provides a comparison of the ERA results with analytical prediction from a NASTRAN finite-element model. The entries in the center of table are correlation coefficients in percent between each ERA-identified mode shape and each NASTRAN mode shape. High correlation values indicate good agreement between the two shapes. The results show reasonable agreement in both frequencies and mode shapes, except for the damping result of the first mode. The main reason for the first mode discrepancy is inadequate data length. Only 50 data points were used which corresponds to less than one cycle of data for the first mode. The results can be improved by using more data points. Note that few high correlations occur for some modes with significantly different frequencies. This is because only 9 sensors were used in comparison. More detailed experimental results for a complex structure are shown in Ref.[19].

CONCLUDING REMARKS

An Eigensystem Realization Algorithm (ERA) is developed for parameter identification and model reduction for dynamical systems. Two developments are given in this paper. First, a new approach is developed to derive the basic ERA formulation of minimum realization for dynamical systems. As by-products of this approach, two alternative less powerful algorithms, identified as A1 and A2, are derived. A special case of A1 is shown to be equivalent to an approach currently in use in structural dynamics. Second, accuracy indicators are developed to quantify the partipation of system modes and noise modes in the realized system model. In other words, degree of controllability and observability for each participated mode is determined. A model reduction can then be made for controller design.

Important features of the ERA algorithm are summarized as follows. (1) From the computational standpoint, the algorithm is attractive, since only simple numerical operations are needed; (2) the computational procedure is numerically stable; (3) the structural dynamics requirements for modal parameter identification and the control design requirements for a reduced state space model are satisfied; (4) data from more than one test can be used simultaneously to efficiently identify the closely spaced eigenvalues; (5) no restrictions on number of measurements are imposed.

REFERENCES

[1] E. G. Gilbert, "Controllability and Observability in Multi-variable Cont[illegible] Systems," SIAM J. Control, Vol. 2, No. 1, [illegible]51, 1963.

[2] R. E. Kalman, "Mathematical Description of Linear Dynamical Systems," SIAM J. Contr., Vol. 1, pp. 152-192, 1963.

[3] B. L. Ho and R. E. Kalman, "Effective Construction of Linear State-variable Models From Input/Output Data," Proc. 3rd Ann. Allerton Conf. Circuit and System Theory, 1965, pp. 449-459; also Reyelungstech, Vol. 14, pp. 545-548, 1966.

[4] A. Tether, "Constructions of Minimum Linear State Variable Models From Input/output Data, "IEEE Trans. on Auto. Contr., Vol. AC-15, No.4, Aug. 1970, pp. 427-436.

[5] L. M. Silverman, "Realization of Linear Dynamical Systems," IEEE Trans. on Auto. Contr., 16, 554(1971)

[6] R. H. Rossen and L. Lapidus, "Minimum Realizations and System Modeling. I.Fundamental Theory and Algorithms," AIChE Journal, Vol.18, No.4, July, 1972, pp. 673-684

[7] R. H. Rossen and L. Lapidus, "Minimum Realizations and System Modeling: II Theoretical and Numerical Extensions," AICHE Journal, Vol. 18, No. 5, Sept. 1972, pp. 881-892.

[8] H. P. Zeiger and A. J. McEwen, "Approximate Linear Realizations of Given Dimension Via Ho's Algorithm," IEEE Trans. Automatic Control, Vol.19,(1974), 153.

[9] S. Kung,"A New Identification and Model Reduction Algorithm Via Singular Value Decomposition," 12th Asilomar Conf., Circuits, Systems and Computers, Nov. 6-8, 1978.

[10] G. H. Golub and C. Reinsch,"Singular Value Decomposition and Least Square Solutions," Numer. Math., Vol. 14, pp. 403-420.

[11] V. C. Klema and A. J. Laub, "The Singular Value Decomposition: Its Computation and Some Application," IEEE Transactions on Automatic Control Vol. AC-25, No.2, April, 1980, pp. 164-176.

[12] R. C. Stroud, S. Smith and G. Hamma,"MODALAB--A New system for Structural Dynamics Testing," Shock and Vibration Bulletin, No. 46, Part 5, August 1976, pp. 153-175.

[13] S. R. Ibrahim and E. C. Mikulcik, "A Method for Direct Identification of Vibration Parameters from the Free Response." The Shock and Vibration Bulletin, No. 47, Sept. 1977, pp. 183-198.

[14] D. L. Brown, R. J. Allemang, R. Zimmerman and M. Mergeay,"Parameter Estimation Techniques for Modal Analysis,"SAE paper 790221, February 1979.

[15] R. N. Coppolino,"A simultaneous Frequency Domain Technique for Estimation of Modal Parameters from Measured Data,"SAE paper 811046, October, 1981.

[16] H. Vold and R. Russell,"Advanced Analysis Methods Improve Modal Test Results," Sound and Vibration, March, 1983, pp 36-40.

[17] J. C. Chen,"Evaluation of Modal Testing Methods," AIAA paper 84-1071, Presented at AIAA Dynamics Specialist Conference, May 1984.

[18] C. T. Chen, Introduction to Linear System Theory, Holt, Rienhart and Winston, Inc., New York, 1970.

[19] R. S. Pappa and J. N. Juang,"Galileo Spacecraft Modal Identification Using an Eigensystem Realization Algorithm," AIAA paper 84-1070-Cp, Presented at the AIAA Dynamics Specialists Conference, Palm Spring, Ca., May, 1984.

[20] R. E. Kalman and R. S. Engler,"Computation of A Minimal Realization," A User Manual for ASPC, Ch. XV, 1966.

[21] F. R. Gantmacher, The Theory of Matrices, Vol. I, Chelsea Publishing Co., New York, New York, 1959.

[22] C. R. Rao,"The Use and Interpretation of Principal Component Analysis in Applied Research,"Sankhya Ser. A, 26, 329-358.

Table 1 : Comparison of the ERA results with the NASTRAN Model

MODE SHAPE CORRELATION		ANALYTICAL FREQUENCY (NASTRAN), HZ										DECAY RATE %	γ	μ
		.362	.612	1.425	2.331	2.826	4.936	5.476	6.429	7.047	9.841			
(ERA) IDENTIFIED FREQUENCY	.363	99	1	21	41	1	42	17	1	0	1	23.1	71	100
	.584	3	99	3	0	1	1	2	98	43	9	0.33	100	99.9
	1.376	22	1	96	36	3	12	45	2	2	3	0.64	99.8	99.9
	2.047	38	0	8	94	7	1	1	1	0	7	0.33	100	100
	2.542	2	6	4	3	96	2	9	3	15	96	0.26	100	99.9
	4.852	48	11	22	35	3	70	65	10	1	3	0.19	100	99.9
	5.095	9	9	29	19	2	46	81	8	6	2	0.61	99.5	97.5
	7.403	4	73	1	5	3	8	0	79	91	10	0.12	100	99.4
	9.519	0	19	8	0	90	2	9	8	22	91	0.24	97.3	99.9

γ : Modal Amplitude Coherence

μ : Modal Phase Collinearity

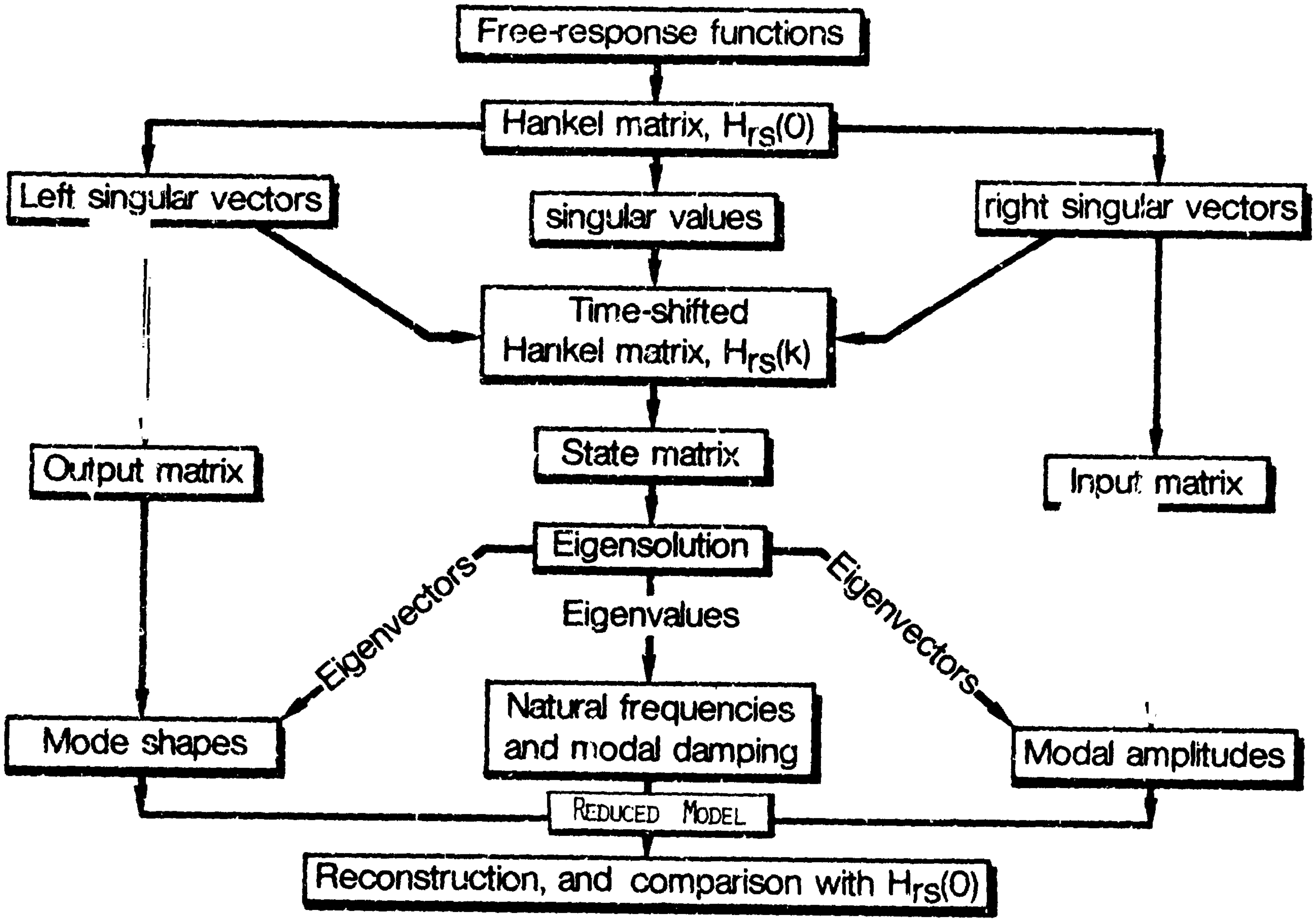

FIGURE 1. FLOW CHART OF ERA

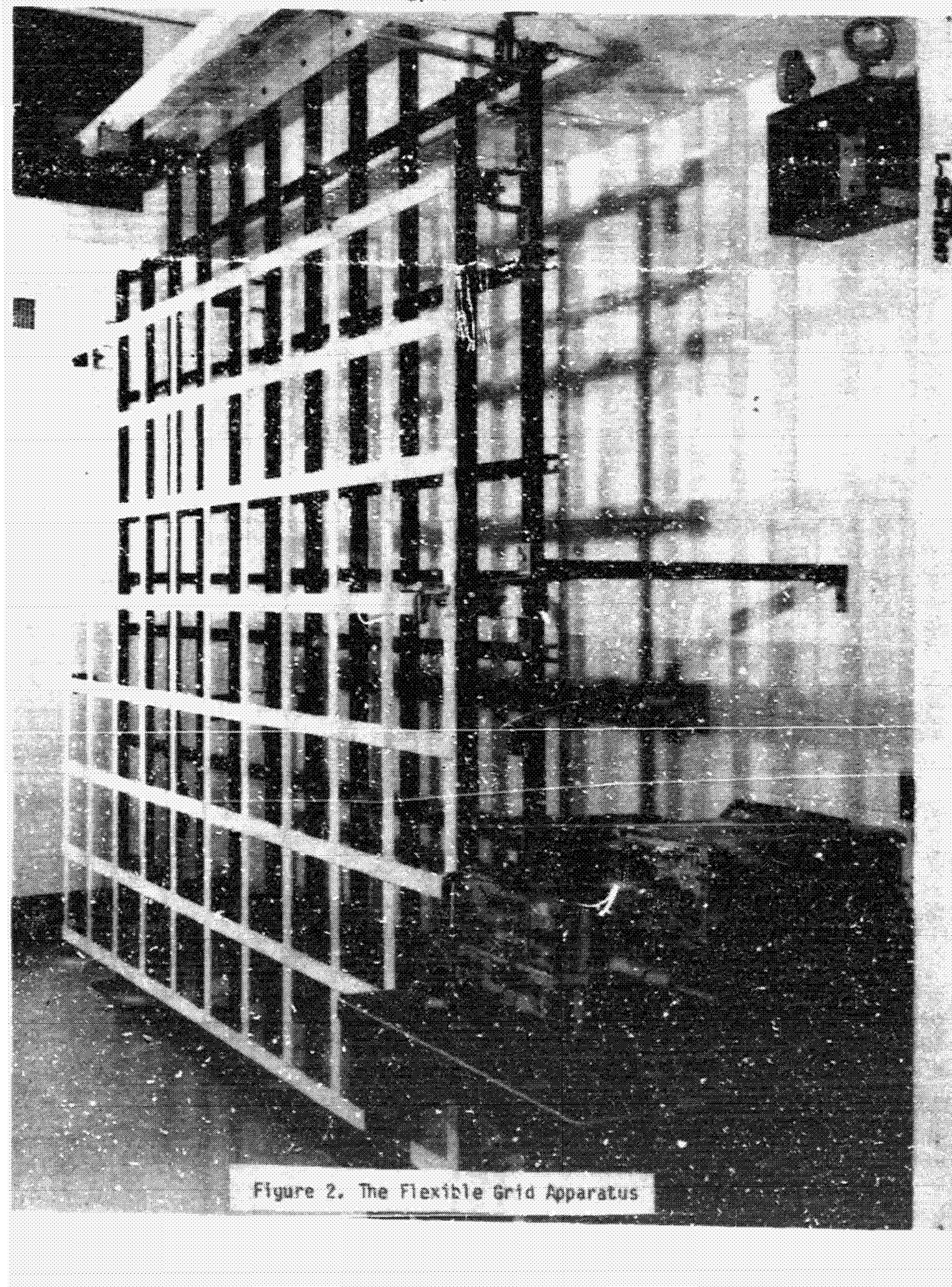

Figure 2. The Flexible Grid Apparatus

N85-31213

A RESIDUALS APPROACH TO FILTERING, SMOOTHING AND IDENTIFICATION FOR STATIC DISTRIBUTED SYSTEMS

G. Rodriguez
Jet Propulsion Laboratory
California Institute of Technology
Pasadena, CA 91109

ABSTRACT

This paper advances an approach for state estimation and identification of spatially distributed parameters embedded in static distributed (elliptic) system models.

The method of maximum likelihood is used to find parameter values that maximize a likelihood functional for the system model, or equivalently, that minimize the negative logarithm of this functional. To find the minimum, a Newton-Raphson search is conducted that from an initial estimate generates a convergent sequence of parameter estimates. Central to the numerical search are a gradient functional and a Hessian operator, which are respectively the first and second function-space derivatives of the negative-log likelihood functional with respect to the parameter distributions being identified. For simplicity, a Gauss-Markov approach is used to approximate the Hessian in terms of products of first derivatives. The gradient and approximate Hessian are computed by first arranging the negative-log likelihood functional into a form based on the square-root factorization of the predicted covariance of the measurement process. The resulting data-processing approach, referred to here by the new term of predicted-data-covariance square-root filtering, makes the gradient and approximate Hessian calculations very simple. Since the parameter estimates are only approximations to the actual parameter values, there is a parameter estimation error inherent in the estimation process. Cramer-Rao bounds are obtained for the covariance of the estimation error in terms of the information operator associated with the likelihood functional. These error covariance bounds are then used to outline methods for optimal input design.

A closely related set of state estimates is also produced by the maximum likelihood method: smoothed estimates that are optimal in a conditional mean sense and filtered estimates that emerge from the predicted-data-covariance square-root filter. The terms "smoothed" and "filtered" are used because the formulas which generate these estimates, when expressed in operator notation, are symbolically very similar to those used in filtering and smoothing for linear dynamical systems. A key similarity is the presence of a predictor-corrector structure containing estimator gains that, as in a Kalman filter, can be expressed in terms of the state estimation error covariances. In addition, a residual process can be defined, in the usual way, as the difference between the actual data and the predicted data obtained from the filtered state estimate. The residuals have properties nearly identical to those of an innovations process: the residuals are white with a unit covariance; and the residuals and measurements can be obtained from each other by means of reciprocal linear transformations. Because these transformations are not Volterra (causal), the residuals are not a bona fide innovations process. Even though they are not a true innovations process, the residuals are very useful, because they lead to state and parameter estimation schemes for elliptic systems that retain conceptually the simplicity of those obtained by the innovations approach to filtering, smoothing and identification for linear dynamical systems.

1. INTRODUCTION AND SUMMARY

The elliptic models considered in this paper can be cast as

$$A(\Theta)u(\Theta) = B(\Theta)\omega + C(\Theta)f, \tag{1.1}$$

$$y = H(\Theta)u(\Theta) + n, \tag{1.2}$$

where A is a formally self-adjoint elliptic differential operator defined over the spatial domain Ω; B and C are appropriately dimensioned operators that model the influence of the process error ω and the input f on the state u; H is an operator that characterizes the state-to-observations map; ω and n are white-noise model errors forming the model error vector $\varepsilon=[\omega,n]$; and f is a deterministic input. Examples of the application of such models to the problem of static shape determination of large space structures are contained in Ref. [1].

The central aim here is to develop a maximum-likelihood approach to the estimation of the parameters Θ (these parameters could in general be spatially distributed) by using the data y and the system model itself. It is assumed that the true value Θ_o of the parameter Θ is a deterministic but poorly known quantity. The input f can be selected to optimize the data generated for estimation. A related but somewhat secondary aim is to develop a methodology for computation of the corresponding state estimates.

<u>A Formula for the Negative-Log Likelihood Ratio</u>

It will be shown in Sec. 3 that the negative-log likelihood functional is specified by

$$J(\Theta;y) = \tfrac{1}{2}\,\mathrm{Tr}\,\log\,[I+R(\Theta)] + \tfrac{1}{2}\,[y-m(\Theta)]^*[I+R(\Theta)]^{-1}[y-m(\Theta)] - \tfrac{1}{2}\,y^*y, \tag{1.3}$$

where

$$m(\Theta) = H(\Theta)\Phi(\Theta)C(\Theta)f \quad \text{and} \quad R(\Theta) = H(\Theta)\Phi(\Theta)B(\Theta)B^*(\Theta)\Phi^*(\Theta)H^*(\Theta).$$

The integral operator $\Phi(\Theta)$ is related to $A(\Theta)$ by $A(\Theta)\Phi(\Theta)=I$, with I the identity. The symbol Φ^* denotes the integral operator adjoint to Φ so that $\Phi^*(\Theta)A^*(\Theta)=I$. It will also be shown in Sec. 3 that $m(\Theta)$ and $R(\Theta)$ are respectively the "suspected" mean and covariance of the data y, under the assumption that the model error vector $\varepsilon=[\omega,n]$ is a spatially distributed white-noise process [1] with a covariance operator $E(\varepsilon\varepsilon^*)=I$ equal to the identity. To simplify Eq. (1.3), the following notation has been used:

$$y^*y = \langle y,y\rangle_s \text{ and } [y-m(\Theta)]^*[I+R(\Theta)]^{-1}[y-m(\Theta)] = \langle [y-m(\Theta)],\,[I+R(\Theta)]^{-1}[y-m(\Theta)]\rangle_s,$$

where $\langle\cdot,\cdot\rangle_s$ indicates an inner product in the function space to which the data belongs.

<u>Predicted-Data-Covariance Square-Root Form of the Likelihood Ratio</u>

A number of alternative formulas for the negative-log likelihood functional are developed in Sec. 4. To solve the above minimization problem, the most convenient formula is:

$$J(\Theta;y) = \mathrm{Tr}\,\log[I+K(\Theta)] + \tfrac{1}{2}\,z^*(\Theta)z(\Theta) - z^*(\Theta)y, \tag{1.4}$$

where

$$z(\Theta) = L(\Theta)y + [I-L(\Theta)]m(\Theta), \tag{1.5}$$

$$L(\Theta) = I - [I+R(\Theta)]^{-1/2}, \qquad K(\Theta) = [I+R(\Theta)]^{1/2} - I. \tag{1.6}$$

Equation (1.5) can be viewed as specifying a filter, characterized by the operator $L(\Theta)$, that processes the data y and the suspected mean $m(\Theta)$ to provide a "filtered" state estimate $z(\Theta)$. This filter $L(\Theta)$ will hereafter be referred to as the predicted data-covariance square-root filter because the key calculation required to specify $L(\Theta)$, as in (1.6), is the evaluation of the square-root of the predicted-data-covariance operator $[I+R(\Theta)]$. The equivalence between (1.3) and (1.4) can be established by substitution of (1.5) and (1.6) into (1.4).

Note for later reference that the definitions in (1.6) imply that $K(\Theta)$ and $L(\Theta)$ are related by

$$[I+K(\Theta)]^{-1} = I-L(\Theta). \tag{1.7}$$

Furthermore, (1.7) implies that $K(\Theta) = L(\Theta)+K(\Theta)L(\Theta) = L(\Theta)+L(\Theta)K(\Theta)$.

Gradient of the Likelihood Functional

The gradient functional $\partial J/\partial\Theta$, to be defined more completely in Secs. 5 and 6, is specified by

$$\partial J/\partial\Theta = \mathrm{Tr}[(\partial L/\partial\Theta)(I+K)] + (z-y)^*(\partial z/\partial\Theta), \tag{1.8}$$

where

$$\partial z/\partial\Theta = (\partial L/\partial\Theta)\bar{y} + (I-L)(\partial m/\partial\Theta), \tag{1.9}$$

with $\bar{y} = y-m$, and $\partial L/\partial\Theta$, $\partial m/\partial\Theta$ being the function-space Frechet derivatives of L and m. These equations can be obtained from (1.4) by function-space differentiation with respect to Θ.

The gradient functional $\partial J(\Theta;y)/\partial\Theta$ in (1.8) is the Frechet derivative [2] of the functional J with respect to the parameter Θ. The derivative is a linear transformation (assumed to be bounded) that maps an admissible parameter perturbation $\delta\Theta$ into the corresponding perturbation $\delta J(\Theta,\delta\Theta;y)$ of the likelihood functional by means of the equation $\delta J(\Theta,\delta\Theta;y) = [\partial J(\Theta;y)/\partial\Theta]\ \delta\Theta$. Detailed computation of the function-space derivatives above is conducted in Sec. 6 using a perturbation analysis of the eigensystem of the covariance operator $R = H\Phi BB^*\Phi^*H^*$ obtained in Sec. 5.
Note that in Sec. 7 it will be established that

$$E[\partial J(\Theta;y)/\partial\Theta]_{\Theta=\Theta_o} = 0, \tag{1.10}$$

so that the expected value of the gradient vanishes at the optimal parameter value Θ_0.

Hessian of the Likelihood Functional

Similarly, differentiation of (1.8) leads to

$$\partial^2 J/\partial\Theta^2 = \mathrm{Tr}\,[(\partial^2 L/\partial\Theta^2)(I+K) + (\partial L/\partial\Theta)(\partial K/\partial\Theta)] + (z-v)^*(\partial^2 z/\partial\Theta^2) + (\partial z/\partial\Theta)^*(\partial z/\partial\Theta); \tag{1.11}$$

and to its expected value at $\Theta=\Theta_0$ of $M(\Theta_0) = E[\partial^2 J/\partial\Theta^2]|_{\Theta=\Theta_0}$, i.e.,

$$E[\partial^2 J/\partial\Theta^2]\,|_{\Theta=\Theta_0} = \mathrm{Tr}\,[(\partial L/\partial\Theta)(I+R)(\partial L^*/\partial\Theta)] + E[(\partial z/\partial\Theta)^*(\partial z/\partial\Theta)]. \tag{1.12}$$

Furthermore, substitution of (1.9) in the last term of (1.12) leads to

$$E[\partial^2 J/\partial\Theta^2]\,|_{\Theta=\Theta_0} = 2\mathrm{Tr}\,[(\partial L/\partial\Theta)(I+R)(\partial L^*/\partial\Theta)] + [(I-L)(\partial m/\partial\Theta)]^*[(I-L)(\partial m/\partial\Theta)]. \tag{1.13}$$

Note that the expected value of the Hessian operator $\partial^2 J/\partial\Theta^2$ evaluated at $\Theta=\Theta_0$ is a sum of two terms each of which is positive definite. Consequently, in a probabilistic sense made precise by (1.13), the likelihood functional is strictly convex in the vicinity of the optimal value $\Theta=\Theta_0$. Note that by definition $M(\Theta_0)$ in (1.13) is also the information operator associated with the likelihood functional.

Newton-Raphson Search for the Optimal Parameter Estimates

Since the problem of minimization of $J(\Theta;y)$ in (1.4) has no closed-form solution, it is necessary to consider iterative numerical search techniques for optimization. The following constitutes a function-space Newton-Raphson iteration:

$$\Theta^{n+1} = \Theta^n - M_n^{-1} g_n, \tag{1.14}$$

where $g_n = \partial J(\Theta^n;y)/\partial\Theta$ is the gradient functional (1.8) evaluated at $\Theta=\Theta^n$; and where

$$M_n = \mathrm{Tr}\,[(\partial L/\partial\Theta)(I+R)(\partial L^*/\partial\Theta)] + (\partial z^*/\partial\Theta)(\partial z/\partial\Theta)|_{\Theta=\Theta_n} \tag{1.15}$$

is an approximation to the Hessian operator $\partial^2 J/\partial\Theta^2$ in (1.11). This approximation is obtained from (1.12) by replacing the second term $E[(\partial z^*/\partial\Theta)(\partial z/\partial\Theta)]$ with the actual value $[(\partial z^*/\partial\Theta)(\partial z/\partial\Theta)]$ obtained in a single realization. Under certain conditions, to be examined in more detail in future work, the sequence Θ^n specified by (1.14) converges to a local minimum of $J(\Theta;y)$, if the initial estimate used to start the search is sufficiently close to the optimal value.

Cramer-Rao Bounds and Optimal Input Design

The above numerical search results in an estimate Θ of the actual parameter value Θ_o. In Sec. 7, a C-R bound for the covariance $E(\Theta_p\Theta_p{*})$ of the estimation error $\Theta_p = \Theta-\Theta_o$ is obtained from the inequality.

$$E(\Theta_p\Theta_p{*}) \geq M^{-1}(\Theta_o), \tag{1.16}$$

where the information operator $M(\Theta_o)$ is specified in (1.13). The related mean-square estimation error is bounded by $E(\Theta_p{*}\Theta_p) \geq Tr[M^{-1}(\Theta_o)]$.

The information operator $M(\Theta_o)$ can also be used to specify criteria for optimal input design. Perhaps the simplest optimal selection method to implement is that which seeks to maximize $Tr\,[M(\Theta_o)]$ with respect to f, subject to the constraint that f satisfy the normalization condition of $f{*}f=1$. This method results in an optimal f which is the eigenvector corresponding to the largest eigenvalue of a positive-definite matrix described in detail in Sec. 7. Other criteria for optimal selection based on calculation of $M^{-1}(\Theta_o)$ may be more difficult to implement but usually lead to superior performance.

The Corresponding State Estimates

Related to the parameter estimation approach are the following two distinct state estimates (denoted by u_o and z_o):

$$u_o = E(u/y) = \Phi Cf + G(y-H\Phi Cf),\quad z_o = \Phi Cf + g(y-H\Phi Cf), \tag{1.17}$$

where G and g are Kalman-like gains (see Sec. 8) specified by

$$G = \sum \sin^2\alpha_k x_k \phi_k{*},\qquad g = \sum (1-\cos\alpha_k)\, x_k\phi_k{*}. \tag{1.18}$$

In these equations, ϕ_k are the eigenvectors of the operator $R = H\Phi BB{*}\Phi H{*}$, so that $R\phi_k = \lambda_k^2\phi_k$, with λ_k^2 being the related eigenvalues. Also, α_k and x_k are defined by $\tan\alpha_k = \lambda_k$ and $x_k = \lambda_k^{-2}\Phi BB{*}\Phi{*}H{*}\phi_k$.

The state estimate $u_o = E(u/y)$ is defined as the conditional expectation of the state given the data y. Since u_o is an optimal estimate of u based on the entire data set (as opposed to a subset), u_o can be viewed as a best smoothed estimate. The other estimate, z_o in (1.17), will be referred to as a filtered state estimate. The filtered estimate has no known probabilistic interpretation similar to $u_o = E(u/y)$ above. However, in spite of the apparent lack of probabilistic meaning, this estimate is useful in simplifying the gradient and Hessian calculations in (1.8) and (1.11). It will be shown in Sec. 8 that z_o in (1.17) and z, the estimate emerging from the predicted-data-covariance square-root filter, are related by $z = Hz_o$. Hence, z_o is a bona fide estimate of the entire state, whereas $z = Hz_o$ is a partial estimate defined only at the observation locations.

Kalman-like Gains and Error Covariances

The gains G and g in (1.17) can alternatively be specified in terms of the covariance of the state estimation error inherent in u_o and z_o, i.e.,

$$G = \bar{P}H^*, \qquad g = pH^*, \tag{1.19}$$

where

$$\bar{P} = E[(u-u_o)(u-u_o)^*], \quad p + p^* = E[(u-z_o)(u-z_o)^*]. \tag{1.20}$$

The corresponding mean-square state estimation error is

$$E[(u-u_o)^*(u-u_o)] = \mathrm{Tr}\,[\bar{P}], \quad E[(u-z_o)^*(u-z_o)] = \mathrm{Tr}\,[p+p^*]. \tag{1.21}$$

Furthermore, $\bar{P}$ and p are related by

$$\bar{P} = p + p - pH^*Hp. \tag{1.22}$$

Since the term pH^*Hp is non-negative, the mean-square estimation error associated with the smoothed estimate u_o is never larger than that of the filtered estimate z_o.

Filtering and Smoothing

While u_o and z_o have been defined somewhat independently in (1.17), they are related by:

$$u_o = z_o + pH^*e, \tag{1.23}$$

where

$$e = y - Hz_o = (I - HpH^*)\bar{y} = (I - L)\,\bar{y} \tag{1.24}$$

is the residual process defined as the difference between the data y and the observed-state estimate Hz_o. The symbol $\bar{y}$ in (1.24) denotes the mean-centered data process $\bar{y} = y - H\Phi Cf$. It will be shown in Sec. 8 that (1.22) and (1.23) constitute a generalization to elliptic systems of the forward/backward sweep method for solution of smoothing problems in linear dynamical systems.

The Residuals as a Pseudo-Innovations Process

The residuals in Eq. (1.24) have two properties that are similar (but not identical) to those of an innovations process:

$$E(ee^*) = I, \tag{1.25}$$

$$e = (I - L)\,\bar{y}, \qquad \bar{y} = (I + K)e. \tag{1.26}$$

Eq. (1.25) reflects whiteness of the residuals. Eq. (1.26) states that the residual and mean-centered data processes e and $\bar{y}$ can be obtained from each other by means of reciprocal transformations, i.e., $(I + K)^{-1} = (I - L)$ as in (1.7). Whiteness of the innovations and reciprocal relationships between innovations and measurements are the two central features of the innovations approach to least-squares estimation for linear dynamical systems. Eqs. (1.25) and (1.26) are similar to these conditions. However, there is a key difference: the transformations $(I + K)$ and $(I - L)$ in (1.26) are Fredholm operators whose domain is the entire measurement space. This is in contrast to the Volterra (causal) operators in the innovations approach for linear dynamical systems. The notion of causality is not even used in this paper, although such a notion can be defined for certain classes of elliptic systems [1]. Because of this difference the residual process is not a bona fide innovations process. However, the residual process is still useful in obtaining the relatively simple formulas in (1.8) - (1.26) for filtering, smoothing and identification.

Paper Outline

This section has at a summary level addressed many of the fundamental issues involved in the maximum likelihood approach to estimation. The subsequent sections of the paper contain a more complete description of the above results.

Section 2. Development of the mathematical framework -- including integral operator models, a priori covariance analysis with white-noise model errors, Fredholm resolvents, and eigenfunction expansions -- required to arrive at formula (1.3) for the likelihood functional and to evaluate the corresponding function-space gradient in (1.8) and the approximate Hessian in (1.15).

Section 3. Derivation of the negative-log likelihood functional in (1.3). This functional is the negative logarithm of the likelihood ratio, associated with the detection of a Gaussian signal in additive Gaussian noise, traditionally encountered in the theory for communication and signal detection.

Section 4. Development of alternative formulas for the likelihood ratio, some of which are more convenient to use than (1.3) in implementing the numerical search for optimization -- in particular, development of the predicted-data-covariance square-root filter form (1.4) upon which the Newton-Raphson search is based. Additional forms of the likelihood ratio which are of interest in their own right (although not subsequently used in the paper) are: a smoothing form expressed in terms of the best mean-square state estimate; an eigensystem expansion form based on the eignenvalues and eigenvectors of the operator $R = H\Phi BB^*\Phi^*H^*$ in (1.3); a trigonometric operator form with which most of the manipulations involved in the maximum likelihood approach can be visualized using their similarities to simple trigonometric formulas for scalars.

Section 5. Development of a first-order perturbation analysis to evaluate the infinitesimal changes in the eigensystem of the operator $R = H\Phi BB^*\Phi^*H^*$ in (1.3) due to similarly small changes $\delta\Theta$ in the parameter distributions being identified. This is the central calculation required to compute the function-space gradients $\partial J/\partial\Theta$, $\partial z/\partial\Theta$, $\partial L/\partial\Theta$ and $\partial m/\partial\Theta$ in (1.8) and (1.9).

Section 6. Calculation of the gradient functional and approximate Hessian of the likelihood functional based on the perturbation analysis of Sec. 5. These are the two calculations which are central to implementation of the Newton-Raphson search and which have been used as a basis for computer programs to implement the maximum likelihood approach.

Section 7. Parameter estimation error covariance analysis and Cramer-Rao bounds based on explicit formulas for the Hessian (information) operator in (1.13). Outline of an optimal input design approach based on using the Cramer-Rao bound as an optimality criterion.

Section 8. Analysis of the filtered and smoothed state estimates embedded in the parameter estimation approach. Analysis of the predicted-data-covariance square-root filter resulting in Kalman-like formulas for the filter gain, evaluation of the state estimation error covariance, and relationships between filtered and smoothed estimates.

Section 9. Summary and explanation of calculations required for implementation of the numerical search for the optimal estimates.

Section 10. Conclusions and directions for future work in the areas of development of asymptotic properties of the estimates and of optimal input design.

2. PRELIMINARIES: Notation, Integral Operator Model, Covariance Analysis, Fredholm Resolvents, and Eigenfunction Expansions

The aim of this section is to develop a set of miscellaneous results that will be useful in subsequent sections in conducting detailed derivation of: the negative-log likelihood functional in (1.3) to be minimized, the corresponding function-space gradient in (1.8), and the approximate Hessian operator in (1.15). The main results of the section can be summarized as follows:

- conversion of the partial differential operator model in (1.1) to an equivalent integral operator formulation. This integral operator formulation is introduced because it simplifies the statement and solution of the estimation problems in (1.1) - (1.3).

- evaluation of the observed state covariance operator $R=H\Phi BB^*\Phi^*H^*$ in (1.3), under the assumption that $\varepsilon = [\omega, n]$ is a spatially distributed white-noise process with a unit covariance operator. Related to evaluation of this covariance operator R is the similar evaluation of the suspected mean $m = H\Phi Cf$ in (1.3).

- evaluation of the dual observed-state covariance operator $Q=B^*\Phi^*H^*H\Phi B$ - which can be viewed as the covariance of the output of a system model dual to (1.1), under the assumption that this dual system is driven by a white-noise process.

- definition of two sets of eigenvectors ϕ_k and ψ_k of R and Q above, with λ_k^2 being a set of common eigenvalues. These two sets of vectors can be used to expand functions in the input space H_1 and the output space H_3.

- definition of the vectors x_k and p_k in the state space H_2 and its dual H_2^*, related to ψ_k and ϕ_k above by $x_k = \lambda_k^{-1}\Phi B\psi_k$ and $p_k = \lambda_k^{-1}\Phi^*H^*\phi_k$. These two sets of vectors x_k and p_k satisfy a boundary-value problem similar to those traditionally encountered as necessary and sufficient conditions for optimality in quadratic optimal control and estimation problems subject to linear constraints.

- analysis of the basic relationship between R and Q above and their corresponding Fredholm resolvents P and S defined as $P = I-(I+R)^{-1}$ and $S = I-(I+Q)^{-1}$. Expansion of the operators R, Q, P and S in terms of the eigenfunctions ϕ_k and ψ_k defined above.

- development of trigonometric operator forms for R and P. These trigonometric forms allow development of interesting trigonometric alternatives to (1.3) in evaluating the likelihood functional.

While the section concentrates on the development of a mathematical framework to be used in subsequent sections, many of the above results (such as the trigonometric operator formulas for the covariance operators) are of interest in their own right, somewhat independently of their subsequent application.

<u>Hilbert Space Notation</u>

There are three Hilbert spaces of primary interest: the input space H_1 to which the process error ω and the deterministic input f belong; the state space H_2 containing the state u; and the measurement space H_3 where the data y and the observation error n belong. The inner product between two arbitrary elements u and v in the space H_i is denoted by $\langle u,v\rangle_i$ or by the simpler notation $u^*v = \langle u,v\rangle_i$. Similarly, uv^* denotes a Hilbert space outer product.

Conversion to Integral Operator Model

It is convenient for subsequent developments to convert (1.1) to an equivalent integral operator formulation. To this end, define the Green's function $\phi(x/\xi)$ of A as the solution of

$$A_x\, \phi(x/\xi) = \delta(x-\xi), \tag{2.1}$$

where δ is the impulsive delta function, and where the subscript x in A_x denotes that the spatial differentiations embedded in A are performed with respect to x (as opposed to being performed with respect to ξ). Define then the integral operator Φ whose kernel is the Green's function, i.e.,

$$\Phi v = \int_{\Omega} \phi(x/\xi) v(\xi) d\xi, \tag{2.2}$$

for all admissible functions v. Note that Φ is the integral operator such that $A\Phi = I$, where I is the appropriately dimensioned identity.

With these definitions at hand, it is possible to recast (1.1) and (1.2) as

$$y = m(\Theta) + H(\Theta)\Phi(\Theta)B(\Theta)\omega + n, \tag{2.3}$$

where $m(\Theta)$ is the "suspected mean"

$$m(\Theta) = H(\Theta)\Phi(\Theta)C(\Theta)f. \tag{2.4}$$

Equation (2.3) can be cast into the following even more compact notation

$$y = m(\Theta) + h(\Theta)\varepsilon, \tag{2.5}$$

where $\varepsilon = [\omega,n]$ is the model error vector [1], and $h(\Theta)$ is the operator $h(\Theta) = [H(\Theta)\Phi(\Theta)B(\Theta) \mid I]$.

Predicted-Data Mean and Covariance

The evaluation of the predicted mean and covariance of y, needed as a preliminary step to arrive at (1.3), is based on the key assumption that the model error vector $\varepsilon = [\omega,n]$ is a zero-mean spatially distributed white-noise process whose covariance operator $E(\varepsilon\varepsilon^*)$ is the identity, i.e.,

$$E(\varepsilon\varepsilon^*) = I, \tag{2.6}$$

where I is the appropriately dimensioned identity. Note that this assumption is not at all restrictive, because the more general case where the model errors $\varepsilon = [\omega,n]$ are correlated (with a nonidentity covariance operator) can be handled within the same formulation by selection of the operator B in (1.1). It is assumed here that BB^* is bounded and trace-class, with kernel $b(x/\xi)$ satisfying $\int_{\Omega} b(x/x)dx < \infty$.

Remark 2.1 The process y is a random field with mean and covariance specified as

$$E(y) = m(\Theta), \qquad E\{[y-m(\Theta)]\,[(y-m(\Theta)]^*\} = I+R(\Theta), \tag{2.7}$$

where $R(\Theta) = H(\Theta)\Phi(\Theta)B(\Theta)B^*(\Theta)\Phi^*(\Theta)H^*(\Theta)$. That $E(y) = m$ follows from (2.5) and the fact that ε is zero-mean. The second of Eqs. (2.7) follows from the following sequence of operations: $E[(y-m)(y-m)^*] = E[h\varepsilon\varepsilon^*h^*] = hE(\varepsilon\varepsilon)h^* = hh^* = I+R$. A more detailed development of the above result is contained in Ref. [1].

Remark 2.2 The process u in (1.1), representing the state of the system, is a random field with mean and covariance specified by

$$E(u) = \Phi Cf, \qquad E[(u-\Phi Cf)(u-\Phi Cf)^*] = \bar{R}(\Theta), \tag{2.8}$$

where

$$\bar{R}(\Theta) = \Phi(\Theta)B(\Theta)B^*(\Theta)\Phi^*(\Theta). \tag{2.9}$$

Note that the state covariance $\bar{R}$ and the "observed-state" covariance R in (2.7) and (2.8) are related by

$$R(\Theta) = H\bar{R}(\Theta)H^*. \tag{2.10}$$

Remark 2.3 The state covariance $\bar{R}$ satisfies the partial differential equation

$$A\bar{R}A^* = BB^*, \tag{2.11}$$

a result which can be established by pre-multiplication of $\bar{R}$ in (2.9) by A and subsequent post-multiplication by A^*.

Remark 2.4 The state covariance operator $\bar{R}$ can be represented as the following integral operator

$$\bar{R}v = \int_\Omega r(x/\xi)\, v(\xi)d\xi, \tag{2.12}$$

where the kernel $r(x/\xi)$ satisfies

$$A_x r(x/\xi) A_\xi = b(x/\xi), \tag{2.13}$$

and where $b(x/\xi)$ is the kernel of BB^*. This result can be established by means of the following sequence of operations. Consider an admissible function v (admissible in the sense that it can be operated on by the operators $A\bar{R}A^*$ and BB^* in (2.11) so that $A\bar{R}A^*v = BB^*v$ makes sense). In terms of the corresponding kernels r and b, this last equation becomes

$$A_x\{\int_\Omega r(x/\xi)\,[A_\xi{}^*v(\xi)]d\xi\} = \int_\Omega [A_x r(x/\xi)A_\xi]\, v(\xi)d\xi = \int_\Omega b(x/\xi)v(\xi)d\xi, \tag{2.14}$$

where the first equality is valid because by definition $A_\xi{}^*$ is the formal adjoint of A_ξ. Since Eq. (2.14) must be valid for all admissible v, then (2.14) implies (2.13).

<u>Remark 2.5</u> The state covariance kernel r in (2.12) can be expressed as

$$r(x/\xi) = \int_\Omega \int_\Omega \phi(x/\eta)\, b(\eta/\beta)\, \phi(\beta/\xi)\, d\eta d\beta, \tag{2.15}$$

where ϕ is the Green's function of A, and b is the kernel of BB^*. This result can be established by expressing (2.9) in terms of the operator kernels ϕ and b of Φ and BB^* and by subsequent reversal of the order of integration.

<u>Remark 2.6</u> In the special case, of interest in many applications, where the process error ω is discretely located at the M locations $[\eta_1,\dots,\eta_M]$, and the sensors are placed at the N locations $[\xi_1,\dots,\xi_N]$, then $R = H\Phi BB^*\Phi^*H^*$ is a matrix whose general element R_{ij} is specified by

$$R_{ij} = \sum_{\ell=1}^{M} \phi(x_i/\eta_\ell)\, \phi(\eta_\ell/\xi_j), \tag{2.16}$$

where the summation is taken over the disturbance locations.

<u>The Dual-Model Covariance Operators</u>

Closely related to R and $\bar{R}$ above are the "dual" operators defined as

$$Q(\Theta) = B^*(\Theta)\Phi^*(\Theta)H^*(\Theta)H(\Theta)\Phi(\Theta)B(\Theta), \quad \bar{Q}(\Theta) = \Phi^*(\Theta)H^*(\Theta)H(\Theta)\Phi(\Theta). \tag{2.17}$$

Note that Q and $\bar{Q}$ can be obtained, from R and $\bar{R}$ respectively, by making the substitutions $\Phi \rightarrow \Phi^*$ and $B \rightarrow H^*$. This observation can be used as the basis for defining the dual system model, illustrated in Fig. 2.1, whose state and output have covariance operators specified by Q and $\bar{Q}$ above.

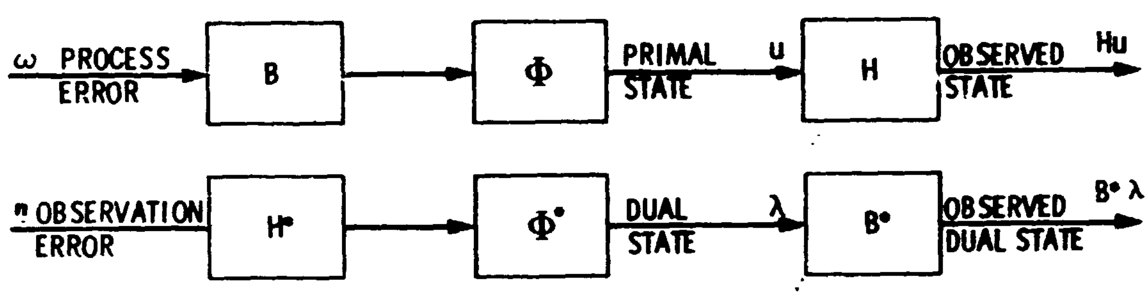

Figure 2.1. Illustration of Primal and Dual Models

The <u>primal</u> system model is based on (2.3), with ω, u and Hu denoting the process error, the system state, and the observed state respectively. For this model, $\bar{R} = E(uu^*)$ is the covariance of the state, while $R = H\bar{R}H^*$ is the corresponding covariance of the observed state. It is assumed for the sake of this discussion that the deterministic input f in (1.1) has been set to zero, so that the suspected mean m in (2.3) is zero also. With this assumption, it is not necessary to show m in the block diagram in Fig. 2.1, and the relationship between the primal and dual models is illustrated more easily. The <u>dual</u> system model is characterized by the dual operators H^*, Φ^* and B^*, by the dual or adjoint state λ, and by the observed dual state $B^*\lambda$. It is assumed that the dual model is driven by a unit-covariance white-noise process so that $E(nn^*) = I$. This input process n driving the dual model can be thought of as being the observation error process in (2.3). For this dual model, $\bar{Q} = E(\lambda\lambda^*)$ and $Q = E(B^*\lambda\lambda^*B)$ are respectively the covariances of the state λ and the observed state $B^*\lambda$. Upon multiplication of λ in Fig. 2.1 by A^*, the following partial differential equations result to describe the dual model

$$A^*\lambda = H^*n. \tag{2.18}$$

Note that the dual state covariance $\bar{Q} = \Phi^*H^*H\Phi$ and the dual observed-state covariance $Q = B^*\Phi^*H^*H\Phi B$ are related by

$$Q = B^*\bar{Q}B. \tag{2.19}$$

In the same spirit used to arrive at (2.11)-(2.16), it is now possible to develop the following properties of the operator $\bar{Q}$ and its corresponding kernel q.

<u>Remark 2.7</u> The dual-state covariance operator $\bar{Q}$ satisfies

$$A^*\bar{Q}A = H^*H, \tag{2.20}$$

a result which can be obtained from $\bar{Q} = \Phi^*H^*H\Phi$ in (2.17) upon multiplication by $A^*(\cdot)A$.

<u>Remark 2.8</u> In terms of its kernel q, the operator $\bar{Q}$ can be expressed as

$$\bar{Q}v = \int_\Omega q(x/\xi)v(\xi)d\xi, \tag{2.21}$$

where q satisfies the differential equation

$$A_\xi q(\xi/x)A_x = h(\xi/x), \tag{2.22}$$

and where $h(\xi/x)$ is the kernel of H^*H. This result can be established by an approach quite similar to that used in arriving at (2.13). The symbol v denotes again an admissible function defined to be admissible if (2.21) makes sense.

<u>Remark 2.9</u> The kernel $q(\xi/x)$ of $\bar{Q}$ can be expressed as

$$q(\xi/x) = \int_\Omega \int_\Omega \phi(\eta/\xi)\, h(\eta/\beta)\, \phi(x/\beta)\, d\eta\, d\beta, \tag{2.23}$$

where h is the kernel of H^*H. This result can be established in a manner analogous to that used in arriving at (2.15).

Remark 2.10 In the special case most typical in applications, where the range of H and B is finite-dimensional, then $Q = B^*\Phi^*H^*H\Phi B$ is a matrix whose general element Q_{ij} can be expressed as

$$Q_{ij} = \sum_{k=1}^{N} q(\eta_k/\xi_i)\, q(x_j/\eta_k), \tag{2.24}$$

where the summation is taken over the set of sensor locations.

Spectral Representations

Recall that $R = H\Phi BB^*\Phi^*H^*$ is the observed-state covariance operator in (2.7). The eigenvalues of R are defined as the nontrivial solutions of

$$R\phi_k = \lambda_k^2\phi_k, \tag{2.25}$$

with ϕ_k being the corresponding eigenvectors. Note that, in cases where H has a finite-dimensional range, the operator R is an N-by-N matrix with a finite number of eigenvectors. In the more general case where the range of H is infinite-dimensional, then R is usually compact and $\lambda_k^2 \to 0$ as $k \to \infty$. In both of these cases, the following Mercer expansions hold for R and its kernel r

$$R = \sum \lambda_k^2\phi_k\phi_k^* \qquad \text{and} \qquad r(x/\xi) = \sum \lambda_k^2\phi_k(x)\phi_k^T(\xi) \tag{2.26}$$

Furthermore, the normalized eigenvectors ϕ_k form an orthonormal basis for the observation space H_3. This implies that $\sum \phi_k\phi_k^* = I$, where I is the identity in H_3.

Closely related to the basis ϕ_k above are the dual vectors ψ_k defined as

$$\psi_k = \lambda_k^{-1}B^*\Phi^*H^*\phi_k, \tag{2.27}$$

which can be viewed as the result of applying an input ϕ_k to the dual system model (2.18) and then "balancing" the output by dividing by the eigenvalue λ_k.

Remark 2.11 The vectors ψ_k defined by (2.27) are the eigenvectors of the dual observed-state covariance $Q = B^*\Phi^*H^*H\Phi B$, i.e.,

$$Q\psi_k = \lambda_k^2\psi_k. \tag{2.28}$$

This result can be established by premultiplication of (2.27) by $H\Phi B$ and use of the condition $R\phi_k = \lambda_k^2\phi_k$. Note that, if the dimension of the input space H_1 is greater than that of the output space H_3, then the ψ_k do not span the input space. They do, however, span the range subspace of the operator $B^*\Phi^*H^*$. Consequently, they cannot be used to expand vectors in the null space of $H\Phi B$.

Remark 2.12 The vectors ψ_k are also related to ϕ_k by the equation

$$\phi_k = \lambda_k^{-1} H\Phi B\psi_k, \tag{2.29}$$

a result that can be obtained from (2.27) upon premultiplication by the operator $H\Phi B$ and use of the condition $R\phi_k = \lambda_k^2\phi_k$.

Remark 2.13 The dual-state covariance operator Q and its corresponding kernel q can be expressed as

$$Q = \Sigma \ \lambda_k^2\psi_k\psi_k^* \qquad q = \Sigma \ \lambda_k^2\psi_k(x)\psi_k^T(\xi) \tag{2.30}$$

a set of equations which are analogous to (2.26). This result can be obtained from the observation that $Q = B^*\Phi^*H^*H\Phi B = B^*\Phi^*H^* (\Sigma\ \phi_k\phi_k^*)\ H\Phi B = \Sigma\ \lambda_k^2\ \psi_k\psi_k^*$. Use has been made of the condition $\Sigma\ \phi_k\phi_k^* = I$.

The vectors ϕ_k span the observation space H_3. While the vectors ψ_k do not span the input space H_1, they do span the range of $B^*\Phi^*H^*$. So far, no attempt has been made to obtain vectors that can be used to expand functions in the state space H_2 or in its dual space H_2^*. To this end, define

$$x_k = \lambda_k^{-1}\ \Phi B\psi_k, \quad p_k = \lambda_k^{-1}\ \Phi^*H^*\phi_k. \tag{2.31}$$

The vector x_k is in the state space whereas the adjoint variables p_k are in the dual space. In general, neither one of these two vectors however spans the state space H_2.

Remark 2.14 The vectors x_k and p_k are orthonormal with respect to H^*H and BB^* respectively, i.e.,

$$x_k^*H^*Hx_m = 0, \quad p_k^*BB^*p_m = 0, \qquad k \neq m, \tag{2.32}$$

$$x_k^*H^*Hx_k = 1, \quad p_k^*BB^*p_k = 1. \tag{2.33}$$

These results can be established by the following sequence of operations: $x_k^*H^*Hx_m = (Hx_k)^*Hx_m = \phi_k^*\phi_m$ and $p_k^*BB^*p_m = (B^*p_k)^*B^*p_m = \psi_k^*\psi_m$. Since ϕ_k and ψ_k are orthonormal, then (2.32) and (2.33) follow.

Remark 2.15 The vectors x_k, ψ_k and p_k, x_k are related by

$$\phi_k = Hx_k \text{ and } \psi_k = B^*p_k. \tag{2.34}$$

This result follows readily from the definitions in (2.27), (2.29) and (2.31).

Remark 2.16 The vectors x_k and p_k satisfy the boundary-value problem:

$$\left[\begin{array}{cc} A & 0 \\ \hline 0 & A^* \end{array}\right] \left[\begin{array}{c} x_k \\ \hline p_k \end{array}\right] = \frac{1}{\lambda_k} \left[\begin{array}{cc} 0 & BB^* \\ \hline H^*H & 0 \end{array}\right] \left[\begin{array}{c} x_k \\ \hline p_k \end{array}\right]. \tag{2.35}$$

This result can be established by operating on x_k in (2.31) by A and on p_k by A^* to obtain

$$Ax_k = \lambda_k^{-1} B\psi_k \text{ and } A^*p_k = \lambda_k^{-1} H^*\phi_k. \tag{2.36}$$

Then, substitution of (2.34) in (2.36) implies (2.35)

Note the similarity between this problem and those traditionally encountered as necessary (and at times sufficient) conditions for optimality in quadratic optimal control and estimation problems for linear systems.

The Fredholm Resolvents of the Covariance Operators Q and R

The Fredholm resolvent of R is defined as that integral operator such that $(I+R)^{-1} = I-P$, a relationship which immediately implies that

$$R = P + RP \text{ and } R = P + PR \tag{2.37}$$

In terms of the corresponding kernels r and p, these equations become

$$r(x/\xi) = p(x/\xi) + \int_\Omega r(x/\eta)p(\eta/\xi)d\eta \tag{2.38}$$

for the case with continuously distributed data. In cases with discrete data, R and P are matrices whose general elements $R_{k,m}$ and $P_{k,m}$ are related by

$$R_{k,m} = P_{k,m} + \sum_{n=1}^{N} R_{k,n}P_{n,m}. \tag{2.39}$$

In both of these equations (2.38) and (2.39), the unknown is the Fredholm resolvent P, whereas the observed-state covariance kernel R is known.

<u>Remark 2.17</u> The integral operator R and its Fredholm resolvent P commute. This result, which can be stated as

$$RP = PR, \tag{2.40}$$

is a direct consequence of (2.37).

<u>Remark 2.18</u> Equations (2.37) also imply that

$$P = (I+R)^{-1}R = R(I+R)^{-1}, \qquad R = (I-P)^{-1}P = P(I-P)^{-1}. \tag{2.41}$$

<u>Remark 2.19</u> In a manner analogous to (2.37) - (2.41), it is possible to define the resolvent S of the dual-state covariance operator Q by the relationship $(I+Q)^{-1} = I-S$ which implies

$$Q = S + QS, \; Q = S + SQ, \; SQ = QS, \tag{2.42}$$

and

$$S = (I+Q)^{-1}Q = Q(I+Q)^{-1}, \qquad Q = (I-S)^{-1}S = S(I-S)^{-1}. \tag{2.43}$$

<u>Remark 2.20</u> The Fredholm resolvents P and S can be expressed as

$$P = \sum \left[\lambda_k^2/(1+\lambda_k^2)\right] \phi_k\phi_k^*, \qquad S = \sum \left[\lambda_k^2/(1+\lambda_k^2)\right]\psi_k\psi_k^*, \tag{2.44}$$

$$p(x/\xi) = \sum \left[\lambda_k^2/(1+\lambda_k^2)\right] \phi_k(x)\phi_k^T(\xi), \quad s(x/\xi) = \sum \left[\lambda_k^2/(1+\lambda_k^2)\right] \psi_k(x)\psi_k^T(\xi). \tag{2.45}$$

These expansions can be established by substituting (2.26) and (2.30) into (2.37) and (2.41).

<u>Trigonometric Operator Forms</u>

<u>Remark 2.21</u> The predicted-data-covariance operator (I+R) can be expressed as

$$I + R = I + \mathrm{TAN}^2\alpha = \mathrm{SEC}^2\alpha, \tag{2.46}$$

where $\mathrm{TAN}^2\alpha$ and $\mathrm{SEC}^2\alpha$ are the operators

$$\mathrm{TAN}^2\alpha = \sum \tan^2\alpha_k\phi_k\phi_k^* = R, \qquad \mathrm{SEC}^2\alpha = \sum \sec^2\alpha_k\phi_k\phi_k^*, \tag{2.47}$$

and $\tan \alpha_k$ is defined by $\tan \alpha_k = \lambda_k$. Note also for later reference that

$$(I+R)^{1/2} = SEC\alpha = \sum \sec\alpha_k \phi_k \phi_k^*, \qquad R^{1/2} = TAN\alpha = \sum \tan\alpha_k \phi_k \phi_k^*. \tag{2.48}$$

Proof: Recall that $R = \Sigma \lambda_k^2 \phi_k \phi_k^* = \Sigma \tan^2\alpha_k \phi_k \phi_k^*$ thereby establishing (2.47). Use of the formal expression $I = \Sigma \phi_k \phi_k^*$ for the identity I implies that $(I+R) = \Sigma (1+\tan^2\alpha_k) \phi_k \phi_k^*$, which leads to (2.46). Equations (2.48) are obtained from (2.46) and (2.47) by performance of the square-root operation.

Remark 2.22 The Fredholm resolvent defined as $P = I - (I+R)^{-1}$ of the covariance operator R can be expressed as

$$P = SIN^2\alpha, \tag{2.49}$$

where $SIN^2\alpha$ is the operator defined by the expansion

$$SIN^2\alpha = \sum \sin^2\alpha_k \phi_k \phi_k^* = \sum [\lambda_k^2/(1+\lambda_k^2)]\phi_k \phi_k^*. \tag{2.50}$$

Proof: This result can be established by substitution of $\tan^2\alpha_k = \lambda_k^2$ in (2.44).

Remark 2.23 Equations (2.47) and (2.48) together imply that

$$P = R(I+R)^{-1} = TAN^2\alpha[I+TAN^2\alpha]^{-1} = TAN^2\alpha\,[SEC^2\alpha]^{-1} = SIN^2\alpha, \tag{2.51}$$

a trigonometric operator identity that can be viewed as a generalization of a similar identity involving scalars.

3. DERIVATION OF THE LIKELIHOOD FUNCTIONAL

Based on the results of the previous section, it is now possible to derive the likelihood functional in (1.3) to be minimized. Since the development required to achieve this is fairly lengthy, it is convenient to summarize in advance the pivotal steps involved in the derivation:

- the integral operator model $y = m + H\Theta B\omega + n$ in (2.3) is first coverted into an equivalent "spectral" form $y_k = m_k + \lambda_k\omega_k + n_k$, where $y_k = \phi_k^* y$, $\omega_k = \psi_k^*\omega$, $n_k = \phi_k^* n$ are the corresponding spectral coefficients.

- the spectral coefficients y_k of the data y are a sequence of independent Gaussian random variables with mean $E(y_k) = m_k$, covariance $\sigma_k^2 = 1 + \lambda_k^2$ and probability density $\rho_k(y_k;\Theta) = \pi^{-1/2}\sigma_k^{-1} \exp[-(y_k-m_k)^2/2\sigma_k^2]$

- a "finite-dimensional" likelihood ratio is then defined as the product of a finite number N of terms involving the probability densities $\rho_k(y_k;\theta)$ above.

- an "infinite-dimensional" likelihood ratio is obtained by letting the number N of spectral coefficients approach infinity. The related negative-log likelihood functional in (1.3) is obtained by taking the negative logarithm of the functional that results from the limiting process. Of course, in cases where the data is finite-dimensional (obtained by means of a finite number of discretely located measurements), the limiting process involved in this last step is not necessary. In this case, the "finite-dimensional" likelihood function obtained in the previous step is the function to be minimized to obtain the parameter estimates.

The remainde of this section contains a more detailed derivation of the foregoing results.

Recall that

$$y = m + H\Phi B\omega + n, \tag{3.1}$$

where $m = H\Phi Cf$ and f is the input. As outlined above, the first step toward evaluating the likelihood function is to convert (3.1) into an equivalent "spectral" form by using the eigenvectors ϕ_k and ψ_k, i.e.,

$$y = \sum y_k\phi_k, \quad \omega = \sum \omega_k\psi_k, \quad n = \sum n_k\phi_k, \quad m \sum m_k\phi_k. \tag{3.2}$$

Substitution of (3.2) and (3.1) and premultiplication of (3.1) by $\phi_k{}^*$ leads to

$$y_k = m_k + \lambda_k\omega_k + n_k. \tag{3.3}$$

<u>Result 3.1</u> y_k, ω_k and n_k are independent Gaussian random variables with mean and covariance given by

MEAN	COVARIANCE
$E(\omega_k) = E(n_k) = 0$	$E(\bar{y}_k^2) = 1 + \lambda_k^2$
$E(y_k) = m_k$	$E(\omega_k^2) = E(n_k^2) = 1$
	$E(\bar{y}_k\bar{y}_m) = 0 \quad m \neq k$

where $\bar{y}_k = y_k - m_k$. Hence, y_k is a sequence of independent Gaussian random variables with mean m_k and covariance $1 + \lambda_k^2$.

Let $y^N = [y_1,\dots,y_N]$ be an N-dimensional vector consisting of the first N spectral coefficients y_k of the data y. Because y_k are independent Gaussian random variables with mean m_k and covariance $\sigma_k^2 = 1 + \lambda_k^2$, their corresponding probability densities $\rho_k(y_k;\Theta) = \pi^{-1/2}\sigma_k^{-1}\exp(-\bar{y}_k^2/2\sigma_k^2)$ can be multiplied to obtain the probability density $\rho(y^N;\Theta)$ of the composite N-dimensional vector y^N, i.e.,

$$\rho(y^N;\Theta) = \prod_{k=1}^{N} \rho_k(y_k;\Theta) = \prod_{k=1}^{N} \sigma_k^{-1}\pi^{-1/2}\exp(-\bar{y}_k^2/2\sigma_k^2). \tag{3.4}$$

In order to obtain a likelihood functional for the identification problem with the function-space process y as the data, it would be desirable to let $N\to\infty$ and obtain what would be in the limit a probability density functional (PDF) for the process y. Unfortunately, this limit may not exist because the right side of (3.4) may not converge as $N\to\infty$, and consequently a PDF for the process y cannot be defined in this manner. However, this can be circumvented by dividing by

$$\rho_0(y^N;\Theta) = \prod_{k=1}^{N} \pi^{-1/2}\exp(-y_k^2/2). \tag{3.5}$$

This results in

$$\Lambda(y^N;\Theta) = \prod_{k=1}^{N} \frac{\exp[-(y_k-m_k)^2/2(1+\lambda_k^2)]}{(1+\lambda_k^2)^{1/2}\exp(-y_k^2/2)}, \tag{3.6}$$

which can be viewed as a likelihood ratio consisting of the PDF of the process y^N with the "signals" ω_k and m_k nonzero, divided by the similar PDF of y^N with the signals ω_k and m_k set to zero. The term likelihood ratio used to describe (3.6) is consistent with terminology common in the theory for detection of Gaussian signals in additive Gaussian noise [3].

Although the limits of $\rho(y^N;\Theta)$ and $\rho_0(y^N;\Theta)$ appearing respectively in (3.4) and (3.5) may not exist when taken independently, the limit of their ratio in (3.6) is a well-defined quantity specified by

$$\Lambda(y;\Theta) = \lim \Lambda(y^N;\Theta) = \frac{\exp[(-½)(y-m)^*(I+R)^{-1}(y-m)]}{[\det(I+R)]^{½}\exp[(-½)y^*y]}. \quad (3.7)$$

This is the desired expression for the likelihood ratio that the maximum-likelihood method seeks to <u>maximize</u>. It can be interpreted as the likelihood ratio for the detection of the "signal" $m + H\Phi B\omega$ in (3.1), in the presence of the noisy Gaussian signal n. Instead of maximizing $\Lambda(y;\Theta)$ directly, it is more convenient to <u>minimize</u> the negative-log likelihood functional defined as $J(\Theta;y) = -\log[\Lambda(y;\Theta)]$, or, more explicitly,

$$J(\Theta;y) = ½ \log\det[I+R(\Theta)] + ½ [y-m(\Theta)]^*[I+R(\Theta)]^{-1}[y-m(\Theta)] - ½ y^*y. \quad (3.8)$$

Note that for the special case with no deterministic input, f=m=0 in (3.1), and the negative-log likelihood in (3.8) reduces to

$$J(\Theta;y) = ½ \log\det[I+R(\Theta)] - ½ y^*P(\Theta)y, \quad (3.9)$$

where $P(\Theta) = I - [I+R(\Theta)]^{-1}$ is the previously defined (in Sec. 2) Fredholm resolvent of the predicted-data-covariance operator R.

The first term in both of these last two equations can be cast into an equivalent and somewhat more convenient form by use of the identity [4]

$$\log\det[I+R(\Theta)] = \mathrm{Tr}\log[I+R(\Theta)]. \quad (3.10)$$

Substitution of (3.10) in (3.9) leads to

$$J(\Theta;y) = ½ \mathrm{Tr}\log[I+R(\Theta)] + ½ [y-m(\Theta)]^*[I+R(\Theta)]^{-1}[y-m(\Theta)] - ½ y^*y, \quad (3.11)$$

which has been recorded previously as (1.3) and constitutes the central aim of this section.

Reorientation

The method of maximum likelihood, as defined here, results in estimates that minimize $J(\Theta;y)$ in (3.11). This minimization problem can be viewed as a function-space nonlinear programming problem subject to the system model constraints that $R(\Theta) = H(\Theta)\Phi(\Theta)^*(\Theta)B^*(\Theta)\Phi^*(\Theta)H^*(\Theta)$ and $m(\Theta) = H(\Theta)\Phi(\Theta)C(\Theta)f$. Since no closed-form solution to this problem exists, it is necessary to use numerical methods for optimization. However, there exist alternative formulas for the likelihood ratio that are more convenient to use in the implementation of the numerical methods. Such formulas are developed in the following section.

4. ALTERNATIVE FORMULAS FOR THE LIKELIHOOD FUNCTIONAL

$\frac{1}{2}\,\mathrm{Tr}\log[I+R(\Theta)] + \frac{1}{2}[y-m(\Theta)]^*[I+R(\Theta)]^{-1}[y-m(\Theta)] - \frac{1}{2}y^*y$	BASIC
$\frac{1}{2}\,\mathrm{Tr}\log[I+R(\Theta)] + \frac{1}{2}[y-m(\Theta)]^*[y-Hu_0(\Theta)] - \frac{1}{2}y^*y$	SMOOTHING
$\frac{1}{2}\sum[\log(1+\lambda_k^2) + (1+\lambda_k^2)^{-1}(y_k-m_k)^2 - y_k^2]$	SPECTRAL
$\mathrm{Tr}\log[I+K(\Theta)] + \frac{1}{2}z^*(\Theta)z(\Theta) - z^*(\Theta)y$	SQUARE-ROOT FILTER
$\mathrm{Tr}\log[SEC\alpha(\Theta)] + \frac{1}{2}z^*(\Theta)z(\Theta) - z^*(\Theta)y$	TRIGONOMETRIC OPERATOR

In the above table, the basic formula is expressed in terms of the suspected mean m and covariance $I+R = I + H\Phi 3B^*\Phi^*H^*$ of the data y. The smoothing form is specified in terms of the optimal smoothed estimate $u_0 = E(u/y)$, representing the conditional mean of the state u given the data y. The spectral formula is obtained by substitution in (1.3) of the eigensystem expansions $R = \Sigma\lambda_k^2\,\phi_k\phi_k^*$, $y = \Sigma y_k\phi_k$, and $m = \Sigma m_k\phi_k$, where λ_k^2 and ϕ_k are the eigenvalues and eigenvectors of the observed-state covariance operator R. The square-root filter formula, previously recorded in (1.4), is based on the factorization of the predicted-data-covariance operator as $(I+R) = (I+R)^{1/2}(I+R)^{1/2}$ and on the definitions $z = Ly + (I-L)m$ and $(I+K) = (I-L)^{-1} = (I+R)^{1/2}$. Finally, the trigonometric operator formula is obtained from the square-root filter expression by use of the identities $I+R = SEC^2\alpha$ and $L = I-COS\alpha$ developed in Sec. 2.

Although the derivation of the above expressions leads to significant insight about the structure of the likelihood functional, it is not within the scope of the paper to investigate all of these alternatives to the same level of detail. The formula involving the predicted-data-covariance square-root filter appears to be the most convenient to implement the numerical search for the optimal estimates. This section, however, aims to first develop the results summarized above.

Formulas Based on the Optimal Smoothed State Estimate

Result 4.1 The negative-log likelihood functional can be expressed as

$$J(\Theta;y) = \tfrac{1}{2}\,\mathrm{Tr}\,\log\,[I+R(\Theta)] + \tfrac{1}{2}\,[y-m(\Theta)]^*[y-Hu_o(\Theta)] - \tfrac{1}{2}\,y^*y, \tag{4.1}$$

$$u_o(\Theta) = G(\Theta)y + [I-G(\Theta)H]\Phi(\Theta)Cf, \tag{4.2}$$

$$G(\Theta) = \bar{R}(\Theta)H^*\,[I+H\bar{R}(\Theta)H^*]^{-1}; \tag{4.3}$$

where $u_o = E(u/y)$ is the conditional expectation of the state u given the data y, and G is the estimator gain.

Proof: It will be shown in Sec. 8 that u_o in (4.2) is the conditional mean and that G in (4.3) is the corresponding estimator gain. Therefore, for the sake of the discussion here, assume that (4.2) and (4.3) are valid. Multiply u_o in (4.2) by H and use (4.3) in the resulting equation to obtain

$$Hu_o = HGy + (I-HG)m, \tag{4.4}$$

and

$$y - Hu_o = (I-HG)\,(y-m), \tag{4.5}$$

where $m = H\Phi Cf$ is as before the suspected mean of the data y. However, recall the identity $HG = H\bar{R}H^*(I+H\bar{R}H^*)^{-1} = I - (I+H\bar{R}H^*)^{-1}$ so that $I-HG = (I+H\bar{R}H^*)^{-1} = (I+R)^{-1}$. Hence, substitution of this last identity in (4.5) leads to

$$y - Hu_o = (I+R)^{-1}(y-m). \tag{4.6}$$

This is the central result required to establish the equivalence between (4.1) and (3.11). To this end, substitute (4.6) into the second term on the right side of (4.1), and observe the equivalence with (3.11) by inspection.

Result 4.2 The negative-log likelihood functional can be expressed as

$$J(\Theta;y) = \tfrac{1}{2}\,\mathrm{Tr}\,\log\,[I+R(\Theta)] + \tfrac{1}{2}\,[E(u)]^*\,H^*H\,[E(u/y)] - \tfrac{1}{2}\,[E(u) + E(u/y)]^*H^*y \tag{4.7}$$

where $E(u) = \Phi Cf$ and $E(u/y)$ are respectively the unconditional and conditional expected values of the state u.

Proof: This result can be established as a corollary to the Result 4.1 by combining the last two terms on the right side of (4.1) and use of the equation $m = H\Phi Cf$.

Both of these results express the likelihood functional in terms of a quantity u_o in (4.2) which is the conditional expectation $E(u/y)$ of the state given the data y. This quantity is also known to be the best linear mean-square estimate as well as the optimal least-squares estimate. The coincidence of the best mean-square estimate and the optimal least-squares estimate, both of which can be computed by the conditional expectation formula (4.2), is explored at length in Ref. [1].

<u>Result 4.3</u> The negative-log likelihood functional can be expressed as

$$J(\Theta;y) = \tfrac{1}{2} \sum \; [\log(1+\lambda_k^2) + (1+\lambda_k^2)^{-1} (y_k-m_k)^2 - y_k^2], \tag{4.8}$$

where $y_k = \phi_k{*}y$ and $m_k = \phi_k{*}m$ are the spectral coefficients of the data and the suspected mean m, and λ_k^2 are the eigenvalues of R. By substitution of $\lambda_k = \tan\alpha_k$ in (4.8), this equation can be cast as

$$J(\Theta;y) = \tfrac{1}{2} \sum \; [\log(\sec^2\alpha_k) + \cos^2\alpha_k (y_k - m_k)^2 - y_k^2]. \tag{4.9}$$

<u>Proof:</u> Equation (4.8) can be established by taking the negative log of $\Lambda(y^N;\Theta)$ in (3.6) and letting $N\to\infty$. Use of the identity $\lambda_k = \tan\alpha_k$ in (4.8) leads to (4.9).

<u>Result 4.4</u> The negative-log likelihood ratio can be expressed as

$$J(\Theta;y) = \sum \; [\tfrac{1}{2} \log(1+\lambda_k^2) + \tfrac{1}{2} z_k^2 - z_k y_k], \tag{4.10}$$

where

$$z_k = L_k y_k + (1-L_k)m_k \quad \text{and} \quad L_k = 1-\cos\alpha_k. \tag{4.11}$$

<u>Proof:</u> Define the "residual" process

$$e_k = y_k - z_k, \tag{4.12}$$

as the difference between the data y_k and the "filtered" estimate z_k. Observe that $e_k = \cos\alpha_k(y_k-m_k)$ by substitution of (4.11) in (4.12). Substitute this last equation into the second term on the right side of (4.9) to obtain (4.10).

The formula for the likelihood functional in (4.10) can be viewed as the "spectral" version of the predicted-data-covariance square-root formula described below.

<u>Predicted-Data-Covariance Square-Root Formula for the Likelihood Functional</u>

<u>Result 4.5</u> The negative-log likelihood functional can be expressed as

$$J(\Theta;y) = \operatorname{Tr} \log [I+K(\Theta)] + \tfrac{1}{2} z^*(\Theta)z(\Theta) - z^*(\Theta)y, \tag{4.13}$$

where

$$z(\Theta) = L(\Theta)y + [I-L(\Theta)]m(\Theta), \tag{4.14}$$

with $L(\Theta)$ and $K(\Theta)$ defined as

$$L(\Theta) = I - [I+R(\Theta)]^{-1/2}, \qquad K(\Theta) = [I+R(\Theta)]^{1/2} - I. \tag{4.15}$$

Proof: Conversion of the first term (1/2) Tr log $[I+R(\Theta)]$ in (3.11) into Tr log $[I+K(\Theta)]$ follows because (1/2) Tr log$(I+R)$ = (1/2) Tr log $(I+K)^2$ = Tr log $(I+K)$. Conversion of the last two terms on the right side of (3.11) into the desired form in (4.15) follows from the identity

$$(y-m)^*(I+R)^{-1}(y-m) = [(I-L)(y-m)]^*[(I-L)(y-m)] = (y-z)^*(y-z), \tag{4.16}$$

where use has been made of the fact that $(I+R)^{-1} = (I-L^*)(I-L)$.

Result 4.6 The operators L and K can be represented in terms of the following eigensystem expansions:

$$L = \sum (1-\cos\alpha_k)\,\phi_k\,\phi_k^* \qquad K = \sum (\sec\alpha_k - 1)\,\phi_k\phi_k^*, \tag{4.17}$$

where $\alpha_k = \tan^{-1}\lambda_k$, and ϕ_k are the eigenvectors of R.

Proof: Let

$$L = \sum L_k\phi_k\phi_k^* \text{ with } L_k = \phi_k^* L\phi_k, \tag{4.18}$$

and then evaluate the as yet undetermined coefficients L_k from $L = I - (I+R)^{-1/2}$ in (4.15). To this end, premultiply L in (4.15) by ϕ_k^* and postmultiply by ϕ_k to obtain $L_k = 1 - (1+\lambda_k^2)^{-1/2} = 1-\cos\alpha_k$, which is the desired result.

Similarly, to obtain the desired expansion for K, seek to determine the coefficients K_k in

$$K = \sum K_k\,\phi_k\phi_k^* \quad \text{with} \quad K_k = \phi_k^* K\,\phi_k. \tag{4.19}$$

Multiplication of K in (4.15) by ϕ_k^* and ϕ_k leads to $K_k = \phi_k^* K\phi_k = (1+\lambda_k^2)^{1/2}-1 = \sec\alpha_k - 1$.

Trigonometric Operator Formulas for the Likelihood Functional

Result 4.7 The log-likelihood functional can be expressed as

$$J(\Theta;y) = \text{Tr}\log[\text{SEC}\,\alpha(\Theta)] + \tfrac{1}{2} z^*(\Theta)z(\Theta) - z^*(\Theta)y, \tag{4.20}$$

where

$$z(\Theta) = [I-COS\alpha(\Theta)]y + COS\alpha(\Theta)m(\Theta), \tag{4.21}$$

with $COS\alpha(\Theta) = [I+R(\Theta)]^{-1/2} = \sum \cos\alpha_k \phi_k \phi_k^*$. (4.22)

Proof: Recognize that (4.17) implies that

$$L(\Theta) = I-COS\alpha(\Theta) \quad \text{and} \quad K(\Theta) = SEC\alpha(\Theta) - I, \tag{4.23}$$

and use these identities in (4.13) and (4.14) to obtain (4.20) and (4.21) respectively.

Result 4.8 The negative-log likelihood functional can be expressed as

$$J(\Theta;y) = \sum [\log \sec\alpha_k(\Theta) + \tfrac{1}{2} z_k^2(\Theta) - z_k(\Theta)y_k(\Theta)], \tag{4.24}$$

where z_k and y_k are the "spectral" coefficients

$$z_k(\Theta) = \phi_k^*(\Theta)z(\Theta), \qquad y_k(\Theta) = \phi_k^*(\Theta)y, \tag{4.25}$$

and as before $\sigma_k = \tan^{-1}\lambda_k$, with λ_k^2 being the eigenvalues of R.

Proof: This result, which is closely related to Result 4.4 above, can be established by observing that $SEC\alpha(\Theta)$, $z(\Theta)$ and y in (4.20) can be expanded as

$$SEC\alpha(\Theta) = \sum \sec\alpha_k \phi_k\phi_k^*, \quad z = \sum z_k\phi_k \quad \text{and} \quad y = \sum y_k\phi_k. \tag{4.26}$$

Selection of Preferred Formula for Numerical Search Implementation

In principle, all of the above formulas for the likelihood functional $J(\Theta;y)$ can be used as a point of departure to compute the gradient $\partial J/\partial\Theta$ and the corresponding Hessian $\partial^2 J/\partial\Theta^2$ - and to thereby obtain the necessary ingredients to implement the Newton-Raphson search for optimization. The calculations involved in the numerical search can vary significantly, however, depending on which of the forms is used as a starting point. It is therefore of interest to conduct a detailed investigation of the relative advantages and disadvantages of the various methods to implement the search that arise from the various forms of the likelihood functional. Such an investigation is currently in progress and will be reported on in future work. In this paper however, the formula selected to compute the gradient and Hessian is that based on the predicted-data-covariance square-root filter in (4.13).

5. COVARIANCE EIGENSYSTEM SENSITIVITY TO SMALL PARAMETER CHANGES

As a preliminary to the evaluation of $\partial J/\partial\Theta$ and $\partial^2 J/\partial\Theta^2$ involved in the numerical search for optimization, it is necessary to conduct an analysis of the perturbations $\delta\lambda_k$ and $\delta\phi_k$ of the eigenvalues and eigenvectors of $R = H\Phi BB^*\Phi^*H^*$, with respect to variations $\delta\Theta$ of the parameter distribution Θ. Such an analysis will provide the mathematical tools that will be used in subsequent sections to evaluate $\partial J/\partial\Theta$ and $\partial^2 J/\partial\Theta^2$.

By definition, λ_k^2 and ϕ_k are the nontrivial solutions of

$$R(\Theta)\phi_k(\Theta) = \lambda_k^2(\Theta)\phi_k(\Theta), \tag{5.1}$$

where the dependence on Θ of R, ϕ_k and λ_k has been explicit. The ultimate objective of this section is to develop analytical formulas for calculating the first-order perturbations $\delta\lambda_k$ and $\delta\phi_k$ of λ_k and ϕ_k with respect to small changes $\delta\Theta$ in the parameter distributions Θ.

Definition of $\delta\lambda_k$, $\partial\lambda_k/\partial\Theta$, $\delta\phi_k$ and $\partial\phi_k/\partial\Theta$

It is assumed here that the Frechet differential [2] of λ_k at Θ exists and that it can be computed by

$$\delta\lambda_k(\Theta;\delta\Theta) = [d\lambda_k(\Theta+\gamma\delta\Theta)/d\gamma]_{\gamma=0}, \tag{5.2}$$

where γ is a scalar and $\delta\Theta$ is an admissible perturbation of Θ. Equation (5.2) is actually the formula typically used for computation of the Gateaux differential. However, it is assumed here that both of these derivatives exist and coincide and that therefore (5.2) can be used to calculate the Frechet derivative.

Since λ_k is Frechet differentiable (admittedly by assumption, as an investigation of the technical conditions required for differentiability is not within the scope of this paper), its differential $\delta\lambda_k(\Theta;\delta\Theta)$ can be expressed as

$$\delta\lambda_k(\Theta;\delta\Theta) = [\partial\lambda_k(\Theta)/\partial\Theta]\delta\Theta, \tag{5.3}$$

where $\partial\lambda_k(\Theta)/\partial\Theta$ is a bounded linear functional referred to as the Frechet derivative of λ_k at Θ. The transformation $\partial\lambda_k/\partial\Theta$ can also be viewed as a function space gradient of λ_k at Θ. Similarly, the eigenvector differential $\delta\phi_k(\Theta;\delta\Theta)$ is defined as

$$\delta\phi_k(\Theta;\delta\Theta) = [\partial\phi_k(\Theta;\delta\Theta)/\partial\Theta]\,\delta\Theta, \tag{5.4}$$

where $[\partial\phi_k(\Theta)/\partial\Theta]$ is the Frechet derivative, assumed to be linear and bounded.

Calculation of $\delta\lambda_k$ and $\partial\lambda_k/\partial\Theta$

Recall that the ϕ_k in (5.1) are orthonormal so that

$$\phi_k^*\phi_k = 1 \quad \text{and} \quad \phi_k^*\phi_m = 0, \qquad m \neq k. \tag{5.5}$$

Multiplication of (5.1) by ϕ_k^* and use of $\phi_k^*\phi_k = 1$ leads to

$$\lambda_k^2 = \phi_k^* R \phi_k, \tag{5.6}$$

which can be taken as the point of departure for calculation of $\delta\lambda_k$ and $\partial\lambda_k/\partial\Theta$.

<u>Result 5.1</u> The Frechet differential $\delta\lambda_k(\Theta;\delta\Theta)$ can be expressed as

$$\delta\lambda_k(\Theta;\delta\Theta) = -\lambda_k^2(\Theta)\,[p_k^*(\Theta)\delta A(\Theta;\delta\Theta)x_k(\Theta)], \tag{5.7}$$

where $\delta A(\Theta;\delta\Theta)$ is the differential of A defined as

$$\delta A(\Theta;\delta\Theta) = [dA(\Theta+\gamma\delta\Theta)/d\gamma]_{\gamma=0} \tag{5.8}$$

and p_k and x_k are the vectors defined as $p_k = \lambda_k^{-1}\Phi^* H^* \phi_k$ and $x_k = \lambda_k^{-1}\Phi B \psi_k$ in Sec. 2.

<u>Proof:</u> Performance of a first-order perturbation on (5.6), and use of the condition $\phi_k^*\delta\phi_k = 0$ leads to

$$\delta\lambda_k = (2\lambda_k)^{-1}\,\phi_k^*\delta R\phi_k, \tag{5.9}$$

where $\delta R(\Theta;\delta\Theta) = [dR(\Theta+\gamma\delta\Theta)/d\gamma]$ evaluated at $\gamma = 0$. However, since $\delta R = \delta(H\Phi BB^*\delta\Phi^*)H^*$, then

$$\delta R = H(\delta\Phi)BB^*\Phi^*H^* + H\Phi BB^*(\delta\Phi^*)H^*. \tag{5.10}$$

It can be observed from (5.10) that evaluation of $\delta\Phi$ is the central calculation required to determine δR. In order to simplify notation, without loss of generality, it has been assumed in arriving at (5.10) that B and H do not depend on Θ. In most practical cases, this assumption is satisfied because the poorly known parameters occur in the operator A.

To compute $\delta\Phi$, as required by (5.10), recall that $A(\Theta)\Phi(\Theta) = I$, so that $(\delta A)\Phi + A(\delta\Phi) = 0$, and

$$\delta\Phi = -\Phi(\delta A)\Phi. \tag{5.11}$$

Substitution of (5.11) in (5.10) leads to

$$\delta R = -H\Phi(\delta A)\Phi BB^*\Phi^*H^* - H\Phi BB^*\Phi^*(\delta A)^*\Phi^*H^*. \tag{5.12}$$

Multiplication by $\phi_k^*(\cdot)\phi_k$ results in

$$\phi_k{}^*\delta R\phi_k = -(\phi_k{}^*H\Phi)\delta A(\Phi BB^*\Phi^*H^*\phi_k) - (\phi_k{}^*H\Phi BB^*\Phi^*)\delta A^*(\Phi^*H^*\phi_k). \tag{5.13}$$

Finally, use of the definitions $p_k = \lambda_k^{-1}\Phi^*H^*\phi_k$ and $x_k = \lambda_k^{-1}\Phi B\psi_k$ in (5.13), and substitution in (5.9), implies (5.7). In performing this last step, it has been assumed that $A = A^*$ is formally self-adjoint, a condition that is valid on most problems of practical interest.

Discussion and Additional Assumptions on A

The above result, although a step in the right direction, is still somewhat intermediate because the differential $\delta\lambda_k$ in (5.7) is expressed in terms of the yet to be determined differential δA. To proceed further, it is convenient to make two additional assumptions (typically satisfied in practice):

- $A(\Theta)$ is linear in Θ so that $A(\Theta_1 + \Theta_2) = A(\Theta_1) + A(\Theta)_2$ for two admissible distributions Θ_1 and Θ_2.
- $A(\Theta)$ can be factored as $A(\Theta) = D^*(\Theta)D$, where D and its corresponding formal adjoint D^* may in general be matrix differential operators.

Based on these assumptions, it is now possible to derive the following more explicit formulas for $\delta\lambda_k$ and $\partial\lambda_k/\partial\Theta$.

Result 5.2 The Frechet derivative $\partial\lambda_k(\Theta)/\partial\Theta$ of λ_k is

$$\partial\lambda_k(\Theta)/\partial\Theta = \lambda_k^2\, Dp_k(\Theta)\cdot Dx_k(\Theta). \tag{5.14}$$

Proof: Since A has been assumed to be linear and factorizable

$$\delta\lambda_k = -\lambda_k^2 p_k{}^*D^*(\delta\Theta)Dx_k = \lambda_k^2 \langle (Dp_k)\,\delta\Theta\,(Dx_k)\rangle_2 \tag{5.15}$$

where the last equality is a consequence of a process analogous to integration by parts.

Result 5.3 Since $\partial\lambda_k/\partial\Theta$ has been assumed to be a bounded linear functional in X, it must be expressible as

$$[\partial\lambda_k(\Theta)/\partial\Theta]\delta\Theta = \langle\partial\lambda_k(\Theta;\cdot)/\partial\Theta,\ \delta\Theta\rangle_X, \tag{5.16}$$

where $\partial\lambda_k(\Theta;\cdot)/\partial\Theta$ is an element of $X^*(\Omega)$. Futhermore, $[\partial\lambda_k(\Theta;\cdot)/\partial\Theta]$ can be evaluated from

$$\partial\lambda_k(\Theta;x)/\partial\Theta = \lambda_k^2\, Dp_k(\Theta;x)\cdot Dx_k(\Theta;x). \tag{5.17}$$

Proof: The rigorous derivation of this result is not as yet available. The result is accepted somewhat formally on the basis that a bounded linear functional can be represented by an element in the dual to the space in which the functional is defined.

Calculation of $\delta\phi_k$ and $\partial\phi_k/\partial\Theta$

Result 5.4 The Frechet differential $\delta\phi_k(\Theta;\delta\Theta)$ of ϕ_k can be expressed as

$$\delta\phi_k(\Theta;\delta\Theta) = \sum_{m\neq k} [(\phi_m{}^*\delta R\phi_k)/(\lambda_k^2 - \lambda_m^2)]\,\phi_m, \tag{5.18}$$

where δR is the differential of the observed-state covariance operator R.

Proof: Since $R\phi_k = \lambda_k^2\phi_k$,

$$(\delta R)\phi_k + R\delta\phi_k = 2\lambda_k(\delta\lambda_k)\phi_k + \lambda_k^2\delta\phi_k. \tag{5.19}$$

Now, seek an expansion for $\delta\phi_k$ in terms of the orthonormal basis ϕ_m, i.e.,

$$\delta\phi_k = \sum_{m\neq k} c_{km}\phi_m, \qquad c_{km} = \phi_m{}^*\delta\phi_k, \tag{5.20}$$

where c_{km} are scalar coefficients to be determined. Note that the orthonormality of ϕ_k implies that $c_{kk} = 0$, so that $\delta\phi_k$ does not have a component in the direction of ϕ_k. To evaluate c_{km}, premultiply (5.20) by $\phi_m{}^*$ to obtain

$$\phi_m{}^*\delta R\phi_m + \phi_m{}^*R\delta\phi_k = \lambda_k^2\phi_m{}^*\delta\phi_k. \tag{5.21}$$

Use of the conditions $\phi_m{}^*R = \lambda_m^2\phi_m{}^*$ and $c_{km} = \phi_m{}^*\delta\phi_k$ and rearrangement of terms leads to

$$c_{km} = (\phi_m{}^*\delta R\phi_k)/(\lambda_k^2 - \lambda_m^2). \tag{5.22}$$

Substitution of (5.22) in (5.20) leads to (5.18), thereby establishing the result.

Equation (5.18) is similar in nature to (5.9) in that it expresses the desired differential in terms of the yet to be determined quantity δR.

Result 5.5 The Frechet differential $\delta\phi_k(\Theta;\delta\Theta)$ of ϕ_k can be expressed as

$$\delta\phi_k(\Theta;\delta\Theta) = \sum_{m\neq k} [\lambda_k\lambda_m/(\lambda_k^2-\lambda_m^2)]\,[\lambda_k p_m{}^*(\delta A)x_k + \lambda_m x_m{}^*(\delta A)^*p_k]\phi_m, \tag{5.23}$$

where $p_k = \lambda_k^{-1}\Phi^*H^*\phi_k$ and $x_k = \lambda_k^{-1}\Phi B\psi_k$.

Proof: Substitute (5.12) in (5.18) and use the definitions for p_k and x_k.

Equation (5.23) is valid without making the additional assumption that $A(\Theta)$ is linear in Θ and factorizable as $A(\Theta) = D^*(\Theta)D$. If these two assumptions are now made, the following result can be obtained.

Result 5.6 The Frechet derivative $\partial\phi_k(\Theta)/\partial\Theta$ is specified by

$$\partial\phi_k(\Theta)/\partial\Theta = \sum_{m\neq k} [\lambda_k\lambda_m/(\lambda_k^2-\lambda_m^2)]\,[\lambda_k Dp_m\cdot Dx_k + \lambda_m Dx_m\cdot Dp_k]\phi_m. \tag{5.24}$$

Proof: This result follows by substitution of $\delta A(\Theta) = D^*(\delta\Theta)D$ in (5.23).

Closely related to $\delta\phi_k$ is the differential

$$\delta(\phi_k\phi_k^*) = \phi_k\delta\phi_k^* + (\delta\phi_k)\phi_k^* \tag{5.25}$$

of the outer product $\phi_k\phi_k^*$. The corresponding Frechet derivative $\partial(\phi_k\phi_k^*)/\partial\Theta$ is evaluated in the following result.

Result 5.7 The Frechet derivative $[\partial(\phi_k\phi_k^*)/\partial\Theta]$ is specified by

$$\partial(\phi_k\phi_k^*)/\partial\Theta = \sum_{m\neq k} [\lambda_k\lambda_m/(\lambda_k^2-\lambda_m^2)]\,[\lambda_k Dp_m\cdot Dx_k + \lambda_m Dx_m\cdot Dp_k]\,[\phi_m\phi_k^* + \phi_k\phi_m^*]. \tag{5.26}$$

Proof: Use (5.24) to evaluate the right side of (5.25) and recall that $\delta(\phi_k\phi_k^*) = [\partial(\phi_k\phi_k^*)/\partial\Theta]\delta\Theta$.

Discussion

The results obtained above provide the key tools required to evaluate the function-space gradient $\partial J/\partial\Theta$ and Hessian $\partial^2 J/\partial\Theta^2$ of the likelihood functional. The most useful formulas are (5.17) for the derivative $\partial\lambda_k/\partial\Theta$ of the eigenvalue λ_k, (5.24) for the derivative $\partial\phi_k/\partial\Theta$ of the eigenvector ϕ_k, and (5.26) for the derivative $\partial(\phi_k\phi_k^*)/\partial\Theta$ of the outer product $(\phi_k\phi_k^*)$. These formulas will be used repeatedly in the following section.

6. SPECTRAL REPRESENTATIONS FOR THE GRADIENT, APPROXIMATE HESSIAN, AND NEWTON-RAPHSON SEARCH

Implementation of the modified Newton-Raphson search for the optimal parameter estimates requires calculation of the gradient $\partial J/\partial\Theta$ and of an approximation to the Hessian operator $\partial^2 J/\partial\Theta^2$. These calculations are best achieved using the predicted-data-covariance square-root filter in Result 4.5 that expresses the likelihood functional as

$$J(\Theta;y) = \mathrm{Tr}\,\log\,[I+K(\Theta)] + \tfrac{1}{2}\, z^*(\Theta)z(\Theta) - z^*(\Theta)y, \tag{6.1}$$

where $z(\Theta) = L(\Theta)y + [I-L(\Theta)]\, m(\Theta)$. Function space differentiation of (6.1) with respect to Θ leads to the gradient functional

$$g(\Theta;y) = \partial J(\Theta;y)/\partial\Theta = \mathrm{Tr}\,[(\partial L/\partial\Theta)\,(I+K)] + (z-y)^*(\partial z/\partial\Theta), \tag{6.2}$$

and to the approximate Hessian operator

$$M(\Theta;y) = \mathrm{Tr}\,[(\partial L/\partial\Theta)\,(I+R)\,(\partial L/\partial\Theta)] + (\partial z/\partial\Theta)^*(\partial z/\partial\Theta), \tag{6.3}$$

upon which the Newton-Raphson numerical search is to be based. An updated estimate $\Theta^{n+1} = \Theta^n - \delta\Theta^n$ is obtained by specification of the parameter change $\delta\Theta^n$ defined as

$$\delta\Theta^n = M^{-1}\,(\Theta^n;y)g(\Theta^n;y). \tag{6.4}$$

The main objective of this section is to replace the operator equations (6.2) and (6.3) with a set of equivalent matrix equations more convenient for calculations. The fundamental approach to be used consists of representing the function space derivatives $\partial L/\partial\Theta$, $\partial m/\partial\Theta$ and $\partial z/\partial\Theta$ - which have only been derived in terms of operator symbols in (6.2) and (6.3) - in terms of a specific orthonormal basis defined by the eigenvectors ϕ_k of the observed-state covariance operator R.

Spectral Representation for the Gradient

Result 6.1 The Frechet derivative $\partial L/\partial\Theta$ of the predicted-data-covariance square-root filter L can be represented as

$$\partial L/\partial\Theta = \sum_k \sum_m a_{km}\phi_k\phi_m^*, \tag{6.5}$$

where the spectral coefficients $a_{km} = \phi_k^*(\partial L/\partial\Theta)\phi_m$ are specified by

$$a_{kk} = \sin^2 a_k Dp_k \cdot Dx_k, \tag{6.6}$$

$$a_{km} = [\lambda_k\lambda_m/(\lambda_m^2-\lambda_k^2)]\,[\cos\alpha_k - \cos\alpha_m]\,[\lambda_k Dp_m \cdot Dx_k + \lambda_m I\, x_m \cdot Dp_k] \quad k\neq m. \tag{6.7}$$

Note that a_{km} defines a matrix whose diagonal elements are provided by (6.6) and whose corresponding nondiagonal elements are given by (6.7).

Proof: Observe $L = \sum (1-\cos\alpha_i)\phi_i\phi_i^*$ implies

$$\partial L/\partial\Theta = \sum \{\sin\alpha_i\,(\partial\alpha_i/\partial\Theta)\phi_i\phi_i^* - \cos\alpha_i\,[\partial(\phi_i\phi_i^*)/\partial\Theta]\}. \tag{6.8}$$

Substitution of this equation in $a_{km} = \phi_k^*(\partial L/\partial\Theta)\phi_m$ and use of orthonormality of ϕ_k lead to

$$a_{kk} = \sin\alpha_k \cos^2\alpha_k\,(\partial\lambda_k/\partial\Theta),\; a_{km} = -\cos\alpha_m\phi_k^*(\partial\phi_m/\partial\Theta) - \cos\alpha_k(\partial\phi_k^*/\partial\Theta)\phi_m, \tag{6.9}$$

where $\partial\lambda_k/\partial\Theta$ and $\partial\phi_k/\partial\Theta$ are the function-space derivatives evaluated in (5.18) and (5.25). Substitution of these two equations from Sec. 5 in (6.9) leads to (6.6) and (6.7) thereby establishing the result.

Result 6.2 The Frechet derivative $\partial m/\partial\Theta$ of the suspected mean $m(\Theta)$ is represented by

$$\partial m/\partial\Theta = \sum (\partial m/\partial\Theta)_k\phi_k, \tag{6.10}$$

with the spectral coefficients $(\partial m/\partial\Theta)_k$ specified by

$$(\partial m/\partial\Theta)_k = \lambda_k\,(Dp_k \cdot D\Phi Cf), \tag{6.11}$$

and ΦCf in (6.11) denoting the suspected value of the state u.

Proof: Since $m = H\Phi Cf$, then $\delta m = H\delta\Phi Cf = -H\Phi A(\delta\Theta)\,\Phi Cf$, where the last equality follows from the condition $\delta\Phi = -\Phi A(\delta\Theta)\Phi$. Define now $(\delta m)_k$ as the k^{th} spectral coefficient of δm, i.e.,

$$(\delta m)_k = \phi_k^*\,\delta m = -\phi_k^*\,H\Phi A(\delta\Theta)\Phi Cf = -\lambda_k p_k^* A(\delta\Theta)\Phi Cf, \tag{6.12}$$

where as before $p_k = \lambda_k^{-1}\Phi^*H^*\phi_k$. Use of the identity $p_k^*A(\delta\Theta)\Phi Cf = -Dp_k \cdot D(\Phi Cf)\delta\Theta$ in (6.12) results in $(\delta m)_k = (\partial m/\partial\Theta)_k\,\delta\Theta$, with $(\partial m/\partial\Theta)_k$ given by (6.11).

Result 6.3 In the special case in which the deterministic input f is assumed to be a vector $f = [f_1,\ldots,f_M]$ of M inputs applied at the discrete locations ξ_i, an alternative to (6.11) in evaluating $(\partial m/\partial\Theta)_k$ is

$$(\partial m/\partial\Theta)_k = \sum_{m=1}^{M} \lambda_k\; Dp_k(x)\cdot D\phi(x/\xi_m)f_m \qquad \text{for } k = 1,\ldots,N, \tag{6.13}$$

where $\phi(x/\xi)$ is the Green's function of the system model operator A.

Result 6.4 The gradient $\partial z/\partial\theta = (\partial L/\partial\theta)y + (I-L)(\partial m/\partial\theta)$ of the filtered state estimate z can be represented as

$$\partial z/\partial\theta = \sum (\partial Z/\partial\theta)_k \phi_k, \tag{6.14}$$

where the spectral coefficients $(\partial z/\partial\theta)_k = \phi_k^*(\partial z/\partial\theta)$ are given by

$$(\partial z/\partial\theta)_k = \sum_{m=1}^{N} a_{km}(x)\,\bar{y}_m + \sum_{m=1}^{M} b_{km}(x) f_m, \tag{6.15}$$

with a_{km} specified in (6.6) and (6.7) and

$$b_{km}(x) = \sin\alpha_k\, Dp_k(x)\cdot D\phi(x/\xi_m). \tag{6.16}$$

Proof: Substitute $\partial L/\partial\theta$ and $\partial m/\partial\theta$ from (6.5) and (6.10) into $\partial z/\partial\theta = (\partial L/\partial\theta)\bar{y} + (I-L)(\partial m/\partial\theta)$ and then compute the spectral coefficients $(\partial z/\partial\theta)_k$ in (6.14) from $(\partial z/\partial\theta)_k = \phi_k^*(\partial z/\partial\theta)$.

Result 6.5 The gradient $g(\theta;y)$ in (6.2) can be represented as

$$g(\theta;y) = \sum [\sin^2\alpha_k \tan\alpha_k (Dp_k\cdot Dx_k) - e_k(\partial z/\partial\theta)_k], \tag{6.17}$$

where $e_k = \phi_k^* e$ are the spectral coefficients of the residual process $e = y-z$, and $(\partial Z/\partial\theta)_k$ are given by (6.15).

Proof: Substitute $\partial L/\partial\theta$ in (6.5), $\partial z/\partial\theta$ in (6.14), $e = \sum e_k\phi_k$ and $I + K = \sum \sec\alpha_k \phi_k\phi_k^*$ into (6.2) and use orthonormality of ϕ_k.

Equation (6.17) provides the means to evaluate the likelihood functional gradient, one of the key ingredients of the Newton-Raphson iteration. The approximate Hessian operator $M(\theta;y)$, which is the other major element required to implement the search, is evaluated below.

Evaluation and Inversion of the Approximate Hessian

Result 6.6 The approximate Hessian $M(\theta;y)$ in (6.3) is an integral operator whose kernel $M(x/\xi)$ is specified by

$$M(x/\xi) = \sum [\sec^2\alpha_k\, a_{kk}(x)\, a_{kk}(\xi) + z'_k(x) z'_k(\xi)], \tag{6.18}$$

where $z'_k = (\partial z/\partial\theta)_k = \phi_k^*(\partial z/\partial\theta)$ is the k^{th} spectral coefficient of $\partial z/\partial\theta$.

Proof: Substitute (2.26) and (6.14) into (6.3) and use the orthonormality of ϕ_k.

Implementation of an iteration step in the Newton-Raphson search requires calculation of $\delta\theta^n = M^{-1}(\theta^n;y)g(\theta^n;y)$, representing the incremental change in the parameter estimate. Inversion of $M(\theta^n;y)$ is therefore required at every step of the search. This inversion is achieved by solving an integral equation as outlined in the following result.

Result 6.7 The incremental parameter change $\delta\theta^n$ can be computed as the solution of the following integral equation

$$\int_\Omega M_n(x/\xi)\,\delta\theta^n(\xi)d\xi = g_n(x), \tag{6.19}$$

where M_n is the approximate Hessian kernel in (6.18), and $g_L(x)$ is the value of the gradient at the spatial location x. The subscript n in M_n and g_n denotes that the corresponding quantities are evaluated at the n^{th} parameter estimate $\theta=\theta^n$.

Proof: Observe that $\delta\theta^n = M_n^{-1}g_n$ implies $M_n\delta\theta^n = g_n$, and express this last equation in terms of the kernel M_n to obtain (6.19).

7. PARAMETER ESTIMATION ERROR, CRAMER-RAO BOUNDS AND OPTIMAL INPUT DESIGN

The objectives here are to obtain a C-R bound for the covariance of the parameter estimation error and to begin an investigation of the problem of optimal input design by using the C-R bound as a criterion for optimal input selection.

Recall that the covariance of an unbiased estimate θ satisfies the inequality

$$E(\theta_p\theta_p^*) \ge M^{-1}(\theta_o), \tag{7.1}$$

where $M(\theta_o)$ is the information operator defined as

$$M(\theta_o) = E[\partial^2 J/\partial\theta^2]_{\theta=\theta_o} = E[(\partial J/\partial\theta)(\partial J/\partial\theta)^*]_{\theta=\theta_o} . \tag{7.2}$$

The corresponding mean-square estimation error $E(\theta_p^*\theta_p)$ satisfies the related inequality

$$E(\theta_p^*\theta_p) \ge Tr[M^{-1}(\theta_o)] \tag{7.3}$$

It can be observed that the key calculation required to obtain the C-R bound is the computation of $E[\partial^2 J/\partial\Theta^2]$ as outlined below.

Cramer-Rao Bound for the Estimation Error

Result 7.1 The information operator $M(\Theta_o)$ is specified by

$$M(\Theta_o) = E[\partial^2 J/\partial\Theta^2]_{\Theta=\Theta_o} = 2\ \mathrm{Tr}[(\partial L/\partial\Theta)(I+R)(\partial L^*/\partial\Theta)] + (\partial m^*/\partial\Theta)(I-L^*)(I-L)(\partial m/\partial\Theta), \tag{7.4}$$

where $R = H\Phi BB^*\Phi^*H^*$ is the data-covariance operator, $(\partial L/\partial\Theta)$ is the derivative of $L = I - (I+R)^{-1/2}$, and $(\partial m/\partial\Theta)$ is the derivative of the data mean $m=H\Phi Cf$.

Proof: Differentiate $g(\Theta;y)$ in (6.2) to obtain

$$\partial^2 J/\partial\Theta^2 = \mathrm{Tr}[(\partial^2 L/\partial\Theta^2)(I+K) + (\partial L/\partial\Theta)(\partial K/\partial\Theta)] + (z-y)^*(\partial z/\partial\Theta) + (\partial z/\partial\Theta)^*(\partial z/\partial\Theta). \tag{7.5}$$

Take the expected value in (7.5) above, evaluate at $\Theta = \Theta_o$, and simplify to obtain

$$E[\partial^2 J/\partial\Theta^2]_{\Theta=\Theta_o} = \mathrm{Tr}\,[(\partial L/\partial\Theta)(I+R)(\partial L/\partial\Theta)] + E[(\partial z^*/\partial\Theta)(\partial z/\partial\Theta)]. \tag{7.6}$$

Finally, use (6.9) in (7.6) to arrive at (7.4).

Result 7.2 In spectral form, the information operator $M(\Theta_o)$ is specified by

$$M(\Theta_o) = \sum [2\sec^2\alpha_k\, a_{kk}(x)\, a_{kk}(\xi) + \cos^2\alpha_k m'_k(x) m'_k(\xi)], \tag{7.7}$$

where a_{kk} and $m'_k = (\partial m/\partial\Theta)_k$ are defined in (6.9) and (6.11) respectively.

Proof: Use an approach similar to that used to arrive at (6.18).

Inspection of (7.4) reveals that the information operator $M(\Theta_o)$ consists of the sum of two terms both of which are positive definite. In the first term, the data-covariance operator $(I+R)$ appears as a "weighting" that is multiplied by the sensitivity filter $\partial L/\partial\Theta$. Note parenthetically that in fact L is self-adjoint so that $L = L^*$. The second term, on the other hand, will be shown to be a quadratic function of the input f.

Result 7.3 Assume that $f = [f_1, \ldots, f_M]$ is a vector of M inputs applied at the M discrete locations ξ_m. The information operator $M(\Theta_o)$ is an integral operator whose kernel $M(x/\xi)$ can be expressed as

$$M(x/\xi) = U(x/\xi) + f^T V(x/\xi) f, \tag{7.8}$$

where

$$U(x/\xi) = \sum_k \sin^4\alpha_k \tan^2\alpha_k \, [Dp_k(x) \cdot \Gamma p_k(x)] \, [Dp_k(\xi) \cdot Dx_k(\xi)], \tag{7.9}$$

$$V(x/\xi) = \sum_k \sin^2\alpha_k \, b_k(x) \, b_k^T(\xi), \tag{7.10}$$

and where $b_k^T(\xi)$ is the M-dimensional vector

$$b_k^T(\xi) = [Dp_k(\xi) \cdot D\phi(\xi/\xi_1), \ldots, Dp_k(\xi) \cdot D\phi(\xi/\xi_M)], \tag{7.11}$$

with ϕ being the Green's function of A in (1.1).

Proof: Substitute the eigensystem expansions for R in (2.26), for L in (4.17), for $(\partial L/\partial\Theta)$ in (6.5), and for $\partial m/\partial\Theta$ in (6.10) into (7.4) to obtain (7.9) and (7.10).

The second term in (7.8) is a quadratic form in the input signal f. This property can be used as a basis for optimal input design.

Optimal Input Design

The information operator can be used to state criteria for optimal input design. While several possible criteria exist, the one that is easiest to use is perhaps the maximization of Tr $M(\Theta_0)$:

$$\max \mathrm{Tr}\, M(\Theta_0) = U + f^T V f, \quad f^T f = 1, \tag{7.12}$$

where

$$U = \int_\Omega U(x/x)dx \text{ and } V = \int_\Omega V(x/x)dx. \tag{7.13}$$

The optimal input f_0, which is the solution to the above optimization problem, is the eigenvector corresponding to the largest eigenvalue of the M-by-M matrix V.

Other criteria for optimal input selection include: minimization of Tr (M^{-1}), which would correspond to minimizing the Cramer-Rao bound; and minimization of $\lambda_{max}(M^{-1})$, where λ_{max} is the maximum eigenvalue of M^{-1}. While these last two criteria could be superior to (7.12), they both have the disadvantage of requiring inversion of the operator $M(\Theta_0)$. However, the requirement for such an inversion may not be a serious additional drawback because a similar calculation is required to implement the Newton-Raphson search outlined in the previous sections.

Vanishing Bias of the Gradient

Closely related to the above analysis is an investigation of the bias in the parameter estimate Θ. The central result is as follows.

Result 7.4 The expected value of the gradient functional $g(\Theta;y)$ vanishes at $\Theta = \Theta_o$, i.e.,

$$E[g(\Theta;y)]\,|_{\Theta=\Theta_o} = 0. \tag{7.14}$$

Proof: Observe that $\partial z/\partial\Theta = (\partial L/\partial\Theta)\bar{y} + (I-L)\,(\partial m/\partial\Theta)$, and recall that $\bar{y} = (I+K)e$. Substitute this in (6.2) and take the expected value. Finally, use the whiteness of the residual process, to be established in (8.46).

8. FILTERING, SMOOTHING AND THE RESIDUAL PROCESS

The central aim of this section is to conduct an analysis of the smoothed estimate u_o and of the filtered state estimate z_o that emerges from the predicted-data-covariance square-root filter. This analysis leads to the following major results:

- The smoothed estimate u_o is optimal in a conditional mean sense.
- The formulas that generate u_o and z_o have a predictor-corrector structure in which the final state estimate is the sum of: a prediction term-based on application of known inputs to the system model; and a correction term based on the difference between the actual and predicted data. The key element in these formulas is an estimator gain that provides the relative weighting between the two terms.
- The covariance of the state estimation error inherent in both estimates can be evaluated by means of equations which, if written in operator notation, resemble those encountered in filtering and smoothing for linear dynamical systems.
- Investigation of a residual process associated with the filtered state estimate z_o that has properties nearly identical to those of an innovations process: the residuals are a white noise process with a unit covariance; the residuals and the measurements can be obtained from each other by means of reciprocal linear transformations. Because these transformations are not causal, the residuals are not a bona fide innovations process. However, they are as useful in deriving filtering, smoothing and identification solutions for elliptic systems as the innovations process is in deriving similar solutions for linear dynamical systems.

- Development of relationships between the filtering and smoothing estimates that can be thought of as extensions to elliptic systems of the forward/backward sweep method for solution of filtering and smoothing problems in linear dynamical systems.

- Development of spectral representations for the predicted-data-covariance square-root filter and the optimal smoother in terms of the eigensystem of the state covariance $\bar{R} = \Phi BB^*\Phi^*$. This leads to simple ways to implement filtering and smoothing solutions on a computer.

Smoothed and Filtered Estimates

The smoothed and filtered state estimates u_0 and z_0 have been defined in (1.17) as

$$u_0 = \Phi Cf + G(y-H\Phi Cf), \qquad z_0 = \Phi Cf + g(y-H\Phi Cf), \tag{8.1}$$

where G and g are Kalman-like gains specified by

$$G = \sum \sin^2\alpha_k x_k \phi_k^*, \quad g = \sum (1-\cos\alpha_k) x_k \phi_k^*. \tag{8.2}$$

The estimate u_0 is referred to as a smoothed estimate because it is the minimum-variance estimate of the state given the entire data set. This is established by the following result.

Result 8.1 The smoothed estimate u_0 in (8.1) is the conditional mean $u_0 = E(u/y)$ of the state given the data. Furthermore, the estimator gain G in (8.2) can be expressed alternatively as

$$G = \bar{R}H^*(I + H\bar{R}H^*)^{-1}, \tag{8.3}$$

in terms of the state covariance $\bar{R} = \Phi BB^*\Phi^*$.

Proof: Recall the general formula

$$E(u/v) = E(uv^*)\,[E(vv^*)]^{-1}v \tag{8.4}$$

derived in [4] for the conditional expected value of a zero-mean random process u given the related zero-mean random process v. Note that this formula requires calculation of the "cross-covariance" operator $E(uv^*)$ and the auto-covariance operator $E(vv^*)$. Define now the mean-centered state $\bar{u} = u-\Phi Cf = \Phi B\omega$ and the mean-centered data $\bar{y} = H\bar{u}+n$. By this definition, $\bar{u}$ and $\bar{y}$ are zero-mean. Therefore (8.4) can be used directly to compute $\bar{u}_0 = E(\bar{u}/\bar{y})$, i.e.,

$$\bar{u}_0 = E(\bar{u}/\bar{y}) = E(\bar{u}\bar{y}^*)\,[E(\bar{y}\bar{y}^*)]^{-1}\bar{y}, \tag{8.5}$$

which indicates that to evaluate $\bar{u}_0$, it is necessary to first evaluate the covariance operators $E(\bar{u}\bar{y}^*)$ and $E(\bar{y}\bar{y}^*)$. These calculations are: $E(\bar{u}\bar{y}^*) = E(\Phi B\omega\omega^* B^*\Phi^*) = \Phi BB^*\Phi^*$ and $E(\bar{y}\bar{y}^*) = E\,[(H\bar{u}+n)\,(H\bar{u}+n)^*] = I + HRH^*$. Use of this in (8.5) leads to

$$E(\bar{u}/\bar{y}) = G\bar{y}. \tag{8.6}$$

This together with the definition of $\bar{u}$ and $\bar{y}$ in terms of u and y implies (8.1). The equivalence between the two different expressions for G in (8.2) and (8.3) is established by use of the spectral expansions in Sec. 2. In particular, use expansions (2.46) - (2.47) for I + R and the definition for x_k in (2.31).

As established by this result, the estimate u_0 has a very well defined probabilistic interpretation. It is not presently known if the filtered estimate z_0 has a similar interpretation. Nonetheless, this estimate plays a very significant role in the filtering, smoothing and identification methodology for elliptic systems under development here. Its role is analogous to that of the filtered estimate emerging from a Kalman filter in the case of dynamical systems. This is further investigated below.

Predictor-Corrector Structure

To examine this structure, consider the equation for u_0 in (8.1) and illustrated in Fig. 8.1. Use of the deterministic input f [1] and the system model ΦC [2] leads to a predicted estimate [3]. The difference process y-HΦCf [4] is then formed and operated on by the estimator gain G [5] to obtain the correction term G(y-HΦCf) [6]. Finally, the correction term is added to the predicted estimate to obtain the optimal estimate u_0. The equation for the filtered estimate z_0 in (8.1) also has a predictor-corrector structure. The key difference between the two equations in (8.1) is that the estimator gains are different. A relationship between these two different gains G and g is explored later in this section.

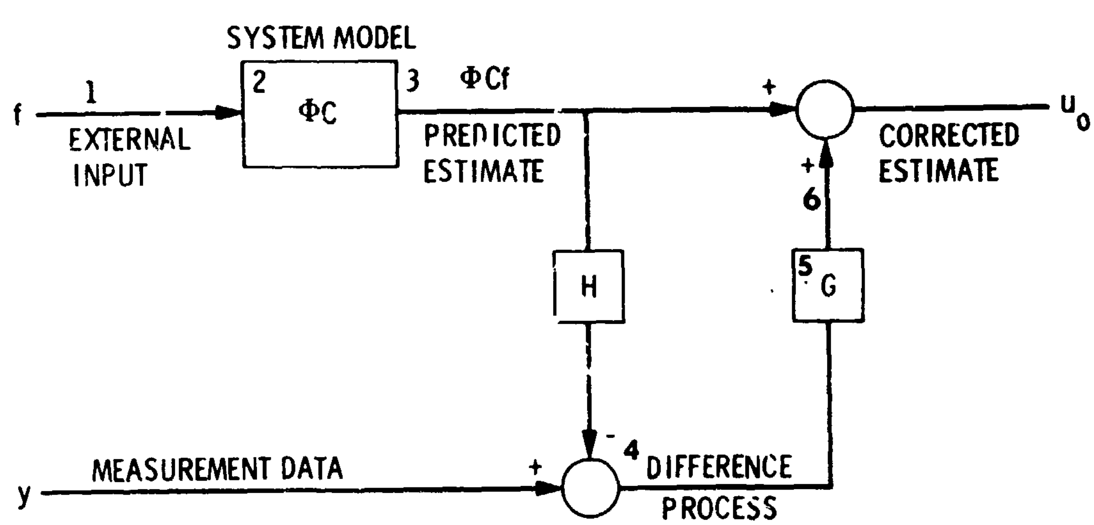

Fig. 8.1 Predictor-Corrector Form of the Smoothed State Estimator

Estimation Error Covariance and Kalman-like Gains: Smoothing

Since u_o and z_o are only estimates of the actual state u, it is of interest to investigate the inherent estimation error $u_p = u-u_o$ and $z_p = u-z_o$. In particular, the aim is to determine the estimation error covariance, under the assumption that the actual model errors ω and n in (1.1) and (1.2) are white-noise processes.

Result 8.2 The covariance $\bar{P} = \bar{P}^* = E(u_p u_p^*)$ of the state estimation error $u_p = u-u_o$ is specified by the following alternative formulas:

$$\bar{P} = (I - GH)\bar{R}(I - GH)^* + GG^*, \tag{8.7}$$

$$\bar{P} = \bar{R} - \bar{R}H^* (I + H\bar{R}H^*)^{-1} H\bar{R}, \tag{8.8}$$

$$\bar{P} = (I - GH)\bar{R} = \bar{R}(I - GH)^*, \tag{8.9}$$

$$\bar{P} = \Phi B (I + B^*\Phi^*H^*H\Phi B)^{-1}B^*\Phi^*. \tag{8.10}$$

Proof: To show (8.7), observe that $u = \Phi Cf + \Phi B\omega$ and $u_o = \Phi Cf + G(y - H\Phi Cf)$ imply that $u_p = u - u_o$ is

$$u_p = (I - GH)\Phi B\omega - Gn. \tag{8.11}$$

Hence $E(u_p u_p^*) = E[(I-GH)\Phi B\omega\omega^*B^*\Phi^* (I-GH)^* + Gnn^*G^*] = (I-GH)\bar{R}(I-GH)^* + GG^*$, where use has been made of the fact that $\epsilon = [\omega,n]$ is a white-noise process with covariance $E(\epsilon\epsilon^*) = I$. To show (8.8), observe that (8.7) implies

$$\bar{P} = \bar{R} - GH\bar{R} - \bar{R}H^*G^* + G(I + H\bar{R}H^*)G^*. \tag{8.12}$$

Substitution of $G = \bar{R}H^* (I + H\bar{R}H^*)^{-1}$ in (8.12) leads to (8.8). To show (8.9), observe that (8.8) can be expressed as $\bar{P} = \bar{R} (I-GH)^* = (I-GH)\bar{R}$ by using $G = \bar{R}H^*(I + H\bar{R}H^*)^{-1}$ in the last two terms of (8.12). To establish (8.10), substitute $\bar{R} = \Phi BB^*\Phi^*$ in (8.8) and use the identities $B^*\Phi^*H^* (I+H\Phi BB^*\Phi^*H^*)^{-1}H\Phi B = (I+B^*\Phi^*H^*H\Phi B)^{-1}B^*\Phi^*H^*H\Phi B = I - (I+B^*\Phi^*H^*H\Phi B)^{-1}$.

Result 8.3 The operator $H\bar{P}H^*$ is the Fredholm resolvent of $H\bar{R}H^*$ so that

$$(I + H\bar{R}H^*)^{-1} = I-H\bar{P}H^*. \tag{8.13}$$

Proof: Compute $H\bar{P}H^*$ from $\bar{P}$ in (7.8) to obtain $H\bar{P}H^* = H\bar{R}H^* [I - (I+H\bar{R}H^*)^{-1}]$. Use the identity $(I+H\bar{R}H^*)^{-1}H\bar{R}H^* = I - (I+H\bar{R}H^*)^{-1}$ twice in this last equation to obtain (8.13).

The aim now is to use (8.13) in (8.2) to obtain an alternative expression for the estimator gain.

Result 8.4 The estimator gain $G = \bar{R}H^*(I+H\bar{R}H^*)^{-1}$ can also be expressed as

$$G = \bar{P}H^*, \tag{8.14}$$

where $\bar{P} = E(u_p u_p^*)$ is the covariance of the smoothed state estimation error u_p.

Proof: Recall that $\bar{P}H^* = (I - GH)\bar{R}H^* = \bar{R}H^*[I - (I + H\bar{R}H^*)^{-1}H\bar{R}H^*]$. Since $(I + H\bar{R}H^*)^{-1}H\bar{R}H = I - (I + H\bar{R}H^*)^{-1}$, then $\bar{P}H^* = \bar{R}H^*(I + H\bar{R}H^*)^{-1} = G$.

Result 8.5 The mean-square smoothed state estimation error is given by

$$E(u_p^* u_p) = \mathrm{Tr}\,[\bar{P}]. \tag{8.15}$$

Proof: This follows from the definition of $\bar{P}$ as $\bar{P} = E(u_p u_p^*)$.

Note that many of the above formulas are very similar in form to the ones traditionally encountered in Kalman filtering for dynamical systems. For instance, Eqs. (8.3) and (8.14) are very similar to those used to compute the gain G for a Kalman filter in which $\bar{R}$ and $\bar{P}$ are the covariances of the estimation error associated with the predicted and corrected state estimates. Note also that (8.8) implies that $\bar{P}$ is always smaller than $\bar{R}$, which implies that the covariance of the estimation error after the observation y has been accounted for is smaller than the error covariance before the estimate correction occurs.

Estimation Error Covariance and Kalman-like Gains: Filtering

The aim here is to obtain results similar to results (8.2) - (8.5) above, but that are applicable to the filtered estimate z_o.

Result 8.6 The covariance $E(z_p z_p^*)$ of the filtered state estimation error $z_p = u - z_o$ is given by

$$E(z_p z_p^*) = (I - gH)\,\bar{R}(I - gH)^* + gg^*, \tag{8.16}$$

where $\bar{R} = \Phi BB^*\Phi^*$ is the state covariance, and g is the filter gain in (8.2).

Proof: Note that $u = \Phi Cf + \Phi B\omega$. This and (8.1) imply that

$$z_p = (I - gH)\,\Phi B\omega - gn, \tag{8.17}$$

where use has been made of $y - H\Phi Cf = H\Phi B\omega + n$ in (8.1). Calculation of $E(z_p z_p^*)$, [illegible] (8.17) and the conditions $E(\omega\omega^*) = I$ and $E(nn^*) = I$, leads to (8.16).

This result applicable to the filtered estimate is analogous to (8.7) of the smoothed estimates. To obtain results that are analogous to (8.8) - (8.10) requires, however, a few preliminary definitions and results. The need for these preliminaries arises from the ultimate desire to find a spectral decomposition for the state covariance $\bar{R} = \Phi BB^*\Phi^*$. It is straightforward to obtain the spectral representation for the observed-state covariance $H\tilde{R}H^*$. However, finding a similar decomposition of $\tilde{R}$ is not as simple. The primary reason for this lack of simplicity is that the vectors $\psi_j = \lambda_j^{-1}B^*\Phi^*H^*\phi_j$ may not necessarily span the entire space H. This is particularly true in cases in which the dimension of the input space H_1 is greater than the dimension of the observation space H_3. In order to consider this case, assume that the operator $H\Phi B$ has finite-dimensional range. This corresponds to the situation where there are only a finite number N of sensors and the observed-state covariance $R = H\Phi BB^*\Phi^*H^*$ is an N-by-N matrix. Assume also that the input space is either infinite-dimensional or finite-dimensional with dimension M greater than N. This second assumption corresponds to cases where the uncertainty is distributed at M discrete locations or throughout the entire spatial domain Ω.

Result 8.7 The identity operator I mapping H_1 into itself can be decomposed as

$$I = I_o + I_\perp, \tag{8.18}$$

where

$$I_o = I - B^*\Phi^*H^*R^{-1}H\Phi B, \qquad I_\perp = B^*\Phi^*H^*R^{-1}H\Phi B, \tag{8.19}$$

and $R = H\Phi BB^*\Phi^*H^*$ is the observed-state covariance. In addition, I_o is in the null-space of the operator

$$R(\cdot) = H\Phi B(\cdot)B^*\Phi^*H^*, \tag{8.20}$$

mapping the space of bounded linear transformations on $H_1 \times H_1$ into the space of N-by-N matrices. Furthermore, I_o and $I_\perp$ are orthogonal complements so that

$$I_o^* I_\perp = \mathrm{Tr}\,[I_o I_\perp] = 0. \tag{8.21}$$

Proof: This result and its corresponding proof are illustrated graphically in Fig. 8.2. Eq (8.18) follows from (8.19). Substitution of I_o in (8.19) into (8.20) shows that $R(I_o) = 0$ so that I_o is in the null space of $R(\cdot)$. That I_o and $I_\perp$ are orthogonal complements follows from substitution of (8.19) in (8.21) by calculation of $\mathrm{Tr}\,[I_o I_\perp]$ using (8.19).

Result 8.8 The identity operator I mapping H_1 into itself can be expressed as

$$I = I_o + \sum_{j=1}^{N} \psi_j \psi_j^* \tag{8.22}$$

SPACE OF BOUNDED LINEAR TRANSFORMATIONS
FROM INPUT SPACE INTO ITSELF

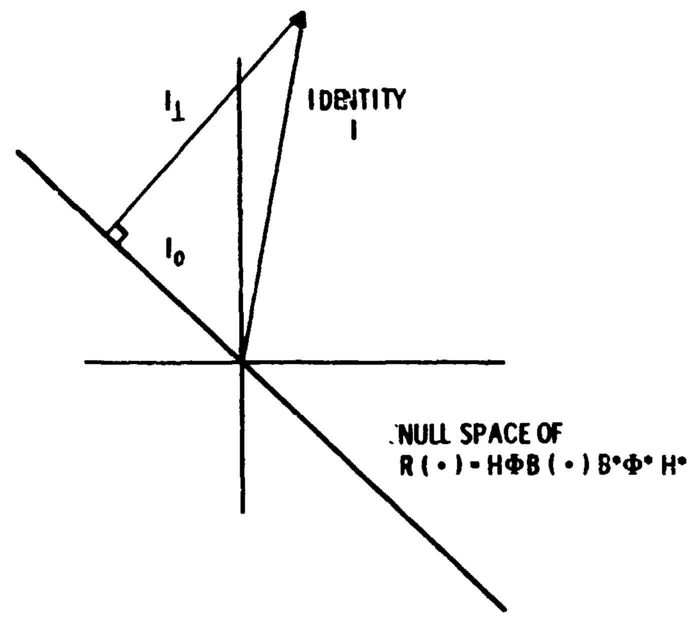

Fig. 8.2 Orthogonal Complement Decomposition of the Identity in $H_1 \times H_1$.

Proof: Substitute $R = \lambda_j^2 \phi_j \phi_j^*$ into $I_\perp$ in (8.19) and use $\psi_j = \lambda_j^{-1} B^* \Phi^* H^* \phi_j$.

The above result simply reflects the fact that the ψ_j do not span H_1, because (by assumption) there are only a finite number of them, and this number is smaller than the dimension of the input space.

Result 8.9 The state covariance $\bar{R} = \Phi BB^*\Phi^*$ can be decomposed as

$$\bar{R} = \bar{R}_o + \sum_{j=1}^{N} \lambda_j^2 x_j x_j^*, \tag{8.23}$$

where

$$\bar{R}_o = \Phi B I_o B^* \Phi^* \tag{8.24}$$

Furthermore,

$$H\bar{R}_o H^* = 0, \; H\bar{R}_o = 0, \; \bar{R}_o H^* = 0. \tag{8.25}$$

Proof: To show (8.23), substitute I from (8.22) into $\bar{R}(I) = \Phi B(I) B^* \Phi^*$, and use $x_j = \lambda_j^{-1} \Phi B \psi_j$. To show (8.25), substitute I_o from (8.19) into (8.24) and (8.25).

<u>Result 8.10</u> The dual state covariance $\bar{Q} = \Phi^*H^*H\Phi$ can be expressed as

$$\bar{Q} = \sum_{j=1}^{N} \lambda_j^2 p_j p_j^* \tag{8.26}$$

where $p_j = \lambda_j^{-1}\Phi^*H^*\phi_j$.

<u>Proof</u>: Since the ϕ_j span the observation space $H_3 = R^N$, then

$$I^N = \sum_{j=1}^{N} \phi_j\phi_j^* \tag{8.27}$$

where I^N denotes the identity in $R^N \times R^N$. To obtain (8.26), substitute (8.27) in $Q = \Phi^*H^*I^NH\Phi$ and use definition of p_j.

Define now the quantities

$$r = (\tfrac{1}{2})\,\bar{R}_0 + \sum_{j=1}^{N} (\sec\alpha_j - 1)\,x_jx_j^*, \quad q = \sum_{j=1}^{N} (\sec\alpha_j - 1)\,p_jp_j^* \tag{8.28}$$

and note the following key identities.

<u>Result 8.11</u> The state covariance $\bar{R} = \Phi BB^*\Phi^*$ and r defined in (8.28) are related by

$$\bar{R} = r + r^* + rH^*Hr. \tag{8.29}$$

Furthermore,

$$I + H\bar{R}H^* = (I+HrH^*)\,(I+Hr^*H^*). \tag{8.30}$$

<u>Proof</u>: Substitute r from (8.28) and $\bar{R}$ from (8.23) into (8.29). Use the orthonormality of x_j with respect to H^*H. This establishes (8.29). Equation (8.30) follows from (8.29) by forming $I+H\bar{R}H^*$ from (8.29) and rearranging terms.

<u>Result 8.12</u> The dual state covariance $\bar{Q}$ in (8.26) and q in (8.28) satisfy the identity

$$\bar{Q} = q + q^* + qBB^*q^*. \tag{8.31}$$

Furthermore,

$$I + B^*\bar{Q}B = (I+B^*qB)\,(I+B^*qB). \tag{8.32}$$

Proof: Substitute $\bar{Q}$ in (3.26) and q in (8.28) into (8.31). Use the orthonormality of p_j with respect to BB^*. This establishes (8.31). To establish (8.32), form $I + B^*\bar{Q}B$ using (8.31, and rearrange terms in the resulting equation.

These are the preliminary results needed to evaluate the covariance of the estimation error associated with the filtered state estimate z_o.

Result 8.13 The filter gain g defined in (8.2) can be expresssed alternatively as

$$g = rH^* (I+HrH^*)^{-1}, \tag{8.33}$$

where r is defined in (8.28).

Proof: Substitute r from (8.28) into (8.33) and use $\bar{R}_o H^* = 0$ and $\phi_j^* = x_j^* H^*$. This recovers g in (8.2).

Note the similarity between (8.3) and (8.33). The equation in (8.3) expresses the smoother gain G in terms of the state covariance $\bar{R} = \Phi BB^*\Phi$. Eq. (8.33) is a similar equation for the filter gain in terms of r. The operator $\bar{R}$ in G can be interpreted as the state covariance. No similar probalistic interpretation for r is known. However, its introduction is very useful because it allows development of formulas for the estimation error covariance and for the filter gain that very closely resemble those obtained for the smoothing solutions.

Result 8.14 The covariance $E(z_p z_p^*)$ of the filtered state estimation error $z_p = u - z_o$ is

$$E(z_p z_p^*) = p + p^*, \tag{8.34}$$

where $p = p^*$ is specified by the alternative formulas

$$p = (I-gH)r(I-gH)^* + gg^* \tag{8.35}$$

$$p = r - rH^* (I+HrH^*)^{-1} Hr, \tag{8.36}$$

$$p = (I-gH)r = r (I-gH)^*, \tag{8.37}$$

$$p = (1/2)\, \bar{R}_o + \sum (1-\cos\alpha_j)\, x_j x_j^*. \tag{8.38}$$

Proof: To establish (8.34) and (8.35), substitute (8.29) in (8.16) and use the identity

$$(I-gH)\, rH^* = rH^* (I + HrH^*)^{-1} = g. \tag{8.39}$$

To establish (8.36), observe that (8.35) implies that

$$p = r - gHr - rH^*g^* + g(I + HrH^*)g^*. \tag{8.40}$$

Substitute $g = rH^* (I + HrH^*)^{-1}$ in (8.40) to obtain (8.36). To obtain (8.37) observe that the second term of (8.36) can be expressed alternatively as gHr and rH^*g^*. To obtain (8.38), substitute r in (8.28) into (8.36) and use orthonormality of ϕ_j.

Result 8.15 The mean-square estimation error associated with the filtered state estimate is given by

$$E(z_p{}^* z_p) = \mathrm{Tr}\,[p + p^*] = \mathrm{Tr}\,[\bar{R}_o] + 2 \sum_{j=1}^{N} (1-\cos\alpha_j)\, x_j{}^* x_j . \tag{8.41}$$

Proof: This result follows from (8.34) and (8.38).

Result 8.16 The filter gain g can be expressed as

$$g = pH^*, \tag{8.42}$$

where p is related to the filtered state estimation error covariance by $E(z_p z_p{}^*) = p + p^*$.

Proof: Since $g = rH^* (I+HrH^*)^{-1}$, then $g = rH^* (I-Hg)^* = rH^* (I-g^*H^*) = r(I-H^*g^*)H^* = r(I-gH)^*H^* = pH^*$.

This equation is analogous to (8.14) in that it expresses an estimator gain in terms of the covariance of the state estimation error.

Result 8.17 The operators $I + HrH^*$ and $I - HpH^*$ are reciprocal, i. e.,

$$(I + HrH^*)^{-1} = I - HpH^*. \tag{8.43}$$

Proof: Recall $(I + HrH^*)^{-1} = I-Hg = I-HpH^*$, where the last equality holds because $g = pH^*$.

Note that this result implies that the operator HpH^* is the Fredholm resolvent of HrH^*. The identity also immediately implies whiteness of the residuals process as investigated in more detail below.

Pseudo-Innovations Properties of the Residuals

Define the residual process in the usual way, as the difference between the actual measurements and the predicted data emerging from the predicted-data-covariance square-root filter, i.e.,

$$e = y - Hz_o \tag{8.44}$$

This process turns out to have two key properties that are nearly identical to those of an innovations process: the residuals are white with a unit covariance; the residuals and the measurements can be obtained from each other by means of reciprocal relationships. These two properties are established in the following results.

Result 8.18 The residual process defined in (8.44) is white with a unit covariance, i.e.,

$$E(ee^*) = I. \tag{8.45}$$

Proof: Observe from (8.1) that $e = (I-Hg)(y-H\Phi cf)$. Hence, $E(ee^*) = (I-Hg)(I+H\bar{R}H^*)(I-Hg)^* = I$. This last equality follows from $E[(y-H\Phi cf)(y-H\Phi Cf)^*] = I + H\bar{R}H^*$ and from (8.42) and (8.43).

Result 8.19 The residuals $e = y-Hz_o$ and the mean-centered measurement process $\bar{y} = y-H\Phi Cf$ can be obtained from each other by means of reciprocal linear transformations, i.e.,

$$e = (I - HpH^*)\bar{y}, \qquad \bar{y} = (I+HrH^*)e \tag{8.46}$$

where

$$(I + HrH^*)^{-1} = (I-HpH^*). \tag{8.47}$$

Proof: Eq. (8.47) has been established in (8.43) and is restated here only to emphasize its relationship to the properties of the residual process. Eq. (8.1) implies $e = (I-Hg)\bar{y}$.

Relationships Between Filtered and Smoothed Estimates

While the smoothed and filtered estimates have been defined somewhat independently of each other, these estimates are in fact very closely related. It is possible to obtain one in terms of the other, as outlined in the following result.

Result 8.20 The smoothed and filtered estimates u_o and z_o are related by

$$u_o = z_o + ge, \tag{8.48}$$

where

$$e = y-Hz_o \tag{8.49}$$

is the residual process, and g is the predicted-data-covariance square-root filter gain.

Proof: Observe that (8.1) and (8.3) imply $u_o = \Phi Cf + \bar{R}H^*(I + H\bar{R}H^*)^{-1}(y-H\Phi Cf)$. Use of (8.46) leads to $u_o = \Phi Cf + \bar{R}H^*(I+HrH^*)^{-1}e$. Similarly, z_o in (8.1) and r in (8.33) lead to $z_o = \Phi Cf + rH^*e$. Hence, $u_o-z_o = [\bar{R}H^*(I+HrH^*)^{-1} - rH^*]e$. Use of the identity (8.29) in this implies that $u_o-z_o = ge$, which is the desired result. Note that (8.48) can be written in the alternative form

$$u_o = (I-gH)z_o + gy. \tag{8.50}$$

Closely related to the above relationship between filtered and smoothed state estimates is a relationship between the corresponding covariances of the state estimation errors. This is developed below.

<u>Result 8.21</u> The filtered state estimation error $z_p = u-z_o$ and the residual process $e = y-Hz_o$ are related by

$$e = n + Hz_p, \tag{8.51}$$

where n is the measurement error.

<u>Proof</u>: Note that $e = y-Hz_o = Hu+n-Hz_o = H(u-z_o)+n = Hz_p + n$

<u>Result 8.22</u> The covariance $\bar{P} = E(u_p u_p^*)$ of the smoothed state estimation error $u_p = u-u_o$ can be expressed as

$$\bar{P} = p + p^* - pH^*Hp, \tag{8.52}$$

where $p + p^* = E(z_p z_p^*)$ is the covariance of the filtered state estimation error $z_p = u-z_o$. Furthermore,

$$I-H\bar{P}H^* = (I-HpH^*)(I-HpH^*). \tag{8.53}$$

<u>Proof</u>: Use (8.52) to obtain

$$E(ez_p^*) = E(nz_p^*) + HE(z_p z_p^*) = E(nz_p^*) + H(p+p^*). \tag{8.54}$$

Now use (8.17) to compute $E(nz_p^*)$, i.e.,

$$E(nz_p^*) = -g^*, \tag{8.55}$$

since $E(n\omega^*) = 0$ by assumption. Substitution of (8.55) in (8.54) and use of $g = pH^*$ leads to

$$E(ez_p^*) = g^*. \tag{8.56}$$

Since $u_p = u-u_o$, then $u_p = z_p - ge$ from (8.48). Hence,

$$E(u_p u_p^*) = E(z_p z_p^*) - g\,E(ez_p^*) - E(z_p e^*)g^* + gE(ee^*)g^*. \tag{8.57}$$

Now use (8.34), (8.43), (8.45) and (8.56) to obtain (8.52). Equation (8.53) follows immediately from (8.52) by forming $I - H\bar{P}H^*$ and rearranging terms in the resulting expression. Note that (8.52) implies that the gains G and g are related by

$$G = g + g - gHg. \tag{8.58}$$

The last three results can be viewed as a generalization to elliptic systems of relationships encountered in filtering and smoothing for dynamical systems. For example, Equation (8.48) is a generalization to elliptic systems of the forward/backward sweep method for solution of two-point boundary-value problems. This method in general terms states that the smoothed states estimates can be obtained as a result of a two-stage process: forward filtering by means of a Kalman filter to obtain a filtered state estimate and a residual process; and backward smoothing to process the residuals and obtain a smoothed state estimate. This two-stage data processing approach has been extensively studied for linear dynamical systems. Eqs. (8.48) and (8.49) have exactly the same structure. This structure is illustrated in Fig. 8.3.

The overall diagram illustrates how the data y[1] and the deterministic input f[2] are processed to arrive at a smoothed estimate u_o[3]. The estimation process consists of two stages: a FILTERING stage that results in a filtered estimate z_o[4] and a residual process[5]. This filtering stage is characterized by a predictor-corrector structure where a predicted estimate[6] is first produced and then corrected by a correction term.[7] The results of the filtering stage are then processed by the SMOOTHING stage. Central to both the filtering and smoothing stages is the gain g[8]. The foregoing structure is nearly identical to that of the forward/backward sweep method in linear dynamical systems. There are, however, some key differences. One of the differences is that the filtering stage in the case of dynamical systems is based on the Kalman filter, whereas in the elliptic case under consideration here, this filter is replaced by the predicted-data-covariance square-root filter. Another key difference is that the Kalman filter is causal whereas the predicted-data covariance square-root filter is not, i.e., the filter gain g is a Fredholm operator as opposed to being a Volterra operator. In the same vein, the smoothing stage for dynamical systems is backward (in time) or anticausal. In the elliptic system case, however, the smoothing stage is also characterized by Fredholm operators. The notion of causality is not even introduced here although it is possible to do this for certain classes of elliptic systems [1].

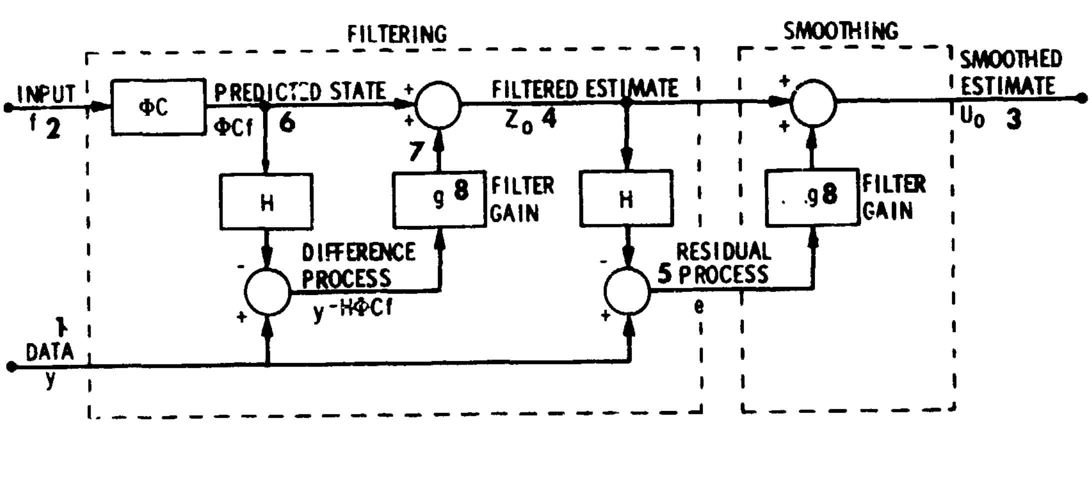

Fig. 8.3 Filtering and Smoothing

Spectral Representations: Smoothing, Filtering, and the Residuals

The aims here are: to obtain spectral representations for the filtered and smoothed estimates u_o and z_o and the corresponding error covariances $\bar{P}$ and p; to explore the predictor-corrector structure of the spectral representations of the filter and smoother; and to investigate the pseudo-innovations properties of the spectral representation of the residual process. The term "spectral representation" means the use of an expansion in terms of the eigensystem ϕ_j of R and of the related functions

$\psi_j = \lambda_j^{-1}B^*\Phi^*H^*\phi_j$, $x_j = \lambda_j^{-1}\Phi B\psi_j$ and $p_j = \lambda_j^{-1}\Phi^*H^*\phi_j$.

Result 8.23 The smoothed state estimate u_o can be represented as

$$u_o = \Phi Cf + \sum \sin^2\alpha_j (y_j - m_j) x_j, \tag{8.59}$$

where $y_j = \phi_j^*y$ and $m_j = \phi_j^*m$ are the spectral components of the data y and the suspected mean $m = H\Phi Cf$. The related observed-state estimate Hu_o is specified by

$$Hu_o = m + HG(y-m), \quad Hu_o = (I-HG)m + HGy. \tag{8.60}$$

In spectral form, $Hu_o = \sum u_o^j\phi_j$ where

$$u_o^j = m_j + \sin^2\alpha_j (y_j - m_j), \quad u_o^j = \cos^2\alpha_j m_j + \sin^2\alpha_j y_j, \tag{8.61}$$

and $u_o^j = \phi_j^*Hu_o$. Let $u_p = u - u_o$ denote the estimation error. The error covariances $\bar{P} = E(u_p u_p^*)$ and $H\bar{P}H^* = E(u_p^*H^*Hu_p)$ are represented by

$$\bar{P} = \bar{R}_o + \sum \sin^2\alpha_j x_j x_j^* \qquad H\bar{P}H^* = \sum \sin^2\alpha_j\phi_j\phi_j^*. \tag{8.62}$$

Furthermore, the corresponding mean-square estimation errors $E(u_p^*u_p) = Tr[\bar{P}]$ and $E(u_p^*H^*Hu_p) = Tr[H\bar{P}H^*]$ are

$$E(u_p^*u_p) = Tr[\bar{R}_o] + \sum \sin^2\alpha_j x_j^*x_j, \quad E(u_p^*H^*Hu_p) = \sum \sin^2\alpha_j \tag{8.63}$$

Proof: To establish (8.59), substitute $y = \Sigma y_j\phi_j$ and $m = \Sigma m_j\phi_j$ in (8.1). To show (8.60) multiply u_o in (8.1) by H and recall that $m = H\Phi Cf$. To establish 8.61, multiply (8.60) by ϕ_j^*. The equation for $\bar{P}$ in (8.62) follows by substitution of (8.23) in (8.8) and use of the conditions $H\bar{R}_o = \bar{R}_oH^* = H\bar{R}_oH^* = 0$. The equation for $H\bar{P}H^*$ in (8.62) follows from $\bar{P}$ and use of $\phi_j = Hx_j$. Eq (8.63) follows from (8.62) and the orthonormality of ϕ_j.

<u>Result 8.24</u> The filtered state estimate z_o can be represented by

$$z_o = \Phi Cf + \sum (1-\cos\alpha_j)(y_j - m_j)\, x_j, \tag{8.64}$$

The related observed state estimate $z = Hz_o$ is

$$z = m + Hg(y-m), \qquad z = (I-Hg)\, m + Hgy. \tag{8.65}$$

In spectral form, $z = \sum z_j \phi_j$

$$z_j = m_j + (1-\cos\alpha_j)(y_j - m_j), \qquad z_j = \cos\alpha_j\, m_j + (1-\cos\alpha_j)\, y_j. \tag{8.66}$$

Let $z_p = z - z_o$ denote the estimation error. The estimation error covariances $E(z_p z_p^*) = p + p^*$ and $E(Hz_p z_p^* H^*) = H(p + p^*)H^*$ can be represented as

$$p = (1/2)\ \bar{R}_o + \sum (1-\cos\alpha_j)\, x_j x_j^*, \qquad HpH^* = \sum (1-\cos\alpha_j)\, \phi_j \phi_j^*. \tag{8.67}$$

Furthermore, the corresponding mean-square estimation errors are

$$E(z_p^* z_p) = Tr(p + p^*), \quad E(z_p^* H^* H z_p) = Tr\,[H(p + p^*)H^*], \tag{8.68}$$

where

$$Tr\,[p] = (1/2)\, Tr\,[\bar{R}_o] + \sum (1-\cos\alpha_j)\, x_j^* x_j, \quad Tr\,[HpH^*] = \sum (1-\cos\alpha_j). \tag{8.69}$$

<u>Proof</u>: To show (<u>8.64</u>), substitute $y = \Sigma y_j \phi_j$ and $m = \Sigma m_j \phi_j$ into z_o in (8.1). Eq. (<u>8.65</u>) follows from multiplication of (8.64) by H and use of $m = H\Phi Cf$. Eq. (<u>8.66</u>) is obtained from (8.65) upon multiplication by ϕ_j^* and use of the orthonormality of ϕ_j. The equation for p in (<u>8.67</u>) has been established in (8.38) and is repeated here only for convenience. The second of Eq. (<u>8.67</u>) follows from use of the identity $\phi_j = Hx_j$. Eq. (<u>8.68</u>) follows from the definition of $p = p^*$ in (8.38). Eq. (<u>8.69</u>) is established by performing the trace operation on (8.67).

<u>Result 8.25</u> The residual process $e = y - Hz_o$ can be represented as

$$e = \sum e_j \phi_j, \quad e_j = \phi_j^* e. \tag{8.70}$$

The spectral components e_j are independent random variables with zero-mean and unit covariance, i.e.,

$$E(e_i e_j) = 0 \text{ for } i \neq j, \qquad E(e_i^2) = 1. \tag{8.71}$$

Furthermore, the spectral components e_i and y_i of the residual and difference processes $e = y - Hz_0$ and $y = \bar{y} - m$ are related by the reciprocal relationships

$$e_i = \cos\alpha_i \, \bar{y}_i, \qquad \bar{y}_i = \sec\alpha_i \, e_i. \tag{8.72}$$

Proof: Eq. (8.70) is valid because ϕ_i are orthonormal in H To show (8.71), observe that $E(e_i e_j) = \phi_i^* \, \Xi(ee^*) \, \phi_j$ and then use (8.45) and the orthonormality of ϕ_j. Equations (8.72) are the spectral representations of the reciprocal relationships (8.47). Note that (8.72) can also be established by the simple trigonometric identity $(1/\cos\alpha_i) = \sec\alpha_i$.

9. NUMERICAL SEARCH CALCULATION SUMMARY

Since the development of the estimation approach is rather lengthy, it is convenient to summarize the steps that are required to implement the numerical search.

It is assumed that the process starts with a known input f, a set of data y and an initial parameter estimate θ^n. To conduct an iteration in the numerical search requires that the following steps be performed:

1. Compute the suspected mean and covariance $m = H\Phi Cf$ and $R = H\Phi BB^*\Phi^*H^*$.
2. Compute the eigenvalues λ_k^2 and eigenvectors ϕ_k of R.
3. Compute the related vectors $p_k = \lambda_k^{-1}\Phi^*H^*\phi_k$, $\psi_k = B^*p_k$ and $x_k = \lambda_k^{-1}\Phi B\psi_k$.
4. Conduct a spectral analysis of the data and of the suspected mean to obtain the spectral coefficients $y_k = \phi_k^*y$ and $m_k = \phi_k^*m$.
5. Use Result 6.5 to evaluate the gradient $\partial J/\partial\theta$ of the likelihood functional.
6. Use Results 6.6 and 6.7 to compute the Hessian M_n and to determine the incremental change $\delta\theta^n$ of the parameter estimates.
7. Obtain a new parameter estimate $\theta^{n+1} = \theta^n - \delta\theta^n$, return to step 1 above, and iterate through steps 1 to 6 until convergence is achieved.

If Cramer-Rao bounds and/or an optimal input are desired use (7.6) - (7.13). If the covariance of the state estimation error is desired use Result 8.2 and/or 8.13.

The calculations involved in conducting a single iteration in the maximum-likelihood parameter estimation approach are summarized in block diagram form in Fig. 9.1 A single iteration consists of all of the computational steps required to obtain an updated parameter estimate θ^{n+1} by processing the available data, the known deterministic input, and the current parameter estimate θ^n.

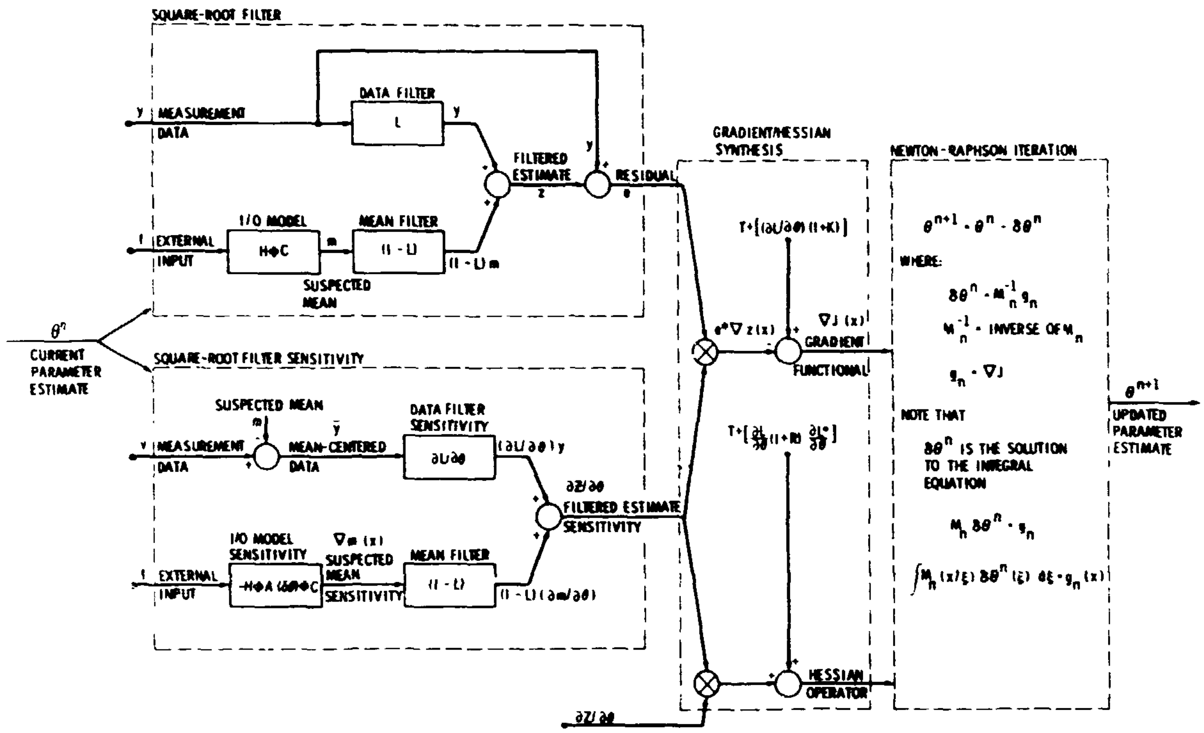

Fig. 9.1 Calculations Required for Single Iteration in Modified Newton-Raphson Search

To simplify the description of these computations, the steps performed in a single iteration have been grouped into the following four major blocks (delineated by the broken lines in the diagram):

- **a SQUARE-ROOT FILTER block that processes the measurement data y and the external input f to obtain a filtered estimate z and a corresponding residual process e, defined as the difference between the data and the filtered state estimate. The square-root filter implements the equations $z = Ly + (I-L)m$ and $e = y-z$. The central computation in the square-root filter block is that provided by the operator $L = I - (I+R)^{-1/2}$ defined in terms of the square-root of the predicted-data-covariance $(I + R)$. This operator appears in two distinct places in the diagram: in the <u>data filter</u>, whose primary function is to process the measurements y; and in the <u>mean filter</u>, whose main function is to process the suspected mean m. The suspected mean is in turn obtained from the known external input by means of the input-output model.**

- a SQUARE-ROOT FILTER SENSITIVITY block that processes the measurement data y and the deterministic input f to obtain the filtered estimate sensitivity $\partial z/\partial\Theta$. This block implements the equation $\partial z/\partial\Theta = (\partial L/\partial\Theta)(y-m) + (I-L)(\partial m/\partial\Theta)$. The computation of the sensitivity $\partial L/\partial\Theta$ is the main calculation performed in this block.

- a GRADIENT-HESSIAN SYNTHESIS block that forms: the function-space gradient $\partial J/\partial\Theta$ of the likelihood functional by means of the equation $\partial J/\partial\Theta = Tr[(\partial L/\partial\Theta)(I+K) - (\partial z/\partial\Theta)e^*]$; and the function-space approximate Hessian by means of the equation $M = Tr\,[(\partial L/\partial\Theta)(I+R)(\partial L^*/\partial\Theta)] + (\partial z/\partial\Theta)^*(\partial z/\partial\Theta)$. Note that the quantity that is actually evaluated in this block is the kernel $M(x/\xi)$ of the Hessian operator. This kernel is a function of two spatial variables x and ξ defined over a "square" domain $(x/\xi)\epsilon\Omega \times \Omega$, where Ω is as before the spatial domain of definition of the system model.

- a NEWTON-RAPHSON ITERATION block whose input is the gradient and the approximate Hessian and that generates as an output the updated parameter distribution Θ^{n+1} for the next iteration. The central calculation in this block is the solution of the integral equation $M_n\delta\Theta^n = g_n$ that results in the parameter estimate update $\delta\Theta^n$.

After specification of the parameter estimate Θ^{n+1}, the square-root filter $L(\Theta^n)$ and its sensitivity $\partial L(\Theta^n)/\partial\Theta$ are redesigned by letting $\Theta^n \to \Theta^{n+1}$, and the steps outlined above are repeated in order to conduct the next step in the iterative process for optimization.

The predicted-data-covariance square-root filter processes the data y and the suspected mean m to produce a filtered state estimate z and a set of residuals $e = y-z$. This is done by means of the equation $z = Ly + (I-L)m$, where $L = I-(I+R)^{-1/2}$. This equation, while providing a very succinct symbolic description of the square-root filter, does not by itself provide a recipe to conduct computations. In order to provide such a recipe, it is convenient to use the corresponding spectral form $z_k = (1-\cos\alpha_k)y_k + \cos\alpha_k m_k$, which expresses the spectral amplitudes $z_k = \phi_k{}^*z$ of the filtered state estimate z as a linear combination of the data and suspected mean spectral amplitudes y_k and m_k. Such a spectral form of the predicted-data-covariance square-root filter is illustrated in Fig. 9.2.

The diagram in the figure illustrates the main calculations involved in the square-root filter. On the upper branch of the diagram, a set of data[1] $y = [y_1,\ldots,y_N]$ is assumed to be available at N discrete locations. A spectral analysis[2] is conducted on this data to obtain the data spectral amplitudes[3] $[y^1,\ldots,y^N]$. These spectral amplitudes are then multiplied by the coefficients $(1-\cos\alpha_k)$ in the data filter[4], resulting in the terms $(1-\cos\alpha_k)y^k$. On the lower branch of the diagram, the deterministic inputs f_i[6] are processed by the input/output system model[7] to obtain the suspected mean $m = [m_1, \ldots, m_N]$[8]. The spectral amplitudes $m^k = \phi_k * m$[9] of the suspected mean are then computed and subsequently multiplied by the coefficients $\cos\alpha_k$ in the mean filter[10] to produce the terms $\cos\alpha_k m^k$ [11]. This last term is then added to $(1-\cos\alpha_k)y^k$ in[5] resulting in the filtered state spectral amplitudes z_k[12] and the residuals e_k[13]. Note that the physical state estimate z and the residual e can be recovered from z_k and e_k by means of the summations $z = \Sigma z_k \phi_k$ and $e = \Sigma e_k \phi_k$, although for simplicity this last transformation is not shown on the diagram.

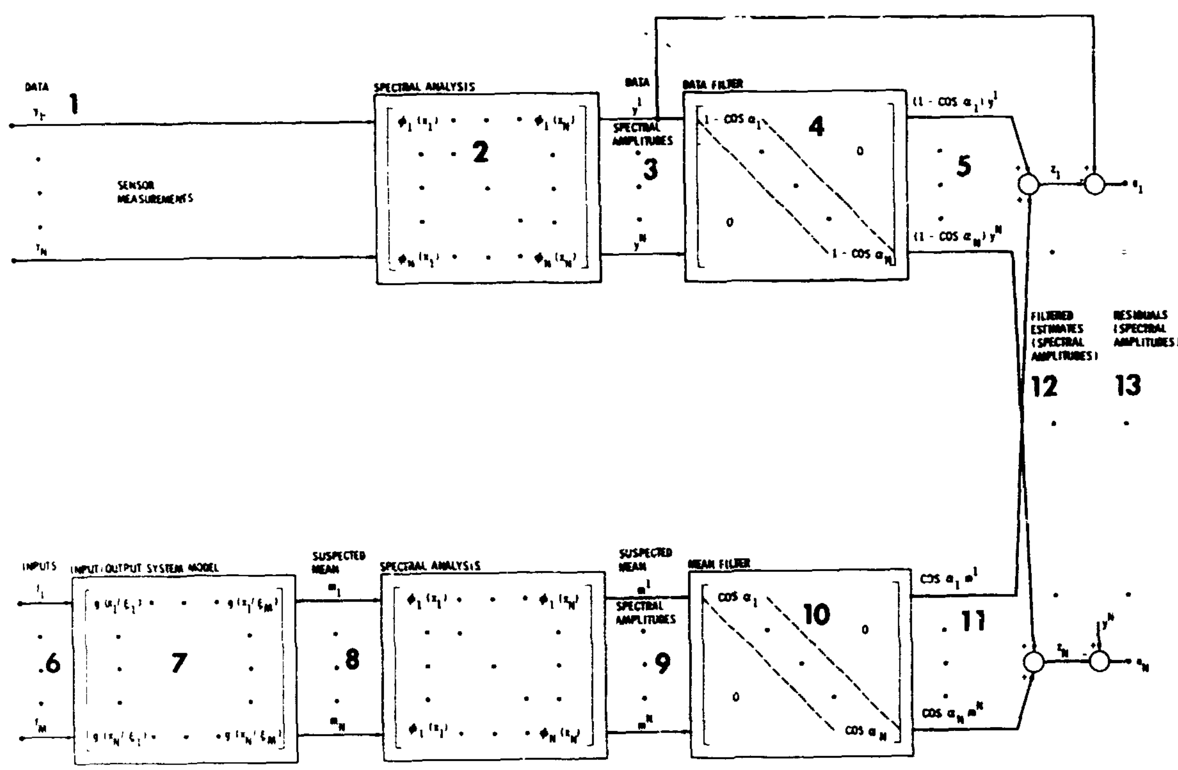

Fig. 9.2 Spectral Form of Predicted-Data-Covariance Square-Root Filter

The foregoing remarks have scrutinized the spectral form of the square-root filter equation $z = Ly + (I-L)m$. The immediate aim now is to conduct a similar detailed analysis of the spectral representation of the square-root filter sensitivity equation $\partial z/\partial\theta = (\partial L/\partial\theta)y + (I-L)(\partial m/\partial\theta)$. The spectral form of this equation is stated in Eq. (6.15) and illustrated in the block diagram in Fig. 9.3. The overall primary function of the square-root filter sensitivity is to process the N mean-centered data spectral amplitudes[1] and the M deterministic inputs[2] in order to obtain the spectral amplitudes of[3] of the filtered state estimate sensitivity $\partial z/\partial\theta$. An intermediate calculation embedded within this overall process involves processing of the mean-centered data spectral amplitudes y^{k}[1] by means of the N-by-N matrix, with general elements a_{km}, representing the data filter sensitivity $\partial L/\partial\theta$[4]. Other intermediate steps involve: processing of the deterministic inputs f_m [2] by the input/output model sensitivity matrix b_{km} [5] to generate the suspected mean spectral amplitudes $(\partial m/\partial\theta)_k$ [6]; and subsequent processing of these coefficients by the mean filter [7] to obtain the terms $\cos\alpha_k\,(\partial m/\partial\theta)_k$ [8].

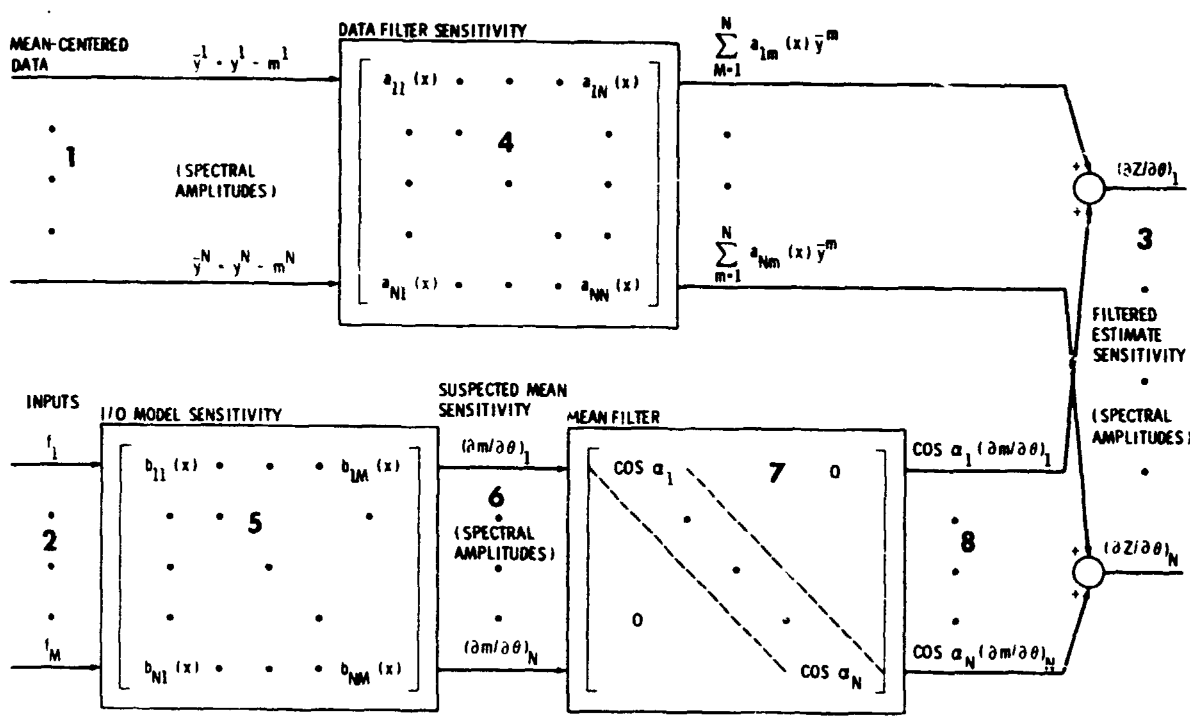

Fig. 9.3 Spectral Form of Square-Root Filter Sensitivity

10. CONCLUDING REMARKS AND FUTURE DIRECTIONS

The area of estimation for elliptic systems is so full of interesting research problems that, in spite of all that this paper has covered, much more remains to be done. These are some of the problems that lie ahead:

- Conduct of an asymptotic statistical property analysis that explores the convergence of the parameter estimates as the number of observations increases.

- Development of approximation approaches that rigorously arrive at finite-dimensional approximations to the infinite-dimensional solutions advanced here.

- More complete investigation of the optimal input design problem. In particular, development of "spectral" domain design approaches which would do for elliptic systems what the frequency domain methods achieve for linear time - invariant dynamical systems.

- Development of more precise mathematical arguments to justify function-space differentiation, eigensystem expansions, covariance calculations, likelihood-ratio derivations, etc.

- Investigation of alternative (to the square-root) factorization of the predicted-data-covariance that could result in easier calculation of the function-space derivatives necessary for the Newton-Raphson search.

- Numerical experimentation with the filtering, smoothing and identification algorithms to gain further insight into the state and parameter estimation approaches and solutions [5].

As a final remark, this paper is a concrete example of the power of the functional analysis approach to estimation advanced in Ref. [4]. Because of the conceptual simplicity of the method, it has been possible to solve in this paper problems that would have defied solution by any other method. It has also made it possible to conceive areas for future research that would otherwise have been left unidentified.

REFERENCES

1. Rodriguez, G., "A Function Space Approach to State and Model Error Estimation for Elliptic Systems," Proceedings of the Workshop on Applications of Distributed System Theory to the Control of Large Space Structures, JPL Publication 83-46, July 1983.

2. Luenberger, D. G., Optimization by Vector Space Methods, Prentice-Hall, 1971.

3. Balakrishnan, A. V., Communication Theory, McGraw-Hill, 1968.

4. Balakrishnan, A. V., Applied Functional Analysis, Springer-Verlag, 1977.

5. Scheid, R. E. and G. Rodriguez, "Numerical Experimentation with Maximum Likelihood Identification in Static Distributed Systems", Proceedings of NASA/JPL/LRC Workshop on Identification and Control of Flexible Space Structures, San Diego, CA., June 1984.

ACKNOWLEDGEMENT

The research described in this paper was carried out at the Jet Propulsion Laboratory, California Institute of Technology, under contract with the National Aeronautics and Space Administration.

N85-31214

NUMERICAL EXPERIMENTATION WITH MAXIMUM LIKELIHOOD IDENTIFICATION IN STATIC DISTRIBUTED SYSTEMS

R. E. Scheid, Jr., and G. Rodriguez
Jet Propulsion Laboratory
California Institute of Technology
Pasadena, CA 91109

1. INTRODUCTION

Many important issues in the control of large space structures are intimately related to the fundamental problem of parameter identification. Very often, a complicated structure can be adequately modeled for certain operations by the fitting of a rather simple model with a number of free parameters. This simple model then can be referenced for necessary control operations. Important applications include the many space station designs which are based on the assembly and joining of discrete modules by crew members. This crew-assisted construction will result in a configuration which is a large-scale composite of many structural elements and whose static and dynamic characteristics cannot be adequately modeled in advance. In fact, any modeling will require periodic updating as more modules are added to the system and as the structural properties of the elements slowly change over the lifetime of the station.

One might also ask how well this identification process can be carried out in the presence of noisy data since no sensor system is perfect. With these considerations in mind our algorithms are designed to treat both the case of uncertainties in the modeling and uncertainties in the data.

This paper serves as a companion to [6] where the analytical aspects of maximum likelihood identification are considered in some detail. Here we focus on the questions relevant to the implementation of these schemes, particularly as they apply to models of large space structures. Our emphasis will be on the influence of the infinite-dimensional character of the problem on finite-dimensional implementations of the algorithms. We highlight those areas of current and future analysis which indicate the interplay between error analysis and possible truncations of the state and parameter spaces.

2. MODELS

As in [6], we consider the systems of the form

$$\begin{aligned} A(\Theta)u(\Theta) &= \sigma_{\omega}B(\Theta)\omega + C(\Theta)f \\ y(\Theta) &= H(\Theta)u(\Theta) + \sigma_{\eta}\eta \end{aligned} \tag{2.1}$$

Here A is a formally self-adjoint elliptic differential operator defined over the spatial domain Ω; the integral operator Φ is related to A by

$$A\Phi = I \quad , \tag{2.2}$$

where I is the identity. B and C are appropriately dimensional operators that model the influence of the process error ω and the input f on the state u. H is an operator that characterizes the state-to-observation map; ω amd η are model errors that form the model error vector

$$\epsilon = [\omega, \eta], \tag{2.3}$$

and f is a deterministic input. Conceptually the error vector ϵ represents spatial white noise and is characterized by the covariance operator

$$E(\epsilon\epsilon^*) = I.$$

σ_ω and σ_η are non-negative scalar weighting parameters that respectively measure the relative importance of the modeling error and the measurement error. Thus, the limit $\sigma_\omega \to 0$ corresponds to the case of perfect modeling while the limit $\sigma_\eta \to 0$ corresponds to the case of perfect measurements.

Θ is the possibly infinite-dimensional parameter which must be estimated. For simplicity we shall generally consider cases where the parameter dependence is restricted to the operator A. Furthermore, we assume as in [6] that the parameter enters linearly into the expression for the potential energy of the system. Thus we assume

$$A(\Theta)u = D^*(\Theta Du) \tag{2.4}$$

where D^* denotes the formal adjoint of D; the corresponding potential energy is given in terms of the appropriate state-space inner-product:

$$\langle A(\Theta)u,u\rangle = \langle \Theta Du, Du\rangle. \tag{2.5}$$

And finally, the deterministic and stochastic forcings will be localized to discrete points which might correspond to actuator locations. Similarly, the observation map returns a vector of observations at discrete points which might correspond to sensor locations. We assumed that there are N_s point-sensors at locations $\{\xi_i\}$ and N_a point-actuations at locations $\{\tilde{\xi}_i\}$.

Because of these last assumptions, many of the relevant calculations outlined in [6] reduce to matrix and vector manipulations. In this paper the notation $\vec{g}$ will refer to a finite-dimensional vector whose k-th component is given by $g^{(k)}$. Similarly $\underset{\sim}{G}$ is the notation for a matrix whose (i,j)-component is given by $G^{(i,j)}$. The relevant dimensions of vector and matrix quantities will always be clear from the context.

After taking formal limits in the system (2.1) we have:

$$\begin{aligned} Au &= \sigma_\omega B\vec{\omega} + C\vec{f} \\ \vec{y} &= Hu + \sigma_\eta \vec{\eta} \end{aligned} \tag{2.6}$$

where

$$\vec{\omega} = (\omega^{(1)}, \ldots, \omega^{(N_a)})^T \tag{2.7a}$$

$$\vec{\eta} = (\eta^{(1)}, \ldots, \eta^{(N_s)})^T \tag{2.7b}$$

$$Hu(x) = (u(\xi_1), \ldots, u(\xi_{N_s}))^T \tag{2.7c}$$

$$H^*\vec{g} = \sum_{i=1}^{N_s} \delta(x-\xi_i) g^{(i)} \tag{2.7d}$$

$$C\vec{f} = \sum_{i=1}^{N_a} \delta(x-\tilde{\xi}_i) f^{(i)} \tag{2.7e}$$

$$C^*u(x) = (u(\xi_1), \ldots, u(\xi_{N_a}))^T \tag{2.7f}$$

$$B\vec{\omega} = \sum_{i=1}^{N_a} \delta(x-\xi_i) \omega^{(i)} \tag{2.7g}$$

$$B^*u(x) = (u(\xi_1), \ldots, u(\xi_{N_a}))^T \tag{2.7h}$$

Even in the case of more general sensing and actuating systems, the modeling requirements for the system can be reduced to solving equations of the form

$$Au = f. \tag{2.8}$$

Thus the discussion in this section will focus on how the infinite-dimensional structure of the system (2.8) influences the choice of finite-dimensional approximations which can be made. In this paper we consider two specific structural models: a string under tension and a wrap-rib antenna.

Let $\hat{x}$ be a distance coordinate measured in meters along a string of Length L which is also given in meters. Let $\hat{u}(\hat{x})$ be the displacement in meters and let $\hat{\alpha}(\hat{x})$ be the tension parameter given in units of newtons. The forcing density is given by $\hat{f}(\hat{x})$ in units of newtons/meter. Then the energy potential [3] is given by

$$\hat{V}(\hat{u}) = \frac{1}{2} \int_0^L \hat{\alpha}(\hat{x})(\hat{u}'(\hat{x}))^2 \, d\hat{x} - \int_0^L \hat{f}(\hat{x}) \, \hat{u}(\hat{x}) \, d\hat{x}. \tag{2.9}$$

Of course the energy potential is given in units of newton-meters. The equations of motion can be derived immediately based on the principles of the calculus of variations but it will be convenient to first transform to dimensionless coordinates. Let $\hat{\alpha}_*$ be some characteristic value of the tension parameter. We introduce the dimensionless variables:

$$x = \frac{\hat{x}}{L}$$

$$\alpha(x) = \frac{\hat{\alpha}(\hat{x})}{\hat{\alpha}_*}$$

$$u(x) = \frac{\hat{u}(\hat{x})}{L} \tag{2.10}$$

$$f(x) = \frac{\hat{f}(\hat{x})L}{\hat{\alpha}_*}$$

$$V(u) = \frac{\hat{V}(\hat{u})}{\hat{\alpha}_* L}$$

and the potential expression becomes

$$V(u) = \frac{1}{2}\int_0^1 \alpha(x)\,(u'(x))^2\,dx - \int_0^1 f(x)u(x)dx. \tag{2.11}$$

For simplicity we prescribe boundary conditions corresponding to fixed end points:

$$u(o) = u(1) = o \tag{2.12}$$

Then arguments based on the calculus of variations give the system

$$\begin{aligned} &(\alpha(x)u'(x))' = f(x) \\ &u(o) = u(1) = 0 \qquad 0 < x < 1 \end{aligned} \tag{2.13}$$

This example has been studied many times in the classical literature but an analogous approach gives comparable expressions for much more complex systems.

We consider now a planar model for a wrap-rib antenna which is used to study out-of-plane vibrations (see Figure 1). The antenna model comprises N gores (subsections) modeled by interconnected ribs and mesh. Since the transformations are similar to those used in the case of the string, we immediately write the potential expression with dimensionless coordinates. Let the vector of rib displacements be $\vec{u}(r)$ where the k-th component of $\vec{u}$ is $u^{(k)}$, the displacement of the k-th rib $(0 < r < 1)$. Let the vector of mesh displacements be $\vec{v}(r,\Theta)$ where the k-th component of $\vec{v}$ is $v^{(k)}$ the displacement of the k-th mesh sector $(0 < r < 1,\ 0 < \Theta < 1)$.

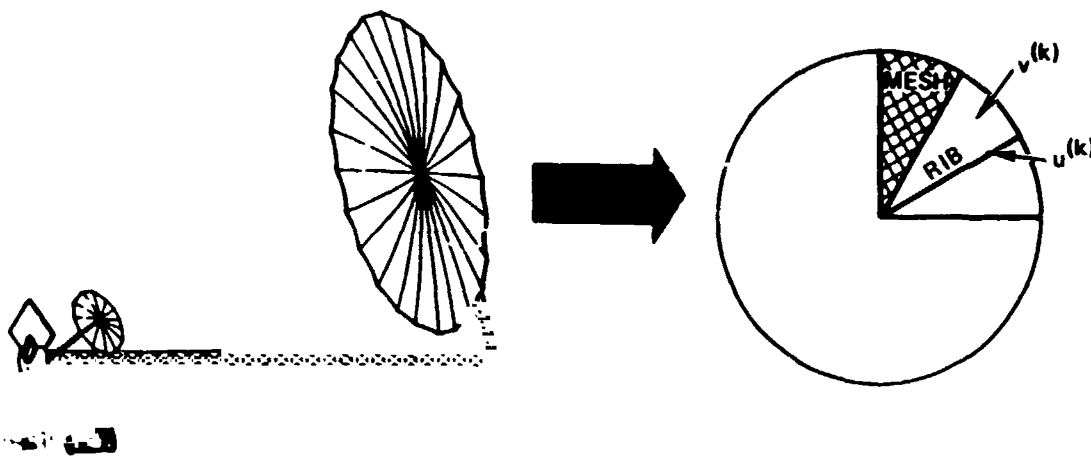

Fig. 1 Simplified model for wrap-rib antenna

Based on analysis of actual antenna designs, our model consists of N identical beams fixed at a central hub. Stretched between the beams are N identical anisotropic membranes. The potential equation is given by

$$V = \frac{1}{2} \int_0^1 G_1 \frac{d^2\vec{u}}{dr^2}^* \frac{d^2\vec{u}}{dr^2} dr + \frac{1}{2} \int_0^1 \int_0^1 G_2 \, r \frac{\partial \vec{v}}{\partial r}^* \frac{\partial \vec{v}}{\partial r} dr\, d\theta + \frac{1}{2} \int_0^1 \int_0^1 G_3 \frac{1}{r} \frac{\partial \vec{v}}{\partial \theta}^* \frac{\partial \vec{v}}{\partial \theta} dr\, d\theta - \int_0^1 \vec{F}_R^* \vec{u}\, dr - \int_0^1 \int_0^1 \vec{F}_M^* \vec{v}\, r\, dr\, d\theta \tag{2.14}$$

Here the coefficients $\{G_i\}$ are related to the physical parameters of the beams and membranes thusly:

$$G_1 = \frac{EI_o}{\sigma L}$$

$$G_2 = \frac{T_r \theta_o L^2}{\sigma} \tag{2.15}$$

$$G_3 = \frac{T_\theta L^2}{\sigma \theta_o} .$$

E and I_o are respectively the Young's modulus and the moment of inertia of the beams. T_r and T_θ are respectively the radial and circumferential tensions of the membrane. L is the radius of the antenna and θ_o is the angular width of a sector; that is, we have

$$\theta_o = \frac{2\pi}{N} \quad , \tag{2.16}$$

where N is the number of gores. Finally, σ is some convenient scaling parameter with the dimensions of energy (nt-m). We note that the physical forcing densities $\vec{F}_R$ and $\vec{F}_M$ having respective dimensions nt/m and nt/m² were rescaled according to

$$\begin{aligned} \vec{F}_R &= \frac{L^2}{\sigma} \hat{\vec{F}}_R \\ \vec{F}_M &= \frac{L^3}{\sigma} \hat{\vec{F}}_M \end{aligned} \tag{2.17}$$

Appropriate geometrical boundary conditions follow from fixing the center and attaching each of the ribs to its adjoining membranes:

$$\begin{aligned} \vec{u}\Big|_{r=o} &= \frac{\partial}{\partial r}\vec{u}\Big|_{r=o} = o \\ \vec{v}\Big|_{\theta=o} &= \underset{\sim}{C}\,\vec{v}\Big|_{\theta=1} = \vec{u} \end{aligned} \tag{2.18}$$

Here $\underset{\sim}{C}$ is an N x N periodic matrix:

$$\underset{\sim}{C} = \begin{bmatrix} 0 & 1 & & & \\ & \ddots & \ddots & & \\ & & \ddots & \ddots & \\ & & & \ddots & 1 \\ 1 & & & & 0 \end{bmatrix} \tag{2.19}$$

As in the case of the string, the equations now follow from arguments based on the calculus of variations:

$$\frac{d^2}{dr^2}\left(G_1 \frac{d^2}{dr^2}\vec{u}\right) - G_3\left(\frac{\partial}{\partial\theta}\vec{v}\Big|_{\theta=0^+} - \underset{\sim}{C}\frac{\partial}{\partial\theta}\vec{v}\Big|_{\theta=1^-}\right) = \vec{F}_R \qquad (2.20a)$$

$$-\frac{1}{r}\frac{\partial}{\partial r}\left(G_2 r \frac{\partial\vec{v}}{\partial r}\right) - \frac{1}{r^2}\frac{\partial^2}{\partial\theta^2}\left(G_3\vec{v}\right) = \vec{F}_M \qquad (2.20b)$$

with the additional natural boundary conditions:

$$\left.\frac{\partial^2\vec{u}}{\partial r^2}\right|_{r=1} = 0$$

$$\left.\frac{\partial^3\vec{u}}{\partial r^3}\right|_{r=1} = 0 \qquad (2.21)$$

$$\left.\frac{\partial\vec{v}}{\partial r}\right|_{r=1} = 0$$

One of the focuses of this study is the consideration of nonmodal approaches in the finite-dimensional approximation schemes. In practice, this generally will mean directly solving a linear system of equations rather than proceeding from some finite modal synthesis. But the infinite-dimensional structure of the system (2.8) also can influence the particular finite-dimensional approximation schemes used. Our approach is sufficiently general so that any adequate finite element model of the system (2.8) should yield adequate numerical approximations. But one can often do much better for a particular model or a particular class of models.

We use the antenna model to illustrate the point and make some observations that should influence the approximation schemes regardless of which finite element or finite difference scheme is employed. We emphasize that these considerations also apply to much more complicated antenna models which share salient features with the system (2.18) - (2.21). First we note that the structure is periodic in the θ-direction. This cyclic symmetry leads to considerable savings in the computation of solutions to (2.8). This can be deduced from either the differential equation or the energy expression (2.14). The periodic matrix $\underset{\sim}{C}$ can be diagonalized by means of a finite Fourier transform [1]. That is, let $\underset{\sim}{U}$ be the N x N matrix whose (j,k) component has the form

$$U^{(j,k)} = \frac{\exp\left(i\,\frac{2\pi}{N}\,(j-1)(k-1)\right)}{\sqrt{N}} \qquad (2.22)$$

We then have:

$$\underset{\sim}{U}^*\underset{\sim}{U} = \underset{\sim}{I}$$

$$\underset{\sim}{U}^*\underset{\sim}{C}\underset{\sim}{U} = \underset{\sim}{\Lambda} = \operatorname*{diag}_{j} \quad \exp\left(i \frac{2\pi}{N}(j-1)\right) \tag{2.23}$$

This transformation decouples the system since the potential expression (2.10) with

$$\begin{aligned} \vec{\tilde{u}} &= \underset{\sim}{U}^* u \\ \vec{\tilde{v}} &= \underset{\sim}{U}^* v \\ \vec{\tilde{F}}_R &= \underset{\sim}{U}^* F_R \\ \vec{\tilde{F}}_M &= \underset{\sim}{U}^* \vec{F}_m \end{aligned} \tag{2.24}$$

has the same form as the original system except that the matrix $\underset{\sim}{C}$ is replaced by the diagnonal matrix $\underset{\sim}{\Lambda}$. The differential system (2.20) is likewise transformed. Thus any particular solution of (2.8) can be expressed in terms of N subsystems each comprising a single rib coupled to a single membrane. Since the cost of solving a m-dimensional linear system is $0(m^3)$ this represents a considerable computational savings.

The balancing of terms in the equation also can influence the choice of discretization. Based on a report by Lockheed on the specifications for a 55-meter wrap-rib antenna with 48 ribs [2], the following nominal parameter ranges were derived :

$$\begin{aligned} L &\sim 27.5\text{m} \\ \Theta_o &\sim 1.31\ 10^{-1} \\ I_o &\sim 1.31\ 10^{-6}\ \text{m}^4 \\ E &\sim 9.72\ 10^{10}\ \text{nt/m}^2 \\ T_R &\sim 1.75\ 10^{-1}\ \text{nt/m} \\ T_\Theta &\sim 3.50\ 10^{-1}\ \text{nt/m} \end{aligned} \tag{2.25}$$

This gives the proper scalings in system (2.20). For simplicity we take $\sigma = T_\Theta L^2/\Theta_o$ and we have

$$G_1 \sim 2.29$$

$$G_2 \sim 8.58\ 10^{-3} \tag{2.26}$$

$$G_3 \sim 1$$

This means that the radial terms of the mesh potential are comparatively small except when the radial derivatives are large. How this affects the structure of the system is demonstrated in the following example (see Figure 2).

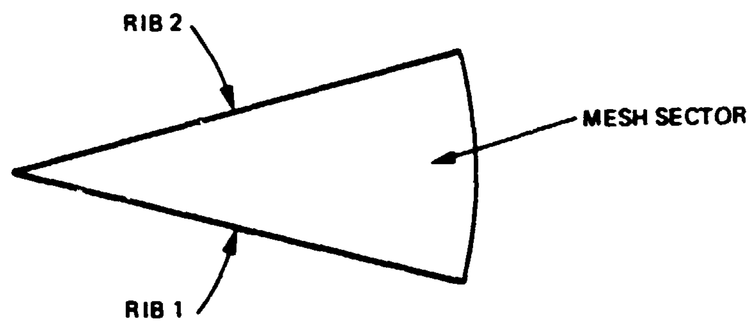

Fig. 2 Single antenna gore

Example:

$$\epsilon \frac{1}{r} \frac{\partial}{\partial r}\left(r \frac{\partial v}{\partial r}\right) + \frac{1}{r^2} \frac{\partial^2 v}{\partial \theta^2} = 0$$

$$v(r,\theta)\Big|_{\theta=o} = f_1(r) \qquad \begin{array}{l} o < r < 1 \\ o < \theta < 1 \end{array} \tag{2.27}$$

$$v(r,\theta)\Big|_{\theta=1} = f_2(r) \quad (f_1(o) = f_2(o) = o)$$

$$\frac{\partial v}{\partial r}(r,\theta)\Big|_{r=1} = o$$

In this example we study the equations for a sector of membrane where the prescribed boundary conditions depend on the adjoining rib displacements ($f_1(r)$ and $f_2(r)$). For simplicity we take the forcing on the mesh to be zero although the more general case could be handled in a similar fashion. We are of course interested in the case where

$$0 < \epsilon << 1 \tag{2.28}$$

which corresponds to the parameter ranges (2.26) in (2.20). Physically one expects that the radial terms contribute little to the static behavior except perhaps at the boundary where the gradients may become large. One is also interested in the behavior near the corners $(r,\Theta) = (1,0)$ and $(r,\Theta) = (1,1)$ since some singular behavior may be possible. Using the techniques of singular perturbations, (see for example [4]), one can show that as ϵ approaches zero we have

$$\begin{aligned} v(r,\Theta) &= f_1(r)(1-\Theta) + f_2(r)\Theta \\ &+ \epsilon^{1/2} \sum^{\infty} \left(-f_1'(1) + f_2'(1)(-1)^n \right) \frac{2}{(n\pi)^2} \exp\left[\frac{n\pi(r-1)}{\epsilon^{1/2}}\right] \sin(n\pi\Theta) \\ &+ O(\epsilon) \quad . \end{aligned} \tag{2.29}$$

This expansion could be continued to higher orders, and, as noted before, a more complicated expression would result from forcings on the membrane. One possible approach to the numerical solution of the system (2.20) would by the elimination of the mesh behavior entirely be substituting an expression similar to (2.29) into the beam equations (2.20a). Then one would have only equations along the beams to solve. If higher-order accuracy on the mesh is required, one could then apply finite-element techniques to the system obtained after linearization about the asymptotic expansion for the mesh behavior. Finally we note the appearance of logarithmic singularities in the mesh gradients $(\partial v/\partial v, \partial v/\partial\Theta)$ as the corners $(r,\Theta) = (1,0)$ and $(r,\Theta) = (1,1)$ are approached from the interior of the mesh. This consideration should also influence any finite element approximation of the mesh.

We emphasize that this analysis applies not only to the simplified antenna model we have considered but would hold for more elaborate configurations where a similar structural balance of terms governs the system. Thus, many modeling options can be considered for parameter identification in important classes of structures if one does not insist on a traditional modal characterization of the system.

3. THE LIKELIHOOD FUNCTIONAL

A detailed discussion of the likelihood principle is given in [6]. The functional we consider is the negative logarithm of the likelihood ratio associated with the detection of a Gaussian signal in additive Gaussian noise; this framework is traditional in the theory of communication and signal detection.

In accordance with the discussion given in [6], and the notation discussed in Section 2 ,the log-likelihood functional is given by,

$$J(\Theta,y) = \frac{1}{2}\,\mathrm{Tr}\,(\log\,[\sigma_\eta^2 \underset{\sim}{I} + \sigma_\omega^2 \underset{\sim}{R}])$$
$$+\frac{1}{2}(\vec{y}-\vec{m}(\Theta))^*\,[\sigma_\eta^2 \underset{\sim}{I} + \sigma_\omega^2 \underset{\sim}{R}]^{-1}(\vec{y}-\vec{m}(\Theta)) \tag{3.1}$$
$$-\frac{1}{2}\;(1/\sigma_\eta)^2\,\vec{y}^*\vec{y}$$

where the expected mean and the covariance operator are given by:

$$\vec{m}(\Theta) = H(\Theta)\;\Phi(\Theta)\;C(\Theta)\,\vec{f}$$
$$\underset{\sim}{R}(\Theta) = H(\Theta)\Phi(\Theta)B(\Theta)B^*(\Theta)\Phi^*(\Theta)H^*(\Theta) \quad . \tag{3.2}$$

Here $\vec{y}_1{}^*\vec{y}_2$ indicates the Euclidian inner product in the N_s-dimensional space to which the observators belong.

From the assumptions of Section 2, it is easy to see that $\underset{\sim}{R}$ is an $N_s \times N_s$ matrix whose (i,j) component is given by

$$R^{(i,j)} = \sum_{k=1}^{N_a} g(\xi_i|\tilde{\xi}_k)\;g\,(\tilde{\xi}_k|\xi_j)$$
$$= \sum_{k=1}^{N_a} g(\xi_i|\tilde{\xi}_k)\;g\,(\xi_j|\tilde{\xi}_k) \tag{3.3}$$

where $g(x|\xi)$ is the point-source solution of the underlying elliptic system

$$Au = \delta(x - \xi) \tag{3.4}$$

with the appropriate boundary conditions. And likewise the expected observation has the form

$$\vec{m} = \underset{\sim}{G}\,\vec{f}$$
$$\vec{f} = (f^{(1)},\ldots,\;f^{(N_a)})^T \tag{3.5}$$
$$G^{(i,j)} = g(\xi_i|\xi_j) \qquad ,$$

where $\underset{\sim}{G}$ is an $N_s \times N_a$ matrix.

We note that (3.1) also differs from (1.3) of [6] in accordance with the introduction of the positive weighting parameters, σ_ω and σ_η, into the system (2.1). An equivalent form for the likelihood functional follows from a rearrangement of terms.

$$J(\Theta,\vec{y}) = \frac{1}{2} \operatorname{Tr} \log [\underset{\sim}{I} + \mu \underset{\sim}{R}]$$

$$+ (1/\sigma_{\eta})^2 (\vec{y}-\vec{m}(\Theta))^* [\underset{\sim}{I} + \mu \underset{\sim}{R}]^{-1} (\vec{y}-\vec{m}(\Theta)) \tag{3.6}$$

$$- \frac{1}{2} (1/\sigma_{\eta})^2 \vec{y}^* \vec{y}$$

where

$$\mu = \frac{\sigma_{\omega}^2}{\mu_{\eta}^2} \tag{3.7}$$

This form is useful since one can arrive at the functional given in [6] directly by the substitutions

$$\underset{\sim}{R} \rightarrow \mu \underset{\sim}{R} = \hat{\underset{\sim}{R}}$$

$$y \rightarrow (1/\sigma_{\eta})\vec{y} = \vec{\hat{y}} \tag{3.8}$$

$$\vec{m} \rightarrow (1/\sigma_{\eta}) \vec{m} = \vec{\hat{m}}$$

This correspondence allows one to use the algorithms derived in [6] directly on the functional

$$J (\Theta,\vec{\hat{y}}) = \frac{1}{2} \operatorname{Tr} \operatorname{Log} [\underset{\sim}{I} + \hat{\underset{\sim}{R}}]$$

$$+ \frac{1}{2} (\vec{\hat{y}} - \vec{\hat{m}}(\Theta))^* [\underset{\sim}{I} + \hat{\underset{\sim}{R}}]^{-1} (\vec{\hat{y}} - \vec{\hat{m}}) \tag{3.9}$$

$$- \frac{1}{2} \vec{\hat{y}}^* \vec{\hat{y}}$$

The goal is to find the parameter value Θ which minimizes the log-likelihood functional; that is, we wish to solve

$$\min_{\Theta} \quad J(\Theta,\vec{\hat{y}}) \quad , \tag{3.10}$$

where Θ ranges over some appropriate infinite-dimensional space. Assuming that the functional has a Frechet derivative and satisfies an appropriate convexity condition, one can restate the problem (3.10) as

$$\partial J/\partial\Theta\, (\Theta,\vec{\hat{y}}) = 0 \tag{3.11}$$

Both problems (3.10) and (3.11) have been studied in a variety of contexts (See, for example, [5]).

Since both the parameter space and the state space are infinite-dimensional, one must make dual approximations in order to achieve problems that are finite-dimensional and therefore computationally tractable. Thus in practice one solves a sequence of problems of the form

$$\min_{\vec{\hat{\theta}}} \hat{J}(\hat{\theta},\vec{\hat{y}}) \tag{3.12}$$

or

$$\partial\hat{J}/\partial\vec{\hat{\theta}}\,(\vec{\hat{\theta}},\vec{\hat{y}}) = 0 \tag{3.13}$$

where the state-space and parameter-space have been replaced by finite dimensional spaces. Then the problem reduces to a finite minimization problem which can be treated numerically by a variety of techniques (see, for example, [1,5]).

The state-space can be approximated by a finite-element space which is appropriate for approximating solutions to (3.4), and the parameter-space can be conveniently represented by a spline-based space. Let N_x be the dimension of the finite-dimensional approximation to the state-space and let N_Θ be the dimensions of the finite-dimensional parameter space. This leads to the natural substitutions

$$\begin{aligned}
& u \to \sum_{k=1}^{N_x} u^{(k)}\,\psi_k(x) \\
& \Theta \to \sum_{k=1}^{N_\Theta} \Theta^{(k)}\,\kappa_k\,(\Theta) \\
& \Theta = [\Theta^{(1)},\ldots,\Theta^{(N_\Theta)}]^T \\
& u = [u^{(1)},\ldots,u^{(N_x)}]^T \quad ,
\end{aligned} \tag{3.14}$$

where the sets $\{\psi_k\}$ and $\{\kappa_k\}$ give the basis elements for the state and parameter spaces respectively.

It will also be convenient to consider the state-space inner-product with a weighting given by the basis elements of the parameter space. Thus we define

$$\begin{aligned}
& < u,v >_j = < u,\ \kappa_j(\Theta)v > \\
& \qquad (j \in \{1,\ldots,N_\Theta\}) \quad .
\end{aligned} \tag{3.15}$$

In the following we restrict our attention to these finite-dimensional problems, and, when the context is clear, we suppress the ^-notation. Questions concerning the convergence of the numerical schemes and the general relationship between the infinite-dimensional and finite-dimensional problems will be discussed more fully in a future report.

Most nonlinear optimization techniques require solving linearized systems iteratively, and consequently one must solve systems of the form (3.4), where the dimension N_x may be quite large. Since the complexity of solving an m-dimensional linear system is $O(m^3)$, the speed of convergence of the iterates is an important consideration. With this in mind, we emphasize the use of quasi-Newton methods for the solution of (3.13). Consequently much of the resulting effort is directed towards deriving adequate approximations for the N_Θ- dimensional Jacobian vector $\partial J/\partial\Theta$ and the $N_\Theta \times N_\Theta$ Hessian matrix $\partial^2 J/\partial\Theta^2$.

We briefly outline the procedure here; as noted previously, a more complete description is given in [6]. In general for the finite problems, the dimension of the state space (N_x) is much larger than the dimension of the parameter space (N_Θ), the number of sensors (N_s) or the number of actuators (N_a), and so it is preferable to carry out the necessary manipulations in spaces whose dimensions do not depend on the dimension of the state space.

Therefore, as in [6] we represent calculations in terms of the eigen-structure of the $N_s \times N_s$ matrix $\underset{\sim}{R}$.

$$\begin{aligned}
&\underset{\sim}{R}\vec{\Phi}_k = \lambda_k^2\vec{\Phi}_k \\
&\lambda_k = \tan\alpha_k \quad (0 \leq \alpha_r < \tfrac{\pi}{2})
\end{aligned} \tag{3.16}$$

From the spectral components of $\underset{\sim}{R}$ we define useful quantities as given in [6].

From (3.2) we have the expected observation

$$\begin{aligned}
&\vec{m} = H\Phi C\vec{f} \\
&m_k = \vec{\Phi}_k{}^*\vec{m} \qquad ,
\end{aligned} \tag{3.17}$$

and also we define the filtered observation

$$\begin{aligned}
&\vec{z} = \underset{\sim}{L}\vec{y} + (\underset{\sim}{I} - \underset{\sim}{L})\,\vec{m} \\
&z_k = \vec{\Phi}_k{}^*\,\vec{z} \qquad ,
\end{aligned} \tag{3.18}$$

where the $N_s \times N_s$ matrix $\underset{\sim}{L}$ is given by

$$\begin{aligned}
\underset{\sim}{L} &= \underset{\sim}{I} - (\underset{\sim}{I} + \underset{\sim}{R})^{-1/2} \\
&= \sum_k (1 - \cos\alpha_k)\,\vec{\Phi}_k\vec{\Phi}_k^*
\end{aligned} \tag{3.19}$$

and the related matrix $\underset{\sim}{K}$ is given by

$$\underset{\sim}{K} = (\underset{\sim}{I} + \underset{\sim}{R})^{1/2} - \underset{\sim}{I}$$
$$= \sum_k (\sec\alpha_k - 1)\,\vec{\Phi}_k \vec{\Phi}_k^* \tag{3.20}$$

For algebraic convenience we also define the residual of the process:

$$\vec{e} = \vec{y} - \vec{z}$$
$$e_k = \vec{\Phi}_k^* \, \vec{e} \tag{3.21}$$

The gradient of L is represented by

$$\partial \underset{\sim}{L} / \partial\theta^{(j)} = \sum_k \sum_{m \neq k} a^j_{km} \vec{\Phi}_k \vec{\Phi}_m^* \tag{3.22}$$

where the coefficients $\{a^j_{km}\}$ are given by:

$$a^j_{km} = \begin{cases} -(\sin \alpha_k)^2 \langle Dp_k, Dx_k \rangle_j & , k = m \\ ((\lambda_m \lambda_k) / (\lambda_k^2 - \lambda_m^2))(\cos\alpha_k - \cos\alpha_m) \cdot & \\ [\lambda_k \langle Dp_m, Dx_k \rangle_j + \lambda_m \langle Dp_k, Dx_m \rangle_j] & , k \neq m \end{cases} \tag{3.23}$$

For later convenience we derive another form for the coefficients $\{a^j_{km}\}$. Using standard trigonometric identities one can easily verify the relation

$$\frac{\cos\alpha_k - \cos\alpha_m}{(\tan\alpha_k)^2 - (\tan\alpha_m)^2} = -\frac{(\cos\alpha_k)^2(\cos\alpha_m)^2}{\cos\alpha_m + \cos\alpha_k} \tag{3.24}$$

This leads to an alternate form for the coefficients

$$a^j_{km} = \begin{cases} -(\cos\alpha_k)^3 [(\lambda_k)^3 \langle Dp_k, Dx_k \rangle_j] & , k{=}m \\ -(\cos\alpha_k \cos\alpha_m)^2 / (\cos\alpha_k + \cos\alpha_m) \cdot & \\ [\lambda_m \lambda_k^2 \langle Dp_m, Dx_k \rangle_j + \lambda_k \lambda_m^2 \langle Dp_k, Dx_m \rangle_j] & , k \neq m \end{cases} \tag{3.25}$$

The point of this last derivation is that the bracketed terms reduce to simpler expressions. From (2.2), (2.7), and (3.4) one can easily show:

$$p_k = \lambda_k^{-1}\, \Phi^*\, H^*\, \phi_k = \lambda_k^{-1} \sum_{j=1}^{N_s} g\,(x|\xi_j)\phi_k^{(j)} \tag{3.26}$$

and also from (2.7) we have:

$$x_m = \lambda_m^{-1} \Phi\, B^* p_m = \lambda_m^{-2} \sum_{k=1}^{N_a} \sum_{j=1}^{N_s} g\,(x|\tilde{\xi}_k)\, g\,(\tilde{\xi}_k|\xi_j)\, \phi_k^{(j)} \quad . \tag{3.27}$$

By this we have:

$$\lambda_k \lambda_m^2 < Dp_k, Dx_m >_j = \vec{\Phi}_k^* \underset{\sim}{A}_j \vec{\Phi}_m \tag{3.28}$$

where the $N_s \times N_s$ matrix $\underset{\sim}{A}_j$ has the form

$$A_j^{(k,m)} = \sum_{i=1}^{N_a} g\,(\xi_i|\xi_m) <Dg\,(x|\xi_k), Dg\,(x|\xi_i) >_j \quad . \tag{3.29}$$

And similarly we have the useful relation

$$\lambda_k <Dp_k, D\bar{u}>_j = \vec{\Phi}_k{}^* \underset{\sim}{B}_j\, \vec{f} \qquad \bar{u} = \Phi C f \tag{3.30}$$

where the $N_s \times N_a$ matrix $\underset{\sim}{B}_j$ is given by

$$B_j^{(k,m)} = <Dg\,(x|\xi_k), Dg\,(x,\tilde{\xi}_m)>_j \tag{3.31}$$

We now give expressions for the gradient and the Hessian in terms of the quantities given above. As in [6] the gradient can be represented as

$$\partial J/\partial\theta^{(j)} = -\sum \sin^2 \alpha_k \tan \alpha_k <Dp_k, Dx_k >_j - \sum e_k\,(\partial z_k/\partial\theta^{(j)}) \tag{3.32}$$

Here the spectral coefficients $\partial z_k/\partial\theta^{(j)}$ are given by

$$\partial z_k/\partial\theta^{(j)} = \sum_m \cos\alpha_m\, a^{\,i}_{km}\, e_k - (\cos\alpha_k)\,[\lambda_k \langle Dp_k, D\vec{u}\rangle_j] \tag{3.33}$$

Exact expressions for the Hessian are given in [6]; in general, however, all terms need not be estimated to give an adequate approximation. In particular, the calculations are much simpler if the terms with second-order derivatives can be ignored. The simplest approximation comes from only keeping those terms which contribute to the expected va[illegible] of the Hessian. Thus, from (1.12) of [6] the (i,j) - component of the $N_s \times N_s$ Hessian approximation $\underset{\sim}{M}$ is given by

$$\begin{aligned} M^{(i,j)} &= \mathrm{tr}\,[\partial \underset{\sim}{L}/\partial\theta^{(i)} (\underset{\sim}{I} + \underset{\sim}{K})\, \partial\underset{\sim}{L}/\partial\theta^{(j)} (\underset{\sim}{I} + \underset{\sim}{K})\,] \\ &\quad (\partial\vec{z}/\partial\theta^{(i)}) * (\partial\vec{z}/\partial\theta^{(j)}) \\ &= \mathrm{tr}\,[\underset{\sim}{V}_i\, \underset{\sim}{V}_j] + \sum_k \partial z_k/\partial\theta^{(i)}\ \partial z_k/\partial\theta^{(j)} \end{aligned} \tag{3.34}$$

where by (3.20) and (3.22) we have $V_i^{(m,k)} = a_i^{mk}\sec\alpha_k$.

This estimate is justified when the covariance is small as one might expect if the number of measurements is large. This point will be investigated more rigorously in a future paper.

We now summarize the search procedure for the system (2.6) where the N_s-dimensional observation vector $\vec{y}$ is given and an initial N_Θ-dimensional parameter estimate $\vec{\Theta}_o$ is available.

First the expected observation $\vec{m}$ and the covariance matrix $\underset{\sim}{R}$ are determined from (3.3) and (3.5). The spectral decomposition of $\underset{\sim}{R}$ as well as the quantities given by (3.17) - (3.33) then can be determined by standard matrix algebra routines. And therefore from (3.32), (3.33) and (3.34) one obtains an N_ε-dimensional gradient approximation g and an $N_s \times N_s$ Hessian approximation $\underset{\sim}{M}$.

The parameter estimate Θ_o can then be updated by making the quasi-Newton correction:

$$\vec{\Theta}_* = \vec{\Theta}_o - \gamma_o \underset{\sim}{M}^{-1}\vec{g} \tag{3.35}$$

Here γ_o is an appropriate scalar chosen to improve the updated parameter estimate. In accordance with the general theory of Newton iterations in function spaces [5], one can repeat this procedure until the solutions of the linearized problems converge to the solution of the underlying nonlinear problem.

This analysis completes our outline of the maximum likelihood identification process. In Section 4 we give examples which illustrate the successful implementation of these schemes in useful applications.

4. EXAMPLES: In this section we give examples of successful implementations of the previously discussed algorithms.

We first consider the string (cf (2.13)

$$
\begin{aligned}
&Au = -(\alpha(x)\, u'(x))' \\
&u(o) = u(1) = 0 \quad .
\end{aligned}
\tag{4.1}
$$

For the case where the unknown tension parameter is constant, the point-source solution can be explicitly given:

$$
\begin{aligned}
&u(x|\xi) = \frac{1}{\alpha}(1 - x_{>})(x_{<}) \\
&x_{>} = \max\{x,\xi\} \\
&x_{<} = \min\{x,\xi\} \quad .
\end{aligned}
\tag{4.2}
$$

And thus, as outlined in Section 2, all calculations could be given in terms of these quantities, without any truncation of the state space or the parameter space.

In general, however, truncations in both spaces are necessary. For the string problem we consider an N_x - dimensional state space of linear splines; the state variable then becomes the vector of nodal values on the corresponding grid. For simplicity we take the grid to be uniform; thus, since the endpoints $x = 0$ and $x = 1$ are fixed, we have:

$$
\Delta x = \frac{1}{N_x + 1} \quad .
\tag{4.3}
$$

The state-space elements are then given by

$$
u = \sum_{i=1}^{N_x} u^{(i)} \kappa_i(x)
\tag{4.4}
$$

where, as illustrated in Figure 3, the basis elements $\{\kappa_i(x)\}$ have the form

$$
\kappa_i(x) = \begin{cases}
\dfrac{x - (i-1)\Delta x}{\Delta x} & , (i-1)\,\Delta x < x < (i)\,\Delta x \\[2ex]
\dfrac{x - (i)\Delta x}{\Delta x} & , (i)\,\Delta x < x < (i+1)\,\Delta x \\[2ex]
0 & , \quad \text{otherwise}
\end{cases}
\tag{4.5}
$$

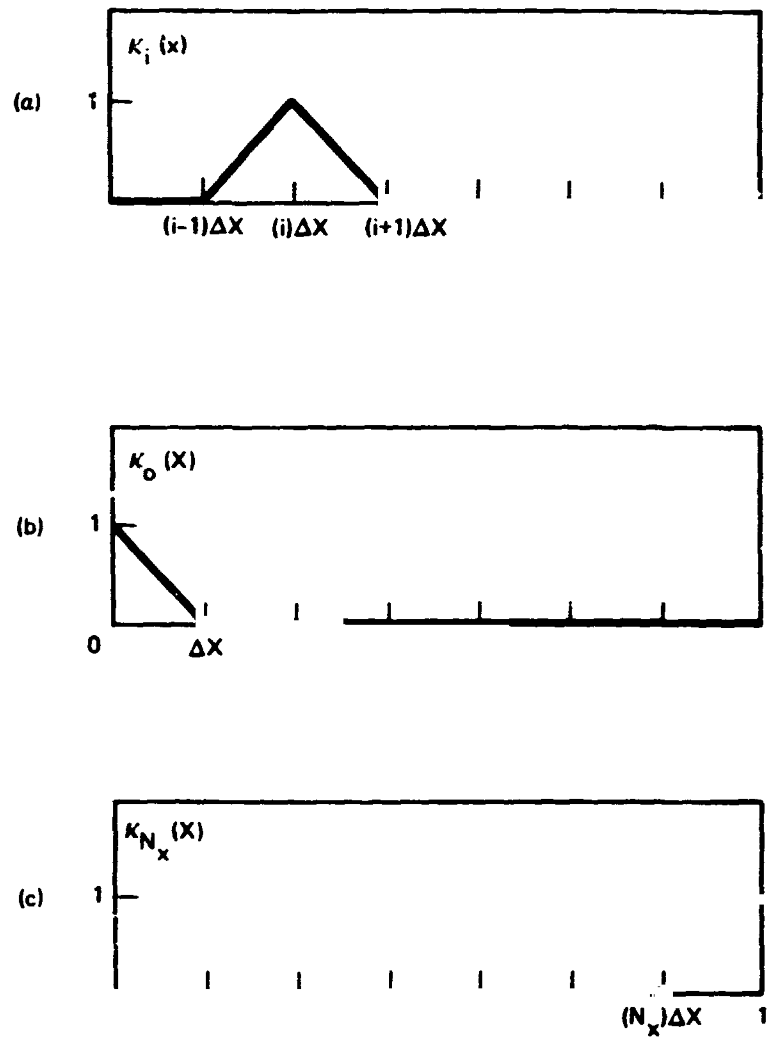

Fig. 3 Linear spline elements

A similar discretization of the parameter space is possible. First we consider the augmented spline space

$$\{\kappa_i(x)\}_{i=0}^{N_x+1} \tag{4.6}$$

where, as illustrated by Figure 3, the endpoint-elements κ_0 and κ_{N_x+1} are given by

$$\kappa_o(x) = \begin{cases} \dfrac{(\Delta x) - x}{\Delta x} & , 0 < x < \Delta x \\ 0 & , \Delta x < x < 1 \end{cases}$$

$$\kappa_{N_x+1}(x) = \begin{cases} 0 & , 0 < x < N_x(\Delta x) \\ \dfrac{x - N_x(\Delta x)}{\Delta x} & , N_x(\Delta x) < x < 1 \end{cases} \qquad (4.7)$$

Thus we have a corresponding parameter element

$$\alpha(x) = \sum_{i=o}^{N_x+1} \alpha^{(i+1)} \kappa_i(x) \qquad (4.8)$$

which would give a parameter space $\{\vec{\alpha}\}$ with dimension N_x+2.

However, as previously noted, the resolution of the parameter space often does not need to be as fine as the resolution of the state-space. We consider then the use of a piecewise linear parameter space of lower dimension where the only requirement is that the nodal points must be a subset of the nodal points of the state-space. The new parameter space is then a subset of the (N_x+2)-dimensional space given by (4.6). Let α be an N_Θ -dimensional parameter element $(N_\Theta \leq N_x+2)$. Then α identifies with an element $\tilde{\alpha}$ of the larger (N_x+2)-dimensional space and the relationship is given by

$$\vec{\tilde{\alpha}} = \underset{\sim}{B}\vec{\alpha} \qquad (4.9)$$

where $\underset{\sim}{B}$ is an $(N_x+2) \times N_\Theta$ matrix. And correspondingly, we have

$$\partial\vec{\tilde{\alpha}}/\partial\vec{\alpha} = \underset{\sim}{B} \quad . \qquad (4.10)$$

This relationship simplifies the algorithms as described below since B is easy to construct, and the more cumbersome calculations which are needed to determine partial derivatives with respect to the parameter space are then specified in terms of the grid associated with the state space. Thus we have:

$$\partial/\partial\vec{\alpha} = \underset{\sim}{B} \; \partial/\partial\vec{\tilde{\alpha}} \qquad (4.11)$$

We illustrate these points with a sample calculation (see Fig. 4). We consider the case where there are seven sensors at the locations

$$\xi \in \{.125, .25, .375, .5, .625, .75, .85\} \tag{4.12}$$

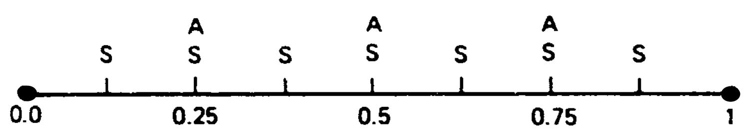

Fig. 4 String tension identification: sensor and actuator locations

and three actuators at the locations

$$\tilde{\xi} \in \{.25, .5, .75\}. \tag{4.13}$$

The data vector was derived from a plant with specifications

$$\begin{aligned} &\alpha_{plant}(x) = 3 + x \\ &C\,\vec{f} = \delta(x-.25) + \delta(x-.5) + \delta(x-.75) \\ &\sigma_{\omega} = .001 \\ &\sigma_{\eta} = .001 \end{aligned} \tag{4.14}$$

For the state space we take the seven-dimensional space of linear splines $\{\kappa_i(x)\}$ with nodes corresponding to the sensor locations (4.12), and for the parameter space we take the five-dimensional subset of linear splines with nodes corresponding to the set

$$\{0, .25, .5, .75, 1.\} \tag{4.15}$$

The relaxation parameter γ_0 in (3.35) was chosen to speed up to the convergence of the iteration; these issues will be discussed more fully in a future report but we give the results of the calculations in Fig. 5. These numerical experiments appear to be very encouraging although with a crude approximation to the Hessian the convergence can be very slow.

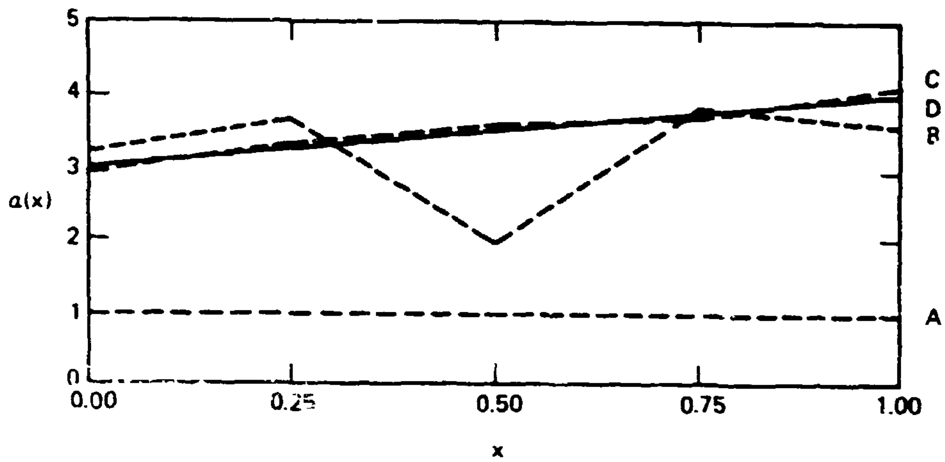

ITERATE	$a^{(1)}$	$a^{(2)}$	$a^{(3)}$	$a^{(4)}$	$a^{(5)}$
A INITIAL	1.00	1.00	1.00	1.00	1.00
B INTERMEDIATE	3.19	3.64	1.98	3.81	3.62
C FINAL	2.98	3.29	3.55	3.68	4.05
D TRUE	3.00	3.25	3.50	3.75	4.00

Fig. 5 Distributed parameter identification via spline analysis

In a similar way, the algorithm was successfully applied to the wrap-rib antenna model (2.4). To simplify the calculations, we assumed here that the stiffness parameters were scalers although one could introduce a spline-based space as in the previous example.

Again for simplicity we consider the case where there are six gores ($N = 6$), where a sensor is placed on the outer endpoint of each rib ($r = 1$), and where an actuator is placed at the midpoint of each rib ($r = .5$). This scheme is outlined in Figure 6.

We introduce the set of N-dimensional unit vectors

$$\left\{ \vec{\hat{e}}_k \right\}_{k=1}^{N} \tag{4.16}$$

where the components of each $\vec{\hat{e}}_k$ are determined by

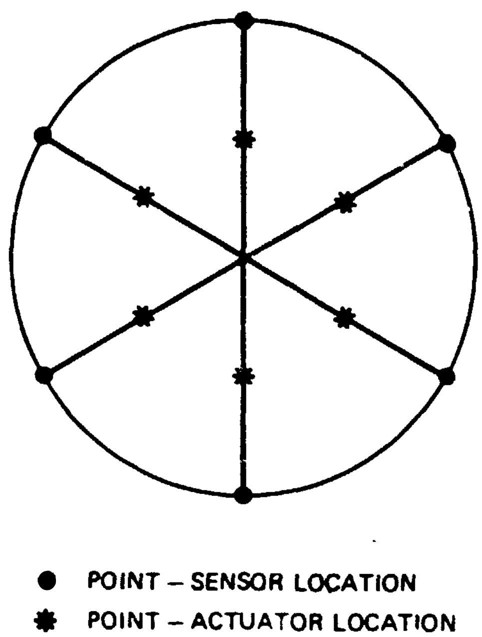

Fig. 6 Rib stiffness identification: sensor and actuator locations

$$\tilde{e}_k^{(i)} = \begin{cases} 1, & i = k \\ 0, & i \neq k \end{cases} \tag{4.17}$$

The parameters of the likelihood functional are then given by

$$\begin{aligned} \sigma_\omega &= .001 \\ \sigma_\eta &= .001 \\ C\vec{f} &= \sum \vec{\tilde{e}}_k \, \delta\,(r - .5) \end{aligned} \tag{4.18}$$

And the stiffness parameters of the plate are given by

$$EI = 1.25 \,.10^{5} \text{ nt-m}^2 \tag{4.19a}$$

$$T_R = 1.75 \,.10^{-1} \text{ nt/m} \tag{4.19b}$$

$$T_\Theta = 3.5 \,.10^{-1} \text{ nt/m} \tag{4.19c}$$

$$L = 2.75 \,.10^{-1} \text{ m} \tag{4.19d}$$

We applied the algorithm then to the case where the unknown parameter was EI while the other stiffness parameters were assumed to be known.

To discretize the state-space eight equal subdivisions were made in the radial direction on each rib and in each mesh sector; in the circumferential direction five equal subdivisions were made in each mesh sector. The shape functions on the ribs were given by Hermite cubics while on the mesh the shape functions were given by splines linear in r and θ. In test cases this discretization produced at least three digits of accuracy in solving problems of the form (3.4). In all calculations the principle of cyclic symmetry (cf. (2.24)) was exploited to reduce the number of calculations.

Convergence of the likelihood algorithm was very fast (see Fig. 7) when the relaxation parameter was taken to be

$$\gamma_o = 2.5 \ .$$

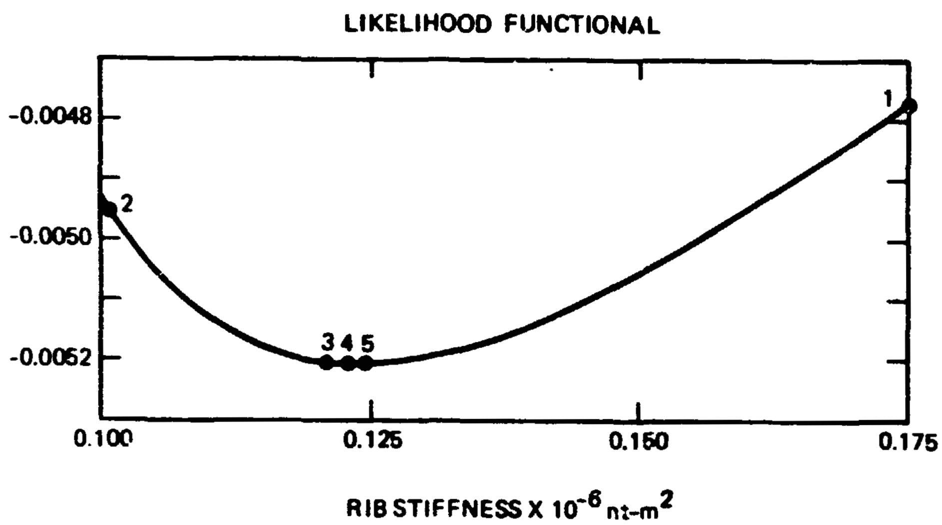

ITERATION NUMBER N	ESTIMATED PARAMETER EI_N	RELATIVE ERROR $\lvert(EI_N-EI_{EST})/EI_{EST})\rvert$
1	$1.75000 \cdot 10^5$	$4. \cdot 10^{-1}$
2	$1.01930 \cdot 10^5$	$2. \cdot 10^{-1}$
3	$1.20484 \cdot 10^5$	$3. \cdot 10^{-2}$
4	$1.23866 \cdot 10^5$	$2. \cdot 10^{-4}$
5	$1.23889 \cdot 10^5$	–

$EI_{PLANT} = 1.25000 \cdot 10^5$

$EI_{EST} = 1.23889 \cdot 10^5$

Fig. 7 Distributed parameter identification of beam stiffness parameter

Numerical experiments also demonstrated an improvement in the sensitivity of the identification schemes as the number of measurements was increased. Thus, Figure 8 illustrates how, for the antenna problem considered, an increase in the number of sensors led to a steepening of the likelihood functional. Here the curves were shifted transversely for illustrative purposes. We note that no corresponding improvement in the parameter estimate occurred in these trials, possibly because of the less favorable signal-to-noise ratio which corresponds to sensing in the interior of the ribs.

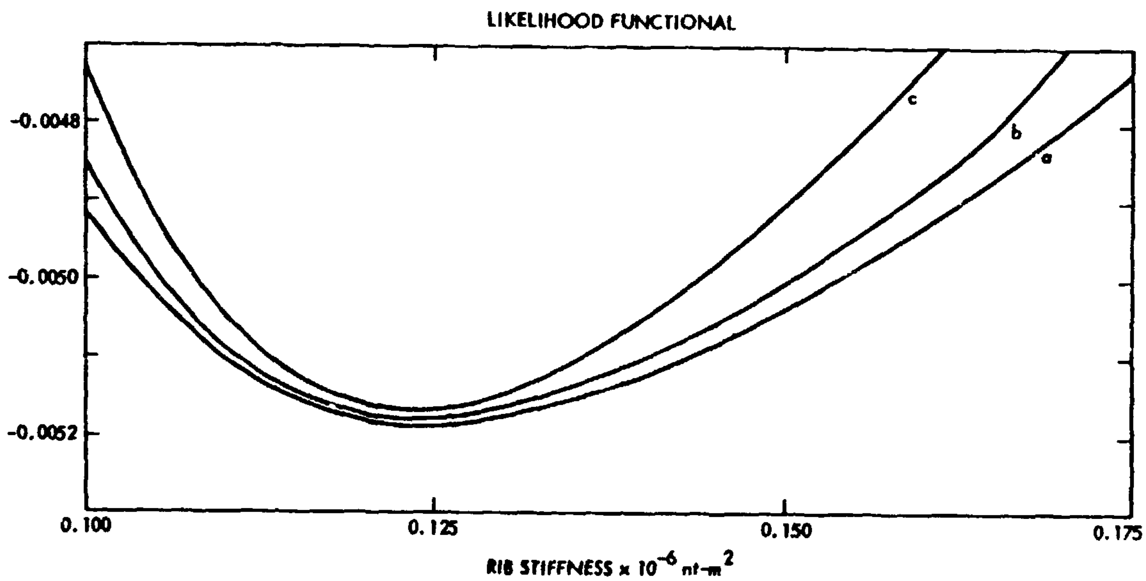

Fig. 8 Sensitivity of antenna stiffness - parameter identification according to number of sensors

(a) One sensor per rib at r = 1.0

(b) Two sensors per rib at r = 0.5, 1.0

(c) Three sensors per rib at r = 0.5, 0.75, 1.0

More detailed numerical experiments with distributed antenna stiffness parameters will be given in a future report. But the results outlined in this report demonstrate already the great potential for these algorithms.

REFERENCES

1. Dahlquist, G. and Bjork, A., Numerical Methods, Prentice Hall, 1974.

2. El-Raheb, M. and Wagner, P., "Static and Dynamic Characteristics of Large Deployable Space Reflectors" AIAA Conference Paper 81-0503-PC, AIAA Dynamics Specialists Conference, Atlanta, Georgia, 1981.

3. Gelfand, I. M., and Fomin, S. V., Calculus of Variations, Prentice-Hall, 1963.

4. Kevorkian, J. and Cole, J., Perturbation Methods in Applied Mathematics, Springer-Verlag, New York, 1980.

5. Luenburger, D. G., Optimization by Vector Space Methods, Prentice-Hall, 1971.

6. Rodriguez, G., "A Residuals Approach to Filtering, Smoothing and Identification for Elliptic Systems", Proceedings of NASA/ACC Workshop on Identification and Control of Large Flexible Structures, 1984.

DISCUSSION—FUTURE RESEARCH DIRECTIONS

Moderator: **Herman A. Rediess,** H. R. Textron, Inc.
Panel Members: **A. V. Balakrishnan,** University of California, Los Angeles,
R. F. Carlisle, NASA Headquarters, **J. L. Lions,** College de France
and Institut National de Recherche en Informatique et en Automatique,
R. E. Skelton, Purdue University, and **W. E. Vander Velde,**
Massachusetts Institute of Technology

SYNOPSIS

The intent in this session was to present several viewpoints on the direction of future research in identification and control of flexible space structures. The panel members were given the option of preparing formal papers or presenting informal comments. Professor Lions was unable to attend the meeting because of a last minute change in plans but did submit a formal written paper which is printed in Session VII of these proceedings. This synopsis attempts to capture the main points discussed but has not been reviewed or endorsed by the speakers.

Professor Vander Velde discussed uncertainty management methodology for large space structures. He identified six major types of uncertainties that are likely to exist in control system design and operation. After assessing the present methodology for handling each type, he suggested the additional technology developments needed. Altogether, he suggested specific research topics covering: sensor noise in nonlinear situations; external or internal disturbances; modeling approximations; model parameter errors; component operational status and reliability; and, spacecraft configuration changes. He introduced, and discussed to some extent, the concept of an on-line system diagnostic monitor for detecting certain types of faults or uncertainties, such as model parameter errors, sensor failures or actuator failures.

Professor Vander Velde concluded that the dynamic character of flexible space structures and the likely complexity of their control systems make them especially likely to have uncertain component operating status. The problem of detecting component failures is coupled with the effects of modeling error whether we like it or not. Perhaps this coupling can be utilized, or at least controlled, in the process of monitoring the health of the system by use of an integrated system diagnostic monitor.

Professor Balakrishnan discussed the important research area of uncertainty modeling from a perspective of estimation and identification problems in random fields. Current estimation and systems identification methods only consider noise with rational spectra. We need to look at signals with non-rational spectra. One area in which non-rational spectra appear naturally is in the area of random fields. Random fields are random processes in which the parameter is no longer time and arise on space structures in describing, for example, deformation in an antenna or mirror. Professor Balakrishnan used a geophysical example of gravity anomalies to illustrate the effectiveness of random field theory in estimation problems when dealing with non-rational spectra. Although there exists substantial research on the theory, there are only a few practical applications in the literature. Techniques are available that can be applied to practical large space structures problems. He suggested that more effort be made to apply these techniques.

Professor Skelton presented his views on the inseparability of the control and modeling problems. When a model is used to derive a control law, then one cannot say how good the model is without knowing what it will be used for and what the control will be. That means that one cannot evaluate the impact of modeling errors until the control is specified. There is a challenge to the community to develop techniques that do the complete model error estimation and compensation problem.

Mr. Carlisle of NASA Headquarters discussed the challenges in controls for the Space Station. He views the problem of designing the Space Station as involving trades among "subsystems". For example, in trades between controls and structures, one uses all of the technology options in both disciplines to optimize the overall design. NASA's plan is for an evolutionary Space Station with the initial operating configuration to be placed in orbit in 1992. Block changes in configuration and maybe in performance will be made subsequently. There is a challenge to the controls community to develop the technology that will provide the flexibility for changes and not be the limiting element in future expansion of the Space Station. There is a five year period to mature technology for the initial system. Periodic block changes will provide opportunities for some later technology to be considered.

Although the Space Station configuration has not yet been determined, it appears likely that it will involve large flexible structures because of the solar arrays, radiators, or even the basic structure as it evolves and grows over many years. Mr. Carlisle described several possible configurations and pointed out the controls challenges. One of the major challenges identified was to devise an affordable scheme for developing and validating the technology for control of flexible structures in view of the high cost of full scale flight experiments.

Dr. Rediess presented his thoughts on the role of experiments in the development of control technology for flexible space structures. The three main points covered were: why experiments are important for developing the technology; the need for a coordinated program from analysis to experiments; and the need for a cooperative program among the various participants to make effective use of the relatively rare experimental data. It will become increasingly more difficult if not impossible to perform ground vibration testing on large flexible space structures. Designers will have to rely more on analytical techniques to predict control/structure interactions. At the same time, control/structure interactions are becoming more important because of increased overlapping of the required controller bandwidth and the structural modes. Damping characteristics, important in the controller design, are probably the most difficult to predict. Even the properties of new materials, such as metal matrix composites, can influence the control/structures design optimization. His conclusion was that experiments on the ground and on-orbit will be necessary to develop and validate the analysis and design techniques. A well coordinated program is needed to bring together the promising analytical methods and the experiments

Dr. Rediess' final point and recommendation was that NASA, the Air Force, and other organizations conducting and/or sponsoring major experiments either in laboratories or on-orbit should establish a cooperative data base with broad access to the technical community. Such experiments are costly and often difficult to get supported. It is imperative that the most effective use be made of these very limited experimental data.

Before opening the discussion to the general audience, Dr. Rediess invited Dr. R. V. Ramnath from Raytheon and an Adjunct Professor of Aeronautics and Astronautics at MIT to present some remarks on the application of asymptotic techniques to control of flexible space structures (to expand on some of the ideas in Professor Lions' paper).

Asymptotic analysis is defined as a study of applied mathematical systems in limiting cases. The following are some of the benefits of using it. In model reduction techniques, an asymptotic ordering of a complicated system into a hierarchical structure can be used in selecting the order of the model. The principle of minimal simplication gives a stopping rule for this process. In solving a complex linear differential equation, the domain of the independent parameter can be extended into a higher dimension. An ordinary differential equation is thus converted into a partial differential equation and solved asymptotically in the new space. The solution is made to coincide with the solution of the original system along certain trajectories. Asymptotic analysis yields a quasianalytic solution which can give insight into stability and controllability of the system. Approximation errors are generally smaller. Dr. Ramnath gave two examples where asymptotic analysis was successfully used to generate the controls. He stressed the need of more applications in control problems of large flexible space structures. These techniques have been used very effectively in other fields such as celestial mechanics and fluid dynamics, among others.

The following are what appeared to be the most important comments and recommendations made during the open discussion period.

- Some people have suggested that Skylab controls technology will be adequate for Space Station. If so, there is no need for controls research to support the Space Station.

- If we rely on Skylab controls technology, we may seriously limit the evolutionary growth of the Space Station.

- It was mentioned earlier in the workshop that NASA cannot afford full scale on-orbit flight experiments. What evidence do we have to say that we can afford <u>not</u> to conduct full scale flight experiments?

- If NASA cannot afford full scale flight experiments, then the project managers will not use the advanced controls technology and will take a more conservative approach.

- There seems to be a change in emphasis in NASA's program away from fundamental research on controls and towards large experimental programs. If that is true, we may be in danger of cutting off new innovative concepts.

- From the perspective of a user of advanced technology, it is necessary to periodically take advanced theory and apply it to practical problems in order to develop an adequate confidence for application to real systems. Without that confidence, the theory would never be used, and we would be reluctant to support more fundamental work. There needs to be a balance of theoretical and applied/experimental effort in NASA's program.

- NASA is to be complimented on the excellent program plan for control of flexible structures that was presented by Mr. Russell at this workshop. It presents a balanced program and a truly integrated controls and structures technology plan.

EDITOR'S NOTE: There follows a synopsis of the prepared remarks given by the panel members.

H. A. REDIESS: I have a particular personal interest in this workshop. About three years ago, when I was at NASA Headquarters and responsible for this technical area of NASA's R&D program, I encouraged G. Rodriguez of JPL and L. W. Taylor, Jr. of Langley Research Center to organize a workshop on control of flexible space structures. The first one was held about two years ago at JPL and was very effective. This, the second one, has been equally as successful, and I am pleased to chair this final plenary session. One objective of this workshop is to provide some feedback to NASA and JPL on research opportunities in controls technology for flexible space structures. We have invited several noted technologists to lead this discussion with you, the workshop participants, to identify these research opportunities. After the prepared remarks by the panelists, the audience will be invited to join in the discussion.

W. E. VANDER VELDE. Uncertainty Management Methodology for Large Space Structures I think it is safe to say that the majority of the papers we have listened to in the last couple of days have dealt with one aspect or another of handling uncertainties in control systems, because, after all, it is one of the fundamental purposes of a feedback control system to accommodate disturbances, noise, and plant uncertainties in certain bandwidth ranges. That is really fundamental in what we are doing. Our purpose here, in this presentation this morning, is to summarize the nature of the uncertainties that we need to deal with, to summarize the technologies that we have available to us to deal with them, and to identify where there are gaps.

Now, suppose you were working onboard a space station, and you gradually became vaguely aware that there was some persistent oscillation going on. In fact, it was getting bigger and bigger, and very soon it was clear to you that you had a problem. The question is, what would you do? Maybe more to the point, would you have designed your control system in such a way that it might have monitored its own behavior and taken some action when it observed that it had a problem? If so, what would that action be? Well, this is one evidence of uncertainty in action, because, of course, based upon our understanding of the dynamics of the system and environment, the system should not behave in this fashion. It is only because we are uncertain about something that we might conceivably get this kind of behavior. But here we are oscillating along in the space station. What are we going to do next? We need to have some fall-back position which is as robust and reliable as possible. It is certainly true that the most robust system you can build is one that does not do anything. Although, in the context of spacecraft control, it may very well be important to at least keep one antenna pointed toward earth to maintain wideband communications. Certainly, the loop that accomplishes that purpose should be extremely low bandwith. It should not attempt to control any flexible mode actively. It should just try to do that one function. Well, suppose we have indeed disengaged our unstable spacecraft system, or at least gone back to a truly robust feedback system. That would then give us a little breathing room, and we would have time to sit back and contemplate what might have gone wrong. What are some of the uncertainties? What are the tools that we need in order to handle these different types of uncertainties? What are some of the research directions that we ought to recommend? I am going to address these questions in my discussion. The list of uncertainties in control system design and operation that I will discuss includes: sensor noise, noise in other components; external or internal disturbances; modeling approximations; model parameter errors; component operational status; and configuration changes.

Sensor noise is a source of uncertainty that has been addressed for a long time. As you well know, if you have a fully linear situation, linear filtering in estimation theory is complete. Even for slightly nonlinear measurements or slightly nonlinear dynamics, approximate extensions of the linear theory, such as various forms of extended Kalman filtering, work well. It is true that if you have a significantly nonlinear problem, a nonlinear set of measurements or dynamics, there is a body of theory which is applicable. But this is very cumbersome to implement. If you cannot assume from the start that you have Gaussian distributions, you have to, in effect, estimate the entire probability density function for the state, given the measurements, and that is inherently an infinite dimensional problem. In the context of spacecraft control, I do not think that the nonlinear situation will be important, unless there are certain types of sensors with nonlinear properties. The only additional technology required are some specialized techniques for handling state estimation for particular types of nonlinear situations. I do not think that it is fruitful to pursue general nonlinear estimation as much as specific techniques that might be applicable to specific problems.

The second category of uncertainties I will discuss includes noise in other components of the system. This is a very important source of noise. There are many instances in which autopilots pick up electronic noise that results in noisy actuator operation. Analytically, this appears as an internal system disturbance. I have included that in my next category, which is internal and external disturbances. Here again, if the system is fully linear, and if these disturbances can be modeled as random processes with rational spectra, then linear system theory is complete. I mention rational spectra, because, if one were to design filters in the frequency domain, one would probably use spectral factorization. This is only easy to do for rational spectra. In any case, for a significantly nonlinear system, the situation is just as it is for sensor noise. Again, I would say it would be more fruitful to pursue specialized analysis techniques that would apply to particular situations.

I have mentioned one other topic under additional technology requirements: internal disturbances that are generated in one part of a spacecraft and propagated to other parts. In fact, just yesterday, we heard one presentation in which it was emphasized that, for multipurpose spacecraft, very often the most significant disturbances are those that one payload imparts to the other payloads. For example, you might have a scanner, with an oscillating mirror or something similar, which is creating a disturbance to other parts of the spacecraft. So, why not try to isolate those disturbances within the modules where they originate. I am sure that this is not a new idea. I list it here and emphasize the fact that active disturbance isolation may make it possible to do this even better than purely passive structure design can do.

This next category is one that has received a great deal of attention in this workshop. This is warranted because we are assured in advance that, in dealing with flexible spacecraft modeling uncertainties, we are going to be working with an inaccurate model of the true dynamics. There a number of methodologies that we are all familiar with to deal with the situation. One such method involves designing a control system on the basis of a reduced-order model and then evaluating it with a higher fidelity model. We know several approaches to the problem of model order reduction. Absolute stability theory is a way of dealing with stability of systems with a nonlinear operator confined only to one sector. And finally, there is a very useful approach using singular values for evaluation of robustness properties of multi-variable systems. There are several additional techniques in modeling approximations that would be very useful. The first one has to do with small but arbitrary damping characteristics of space systems. The characteristics of flexible structures which will be least understood in advance will be their damping properties. But, if the damping is small, you have the impression that you should be able to design a control system which does not really depend on what is the specific damping. I have not attempted to do this. It just seems to me that it might be possible. In a similar spirit, slight nonlinearities and uncertain stiffness properties in higher order systems may not be important under steady regulation. They might be important, for example, under slew maneuvers. The idea of design procedures for control systems, in which modeling inaccuracies of an unspecified form are incorporated directly, is a highly desirable objective but a difficult one to be sure.

Model parameter errors are a somewhat more structured kind of uncertainty in the plant. Our conception is that we have a model which is adequate in some sense. We just do not know quite what the values of the parameters are. The standard approaches available to us include passively robust controllers and adaptive systems. There are two basic types of adaptive systems: in one you explicitly identify parameters; in the other you do not. We have already heard some interesting things about adaptive systems at this workshop. Under the heading of robust controllers, it is always my impression that robustness normally is bought at the cost of some aspect of performance. It would be well to work on that trade-off and attempt to improve it. Under parameter identification, the issue of how to efficiently model a system is important from the standpoint of the original design, as well as from the standpoint of identifying the system. One of the thoughts in an earlier paper at this workshop appeals very much to me. The idea is to model certain modules of the system as distributed parameter models and then piece them together at the boundaries. It strikes me that this might be an efficient way to handle some configurations at least. The idea of optimizing inputs for identification is not a new thought by any means. It is true that, in order to identify all of the properties of the system, you have to push on the system with your own actuators and measure the effect on the output variables. You would like to do it in a way that affords you the best identification. In the context of flexible spacecraft, that has to be done carefully. I mention the problem of adjusting the controller following identification of the plant simply because of the fact that the design of the controller in the first place is such a difficult chore in the large space structure applications. If we indeed identify the plant, and find it to be slightly different than the model we have in the original design process, then the controller has to be adjusted to account for the differences. That may not be a trivial thing to do. In our present state of knowledge about the design of these systems, control design seems to be very tricky. The designs have to be tuned just about right in order to perform well.

Finally, under adaptive control we actually heard some interesting results on stability theory yesterday. It is still true that it is somewhat of a risky business. The conditions for stability generally depend on the relative magnitude of things like disturbances relative to known inputs. It would be very well if we could use and depend upon adaptive controllers. Any research that can be done to clarify stability properties of adaptive controllers would be helpful.

Component operational status has to do with the failure status of the components of the system. We do have a number of methods for failure detection and isolation (FDI). Less work has been done on the problem of reconfiguring the system following the detection of a failure. In the area of computers and signal transmission networks, there is quite a substantial background of work. Under additional technology, I mention the fact that FDI system concepts are needed that are less sensitive to unmodeled dynamics. It is true that, if your FDI depends upon system dynamics modeling, then it suffers from unmodeled dynamics, just like the controller design problem suffers from unmodeled dynamics - and maybe in an even more sensitive manner. Methods for reliable reconfiguration are certainly not settled at this point. In effect, we have to do a redesign of the system using one less component once we discover a failure. The redesign process is not all that simple because the design process is difficult in this application.

I mentioned fault tolerant assembly of loosely coupled computers only to suggest that the fault tolerant computer assemblies that we are dealing with now, for the most part, are based upon varying degrees of synchronism - very tight synchronism in some cases and looser in other cases. In a large spacecraft - particularly one that has been assembled in space out of a number of modules, with each module controlled separately prior to its assembly with the rest - you will have control systems with asynchronous computers. You would like to be able to monitor those for their failure performance as well. And finally, a very important item is the validation of the operational software which is executed in the system.

The last category of uncertainti 's configuration changes. This is very important for the space station, which is to be a ,owing system. It does seem to me that we will need to use pre-programmed changes in the controllers to coincide with configuration changes. I suspect that we will use a low bandwidth robust controller during the period of a change. Someone observed yesterday that it would be nice to avoid the need for that by using adaptive controllers that were adequate to handle configuration changes. You certainly would have to suppress transients in the control system when a change in a controller is made, but I think that is not hard to do. Another problem will be the isolation of the disturbance due to mating a new module with the existing assembly. One should isolate the effect of that to the local region, if possible, to prevent the disturbance from propagating throughout the structure.

These are some of the different types of uncertainties and the technology that we have to deal with. But, what about the unstable spacecraft I mentioned at the beginning? We still have it in the backup mode and have not yet figured out what is wrong. Do the methodologies that we talked about answer this question? Are they adequate to help us discover what happened? Well, I would say not really. Nothing of what we spoke of is directly applicable to the diagnosis of a problem like this. So, it would be very nice to have an additional tool, which I am calling here a System Diagnostic Monitor. A System Diagnostic Monitor has the property that it monitors the health of the system. Not only does it monitor the health and give a go/no-go indication. When it is no-go, it isolates the failure. This is helpful in figuring out what has happened. In particular, you might be able to monitor parameter values in the model to detect changes as well as monitoring for failures in components. A desirable property of such a monitor would be that it can be reconfigured from time to time so that it can monitor different characteristics of the system. A suggested possible structure for such a system monitor is shown in Figure 1. The controller can either be in operation or not. It does not make any difference as far as the monitor is concerned. The lower part of the figure shows a failure detection filter which has the same structure as a Kalman filter or any other linear filter. In fact, if the gain matrix D which operates on the measurement residual were chosen to be the Kalman gain

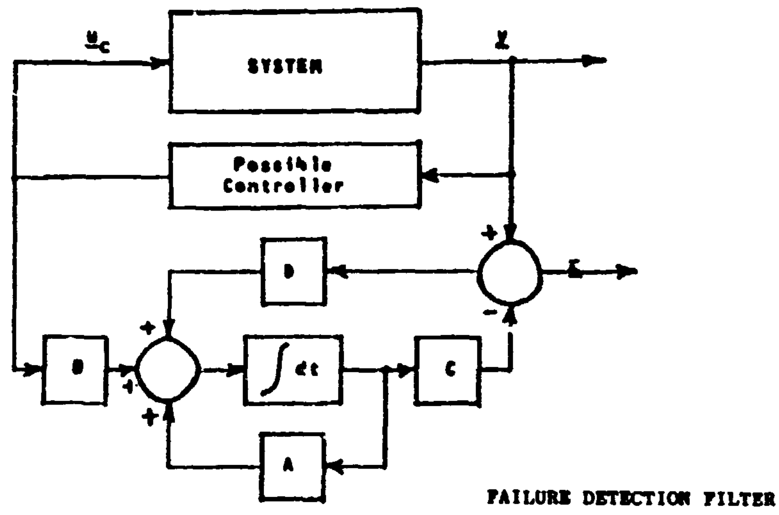

Figure 1. A Possible Structure for the System Diagnostic Monitor

matrix, this would be a Kalman filter. But it is possible to design the gain matrix in different ways. In particular, it is possible to design that gain matrix such that, for certain selected events, the residual can be constrained at the output to lie in a fixed direction. This idea was first proposed for the purpose of doing component failure detection, but it can also be used to detect individual parameters of a model that have been mismatched I will just give you a quick illustration of this in Figure 2.

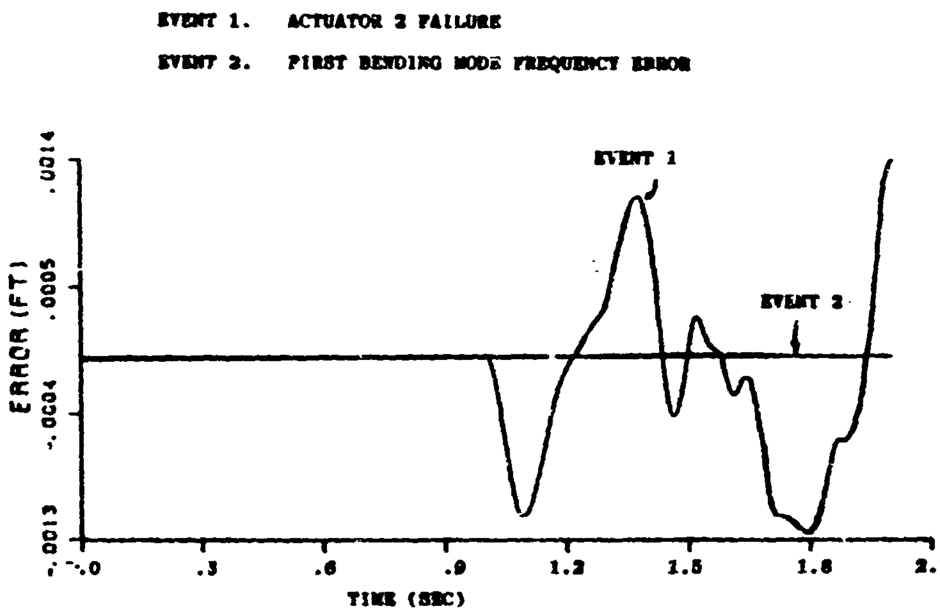

Figure 2. Simulation of the System Diagnostic Monitor
(Actuator 2 Failing off at 1 Sec)

Figure 2 shows a dynamic system modeled with this type of filter or monitor designed to monitor two events: a failure in actuator number 2 (there are four actuators in this model); and a mismatch in the frequency of the first bending mode. The graph is a time history of two output indicators for the two events. Initially, everything is nominal, and the outputs are indistinguishable from zero. But after one second, we simulate a failure in actuator 2. At that point, the output indicator of the first event becomes non-zero, while the output indicator of the second event, which is related to the frequency, still remains zero. If the system were configured to monitor these two events, you could clearly say what was wrong. The other case would be if the value model of that first bending mode frequency were wrong, as is shown in Figure 3. In that case, the monitoring system is being excited right from the start. The second event indicator is nonzero, where as the first-event indicator, corresponding to the actuator failure, stays zero. Again in this case, the monitor would be helpful in discovering what had gone wrong. I do not claim that this is a closed book. In particular, the effect of modeling inaccuracy on this kind of a monitor has not been resolved and is very important. We have made other runs for the case where some additional bending modes, beyond those that were involved in the design of the filter, were simulated. That thoroughly confuses the monitor because of the leakage of the unmodeled dynamics through the filter to the indicator outputs.

In conclusion, the management of uncertainty is certainly nothing new in control system work. Basically, controlling uncertainties is a fundamental reason for feedback in controllers. The large space structure problem is especially sensitive to some of these uncertainties. It is especially susceptible to component failures. Now, whether we like it or not, the problem of trying to detect component failures is coupled with the problems of modeling inaccuracies or model error parameter errors. I would suggest that if the coupling cannot be used to our advantage, then at least it could be used in monitoring of the health of the system.

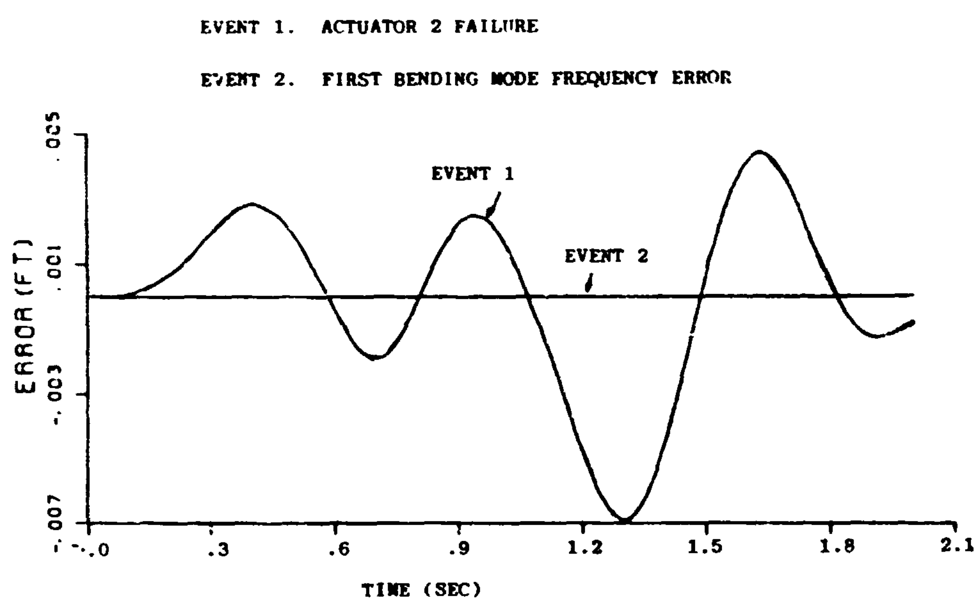

Figure 3. Simulation of the System Diagnostic Monitor
(First Bending Mode Frequency 10 Percent Low)

A. V. BALAKRISHNAN: Some Estimation and Identification Problems in Random Fields In this lecture, the usefulness of random field theory in the estimation and control of large space structures is outlined. Random field theory can be used to characterize the deformation of surfaces of antennas or of other flexible structures. Professor Balakrishnan has developed a filtering technique for random fields which processes data to obtain estimates of the shape and model parameters. Most of the current filtering techniques exploit time dependency and the rational power density spectra of the signal. Random fields often generate a nonrational power spectral density of the signal and they do not have a time parameter. They have 2 or more parameters. Therefore, current filtering techniques cannot be used. Batch estimation is cumbersome to apply because it requires all the data to be processed at the same time. Hence, scanning schemes are superior. In two-dimensions, if the data is scanned in certain directions, the problem is converted to a one dimensional problem, and Kalman filtering can be applied. Professor Balakrishnan has suggested an improved method. Instead of considering one scan line at a time, consider many scan lines simultaneously. Thus, in a direction orthogonal to the scan line, a vector can be constructed consisting of states at points on the scanning lines. Thus, the problem is converted into a vector filtering problem. If the spectral model satifies certain sufficiency conditions, infinite-dimensional Kalman filters can be used. Necessary conditions are not known to date. However, the resulting Kalman filters can be used to handle two dimensional data very efficiently.

R. E. SKELTON: Model Error Structure and the Inseparability of the Control and Identification Problems This morning I would like to share with you my views on some of the problems we all face in the modeling and control of large space structures. Specifically, we will be reminded, in several different ways, that the modeling and control problems are not independent, and that this fact has consequences in the field of identification, a major subject of this workshop.

A Simple Experiment

A graphic demonstration of the inseparability of the modeling and control problem is presented in [1]. The essence of this experiment is as follows. Let S_1 denote a model of the system S, but $S_1 \neq S$ due to modeling errors. Let S_2 be another model of the system S, but also $S_2 \neq S$. In the experiment of [1], S was represented as the first 44 elastic modes of a flexible spacecraft, S_1 was one subset of these modes {1, 2, 5, 9, 17}, and S_2 was another subset of these modes {1, 2, 17, 4 10}. Now, let S_{c1} denote the controller which is optimal with respect to the model S_1, and let S_{c2} denote the controller which is optimal with respect to model S_2. Let the performance of these two controllers be evaluated when driving the "real" system S. Which model should be better for control design S_1 or S_2? Fig. 1 illustrates that the answer is that neither model is always best. For a particular range of control gains S_1 is best, and for another range S_2 is best. In other words, one cannot say which model is best independently of some statement of the control law. This reinforces the notion that "one cannot say what is a good model without saying (precisely) what the model is going to be used for".

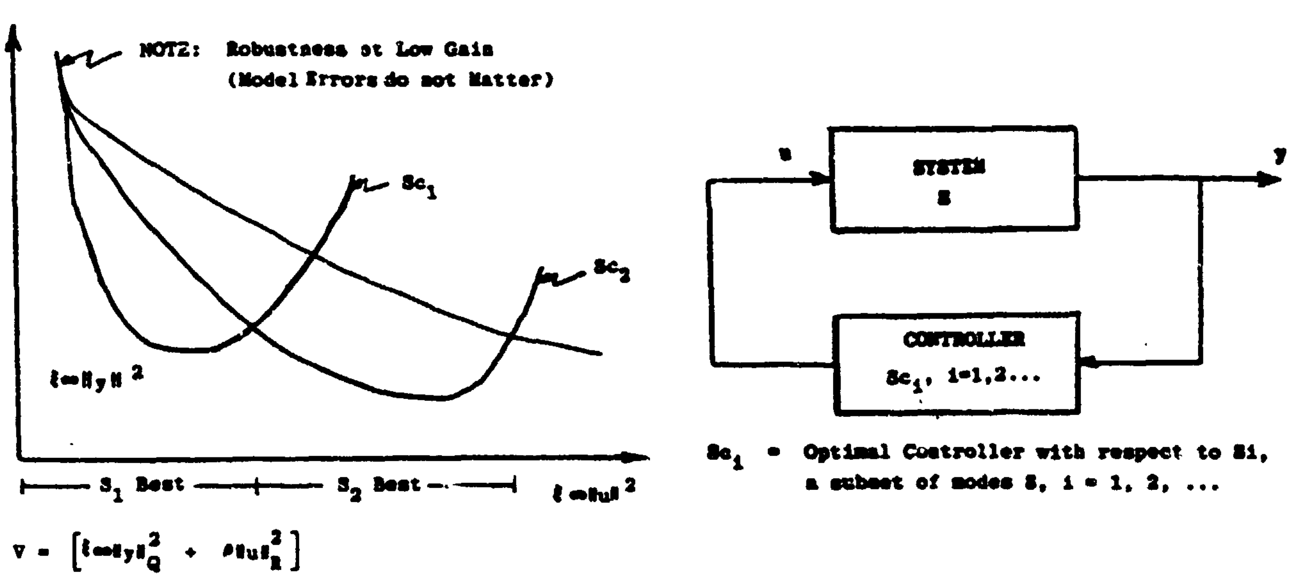

Figure 1. Any given model not always best for control design

Now, if there exists a model S_2 for which the control design cannot be improved (Fig. 2), then the modeling and control problem can be called separable with respect to that model S_2. Of course, such notions involve all possible (infinite in number) models, and the question makes sense only with respect to a given control design methodology (LQG in the case of Fig. 1).

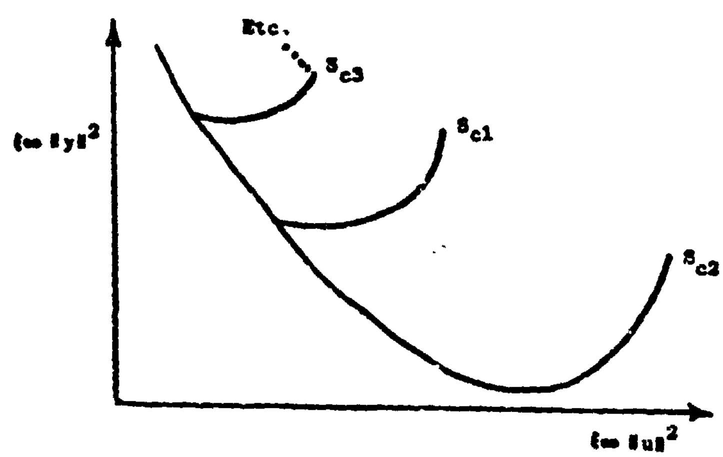

Figure 2. Modeling and control problems separable with respect to S_2.

Nonetheless, this inseparability of the modeling and control problems holds without regard to the method of producing the model, whether that method be modeling from first principles (known physical laws, F = MA, etc.), or whether that method be modeling from on-line data, commonly called the identification problem. Our experience at Purdue has always produced the inseparability described in Fig. 1 and never the separability phenomenon of Fig. 2.

The theory of Root Locus requires the model to be the same for all control gains. Hence, the Root Locus method seems useful only when the modeling and control problems are separable. In the original Root Locus work of Evans [2], he imagined that the most appropriate representation of the plant model remained the same for all controls (as it turns out, this is equivalent to the assumption of no error in the plant representation). Since modeling error creates such havoc with our textbook theories, it is worthwhile to look more closely at the nature of modeling errors.

Model Error Structure

Considering only linear systems, let us label the state of our finite dimensional representation of the plant as x_R and the interconnection with the remaining states as x_T. Hence, the system actually obeys equations (1)

$$\begin{bmatrix} \dot{x}_R \\ \dot{x}_T \end{bmatrix} = \begin{bmatrix} A_R & A_{RT} \\ A_{TR} & A_T \end{bmatrix} \begin{bmatrix} x_R \\ x_T \end{bmatrix} + \begin{bmatrix} B_R \\ B_T \end{bmatrix} u + \begin{bmatrix} w_R \\ w_T \end{bmatrix} \tag{1}$$

$$y = \begin{bmatrix} C_R & C_T \end{bmatrix} \begin{bmatrix} x_R \\ x_T \end{bmatrix}$$

but the representation available to the control designer is

$$\dot{x}_R = Ax_R + Bu \qquad y = Cx_R \tag{2}$$

$$A_R = A + \Delta A, \quad B_R = B + \Delta B, \quad C_R = C + \Delta C$$

subject to parameter errors in ΔA, ΔB, ΔC. But, rewriting (1) using these definitions

$$e_i \triangleq \int_o^t A_{RT} A_T^{i-1} e^{A_T(t-\sigma)} A_{TR} x_R(\sigma) d\sigma = P_i x_R \tag{3}$$

$$f_i \triangleq \int_o^t A_{RT} A_T^{i-1} e^{A_T(t-\sigma)} B_T u(\sigma) d\sigma = Qu \tag{4}$$

$$e_t \triangleq w_R + A_{RT} [e^{A_T t} x_T(0) + \int_o^t e^{A_T(t-\sigma)} w_T(\sigma) d\sigma] \tag{5}$$

allows x_T to be eliminated in (1), yielding,

$$\dot{x}_R = A_R x_R + B_R u + e_t(t) + e_1(x_R) + f_1(u) \tag{6}$$

$$y = C_R x_R \tag{7}$$

$$e_i = P_i x_R + e_{i+1} \quad i = 1, \ldots, \infty, \quad P_i \triangleq A_{RT} A_T^{i-1} A_{TR} \tag{8}$$

$$f_i = Q_i u + f_{i+1} \quad i = 1, \ldots, \infty, \quad Q_i = A_{RT} A_T^{i-1} B_T \tag{9}$$

where we have fixed the coordinates in (1) so that $C_T = 0$. Such coordinates always exist if dim y $\leq$ dim x_R. It is also possible to imagine coordinates for which $A_{RT} = 0$, $C_T \neq 0$. In this case the error term of the sort $(e_t + e_1 + f_1)$ appears in the output eq. (7) instead of the state eq. (6). But, these variations do not alter the story, so I shall stick to the form (6) - (9), which is now a representation of the exact model error system. Comparing (2) and (6) - (7), it is clear that any model (2) which we may write for a linear system always has an associated model error vector of the form $e = e_t(t) + e_1(x_R) + f_1(u) + e_\Delta$, which is the sum of four types of modeling errors: $e_t(t)$ = errors which are functions of time (we usually call these external and internal disturbances), $e_1(x_R)$ = errors in model order (an integral operator P on x_R), $f_1(u)$ = errors in model order (an integral operator Q on u), $e_\Delta(\Delta A, \Delta B)$ = errors in parameters = $(\Delta A x_R + \Delta B u)$. Note especially that due to $f_1(u)$, the impact of the model error $e = e_t + e_1 + f_1 + e_\Delta$ cannot be determined independently of the control input u. The integral operator $f_1 = Qu$ is an explanation of the inseparability of the modeling and control problem. Model reduction theories concern themselves with the term $e_1 + f_1$. Disturbance accommodation techniques concern themselves with e_Δ. There is no control theory which promises the simultaneous accommodation of all four types of modeling error.

More importantly, note that the phrase "parameter error" has no precise meaning, since the submatrix $A_R = A + \Delta A$ is coordinate dependent (even though we have a specific A in mind) and, in fact, this coordinate choice affects all the four model error terms. Therefore, each term of the model error vector is nonunique. The challenge here is this: If we succeed (by choice of coordinates or by compensation) in reducing or eliminating one type of error, another type may get worse.

In the future, I think we must find ways to estimate the entire model error vector and not just certain terms in it. Because the subject of model error estimation embraces a broader class of errors, it has no substantial progress yet to report. One attempt [3] writes the model error systems (6-9) in the form

$$\begin{aligned} \dot{x} &= Ax \\ y &= Cx \end{aligned} \tag{10}$$

where $x = (x_R, e_1^T, e^T, \ldots, f^T, f^T, \ldots, \gamma^T)$. (The time dependent error e has for convenience been written in the form $e_t = P_\gamma(t)$, where the equality is only in a mean-squared sense and holds when the independent basis functions $\gamma^T(t) = (\gamma_1(t), \gamma_2(t), \ldots)$ form a complete set.) The matrix A has a specific form dictated by the aggregation of equations (6-9) to form (10). The model error vector is estimated if x is, since $(x_R^T, e_1^T, f_1^T, \gamma^T) = x^T C_1$ for some C_1. The parameter A and the state x can be estimated under certain conditions [3].

The dynamical system described by

$$\dot{\hat{x}} = \hat{A}\hat{x} + F(y - C\hat{x})$$
$$\dot{\hat{A}} = Q^{-1}C^TQ(y - C\hat{x})\hat{x}^T \tag{11}$$

drives this Liapunov function downhill ($\dot{V} \leq 0$),

$$V = ||y - C\hat{x}||_Q^2 + ||A - \hat{A}||_Q^2 \tag{12}$$

provided

$$C^TQC(A - FC) + (A - FC)^TC^TQC + L^TL = 0 \tag{13}$$

is satisfied for some L.

The <u>good news</u> is that estimators of the form (11), when used in the above spirit, embrace a broader class of model errors. The <u>bad news</u> is that condition (13) is unverifiable even when it is satisfied (A is unknown). Partitioned parts of (13) yield certain specialized results, reported in [4]. Most adaptive control and estimation algorithms can be explained in terms of simplications of problem (11-13). Adaptive control ignores (e_i, f_i, γ) in the x of (10). Orthogonal filters [4] ignore (e_i, f_i) in the x of (10).

A more direct approach to model error estimation was posed by Rodriguez [5,6]. By lumping $e_1 + f_1 + e_t$ into one term $e_x = e_1 + f_1 + e_t$, and allowing error terms also in the output equation, $y = Cx_R + e_y$, the model error system (6-9) can be written

$$\dot{x}_R = Ax_R + Bu + e_x$$
$$y = Cx_R + e_y \tag{14}$$

or in operator notation (assuming zero initial conditions)

$$y = K_1u + K_2e_x + e_y = K_1u + [K_2 I] \begin{bmatrix} e_x \\ e_y \end{bmatrix} \tag{15}$$

where the operators are defined by

$$K_1u \triangleq \int_0^t Ce^{A(t-\sigma)}Bu(\sigma)d\sigma$$
$$K_2e_x \triangleq \int_0^t Ce^{A(t-\sigma)}e_x(\sigma)d\sigma \tag{16}$$

Hence (15) may be written

$$y \stackrel{\Delta}{=} y - K_1 u \stackrel{\Delta}{=} Ke \quad , \; K = [K_2, I]$$

$$e^T \stackrel{\Delta}{=} (e_x^T \; e_y^T) \tag{17}$$

and has the minimum norm solution

$$e = K^* y. \tag{18}$$

The good news is that the model error estimation (18) requires no decomposition of the model error vector as in (6). (This is an advantage due to the nonuniqueness of the decomposition.) The bad news is that the pseudo inverse of an integral operator K^* is required, and this is not an on-line calculation. Some numerical examples are given in [6].

Identifying Structures Under Control

We now look at the parameter identification problem as a modeling method. Having already reminded ourselves that the modeling and control problems are not independent, we certainly expect that the identified model will be dependent upon the control inputs. Suppose that the closed loop system of Fig. 3 is "identified" as G'(s). Then, since the controller H(s) is known, the identified plant is recovered from knowledge of G'(s) and H(s),

$$G(s) = \frac{G'(s)}{1 - G'(s)H(s)} \tag{19}$$

Now, the interesting observation here is the "identified plant" G'(s) is a function of the controller H(s). Hence, if the controller H(s) is changed, the plant as the controller sees it is different. The fact that the plant looks different with each controller (hence with and without control) has not penetrated the identification research, judging from a sparsity of papers on the subject of identification under feedback.

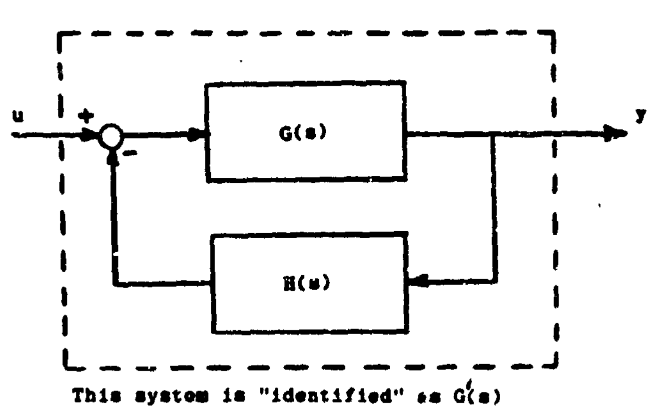

Figure 3. Identifying structures under control

Since the identified closed loop system $G'(s)$ is obviously a function of the feedback law $H(s)$, let us write $G'(H(s),s)$. Then, it is clear that the identification and control problems are separable iff $G'(s)$ is invariant under $H(s)$; that is, iff

$$G'(s) = \frac{G(s)}{1 + G(s)H(s)}$$

But this can happen only if there are no modeling errors ($G'(s)$ is exactly correct). Hence, the inevitable modeling errors force the inseparability of the modeling and control problems.

The conclusion here is that it is very difficult to define a meaningful identification experiment, one that provides improved knowledge with which to design a control law. One logical approach to this dilemma is to reject any identification result which does not produce the correct $H(s)$. That is, apply an identification method to the closed loop system treating both plant and controller as unknowns. Then reject the "identified" plant unless the "identified" controller matches the known controller This is not a sufficient condition for a successful identification experiment, however. The problems involved in such a unified identification plan include:

1. One identification approach may satisfy these conditions and another may not, even though both methods may have convergence "proofs" (which are based upon the assumption that only parameter errors are present in the model error vector).

2. Even after identification, the mathematical techniques used to separate the identification of the plant and controller subsystems will affect the results and conclusions.

3. Convergence criteria need to be established to determine when identification under feedback is successful.

Conclusions

Both dynamics and control textbooks are written as though the modeling problem and the control problem are separable. However, due to inevitable modeling errors, they are not separable. Moreover, since the modeling and control problems are not separable, neither are the identification and control problems. Research is needed to identify structures under feedback control. Otherwise, it is not clear that open loop identification experiments will be useful for providing models for control design. R. A. Frosch put it well this morning in his ACC plenary talk when he said, "We are not sure of what we are doing when we abstract the real world".

REFERENCES

[1] R. E. Skelton, J. Davis, and Y. Yousuff, "A Computer Aided Design for Suboptimal LQG Control", IFAC Symposium on Computer-Aided Design, West Lafayette, IN., Sept. 1982.

[2] W. R. Evans, "Graphical Analysis of Control Systems", AIEE Trans. Part II 67, 1948, pp. 547-551.

[3] R. E. Skelton, Course Notes, AAE 664, Purdue University, West Lafayette, IN., 1983.

[4] R. E. Skelton, "Adaptive Orthogonal Filters for Compensation of Model Errors in Matrix Second Order Systems", J. Guid. & Control, Vol. 4, No. 2, March, 1981.

[5] G. Rodriguez, "Model Error Estimation for Large Space Systems", JACC, 1980, San Francisco.

[6] G. Rodriguez, "A Function Space Approach to Smoothing with Applications to Model Error Estimation for Flexible Spacecraft Control", IEEE CDC, 1981.

R. F. CARLISLE: Future Research Technology Directions for Space Station* What we are attempting to do, using the available literature and expertise, is to get a solution that can optimize the station by further application of controls. In the world of spacecraft systems, when the power subsystem fellows tell me to bring on-line improvements in power, I tell them to forget it. This is an expense that I do not think the system can afford. We will go back to the user and reduce the power requirements by applying other techniques. We are dealing with trades in the integration of subsystems. Thus, when a control system designer says I cannot solve your problem, I go back to structures. We just have to beef it up and fly it anyway. When I cannot afford the structure and the weight to do that, then I go back to the control people and say how can you help me. That is the world that we are dealing with.

On the space station, as you know, we have a planned approval for the program. We are all anxiously waiting for the approved budget this year. If successful this year, we are looking for a flight date approximately in the 1992 time frame. In the world of research and technology and advanced development and design, that means we can expedite some promising hings in the pipeline. This will be done by increasing funding for certain technologies and bringing them to a state of maturity and readiness that perhaps can improve the initial space station design. Let me share with you some of the things that I see in the design profile.

First, we have a ground rule that says the space station is going to be an evolutionary design. That means it is going to grow and change with time. There will be block changes in configuration, and maybe block changes in performance. Therefore, it behooves us to do the best we can in the initial design, so that we can evolve gracefully and economically to meet those challenges. If we lock ourselves in with a design that does not have flexibility and growth potential, then the control system may be one of the things that bounds the extent of evolution that we could hope to achieve. All of the sub-systems are trying to bring robustness, flexibility, and evolution of growth, so that they are not the ones to bound the potential for space station evolution. Another interesting thing in space, as opposed to aeronautics, is that the space station is essentially the first time (really the shuttle was) we can repair on-orbit. We are asking for 20 years continuous life with on-orbit maintenance. That gets into the practical world of hardware and failure analysis. It also gets into the question of how we accept failures in the most economical way, and whether we want to have built-in redundancy and fault tolerance or repair on-orbit. Repairing on-orbit means we need tests and analysis in order to locate failures, and a means of accomplishing the repairs. Thus, we are looking at extremely interesting challenges with the space station. Essentially, we have 5 years to mature promising technology and applications. But in an evolutionary sense, promising research that could be made into a block change is also an opportunity. Overall, it is a world of opportunity that I do not think I have ever seen before. Thus, I want to illustrate just a little more what I think the problem is, and review with you what I understand of where NASA has gone with their funding that is applicable to space station. Finally, want to leave with you our definition of what we are looking for that is in the spirit of opportunities for future research.

*The speaker refers to slides used in the oral presentation that were not available for inclusion in this written report; however, the major points are evident even without the slides.

If this were our initial space station-and it is not, it is just typical-each one of these would be a payload flight for the shuttle. So you place one of these in orbit and leave it there, and then you bring the shuttle up and bring another module to it. Now, I think this is fairly complex for the initial operating configuration, but let us just assume that for now and walk through the control problems. You have to be able to stabilize something like this. You have to be able to hold it well enough in attitude so you can mate to it, and mate to it with only the resolution of what the shuttle can do, or what this can do. As that changes, there are obviously major shifts in mass distribution. Maybe two modules hooked together can still be considered a rigid body. But, as it grows in size, as the whole structure gets larger, then you begin to wonder what the relative rigidity of these joints is. The initial space station has a requirement for 75 kw useful on-board power. That is a solar array of about 20,000 square feet, half an acre and about 20,000 pounds. So, it is not trivial. There are significant distributed low-frequency appendages on this structure. This is the radiator, which dumps the waste heat. Because of the efficiency of a closed cycle like this, there is almost 75 kw being radiated out. So, this is not a trivial appendage either.

This is another illustration of a larger space station. Now look what we have done to ourselves. If these were rigid bodies with classical control, and then somehow this whole matrix grew to this configuration with these appendages, then I wonder if that original classical control design would stand some graceful economic evolution to control that cluster as it is shown there. I would say that is reasonably realistic as to what the evolution would be. Going a bit further, this is a collection of conceptual drawings of what it may grow to eventually. I cannot define anyone of those as being realistic, but any of them could be. We would like to drive in that direction. The challenge to you is that control systems of the original configuration should not constrain us, if that is a reasonable request. I do not know whether it is or not.

Let me go back then to a very quick review of where we have been in NASA funding for control of large flexible structures. In about 1978, we started working on a large structures program. Initially, we homed in on antennas. These are two antenna configurations: the hoop column and the wrap rib, representing Harris Corporation and Lockheed designs. In the control area, we dealt with the problem of maintaining the relationship between critical points of the feed and the reflector. We also dealt with the problem of surface control. This program started as a structures program. As we got into the program, we recognized that we were not dealing with a system unless we addressed the control problem and the RF characteristics. We had a ground test program that built up full-size segments of these antennas. Here is a section of four gores of the hoop column. This shows it built up on the ground and spreading the mesh. These are small reflectors that are out on the mesh for lining up the mesh. They can also be used to close the loop around to measure and control the surface conditions. This is a full scale model of the wrap rib, with the mesh deployed. The ribs cannot support themselves in one G. They are hung from spring assemblies attached to the ceiling and to the floor. We hoped when we started that we could measure some dynamic characteristics. In retrospect, I have to say that it was successful research since we learned that we failed. We could not get significant resolution of any importance to measure dynamics. We did not spend enough money or time to get the precision of realistic measurements for dynamics. This led us to conclude that since we did not know what to do on the ground anymore, we were going to have to fly. We proposed a flight program planning exercise in-house. We recognized the expense in undertaking such ambitious planning, but we felt it had to be done. The plan grew to the point that we killed it with economics. We ended up with an in-house estimate of approximately 350 million dollars to run perhaps a single flight that would only learn something about control dynamics. Figuring the system would not stand that much expense, we decided try to get a payload to share expenses with us. We couldn't find a payload willing to take the risk of committing to an unproven structure. Since nobody wanted to go with us, and we could not afford it alone, we stopped that program and faced the fact that we do not know how to go full size in flight. We are still working on the problem. I think, and several others agree, that we are developing powerful technology. We want to achieve that plateau of technology where we can handle control of low frequency interactive modes. We are now planning an exhaustive ground test on a much smaller article. The question is how do we proceed to validate that design. Can we get sufficient measurements on the ground, with instrumentation and fixturing errors, to have the confidence to fly full scale, larger vehicles? Or do we need a flight test to validate the ground test? If we have to have a flight test, how do we scale? If we use a small ground sample and fly that same sample, to get the relationship between the on-orbit and ground characteristics, do we gain enough confidence to fly full-size structures? Those are the things that we are really worrying about. In the current planning of the space station, there are several configurations. The real configuration has not been decided. The eight contractors that have been working with us all recognize that controllability is a critical issue for confidence in the original design. This configuration, called the delta, has a rigid structure. It is an inherently stiff design, with the modules lined up at the ends of the triangle of a pyramid. It is the most rigid design. It is also probably the one with the least growth potential. These two are quite similar, with the modules gathered in a fairly stiff arrangement and with a flexible appendage. This design offers the opportunity and advantage that the shuttle can come in and berth to it away from the solar arrays; but it can, if it grows in evolution, significantly change and complicate the control problem. The question that I pose is: how can you help us with the tough decisions that we have to make in the next five years? What is the original control configuration that can meet most of the desirable features that I mentioned earlier? Our problem may be summarized as evolutionary growth, size and complexity, possible need for on-orbit test, and a long-life requirement. We have the opportunity for solving it with control technology or with structures technology or by some combination of each. No matter what that combination is, we still have challenge of how the initial design should give us the most options.

H. A. REDIESS: The Role of Experiments in the Development of Control Technology*
Experiments, both in laboratories on the ground and flight experiments on-orbit, are necessary in the development and validation of controls technology for large flexible space structures. I was pleased to see that it was recognized in this workshop, and that there were so many papers that touched on experiments. I have not prepared a formal paper on this subject, and for the most part I am singing to the choir. However, there are three points that I would like to discuss:

- Why experiments are important for developing the technolog

- The need for a coordinated program to validate techniques from analysis to simple experiments to complex experiments.

- The need for a cooperative program among government, university and industry to make the most effective use of experimental data.

Why Experiments are Important. We are beginning a new era with large space systems that will tax our current methods of developing spacecraft. We are considering space systems that are sufficiently large that they must be developed in space in sections and assembled. The systems will be designed for the zero-g vacuum environment of space, and we will not be able to fully assemble and test the entire system on the ground before deployment. We will not be able to do complete ground vibration testing.

Ground vibration testing has been an important aspect of developing control systems for aerospace vehicles where there are significant structures and controls interactions. We currently do the best job we can in modeling the structural dynamics of a vehicle, but we have an opportunity to fine-tune our models and, in turn, the control systems with ground vibration data.

If we cannot test the complete space system, we need to have a higher degree of confidence in our modeling and design methods than we currently have. We may have to do on-orbit systems identification of the complete space system, or even as it is being constructed in the case of a space station, before the attitude control system can be operated. We must have confidence in our systems identification methods before we get to operational systems.

There are other factors that further complicate the problem of having confidence in our analysis and design methods. Three significant ones are:

1. Structural modes will be overlapping the required controller bandwidth.

2. Uncertainties in predicting damping.

3. Introduction of new composite materials.

Figure 1 points out the trend we expect to see in the control and structure interactions of future spacecraft, as they get much larger and hence more flexible. In today's spacecraft, the structural modes are sufficiently separated from the controller bandwidth that relatively simple filtering is adequate to deal with the interaction. In future flexible spacecraft, the structural modes are expected to overlap the required

*Several of the charts used by H. A. Rediess are from a NASA presentation on Control of Flexible Structures and were used with NASA permission.

controller bandwidth. Requirements for rapid slewing, precise pointing, and very accurate shape control will force the designer to consider the control and structure interactions. Active structural mode suppression may be necessary to achieve effective and affordable designs. We need a higher degree of confidence in our structural modeling and control design techniq   for active controls.

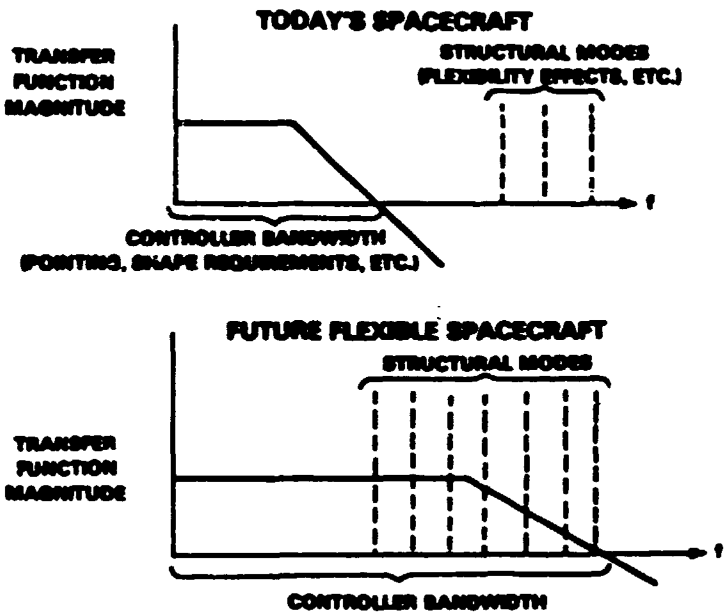

Figure 1. Trends in spacecraft control and structures interactions (From R. A. Russell of NASA Headquarters).

The second factor that complicates the problem is the uncertainty in predicting the inherent damping of space structures. Professor Vander Velde mentioned earlier that damping characteristics are probably the most difficult to predict and yet are very important in control design problems. Damping characteristics of complicated structures, such as a large tetrahedral truss antenna with a long offset feed, can be very different in the space environment than on the ground. Figure 2 shows experimental data on simple-joint damping obtained by Professor Mead of South Hampton University. Test results are shown for a no-joint specimen and for a joint specimen in air and in a vacuum. Note that joint damping in vacuum is about one-third that in air. These data are for one simple type of joint, for one type of material (aluminum), and for the fundamental vibration mode in oscillating tension and compression. Considering the multitude of types of joints, materials, and vibration modes, one can see the difficulty in predicting damping of large complex space structures. There is a need for a series of experiments on small and full scale specimens. If possible, these experiments should be conducted in the space environment to develop an adequate data base and prediction techniques.

The third factor is due to the introduction of new composite materials, such as metal matrix composites (MMC). MMC have several characteristics which make them particularly well suited for spacecraft applications. They have a high strength to

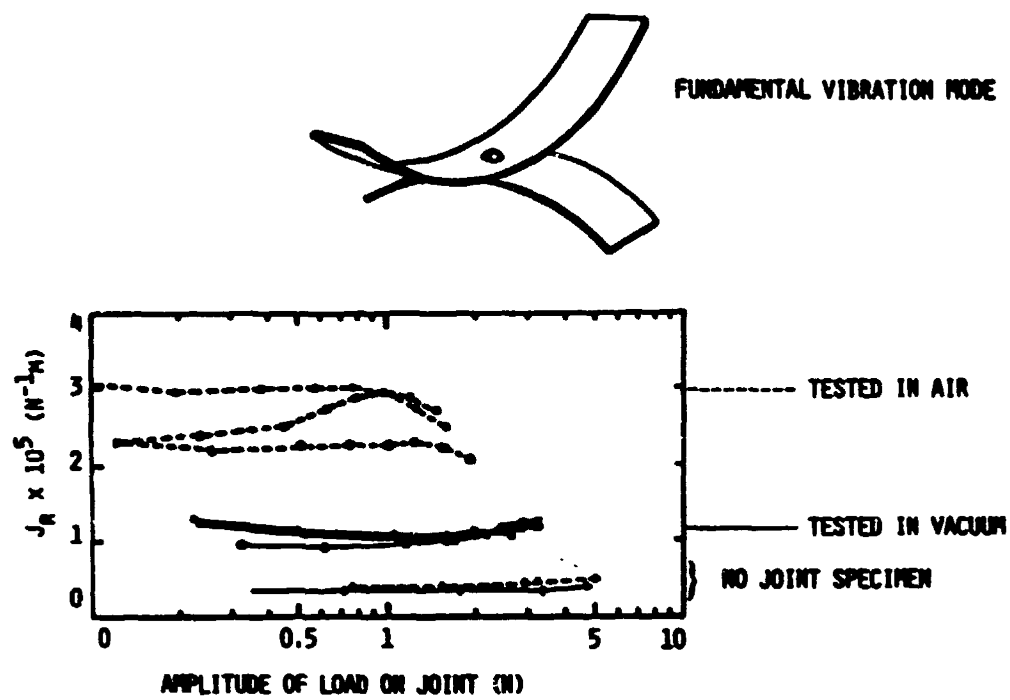

Figure 2. Joint damping data for oscillating tension/compression tests (From Prof. Mead of South Hampton University).

weight ratio, excellent dimensional stability, and low coefficients of expansion. Certain important characteristics, such as stiffness and damping, can be changed and tailored by the way the MMC is made. The effect of material characteristics could have on spacecraft performance is illustrated in Figure 3. It depicts the elements of a study being conducted by HR Textron for the Naval Sea Systems Command. The spacecraft is a hypothetical surveillance system that is required to maneuver for survivability and yet meet stringent pointing and shape control requirements even while maneuvering. The chart in the center illustrates the effect of one material parameter, stiffness, on line-of-sight error at various maneuver acceleration levels. It is necessary to characterize these new materials in laboratory tests in order to assess the effects on spacecraft performance. That would, in turn, improve the ability to predict the structural dynamics characteristics. Control and structural interactions will become more significant in future large space structures. The ability to predict accurately the damping characteristics is important for effective controller design. Characterization of MMC properties could lead to optimization of new materials, structures, and controls for flexible space structures. These and other factors will require a variety of experiments in laboratories in space to develop the technology with confidence.

Need for a Coordinated Program The second major point I wanted to make was the need for a well coordinated program to validate techniques from analysis to simple experiments to complex experiments. The final report of the NASA Space Systems Technology Advisory Committee, ad hoc Subcommittee on Controls/Structures Interactions, dated June 8, 1983, strongly supported the need for ground and on-orbit testing for developing control/structures interaction (CSI) technology. Figure 4 is from that report and shows the ad hoc Subcommittee's recommendation for a coordinated

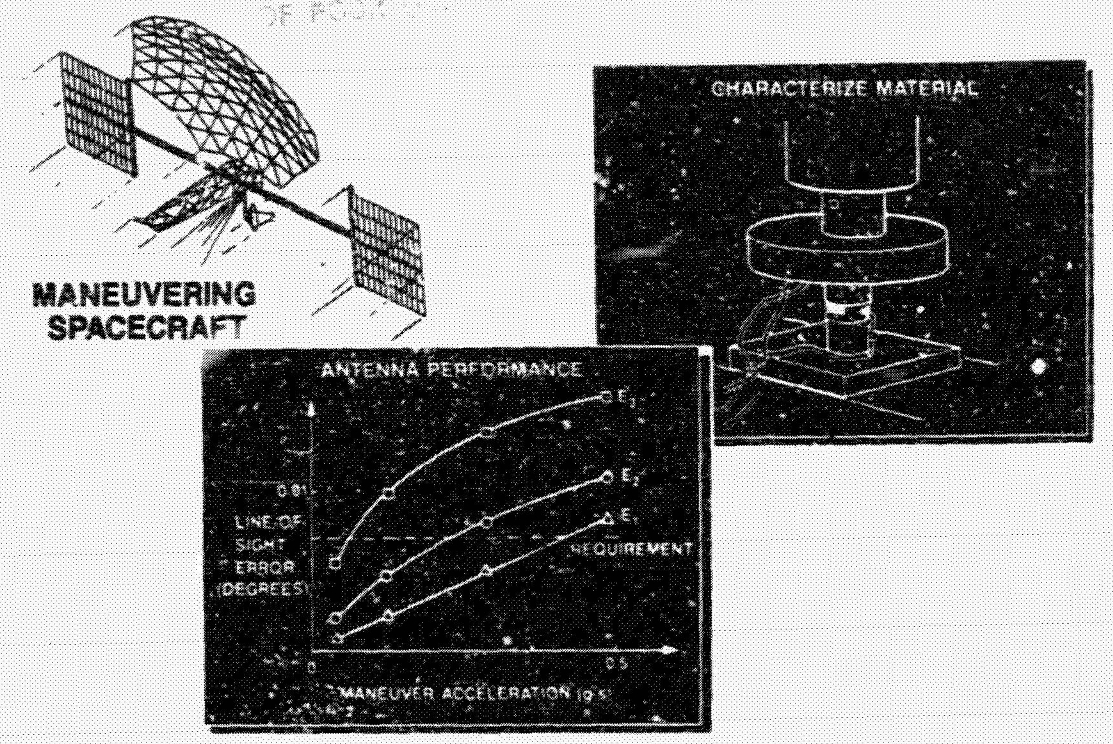

Figure 3. Effects of material stiffness on spacecraft performance.

experimental program to develop and validate the technology. It also suggests a time frame for various elements in order to reach a high-confidence level by the early 1990's. The process is iterative and involves technique development, ground testing, and on-orbit testing. An important part of on-orbit testing is the validation of ground-testing techniques. The report suggests a major control/structures interaction flight demonstration to validate the techniques once the analysis tools and ground testing procedures are refined. The report indicated that such a flight demonstration could be conducted in the early 1990's. That is the type of coordinated analysis, ground, and flight test program that I also believe is needed to adequately validate the technology.

Figure 5 shows one element of NASA's planned program for developing this technology for multibody configurations with flexible appendages. The approach is to start with a relatively simple configuration and to progress to more complicated and realistic ones as the techniques are refined. Even though these are ground tests, they can be very expensive. A well coordinated program is needed to make it cost effective.

Need for a cooperative government, university, industry data base program. My third and last point is on the need for a cooperative data base among NASA, Air Force, industry, and universities to make the most effective use of experimental data. Figure 6 shows the major test elements planned in NASA's control of flexible structures program. It is envisioned that these will include extensive and costly experiments on the ground and on-orbit. The Air Force is also conducting extensive ground and flight test activities. The nation will only be able to afford a limited number of these test programs. Therefore, it is vital that the data be made available to a broad cross-section of the controls technology community. I recommend that NASA

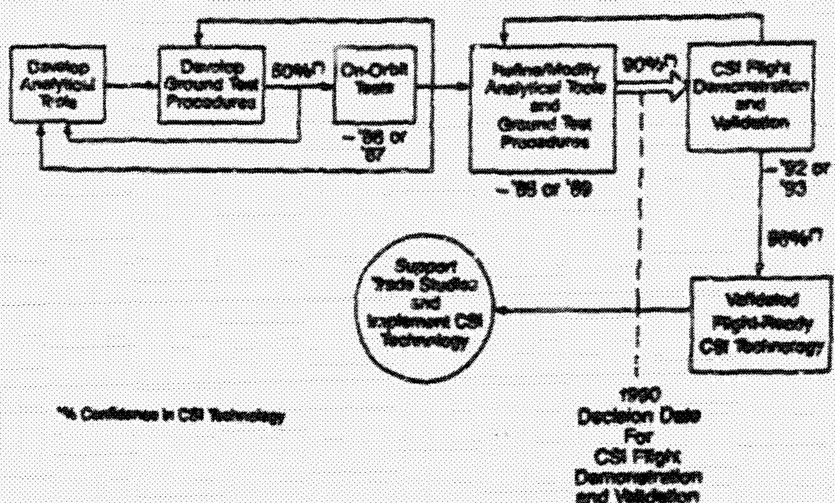

Figure 4. Role of ground and on-orbit testing in control/structure interaction technology development (From final report of the NASA ad hoc Advisory Subcommittee on Control/Structure interactions).

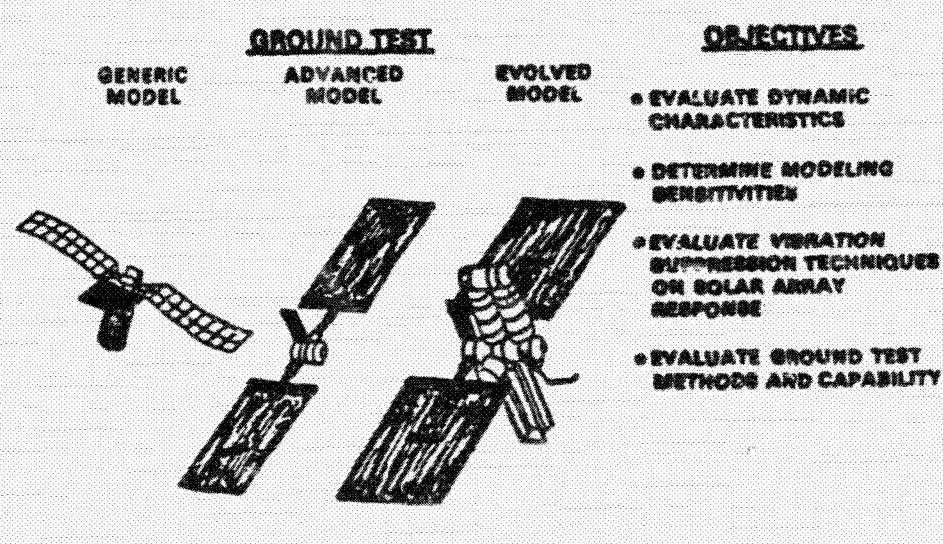

Figure 5. Examples of multibody dynamics models considered in NASA's control of flexible structures program (From R. H. Russell of NASA Headquarters).

and the Air Force develop a national cooperative data base for these major ground and on-orbit experiments. The controls/structures technical community - including universities, industry, and government laboratories - should be involved in establishing the experiment and data requirements. A data base should be established so that many of the different techniques for modeling and controlling of structures could be tested and validated. There must have been at least 50 different ones discussed at this workshop alone. The data base should be devised in such a manner that it can be easily accessed and used without extra programming by each user. It should be available at a low enough cost that universities could use the data in relatively small research grants. If these requirements are considered and included at the outset, there should be minimal impact on cost and schedule of the programs.

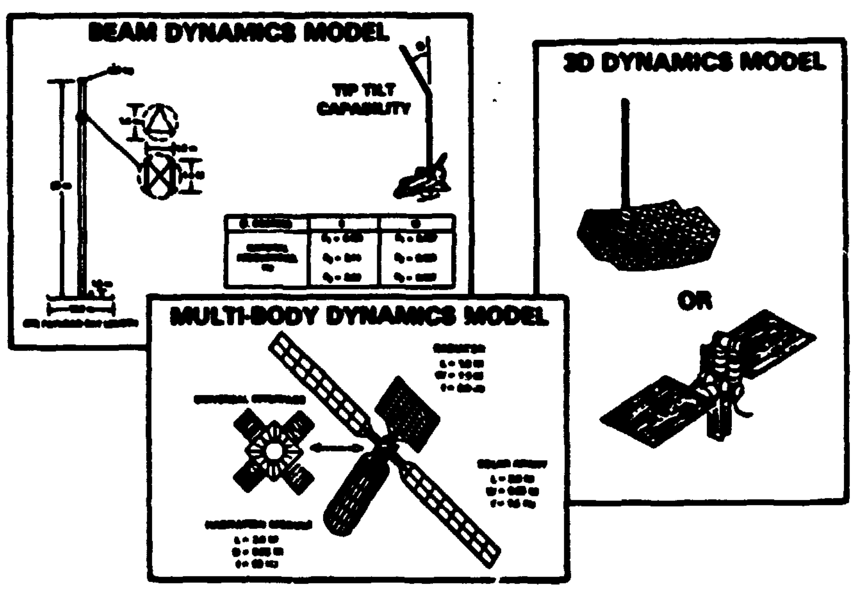

Figure 6. Test model descriptions for NASA's control of flexible structures program (From R. H. Russell of NASA Headquarters).

It will not be possible to rerun these experiments with each new analysis technique or control concept. It also gets very expensive to re-analyze experimental data with a second or third researcher, if the data are not already in a good user format. With appropriate pre-planning and setting up of a multi-user data base, the cost for additional analysis by alternate researchers should be quite small.

In conclusion, my three main points were that: ground and flight test experiments will be necessary to have high confidence in our systems identification and controls/structures interaction design techniques; a well coordinated program is needed that involves analysis, ground testing and flight testing; and, lastly, an interagency cooperative data base should be set up for all major ground and flight test programs to achieve the most effective use of the very rare experimental data. I would like to commend NASA on constructing an excellent program plan for developing and validating the technology for control of flexible structures as presented in Mr. Russell's paper.

<u>EDITOR'S NOTE:</u> This concludes the formal remarks made by the panel members. There follows a discussion period between the panel members and audience participants.

R. V. RAMNATH: I would like to share with you some of my experiences, interests, and aspirations in the area of asymptotic analysis. Asymptotic methods have been used with great success in many branches of the physical sciences, mathematics, physics, celestial mechanics, mechanics, etc. It is my feeling that asymptotic methods have not been used as well as they should have been in the areas of large space structures, structural dynamics, and control. There have been a sprinkling of papers using perturbation methods and asymptotic analysis in the last ten or twenty years. Professor Lions' paper highlights some of the issues. We have been working in this area for sometime. I would like to tell you about our experience.

Asymptotic Analysis. We all agree that real physical problems are very hard to pose exactly, and, even if they can be posed, they will result in highly nonlinear coupled equations, for which closed form analytical solutions are hard to obtain. For example, large flexible space structures are described by partial differential equations with variable parameters. Even worse, these parameters may be nonlinear functions. For such problems, it is very hard to obtain closed form solutions. So what we do is try to get some kind of an approximation. Historically, approximations have been tried as long as people have been analyzing real problems. Asymptotic analysis is one way of approximating the problems, and we have used it fairly successfully.

I would like to define asymptotic analysis as a study of applied mathematical systems in limiting cases. There seems to be a little bit of confusion in the literature about the convergence and the asymptoticity of equations. These two words are used interchangeably. We can discuss the difference in the context of a simple example. Consider a slowly decaying exponential function exp (-at), where a is a small parameter. The series representation of this function is convergent within an infinite radius of convergence. But, in order to get the approximation by truncating the series, one has to be careful. If the argument is very large, while the series converges, it converges very, very slowly. Thus, if one takes a few terms to represent the series, one gets very poor results. Thus, this is an example of a convergent series that is not asymptotic in certain domains. Also, there are other functions which diverge everywhere, but for certain values are known to be asymptotic.

Asymptotic analysis is considered as an art and science by practitioners. The science is what mathematicians worry about. For example, they worry about how to calculate these functions, etc. On the other hand, engineers are faced with unknown parameters, so that there is some kind of judgement required. This is the art side of the problem.

Asymptotic analysis can be used in simplifying complicated problems. The principle of simplification states that in the asymptotic limit the system simplifies. Professor Lions talks about the need for more asymptotic analysis in his paper, mainly because it leads to simple descriptions of very complicated systems.

The principle of minimum simplification or maximum balance states that there exists a representation of the problem which retains most of the prominent features of the problem, while it is simple enough to obtain a closed form solution to it. The real problem may not be amenable to a closed form solution. These two principles are not theorems but give a guideline for approximating problems which I have found very useful.

Simplicity is obtained basically by neglect of terms im the mathematical model, but if one throws away too many terms, the problem posed may be useless. Thus, an optimum has to be found. I have found that this principle of minimal simplification or maximal balance is very useful in this regard. There are a lot of ways of simplifying a system, but a particular approach that I like is that of asymptotically ordering a complicated system. Asymptotic ordering puts a complicated system into a hierarchical structure, where you start with the simplest system and add on to it another sub-system which is a little bit more complicated. Thus, one achieves some kind of ordering and a cascade of systems of greater and greater complexity. Then one stops when the systems become too complicated to solve.

We have applied this to model the space shuttle. It has a 50-state differential equation describing rigid body motion, flexible body motion, control actuator dynamics, etc. The hierarchical structure could be obtained because we could differentiate by time scaling. This approach is called the multiple scale approach.

Multiple Scale Approach. This approach consists of taking an independent variable in the differential equation and extending its domain into a space of higher dimension. When the problem is restated in this new space, the problem gets simplified considerably.

For example, a dynamic phenomenon which exhibits qualitatively different behavior, such as fast motion combined with slow motion, can be converted into two problems. The independent variable, time, will have two scales, one for the fast motion and the other for the slow motion. With these two new independent variables, two partial differential equations can be written in the place of one differential equation.

Physically, it is of interest to think of the following experiment. Imagine there are observers with clocks observing a phenomenon. Each clock counts time on a different scale. Thus, each observer observes only certain aspects of the phenomenon which may be different from the others. The observer with the fast clock observes the fast changes of the dynamics while the observer with the slow clock observes only slow changes. Thus, it is possible to separate all the motions and then combine them together to get a composite type of representation. Now, one solves this new problem in higher dimensions asymptotically and requires the solution to match with the solution of the original problem along certain lines which are called trajectories. Thus, we are able to get back to the original problem.

Applications. The multiple scale approach was used to solve the problem of electrostatically controlling the membrane mirror of a space antenna which would be used in radio astronomy experiments. A membrane made of Mylar is preferable because it is light and can be folded. Thus, it is convenient to carry in space. The shape of this membrane is to be controlled by an electrostatic field generated by electrodes. Even though the electrodes are finite, the electrostatic field is continuous. Thus, a continuous membrane is to be controlled by a discontinuous force. If the shape of the membrane is a perfect circle, the mode shapes are give by Bessel functions. But when the shape is not circular, solving for the mode shapes is very difficult. But, our experience tells us that this is where art comes into play. The independent variable can be split into two variables that are nonlinear functions. Then, a solution in terms of Bessel functions can be obtained, whose arguments are these nonlinear functions. Thus, one obtains an asymptotic solution for the mode shapes of the membrane.

The payoff of this asymptotic solution is that we can understand the dynamics of the model asymptotically. The error is not zero, but it is not large. We are able to think of a feedback solution for the control problem. The solutions have a Bessel function of a different kind with the feedback gain embedded in its arguments. Also, we can study its stability and controllability and come up with a constructive procedure to calculate feedback gains and stability.

Conclusions: It is my feeling that more and more studies would indicate the usefulness of approximations using asymptotic methods for problems which are very difficult to solve analytically. The advantages of asymptotic methods are that one obtains analytical or quasi-analytical solutions to these problems. This helps in studying the properties of the system, such as stability and controllability. Also, the methods can be used to solve control problems. Even though the errors are not zero, they are rather small compared to other methods. So I want to reiterate Professor Lions' suggestion of looking at asymptotic solutions of distributed parameter systems.

QUESTION: There are a range of opinions on Space-Station controls, some of which say that it is just another Skylab. If that is true, why can't we merely use the control laws from that program?

RAMNATH: I want to paraphrase what R. A. Frosch said, "We are not sure of what we are doing when we abstract the real world." When we develop models for these things, we cannot know the importance of modeling errors until we fly. Therein lies the rub. It depends on the performance requirements of the Space Station. If the performance requirements are benign, we can use Skylab technology. If you are asking for complicated requirements, that require control systems bandwidths less than the order of hours, then we should worry about flexibility.

CARLISLE: I think it is reasonable to assume that experiments that require very precise pointing would have some control system just as they did in Skylab. What concerns me the most is that we have to be able to hold a large station stable enough to rendezvous and dock with virtually zero energy transfer. Then we want to be able to evolve. The evolution is "to be determined". We just do not know what its nature is. The question is: what can we put in the first one as a control system architecture that will give us flexibility to evolve in the future? I think if we go with Skylab technology, the control system is going to bound the evolutionary growth prematurely.

REDIESS: I think that the available controls technology has got to be self-fulfilling in terms of the type of space station one might have. For example, if we rely on the technology that presently exists, which was adequate for Skylab, we are going to be limited to a type of space station that is compatible with that or suffer very expensive modifications in space at some later time when we want to expand that capability.

SKELTON: It was mentioned earlier that we cannot afford to do full scale testing in space. What evidence do we have that we can afford not to -- in other words, it may turn out to be less expensive in the long run.

CARLISLE: The problem is: if we have to have full scale testing in space to validate new technology, and the system says we cannot afford it, then we are bound to live with something less than the potential technology that control analysis and research shows is very promising.

QUESTION: In various meetings in which I have participated recently, I have sensed an opinion that we have had a lot of effort on theoretical development directed toward large space structures. There seems to be an unjustified impatience with theoretical developments, and a concern that researchers are going off in the wild blue yonder trying to address problems that may not exist. The impression is that it is more appropriate to develop an extensive experimental plan and defer further emphasis on theoretical activities. I would like to get the panel to comment on this.

CARLISLE: I think research is very promising. However, in the world of program management, unless we validate the research, it will never get used. The question is, how do you get your kicks? In pure research, you can get your kicks by doing analysis and identifying a promising application. Then, you get bored with it and want to take on another new idea. If nobody else picks it up, develops feasibility, and validates your first idea, that idea will never get used. I think there is a necessity for all phases of research. I think it is terrific to do fundamental work. I think it more imporant that research be developed to the point that there is enough confidence in it to be used. That is a tough decision. I have had some experience with program management. I can tell you that, when I was running a major program, I was not interested in research unless I had a critical problem. When I had a critical problem, I needed all the help I could get. I would take as many chances as I had to, to meet my obligation as program manager. Unless I had that critical need, I did not have any incentive to add complexity in maturing an experimental technology. A program manager has no incentive to do that. It has to be done in the pre-development phase. This relates to my concern on Space Station. We have five years to mature promising ideas. I am not satisfied that we are paying enough attention to sort out which are the most promising views. With an evolutionary approach to the Space Station, we should not go with last year's technology, we should go with next year's technology, with a plan to evolve to the future -- do something even better. I feel quite strongly that there is a necessity for several views and that we need to coordinate all those in some complementary way. I also believe that there is a personality clash between the types of people with original ideas and those required to carry out the applications. We have to do something as a community to improve the communication and cooperation, so that we can sort out the really promising ideas and get them used. The more new ideas get used, the more the whole discipline will proceed. Soon the rest of the Space Station will be doing things with structures that we never did before, because the control system technology is needed. I do not think we are really up to speed now in that area, and I would like to encourage it.

QUESTION: As program manager of a Space Station program, would you be satisfied to incorporate methodology in control systems or operations that you had not demonstrated in some kind of space experiment?

CARLISLE: It depends. That is a point I tried to touch on earlier today. If the technology is too expensive to mature full-scale in orbit, then the problem is to gain confidence to use it the first time full scale. We flew the shuttle, and we did not do as much flight testing on the shuttle as we do on aircraft. When the first Shuttle flew, it was a brand new thing in space. We had enough maturity, confidence, and experience, so that was a good decision. I also think that the decision to use new technology varies with the experience of the decision maker. You think of your own field. If somebody suggests a new technology to you, you get comfortable based on your own experience. If somebody suggests something in a field foreign to you, and you are a good researcher or engineer, you will have all kinds of doubts, without the experience to back them up, and you will never buy the proposal.

SKELTON: I would just like to make a point about the problem with waiting until there is a need for a new method before we start worrying about it. We do not have a continuity that serves as a basis for a continuous flow of ideas into the system. One of the things that strikes me as odd is that in this country, and in the western world, there is no institute of significant size that focuses on control and system science issues, as there is in the Soviet Union. The Soviets have more than a dozen institutes, sponsored by the Academy of Sciences, each one employing 3 to 4 thousand engineers with advanced degrees. They have the responsibility to carry on research all the way from the very theoretical to the applied and experimental in system topics such as control, identification, artificial intelligence, and all of their interactions. It seems to me, if you look at our organization charts, we find guidance and control blocks somewhere along the line. That narrow view of it may have covered the subject 30 years ago. I do not think it does today nor it will tomorrow. I am wondering, where in the western world it should be covered, whether it should in the Air Force, in NASA, or somewhere else. I think everybody is expecting the other guy to do it. There is no consistent substantial support of the size and focus required to address the issues that we deal with. When we launched the Saturn V vehicle, we had interaction problems between propulsion systems and control. Then, we had interaction problems between the structural dynamics and controls. We can name a number of instances and examples where we defined the control concept too narrowly. We thought of it as a little black box to be added to the system after everything else was done. I think the controls community has a much broader view today than it did 10 years ago. However, in terms of the organizations that sponsor research, there is still only a very small segment that understands this broader view.

CARLISLE: What constructive actions are suggested?

SKELTON: One concern is this. We should determine whether or not to create an institute on systems science or control systems issues, or whatever you want to call it. There may be good reasons for not creating such an institute, but there should be a study to decide. The decision not to do it should be a conscious effort. Let us not lose the technological leadership by default.

VANDER VELDE: I would like to comment on your concern about combining control theory with other disciplines. We see this phenomenon at MIT (I assume you do also at Purdue): the graduate students today very commonly study quite a good deal in control and structural dynamics. This interest has been stimulated by the problem of large spacecraft control, which they look upon as an interesting challenge. It was very uncommon a number of years ago for our students to study those two areas very much.

CARLISLE: I would like to comment that in the last four or five years, within the sphere of NASA we have made a significant change. Funding for controls has gone up by a factor of 10 or more. We have this visibility that was talked about -- the necessity of addressing the problem of structures and control dynamics interactions. We have visibility in the budget and are looking for further expansion. I think that we have a thing going now because of this recognition. This is a powerful tool and can make a big difference in Space Station. We should try to pay attention to it and take advantage of that exposure.

SKELTON: I agree there is progress.

BALAKRISHNAN: I just want to make a comment on an earlier statement maintaining that structures students have discovered control theory. Actually, the number of students going into controls is much more smaller than it used to be. At UCLA, many more are going into communications. I have a question regarding the evolutionary design concept. Is this something new for NASA, or has NASA had any experience doing something like that before? What kind of comments from university, industry and scientific communities are taken before such decisions are made? Is there any formal mechanism, or does somebody just make the decision?

CARLISLE: I think the opportunity for permanent presence in space just spontaneously developed the evolutionary idea among those of us who have worked on it. The only way to achieve permanent presence is by service and maintenance. The Shuttle gives us the opportunity to evolve. I think we are in the infancy of even understanding what we mean when we say that. I do not know of any formal way that we consulted with anybody. It was just handled spontaneously, with a very preliminary plan which could go in any direction. The system engineering and integration task on the Space Station has been planned to be done within the agency with contractor support. Though the program is very new, we have been planning technology for a couple of years. But we are really in an infancy state. I meant what I said. I do not think we know what we mean when we say evolutionary design, except that we know we do not want to be bounded with last year's technology. We want to open it up to take advantage of the Shuttle and logistics and have it grow.

QUESTION: Is the project pretty definite?

CARLISLE: It is definite that we did not yet win a vote in Congress, but we did win the vote of the President. In his speech of last January, it was one of the things that he quoted as being one of the future commitment in space for this country.

REDIBSS: I would like to go back to the point R. E. Skelton raised about the institute in control. In part, it relates to my experience within NASA, particularly in the controls area. I think there is a long term fundamental outlook within NASA of not really having treated controls as a science and discipline. It has been treated more as an engineering area. It takes quite a bit of effort for an organization like NASA to turn that around. There are times where we have received substantial increases in support in the area. It is due largely to program managers such as R. S. Carlisle, who understands controls and its real difficulties and concerns, and who provides personal support. When major projects come along that clearly require some new technology in controls, there is an opportunity to increase the support for developing the technology, particularly towards the more costly end of it. I think there still is a difficulty in really recognizing controls as an equal disciplinary area with some of the more well established disciplines, which have had decades of support with NASA. There are a number of people who are aware of that within NASA. It is just a difficult institutional thing to turn around.

QUESTION: Do you think it is a reflection of their evaluation of the relative importance of the subject?

REDIBSS: No, I think the problem is that it is often treated as an engineering problem which can be solved through a good engineering approach-as compared with developing the fundamental concepts, methods, and tools as a discipline, such as we do in aerodynamics, materials and other disciplines.

VANDER VELDE: In aeronautics, we are all familiar with the term control-configured aircraft. In fact, NASA has done work in-house and has sponsored a certain amount of work in that area. You never hear the term control-configured spacecraft, even though you mentioned the requirement this morning for integrated design. It seems as if there may be perhaps more to be gained in the large spacecraft area through the integrated design of the configuration, assuming from the onset that there will be some form of control. That would really be a control configured spacecraft.

CARLISLE: I think aeronautics is ahead of space technology in the integration of structures and controls.

SKELTON: I think the universities should take some blame for this problem. In the past, students would take a dynamics course, and they were told: this is what you want to model, and this is how you model it. They take a controls course, and they hear: if that is a model of a system, then this is what you do with it. However, there is a big world in-between for which we are here assembled. I think the universities have to raise a new breed that understands integration of the disciplines. At Purdue, we are really concerned about the integration of disciplines, and we are now revising our curriculum accordingly. Structures and dynamics have had a 150-year history of development of very sophisticated methods to answer specific needs. Even though controls is in its infancy (being only a 50-year old subject), it has grown very rapidly and has achieved some sophisticated level. On the other hand, the premises upon which each of these two disciplines are based fall apart when put together. I do not think it is possible to take formally trained structural designers and ask them to understand enough about "controls" to do the job. Conversely, it is not possible to ask formally trained control engineers to learn enough about structures to do the job. I think you need the universities to take it upon themselves to merge those disciplines at the fundamental educational level.

REDIESS: I would like to come back to one other point. There was a presentation by R. A. Russell from NASA Headquarters on a program plan for the control of flexible structures. I do not know how many of you had an opportunity to hear him, but it is in part responding to a special ad hoc subcommittee that was established by NASA to look at the control of flexible space structures. That particular subcommittee was a combination of controls and structures experts. I personally feel they did a very good job of reviewing NASA's program and making some recommendations. I also find that the particular plan put together in responding to that is an excellent plan. I have had involvement for two years in trying to put together these types of plans for NASA. I think the people who did this should be commended, because they present an approach that really couples the disciplines of controls and structures. Often, when we have tried to put together such a program, we ended up packaging in one plan, a controls program and a separate structural dynamics program. I think this plan brings the two disciplines together. I would like to encourage that NASA implement as much of it as possible. I understand that it has been favorably received up to this point. I fully understand the problems of funding these programs, since they get to be extremely expensive. I would encourage them to proceed and accomplish as much as possible.

CARLISLE: I do not know if you are aware, but that was one of two specific new thrusts for next year's budget. So, we in NASA are trying to proceed. I suggest that the universities help. If the government and universities can get together to recognize the problem, it might help.

REDIBSS: The plan proposed was indeed a combination of analytical and theoretical work up through significant ground and flight testing. I think it really is responsive to the community's needs for technology.

BALAKRISHNAN: I just wanted to say that we must not forget the scale of things. In microelectronics, we have projects at the level of $20 million in the universities. As you mentioned, your NASA project is coming along. However, if each group is given only $10K to carry on and participate, you will not get major results. That kind of thing has to change if you want large scale involvement.

SKELTON: I would like to turn the question around to the audience. I am on the Aeronautics and Space Engineering Board (ASEB) of the National Research Council. A committee of the ASEB is looking at the relationships between faculty, industry, and universities. I would appreciate those of you who have specific concerns or ideas on how those relationships can be improved to drop me a note, or somehow register those thoughts, so that I might take them into account. The concern is that in the universities a lot of our potential graduate students are not going on to higher education. If you have concerns that would help to broaden my own perspective in formulating ideas and getting points of view, I would certainly appreciate hearing them.

TECHNICAL EVALUATION REPORT OF THE WORKSHOP ON IDENTIFICATION AND CONTROL OF FLEXIBLE SPACE STRUCTURES

H. A. Rediess and N. Nayak
H. R. Textron, Inc.
Irvine, CA 92714

INTRODUCTION

The main objectives of the workshop were:

- to provide a forum for exchanging ideas and thoughts on how to effectively control large flexible multibody spacecraft; and

- to identify the important unsolved problems of current and future interest leading to possible future collaborative NASA/University/Industry efforts.

The workshop was organized with several sessions addressing the major technical and theoretical issues through invited and contributed papers, three panel discussions, and a final wrap-up session. The workshop agenda is presented in Appendix A. The list of attendees is presented in Appendix B. The purpose of this report is to present a technical evaluation of the workshop that synthesizes the most important results, conclusions, and recommendations for future research.

The workshop covered a wide spectrum of issues involved in the identification and control of flexible space structures. Many different concepts, ideas, and novel solutions were presented in this workshop. A new trend in the workshop was visible. There was a consensus that an integrated approach be adopted to solve the complex and challenging problem of control of large flexible space structures. A me[illegible]ng of control theory, structural design, and materials among others can produce [illegible]ent solution to the problem.

Since NASA is planning for the deployment of large space structures, such as space station and antennas, it was felt that much of the theory that has been developed has to be validated by doing laboratory experiments both on the ground and onboard in space. Of course, there is a continuing need for more basic research in many areas to refine the ideas and concepts and to develop new solutions.

The recommendations outlined below are believed to represent a consensus view from the workshop and draw heavily on the results of the panel discussions and the papers presented. One should not conclude, nor is there any intent to imply, that all participants of the workshop or the wrap-up panel discussion endorsed these recommendations.

MAJOR RECOMMENDATION FOR AREAS OF FUTURE RESEARCH

1. An integrated approach to modeling, control law design, and optimization of space structures

Rationale: Future space structures will be very large and complex with stringent performance requirements. Thus, the control requirements for slewing and stabilizing the structure, and for providing shape control and vibration suppression, necessitate careful review. To minimize control problems, these control requirements must be an integral part of the structure design process. Since a failure-proof control strategy satisfying these requirements does not exist, it is important that additional research be focused on structural modeling and design problems from a controls viewpoint.

2. Model reduction and robustness

Rational: Because of the large size and light weight, the space structure will exhibit a very large number of flexible mode shapes with low frequencies that will interact with the controllers. To control such structures, it is imperative to model the structure very carefully. To keep the model reasonably tractable from a computational point of view, a reduced order model has to be obtained. Some new results are now available to give guidelines in obtaining reduced order models, but good definitions and techniques are needed to measure robustness.

3. Interdisciplinary approach in the control of flexible structures

Rationale: The control of a large flexible space structure is a complex and challenging problem. In order to keep the control simple, functional, and tractable, all the available adjustable parameters must be exploited. For example, by changing certain material properties, the amount of power required for control can be decreased. Thus, by considering options offered through the material and structural properties involved, the control problem can be alleviated considerably. Researchers and engineers are recognizing the potential of this interdisciplinary approach.

4. Adaptive control, estimation and identification

Rationale: Some large space structures, such as space station, will undergo changes in their be dynamic characteristics. Adaptive control is potentially suitable under such conditions, but there is a need for extensive research. In addition, for adaptive control to be effective, a good estimation and identification scheme is needed.

5. Control of distributed systems

Rationale: Since the proposed space structure will be large, it can be viewed as a distributed parameter system. Results obtained in a distributed parameter setting can give a good understanding and insight into choosing a proper control strategy. Control of distributed systems can be viewed as a limiting case of lumped parameter system control. Thus, one can exploit the strong theoretical results of distributed parameter systems theory to study the limiting behavior of lumped parameter systems.

6. Ground and flight experiments

Rationale: There were a considerable number of laboratory experimental results presented at the workshop. These experiments are necessary to validate theory. There should be one or more benchmark test articles set up where various control/estimation/identification algorithms can be tested and compared to provide a better understanding of the overall control problem. Carefully selected and well designed on-orbit experiments should be conducted to further validate identification and control techniques. Particular emphasis should be placed on validating ground testing techniques and techniques for estrapolating ground test data to the space environment. The program should be well coordinated going from analysis, to simple experiments, and to full-blown realistic experiments.

7. Sensor/Actuator placement and development

Rationale: A proper sensor/actuator set on a flexible space structure can be highly effective in controlling the structure. Large and unique space structures will probably need different types of sensors and actuators.

8. Control system fault detection and tolerance research

Rationale: It is important to detect the faults and failures of sensors and actuators in time to control flexible space structures properly. This is particularly critical for stringent performance criteria. After fault detection, the control must be able to reconfigure to the new and smaller set of sensors and actuators.

9. Nonlinear control

Rationale: Because of the complex nature of the flexible structure, nonlinearity may be a part of designing a good control law. More attention needs to be paid to this area to develop a more mature and practical theory.

OTHER RECOMMENDATIONS

1. Real-time processor control laws

   High speed of computation (10 to 100 million operations per second)

   High reliability and durability

   Software languages, verification, validation, and fault tolerance

2. Nonlinear state estimation

3. Active disturbance isolation for Space Station

4. Analysis of high order structural systems with slightly nonlinear stiffness properties

5. Theory of asymptotic properties of systems

6. Applications of random field theory to estimation and system identification

7. Combined treatment of identification and control problem accounting for modeling errors

8. A cooperative program among NASA, DoD, universities and industry to make the most effective use of limited data from major ground and flight experiments

APPENDIX A

PROGRAM SCHEDULE *

WORKSHOP ON
IDENTIFICATION AND CONTROL OF
FLEXIBLE SPACE STRUCTURES

June 4-6, 1984

Hyatt Islandia Hotel
San Diego, California

National Aeronautics and
Space Administration

Jet Propulsion Laboratory
4800 Oak Grove Drive
Pasadena, California 91109

Langley Research Center
Hampton, Virginia 23665

G. Rodriguez, Technical Program Chairman

* EDITOR'S NOTE: This is the final agenda for the workshop including the order in which sessions were held and papers presented. For convenience, the order of some of the papers and sessions was changed before compilation of the proceedings.

WORKSHOP ON IDENTIFICATION AND CONTROL OF FLEXIBLE SPACE STRUCTURES

June 4-6, 1984

Hyatt Islandia Hotel
San Diego, California

OBJECTIVES

The main objective of the Workshop is to explore the application of state-of-the-art modeling, estimation, identification and control methodologies to the control of flexible space structures. The Workshop responds to the rapidly growing interest within NASA in developing the new control technology required for large flexible space systems (platforms, stations, antennas, flight experiments) currently under design. These systems, much larger than any spacecraft flown to date, must satisfy very stringent performance requirements. The Workshop will provide a forum where leading researchers can share ideas, procedures and results on theory and methodology, as well as on practical experience with the emerging flexible space structures.

The Workshop will consist of surveys, tutorial and contributed papers, and open discussion sessions in the following areas:

MISSIONS OF CURRENT INTEREST - Space platforms, antennas, flight experiments, space station.

CONTROL/STRUCTURE INTERACTIONS - Dynamics modeling, distributed system theory, integrated design and optimization, maneuver designs, attitude control and stabilization, shape control.

UNCERTAINTY MANAGEMENT - Parameter identification, model error estimation/compensation, adaptive control, robust control, fault detection, modular control, growth accommodation.

EXPERIMENTAL EVALUATION - Ground experiment demonstrations, flight experiment designs.

Sponsors
National Aeronautics and Space Administration; Jet Propulsion Laboratory, California Institute of Technology, Pasadena, CA; Langley Research Center, Hampton, VA.

Steering Committee
A. E. Bryson, Jr. - Stanford; J. P. Garibotti - H. R. Textron; V. O. Hoehne - AFWAL; S. M. Joshi, L. W. Taylor, Jr. - NASA-LRC; D. McIver - NASA Headquarters; D. L. Mingori, J. S. Gibson - UCLA; G. Rodriguez, S. Z. Szirmay, A. F. Tolivar - JPL; W. E. Vander Velde - MIT.

MONDAY MORNING

June 4, 1984

PLENARY SESSION 1

8:30-9:45 (I) Regency A

Chairmen: G. Rodriguez, Jet Propulsion Laboratory
L. W. Taylor, Jr., NASA Langley Research Center

NASA Space Controls Research and Technology Program
R. W. Key and D. McIver
National Aeronautics and Space Administration

AFWAL Control Technology Program
V. O. Hoehne
Air Force Wright Aeronautical Laboratories

NASA LSS Missions of Current Interest
A. F. Tolivar and J. B. Dahlgren
Jet Propulsion Laboratory

CODING:
- MA = Monday morning
- MP = Monday afternoon
- TA = Tuesday morning
- TP = Tuesday afternoon
- WA = Wednesday morning
- WP = Wednesday afternoon
- (I) = Invited Paper

MONDAY MORNING
June 4, 1984

SESSION MA1: Regency A

CONTROL OF SPACE STATIONS

Chairman: J. B Dahlgren
Jet Propulsion Laboratory

10:00 10:30
A Multivariable Control Technique for a Control Configured Space Station
J. W. Sunkel, NASA Johnson Space Center
A. F Hotz, McDonnell Douglas Company

10:30-11:00
A Dual Spin Space Station Design
M. A. Paluszek, C S Draper Laboratory

11:00-11:30
Dynamics and Control of a Dual Spin Space Station
J. R. Velman and J. J McEnnan, Hughes Aircraft Company

11:30-12:00
Automatic Assembly of Space Stations
P.K.C. Wang, University of California, Los Angeles

12:00-12:30
Space Station Dynamic Modeling, Disturbance Accommodation, and Adaptive Control
S J Wang, C. Ih, Y H. Lin and E. Mettler
Jet Propulsion Laboratory

SESSION MA2 Regency B

FLEXIBLE MULTIBODY DYNAMICS AND CONTROL

Chairman: S M Joshi
NASA Langley Research Center

10:00 10:30
A Reducing Transformation for Dynamics Modeling of a Cluster of Contiguous Flexible Structures with Constraints
R P Singh, Honeywell, Inc
P W Likins, Lehigh University

10:30 11:00
Vibration/Libration Interaction Dynamics and Control During the Orbiter Based Deployment of Flexible Members
V J. Modi and A M Ibrahim, University of British Columbia

11:00-11:30
Design of Multivariable Controllers Using the Integrated Analysis Capability (IAC)
J. A Bossi, University of Washington
S A. Winkleblack, G A. Price, Boeing Aerospace Co.

11:30 12:00
Simulation of Spacecraft Control/Structure Interaction Using Structural System Dynamic Analysis Software
J. W. Young, SDRC, Inc.

12:00-12:30
Attitude Control Tradeoff Study Between a Flexible Beam and a Tether Configuration
S. H. Graff, Jet Propulsion Laboratory

SESSION MA3: Regency C

MODELING AND MODEL REDUCTION

Chairman: J. Sesak
General Dynamics Co.

10:00-10:30
An Overview of Modeling and Control of Large Flexible Space Structures
J B. Santiago, W. J. Lange, Jr., and M. Jamshidi
University of New Mexico

10:30-11:00
Frequency Domain Control Design of Large Space Structures: A Practical Approach
A. Das, R. Harding, General Electric Space Center

11:00-11:30
Model Reduction Based on Frequency Response for Control System Design
D. Enns, Honeywell Systems and Research Center

11:30-12:00
A Control Concept for Large Flexible Spacecraft Using Order Reduction Techniques
G. Thieme and H. Roth, Dornier-System GMBH, West Germany

12:00-12:30
Wideband Disturbance Accommodation in Precision Flexible Space Structures
D. R. Hegg and G J. Kissel, C.S. Draper Laboratory

MONDAY AFTERNOON
June 4, 1984

SESSION MP1 Regency A

CONTROL OF LARGE ANTENNAS

Chairman: V. O. Hoehne
Air Force Wright Aeronautical Laboratories

1:45 2:30
Dynamic Performance of Several Large Antenna Concepts
G. C. Andersen and L. R. Garrett, NASA Langley Research Center
R. E. Calleson, Keutron International

2:30 3:00
Antenna Pointing of Large Flexible Telecommunications Spacecraft
B. Govin and A. Bousquet, MATRA Space Branch, France

3:00 3:30
Design and Evaluation of Control Systems for Large Communications Satellites
M. E. Stieber, Communications Research Centre, Canada

3:30 4:00
Control of Large Antennas Based on Electromagnetic Performance Criteria
Y. H. Lin, M. Hamidi, F. Manshadi, Jet Propulsion Laboratory

4:00 4:30
Vibration Control Experiment Design for the 15-M Hoop/Column Antenna
F. M. Ham and D. C. Hyland, Harris Corporation

4:30 5:00
A Hardware Demonstration of Distributed Control for a Flexible Offset-Feed Antenna
D. B. Schaechter and N. C. Nguyen, Lockheed Missiles and Space Company

5:00-5:30
Model Development for Spacecraft Pointing and Shape Control
J. Sesak, General Dynamics Corporation

SESSION MP2. Regency B

CONTROL OF DISTRIBUTED PARAMETER SYSTEMS

Chairman: P. K. C. Wang
University of California, Los Angeles

1:45 2:30 (I)
The MIPAC Facility: Investigation of Properties of Distributed Parameter Systems
D. L. Russell, University of Wisconsin

2:30 3:00
Finite Control in Underdamped Distributed Parameter Systems
D. J. Inman, State University of New York, Buffalo

3:00 3:30 (I)
New Directions in Asymptotically Stable Finite-Dimensional Adaptive Control of Linear Distributed Parameter Systems
M. J. Balas, Rensselaer Polytechnic Institute

3:30-4:00
Factorization Approach to Optimal Control Design
M. H. Milman, Jet Propulsion Laboratory

4:00 4:30 (I)
Estimation of Parameters in Distributed Models for Large Space Structures
H. T. Banks, Brown University
I. G. Rosen, C.S. Draper Laboratory

4:30 5:00
Space Station Parametric Models
M. Hamidi and S. J. Wang, Jet Propulsion Laboratory

SESSION MP3: Regency C

MODEL REDUCTION AND ROBUSTNESS

Chairman: A. F. Tolivar
Jet Propulsion Laboratory

1:45-2:30
Study on the Control of 3rd Generation Spacecraft
E. J. Davison and W. Gesing, University of Toronto, Canada

2:30-3:00
Sensor/Actuator Selection for the Constrained Variance Control Problem
M. L. DeLorenzo, R. E. Skelton, Purdue University

3:00-3:30
Eigenvalue Assignment by Constrained Optimization
S. M. DeCaro, D. J. Inman, State University of New York, Buffalo

3:30 4:00
Matrix Transfer Function Control Design for Flexible Structures: An Application
T. J. Brennan, A. V. Compito, A. L. Doran, C. L. Gustafson, C. L. Wong, Aerospace Corporation

4:00-4:30
Robust Control Design for Large Space Structures
W. L. Eastman, McDonnell-Douglas, Houston
J. A. Bossi, University of Washington

4:30-5:00
Influence of Structural Parameter Uncertainties on Flexible Space Structure Control Performances
L. Passeron, Aerospatiale, France

5:00-5:30
On the Stability of Collocated Controllers in the Presence of Uncertain Nonlinearities and Other Perils
S. M. Joshi, NASA Langley Research Center

MONDAY EVENING 7:00-9:00 DINNER REGENCY

TUESDAY MORNING
June 5, 1984

SESSION TA1: Regency A

DYNAMICS AND CONTROL EXPERIMENTS

Chairman: R. A. Russell
NASA Headquarters

8:15-9:00 (I)
Large Space Structure Dynamics and Control Experiments
J. Pearson, Air Force Wright Aeronautical Laboratories

9:00-9:30 (I)
Control of Flexible Structures Ground Experiment Plans
R. A. Russell, NASA Headquarters

9:30-10:00
Space Station Configuration and Flight Dynamics ID
E. Mettler and M. Milman, Jet Propulsion Laboratory

10:00-10:30
Current Status of NASA/IEEE Control Design Challenge
L. W. Taylor, Jr., NASA Langley Research Center

10:30-11:00
Large Space Structure Flight Experiment
S. J. Wang, Jet Propulsion Laboratory
D. C. Schwab, Lockheed Missiles and Space Company

11:00-11:30
Time-Optimal Bang-Bang Slew of Rigidized SCOLE Configuration
J. G. Lin, Northeastern University and Control Research Corporation
L. W. Taylor, Jr., NASA Langley Research Center

11:30-12:00
NASA/MSFC Ground Experiment for Large Space Structures Control Verification
S. M. Seltzer, Control Dynamics Company
H. B. Waites, NASA Marshall Space Flight Center

SESSION TA2: Regency B

INTEGRATED MODELING, DESIGN AND OPTIMIZATION

Chairman: G. T. Tseng
Aerospace Corporation

8:15-9:00
Approximation of Optimal Finite-Dimensional Compensators for Flexible Structures
J. S. Gibson, D. L. Mingori, A. Adamian, and F. Jabbari
University of California, Los Angeles

9:00-9:30
Control of a Flexible Space Antenna: A Finite-Dimensional Solution Based on Distributed Parameter Theory
D. L. Mingori, J. S. Gibson, P. Blelloch, and A. Adamian
University of California, Los Angeles

9:30-10:00
An Integrated Control and Minimum Mass Structural Optimization Algorithm for Large Space Structures
A. Messac, J. D. Turner, and K. Soosar, C. S. Draper Laboratory

10:00-10:30
Characteristic Elastic Systems of Time-Limited Optimal Maneuvers
A. L. Hale and R. J. Lisowski, Department of Aeronautical and Astronautical Engineering, University of Illinois, Urbana Champaign, Illinois

10:30-11:00
ISAAC (Integrated Structural Analysis and Control) via Continuum Modeling and Distributed Frequency Domain Design Techniques
C. L. Gustafson, M. Aswany, A. L. Doran, and G. T. Tseng
Aerospace Corporation

11:00-11:30
Control/Structure Optimization
M. Hamidi, M. Salama, and L. Demsetz, Jet Propulsion Laboratory

11:30-12:30
Panel Discussion: Panel will discuss the relationship between the various integration approaches currently under development.

SESSION TA3: Regency C

ADAPTIVE CONTROL

Chairman: R. W. Montgomery
NASA Langley Research Center

8:15-9:00 (I)
Adaptive Control - Actual Status and Research Trends
Y. D. Landau, Laboratoire d'Automatique de Grenoble, France

9:00-9:30
A Nonlinear Dual-Adaptive Control Strategy for Identification and Control of Large Space Structures
F. E. Thau, City College of the City University of New York

9:30-10:30
Stable Direct Adaptive Control of Linear Infinite-Dimensional Systems Using a Command Generator Tracker Approach
M. J. Balas and H. Kaufman, Rensselaer Polytechnic Institute

10:00-10:30
Self-Tuning Adaptive Controller Using Online Frequency Identification
W. W. Chiang and R. H. Cannon, Jr., Stanford University

10:30-11:00
Adaptive Control for Large Space Structures - A Closed-Form Filtering Solution
H. E. Rauch and D. B. Schaechter, Lockheed, Palo Alto Research Laboratory

11:00-11:30 (I)
Robust Algorithms for Adaptive Control
K. S. Narendra, Yale University

11:30-12:30
Panel Discussion: Panel will discuss the role that adaptive control theory can play in the control of flexible space structures.

TUESDAY AFTERNOON
June 5, 1984

SESSION TP1 Regency A

CONTROL/STRUCTURE INTERACTION EXPERIMENTS

Chairman: J. A. Breakwell
Lockheed. Palo Alto Research Lab

1:45-2:30 (I)
Flexible Robot for Space Applications
R. Gran, Grumman Aerospace Company

2:30-3:00
Experiments in Structural Dynamics and Control Using a Grid
R. C. Montgomery and N. Sundararajan, NASA Langley Research Center

3:00-3:30
The Computer-Controlled Experimentation of a Two-Dimensional Hyperbolic System
Y. Yam, University of California, Los Angeles
J. H. Lang and D. H. Staelin, MIT
T. L. Johnson, Bolt Beranek and Newman Inc.

3:30-4:00
Ratio[illegible] for an Experimental Test for Flexible Space Stru[illegible] Attitude Control
Th[illegible], G. Heimbold, B. Schafer, H. Holzach, DFVLR, FRG

4:00-4:30
Numerical and Experimental Evaluation for Single-Axis Control of an LSS Laboratory Model
Y. Ohkami, O. Okamoto, S. Yoshimura, Y. Kida, and I. Yamaguchi, National Aerospace Laboratory, Japan

4:30-5:00
Measurement of Material Damping in a Simulated Space Environment
[illegible] Iberg, Stanford University

5:00-5:30
Optimal Er[illegible] for Damping Identification Experiments
D. B. Eldred, Jet Propulsion Laboratory

SESSION TP2: Regency B

PARAMETRIC AND NONLINEAR CONTROL

Chairman: M. Hamidi
Jet Propulsion Laboratory

1:45-2:30
Parametric Stiffness Control of Flexible Structures
F. C. Moon and R. H. Rand, Cornell University

2:30-3:00
Vibrational Stabilization of Flexible Structures
M. Zak, Jet Propulsion Laboratory

3:00-3:30
Stiffness Control of Large Space Structures
J. L. Fanson, J. C. Chen, Jet Propulsion Laboratory

3:30-4:00
Sub-Optimal Control of Nonlinear Flexible Space Structures
J. Dehaghanyar, S. F. Masri, R. K. Miller, and G. A. Bekey, University of Southern California
T. K. Caughey, California Institute of Technology

4:00-4:30
BREAK

4:30-5:30
Panel Discussion: Interdisciplinary Issues in the Control of Flexible Structures
Tentative Participants: J. F. Garibotti, Moderator; D. L. Mingori, UCLA; V. B. Venkayya, AFWAL; A. Nayak, H. R. Textron; I. Sesak, General Dynamics Co.

SESSION TP3: Regency C

ESTIMATION/IDENTIFICATION

Chairman: L. W. Taylor, Jr.
NASA Langley Research Center

1:45-2:30 (I)
Maximum Likelihood Estimation with Emphasis on Aircraft Flight Data
K. W. Iliff, NASA Ames Research Center
Dryden Flight Research Facility

2:30-3:00
Optimal Sensor Locations for Structural Identification
F. E. Udwadia, University of Southern California
J. A. Garba, Jet Propulsion Laboratory

3:00-3:30
Combined State and Parameter Estimation for a Static Model of the Maypole (Hoop/Column) Antenna Surface
H. T. Banks, Brown University
P. K. Lamm, Southern Methodist University
E. S. Armstrong, NASA Langley Research Center

3:30-4:00
Experimental Verification of Identification Algorithms for Control of Flexible Structure
B. Sridhar, J. N. Aubrun, and K. R. Lorell, Lockheed Palo Alto Research Laboratory

4:00-4:30
An Eigensystem Realization Algorithm (ERA) for Modal Parameter Identification
N. Juang and R. S. Pappa, NASA Langley Research Center

4:30-5:00
A Function Space Approach to Maximum Likelihood Identification of Parameters in Elliptic Systems
G. Rodriguez and R. Scheid, Jet Propulsion Laboratory

TUESDAY EVENING 6:30 - 8:30 NO HOST SOCIAL PERIOD

WEDNESDAY MORNING

June 6, 1984

*PLENARY SESSION 1 - AMERICAN CONTROL CONFERENCE

8:30-9:30 **Regency Room**

CHAIRMAN:	Herbert E. Rauch, Lockheed, Palo Alto Research Lab
CO-CHAIRMAN:	Leonard Shaw, Polytechnic Institute of New York
KEYNOTE ADDRESS:	Getting It All Under Control Robert A. Frosch, Vice President, General Motors Research Laboratories

*This plenary session constitutes the initiation of the 1984 American Control Conference. While the session is not part of the Identification and Control Workshop, all workshop participants are welcome to attend at no additional cost. Because it was anticipated that this plenary lecture by a former NASA administrator would generate significant interest among the workshop participants, no other workshop activities have been scheduled in this time period. A workshop plenary session described on the following page has been scheduled immediately following the ACC plenary session lecture.

WEDNESDAY MORNING

June 6, 1984

PLENARY SESSION 2

9:45-1:00 (I) **Regency A**

TITLE: **FUTURE RESEARCH DIRECTIONS**

CHAIRMAN: **H. A. Rediess, H. R. Textron**

Uncertainty Management Methodology for Large Space Structures
W. E. Vander Velde, MIT

Some Estimation and Identification Problems in Random Fields
A. V. Balakrishnan, University of California, Los Angeles

Some Trends and Problems in Control Theory of Distributed Parameter Systems
J. L. Lions, I.N.R.I.A. and College de France

Model Error Structure and the Inseparability of the Control and Identification Problems
R. E. Skelton, Purdue University

The Role of Experiments in the Development of Control Technology
H. A. Rediess, H. R. Textron

Future Research and Technology Directions for Space Station
R. F. Carlisle, NASA Headquarters

Panel Discussion: Panel will discuss the state-of-the-art in modeling, estimation, identification and adaptive control and will identify potential research opportunities for NASA consideration. This wrap-up session will also provide a forum for all participants to further comment on the papers and issues presented and to contribute recommendations.

APPENDIX B

WORKSHOP ON IDENTIFICATION AND CONTROL OF FLEXIBLE SPACE STRUCTURES

ATTENDEES/PARTICIPANTS

A. Adamian
UCLA
4731 Boelter Hall
Los Angeles, CA 90024

A. Alexandridis
GM Research Labs
Dept. 15
Warren, MI 48090

*G. Andersen
LaRC M/S 364

R. Araya
UCLA
BYH 4531
Los Angeles, CA 90024

*E. S. Armstrong
LaRC M/S 161

M. Aswani
The Aerospace Corp.
M/S M4/921
P. O. Box 92957
Los Angeles, CA 90274

C. B. Auchter
United Space Boosters
P. O. Box 1626
Huntsville, AL 35807

+W. E. Bachman
JPL M/S 198-112C

T. Baker
U.C. Berkeley
262 Cory Hall
Berkeley, CA 90026

A. V. Balakrishnan
University of California
Los Angeles
Los Angeles, CA 90024

M. J. Balas
ESCE Department
Rensselaer Polytechnic Institute
Troy, NY 12181

S. S. Banda
Flight Dynamics Lab
AFWAL/FIGC
Wright Patterson AFB
OH 45433

H. T. Banks
Applied Math Dept.
Brown University
Providence, RI 02912

M. Barrett
Honeywell, Inc.
2600 Ridgway Parkway
Box 312
Minneapolis, MN 55440

D. Barrows
MDAC
5301 Bolsa Avenue
Huntington Beach, CA 92647

L. Bindin
ISA
P.T. Arun NGL
Singapore

P. Blelloch
UCLA
4731 Boelter Hall
Los Angeles, CA 90024

J. A. Bossi
University of Washington
Dept. of Aero. & Astro. FS-10
Seattle, WA 98195

J. Breakwell
Lockheed Research Labs
3251 Hanover Street
Palo Alto, CA 94304

+Affiliated with Jet Propulsion Laboratory, California Institute of Technology, 4800 Oak Grove Drive, Pasadena, CA 91109

*Affiliated with NASA Langley Research Center, Hampton, VA 23665

T. Brennan
Aerospace Corporation
M4/971
P. O. Box 92957
Los Angeles, CA 90009

P. E. Brey
Wayne State University
Dept. of Mech. Engineering
667 Merrick
Detroit, MI 48128
Toronto, Ontario, Canada M5S1A4

+J. Cameron
JPL M/S 198-326

R. Carlisle
NASA Headquarters
Code S, B-536
Washington, D.C. 20546

D. Carlstrom
Frito-Lay Research
900 N. Loop 12
Irving, TX 75206

M. J. Chang
Goodyear Aerospace Corp.
1210 Massillon Road
Akron, OH 44315

R. Chang
TRW Systems 82/2024
One Space Park
Redondo Beach, CA 90278

+J. C. Chen
JPL M/S 157-316

W. W. Chiang
Stanford University
Durand 017, Dept. of Aero/Astro
Stanford, CA 94305

E. M. Cohen
The Foxboro Co.
D835, Bristol Park
Foxboro, MA 02035

A. Compito
Aerospace Corporation
2350 E. El Segundo Blvd.
El Segundo, CA 90250

+J. J. Cucchissi
JPL M/S 511-202

+J. B. Dahlgren
JPL M/S 198-326

A. Das
AFRPL
AFRPL/DYS/Stop 24
Edwards Air Force Base
CA 93534

E. J. Davison
Dept. of Electrical Engineering
Toronto, Ontario, Canada M5S1A4

F. De Canio
C. S. Draper Laboratories
555 Technology Square
Cambridge, MA 02139

R. DeCarlo
Purdue University
School of Elec. Engineering
West Lafayette, IN 47906

S. M. DeCaro
A.T. & T. Bell Labs
7 Hamilton Rd., Apt. 3C
Morristown, N. J.

+L. Demsetz
JPL M/S 157-316

J. A. Donaldson
Howard University
Mathematics Dept.
Washington, D.C. 20059

A. Doran
UCLA
5713 Boelter Hall
Los Angeles, CA 90024

W. L. Eastman
McDonnell-Douglas
16441 Space Center Blvd, E-2
Houston, TX 77062

D. L. Edberg
Stanford University
Dept. of Aero & Astro
Stanford, CA 94305

+Affiliated with Jet Propulsion Laboratory, California Institute of Technology, 4800 Oak Grove Drive, Pasadena, CA 91109

+D. B. Eldred
JPL M/S 198-326

J. Garibotti
H. R. Textron, Inc.
2485 McCabe Way
Irvine, CA 92714

+ S. Graff
JPL M/S T1201

R. Gran
Grumman Aerospace
Bethpage, NY 11714

C. L. Gustafson
Aerospace Corporation
P. O. Box 92957
Los Angeles, CA 90009

A. L. Hale
University of Illinois, AAE Dept.
104 S. ... hews Avenue
Urbana, IL 61801

D. R. Haley
BITS, Inc.
10210 Greenbelt Road
Suite 440
Seabrook, MD 20706

F. M. Ham
Harris Corp. (GASD)
P. O. Box 94000
M/S 15-500A
Melbourne, FL 32902

M. Hamidi
JPL M/S 198-326

R. Harding
General Electric
Valley Forge, PA 19481

D. R. Hegg
C. S. Draper Laboratories
M/S 60
555 Technology Square
Cambridge, MA 02139

D. Herrick
R & D Associates
International Airport, ATO 9377
Albuquerque, NM 87119

V. O. Hoehne
AFWAL/FIGC
Wright Patterson AFB
OH 45433

+C. Ih
JPL M/S 198-326

K. Iliff
NASA Ames/Dryden
M/S D-OFD
P. O. Box 273
Edwards, CA 93523

D. J. Inman
University of Buffalo
Dept. of Mech. & Aerospace Eng.
SUNYAB
Buffalo, NY 14260

F. Jabbari
UCLA
Los Angeles, CA 90024

S. Jacobs
USBI
P. O. Box 1626
Huntsville, AL 35801

W. J. Jasper
Hughes Aircraft Co.
Bldg. S41, MS B323
P. O. Box 92919, Airport Station
Los Angeles, CA 90009

*S. M. Joshi
LaRC M/S 161

*J. N. Juang
LaRC M/S 230

C. Karl
MIT
77 Massachusetts Avenue
Rm 10-025
Cambridge, MA 00213

+Affiliated with Jet Propulsion Laboratory, California Institute of Technology, 4800 Oak Grove Drive, Pasadena, CA 91109

*Affiliated with NASA Langley Research Center, Hampton, VA 23665

J. Kelly
McDonnell Douglas Astronautics
5301 Bolsa Avenue
Huntington Beach, CA 92647

+R. Key
JPL M/S 180-701

M. J. Klepl
Rockwell International
201 N. Douglas Street
P. O. Box 92098
Los Angeles, CA 90009

D. Klinger
LMSC
7538 Waterford Dr.
Cupertino, CA 95014

I. Landau
C.N.R.S. "Systemes Adaptatifis"
Ensieg BP 46
38402 St. Martin D'Heres, France

Th. Lange
DFVLR, WT RM
8031 Oberpfaffenhoten
Post Webling, FRG

W. J. Lange
Kirtland AFB
7640 Arroyo del Oso NE
Albuquerque, NM 87109

J. H. Lilly
Electrical Engineering Dept.
University of Kentucky
Lexington, KY 40506

J. G. Lin
Control Research Corp.
6 Churchill Lane
Lexington, MA 02173

+Y H. Lin
JPL M/S 198-326

K. R. Lorell
Lockheed Research Labs
3251 Hanover Street
Palo Alto, CA 94306

M. Lukich
TRW Electronics & Defense
One Space Park
Bldg. R4, Rm 1189
Redondo Beach, CA 90278

P. Mak
Aerospace Corp.
M/S M4-971
2350 E. El Segundo Blvd.
El Segundo, CA 90245

D. B. Malkoff, M.D.
Navy Personnel & Develop. Center
Code 71
San Diego, CA 92152

L. Markus
University of Minnesota
Mathematics Dept.
Minneapolis, MI 55455

+N. Marzwell
JPL M/S 198-326

G. Y. Matsumoto
TRW
One Space Park, R4/1082
Redondo Beach, CA 90278

M. Masubuchi
Osaka University
Dept. of Mech. Engineering
Suita, Osaka, Japan

W. A. Matthews
Rockwell Int'l.
16323 Parksley Drive
Houston, TX 77059

+E. Mettler
JPL T-1201

C. J. Meyers
U.S. Air Force
Kirtland AFB
Albuquerque, NM 87109

R. K. Miller
University of So. California
Dept. of Civil Engineering
Los Angeles, CA 90089-0242

+Affiliated with Jet Propulsion Laboratory, California Institute of Technology, 4800 Oak Grove Drive, Pasadena, CA 91109

T. R. Miller
IBM Corporation, Dept. 235
1701 North Street, Bldg. 250-2
Endicott, NY 13760

+M. Milman
JPL M/S 198-326

D. L. Mingori
UCLA
4731 Boelter Hall
Los Angeles, CA 90024

V. J. Modi
Dept. of Mechanical Engineering
University of British Columbia
Vancouver, B.C., Canada

*R. C. Montgomery
LaRC M/S 161

F. Moon
Cornell University
Dept. of Theoretical & Appl. Mech.
Thurston Hall
Ithaca, NY 14853

A. P. Nayak
H. R. Textron
2485 McCabe Way
Irvine, CA 92714

Y. Ohkami
National Aerospace Laboratory
1880 Jindaiji Chotu
Tokyo, Japan

H. Okubo
University of Osaka Prefecture
Dept. of Aeronautical Engineering
Sakai, Osaka 591
Japan

H. H. Ottesen
IBM
5905 Chateau Rd. N.W.
Rochester, MN 55901

C. Partin
Lockheed Engineering &
Management Services
1830 Nasa Road One
Houston, TX 77223

M. Paluszek
C. S. Draper Laboratories
555 Technology Square, M/S 60
Cambridge, MA 02139

L. R. Passeron
Aerospatiale
100 Boulevard du Midi
06322 Cannes La Bocca Cedex
B.P. 99, France

A. N. Payne
Lawrence Livermore Laboratory
P. O. Box 5540, L-153
Livermore, CA 94550

J. Peebles
McDonnell Douglas Astronautics
5301 Bolsa Avenue
A3-222-13-3
Huntington Beach, CA 92647

M. P. Polis
National Science Foundation
1800 G. Street, N.W.
Washington, D. C. 20550

T. A. Posbergh
University of Maryland
College Park, MD 20742

G. A. Price
101 228th Avenue, S. E.
Redmond, WA 98053

R. V. Ramnath
Raytheon
12 Fessenden Way
Lexington, MA 02173

A. S. S. R. Reddy
Howard University
Dept. of Mech. Engineering
Washington, D.C. 20059

H. A. Rediess
H. R. Textron, Inc.
2485 McCabe Way
Irvine, CA 92714

D. B. Ridgely
Flight Dynamics Laboratory
AFWAL/FIGC
Wright Patterson AFB, Ohio 45433

+Affiliated with Jet Propulsion Laboratory, California Institute of Technology, 4800 Oak Grove Drive, Pasadena, CA 91109

*Affiliated with NASA Langley Research Center, Hampton, Virginia 23665

+G. Rodriguez
JPL M/S 198-326

G. Rosen
C. S. Draper Laboratories
555 Technology Square, M/S 60
Cambridge, MA 02139

D. L. Russell
University of Wisconsin
480 Lincoln Drive
Madison, WI 53706

*R. Russell
LaRC M/S 162

+M. Salama
JPL M/S 157-326

R. L. Sanders
United Technologies
Huntsville, AL 35804

C. M. Satter
C. S. Draper Laboratories
555 Technology Square
Cambridge, MA 02139

D. Schaechter
Lockheed Palo Alto Research Labs
3251 Hanover Street, B205,O 92-30
Palo Alto, CA 94304

+R. E. Scheid, Jr.
JPL M/S 198-326

J. R. Sesak
General Dynamics Convair
P. O. Box 85357, M/S 21-9530
San Diego, CA 92138

M. Shafer
NASA Ames/Dryden
M/S D-OFDD
P O. Box 273
Edwards, CA 9352

D. C. Schwab
LMSC
1111 Lockheed Way, Bldg. 104
Dept. 62-11
Sunnyvale, CA 94089

R. P Singh
Honeywell, Inc.
13350 U. S. Highway 19 South
Clearwater, FL 33563

+S. W. Sirlin
JPL M/S 198-326

R. E. Skelton
Purdue University
North Lafayette, IN 47907

G. Smit
Aerospace Corporation
2350 E. El Segundo Blvd.
El Segundo, CA 90245

B. Sridhar
Lockheed Research Labs
3251 Hanover Street
Palo Alto, CA 94304

D. S. Stauffer
NTI
Bradford Drive
Huntsville, AL 35805

M. Stieber
Communcations Research Centre
P. O. Box 11490, Station H
3701 Carling Avenue
Ottawa, Ontario, Canada U2H852

+S. Z. Szirmay
JPL M/S 198-326

*L. W. Taylor, Jr.
LaRC M/S 161

+Affiliated with Jet Propulsion Laboratory, California Institute of Technology. 4800 Oak Grove Drive, Pasadena, CA 91109

*Affiliated with NASA Langley Research Center, Hampton, VA 23665

F. E. Thau
City College of the City
University of New York
New York, NY 10031

G. Thieme
Dornier System GMBH
Dept. ERMR
Postfach 1360
D-7990 Friedrichshafen 1
West Germany

+A. F. Tolivar
JPL M/S 198-326

S. S. Tripathi
Perkin-Elmer Corporation
100 Wooster Heights Road
Danbury, CT 06810

C. T. Tseng
The Aerospace Corporation
P. O. Box 92957, M4/971
Los Angeles, CA 90009

F. Tung
One Space Park
Redondo Beach, CA 90278

J. D. Turner
Cambridge Research
Belmont, MA 02178

F. E. Uwadia
USC
University Park, 364 DRB
Los Angeles, CA 90007

S. Utku
Duke University
122 Engineering
Durham, NC 27706

B. Venkayya
AFWAL/FIBR
Wright Patterson AFB
OH 45433

W. E. Vander Velde
Mass. Institute of Technology
Room 33-109
Cambridge, MA 02139

D. Vervaerde
Dornier System GMBH
BP 27,94190 Villeneuve
St. Georges, France

L. Q. Vu
University of California
Davis Hall #516
SESM Division
Berkeley, CA 94720

+B. Wada
JPL M/S 157-507

P.K.C. Wang
UCLA
4531 Boelter Hall
Los Angeles, CA 90024

+S. J. Wang
JPL M/S 198-326

D. Washburn
R&D Associates
105 E. Vermijo, Suite 450
Colorado Springs, CO 80903

T. Weber
General Motors Research Labs
GM Technical Center
Power Systems Research Dept.
Warren, MI 48090-9057

M. Webster
McDonnell Douglas Astronautics
Huntington, Beach, CA 92647

P. Wei
Lockheed-Georgia Company
Dept. 72-42, Zone 418
South Cobb Drive
Marietta, GA 30063

N. Wright
TRW
One Space Park, 82/2754
Redondo Beach, CA 90248

H. Woo
Rockwell, Int'l
12214 Lakewood Blvd.
Downey, CA 90241

+Affiliated with Jet Propulsion Laboratory, California Institute of Technology, 4800 Oak Grove Drive, Pasadena, CA 91109

AFWAL/FIGC
Wright Patterson AFB
OH 45433

Y. Yeung
1326 Federal Avenue, Apt. 3
West Los Angeles, CA 90025

Y. Yez-Pien
UCLA
500 Landfair Avenue, 717
Los Angeles, CA 90024

K. Yong
The Aerospace Corporation
2350 E. El Segundo Blvd.
El Segundo, CA 90245

J. W. Young
SDRC, Inc.
11055 Roselle Street
San Diego, CA 92121

+M. Zak
JPL M/S 157-102

+Affiliated with Jet Propulsion Laboratory, California Institute of Technology, 4800 Oak Grove Drive, Pasadena, CA 91109

NASA—JPL—Coml., L.A., Calif.